

INDIAN JOURNAL OF PHYSICS

VOL. 33

AND

PROCEEDINGS

OF THE

Indian Association for the Cultivation of Science, Vol. 42

(Published in Collaboration with the Indian Physical Society)

(With Twelve Plates)

Printed by Kalipada Mukherjee, Eka Press, 204/1, B. T. Road, Calcutta
and published by the Registrar, Indian Association for the Cultivation
of Science, Jadavpur, Calcutta 32

1959

BOARD OF EDITORS

R. K. ASUNDI	P. S. GILL
K. BANERJEE	S. K. MITRA
D. M. BOSE	P. RAY
S. N. BOSE	K. R. RAO
K. R. DIXIT	S. C. SIKKAR (<i>Secretary</i>)

B. N. SRIVASTAVA

EDITORIAL COLLABORATORS

PROF. D. BASU, PH.D.
DR. A. BOSE, D.SC.
DR. N. N. DASGUPTA, M.SC., PH.D.
PROF. A. K. DUTTA, D.SC. F.N.I.
DR. S. GHOSH, D.SC.
DR. S. R. KHASTGIR, D.SC., F.N.I., F.R.S.E.
PROF. P. K. KICHLU, D.SC., F.N.I.
PROF. D. S. KOTIARI, D.SC., F.N.I.
DR. K. S. KRISHNAN, D.SC., F.R.S.
PROF. B. D. NAG CHOWDHURY, PH.D.
PROF. S. R. PALIT, D.SC., F.R.I.C., F.N.I.
DR. S. PARTHASARATHY, D.SC., F.N.I.
DR. H. RAKSHIT, D.SC., F.N.I.
DR. R. GOPALAMURTY RAO.
DR. VIKRAM A. SARABHAI, M.A., PH.D.
PROF. N. R. TAWDE, D.SC., F.N.I.
DR. P. VENKATESWARLU.

ASSISTANT EDITOR

SRI MONOMOHAN MAZUMDER, M.Sc.

Annual Subscription—

Inland Rs. 20

Foreign £ 2 or 6

NOTICE TO INTENDING AUTHORS

Manuscripts for publication should be sent to the Assistant Editor, Indian Journal of Physics, Jadavpur, Calcutta-32.

The manuscripts submitted must be type-written with double space on thick foolscap paper with sufficient margin on the left and at the top. The original copy, and not the carbon copy, should be submitted. Each paper must contain an ABSTRACT at the beginning.

All REFERENCES should be given in the text by quoting the surname of the author, followed by year of publication, e.g., (Roy, 1958). The full REFERENCE should be given in a list at the end, arranged alphabetically, as follows; Roy, S. B., 1958, *Ind. J. Phys.*, **32**, 323.

Line diagrams should be drawn on white Bristol board or tracing paper with black Indian ink, and letters and numbers inside the diagrams should be written neatly in capital type with Indian ink. The size of the diagrams submitted and the lettering inside should be large enough so that it is legible after reduction to one-third the original size. A simple style of lettering such as gothic, with its uniform line width and no serifs should be used, e.g.:

A·B·E·F·G·M·P·T·W·

Photographs submitted for publication should be printed on glossy paper with somewhat more contrast than that desired in the reproduction, and should, if possible, be mounted on thick white paper.

Captions to all figures should be typed in a separate sheet and attached at the end of the paper.

The mathematical expressions should be written carefully by hand. Care should be taken to distinguish between capital and small letters and superscripts and subscripts. Repetition of a complex expression should be avoided by representing it by a symbol. Greek letters and unusual symbols should be identified in the margin. Fractional exponents should be used instead of root signs.

INDIAN JOURNAL OF PHYSICS. 33, 1959

CONTENTS

No. 1. January

	PAGE
1. A Study of Neon F_2 Ionization in Relation to Geomagnetic Coordinates—J. N. Bhar and P. Dhar Bhowmik	1
2. A Case for Efficacy of Hulburt-Hirschfelder Potential Function N. R. Tawde and M. R. Katti	18
3. Resonance Curves of a Synchronised Oscillator—B. R. Nag	23
4. A Micro-Calorimeter for Measurement of small Heat Changes—S.N. Bhattacharya and S. K. Das	36
5. Electronic Spectra of 1, 3, 5-Trimethylbenzene in the Liquid State and in the Solid State at -180°C —S. K. Sen	41
6. Polarised Electronic Spectra of Single Crystals of Para Dichlorobenzene—S. C. Sirkar and T. N. Misra	45

No. 2. February

7. Dipole Moments of some Aliphatic Amines—D. V. G. L. Narasimha Rao	51
8. Study of an Oscillator with two Degrees of Freedom by a Differential Analyser—B. R. Nag	57
9. Light Absorption in Paramagnetic Ions in State of Solution. Part I—Cupric Ions—A. Mookherji and N. S. Chhonkar	74
10. A Test for Hulburt-Hirschfelder Potential Function—N. R. Tawde and M. R. Katti	89
11. Raman Spectra of Solutions of Ethylene Dichloride, Ethylene Dibromide and Ethylene Chlorhydrin at low Temperatures—Monomohan Mazumder	92

LETTERS TO THE EDITOR

1. Studies on Phase Transition of Synthetic $\gamma\text{-Fe}_2\text{O}_3 \cdot \text{H}_2\text{O}$ —S. Ray and A. Roy	101
---	-----

No. 3. March

12. Calculations of the Nuclear Quadrupole Coupling Constant for I_2 —D. V. G. L. Narasimha Rao	103
13. Crystal Structure of 1, 2-Cyclo-Pentenophenanthrene—B. S. Basak and M. G. Basak	107
14. A Simple Phase-Meter for Laboratory Use—B. Chatterjee	111
15. Investigations on the Paramagnetic Resonance in Coal with a Transmission Type Electron Paramagnetic Resonance Spectrometer—G. N. Sarkar, A. Mukherji, R. N. Chatterjee and U. S. Ghosh	117

	PAGE
16. Renninger Effect in Naphthazarin—P. Srivastava	123
17. A Note on the Dependence of the Sputtering Produced by Bombardment by Canal Rays on their Angle of Impact—V. T. Chiplonkar and B. N. Varadrajan	127
18. Intensity of Brillouin Components in Light Scattered by Some Liquids—K. C. Medhi	135
19. A Magnetic Spectrometer for Charged Particles—S. B. Karmohapatro	139

No. 4. April

20. Construction of a 14 MeV Neutron Generator Utilizing $T^3(d, n) He^4$ Reaction and Measurement of fast Neutron Flux—Bimalendu Mitra	149
21. Energy Distribution of Neutrons from RaD-Be Source—B. Sen ...	158
22. Magnetic Study of Iron-Containing Glasses at Room Temperature—Bhupati Kumar Banerjee	165
23. Proton-Nucleus Scattering at 96 MeV—Arundhati Ghose ...	177
24. Some Studies on the Effects of Limiting in a Position Control Servo Containing Backlash—A. K. Mahalanabis	183

No. 5. May

25. Elastic Scattering and Polarization of 300 MeV Protons—Arundhati Ghosh	197
26. Magnetic Study of Iron-Containing Glasses at low Temperature—Bhupati Kumar Banerjee	201
27. Singlet→Triplet Transition in Para-chlorotoluene—J. K. Roy ...	209
28. Polarisation of Nucleons due to Anomalous Magnetic Moment in Higher Born Approximation—S. Sarkar	213
29. Unlike Molecular Interactions from Viscosity and Inter-Diffusion—A. K. Barua	221
30. The Temperature Dependence of Inter-Diffusion Coefficient for Some Pairs of Rare Gases—K. P. Srivastava and A. K. Barua ...	229

LETTERS TO THE EDITOR

2. Spectra of Dimethoxybenzenes. Part I—Metadimethoxybenzene K. Sreeramamurty	241
--	-----

N. 6. June

31. An Investigation into the Momentum Distribution in Light Nuclei—C. M. Pujara and K. M. Gatha	243
32. Design of Pulse Amplifier—R. C. Ganguli	263
33. On Polarised Electron Spectrum of Single Crystal of Paradibromobenzene At $-180^{\circ}C$ —T.N.Misra	276

LETTERS TO THE EDITOR

- | | |
|--|-----|
| 3. Effect of Chemical Treatment on the Structure and Properties of Graphite—S. Ray | 282 |
|--|-----|

No. 7. July

- | | |
|--|-----|
| 34. A Reinvestigation of the Decay of Na-22—M. K. Ramaswamy | 285 |
| 35. The Infrared Spectra of Ortho, Meta and Para Thiocresols
—R. N. Bapat | 295 |
| 36. The Space Group of Meta Toluic Acid—R. C. Srivastava | 305 |
| 37. On Wave Solution of Field Equations in Einstein's Unified Field Theory—N. N. Ghosh | 307 |
| 38. Gyro-Frequency in the Ionospheric Regions—S. Datta and R. N. Datta | 316 |
| 39. The Magnetic Behaviours of Titanium Caesium Sulphate Alum
—A. Bose, A. S. Chakravarty and R. Chatterjee | 325 |

No. 8. August

- | | |
|--|-----|
| 40. The Raman Spectra of Ortho-, Meta-, and Para-Thiocresols—
R. N. Bapat | 329 |
| 41. Low-Energy Spectrum of the Sea-level Electrons and Muons at 12°N—Nilima Mishra (Basu) and M. S. Sinha | 335 |
| 42. Infrared Absorption Spectra of Ethylene Chlorhydrin in the Vapour State and in Solution in Different Solvents—Monomohan Mazumder | 346 |
| 43. A Simple Method for the Energy Estimation of Electron Pairs
—P. K. Aditya | 357 |
| 44. Powder Data, Unit Cell and Space Group for Ferrous Sulphate
C. W. F. T. Pistorius | 363 |

LETTERS TO THE EDITOR

- | | |
|---|-----|
| 4. Absorption of 8-Millimetre Waves in Ethyl Bromide—G. P. Srivastava | 367 |
|---|-----|

No. 9. September

- | | |
|---|-----|
| 45. Space Group of 1, 3, 5-Trichlorobenzene—S. G. Biswas | 371 |
| 46. Visible Absorption Spectrum of Benzoquinone—Rama Shankar Singh | 376 |
| 47. Level Scheme of Pr ¹⁴⁴ —A. K. Sngupta, R. Bhattacharyya, J. Lahiri and P. N. Mukherjee | 388 |
| 48. Neutron Strength Function $\bar{\Gamma}n^0/D$ with Complex Diffuse Boundary Potential—Arundhati Ghosh | 395 |
| 49. Space Group of Cyclohexanone at -180°C—G. S. R. Krishna Murti | 401 |

	PAGE
LETTERS TO THE EDITOR	
5. Increase in Breakdown Potential of a Gas in Electrodeless Discharge in the Presence of a Transverse Magnetic Field and the Concept of Equivalent Pressure—S. N. Goswami	405
6. Effect of Chemical Treatment on the Electrical Conductivity of Graphite—R. Bhattacharyya	407
7. Magnetic Anisotropy of Fe^{++} Ion in Siderite—A. Mookherji and S. C. Mathur	41

No. 10. October

50. The Question of the Existence of ($\Delta^\circ P$), ($\Sigma^+ P$) and ($\Sigma^- n$) Hyper-fragments—R. C. Kumar	411
51. A Statistical Analysis to test the Reliability of Measuring Atmospheric Noise Subjectively by a small Group of People—B. B. Ghosh	415
52. Velocity of Sound in Water as a Function of Temperature and Pressure—Arvind Mohan Srivastava and Y. P. Varshni ...	423
53. Some Possible arrangements of Parametric Amplifiers Employing Lower Frequency Pumping—N. B. Chakrabarti and K. D. Dikshit	431
54. Electron Temperature in Electrodeless Discharge Subjected to a Transverse Magnetic Field—S. N. Goswami ...	452

LETTERS TO THE EDITOR

8. Preliminary Report on the Crystal Structure of Anthrone—Surendra Nath Srivastava	456
9. On the Crystal Structure of Methanol at -180°C —G. S. R. Krishna Murti	459

No. 11. November

55. Action Principle and Lagrangian with higher order Derivatives—S. P. Misra	461
56. X-Ray Small Angle Measurements on 1% Solution of Haemoglobin Corpuscular Protein—T. Ratho	469
57. Spectroscopic Constants of Molecules VII. Relation Between Force Constant and Equilibrium Internuclear Distance for Hydride Diatoms—Yatendra Pal Varshni, Shashanka Shekhar Mitra and Ramesh Chandra Shukla	473
58. Studies on the Magnetic Susceptibility of some V^{3+} Alums and Ti^{3+} Caesium Alum in the Range 300°K to 100°K —S. K. Dutta-Roy, A. S. Chakravarty and A. Bose	483
59. On the Absorption of 3.18 cm Microwaves in Ethylene Chlorhydrin and its Solutions—T. J. Bhattacharyya	498

	PAGE
LETTERS TO THE EDITOR	
10. Relationship between Ultrasonic Velocity and other Physical Properties of Pure Organic Liquids—Satish Chandra Srivastava ...	503
No. 12. December	
60. The Evaluation of the Electronic Transition Moment for the $b^3\Sigma^+ \rightarrow a^3\pi$ System of CO.—N. R. Tawde and B. S. Patil ...	505
61. Temperature Variation of Dielectric Relaxation in six Polar Liquids —J. Sobhanadri ...	511
62. Application of Schwinger's Action Principle to Quantise a fourth Order Meson Field—S. P. Misra ...	520
63. A Short Note on the Crystalline Electric Fields in Hydrated Co^{2+} Salts—A. S. Chakravarty and R. Chatterjee ...	531
64. Influence of Interatomic Resonance on the Frequency of Re-Emitted Resonance Radiation—G. S. Kastha ...	534
65. Effect of Annular Solar Eclipse of 19th April, 1958 (at Sunrise) on the F_2 Layer of the Ionosphere—S. N. Mitra and B. C. Narasinga Rao ...	540
LETTERS TO THE EDITOR	
11. A Note on the Spectrum of Br IV—Y. Bhupala Rao ...	546
12. On the Magnetic Perturbation of an Electron Beam —S. Yamaguchi	547

AUTHOR INDEX

AUTHOR	SUBJECT	PAGE
Aditya, P. K.	A simple method for the energy estimation of electron pairs	357
Banerjee, Bhupati Kumar	Magnetic study of iron-containing glasses at room temperature	165
,,	Magnetic study of iron-containing glasses at low temperature	201
Bapat, R. N.	The infrared spectra of ortho, meta and para thiocresols	295
,,	The Raman spectra of ortho, meta, and para-thiocresols	329
Barua, A. K.	Unlike molecular interactions from viscosity and inter-diffusion	221
,,	See Srivastava, K. P.	229
Basak, B. S. and M. G. Basak	Crystal structure of 1, 2-cyclo-pentenophenanthrene	107
Basak, M. G.	See Basak, B. S.	107
Bhar, J. N. and P. Dhar Bhowmik	A study of noon F_2 ionisation in relation to geomagnetic co-ordinates	1
Bhattacharyya, R.	Effect of chemical treatment on the electrical conductivity of graphite (L)	407
,,	See Sengupta, A. K.	388
Bhattacharya, S. N. and S. K. Das	A micro-calorimeter for measurement of small heat changes	36
Bhattacharyya, T. J.	On the absorption of 3.18 cm microwaves in ethylene chlorhydrin and its solutions	498
Biswas, S. G.	Space group of 1,3,5-trichlorobenzene	371
Bose, A.	See Dutta-roy, S.K.	483
Bose, A., A. S. Chakravarty and R. Chatterjee	The magnetic behaviour of titanium caesium sulphate alum	325
Chakravarty, A. S.	See Bose, A.	325
Chakravarty, A. S. and R. Chatterjee	A short note on the crystalline electric fields in hydrated Co^{2+} salts	531
Chakravarty, A. S.	See Dutta-Roy, S. K.	483
Chakrabarti, N. B. and K. D. Dikshit	Some possible arrangements of parametric amplifiers employing lower frequency pumping	431
Chatterjee, B.	A simple phase-meter for laboratory use	111

AUTHOR	SUBJECT	PAGE
Chatterjee, R.	See Bose, A.	325
„	See Chakravarty, A. S.	531
Chatterjee, R. N.	See Sarkar, G. N.	117
Chhonkar, S.	See Mookherji, A.	74
Chiplonkar, V. T. and B. N. Varadrajan	A note on the dependence of the sputtering produced by bombard- ment by canal rays on their angle of impact	127
Das, S. K.	See Bhattacharya, S. N.	36
Dutta, R. N.	See Datta, S.	316
Datta, S. and R. N. Datta	Gyro-frequency in the ionospheric regions	316
Dhar Bhownik, P.	See Bhar, J. N.	1
Dikshit, K. D.	See Chakrabarti, N. B.	431
Dutta-Roy, S. K., A. S. Chakravarty and A. Bose	Studies on the magnetic susceptibility of some V^{3+} alums and Ti^{3+} caesium alum in the range 300°K to 100°K	483
Ganguli, R. C.	Design of pulse amplifier	263
Gatha, K. M.	See Pujara, G. M.	243
Ghosh, Arundhati	Proton-nucleus scattering at 96 MeV Elastic scattering and polarization of 300 MeV protons	177 197
	Neutron strength function $\Gamma n^0/D$ with complex diffuse boundary potential	395
Ghosh, B. B.	A statistical analysis to test the reliability of measuring atmospheric noise subjectively by a small group of people	415
Ghosh, N. N.	On wave solution of field equations in Einstein's unified field theory	307
Ghosh, U. S.	See Sarkar, G. N.	117
Goswami, S. N.	Increase in breakdown potential of a gas in electrodeless discharge in the presence of a transverse mag- netic field and the concept of equi- valent pressure (L)	405
	Electron temperature in electrodeless discharge subjected to a transverse magnetic field	452
Karmohapatro, S. B.	A magnetic spectrometer for charged particles	139

AUTHOR	SUBJECT	PAGE
Kastha, G. S.	Influence of interatomic resonance on the frequency of re-emitted resonance radiation	534
Katti, M. R.	See Tawde, N. R.	18
"	See Tawde, N. R.	89
Krishna Murti, G. S. R.	Space group of cyclohexanone at -180°C	401
"	On the crystal structure of methanol at -180°C (I.)	459
Kumar, R. C.	The question of the existence of ($\wedge^{\circ}\text{P}$), ($\Sigma^+\text{P}$) and ($\Sigma^-\text{n}$) hyper-fragments	411
Lahiri, J.	See Sengupta, A. K.	388
Mahalanabis, A. K.	Some studies on the effects of limiting in a position control servo containing backlash	183
Mathur, S. C.	See Mookherji, A.	410
Mazumder, Monomohan	Infrared absorption spectra of ethylene chlorhydrin in vapour state and in solution in different solvents	346
	Raman spectra of solutions of ethylene dichloride, ethylene dibromide and ethylene chlorhydrin at low temperatures	92
Medhi, K. C.	Intensity of Brillouin components in light scattered by some liquids.	135
Misra (Basu), Nilima and M. S. Sinha	Low energy spectrum of the sea-level electrons and muons at 12°N	335
Misra, S. P.	Application of Schwinger's action principle to quantise a fourth order meson field	520
	Action principle and Lagrangian with higher order derivatives	461
Misra, T. N.	On polarised electronic spectrum of single crystal of paradibromobenzene at -180°C	276
	See Sirkar, S. C.	45
Mitra, Bimalendu	Construction of a 14 Mev neutron generator utilizing $\text{T}^3(\text{d}, \text{n}) \text{He}^4$ reaction and measurement of fast neutron flux	149
Mitra, Shashanka Shekhar	See Varshni, Y. P.	473

AUTHOR	SUBJECT	PAGE
Mitra, S. N. and B. C. Narasinga Rao	Effect of annular solar eclipse of 19th April, 1958 (at sunrise) on the F_2 layer of the ionosphere	540
Mookherji, A. and N. S. Chhonkar	Light absorption in paramagnetic ions in state of solution. Part I —cupric ions	74
Mookherji, A and S. C. Mathur	Magnetic anisotropy of Fe^{+2} ion in siderite (L)	410
Mukherjee, P. N.	See Sengupta, A. K.	388
Mukherjee, A.	See Sarkar, G. N.	117
Nag, B. R.	Resonance curves of synchronised oscillator	23
	Study of an oscillator with two degrees of freedom by a differential analyser	57
Patil, B. S.	See Tawde, N. R.	505
Pistorius, C. W. F. T.	Powder data, unit cell and space group for ferrous sulphate	363
Pujara, C. M. and K. M. Gatha	An investigation into the momentum distribution in light nuclei	243
Ramaswamy, M. K.	A re-investigation of the decay of Na-22	285
Rao Narasimha, D. V. G. L.	Dipole moments of some aliphatic amines	51
	Calculations of the nuclear quadrupole coupling constant for I_2	103
Rao, Y. Bhupala	A note on the spectrum of Br IV (L)	546
Ratho, T.	X-ray small angle measurements on 1% solution of haemoglobin corpuscular protein	469
Ray, S.	Effect of chemical treatment on the structure and properties of graphite (L)	282
Ray, S. and A. Roy	Studies on phase transition of synthetic $\gamma\text{-Fe}_2\text{O}_3 \cdot \text{H}_2\text{O}$ (L)	101
Roy, A.	See Ray, S.	101
Roy, J. K.	Singlet \rightarrow triplet transition in parachlorotoluene	209
Sarkar, G. N., A. Mukherji, R. N. Chatterjee and U. S. Ghosh	Investigations on the paramagnetic resonance in coal with a transmission type electron paramagnetic resonance spectrometer	117

Author Index

xx

AUTHOR	SUBJECT	PAGE
Sarkar, S.	Polarisation of nucleons due to anomalous magnetic moment in higher born approximation	213
Sen, B.	Energy distribution of neutrons from RaD-Be source	158
Sen, S. K.	Electronic spectra of 1,3, 5-trimethyl benzene in the liquid state and in the solid state at -180°C	41
Sengupta, A. K., R. Bhattacharyya, J. Lahiri and P. N. Mukherjee	Level scheme of Pr^{141}	388
Shukla, Ramesh Chandra	See Varshni, Y. P.	473
Sinha, M. S.	See Mishra (Basu), Nilima	335
Singh, Rama Shankar	Visible absorption spectrum of benzoquinone	376
Sirkar, S. C. and T. N. Misra	Polarised electronic spectra of single crystal of para dichlorobenzene	45
Sobhanadri, J.	Temperature variation of dielectric relaxation in six polar liquids	511
Sreeramamurty, K.	Spectra of dimethoxybenzenes. Part I. Meta dimethoxybenzene (L)	241
Srivastava, Arvind Mohan and Y. P. Varshni	Velocity of sound in water as a function of temperature and pressure	423
Srivastava, G. P.	Absorption of 8-millimetre waves in ethyl bromide (L)	367
Srivastava, K. P. and A. K. Barua	The temperature dependence of inter-diffusion coefficient for some pairs of rare gases	229
Srivastava, P.	Renninger effect in naphthazarin	123
Srivastava, R. C.	The space group of meta toluic acid	305
Srivastava, Satish Chandra	Relationship between ultrasonic velocity and other physical properties of pure organic liquids (L)	503
Srivastava, Surendra Nath	Preliminary report on the crystal structure of anthrone (L)	456
Tawde, N. R., and B. S. Patil	The evaluation of the electronic transition moment for the $b^3\Sigma^+ - a^3\Pi$ system of CO	505
Tawde, N. R. and M. R. Katti	A case for efficacy of Hulburt-Hirschfelder potential function	18

AUTHOR	SUBJECT	PAGE
Tawde, N. R. and M. R. Katti	A test for Hulburt-Hirschfelder potential function	89
Varadrajan, B. N.	See Chiplokar, V. T.	127
Varshni, Y. P.	See Srivastava, Arvind Mohan	423
Varshni, Y. P., Shashanka Shekhar Mitra and Ramesh Chandra Shukla	Spectroscopic constants of molecules VII. Relation between force constant and equilibrium internuclear distance of hydride diatoms	473
Yamaguchi, S.	On the magnetic perturbation of an electron beam (L)	547

SUBJECT INDEX

SUBJECT	AUTHOR	PAGE
Absorption of 3.18 cm microwaves in ethylene chlorhydrin and its solutions. On the	T. J. Bhattacharyya	498
Absorption of 8-millimetre waves in ethyl bromide (L)	G. P. Srivastava	367
Action principle and Lagrangian with higher order derivatives	S. P. Misra	461
Breakdown potential of a gas in electrodeless discharge in the presence of a transverse magnetic field and the concept of equivalent pressure. Increase in (L)	S. N. Goswami	405
Control servo containing backlash. Some studies on the effects of limiting in a position	A. K. Mahalanobis	183
Crystal structure of anthrone. Preliminary report on the (L)	Surendra Nath Srivastava	456
Crystal structure of methanol at -180° C. On the (L)	G. S. R. Krishna Murti	459
Crystal structure of 1, 2-cyclopenteno-phenanthrene	B. S. Basak and M. G. Basak	107
Crystalline electric fields in hydrated Co^{2+} salts. A short note on the	A. S. Chakravarty and R. Chatterjee	531
Decay of Na-22. A reinvestigation of the	M. K. Ramaswamy	285
Dielectric relaxation in six polar liquids. Temperature variation of	J. Sobhanadri	511
Dipole moments of some aliphatic amines	D. V. G. L. Narasimha Rao	51
Electrical conductivity of graphite. Effect of chemical treatment on the (L)	R. Bhattacharyya	407
Elastic scattering and polarization of 300 MeV protons	Arundhati Ghosh	197
Electron temperature in electrodeless discharge subjected to a transverse magnetic field	S. N. Goswami	452

SUBJECT	AUTHOR	PAGE
Electronic transition moment for the $b^3\Sigma^- \rightarrow a^3\Pi$ system of CO. The evaluation of the	N. R. Tawde and B. S. Patil	505
Energy distribution of neutrons from RaD-Be source	B. Sen	158
Energy estimation of electron pairs. A simple method for the	P. K. Aditya	357
Existence of (Λ^0P), (Σ^+P) and (Σ^-n) hyperfragments. The question of the	R. C. Kumar	411
F ₂ ionization in relation to geomagnetic co-ordinates. A study of noon	J. N. Bhar and P. Dhar Bhowmik	1
Gyro-frequency in the ionospheric regions	S. Datta and R. N. Datta	31
Hulburt-Hirschfelder potential function. A test for	N. R. Tawde and M. R. Katti	89
Hulburt-Hirschfelder potential function. A case for efficacy of	N. R. Tawde and M. R. Katti	18
Inter-diffusion coefficient for some pairs of rare gases. The temperature dependence of	K. P. Srivastava and A. K. Barua	229
Level scheme of Pr ¹⁴⁴	A. K. Sengupta, R. Bhattacharyya J. Lahiri and P. N. Mukherjee	388
Light absorption in paramagnetic ions in state of solution. Part I. Cupric ions	A. Mookherji and N. S. Chhonkar	74
Low-energy spectrum of the sea-level electrons and muons at 12°N	Nilima Mishra (Basu) and M. S. Sinha	335
Magnetic anisotropy of Fe ⁺⁺ ion in siderite (L)	A. Mookherji and S. C. Mathur	410
Magnetic behaviours of titanium caesium sulphate alum. The	A. Bose, A. S. Chakravarty and B. Chatterjee	325
Magnetic study of iron-containing glass at room temperature	Bhupati Kumar Banerjee	165
Magnetic study of iron-containing glasses at low temperature	Bhupati Kumar Banerjee	201
Magnetic perturbation of an electron beam. On the (L)	S. Yamaguchi	547

Subject Index

xv

SUBJECT	AUTHOR	PAGE
Magnetic susceptibility of some V^{3+} alums and Ti^{3+} caesium alum in the range 300°K to 100°K. Studies on the	S. K. Dutta-Roy, A. S. Chakravarty and A. Bose	483
Micro-calorimeter for measurement of small heat changes. A	S. N. Bhattacharya and S.K. Das	36
Molecular interactions from Viscosity and inter-diffusion. Unlike	A. K. Barua	221
Momentum distribution in light nuclei. An investigation into the	C. M. Pujara and K. M. Gatha	243
Neutron generator utilizing $T^3(d, n) He^4$ reaction and measurement of fast neutron flux. Construction of a 14 Mev	Bimalendu Mitra	149
Neutron strength function $\Gamma n^0/D$ with complex diffuse boundary potential	Arundhati Ghosh	395
Nuclear quadrupole coupling constant for I_2 . Calculations of the	D. V. G. L. Narasimha Rao	103
Oscillator with two degrees of freedom by a differential analyser. Study of an	B. R. Nag	
Paramagnetic resonance in coal with a transmission type electron paramagnetic resonance spectrometer. Investigations on the	G. N. Sarkar, A. Mukherji, R. N. Chatterjee and U. S. Ghosh	117
Parametric amplifiers employing lower frequency pumping. Some possible arrangements of	N. B. Chakrabarti and K. D. Dikshit	431
Phase-Meter for laboratory use. A simple	B. Chatterjee	111
Phase transition of synthetic $\gamma-Fe_2O_3$, H_2O . Studies on (L)	S. Ray and A. Roy	101
Polarization of nucleons due to anomalous magnetic moment in higher born approximation	S. Sarkar	213
Powder data, unit cell and space group for ferrous sulphate	C.W.F.T. Pistorius	363
Proton-nucleus scattering at 96 MeV	Arundhati Ghosh	177
Pulse amplifier. Design of	R. C. Ganguli	263
Reimering effect in naphthazarin	P. Srivastava	123
Resonance curves of a synchronised oscillator.	B. R. Nag	23

SUBJECT	AUTHOR	PAGE
Schwinger's action principle to quantise a fourth order meson field. Application of	S. P. Misra	520
Singlet-Triplet transition in para-chlorotoluene	J. K. Roy	209
Solar eclipse of 19th April, 1958 (at sunrise) on the F_2 layers of the ionosphere. Effect of annular	S. N. Mitra and B. C. Narashinga Rao	540
Space group of cyclohexanone at -180°C	G. S. R. Krishna Murti	401
Space group of 1, 3, 5-trichlorobenzene	S. G. Biswas	371
Space group of meta toluic acid. The	R. C. Srivastava	305
SPECTRA :		
Brillouin components in light scattered by some liquids. Intensity of	K. C. Medhi	135
Electronic spectra of 1, 3, 5-trimethylbenzene in the liquid state and in the solid state at -180°C	S. K. Sen	41
Frequency of re-emitted resonance radiation. Influence of interatomic resonance on the	G. S. Kastha	534
Infrared absorption spectra of ethylene chlorhydrin in the vapour state and in solution in different solvents	Monomohan Mazumder	346
Infrared spectra of ortho, meta and para thiocresols	R. N. Bapat	295
Magnetic spectrometer for charged particles	S. B. Karmohapatro	139
Polarised electronic spectra of single crystal of para dichlorobenzene	S. C. Sirkar and T. N. Misra	45
Polarised electronic spectrum of single crystal of paradibromobenzene at -180°C	T. N. Misra	276
Raman spectra of ortho, meta, and para-thiocresols. The	R. N. Bapat	329
Raman spectra of solutions of ethylene dichloride, ethylene dibromide and ethylene chlorhydrin at low temperatures.	Monomohan Mazumder	92
Spectrum of Br. IV. A note on the (L)	Y. Bhupala Rao	546
Spectra of dimethoxybenzenes. Part I Metadimethoxybenzene (L)	K. Sreeramamurty	241

SUBJECT	AUTHOR	PAGE
Spectroscopic constants of molecules		
VII. Relation between force constant and equilibrium internuclear distance for hydride diatoms	Y. P. Varshni, Sashanka Shokhar Mitra and Ramesh Chandra Shukla	473
X-ray small angle measurements on 1% solution of haemoglobin corpuscular protein	T. Rath	469
Visible absorption spectrum of benzoquinone	Rama Shankar Singh	376
Sputtering produced by bombardment by canal rays on their angle of impact.	V. T. Chiplonkar and	
A note on the dependence of the	B. N. Varadrajan	127
Statistical analysis to test the reliability of measuring atmospheric noise subjectively by a small group of people.		
A	B. B. Ghosh	415
Structure and properties of graphite.		
Effect of chemical treatment on the (L)	S. Ray	282
Ultrasonic velocity and other physical properties of pure organic liquids.		
Relationship between (L)	Satish Chandra Srivastava	503
Velocity of sound in water as function of temperature and pressure	Arvind Mohan Srivastava and Y. P. Varshni	423
Wave solution of field equations in Einstein's unified field theory. On	N. N. Ghosh	307

A STUDY OF NOON F_2 IONIZATION IN RELATION TO GEOMAGNETIC CO-ORDINATES

J. N. BHAR AND P. DHAR BHOWMIK

INSTITUTE OF RADIO PHYSICS AND ELECTRONICS, UNIVERSITY OF CALCUTTA

(Received for publication, October 10, 1958)

ABSTRACT. The relation of F_2 layer noon critical frequency with magnetic dip and geomagnetic latitude is studied for constant values of solar zenithal angle. The constant- X plots show two maxima situated on the two sides of the magnetic equator. An asymmetry between the northern and southern hemispheres is also revealed.

For chosen values of solar zenith distance the ratio of noon fF_2 at sunspot maximum to that at sunspot minimum is studied in relation to magnetic dip. The ratio is found to vary with magnetic dip displaying a minimum to the north of the magnetic equator.

1. INTRODUCTION

Chapman's theory of solar ultraviolet radiation producing the ionospheric layers in the upper atmosphere was based on certain simplifying assumptions. In spite of this, the theory explains with remarkable success* not only the variations in time of the E layer ionization but also its geographical distribution. Routine ionospheric soundings carried out for nearly two decades at stations scattered all over the world have firmly established the validity of this theory in the case of the E layer, so much so that the nature of variations following from Chapman's Law has come to be regarded as "normal". Any departure from this is considered as abnormal or anomalous.

In this sense, the observed variations of the F_2 layer characteristics are found to be anomalous. One aspect of such anomaly was first disclosed by Appleton and Naismith (1935) who in their studies of the seasonal variations of F_2 layer ionization noticed that, fF_2 was less at summer noon than at winter noon, contrary to what is expected from Chapman's theory. Another aspect of the anomalous behaviour of the F_2 layer was also strikingly demonstrated by Appleton (1946) who showed that under equinox noon conditions "there is a belt of low values of f_0F_2 circling the earth and centred roughly on the magnetic equator".

This equatorial belt effect has been studied subsequently by many workers (Appleton 1950, 1954; Liang 1947; Bailey 1948; Maeda 1955); however, these studies have been made by plotting the value of fF_2 at a given local time at a particular

*The remarks apply in regard to the general behaviour of E layer ionization. In finer details, however, certain departures from Chapman's Law have been revealed, attention to which has been drawn by Appleton and Lyons (1957).

epoch of the annual solar cycle against one or other of the geomagnetic co-ordinates. Such a plot obviously includes the possible variations of fF_2 due to varying zenithal angle χ of the sun for stations situated at different geographical latitudes. For example, the solar zenith distance at Singapore (Geographical Latitude 1.3°N) at noon on the equinox day is about 1° , while on the same day the noon value of χ at Slough (Geographical Latitude 51.5°N) is about 52° . According to Chapman's theory the wide difference in the χ value must by itself produce substantial difference in fF_2 at the two stations. In order to have a correct picture of the dependence of F_2 ionization on the geomagnetic field, this contamination due to variation of solar zenith distance must be eliminated. Such a plot should be very useful in examining the manner in which the terrestrial magnetic field might, to the exclusion of other factors, control the geographical distribution of ionization produced by the solar rays.

In a recent note (Bhar 1957) published elsewhere the true relation between noon fF_2 and magnetic dip after the elimination of the effect of solar zenith distance variation from place to place has been depicted using data for the year 1953. In the present paper, the same work has been extended making use of data collected over the period 1952-1955. Certain important aspects of fF_2 behaviour have been discussed on the basis of the observed data.

2. CONSTANT- χ PLOTS

The effect on noon fF_2 caused by the difference in solar zenith distance at different stations has been eliminated by plotting the noon values of fF_2 against magnetic dip or geomagnetic latitude—keeping the solar zenith distance χ as a fixed parameter instead of the equinox or any other epoch of the year. In other words, for stations at different geographical latitudes, such days of the year are selected as to give the same value of χ at noon for all the stations. For convenience, a table may first be prepared showing the dates on which χ_{noon} assumes certain selected values at the different stations. Table I given below is compiled to indicate the dates during the year on which χ_{noon} at the different stations assume the values 0° , 10° , 20° , 30° , 40° , and 50° . (This is followed by Table II which gives the location of each station in geographical as well as in geomagnetic co-ordinates). For each year, for a particular value of χ_{noon} and for a given station, noon fF_2 data for five days centred round the date shown in Table I is averaged. In cases where a particular value of χ_{noon} is attained on more than one date, five days centred round each of these dates are taken and values of noon fF_2 for all these days are averaged. This average value is taken as the representative value of noon fF_2 of the station concerned for the chosen zenith distance. A graph obtained by plotting such values of fF_2 against location (i.e., geographical latitude, geomagnetic latitude or

magnetic dip) for different stations for a particular χ_{noon} will, for the sake of brevity, be called a constant- χ plot.

TABLE I

Dates on which solar zenith distance χ assumes certain specified values at noon at different stations

Station	Dates for which $\chi_{noon}=0^{\circ}$	Dates for which $\chi_{noon}=10^{\circ}$	Dates for which $\chi_{noon}=20^{\circ}$	Dates for which $\chi_{noon}=30^{\circ}$	Dates for which $\chi_{noon}=40^{\circ}$	Dates for which $\chi_{noon}=50^{\circ}$
Akita	—	—	May 19 July 25	Apr. 15 Aug. 28	Mar. 20 Sep. 24	Feb. 23 Oct. 20
Bagnoux	—	—	—	May 15 July 29	Apr. 12 Aug. 31	Mar. 18 Sep. 26
Bombay	May 16 July 28	Apr. 13 Aug. 30	Mar. 18 Sep. 26	Feb. 21 Oct. 22	Jan. 17 Nov. 27	—
Brisbane	—	Feb. 12 Nov. 1	Mar. 13 Oct. 1	Mar. 17 Sep. 27	Apr. 23 Aug. 20	June 5 July 8
Calcutta	June 7 July 7	Apr. 23 Aug. 20	Mar. 27 Sep. 17	Mar. 2 Oct. 12	Feb. 1 Nov. 11	—
Canberra	—	—	Feb. 8 Nov. 4	Mar. 7 Oct. 7	Apr. 2 Sep. 11	Apr. 30 Aug. 13
Capetown	—	—	Feb. 12 Nov. 1	Mar. 10 Oct. 4	Apr. 5 Sep. 8	May 4 Aug. 9
Casablanca	—	—	Apr. 27 Aug. 17	Mar. 30 Sep. 14	Mar. 4 Oct. 10	Feb. 5 Nov. 8
Christchurch	—	—	Dec. 22	Feb. 14 Oct. 29	Mar. 12 Oct. 2	Apr. 6 Sep. 6
Dakar	Apr. 30 Aug. 13	Apr. 1 Sep. 11	Mar. 7 Oct. 7	Feb. 7 Nov. 7	—	—
Delhi	—	May 14 July 30	Apr. 12 Sep. 1	Mar. 17 Sep. 27	Feb. 20 Oct. 23	Jan. 15 Nov. 29
Djibouti	Apr. 20 Aug. 23	Mar. 24 May 28 July 15 Sep. 19	Feb. 28 Oct. 15	Jan. 28 Nov. 15	—	—
Falkland Is.	—	—	—	Jan. 13 Dec. 1	Feb. 20 Oct. 24	Mar. 16 Sep. 27
Freiburg	—	—	—	May 12 Aug. 1	Apr. 11 Sep. 2	Mar. 16 Sep. 27
Hobart	—	—	Jan. 4 Dec. 9	Feb. 16 Oct. 27	Mar. 14 Sep. 30	Apr. 8 Sep. 4
Huancayo	Feb. 18 Oct. 25	Jan. 11 Mar. 16 Sep. 28 Dec. 3	Apr. 10 Sep. 2	May 12 Aug. 1	—	—

TABLE I (contd.)

Station	Dates for which $\chi_{noon}=0^\circ$		Dates for which $\chi_{noon}=10^\circ$		Dates for which $\chi_{noon}=20^\circ$		Dates for which $\chi_{noon}=30^\circ$		Dates for which $\chi_{noon}=40^\circ$		Dates for which $\chi_{noon}=50^\circ$	
Ibadan	April Sept.	9 4	Mar. May Aug. Sep.	14 9 4 30	Feb. Oct.	16 27	Jan. Dec	6 7	—			
Inverness									May Aug.	9 4	Apr. Sep.	9 4
Johannesburg	—		Feb. Nov.	5 7	Mar. Oct.	5 9	Mar. Sep.	30 13	Apr. Aug.	27 16	June	21
Khartoum	May Aug.	3 10	Apr. Sep.	4 9	Mar. Oct.	9 4	Feb. Nov.	11 1	—		—	
Macquarie									Feb. Nov.	11 1	Mar. Oct.	9 5
Madras	Apr. Aug.	25 19	Mar. June July Sep.	28 10 3 15	Mar. Oct.	3 11	Feb. Nov.	3 10	—		—	
Mau	May July	24 19	Apr. Aug.	18 25	Mar. Sep.	23 21	Feb. Oct.	26 17	Jan. Nov.	25 18	—	
Nairobi	Mar. Sep.	18 26	Feb. Apr. Aug. Oct.	21 13 30 22	Jan. May July Nov.	17 16 28 27	—		—		—	
Okinawa	—		May Aug.	5 8	Apr. Sep.	6 7	Mar. Oct.	11 3	Feb. Nov.	7 5	—	
Panama	Apr. Aug.	14 29	Mar. May July Sep.	19 18 26 25	Feb. Oct.	22 21	Jan. Nov.	19 24	—		—	
Puerto Rico	May July	14 30	Apr. Sep.	12 1	Mar. Sep.	17 27	Feb. Oct.	20 23	Jan. Nov.	15 28	—	
Poitiers	—		—		—		May Aug.	6 7	Apr. Sep.	7 6	Mar. Oct.	12 2
Raratonga	Jan. Nov.	15 28	Feb. Oct.	20 23	Mar. Sep.	17 26	Apr. Aug.	12 31	May July	13 31	—	
Shibata	—		—		May Aug.	11 2	Apr. Sep.	10 2	Mar. Sep.	15 28	Feb. Oct.	18 25
Singapore	Mar. Sep.	24 20	Feb. Apr. Aug. Oct.	27 20 24 16	May July	27 17	—		—		—	
Slough	—		—		—		May July	28 15	Apr. Aug.	20 28	Mar. Sep.	24 19
Tananarive	Jan. Nov.	27 17	Feb. Oct.	27 16	Mar. Sep.	24 20	Apr. Aug.	19 24	May July	27 17	—	

TABLE I (contd.)

Station	Dates for which $\chi_{noon}=0^\circ$	Dates for which $\chi_{noon}=10^\circ$	Dates for which $\chi_{noon}=20^\circ$	Dates for which $\chi_{noon}=30^\circ$	Dates for which $\chi_{noon}=40^\circ$	Dates for which $\chi_{noon}=50^\circ$
Tiruchly	Apr. 18 Aug. 25	Mar. 23 May 24 July 20 Sep. 21	Feb. 26 Oct. 17	Jan. 25 Nov. 18	—	—
Tokyo	—	—	May 3 Aug. 10	Apr. 4 Sep. 8	Mar. 10 Oct. 4	Feb. 11 Nov. 1
Townsville	Jan. 25 Nov. 19	Feb. 26 Oct. 17	Mar. 22 Sep. 21	Apr. 18 Aug. 25	May 24 July 20	—
Upsala	—	—	—	—	May 19 July 25	Apr. 15 Aug. 28
Wakkanai	—	—	—	May 2 Aug. 11	Apr. 3 Sep. 9	Mar. 9 Oct. 4
Washington	—	—	May 15 July 20	Apr. 12 Aug. 31	Mar. 17 Sep. 26	Feb. 20 Oct. 23
Yamugawa	—	May 27 July 17	Apr. 19 Aug. 24	Mar. 24 Sep. 20	Feb. 27 Oct. 16	Jan. 27 Nov. 17

In demonstrating the geomagnetic influence on the worldwide distribution of F_2 region ionization, different workers have plotted fF_2 against different geomagnetic co-ordinates. Of these, geomagnetic latitude has the merit that plots against it are more convenient for mathematical analysis, whereas plots against magnetic dip* generally show the least amount of scatter. In the present paper, fF_2 data are plotted against both geomagnetic latitudes and magnetic dips of the stations.

3. THEORETICAL CONSIDERATIONS

In examining the observed worldwide distribution of local noon ionization of the ionospheric layers it is interesting first of all to know what one should expect from theoretical considerations. Evidently, Chapman's theory provides a good starting point for this purpose. The simplifying assumptions made by Chapman were that the upper atmosphere is isothermal—the constituent gases being distributed accordingly, that the ionizing radiation from the sun is monochromatic, and that the electrons and ions produced decay by simple recombination. It is now known that these assumptions are substantially valid for the case of the E and F_1 layers; or at any rate, if there are departures from these

*Magnetic \downarrow dip [as distinguished from geomagnetic dip given by $I = \tan^{-1} 2 \tan \lambda$, where λ is the geomagnetic latitude.

TABLE II

Values of geographical coordinates, geomagnetic latitude and magnetic dip of the respective stations

Station	Geog. Latitude	Geog. Longitude	Geomag. Latitude	Magnetic Dip
Akita	39 7°N	140.1°E	29.5°N	53°N
Bagneux	48.8°N	2.3°E	51.3°N	64°N
Bombay	19°N	73°E	9.7°N	24°N
Brisbane	27.5°S	153°E	35.9°S	56°S
Calcutta	22 6°N	88.4°E	11 9°N	31°N
Canberra	35.3°S	149°E	44°S	64.5°S
Capetown	34.2°S	18 3°E	33°S	60.5°S
Casablanca	33.6°N	7 6°W	38 5°N	50 5°N
Christchurch	43.5°S	172.7°E	48°S	68°S
Darkar	14.6°N	17.4°W	21.6°N	26°N
Delhi	28.6°N	77.1°E	18.9°N	41°N
Djibouti	11.5°N	43.1°E	6.8°N	5°N
Falkland Is.	51.7°S	57 8°W	40.4°S	46°S
Freiburg	48.1°N	7.8°E	49.4°N	63.5°N
Hobart	42 8°S	147 4°E	51 4°S	71.5°S
Huancayo	12°S	75.3°W	0.6°S	0°
Ibadan	7.4°N	4°E	10 4°N	2.5°S
Inverness	57 4°N	4.2°W	60.8°N	70.6°N.
Johannesburg	26.2°S	28°E	26.7°S	59°S
Khartoum	15 6°N	32.6°E	12.9°N	13°N
Macquarie	54.5°S	159°E	61°S	79°S
Madras	13°N	80 2°E	3.1°N	11°N
Maui	20.8°N	156.5°W	20.7°N	38.5°N
Nairobi	1°S	37°E	4 2°S	25°S
Okinawa	26.3°N	172.8°E	15.3°N	36°N
Panama	9.4°N	79.9°W	20.7°N	35.5°N
Puerto Rico	18.5°N	62.2°W	30°N	51°N
Poitiers	46.6°N	0.3°E	49.1°N	62.5°N
Rararonga	21.3°S	159.8°W	21.8	38.5°S
Shibata	37.9°N	139.3°E	27.6°N	51°N
Singapore	1.3°N	103.8°E	10.1°S	16°S
Slough	51.5°N	0.6°W	54.3°N	66°N
Tananarive	18.8°S	47.8°E	23.8°S	52.5°S
Tiruchy	10.8°N	78.8°E	1°N	5°N
Tokyo	35.7°N	139.5°E	25.5°N	49°N
Townsville	19.3°S	148.8°E	28.4°S	46°S
Upsala	59.8°N	17.6°E	58.4°N	70.5°N
Wakkanai	45.4°N	141.7°E	35.4°N	59°N
Washington	38.7°N	77.1°W	50°N	70°N
Yamagawa	31.2°N	130.6°E	20.3°N	43.5°N

assumptions, these are not likely to affect substantially the behaviour of these layers so far as the latitude distribution of the ionization at local noon is concerned.

E and F_1 layers :

The basic continuity equation resulting from Chapman's simple theory is

$$\frac{dN}{dt} = q - \alpha N^2 \quad \dots (1)$$

where N is the density of ionization, q is the rate of electron production per c.c. and α is the coefficient of recombination.

It is now established from observed data that in the case of E and F_1 layers, quasi-stationary conditions obtain roundabout noon; that is, dN/dt is negligible compared to the other two terms of the above equation. Under this condition the maximum value of N for the layer near noon is given by

$$N_m = \sqrt{\frac{q_0 \cos \chi}{\alpha}} \quad \dots (2)$$

where χ is the sun's zenith distance at the time and q_0 is the value of q for $\chi = 0^\circ$. At any station and in any season χ attains its daily maximum value at noon which we shall denote by χ_{noon} . The noontime maximum electron density is thus

$$N_{noon} = \sqrt{\frac{q_0 \cos \chi_{noon}}{\alpha}} \quad \dots (3)$$

The expression indicates that N_{noon} and hence noon-time critical frequency of the layer is uniquely determined by χ_{noon} in a particular epoch of the solar cycle, and is independent of the location of the station.

Thus, if fE_{noon} or fF_{1noon} is plotted against the location of a station (i.e., geographical latitude, geomagnetic latitude or magnetic dip) for a fixed value of χ_{noon} , the resulting constant- χ plot is expected to be a straight line.

F_2 layer :

An attempt to make a theoretical deduction regarding the latitude distribution of noon F_2 ionization presents formidable difficulties. Even assuming that there is no appreciable departure from the assumptions made in Chapman's theory, which appears improbable, a complication arises in the case of the F_2 layer due to the fact that dN/dt is not negligible i.e. quasi-stationary conditions do not obtain even at noon and the simple $(\cos \chi)^4$ law (Eq. 2) for N_m does not hold. In order to estimate the latitude distribution one has to resort to numerical solutions of Eq. 1. This was done by Millington (1932) who gave a series of curves representing the diurnal variation of ionization of the layer at different latitudes and in different seasons. From the curves for $\sigma_0 = 1$ ($\sigma_0 = 1/1.37 \times 10^4 \sqrt{q_0 \alpha}$) which may be assumed to fit the F_2 layer for the sunspot minimum period, one

can estimate the values of N_{noon} for the F_2 layer at different geographical latitudes for a series of chosen values of χ_{noon} , say 0° , 10° , 20° , 30° and 40° . It is found that the plot of noon fF_2 against latitude for any of these values of χ_{noon} is a straight line with deviations not greater than $\pm 5\%$.

Thus, according to Chapman's theory the constant- χ curves for the F_2 layer would also be straight lines for all practical purposes.

Evidences, both theoretical and observational, collected during recent years, indicate, however, that the assumptions made in Chapman's theory require considerable modification. This is true in particular for the assumption regarding the process of electron decay. Extensive work has been done on various possible processes of electron decay in the F_2 region levels and it is believed that a decay rate represented by the αN^2 law may not be true for this region. Nevertheless, if the electrons produced are assumed to appear and disappear at the same spot in the ionosphere, as is implied in Chapman's theory, it is likely that the noon-time ionization of the F_2 region for a given value of χ_{noon} will not vary substantially from place to place over a wide range of latitudes, whatever be the actual process or processes of electron decay. In other words, the constant- χ plots would still approximate straight lines.

Recent studies indicate, however, that the appearance and disappearance of the electrons do not take place at the same spot. The electrons (and ions) produced by solar ultraviolet radiation are subject to tidal and other forces, which cause them to drift (Martyn 1947, 1954). It now appears that the resulting motion of the electrons under the influence of the earth's magnetic field plays an active part in determining the ionization density of the upper regions of the ionosphere in relation to the terrestrial magnetic co-ordinates, and thus controls the worldwide distribution of the F_2 ionization.

4. DISCUSSION OF OBSERVED DATA

(i) *Constant- χ plots*: In figure 1 (a, b, c, & d) constant- χ plots of noon fF_2 against magnetic dip have been depicted for the four years 1952-55 which are centred more or less round the period of minimum sunspot activity. Figure 2 (a, b, c & d) shows the same plots depicted against geomagnetic latitude. For the sake of comparison constant- χ plots of noon fF_2 depicted against magnetic dip and against geomagnetic latitude are also shown for the sunspot maximum year 1948 in figures 3 and 4. It will be seen that the plots against magnetic dip show less scatter than those against geomagnetic latitude.

It is noted that the features reported previously (Bhar, 1957) on the basis of the data for 1953 are repeated in all the years. For example, for $\chi = 0^\circ$, noon fF_2 is minimum at the magnetic equator and attains maximum values roughly at $\pm 30^\circ$ magnetic dip. The variation of fF_2 with magnetic dip follows nearly

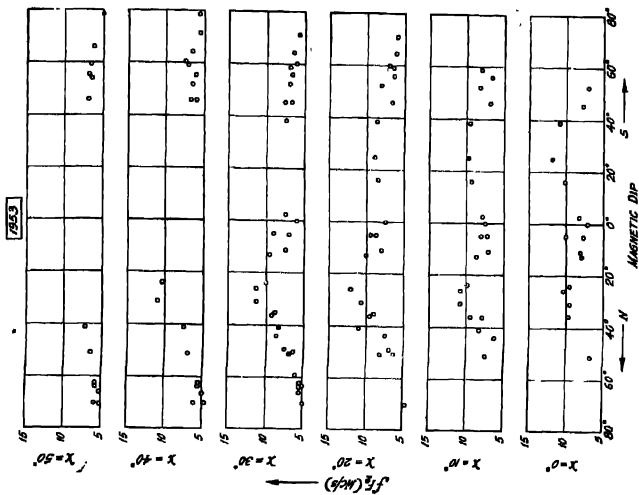


Fig. 1(b). Constant X plots of noon fF_2 against magnetic dip for $X = 0^\circ, 10^\circ, 20^\circ, 30^\circ, 40^\circ$ and 50° for 1953.

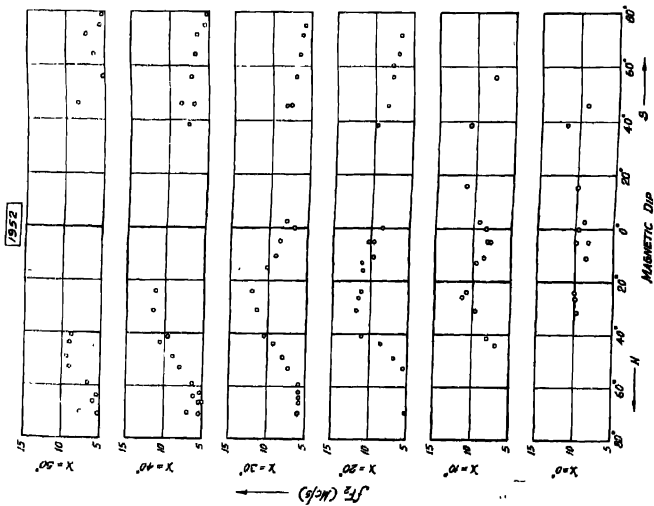


Fig. 1(a). Constant X plots of noon fF_2 against magnetic dip for $X = 0^\circ, 10^\circ, 20^\circ, 30^\circ, 40^\circ$ and 50° for 1952.

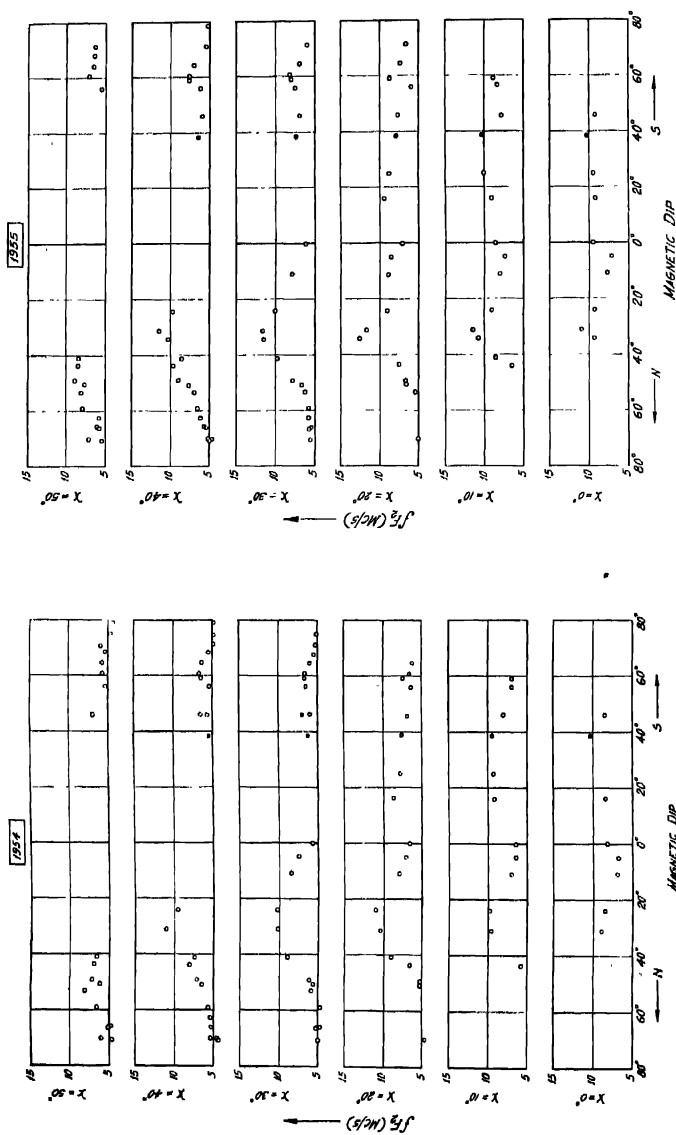


Fig. 1(c). Constant x plots of noon fF_2 against magnetic dip for $x = 0^\circ, 10^\circ, 20^\circ, 30^\circ, 40^\circ$ and 50° for 1954.

Fig. 1(d). Constant x plots of noon fF_2 against magnetic dip for $x = 0^\circ, 10^\circ, 20^\circ, 30^\circ, 40^\circ$ and 50° for 1955.

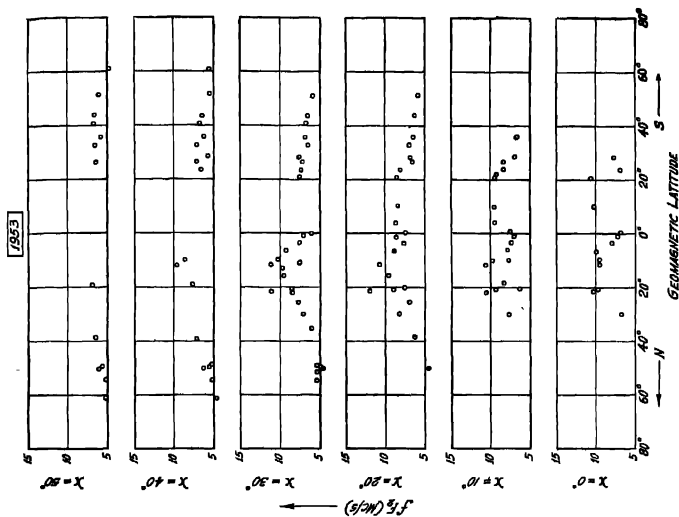


Fig. 2(b). Constant- X plots of noon fF_2 against geomagnetic latitude for $X = 0^\circ, 10^\circ, 20^\circ, 30^\circ, 40^\circ, 50^\circ$ for 1953.

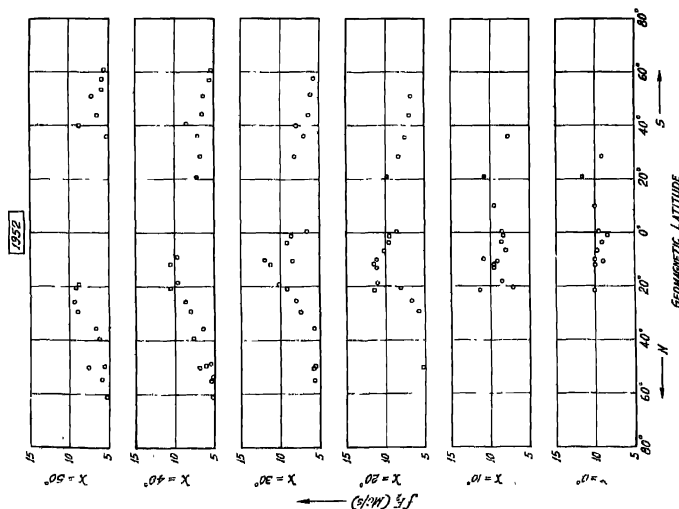


Fig. 2(a). Constant- X plots of noon fF_2 against geomagnetic latitude for $X = 0^\circ, 10^\circ, 20^\circ, 30^\circ, 40^\circ, 50^\circ$ for 1952.

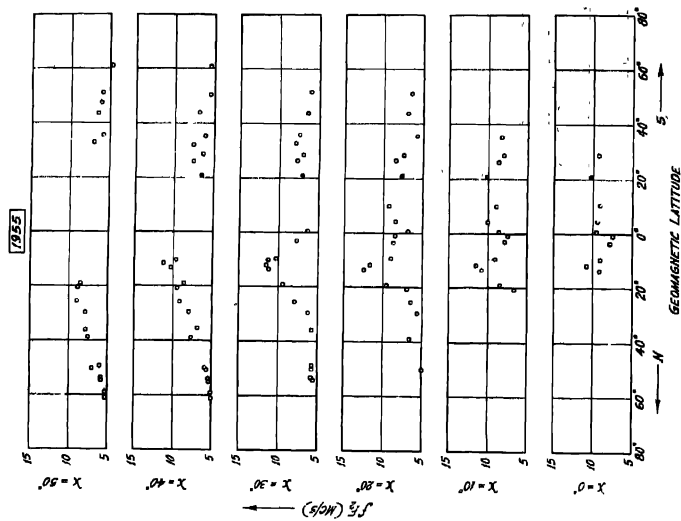


Fig. 2(d). Constant- x plots of noon fF_2 against geomagnetic latitude for $x = 0^\circ, 10^\circ, 20^\circ, 30^\circ, 40^\circ$ and 50° for 1955.

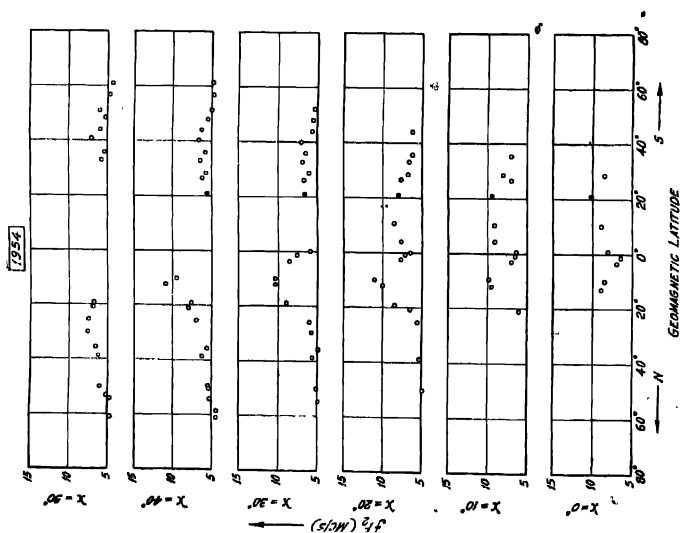


Fig. 2(c). Constant- x plots of noon fF_2 against geomagnetic latitude for $x = 0^\circ, 10^\circ, 20^\circ, 30^\circ, 40^\circ$ and 50° for 1954.

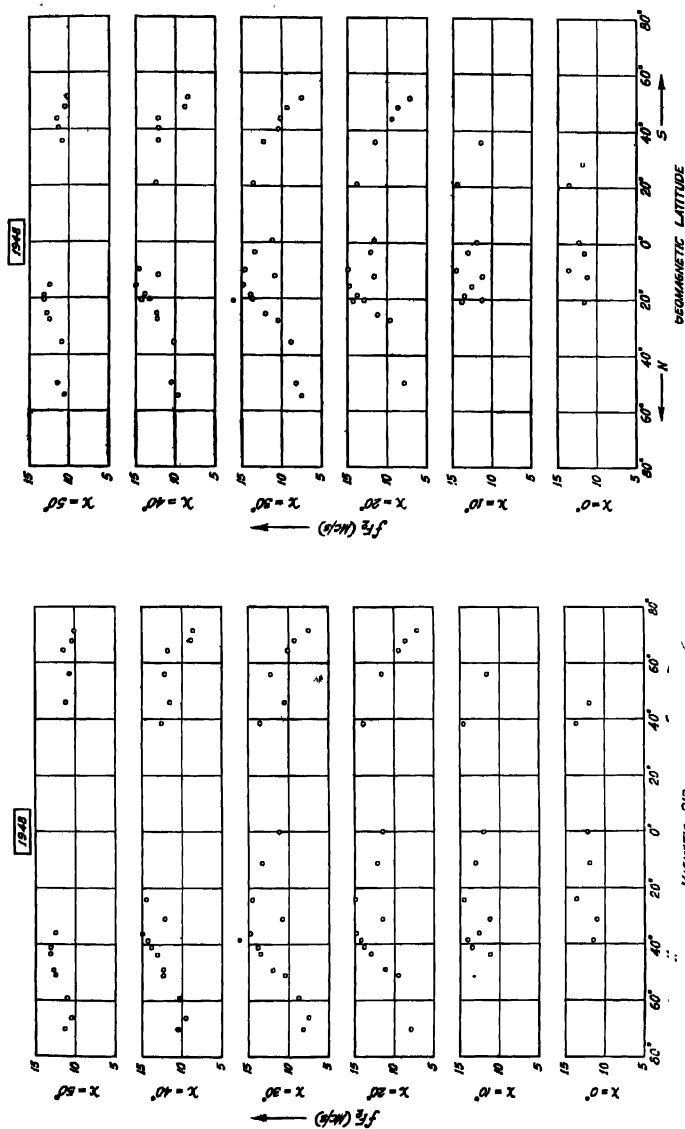


Fig. 3. Constant- X plots of noon fF_2 against magnetic dip for the sunspot maximum year 1948.

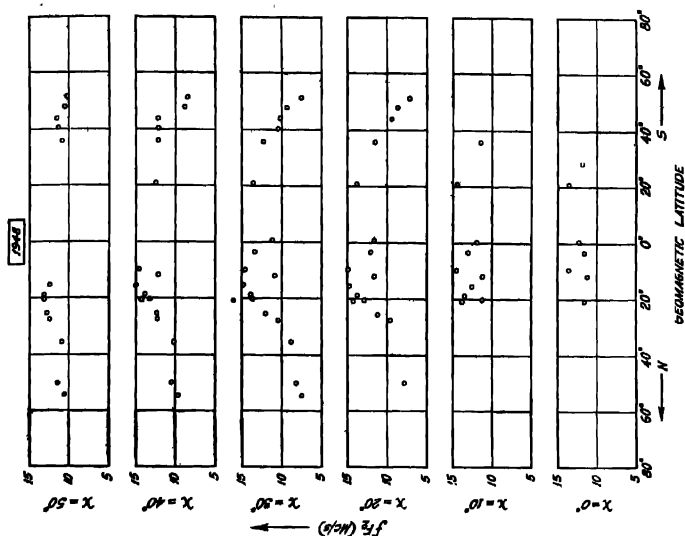


Fig. 4. Constant- X plots of noon fF_2 against geomagnetic latitude for the sunspot maximum year 1948.

the same trend for $\chi = 10^\circ$. For $\chi = 20^\circ$ and 30° respectively the peak on the north and the minimum at the magnetic equator are clearly maintained. But the peak to the south of the magnetic equator loses prominence. The southern peak gets flattened out as χ increases from 0° to higher values.

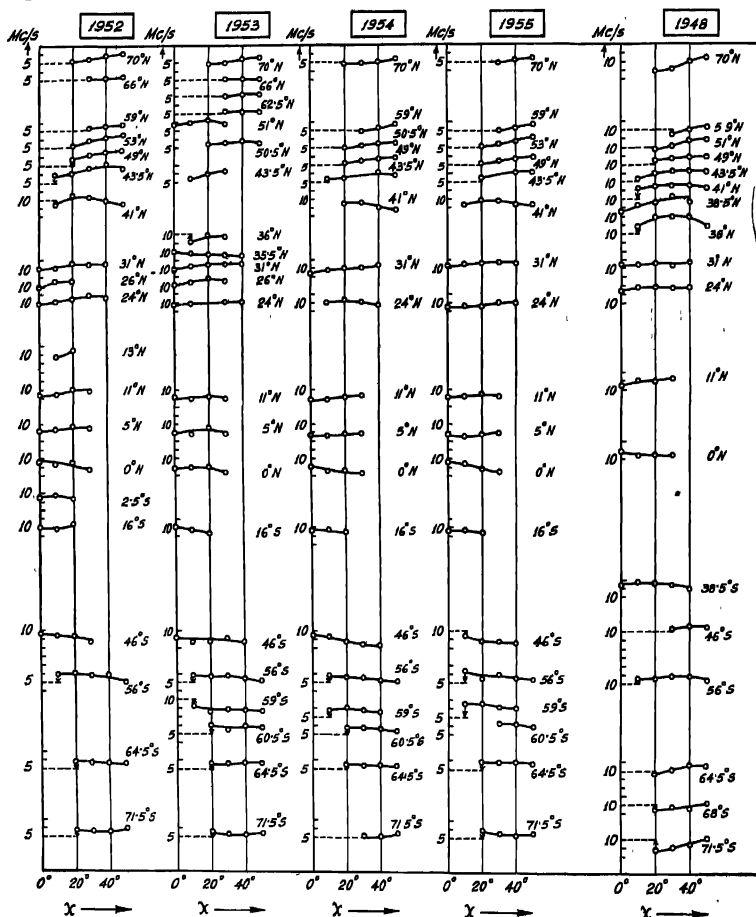


Fig. 5. Variation of average fF_2 against noon χ -values for respective stations for the years 1952-55 and 1948. Stations are arranged in order of magnetic dip (magnetic dip value is indicated on right hand side of each curve). Scale of ordinate:—Each small division represents 2.5 Mc/s. Arrows indicate reference levels.

In the plots against geomagnetic latitude (figures 2 and 4), the peaks appear at 10° to 15° north and south; the flattening of the southern peak for higher values of χ is also clearly noticeable in these figures.

(ii) *North-South anomaly in fF_2-I relation*: Although paucity of data in the southern hemisphere dictates caution in making inferences in any detail, there seems to be no escape from the conclusion that the relation between noon fF_2 and magnetic dip (for constant χ) exhibits some amount of asymmetry in behaviour about the magnetic equator. The observed facts on which this statement is based are discussed below.

In the first place, as observed above, for high values of χ (20° onward) the southern peak of each plot appears to be more or less flat in contrast with the northern portion.

Secondly, if the variations of noon values of fF_2 with season, i.e., with χ is plotted for different stations north and south of the magnetic equator, the curves obtained exhibit dissimilar nature in the two hemispheres. Had the relation between noon fF_2 and I (magnetic dip) been symmetrical about the magnetic equator the fF_2-I curves of figures 1 to 4 should have been substantially alike in both the hemispheres. In fact, speaking in a very general way, noon fF_2 appears to increase with χ for northerly stations whereas it decreases with χ for southerly stations. Figure 5 shows this for the four years from 1952 to 1955. Such north-south anomaly in the seasonal behaviour of noon fF_2 has also been noticed earlier (Berkner and Wells, 1938). It is found, however, that similar curves drawn for the sunspot maximum year 1948 and depicted in the same figure for comparison, do not show this north-south anomaly. On the contrary, the curves exhibit a general increase of fF_2 from low to high values of χ_{noon} in both hemispheres.

(iii) *Decrease of noon fF_2 from sunspot maximum (1948) to sunspot minimum (1954)*: It is known that the value of noon fF_2 at a particular station follows the solar cycle attaining a maximum during the epoch of maximum sunspot activity. Figure 6 depicts the ratio of noon fF_2 at the epoch of sunspot maximum (1948) to that at the epoch of sunspot minimum (1954) plotted against magnetic dip for chosen constant values of χ_{noon} . In plotting the curves, the values of noon fF_2 have been estimated from the plots of figures 1 and 3 by interpolation.

The plots show that the ratio varies with magnetic dip exhibiting clearly a minimum north of the magnetic equator. This means that the decrease of noon fF_2 from sunspot maximum to sunspot minimum is not in the same proportion at all places.

5. CONCLUDING REMARKS

The information obtained from the analysis presented here indicates clearly that for constant solar zenith distance noon F_2 ionization is not the same everywhere but varies with magnetic dip or geomagnetic latitude. Furthermore, the

shape of the constant- χ plots varies with the sunspot cycle. To explain these facts, which are not expected from Chapman's theory, two alternative possibilities suggest themselves. In the first place, the source of ionization of the F_2 region is not the sun or at least predominantly not so. Alternatively, the solar

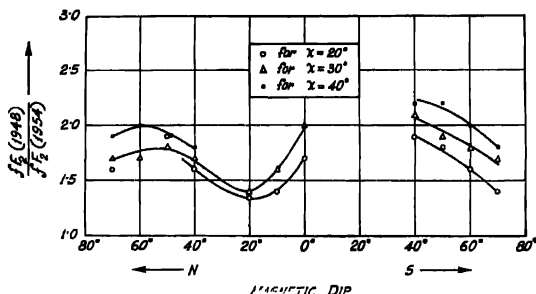


Fig. 6. Ratio of noon fF_2 in sunspot maximum year 1948 to that in sunspot minimum year 1954 plotted against magnetic dip for three different values of solar zenith distance.

ultraviolet radiation is the main source of ionization but the observed variation with magnetic co-ordinates of the earth is the result of a balance between gain and loss of electrons at the site of observation, produced by processes more complicated than envisaged earlier. The authors believe that the latter alternative is more likely to be the correct explanation and that, besides the primary processes of solar photon absorption producing electrons and of recombination, attachment, etc., causing electron decay, the transport of electrons from one place to another under the influence of the terrestrial magnetic field govern both the gain and loss of electrons at any site.

Another phenomenon revealed by the analysis of the 1952-55 data is that even though the variation of noon F_2 ionization has a dip near the terrestrial magnetic equator with peaks on either side, the variation is by no means symmetrical about the equator. We consider this asymmetric behaviour in the two hemispheres as a significant phenomenon and any theory attempting to explain the equatorial depression of F_2 ionization should, in order to be complete, also explain this asymmetry.

ACKNOWLEDGMENTS

The authors are indebted to Professor S. K. Mitra for his kind interest in the work.

One of the authors (P.D.) is grateful to the Ministry of Scientific Research and Cultural Affairs, Government of India, for the grant of a Senior Research Training Scholarship.

REFERENCES

- Appleton, E. V., 1946, *Nature*, 157, 691.
 ,, 1950, *J. Atmos. Terr. Phys.*, 1, 106.
 ,, 1954, *J. Atmos. Terr. Phys.*, 5, 349.
Appleton, E. V. and Lyon, A. J., 1957, *J. Atmos. Terr. Phys.*, 10, 1.
Appleton, E. V. and Naismith, R., 1935, *Proc. Roy. Soc. A.*, 150, 685.
Bailey, D. K., 1948, *Terr. Mag. Atmos. Elect.*, 53, 35.
Berkner, L. V. and Wells, H. W., 1938, *Terr. Mag. Atmos. Elect.*, 43, 15.
Bhar, J. N., 1957, *J. Atmos. Terr. Phys.*, 10, 168.
Liang, P. H., 1947, *Nature*, 160, 642
Maeda, H., 1955, *Rep. Ionos. Res., Japan*, 9, 60.
Martyn, D. F., 1947, *Proc. Roy. Soc. A*, 189, 241.
 ,, 1954, *The Physics of the Ionosphere*, p. 254 (Phys. Soc., London)
Millington, G., 1932, *Proc. Roy. Soc. A*, 44, 580.

A CASE FOR EFFICACY OF HULBURT-HIRSCHFELDER POTENTIAL FUNCTION

N. R. TAWDE AND M. R. KATTI

DEPARTMENT OF PHYSICS, KARNATAK UNIVERSITY, DHARWAR

(Received for publication, November 6, 1958)

ABSTRACT The Hulburt-Hirschfelder potential energy function has been tested for its efficiency in relation to Morse expression. Its five-parameter character has been converted to four-parameter one, with a view to derive the fifth parameter a_e . The calculated data are then compared to the accurately known experimental data of a large number of diatomic molecules. The expression proves much superior to Morse's and even to some others, known to be better than Morse's.

In a recent exhaustive review, Varshni (1957) has made a critical assessment of the relative merits of various potential energy functions of diatomic molecules. The test has been confined only to the functions which do not assume, but which predict the molecular constants α_e or $\omega_e x_e$. These latter are then compared with the actual measured values. Obviously a test of this type is not possible with functions, such as Hulburt-Hirschfelder (H-H, 1941), which employ all the known experimental constants. Hence this function does not figure in the above study. However, if this five-parameter function of H-H is converted into a four-parameter one and then the fifth parameter predicted from it, one could still carry out the test in the manner given by Varshni. This is proposed to be done in the present paper.

Varshni starts by expanding $U(r)$ near the equilibrium value ($r = r_e$). The expansion is given by

$$U(r) = \frac{1}{2!} U''(r_e)(r-r_e)^2 + \frac{1}{3!} U'''(r_e)(r-r_e)^3 + \frac{1}{4!} U^{IV}(r_e)(r-r_e)^4 + \dots \quad (1.1)$$

Here the value of the first derivative $U'(r_e)$ does not appear as it is obviously zero. Relations first deduced by Kratzer (1920) and modified for the above form of the expansion, provide values of these derivatives in terms of the spectroscopic constants. Later Dunham (1932) has shown that

$$\alpha_e = - \left[\frac{c_3}{c_2} r_e + 1 \right] \frac{6B_e^2}{\omega_e} \quad \dots \quad (1.2)$$

and

$$\mu \omega_e x_e = \left[\frac{15}{8} \left(\frac{c_3}{c_2} \right)^2 - \frac{3}{2} \left(\frac{c_4}{c_2} \right) \right] h/8\pi^2 c \quad \dots \quad (1.3)$$

where

$$c_2 = U^{II}(r_e)/2!, \quad c_3 = U^{III}(r_e)/3! \quad \text{and} \quad c_4 = U^{IV}(r_e)/4! \quad \dots \quad (1.4)$$

After putting

$$U^{III}(r_e)/U^{II}(r_e) = X \quad \dots \quad (1.5)$$

$$U^{IV}(r_e)/U^{II}(r_e) = Y \quad \dots \quad (1.6)$$

one obtains

$$\alpha_e = - \left[\frac{Xr_e}{3} + 1 \right] 6B_e^2/\omega_e \quad \dots \quad (1.7)$$

and

$$\omega_e x_e = \left[\frac{5}{3} X^2 - Y \right] \frac{W}{\mu_A} \quad \dots \quad (1.8)$$

with $W = 2.1078 \times 10^{-16}$

In the above equations (1.7) and (1.8), it is only the quantities $\left[\frac{Xr_e}{3} + 1 \right]$

and $\left[\frac{5}{3} X^2 - Y \right]$ which will be different for different functions.

Using the most generally adopted Morse's (1929) function

$$U = D_e [1 - e^{-a(r-r_e)}]^2 \quad (1.9),$$

we have the derivatives

$$U^{II}(r_e) = 2a^2 D_e \quad (2.0)$$

$$U^{III}(r_e) = -6a^3 D_e \quad (2.1)$$

and

$$U^{IV}(r_e) = 14a^4 D_e \quad (2.2)$$

From these, the values of X and Y turn out to be

$$X = -3a \quad \dots \quad (2.3)$$

$$Y = 7a^2 \quad \dots \quad (2.4)$$

Using the above in eqs. (1.7) and (1.8), Varshni has evaluated the constants α_e and $\omega_e x_e$ in the case of 23 neutral diatomic molecules for which reliable experimental data of molecular constants is available. The comparative study of the calculated and observed constants by him has revealed that the percentage dispersion between the two is of the order of ± 33.1 for α_e and ± 31.2 for $\omega_e x_e$. In comparison to the dispersions given by Morse function, other functions give either smaller or larger departures. A function giving smaller dispersion than that of Morse is considered as more satisfactory. Thus the superiority of a function is judged in terms of the accuracy given by Morse's. As for the reproduction of α_e is concerned, there are functions examined by Varshni giving percentage error as low as ± 22.1 and thus proving superior to Morse's.

Some calculational slips have been noticed in Table XIa reduce the percentage error in case of Morse function from \pm

thus provide relatively better accuracy for it. These slips relate to OH, HF, HI, N₂ (two cases), SO, and ICl (cf. Table I here for corrections).

In the light of the objective outlined in para 1, the H-H function can now be viewed as a four-parameter function to predict the value of α_e . Hulburt-Hirschfelder's expression is of the form

$$U = D[(1 - e^{-x})^2 + cx^3e^{-2x}(1 + bx)] \quad \dots (2.5)$$

which is the same as that of Morse, except for an additional term which acts as a correction term. Here

$$x = 2\beta\xi = \frac{\omega_e}{2(B_e D_e)^{1/2}} \cdot \frac{r - r_e}{r_e} \quad \dots (2.6)$$

and b and c are simple algebraic functions of the five spectroscopic constants K_e , r_e , D_e , α_e and $\omega_e x_e$

$$c = 1 - a_1(D/a_0)^{1/2} \quad \dots (2.7)$$

$$b = 2 - \left[\frac{7}{12} - \frac{Da_2}{a_0} \right] / c \quad \dots (2.8)$$

where a_0 , a_1 , and a_2 are the Dunham coefficients

$$a_0 = \omega_e^2 / 4B_e, \quad a_1 = -1 - \alpha_e \omega_e / 6B_e^2, \quad a_2 = \frac{5}{4} a_1^2 - \frac{2\omega_e x_e}{3B_e}$$

The function (2.5) on differentiation gave

$$U^{II}(r_e) = 2a^2 D_e \quad \dots (2.9)$$

$$U^{III}(r_e) = 6a^3(c-1)D_e \quad \dots (3.0)$$

$$U^{IV}(r_e) = 2a^4[7+12c(b-1)]D_e \quad \dots (3.1)$$

and

$$X = U^{III}(r_e)/U^{II}(r_e) = 3a(c-1) \quad \dots (3.2)$$

$$Y = U^{IV}(r_e)/U^{II}(r_e) = a^2[7+12c(b-1)] \quad \dots (3.3)$$

It may be seen from (3.2) above that it involves α_e and thus assumes its value. Hence this quantity in the present form cannot be used for the prediction of α_e . If we modify the expression

$$a_1 = -1 - \alpha_e \omega_e / 6B_e^2 \quad \dots (3.4)$$

$$\text{by putting} \quad \alpha_e = \frac{6\sqrt{\omega_e x_e B_e^3}}{\omega_e} - \frac{6B_e^2}{\omega_e} \quad \dots (3.5)$$

a relation due to Pekeris (1934), we make the quantity c independent of α_e . The above substitution is justified by the fact that the Pekeris relation (3.5) is derived from the Morse function which forms an integral part of H-H's function. Thus c will be determined by

$$a_1 = -\sqrt{\frac{\omega_e x_e}{B_e}} \quad \text{and} \quad a_0 = \omega_e^2 / 4B_e \quad \dots (3.6)$$

and thus made independent of α_e .

Such an operation is not possible in the case of Y in order to make it independent of $\omega_e x_e$ and thus to predict $\omega_e x_e$, as too many quantities are involved. This led us to restrict ourselves to the deduction of α_e only. The results of α_e evaluated from Morse and H-H function used as above, are shown in the Table I. The various molecular constants employed in the present paper are uniform with those employed by Varshni.

TABLE I

Molecule	α_e		α_e	
	Morse Present calc.	% Error	H-H function Present calc.	% Error
H ₂	2.222	-25.8	1.984	-33.7
ZnH	0.4248	+69.9	0.3118	+24.73
CdH	0.3599	+65.1	0.2379	+9.13
HgH	0.5090	+63.1	0.3818	+22.38
CH	0.5238	+1.9	0.4861	+8.97
OH	0.7076* (0.7141)	-9.0* (0.0)	0.6268	-12.21
HF	0.6055* (0.5822)	-8.2* (-24.4)	0.6662	-13.53
HCl	0.3109	+3.3	0.2741	-9.21
HBr	0.2540	+7.9	0.2131	-5.71
HI	0.2588* (0.2015)	+41.1* (-19.2)	0.1295	-29.23
Li ₂	0.0103	+46.3	0.00744	+5.68
Na ₂	0.00146	+84.8	0.001051	+33.04
K ₂	0.000412	+88.1	0.0003088	+41.02
N ₂ (1)	0.02442* (0.02864)	+29.5* (+53.2)	0.01727	-7.65
N ₂ (2)	0.01969* (0.01996)	+5.3* (+6.2)	"	"
P ₂	0.00177	+24.7	0.001443	+0.41
O ₂	0.00175	+10.8	0.01244	-21.21
SO	0.00719* (0.01095)	+27.9* (+94.8)	0.005197	-7.53
Cl ₂	0.00190	+11.8	0.001925	+13.22
Br ₂	0.000423	+53.8	0.0003357	+22.08
I ₂	0.000154	+31.6	0.0001018	-12.99
Iod	0.000670* (0.000654)	+25.0* (+22.0)	0.0005257	-1.92
CO(1)	0.01912	+9.4	0.01691	-3.26
CO(2)	0.01844	+5.5	"	"
CO(3)	0.01643	-6.0	"	"
NO(1)	0.0228	+28.1	0.01707	-4.10
NO(2)	0.0198	+11.2	"	"
Average		± 31.9 (± 33.1)		± 15.3

N.B. Figures with asterisk are our corrected values; bracketed are reproduced from Varshni.

It is seen from the Table I that as far as the reproduction of α_e is concerned, the results obtained with H-H's function show the average percentage error to be ± 15.3 , which is much less than that given by Morse's function. Comparing this accuracy with the other three functions examined by Varshni, the H-H's function used in the manner given above, proves to be much superior to all of them. This is evident from the comparative figures of the magnitude of percentage errors recorded in Table II.

TABLE II

Comparative percentage errors in the α_e estimates

Function	% Error
Morse	± 31.9
Rydberg	$+28.0$
Third	± 22.9
Empirical	± 22.1
{ Hulburt & Hirschfelder (Present paper)	± 15.3

Another feature which is apparent is that after the modifications α_e becomes independent of D_e . In view of these findings the relation $c = 1 - \left(\frac{Dx_e}{\omega_e} \right)^{\frac{1}{2}}$ becomes preferable to one originally given by H-H, viz., $c = 1 + a_1(D/a_0)^{\frac{1}{2}}$. Further work on these lines is in hand.

ACKNOWLEDGMENTS

The junior author (M.R.K) is grateful to Mr. M. I. Savadatti of this department for numerous helpful discussions.

REFERENCES

- Dunham, J. L., 1932, *Phys. Rev.* **41**, 713, 721.
 Hulburt H. M. and Hirschfelder, J. O., 1941, *J. Chem. Phys.* **9**, 61.
 Krutzer, A., 1920, *Z. Physik*, **3**, 289
 Morse, P. M., 1929, *Phys. Rev.*, **34**, 57
 Pekeris, C. L., 1934, *Phys. Rev.*, **45**, 98.
 Varshni, Y. P. 1957, *Rev. Mod. Phys.*, **29**, 664.

RESONANCE CURVES OF A SYNCHRONISED OSCILLATOR

B. R. NAG

INSTITUTE OF RADIO PHYSICS AND ELECTRONICS, CALCUTTA UNIVERSITY

(Received for publication, September 30, 1958)

ABSTRACT. Resonance curves of an oscillator with an external synchronising electromotive force capable of delineating the features of hysteresis effect have been determined experimentally with the help of a differential analyser. Theoretical resonance curves of an oscillator with a break-point non-linearity are deduced and compared with experimental curves. From the experimental curves the range of hysteresis is determined.

1. INTRODUCTION

Resonance curves of an oscillator with an external synchronising electromotive force have been studied both theoretically and experimentally by many workers (Appleton, 1922; Appleton and Van der Pol, 1922; Golz, 1922, Van der Pol, 1927, 1934; Andronov and Witt, 1930; Gapanov, 1935; Tucker, 1946; Cartwright, 1948; Gillies, 1949, 1954). However, the experimental measurements made by previous workers were only adequate to verify portions of the resonance curves obtained theoretically. Some important details of these theoretical curves have remained yet to be verified. For instance, it follows from theoretical analysis that the resonance curves of an oscillator obeying Van der Pol equation should show hysteresis over a range of synchronising voltages on the 'border line between strong and weak signals' (Cartwright, 1948), the exact range suggested by different authors being different. Nevertheless, as far as the present author is aware, the hysteresis effect has not been experimentally obtained by any worker. This is possibly due to the fact that the hysteresis occurs for values of parameters which are very close together and it is difficult to provide such close variation of the parameters in a determined way on an experimental oscillator. On a differential analyser, however, an oscillator may be easily realised of which the describing differential equation is definite and the parameters admit of accurate control. The resonance curves of the oscillator may thus be obtained with the help of a differential analyser in greater detail than is otherwise possible.

The work, described in the present paper, was first concerned with the Van der Pol oscillator and the experimental resonance curves were obtained on a differential analyser. Hysteresis effect was found to exist in these curves but the range was too small to be determined exactly. Moreover, a very accurate realisa-

tion of the cubic non-linearity of Van der Pol equation is difficult. The study was therefore extended to an oscillator which is stabilised by a break-point non-linearity, easily representable on the analyser and for which the range of hysteresis is wider. The theoretical resonance curves of this type of oscillator are not available and hence these have also been calculated.

2. THEORETICAL RESONANCE CURVES OF AN OSCILLATOR WITH AN EXTERNAL ELECTROMOTIVE FORCE

The differential equation describing an oscillator with an external electromotive force can be written as

$$\ddot{x} + \mu f(x, \dot{x}) + \omega_0^2 x = E \sin \omega_1 t, \quad (1)$$

where $\mu f(x, \dot{x})$ represents the non-linearity in the oscillator.

The solution of the above equation for small values of μ may be assumed to be given by

$$x = A \sin (\omega_1 t + \phi) \quad \dots (2)$$

where A and ϕ are functions of time.

Differentiating (2)

$$\dot{x} = \omega_1 A \cos (\omega_1 t + \phi) + \dot{A} \sin (\omega_1 t + \phi) + A \dot{\phi} \cos (\omega_1 t + \phi) \quad \dots (3)$$

Differentiating again and keeping only the first order terms (terms involving \ddot{A} , $\ddot{\phi}$ or $\dot{A} \dot{\phi}$ are neglected).

$$\ddot{x} = -\omega_1^2 A \sin (\omega_1 t + \phi) + 2\omega_1 \dot{A} \cos (\omega_1 t + \phi) - 2\omega_1 A \dot{\phi} \sin (\omega_1 t + \phi) \quad \dots (4)$$

Substituting for \ddot{x} , \dot{x} and x in Eqn. (1) from Eqns. (4), (3) and (2) respectively and retaining the first order terms only

$$\begin{aligned} (\omega_0^2 - \omega_1^2) A \sin (\omega_1 t + \phi) + 2\omega_1 \dot{A} \cos (\omega_1 t + \phi) - 2\omega_1 A \dot{\phi} \sin (\omega_1 t + \phi) \\ = E \sin \omega_1 t - \mu f\{A \sin (\omega_1 t + \phi), \omega_1 A \cos (\omega_1 t + \phi)\}. \end{aligned} \quad \dots (5)$$

Now, $\mu f\{A \sin (\omega_1 t + \phi), \omega_1 A \cos (\omega_1 t + \phi)\}$ may be written as

$$\mu f\{A \sin (\omega_1 t + \phi), \omega_1 A \cos (\omega_1 t + \phi)\} = g \cos (\omega_1 t + \phi) + h \sin (\omega_1 t + \phi) \quad \dots (6)$$

+ terms involving harmonics of ω_1 .

where

$$g = \frac{1}{\pi} \int_0^{2\pi} \mu f\{A \sin (\omega_1 t + \phi), \omega_1 A \cos (\omega_1 t + \phi)\} \cos (\omega_1 t + \phi) d(\omega_1 t) \quad \dots (7)$$

and

$$h = \frac{1}{\pi} \int_0^{2\pi} \mu f\{A \sin (\omega_1 t + \phi), \omega_1 A \cos (\omega_1 t + \phi)\} \sin (\omega_1 t + \phi) d(\omega_1 t) \quad \dots (8)$$

Equating the co-efficients of $\cos(\omega_1 t + \phi)$ and $\sin(\omega_1 t + \phi)$ on the two sides of Eqn. (5)

$$\omega_1 \dot{A} = -\frac{1}{2} g - \frac{E}{2} \sin \phi. \quad \dots (9)$$

$$\omega_1 A \dot{\phi} = \frac{1}{2} h - \frac{A}{2} (\omega_1^2 - \omega_0^2) - \frac{E}{2} \cos \phi. \quad \dots (10)$$

For periodic oscillations, the equilibrium values of A and ϕ are obtained on putting $\dot{A} = 0, \dot{\phi} = 0$ in Eqs. (9) and (10).

Thus,

$$-g = E \sin \phi. \quad \dots (11)$$

$$h = A(\omega_1^2 - \omega_0^2) + E \cos \phi. \quad \dots (12)$$

On eliminating ϕ

$$E^2 = [h - (\omega_1^2 - \omega_0^2)A]^2 + g^2. \quad \dots (13)$$

Eqn. (13) gives the amplitudes of periodic oscillations for different excitations and detuning. The plots of A^2 or normalised values of A^2 against $\frac{\omega_1^2 - \omega_0^2}{\omega_1}$ are referred to as the resonance curves of the oscillator.

Resonance Curves of the Van der Pol Oscillator

For the Van der Pol oscillator,

$$\mu f(x, \dot{x}) = c \dot{x}^3 - ax. \quad \dots (14)$$

Hence

$$g = \left(\frac{3}{4} c \omega_1^2 A^2 - a \right) \omega_1 A. \quad \dots (15a)$$

$$h = 0 \quad \dots (15b)$$

On substituting in Eqn. (13)

$$E^2 = [(\omega_1^2 - \omega_0^2)A]^2 + \left[\left(\frac{3}{4} c \omega_1^2 A^2 - a \right) \omega_1 A \right]^2 \quad \dots (16)$$

Putting $\frac{4a}{3c} = A_0^2, \quad \frac{\omega_1}{A_0} A = \rho, \quad \frac{\omega_1^2 - \omega_0^2}{\omega_1 A_0} = \sigma, \quad \frac{E}{a A_0} = F$

$$F^2 = \rho^2 [\sigma^2 + (1 - \rho^2)^2] \quad \dots (17)$$

In the resonance curves shown in figure 1, ρ^2 is plotted against σ with F^2 as parameter. Since the plots are symmetrical about σ , the portions for positive values of σ are only shown.

It is observed that for low values of F^2 , the resonance curves have two branches and there are three values of ρ^2 for low values of σ . With increase in F^2 , the two branches approach each other and meet on the $\sigma = 0$ axis for $F^2 = \frac{1}{4}$; with further increase in F^2 the curve opens out but continues to have triple value of ρ^2 for some values of σ till $F^2 = \frac{1}{4}$. For larger values of F^2 the resonance curves are single-valued.

The equilibrium values of ρ^2 as given by Eqn. (17) are not all necessarily stable. The stability can be judged on considering the singularities of the first order differential equation, (Andronov and Witt, 1930) which may be derived, from Eqns (9) and (10) as

$$\frac{d\rho}{d\phi} = \rho \frac{-(\rho^2 - 1)\rho - F \sin \phi}{-\sigma\rho - F \cos \phi} \quad \dots (18)$$

The singularities of this equation are of the form shown in figure 1. The equations for the critical lines are given by

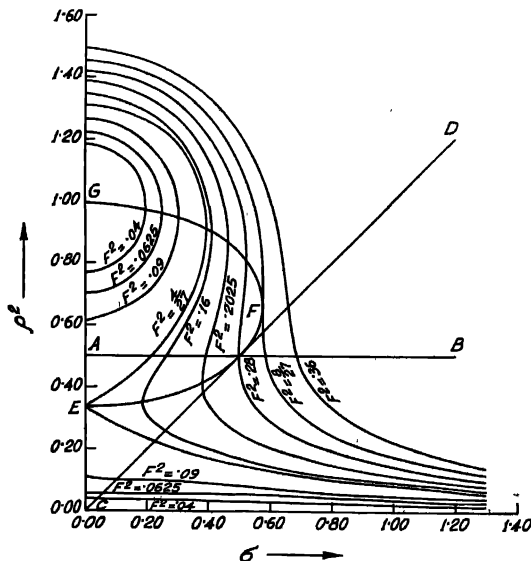


Fig. 1(a). Theoretical resonance curves of Van der Pol oscillator.

- | | |
|---|----------------|
| (i) $\rho^2 = \frac{1}{2}$ | (line A B) |
| (ii) $\rho^2 = \sigma$ | (line C D) |
| (iii) $\sigma^2 = -(1 - \rho^2)(1 - 3\rho^2)$ | (Curve E F G). |

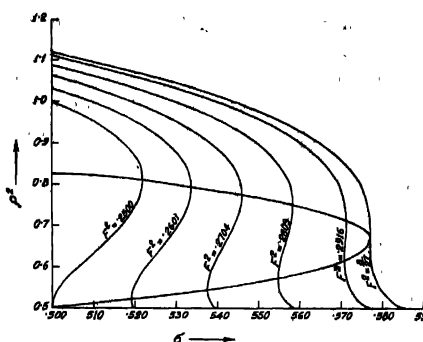


Fig. 1(b) Theoretical resonance curves of Van der Pol oscillator showing the region of hysteresis.

Evidently in the regions where the singularities are of the nature of saddles, unstable nodes or unstable spirals, the values of ρ^2 given by the resonance curves represent unstable equilibrium. Now, when a periodic solution becomes unstable, the oscillator will execute the other stable periodic oscillation, if there be any in the region. In regions where no periodic stable oscillation is possible, the oscillator will execute the other possible oscillation which has been called the quasi-periodic oscillation. In that case \dot{A} and $\dot{\phi}$ do not become zero but vary periodically giving rise to a limit cycle in the $A-\phi$ plane.

On the basis of the above considerations, the transformation from periodic to quasi-periodic oscillation or vice versa can be readily predicted. The $\rho^2-\sigma$ plane can be divided into three regions characterised by the different ways in which the transformation from periodic to quasi-periodic oscillation or vice versa takes place.

(i) *Region extending from $F^2 = 8/27$ upwards*: For such values of F^2 , the periodic oscillation becomes unstable on AB . Hence as σ is varied from lower to higher values the periodic oscillation continues following the resonance curve till it reaches the line AB . Quasi-periodic oscillations will thereafter be excited, i.e., a limit cycle will appear round the unstable focus which will continue for higher values of σ ; the r.m.s. value of the amplitude will gradually increase to the free oscillation value. The curves will be reversible.

(ii) *Region extending from $F^2 = 4/27$ downwards*: In this case the transformation will take place on the upper part of the curve $EF G$; the limit cycle will transform to a separatrix through the double singularity. The resonance curves again will be reversible.

(iii) *Region extending from $F^2 = 4/27$ to $F^2 = 8/27$* : The transformation from periodic to quasi-periodic oscillation or vice versa cannot be so readily

predicted in this case. For values of $F^2 \geq 9/32$, for which the resonance curves cut the upper part of the curve EEG at a lower value of σ than that for the lower part, the limit cycle is expected to penetrate the curve EEG and transformation will take place on AB . The response curve will show hysteresis. As σ is decreased the r.m.s. amplitude of quasi-periodic oscillation will gradually decrease and the oscillation transforms to periodic oscillation on AB . With further decrease in σ , the amplitude will follow the resonance curve till it cuts the lower part of EEG . At this point it will jump to the higher stable value. For further reduction of σ it will again follow the resonance curve. When σ is increased from lower to higher values the amplitude of oscillation follows the resonance curve till it meets the upper part of EEG . At this point the amplitude jumps to the lower stable value. It will be seen that this downward jump occurs for a value of σ higher than that for which the upward jump occurs for the reverse variation of σ .

For values of F^2 lower than $9/32$, however, the transformation can not be definitely predicted. The point of transformation may shift suddenly from AB to the upper part of EEG for $F^2 < 9/32$. In that case the hysteresis effect will be exhibited only in the periodic oscillations. The range of hysteresis will extend from $F^2 = 9/32$ to $F^2 = 8/27$ (Gapanov, 1935). It has been suggested by Cartwright (1948) that this discontinuous behaviour on the two sides of $F^2 = 9/32$ is improbable and that the quasi-periodic oscillation will continue to transform to periodic oscillation on AB upto $F^2 = 1/4$ as in the above case. Then the transformation point will gradually move up i.e. the limit cycle instead of vanishing through a focus will vanish through a saddle point. However, this transformation point will move up to the upper part of EEG before $F^2 = 4/27$. If this suggestion is correct, the response curve will show jumps from lower periodic oscillations to upper periodic oscillations in the region $1/4 \leq F^2 \leq 9/32$ and from lower quasi-periodic to upper periodic oscillation in the region $4/27 \leq F^2 \leq 1/4$. The downward jumps will be from upper periodic oscillation to lower quasi-periodic oscillation. The region of hysteresis will extend from $F^2 = 4/27 + \delta$ to $F^2 = 8/27$, δ being an undetermined positive number.

Alternatively it has been suggested by Gillies (1954) that the transformation will continue to take place on the upper part of the curve EEG even for $F^2 > 1/4$. But in between $F^2 = 1/4$ and $F^2 = 9/32$, there will be some value of F^2 for which the limit cycle passes through a second order singularity on the upper part of EEG , but instead of degenerating to a separatrix when the singular points separate, a new limit cycle will appear which will continue to exist shrinking up round the unstable focus to vanish on AB . For larger values of F^2 the second order singularity appears outside the limit cycle and the latter therefore will continue to exist upto AB when it vanishes to a focus. Accordingly hysteresis should extend from $F^2 = 1/4 + \delta$ to $F^2 = 8/27$. Numerical integrations performed by Gillies seem to indicate that $\delta > 1/108$.

It is difficult to ascertain which one of the above suggestions is correct. A proper experimental determination of the range of hysteresis is also not easy in this case, since the range is very small. For example, for $a = 0.1$, $A_0 = 1$ the hysteresis range for E^2 as given by the three solutions are (1) .053—.0545, (Gapanov), (2) .050— δ —.0545 (Cartwright), (3) .050+ δ —.0545 (Gillies). Thus a decision can be reached only when the experimental accuracy is of the order of 1 in 1000; this is difficult to be attained on an electronic differential analyser.

Resonance Curves of an Oscillator Stabilised by Break-point Non-linearity

We next consider an oscillator for which

$$\mu f(x, \dot{x}) = f_1(x) - a\dot{x}$$

$$f_1(x) = \dot{x} - E_0, \quad \text{for } \dot{x} > E_0$$

$$= 0, \quad \text{for } -E_0 < \dot{x} < E_0$$

$$= \dot{x} + E_0, \quad \text{for } -E_0 > \dot{x}$$

This non-linearity has been called the break-point non-linearity and is shown graphically in figure 2. It may be mentioned that the operating conditions of a

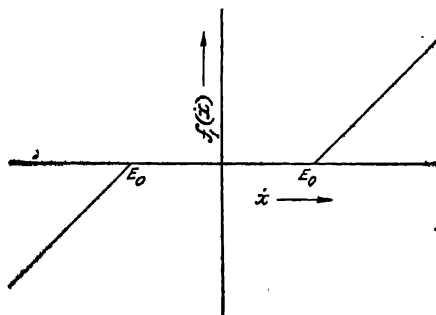


Fig. 2. The break-point non-linearity.

practical oscillator are such that this type of non-linearity is nearer to the actual conditions than the cubic non-linearity.

In this case, from Eqns. (7) and (8),

$$-g = \omega_1 A \left[a - \frac{2}{\pi} \cos^{-1} \frac{E_0}{\omega_1 A} + \frac{2}{\pi} \left(\frac{E_0}{\omega_1 A} \right) \sqrt{1 - \left(\frac{E_0}{\omega_1 A} \right)^2} \right], \quad \text{for } \omega_1 A > E_0$$

$$= \omega_1 A a, \quad \text{for } \omega_1 A < E_0$$

$$h = 0$$

$$\dots (18)$$

Substituting these values of g and h in Eqn. (13) and putting

$$\frac{\omega_1 A}{E_0} = \rho_b, \quad \frac{\omega_1^2 - \omega_0^2}{\omega_1} = \sigma_b, \quad \frac{E}{E_0} = e$$

$$\left. \begin{aligned} \frac{e^2}{\rho_b^2} &= \left[a - \frac{2}{\pi} \cos^{-1} \frac{1}{\rho_b} + \frac{2}{\pi} \frac{1}{\rho_b} \sqrt{1 - \frac{1}{\rho_b^2}} \right]^2 + \sigma_b^2, \text{ for } \rho_b > 1 \\ &= a^2 + \sigma_b^2, \text{ for } \rho_b < 1 \end{aligned} \right\} \quad \dots (19)$$

In contrast to the previous case normalised (with respect to a) plots of the resonance curves cannot be given. Plots for the particular value of $a = 0.1$ are shown in figure 3.

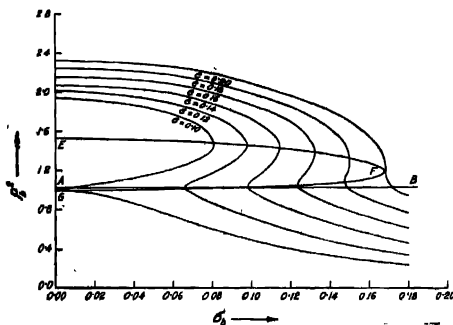


Fig. 3(a). Theoretical resonance curves of an oscillator with break-point non-linearity.

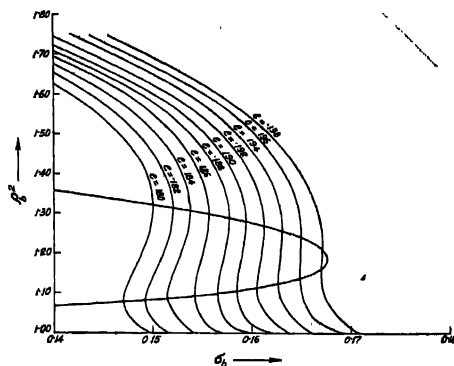


Fig. 3(b). Theoretical resonance curves of an oscillator with break-point non-linearity showing the region of hysteresis.

The general characteristics of the curves are similar to those of figure. 1. For $\epsilon < 0.1$, there are three values of ρ_b for low values of σ_b , while for $\epsilon > 0.198$ there is only one value of ρ_b for any value of σ_b . For intermediate values of ϵ there are three values of ρ_b for some intermediate values of σ_b .

The equations for the critical lines separating the ρ_b^2 - σ_b plane into different regions characterised by different types of singularities are

$$(i) \quad \frac{1}{\rho_b} = \cos \frac{\pi}{2} a. \quad (\text{line } AB)$$

$$(ii) \quad \frac{1}{\rho_b} \left(1 - \frac{1}{\rho_b^2} \right)^{1/2} = \frac{\pi}{2} \sigma_b. \quad (\text{curve } CD)$$

$$(iii) \quad \sigma_b^2 = - \left(a - \frac{2}{\pi} \cos^{-1} \rho_b^{-1} \right)^2 + \left(\frac{2}{\pi} \frac{1}{\rho_b} \sqrt{1 - \frac{1}{\rho_b^2}} \right)^2$$

(Curve *EEFG*)

The reversible transformations from periodic to quasi-periodic oscillation or vice versa on the upper part of *EEFG* occur for $\epsilon < 0.139$ and on *AB* for $\epsilon > 0.1985$. The range of hysteresis according to Cartwright's solution should extend from $\epsilon = 0.139 - \delta$ to $\epsilon = 0.1985$; according to that of Gillies from $\epsilon = 0.139 + \delta$ to $\epsilon = 0.1958$; and according to that of Gapanov from $\epsilon = 0.184$ to $\epsilon = 0.1985$. It is observed that the range of hysteresis for this oscillator is wider than in the case of the van der Pol oscillator for the same value of initial damping ($a = 0.1$). The study of the resonance curves of this oscillator is thus expected to yield more definite results.

3. EXPERIMENTAL ARRANGEMENT

The set up of the differential analyser for solving Eqn. (1) is shown in figure

4. The solution x appears at *A* and \dot{x} at *B*. The sinusoidal synchronising voltage

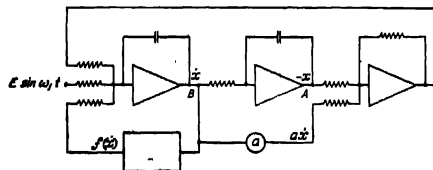


Fig. 4. Set up of the differential analyser for solving the equation;

$$\ddot{x} + f(x) - ax + \omega_0^2 x = E \sin \omega_1 t.$$

is supplied by an oscillator, stabilised by biased diodes, set on the analyser. Different values of σ are set by adjusting the frequency of the synchronising voltage which can be varied accurately by amounts as small as 0.01 per cent. The mean square amplitude of \dot{x} is measured by a thermocouple in conjunction

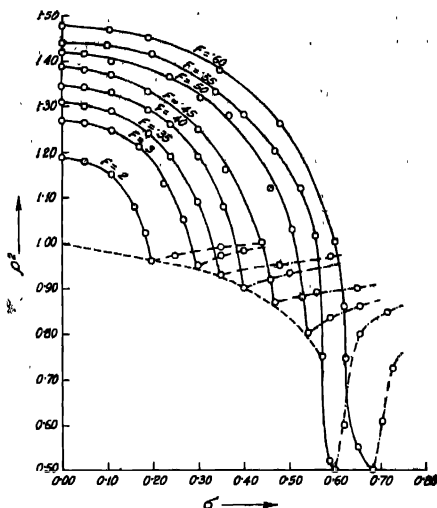


Fig. 5(a). Experimental resonance curves of Van der Pol oscillator.

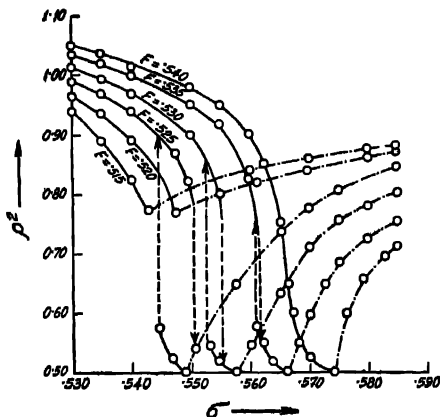


Fig. 5(b). Experimental resonance curves of Van der Pol oscillator showing the region of hysteresis.

with a d.c. millivoltmeter. The oscillator frequency is so chosen that the thermal inertia of the heater element of the thermocouple is large enough to give the average value. It may be noted that the accuracy of the differential analyser as obtained by test solutions is better than 1%.

4. EXPERIMENTAL RESULTS

The experimental plots of the resonance curves of the van der Pol oscillator are shown in Figure 5 and those for the oscillator with break-point non-linearity for $a = 0.1$ in figure 6.

Figures. 5(a) and 6(a) indicate very close qualitative agreement between the experimental and the theoretical curves. The reversible transformations from periodic to quasi-periodic oscillation or vice versa on the upper part of the curves EFG for low values of F and e and on the line AB for high values of F and e are clearly shown

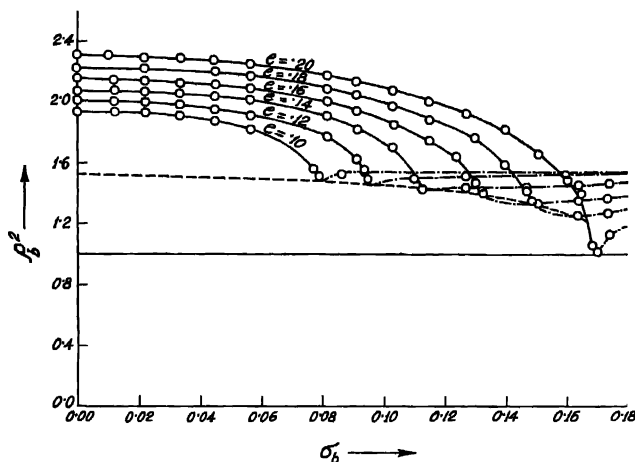


Fig. 6(a). Experimental resonance curves of an oscillator with break-point non linearity.

The detailed resonance curves shown in figures 5(b) and 6(b) show that hysteresis effect occurs in both the cases. The range of hysteresis of Van der Pol oscillator being comparatively narrow, detailed examination of the resonance curves in the hysteresis region is almost ruled out. But the curves for the oscillator with break-point non-linearity show all the details expected theoretically. The jump from low values of periodic oscillation to high values or vice versa is shown within the range $0.184 \leq e \leq 0.194$. It is further observed that hysteresis is obtained upto $e = 0.180$. In the region $0.180 \leq e \leq 0.184$, the upward jump continues to be from low periodic to high periodic oscillation, while the downward jump occurs from high periodic to low quasi-periodic oscillation. Jump from low quasi-periodic oscillation to high periodic oscillation as suggested by Cartwright has not been observed. The range of hysteresis extends from 0.196 to values of

ϵ definitely greater than 0.178 and less than 0.184 and agrees more closely with Gillies's solution. However, the mechanism of shift of the transformation point from the line AB to the upper part of EFG appears to be different. Previous theoretical analyses indicated that with decrease in σ_b , the limit cycle should always shrink. Experimental curves show, however, that for $\epsilon > 0.198$ the limit cycles shrink with decrease in σ_b to vanish through a focus. But for values of $\epsilon < 0.180$ the limit cycle at first shrinks and then expands to vanish through a separatrix on the upper part of EFG .

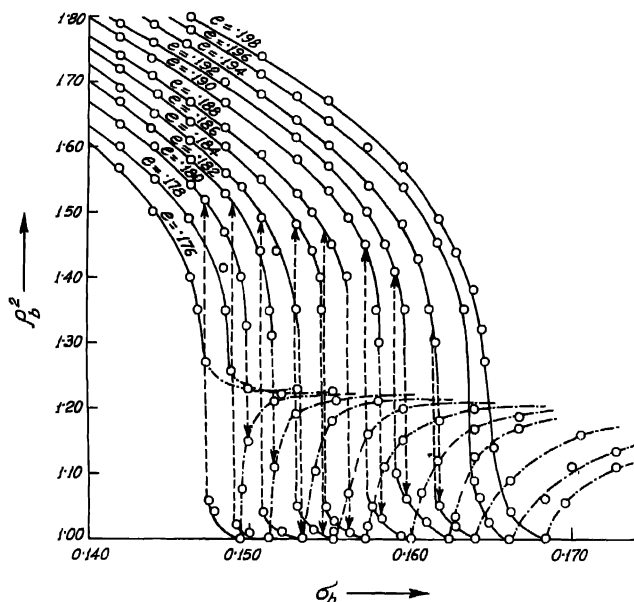


Fig. 6(b). Experimental resonance curves of an oscillator with break-point non-linearity showing the region of hysteresis

5. CONCLUSION

The experimental resonance curves obtained by a differential analyser agree very closely with the theoretical curves obtained by Van der Pol's method. The hysteresis phenomenon is clearly shown by the experimental curves. The range of hysteresis is found to be in good accord with the solution due to Gillies. In the oscillator with break-point non-linearity, the quasi-periodic oscillation in the border region shows a minima in amplitudes.

ACKNOWLEDGMENT

The author is indebted to Professor J. N. Bhar, D.Sc., F.N.I., for his constant guidance during the progress of the work.

REFERENCES

- Appleton, E. V., 1922, *Proc. Cambr. Phil. Soc.*, **21**, 231.
 Appleton, E. V. and Van der Pol, B., 1922, *Phil. Mag.*, **43**, 189.
 Andronov, A. and Witt, A., 1930, *Archiv fur Electrotechnik*, **24**, 99.
 Cartwright, M. L., 1948, *J.I.E.E.*, Part III, **95**, 88.
 Gapanov, W. I., 1935, *Journal of Technical Physics*, **5**, 821.
 Golz, J., 1922, *Jahrbuch der drahtlosen Telegraphie und Telephonie*, **19**, 281.
 Gillies, A. W., 1949, *Proc. I.E.E.*, Part III, **96**, 453.
 Gillies, A. W., 1954, *Quart. Jour. Mecha. Appl. Math.* Part II, **7**, 152.
 Kryloff, N. and Bogoliuboff, N., 1949, 'Introduction to Non-linear Mechanics', Princeton University Press, Pp 79-87.
 Minorsky, N., 1947, 'Introduction to Non-linear Mechanics', Edwards Brothers, Inc., Pp. 341-354.
 Tucker, D. G., 1946, *J.I.E.E.*, Part III, **92**, 226.
 Van der Pol, B., 1927, *Phil. Mag.*, **3**, 65
 Van der Pol, B., 1934, *Proc. I.R.E.*, **22**, 1051.

A MICRO-CALORIMETER FOR MEASUREMENT OF SMALL HEAT CHANGES

S N BHATTACHARYA and S. K. DAS.

INDIAN ASSOCIATION FOR THE CULTIVATION OF SCIENCE, CALCUTTA-32

(Received for publication, July 10, 1958.)

ABSTRACT. A calorimeter has been designed to study the heats of mixing of binary liquid systems. The accuracy of the calorimeter is better than $\pm .5\%$ and sensitivity is $.002$ J/mm. The vapour phase has been eliminated and the idea of thermally lagged multijacket has been achieved in practice.

INTRODUCTION

In modern experimental work on thermodynamic properties of mixtures, systems which show only small deviation from ideality and possess small heats of mixing are of great importance from the theoretical standpoint. In measuring small heats of mixing, the most important task is to eliminate errors due to evaporation. The recent work of MacGlashan and Adcock (1954) seems to be the most successful effort so far in this line. Since then a few groups of workers are pursuing this line but many systems could not be studied by this time, the need of which can not be over-stressed. In order to add more reliable data in this field a calorimeter has been constructed with certain important modifications to the MacGlashan-Adcock model to reduce the background fluctuation of temperature and uncertainty in the heat of stirring. The calorimeter is designed to use small quantities of liquids. It has been tested for a system for which standard data exist

DESCRIPTION OF THE CALORIMETER

Utilising the idea of Culvet (1945) and more recently by Tompa (1952) the troublesome vapour phase has been eliminated here by confining the liquid before and after the mixing under mercury. The calorimeter shown in figure 1 consists of two unsilvered, double walled pyrex vessels each containing two bells. In the mixing vessel, the heat absorbed on mixing is compensated by an electrical heater, wound non-inductively on the outer bell, while the other vessel acts as a reference bath for the thermocouple. The concentric bells can be lowered or raised independent of each other, the inner one having a thin glass membrane at the top. The outer bell has a glass pointer projected inwards by means of which the membrane can be punctured. Weighed amounts of liquids can be introduced, one into the inner bell and the other in the annular space

between the bells, by displacement of mercury. The reference vessel has exactly the same arrangement. By means of a mechanical coupling the outer and inner bells were connected in such a manner that this movement is simultaneous and identical in both the vessels. This is to eliminate the uncertainty due to

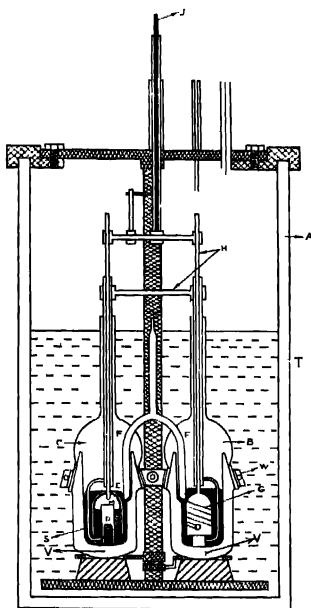


Fig. 1.

A—Lagged submarined jacket, B—Reaction vessel, C—Reference vessel, D—Inner bell, E—Outer bell, F—Ten junction thermocouple, G—Compensation heater, H—Mechanical coupler, J—Puncture rod, V—Outlet for evaporation, T—Outer thermostat.

heat produced by stirring. A ten-junction thermocouple with its ends insulated with "araldite" cement was used to measure the temperature difference. The jacket of the vessels can be connected to high vacuum line.

The calorimeter is mounted on a stout brass holder which can be suspended rigidly from a heavy brass lid of a thermally lagged jacket containing water. It is kept immersed under water in the water-tight jacket provided with outlets through which the mechanical coupler and electrical connections can be brought out. The thermally lagged jacket in its turn is kept submarined in a large thermostat fitted with a mercury-toluene regulator of 1.5 litre capacity and

efficient stirrers. The temperature of the outer bath is kept constant within $\pm 0.005^{\circ}\text{C}$.

The calorimeter is allowed to stand for 24 hours to attain equilibrium without any stirring inside the thermally lagged jacket. This is done to achieve in practice the idea of thermally lagged multi-jacket proposed by Tian (1922, 1923). Once the equilibrium is attained any fluctuation in the outer bath will have only a greatly reduced effect on the calorimeter itself due to thermal damping introduced by the lagged jacket. Thus an excellent reduction of background fluctuations of temperature can be achieved. Small temperature gradients may, however, be set up inside the thermally lagged jacket and this may vary slowly with time but the whole measurement lasts only for a short interval (not more than 10 min) and as such, the gradients can be taken as permanent in nature during this interval. Also as the heat absorbed in the system is practically compensated and the mixer vessel is kept heavily damped by its highly evacuated wall during the experiment, the temporary small disturbance in the mixer vessel will practically have no effect on the permanent temperature gradients, if there be any. These gradients may cause only a small galvanometer deflection which remains fairly steady for short interval during the measurement. This can be taken as the zero of the galvanometer reading.

The jackets of the mixer and reference vessel are evacuated two hours before the measurements. Half an hour before the measurements, galvanometer deflections are observed at an interval of 10 min. The membrane separating the two liquids is then punctured with a gentle push of the outer bell. Compensating current is switched on, for a predetermined period and the bells are raised up and down slowly to mix the two components properly. The galvanometer deflection after compensation is noted at definite intervals of time and a known amount of energy is again supplied to the system to account for the net uncompensated or over-compensated part.

To check the uncertainty due to heat of stirring and heat produced due to puncture of the membrane, the bells in the mixer vessel is filled with the same component. The corresponding inside bell of the reference vessel is without any membrane. No measurable quantity of heat is found to develop for the latter. As for the former, it is observed that if the stirring is very gentle and the quantity of mercury taken in both the vessels remains almost equal, then compensation due to heat of stirring is excellent and the galvanometer-zero remains completely unaffected by stirring.

Time intervals of compensating and calibrating currents are measured by means of a calibrated 50 cycle pulse generator and a scalar unit with a scale of ten. The output of the pulse generator is fed to the scalar unit via one pole of a D. P. D. T. switch. The other pole connects the heating circuit of the calorimeter to the storage cells. During the interval when current is sent to the

heating coil, the pulse generator is connected simultaneously to the scalar unit, from the count of which the time can be calculated with an accuracy of .02 seconds. The advantage of this type of arrangement lies in that it eliminates personal error without introducing any cumbersome mechanical systems like moving paper strips etc.

The electrical arrangement is similar to that of McGlashan and Adecock (1954) and the possible experimental errors have been fully discussed by them. Extending their estimate to that of our case, an accuracy better than $\pm 0.5\%$ has been attained. The sensitivity of the calorimeter is approximately .002 Joules/mm.

EXPERIMENTAL

In order to test the calorimeter the heat of mixing of the system carbon tetrachloride and cyclohexane was studied at 40°C for which reliable data exist.

Anal. carbon tetrachloride was refluxed at 50°–60°C with an alcoholic solution of potassium hydroxide (1:1 by weight). The alcohol was then removed by shaking with water followed by shaking with small portions of concentrated sulphuric acid, until there was no colour. It was then first distilled in an all glass assembly and finally fractionated through a column of 40 theoretical plates. Only the middle fraction was collected. The purity of the sample was checked by measuring the density. At 25°C the density of the sample was found to be 1.58423 gm/cc which possibly can be compared to 1.5858 gm/cc obtained by McGlashan *et al.* (1954) and 1.58452 gm/cc by Scatchard at the same temperature

RESULTS

TABLE I

At temperature 40°C

Wt. of carbon tetrachloride	Wt. of cyclo-mole hexane	fraction of CCl ₄ in mixture	<i>h</i> in J	<i>H_m</i> in J/mole
1.5829	.8261	.488	2.85	141.9
2.0576	.5512	.329	2.46	124.7
2.3748	.3937	.233	2.03	100.7
2.6909	.2361	.138	1.35	66.5
1.1077	1.0228	.628	2.53	130.8
.7922	1.0808	.731	2.09	109.2
.4751	1.3382	.837	1.45	76.1

Anal. cyclohexane was washed several times with a cold mixture of concentrated sulphuric and nitric acids to nitrate any benzene that might have been

present. After repeated washings with distilled water it was dried and distilled over metallic sodium. Finally it was fractionated through a column of 40 theoretical plates. The density of the sample measured at 25°C was 0.77395 gm/cc while those obtained by McGlashan *et al.* (1954) and Scatchard at 25°C is 0.77375 gm/cc and 0.77383 gm/cc respectively.

The results of our work and that of McGlashan *et al.* have been plotted on the same graph in figure 2. The agreement is found to be quite satisfactory.

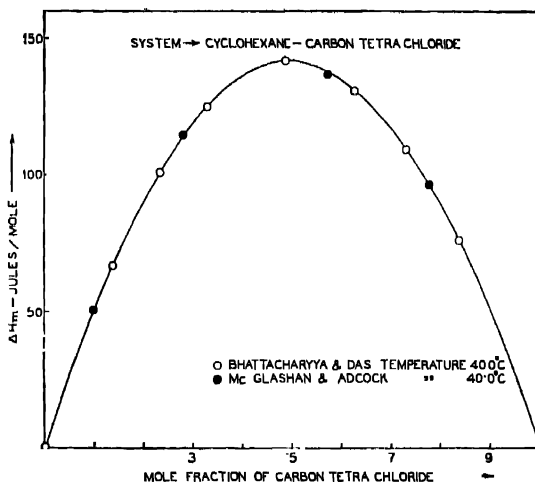


Fig. 2

ACKNOWLEDGMENTS

The authors are grateful to Professor S. R. Palit for his valuable suggestions and keen interest throughout the progress of this work. They are also indebted to the Council of Scientific and Industrial Research for financial assistance.

REFERENCES

- Culvet, E., 1945, *Mem. Serv. Chim. d'Etat*, **32**, 168.
 McGlashan, M. L. and Adcock, D. S., 1954, *Proc. Roy. Soc.*, **226**, 266.
 Tian, A., 1922, *Bull. Soc. Chim. France*, (4), **31**, 535.
 Tian, A. J., 1923, *Chim. Phys.*, **20**, 132.
 Tompa, H. J., 1953, *Polymer. Sci.*, **8**, 51.

ELECTRONIC SPECTRA OF 1, 3, 5-TRIMETHYLBENZENE IN THE LIQUID STATE AND IN THE SOLID STATE AT -180°C^*

S. K. SEN

OPTICS DEPARTMENT, INDIAN ASSOCIATION FOR THE CULTIVATION OF SCIENCE,
JADAVPUR, CALCUTTA-32

(Received for publication, November 18, 1958)

ABSTRACT. The ultraviolet absorption spectra of 1, 3, 5-trimethylbenzene in the liquid and solid states have been analysed and the results have been compared with those reported by previous workers for the same substance in the vapour state and for other similar compounds in different states. The 0, 0 band, which is forbidden in the vapour state, is found to appear with moderate intensity in the spectra due to the liquid and the solid at -180°C indicating a distortion of the three-fold symmetry of the molecules owing to the influence of the surrounding molecules of the same type. It is pointed out that such a distortion takes place even in absence of any halogen atom in the molecule.

INTRODUCTION

Sponer and Stallcup (1948), while analysing the absorption spectrum of 1, 3, 5-trimethylbenzene in the vapour state, observed that the 0, 0 band was absent. They ascribed the first strong band at 37000 cm^{-1} to $0 \rightarrow 1$ vibrational transition coupled to the electronic transition and a much weaker band at 36041 cm^{-1} to such a coupling of $1 \rightarrow 0$ transition and thus found the position of the 0,0 band to be at 36557 cm^{-1} . They pointed out that as the molecule possesses the symmetry D_{3h} , the 0,0 band is forbidden.

Banerjee (1957) observed that in the spectrum due to 1, 3, 5-trichlorobenzene in the solid state at -180°C , the forbidden 0,0 band appears with weak intensity. This has been explained on the assumption that the symmetry of the molecule is partially destroyed due to the formation of weak bands between chlorine atom of one molecule and a hydrogen atom of a neighbouring molecule.

Roy (1957) studied the absorption spectra of solutions of 1, 3, 5-trimethylbenzene and 1, 3, 5-trichlorobenzene in different solvents and observed that in the former case when the molecule of the solvent contains a chlorine atom or an OH group, weak intermolecular bonds are formed so as to distort the symmetry of the molecule and the 0, 0 band appears with weak intensity. In the latter case, solvents with molecules containing hydrogen atoms showed greater influence to produce the 0,0 band.

* Communicated by Prof. S. C. Sirkar.

In the present investigation the absorption spectra of 1, 3, 5-trimethylbenzene in the liquid and solid states have been studied to find out whether the surrounding molecules of the same type exert any influence on the electronic state of the molecule so as to destroy its three-fold axis of symmetry

EXPERIMENTAL

Chemically pure sample of 1, 3, 5-trimethylbenzene (B.D.H.) was distilled several times under reduced pressure.

The experimental set up was the same used in an earlier investigation by the author (Sen, 1955). Spectrograms were taken on HP3 films with Hilger E1 Quartz spectrograph having a dispersion 3 Å.U per mm. in the region 2600 Å. Very thin films of thickness of the order of a few microns were required for the spectrum due to the liquid state, the time of exposure varying from 10 to 15 minutes. The spectrum in the solid state was photographed with one hour's exposure time. Iron arc spectrum was taken in each spectrogram as comparison. Microphotometric records were obtained with a self-recording microphotometer of Kipp and Zonen type. The frequencies of the bands were measured using the microphotometric records of iron lines as in the earlier investigation (Sen, 1956). The slit width was 0.3 mm ($\approx 15 \text{ cm}^{-1}$) in the region 2600 Å.

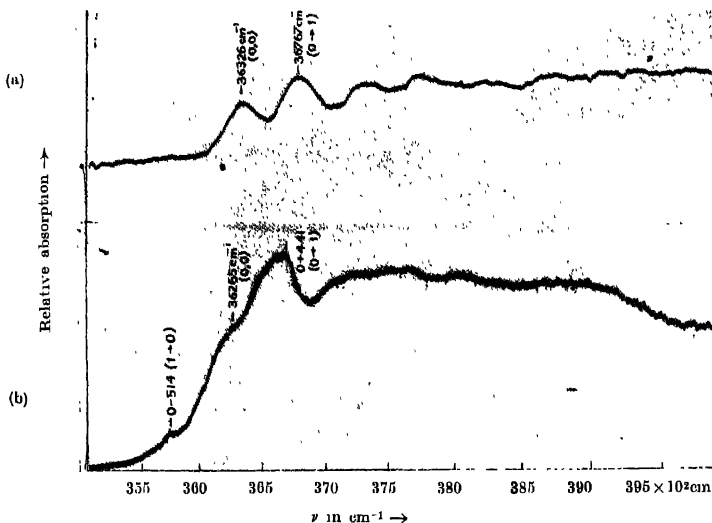


Fig. 1. Microphotometric records of the ultraviolet absorption spectra of 1, 3, 5-trimethylbenzene.

RESULTS

The microphotometric records of the spectra are reproduced in figure 1 and the wave numbers of the bands with approximate intensities and probable assignments are given in Table I.

DISCUSSION

It is seen from Table I that the first band at 36326 cm^{-1} due to the compound at -180°C is at a distance of 441 cm^{-1} from the next stronger band at 36767 cm^{-1} . In the spectrum due to the vapour state (Sponer and Stallcup, 1948) the distance between the first two bands is 959 cm^{-1} . These two bands were assigned to $1 \rightarrow 0$ and $0 \rightarrow 1$ vibrational transitions, the corresponding vibrational frequencies being 516 cm^{-1} and 443 cm^{-1} respectively. In the spectrum due to the solid state at -180°C , the first band at 36326 cm^{-1} cannot be due to $1 \rightarrow 0$ transition as there is no corresponding stronger band on the shorter wavelength side of the band at 36767 cm^{-1} . Hence the weaker band at 36326 cm^{-1} is to be assigned as the $0, 0$ band and the band at 36767 cm^{-1} would correspond to the vibrational transition $0 \rightarrow 1$, the excited state vibrational frequency being 441 cm^{-1} . The band corresponding to the vibrational transition $1 \rightarrow 0$ corresponding to the ground state vibrational frequency 516 cm^{-1} is absent as the population of molecules at this frequency cannot be high in the solid state at -180°C . Further, in

TABLE I
Absorption bands of 1, 3, 5-trimethylbenzene in the
liquid and solid states

Vapour (Sponer and Stallcup, 1948)	Solid at -180°C		Liquid at 30°C	
ν in cm^{-1} (Prominent bands)	ν in cm^{-1}	Assignment	ν in cm^{-1}	Assignment
36041 (vw) (1, 0)			35751 (vw)	0—514 (1, 0)
36557 (calculated 0, 0)	36326 (s)	0, 0	36265 (w)	0, 0
37000 (s) (0, 1)	36767 (vs)	0+441 (0, 1)	36705 (s)	0+441 (0, 1)
37968 (s)	37288 (m)	0+962	37225 (m)	0+960
38300 (ms)	37724 (m)	0+962+441	37667 (m)	0+960+440
	38244 (m)	0+962×2	38185 (w)	0+960×2
	38688 (m)	0+962×2+441	38028 (vw)	0+960×2+440
	39210 (w)	0+962×3	39142 (vw)	0+960×3
	39645 (w)	0+962×3+441		

the spectrum due to the solid state at -180°C , progressions of $0+n\times 962$ and $0+441+n\times 962$ are observed while in the vapour state there is only the progression of $0+443+n\times 968$. It is thus seen that the symmetric oscillation coupled to the 0, 0 electronic transition itself is allowed. This shows that the three-fold axis of the molecule is not present in the solid state at -180°C and the 0,0 band is therefore not forbidden in the solid state.

The 0,0 band shifts in this case by 241 cm^{-1} towards longer wavelengths from the calculated position of the 0,0 band due to the vapour state. The corresponding shifts observed in the case of benzene (Kronenberg, 1930) and 1, 3, 5-trichlorobenzene (Banerjee, 1957) are 261 cm^{-1} and 279 cm^{-1} respectively.

The spectrum due to the liquid state at room temperature exhibits system of bands, of which the first band at 35751 cm^{-1} is very weak and is at a distance of 514 cm^{-1} from the second band. The first band thus corresponds to $1\rightarrow 0$ vibrational transition and the second band 36265 cm^{-1} can be assigned to 0,0 transition. This system of bands is thus shifted towards longer wavelengths with reference to the system due to the solid state by 61 cm^{-1} .

It is concluded from the above results that even when the molecules of 1, 3, 5-trimethylbenzene are surrounded by other molecules containing only CH_3 groups, the three-fold symmetry of the six π -electrons in the ring is disturbed and this influence is intensified when the liquid is frozen and cooled to -180°C . Such an influence is expected in the case of 1, 3, 5-trichlorobenzene from the usual chemical point of view, but the results of the present investigation furnish some evidence for the existence of the influence even in the case of the trimethyl compound.

ACKNOWLEDGMENT

The author is indebted to Professor S. C. Sirkar, D.Sc., F.N.I., for his kind interest and constant guidance throughout the progress of the work.

REFERENCES

- Banerjee, S. B., 1957, *Ind. J. Phys.*, **31**, 483.
 Kronenberg, A., 1930, *Zets. f. Physik*, **63**, 494.
 Roy, S. B., 1957, *Ind. J. Phys.*, **31**, 588.
 Sponer, H. and Stalleup, Mary Jane, 1948, *Contribution a l'Etude de la Structure Molculaire* (Deosol, Liege), p. 222.
 Sen, S. K., 1955, *Ind. J. Phys.*, **29**, 561.
 „ 1956, *Ind. J. Phys.*, **30**, 56.

POLARISED ELECTRONIC SPECTRA OF SINGLE CRYSTALS OF PARA DICHLOROBENZENE

S. C. SIRKAR AND T. N. MISRA

OPTICS DEPARTMENT, INDIAN ASSOCIATION FOR THE CULTIVATION
OF SCIENCE, CALCUTTA-32

(Received November 18, 1958)

Plate I

ABSTRACT. The polarisation of the ultraviolet absorption spectra of very thin single crystals of *p*-dichlorobenzene has been studied by photographing simultaneously the two components with the light vector respectively parallel to the *b*-axis and the *c*-axis. It is observed that although the bands due to $0 \rightarrow v$ transitions are equally sharp in the vertical and horizontal components the 0,0 band is sharp only in the vertical component, but it has a triplet structure in the horizontal component. Analysis of the bands in the horizontal component shows that an intermolecular vibration of frequency about 53 cm^{-1} is coupled with the 0,0 transition only in this component and also two other new $0 \rightarrow v$ transitions not observed in the vertical component take place in this component. It is pointed out that these vibrational transitions occur when the light vector is along the short axis of the molecule and they always appear in the vapour.

The identical positions of some of the bands due to $0 \rightarrow v$ transitions in both the components indicate that there is no Davydov splitting in this case. The expected Davydov splitting due to interaction of nearest neighbours has been calculated and found to be 22 cm^{-1} . Such a splitting could be easily detected. The absence of this splitting is explained on the assumption that the usual expression for the mean square transition moment cannot be used in this case, because only a few nearest neighbouring molecules are effective in producing the splitting, and the oscillator strength being very low, the mean moment is derived from the absorption by a large number of molecules.

INTRODUCTION

It was observed by Craig and Hobbins (1955) that in the two components of the ultraviolet absorption band system of single crystal of anthracene with the light vectors respectively parallel and perpendicular to the *b*-axis the component with light vector parallel to the *b*-axis consists of two bands at 2680 \AA and 2595 \AA respectively, but in the other component the bands shift to 2300 \AA . They calculated the shift expected on the theory put forward by Davydov (1948) and found that the calculated values were in agreement with the experimental results.

The crystal of *p*-dichlorobenzene has a structure similar to that of anthracene with two molecules in the unit cell and the orientations of these molecules in the lattice have been found out accurately by Croatto *et al.* (1952). It would,

therefore, be quite easy to extend the calculations on Davydov's theory to this particular crystal. It was formerly observed by Swamy (1953) that the near ultraviolet absorption band system of polycrystalline mass of *p*-dichlorobenzene at -180°C consists of sharp bands and there is no indication of presence of a second system slightly displaced from the first system in this spectrum, as would be expected if the two components were slightly displaced from each other. On the other hand, in the case of *o*-dichlorobenzene at -180°C the band system indicated a splitting of each band into three components widely separated from each other, and later, Roy and Sirkar (1957) observed that when the molecules of *o*-dichlorobenzene are dispersed in frozen alcohol at -180°C no such splitting occurs. These results indicate that the splitting is produced by the interaction of the permanent dipoles in the crystal on the transition moments

In the case of *p*-dichlorobenzene crystals it was difficult to come to a definite conclusion regarding the absence of the splitting, because if one of the two components were very much weaker than the other it would be difficult to separate the two components from each other in the spectrum due to the polycrystalline mass. So, it was thought worthwhile to study the polarisation of the ultraviolet band system of *p*-dichlorobenzene to find out the structure and relative positions of the two systems. It was also intended to calculate the splitting expected on Davydov's theory in this case.

EXPERIMENTAL

Very thin single crystals of *p*-dichlorobenzene were prepared from saturated solutions in alcohol at room temperature. The crystal elongated along *c*-axis was mounted with its *c*-axis vertical between two fused silica discs in a brass frame, the lower portion of which was immersed in liquid oxygen contained in a Dewar vessel of fused silica. The crystal was held with its *bc*-face normal to the incident rays from a hydrogen discharge tube and the light transmitted by the crystal was focussed on the slit of a Hilger large quartz spectrograph with a fused silica lens. A double-image prism of quartz was used to separate the components having light vectors vertical and horizontal respectively.

Microphotometric records of the spectra were taken with a Kipp and Zonen type self-recording microphotometer and before taking the records of the two components, a linear mark parallel to a prominent iron line in the iron arc comparison spectrum was made by cutting across both the components of the spectrum with a sharp razor blade. The mark produced a very narrow peak in the microphotometric record and distances of the sharp bands in the records of the two components of the spectrum from this mark could be measured very accurately. The dispersion in the record was about 2\AA or 24 cm^{-1} per mm in the region of 2800\AA . A shift of the sharp bands larger than 6 cm^{-1} could be easily measured by this method.

RESULTS AND DISCUSSION

(a) Assignment of the bands.

The vertical and horizontal components of the polarised electronic absorption spectrum are reproduced in figure 1 and the microphotometric records of the bands are shown in figure 2 in Plate I. The frequencies of the bands in the vertical and horizontal components are given in Table I. Care was taken to measure the distance of the bands from the mark *F* mentioned earlier. The frequencies of the bands due to the vapour reported by earlier workers are also included in the table.

It can be seen from figure 2 that although the bands on the shorter wavelength side of the 0,0 band are equally sharp in both the vertical and horizontal components, the 0,0 band in the horizontal component is much broader than that in the vertical component. Table I shows that the bands at 36051 cm^{-1} and 36247 cm^{-1}

TABLE I
Polarised absorption bands of *p*-dichlorobenzene

Vapour (Sponer, 1942) for comparison		Light vector parallel to c-axis		Light vector parallel to b-axis	
ν in cm^{-1}	Assignment	ν in cm^{-1}	Assignment	ν in cm^{-1}	Assignment
35783 vs	0, 0(ν_0)	35672 s	0 0(ν_0)	35629 s	ν_0-53
				35672 s	0,0(ν_0)
36070 m	ν_0+357	36051 vw	ν_0+379	35725 s	ν_0+53
				36051 w	ν_0+379
36274 ms	ν_0+431	36247 m	ν_0+575	36111 m	ν_0+439
				36247 m	ν_0+575
36438 m	ν_0+695	36419 m	ν_0+747	36366 m	ν_0+694
36471 s	ν_0+728	36539 w	ν_0+867		
36544 w	ν_0+801	36736 s	ν_0+1064		
36808 vs	ν_0+1065	36930 w	ν_0+1258		
36998 m	ν_0+1255	37172 m	$\nu_0+2 \times 750$		
37069 w	$\nu_0+801+531$	37308 m	$\nu_0+1064+572$		
37136 w	$\nu_0+1065+327$	37489 m	$\nu_0+1064+753$		
37205 vw	$\nu_0+2 \times 731$	37601 w	$\nu_0+1064+865$		
37340 vw	$\nu_0+1065+531$	37804 s	$\nu_0+2 \times 1066$		
37546 m	$\nu_0+1065+728$	37994 m	$\nu_0+1064+1258$		
37856 vs	$\nu_0+2 \times 1065$	38229 m	$\nu_0+1064+2 \times 747$		
38040 w	$\nu_0+1065+695$	38547 m	$\nu_0+2 \times 1067+747$		
	+531				
38195 w	$\nu_0+2 \times 1065+327$	38853 s	$\nu_0+3 \times 1060$		
38274 ms	$\nu_0+1065+2 \times 728$				
38602 w	$\nu_0+2 \times 1065+728$				
38937 s	$\nu_0+3 \times 1065$				

are present in both the components exactly at same positions. So there is no shift of these bands in the horizontal component from the positions of the corresponding bands in the vertical component by more than 6 cm^{-1} , which is the maximum probable error in the measurement. The bands at 36111 cm^{-1} and 36366 cm^{-1} in the horizontal component are quite strong, but they are absent in the vertical component. Careful examination of the $0,0$ band in the horizontal component shows that it consists of two adjacent peaks separated by about 80 cm^{-1} , one of the bands being twice as broad as the other. If it is assumed that this structure is produced by splitting of the energy level into two components, the other bands due to $0 \rightarrow v$ transitions cannot be assigned properly. On the other hand, if it is assumed that the $0,0$ band in this case is at the same position as in the vertical component some of the excited state frequencies given by the bands at 36051 cm^{-1} and 36247 cm^{-1} are found to be exactly the same as those given by the corresponding bands in the vertical component as shown in Table I. The remaining bands in the horizontal component are found to be missing in the vertical component and these bands give some new excited state frequencies 439 cm^{-1} and 694 cm^{-1} as shown in Table I.

The structure of the $0,0$ band in the horizontal component can be explained on the assumption that when the light vector is parallel to the b -axis some inter-molecular vibration of frequency 53 cm^{-1} is coupled to the electronic transition, but when the vector is along the c -axis no such coupling takes place. Actually both $v \rightarrow 0$ and $0 \rightarrow v$ transitions produce strong bands on the two sides of the $0,0$ band. Further, the appearance of the new bands in the horizontal component can also be explained by assuming that in this case some new modes of vibration are excited, but they are not excited when the light vector is along the c -axis and makes a large angle with the short axis of the molecule.

It can be seen from Table I that the excited state vibrational frequencies deduced from the bands in the horizontal component all agree with those observed in the case of the vapour, but some of these bands are absent in the vertical component. It appears, therefore, that the vibrations of excited state frequencies 439 cm^{-1} and 694 cm^{-1} are excited only when the light vector is almost parallel to the short axis of the molecule. In the vapour the molecules have random orientation and therefore, all the modes of vibration are excited. This information given by the polarised spectra may be helpful in assigning the vibration frequencies of the molecule unequivocally.

(b) *Search for the Davydov splitting*

The splitting of the $0,0$ band expected from Davydov's theory has been calculated in this case for the molecules in the bc -plane taking into account only the interaction of nearest neighbours.

If A be the value of interaction integral for interaction between translationally equivalent molecules along a -axis, B that between similar molecules along



Fig 1. Polarised electronic spectrum of single crystals of *p*-dichlorobenzene at -180°C , with light vector (a) parallel to *c*-axis, (b) parallel to *b*-axis.

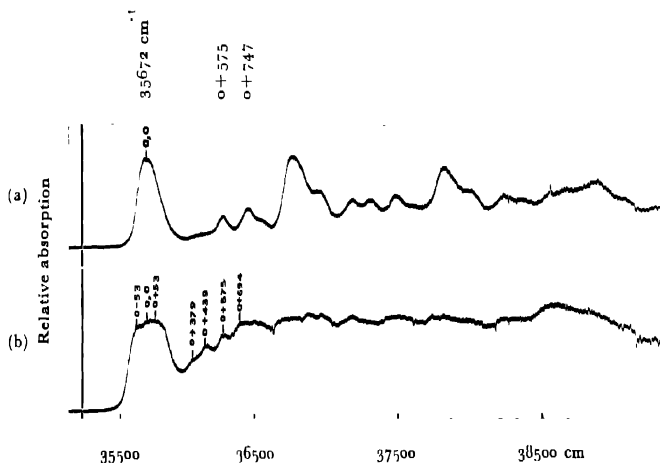


Fig 2. Microphotometric records of the polarised electronic spectrum of single crystals of *p*-dichlorobenzene at -180°C , with light vector (a) parallel to *c*-axis, (b) parallel to *b*-axis.

b -axis and C that for interaction between the two molecules in the unit cell, the splitting between the two components is given by 8C. Actually it has been shown by Davydov (1948) that if only dipole-dipole interaction is taken into account, the interaction integral I_{lk} is given by

$$I_{lk} = - \left(\frac{e^2}{r_{lk}^3} \right) |M|^2 \{ 2 \cos \theta_{l1} \cos \theta_{k1} - \cos \theta_{l2} \cos \theta_{k2} - \cos \theta_{l3} \cos \theta_{k3} \} \dots (1)$$

where θ_{l1} , θ_{l2} and θ_{l3} are angles made by the transition moment of the l -th molecule with the three rectangular axes, M is the molecular transition moment and r_{lk} the distance between the centres of the two molecules. The values of A , B and C calculated from eqn.(1) are given in Table II for the p -dichlorobenzene crystal. The unit is cm^{-1} and that for $|M|$ is \AA .

TABLE II

	Long axis- transition	Short axis- transition
$A/ M ^2$	48	25
$B/ M ^2$	613	1771
$C/ M ^2$	407	170

As the component parallel to b -axis is more strongly absorbed than the other component, and the molecule is inclined at 62°C to the b -axis the transition in this particular case is a short-axis one. Hence the splitting expected is $1360 |M|^2$. The value of $|M|^2$ can be found out from that of f , the oscillator strength from the relation

$$|M|^2 = \frac{3hf}{8\pi^2mc\nu} \dots (2)$$

where c is the velocity of light, h the Planck's constant, m , the electronic mass and ν the frequency of the band in cm^{-1} . The value of f can be obtained from the relation

$$f = 2.3 \times \frac{nc^2m}{N\pi e^2} 10^3 \int \epsilon d\nu \dots (3)$$

where n is the refractive index, N the Avogadro number and ϵ is given by the relation

$$\epsilon = \left(\frac{1}{cd} \right) \log_{10} (I_0/I)$$

c being the concentration in moles per litre.

The values of $\int \epsilon d\nu$ for solutions of p -dichlorobenzene and benzene were reported by Conrad-Billroth (1932) and subtracting the value of $\int \epsilon d\nu$ for benzene

from that for *p*-dichlorobenzene we get the oscillation strength for the migration in the ring in the *p*-dichlorobenzene molecule. The value of f is found to be 6.4×10^{-3} , and this leads to a value $16.3 \times 10^{-3} \text{ \AA}^2$ for $|M|^2$. Hence, the splitting expected in the case of *p*-dichlorobenzene is about 22 cm^{-1} . The bands in the horizontal component should shift towards red relative to those in the vertical component by about 22 cm^{-1} . As mentioned earlier, such a splitting is not actually observed in figures 1 and 2.

The discrepancy mentioned above may be due to two alternative causes. First, the value of oscillator strength calculated from the extinction coefficients reported by Conrad-Billroth (1932) may be a little too high. But if it is assumed that the value of f is not far from the true value, the alternative cause of the discrepancy may be the non-applicability of the expression for the transition moment in this particular case. It can be seen that in Davydov's theory it is assumed that all the neighbouring molecules have the transition moment produced simultaneously, the magnitude of this moment being determined by the probability of excitation and is taken as the mean transition moment. Such an assumption will lead to a correct value to extinction coefficient, because a large number of molecules is contained in a small volume. In calculating the influence of the neighbouring dipoles on the transition moment, however, we are concerned only with the molecules in a few unit cells and a correct value of the mean square transition moment in this case cannot be given by the theory. It may so happen that when a molecule is excited none of its nearest neighbours is excited simultaneously and when the oscillator strength is very low there is high probability of occurrence of such an event. This may produce a horizontal component undisplaced from its original position. When the oscillator strength is high there is high probability of simultaneous excitation of the neighbouring molecules in a few unit cells, and therefore, the theoretical values of the splitting may agree with the observed values as in the case of anthracene (Craig and Hobbins, 1955).

It is quite clear, however, that when the transition takes place in the field of permanent dipoles a large splitting occurs, as in the case of *o*-dichlorobenzene. As the crystal structure of *o*-dichlorobenzene has not been determined yet with sufficient accuracy it is not possible to calculate the splitting on Davydov's theory.

DIPOLE MOMENTS OF SOME ALIPHATIC AMINES

D. V. G. L. NRASIMHA RAO

PHYSICS DEPARTMENT, ANDRA UNIVERSITY, WALT AIR

(Received, December 12, 1958)

ABSTRACT. The dipole moments of eight higher members of the aliphatic amines have been determined in solution in benzene at 30°C and the results are discussed in the light of their molecular structure. Apart from the fact that the reported values of the dipole moments are new, the investigation was undertaken as a complementary to measurements on the same molecules in the centimetric region.

INTRODUCTION

The apparent polarisations of ammonia and its mono-, di-, tri- methyl and ethyl derivatives have been studied in the solvent benzene by Le Fevre and Russell (1947) and Barclay, Le Fevre and Smythe (1950). The latter authors have also extended the investigations (1951) to *n*-propyl and *n*-butyl amines for which the variation of moment with state is studied and also the apparent moments in solution of certain other amines. A positive solvent effect is noted by all these investigators. From a study of the moments of eighteen aliphatic and aromatic amines in seven non-polar solvents and of fifteen liquid amines in the pure state, Cowley (1952) could show that in most cases the solvent effect is small. The solvents benzene, toluene and dioxane gave small positive solvent effects confirming the previous results but with other solvents a small negative solvent effect is the more usual observation. Variation of polarisation with change of concentration from infinite dilution to the pure solute is also studied and is shown to depend on the type of amine and also on the value of its dielectric constant. The dipole moment values are corrected for the atom polarisation which is assumed as 5 per cent of the electron polarisation.

The aliphatic amines may be considered as substitution products of ammonia in which one hydrogen atom is replaced by an alkyl group. The bond angle of ammonia (109°) may be taken as evidence of the existence of hybridized orbitals. It has been found that the lone-pair contribution to the resultant moment is much higher than in the case of water. Arguments similar to those of ammonia also apply to the aliphatic amines. The low moment of tri-methylamine may be explained as due in part to the wider bond angle compared to that in ammonia, with the result that the lone-pair orbital has less *s*-character and hence makes a smaller contribution to the dipole moment.

Till now all observations are confined only up to butylamine. There are no investigations on the still higher aliphatic amines. A systematic study of eight higher members of the homologous series, starting from amylamine to decylamine, is made by the author, the measurements being carried out in solution in benzene at 30°C. Not only do the results serve as an extension of the previous work, they also provide a useful check on the values derived by the author from measurements made on the same molecules in the microwave region (to be published shortly).

EXPERIMENTAL

The experimental technique and the method of computing the moment from the observed data are described in an earlier publication of the author (1956).

RESULTS AND DISCUSSION

The detailed observations of dielectric constant and refractive index are presented in Tables I to VIII and the consolidated results are shown in Table IX. For completeness, literature values on the lower members of the series (Smith, 1955a) are also given in Table IX.

Let us assume a bond angle of 110° in methylamine, a set of reference axes with the N atom at the origin and fix the x -axis in the axis of symmetry (of the parent NH_3) and choose the xy -plane to pass through the C atom. The moment components outside the plane of symmetry cancel one another. The bond moments may be derived from the values for ammonia (1.45D) and trimethylamine (0.64 D) as

$$\begin{aligned} 3(\text{H}-\text{N}) \cos 68^\circ &= 1.45 & \text{H}-\text{N} &= 1.29 \\ 3(\text{R}-\text{N}) \cos 70^\circ &= 0.64 & \text{R}-\text{N} &= 0.62 & \text{C}-\text{N} &= 0.22 \end{aligned}$$

Using these values, we get for methylamine

$$\begin{aligned} m_x &= (\text{R}-\text{N}) \cos 70^\circ + 2(\text{H}-\text{N}) \cos 70^\circ = 1.09 \\ m_y &= -(\text{R}-\text{N}) \sin 70^\circ + 2(\text{H}-\text{N}) \sin 70^\circ \sin 30^\circ = -0.63 \\ \mu &= (m_x^2 + m_y^2)^{\frac{1}{2}} = 1.26. \end{aligned}$$

The calculated value thus agrees well with the gas value of 1.28. It may be shown that the angle between the molecular dipole axis and the C-N bond direction is $30^\circ + 70^\circ = 100^\circ$ (Smyth, 1955). The calculated value for all the other higher amines (only one H atom of NH_3 is substituted) is the same as for methylamine, except for some induced effects of the primary dipole on the hydrocarbon chains. It is known that the dipole axis in methylamines is not far from perpendicular to the direction of maximum polarisability and hence the solvent effect causes the apparent moments in solution to be higher than the

TABLE I
n-Amylamine

w	ϵ_{12}	$\Delta\epsilon$	$\Delta\epsilon/w$	n_{12}	n_{12}^2	Δn^2 (-)	$\Delta n^2/w$ (-)
0.01635	2.3065	0.0425	2.600	1.49298	2.22900	0.00558	0.341
0.04442	2.3796	0.1156	2.603	1.48976	2.21939	0.01519	0.342
0.06269	2.4283	0.1643	2.620	1.48798	2.21409	0.02049	0.327
0.08900	2.4951	0.2311	2.596	1.48553	2.20681	0.02777	0.312
0.10210	2.5283	0.2643	2.589	1.48305	2.19945	0.03513	0.344
0.11950	2.5738	0.3098	2.593	1.48120	2.19395	0.04003	0.340
0.13090	2.5987	0.3347	2.557	1.47980	2.18981	0.04477	0.342

$$A = (\Delta\epsilon/w)_w \rightarrow 0 = 2.605 \quad P_0 = 48.61 \text{ c.c.}$$

$$B = (\Delta n^2/w)_w \rightarrow 0 = -0.339 \quad \mu = 1.55 D.$$

TABLE II
n-Hexylamine

w	ϵ_{12}	$\Delta\epsilon$	$\Delta\epsilon/w$	n_{12}	n_{12}^2	Δn^2 (-)	$\Delta n^2/w$ (-)
0.01931	2.3083	0.0443	2.292	1.49436	2.22798	0.00660	0.342
0.03386	2.3389	0.0749	2.211	1.49102	2.22312	0.01145	0.338
0.04774	2.3667	0.1027	2.150	1.48964	2.21902	0.01556	0.326
0.07396	2.4180	0.1640	2.082	1.48686	2.21076	0.02382	0.322
0.08950	2.4458	0.1818	2.031	1.48500	2.20522	0.02936	0.328
0.10280	2.4654	0.2014	1.959	1.48339	2.20045	0.03413	0.332

$$A = 2.320 \quad B = -0.331 \quad P_0 = 50.81 \text{ c.c.} \quad \mu = 1.59 D$$

TABLE III
n-Heptylamine

w	ϵ_{12}	$\Delta\epsilon$	$\Delta\epsilon/w$	n_{12}	n_{12}^2	Δn^2 (-)	$\Delta n^2/w$ (-)
0.01372	2.2916	0.0276	2.011	1.49325	2.22981	0.00477	0.348
0.02904	2.3231	0.0591	2.036	1.49158	2.22482	0.00976	0.336
0.04256	2.3483	0.0843	1.982	1.49003	2.22020	0.01438	0.338
0.06176	2.3837	0.1197	1.937	1.48810	2.21444	0.02014	0.326
0.07504	2.4069	0.1429	1.904	1.48678	2.21050	0.02408	0.321
0.09217	2.4374	0.1734	1.881	1.48467	2.20425	0.03033	0.325
0.10490	2.4510	0.1870	1.782	1.48340	2.20048	0.03410	0.325

$$A = 2.040 \quad B = -0.332 \quad P_0 = 51.76 \text{ c.c.} \quad \mu = 1.60 D.$$

TABLE IV
n-Octylamine

w	ϵ_{12}	$\Delta\epsilon$	$\Delta\epsilon/w$	n_{12}	n_{12}^2	Δn^2 (-)	$\Delta n^2/w$ (-)
0.00673	2.2732	0.0092	1.374	1.49423	2.23272	0.00186	0.276
0.01253	2.2809	0.0169	1.351	1.49364	2.23097	0.00361	0.288
0.02077	2.2920	0.0280	1.345	1.49292	2.22880	0.00578	0.278
0.03260	2.3070	0.0430	1.320	1.49182	2.22552	0.00906	0.278
0.05841	2.3386	0.0746	1.277	1.48791	2.21899	0.01559	0.267
0.09126	2.3768	0.1128	1.236	1.48702	2.21123	0.02335	0.256
0.11300	2.3926	0.1286	1.139	1.48525	2.20597	0.02861	0.253
$A = 1.380$		$B = -0.271$	$P_0 = 40.45$ c.c.		$\mu = 1.42 D$		

TABLE V
n-Decylamine

w	ϵ_{12}	$\Delta\epsilon$	$\Delta\epsilon/w$	n_{12}	n_{12}^2	Δn^2 (-)	$\Delta n^2/w$ (-)
0.00615	2.2706	0.0066	1.078	1.49433	2.23301	0.00157	0.256
0.01369	2.2785	0.0145	1.057	1.49377	2.23135	0.00323	0.236
0.02216	2.2877	0.0237	1.070	1.49313	2.22944	0.00514	0.232
0.02956	2.2940	0.0300	1.014	1.49257	2.22777	0.00681	0.230
0.03749	2.3014	0.0374	0.997	1.49171	2.22520	0.00938	0.250
0.04500	2.3082	0.0442	0.983	1.49111	2.22342	0.01116	0.248
0.06039	2.3219	0.0579	0.059	1.48971	2.21925	0.01533	0.254
$A = 1.090$		$B = -0.244$	$P_0 = 39.77$ c.c.		$\mu = 1.41 D$		

TABLE VI
Isoamylamine

w	ϵ_{12}	$\Delta\epsilon$	$\Delta\epsilon/w$	n_{12}	n_{12}^2	Δn^2 (-)	$\Delta n^2/w$ (-)
0.01242	2.2950	0.0310	2.494	1.49348	2.23048	0.00410	0.330
0.02973	2.3394	0.0754	2.536	1.49167	2.22507	0.00951	0.320
0.04033	2.3672	0.1032	2.560	1.49041	2.22132	0.01326	0.329
0.05860	2.4141	0.1501	2.562]	1.48829	2.21601	0.01957	0.334
0.06960	2.4404	0.1764	2.535	1.48720	2.21175	0.02283	0.328
0.09185	2.4913	0.2273	2.475	1.48465	2.20418	0.03040	0.331
0.10550	2.5200	0.2560	2.426	1.48295	2.19913	0.03545	0.336
$A = 2.540$		$B = -0.330$	$P_0 = 47.40$ c.c.		$\mu = 1.53 D$		

TABLE VII
Isohexylamine

w	ϵ_{12}	$\Delta\epsilon$	$\Delta\epsilon/w$	n_{12}	n_{12}^2	Δn^2 (—)	$\Delta n^2/w$ (—)
0.01114	2.2929	0.0289	2.592	1.49371	2.23117	0.00341	0.306
0.02310	2.3235	0.0595	2.575	1.49255	2.22770	0.00688	0.298
0.03402	2.3536	0.0896	2.632	1.49152	2.22464	0.00994	0.292
0.04381	2.3845	0.1205	2.761	1.49057	2.22179	0.01279	0.292
0.05331	2.4137	0.1497	2.809	1.48973	2.21928	0.01530	0.287
0.06032	2.4379	0.1739	2.883	1.48907	2.21733	0.01725	0.286
$A = 2.390$		$B = -0.294$	$P_0 = 51.44$ c.c.	$\mu = 1.60 D.$			

TABLE VIII
Tertioctylamine

w	ϵ_{12}	$\Delta\epsilon$	$\Delta\epsilon/w$	n_{12}	n_{12}^2	Δn^2 (—)	$\Delta n^2/w$ (—)
0.01243	2.2750	0.0119	0.955	1.49373	2.23122	0.00336	0.270
0.01972	2.2825	0.0185	0.938	1.49303	2.22913	0.00545	0.276
0.04153	2.3050	0.0410	0.988	1.49152	2.22463	0.00995	0.240
0.05181	2.3123	0.0483	0.931	1.49018	2.22064	0.01394	0.269
0.06963	2.3306	0.0666	0.956	1.48845	2.21547	0.01911	0.275
0.07893	2.3390	0.0750	0.950	1.48786	2.21373	0.02085	0.264
0.09919	2.3589	0.0949	0.957	1.48581	2.20763	0.02695	0.272
0.11660	2.3748	0.1108	0.950	1.48458	2.20397	0.03061	0.262
$A = 0.950$		$B = -0.206$	$P_0 = 29.79$ c.c.	$\mu = 1.22 D.$			

TABLE IX

Compound	Formula	Author	Literature values	
		μ_B	μ_B	μ_V
Ammonia	NH ₃	—	1.40*	1.45D
Methylamine	CH ₃ NH ₂	—	1.46	1.28
Ethylamine	CH ₃ CH ₂ NH ₂	—	1.37	0.99
n-Propylamine	CH ₃ (CH ₂) ₂ NH ₂	—	1.32	1.17*
n-Butylamine	CH ₃ (CH ₂) ₃ NH ₂	—	1.32	1.00*
sec-Butylamine	CH ₃ CH(NH ₂)CH ₂ CH ₃	—	1.28	—
tert-Butylamine	(CH ₃) ₃ CNH ₂	—	1.29	—

n-Amylamine	CH ₃ (CH ₂) ₄ NH ₂	1.55	—	—
n-Hexylamine	CH ₃ (CH ₂) ₅ NH ₂	1.59	—	—
n-Heptylamine	CH ₃ (CH ₂) ₆ NH ₂	1.60	—	—
n-Octylamine	CH ₃ (CH ₂) ₇ NH ₂	1.42	—	—
n-Decylamine	CH ₃ (CH ₂) ₉ NH ₂	1.41	—	—
Isoamylamine	(CH ₃) ₂ CH(CH ₂) ₃ NH ₂	1.53	—	—
Isohexylamine	(CH ₃) ₂ CH(CH ₂) ₄ NH ₂	1.60	—	—
Tertioctylamine	(CH ₃) ₃ CNH ₂ (CH ₂) ₄	1.22	—	—

*value of Le Fèvre and Russell (1947)

**values of Barolay, Le Fèvre and Smythe (1951)

 μ_B values in solution in benzene μ_V values in the vapour state.

gas values (i.e., a positive solvent effect). It is seen that for all the amines listed in Table IX for which the vapour values are available $\mu_B > \mu_V$. Cowley (1952) also observed a positive solvent effect for *n*-propyl and *n*-butyl amines in all the solvents he used. This may perhaps explain the values obtained in this investigation. But, when compared to the literature values on the lower members, the author's values appear to be slightly high for some of the molecules. The following points may be noted.

(1) As we go higher up in the homologous series, there is a tendency for a decrease in the moment. This is in conformity with the conclusions of Smith (1955b). As is already shown the resultant moment of the primary dipole is inclined at an angle of 100° with the C-N bond. Consequently there is rather a greater change of the induced moments opposing the primary moment than assisting it.

(2) The moments of the normal and iso- compounds are almost the same.

(3) The moment of the tertiary amines is a little less than that of the normal compound. A difference of 0.20 is obtained between *n*-octylamine and tert-octylamine. The corresponding difference is 0.11 for the butylamines (cf. Table IX).

(4) A small positive solvent effect in benzene appears reasonable. It is probable that a considerable change in the angle from 90° between the molecular dipole axis and the axis of maximum polarisability lowers the solvent effect so that the difference between vapour and solution values becomes much less.

ACKNOWLEDGMENTS

The author is deeply indebted to Prof. K. R. Rao for his kind and invaluable guidance throughout the progress of work. He is also grateful to the Council of Scientific and Industrial Research for financial assistance.

REFERENCES

- Barclay, Le Fevre and Smythe, 1950, *Trans. Farad. Soc.* **46**, 812.
Barclay, Le Fevre and Smythe, 1951, *Trans. Farad. Soc.*, **47**, 357.
Cowley, 1952, *J. Chem. Soc.*, 3557.
Le Fevre and Russell, 1947, *Trans. Farad. Soc.*, **43**, 374.
Narasimha Rao, 1956, *Ind. J. Phys.* **30**, 91.
Smith, 1955a, Electric Dipole Moments, Butterworths scientific publications, London, pp. 194.
Smith, 1955b, *ibid.*, pp. 195.
Smyth, 1955, Dielectric Behaviour and Structure, McGraw Hill Book Co. Inc. N.Y. pp. 311.

STUDY OF AN OSCILLATOR WITH TWO DEGREES OF FREEDOM BY A DIFFERENTIAL ANALYSER

B. R. NAG

INSTITUTE OF RADIO PHYSICS AND ELECTRONICS, UNIVERSITY OF CALCUTTA

(Received, June 17, 1958)

ABSTRACT. Equations giving the stable amplitudes of oscillation and the conditions of stability of all the possible modes of oscillation of an oscillator with two degrees of freedom and stabilised by a non-linearity which can be described by a third degree polynomial are given. The use of a differential analyser for the verification of these equations is illustrated. Also a method of graphically representing the transient oscillations on the analyser is described.

INTRODUCTION

Oscillators described by two simultaneous differential equations of the second order have two possible frequencies of oscillation. If the non-linearity of the circuit is neglected, it follows that oscillations will occur independently at both the frequencies, the amplitude at any one frequency being determined only by losses at that frequency. However, the non-linearity which is essential for limiting the amplitudes of oscillation introduces interdependence. Due to this interdependence there are two distinct modes of oscillations. In the one, the oscillator may oscillate at any one of the two frequencies and the amplitude of oscillation is then determined by the losses at the oscillation frequency; in the other it may oscillate at both the frequencies simultaneously and the amplitudes in that case are determined by the losses at both the frequencies. The detailed characteristics of such an oscillator may be obtained by solving the differential equations taking into account the contributions due to non-linearity. In the present paper, the solutions as obtained by the variation of parameter method are presented (Van der Pol, 1922; Fontana 1951; Schaffner, 1954).

Experimental verification of the theoretical results were obtained earlier by actual oscillator circuits, the non-linear terms being realised by vacuum tubes (Fontana, 1951). A closer and more detailed representation of the non-linear terms is possible with a differential analyser. The author has made use of a differential analyser with a view to verify the theoretical derivations for non-linearities expressible by a polynomial of the third degree. The results obtained are presented in this paper.

In visualising the growth of a particular mode of oscillation from the initial conditions, plots of the transient oscillations are very helpful. Theoretically, the transient plots are obtained by the method of isoclines and involve considerable labour (Schaffner, 1954). A simple method of obtaining graphical repre-

sensation of the transient oscillations by depicting experimentally the trajectories in the A_1-A_2 plane on the analyser is also described.

TYPICAL OSCILLATORS DESCRIBED BY TWO SIMULTANEOUS SECOND ORDER DIFFERENTIAL EQUATIONS

In general, oscillators consisting of two separately tuned circuits coupled together are described by two simultaneous differential equations of the second order. The tuned grid tuned plate oscillator is an example. The equivalent circuit of a $TG-TP$ oscillator is shown in figure 1.

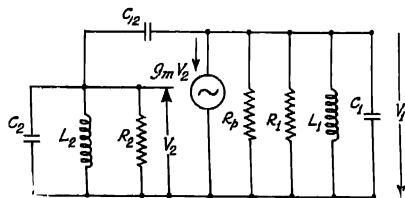


Fig. 1. Equivalent circuit of a tuned grid tuned plate oscillator.

The differential equations describing the oscillator are given by

$$\frac{d^2 V_1}{dt^2} + \frac{1}{C_1 + C_{12}} \frac{d}{dt} \left(\frac{1}{R_1} + \frac{1}{R_p} \right) V_1 + \frac{V_1}{L_1(C_1 + C_{12})} + \frac{C_{12}}{(C_1 + C_{12})} \frac{d^2 V_2}{dt^2} = \frac{1}{(C_1 + C_{12})} \frac{d(g_m V_2)}{dt}, \quad \dots \quad (1a)$$

$$\frac{d^2 V_2}{dt^2} + \frac{1}{(C_2 + C_{12})} \frac{1}{R_2} \frac{dV_2}{dt} + \frac{V_2}{L_2(C_2 + C_{12})} + \frac{C_{12}}{C_2 + C_{12}} \frac{d^2 V_1}{dt^2} = 0. \quad \dots \quad (1b)$$

If R_p is very large compared to R_1 , the non-linearity is introduced by g_m only. g_m can be generally expressed as a function of V_2 in the form of a polynomial

Common single tuned circuit oscillators when supplying the output to a tuned load directly coupled to it are also described by two simultaneous differential

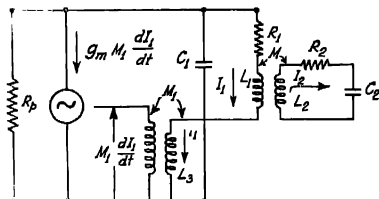


Fig. 2. Equivalent circuit of a tuned plate oscillator coupled to a tuned circuit.

equations of the second order. Such coupling is usual in the R.F. extra high tension supplies. The equivalent circuit for a tuned plate oscillator coupled to a tuned load by mutual inductance is shown in figure 2.

The differential equations for this circuit are

$$\frac{d^2 I_1}{dt^2} + \left[\frac{R_1}{(L_3 + L_1)} + \frac{1}{C_1 R_p} + g_m \frac{M_1}{(L_3 + L_1) C_1} \right] \frac{dI_1}{dt} - \frac{M}{(L_3 + L_1) C_1 R_p} \frac{dI_2}{dt} + \frac{I_1}{(L_3 + L_1) C_1} \left(1 + \frac{R_1}{R_p} \right) - \frac{M}{(L_3 + L_1)} \frac{d^2 I_2}{dt^2} = 0. \quad \dots (2a)$$

$$\frac{d^2 I_2}{dt^2} + \frac{R_2}{L_2} \frac{dI_2}{dt} + \frac{1}{L_2 C_2} I_2 - \frac{M}{L_2} \frac{d^2 I_1}{dt^2} = 0. \quad \dots (2b)$$

SOLUTION BY THE VARIATION OF PARAMETER METHOD

The above differential equation may, in general, be written in the form

$$\frac{d^2 x_1}{dt^2} + \omega_1^2 x_1 + K_2 \frac{d^2 x_2}{dt^2} = F_1 \left(x_1, \frac{dx_1}{dt}, x_2, \frac{dx_2}{dt} \right), \quad \dots (3a)$$

$$\frac{d^2 x_2}{dt^2} + \omega_2^2 x_2 + K_1 \frac{d^2 x_1}{dt^2} = F_2 \left(x_2, \frac{dx_2}{dt}, x_1, \frac{dx_1}{dt} \right), \quad \dots (3b)$$

In what follows it is assumed that

$$F_2 \left(x_1, \frac{dx_1}{dt}, x_2, \frac{dx_2}{dt} \right) = -a_2 \frac{dx_2}{dt}, \quad \dots (4a)$$

and $F_1 \left(x_1, \frac{dx_1}{dt}, x_2, \frac{dx_2}{dt} \right) = a_1 \frac{dx_1}{dt} - a_1 f(x_1) \frac{dx_1}{dt} \quad \dots (4b)$

Eliminating x_2 and neglecting terms involving the product $a_1 a_2$, which is assumed to be small, one gets

$$\begin{aligned} & \frac{d^4 x_1}{dt^4} + (\omega_1^2 + \omega_2^2) \frac{d^2 x_1}{dt^2} + \omega_1^2 \omega_2^2 x_1 - K_1 K_2 \frac{d^4 x_1}{dt^4} \\ &= -a_2 \left[\frac{d^3 x_1}{dt^3} + \omega_1^2 \frac{dx_1}{dt} \right] + a_1 \left[\frac{d^3 x_1}{dt^3} + \omega_2^2 \frac{dx_1}{dt} \right] \\ & \quad - a_1 \left[\frac{d^2}{dt^2} f(x_1) \frac{dx_1}{dt} + \omega_2^2 f(x_1) \frac{dx_1}{dt} \right]. \quad \dots (5) \end{aligned}$$

When $a_1 = a_2 = 0$, solution of Eqn. 4 is given by

$$x_1 = A_1 \cos(\omega_{10}t + \phi_1) + A_2 \cos(\omega_{20}t + \phi_2), \quad \dots (6)$$

where

$$\omega_{10}^2 = \frac{\omega_1^2 + \omega_2^2 - [(\omega_1^2 - \omega_2^2)^2 + 4K_1K_2\omega_1^2\omega_2^2]^{\frac{1}{2}}}{2(1 - K_1K_2)} \quad \dots (7a)$$

$$\omega_{20}^2 = \frac{\omega_1^2 + \omega_2^2 + [(\omega_1^2 - \omega_2^2)^2 + 4K_1K_2\omega_1^2\omega_2^2]^{\frac{1}{2}}}{2(1 - K_1K_2)} \quad \dots (7b)$$

A_1, A_2, ϕ_1 and ϕ_2 are constants determined by the initial values of x_1 and its derivatives.

When a_1 and a_2 are finite A_1, A_2, ϕ_1 and ϕ_2 are not constant but are functions of time. In that case we may rewrite Eqn. (6) as

$$x_1 = A_1(t) \cos[\omega_{10}t + \phi_1(t)] + A_2(t) \cos[\omega_{20}t + \phi_2(t)], \quad \dots (7)$$

and substitute this value in Eqn. (5). Since a_1 and a_2 are small, though finite, an approximate solution may be obtained retaining the first order derivatives only. Thus

$$\frac{dA_1}{dt} = - \frac{F \sin(\omega_{10}t + \phi_1)}{\omega_{10}(\omega_{20}^2 - \omega_{10}^2)}, \quad \dots (8a)$$

$$\frac{dA_2}{dt} = \frac{F \sin(\omega_{20}t + \phi_2)}{\omega_{20}(\omega_{20}^2 - \omega_{10}^2)}, \quad \dots (8b)$$

$$\frac{d\phi_1}{dt} = - \frac{1}{A_1} \frac{F \cos(\omega_{10}t + \phi_1)}{\omega_{10}(\omega_{20}^2 - \omega_{10}^2)}, \quad \dots (8c)$$

$$\frac{d\phi_2}{dt} = \frac{1}{A_2} \frac{F \cos(\omega_{20}t + \phi_2)}{\omega_{20}(\omega_{20}^2 - \omega_{10}^2)}, \quad \dots (8d)$$

where

$$\begin{aligned} (1 - K_1K_2) F = & -a_2 \left[\frac{d^3x_1}{dt^3} + \omega_1^2 \frac{dx_1}{dt} \right] + a_1 \left[\frac{d^3x_1}{dt^3} + \omega_2^2 \frac{dx_1}{dt} \right] - \\ & - a_1 \left[\frac{d^2}{dt^2} f(x_1) \frac{dx_1}{dt} + \omega_2^2 f(x_1) \frac{dx_1}{dt} \right]. \quad \dots (9) \end{aligned}$$

Since a_1 and a_2 are assumed to be small, $\dot{A}_1, \dot{A}_2, \dot{\phi}_1, \dot{\phi}_2$, which vary little over a period of oscillation can be approximately taken to be equal to their average values over the period.

Now, if $f(x_1)$ is given by a polynomial, F can be expanded into a Fourier series of the two fundamental periods $\frac{2\pi}{\omega_{10}}$ and $\frac{2\pi}{\omega_{20}}$. Let a_{10} , a_{20} , b_{10} , b_{20} , be the coefficients of $\sin(\omega_{10}t + \phi_1)$, $\sin(\omega_{20}t + \phi_2)$, $\cos(\omega_{10}t + \phi_1)$, $\cos(\omega_{20}t + \phi_2)$ respectively in the expansion, then

$$\frac{dA_1}{dt} = -\frac{1}{2} \frac{a_{10}}{\omega_{10}(\omega_{20}^2 - \omega_{10}^2)}, \quad \dots \quad (10a)$$

$$\frac{dA_2}{dt} = \frac{1}{2} \frac{a_{20}}{\omega_{20}(\omega_{20}^2 - \omega_{10}^2)}, \quad \dots \quad (10b)$$

$$\frac{d\phi_1}{dt} = -\frac{1}{2} \frac{b_{10}}{A_1 \omega_{10}(\omega_{20}^2 - \omega_{10}^2)}, \quad \dots \quad (10c)$$

$$\frac{d\phi_2}{dt} = \frac{1}{2} \frac{b_{20}}{A_2 \omega_{20}(\omega_{20}^2 - \omega_{10}^2)}. \quad \dots \quad (10d)$$

If ω_{10} and ω_{20} are not integrally related, the only conditions for equilibrium are $\dot{A}_1 = 0$, $\dot{A}_2 = 0$, and the equilibrium values of A_1 and A_2 may be obtained therefrom. Also, the equilibrium is stable if the roots of the equation

$$\begin{vmatrix} p - \frac{\partial \dot{A}_1}{\partial A_1} & -\frac{\partial \dot{A}_1}{\partial A_2} \\ -\frac{\partial \dot{A}_2}{\partial A_1} & p - \frac{\partial \dot{A}_2}{\partial A_2} \end{vmatrix} = 0 \quad \dots \quad (11)$$

have their real parts negative for the equilibrium values of A_1 and A_2 .

If ω_{10} and ω_{20} are integrally related, i.e., $\frac{\omega_{20}}{\omega_{10}} = \frac{p}{q}$, $\frac{p}{q}$ being an integral ratio, then for equilibrium in addition to the conditions $\dot{A}_1 = 0$, $\dot{A}_2 = 0$, it is required that

$$\dot{\phi} = p\dot{\phi}_1 - q\dot{\phi}_2 = 0. \quad \dots \quad (12)$$

In this case stable equilibrium will require the roots of the equation

$$\begin{vmatrix} p - \frac{\partial \dot{A}_1}{\partial A_1} & -\frac{\partial \dot{A}_1}{\partial A_2} & -\frac{\partial \dot{A}_1}{\partial \phi} \\ -\frac{\partial \dot{A}_2}{\partial A_1} & p - \frac{\partial \dot{A}_2}{\partial A_2} & -\frac{\partial \dot{A}_2}{\partial \phi} \\ -\frac{\partial \dot{\phi}}{\partial A_1} & -\frac{\partial \dot{\phi}}{\partial A_2} & p - \frac{\partial \dot{\phi}}{\partial \phi} \end{vmatrix} = 0 \quad \dots \quad (13)$$

to have negative real parts. The derivatives are to be evaluated at the equilibrium values of A_1 , A_2 and ϕ .

It may be noted that small deviations in the ratio of $\frac{\omega_{20}}{\omega_{10}}$ from the integral value may be compensated by ϕ . In that case for equilibrium condition (12) will be replaced by

$$\Delta\omega + \dot{\phi} = 0,$$

$$\text{where} \quad \Delta\omega = p\omega_{10} - q\omega_{20}. \quad \dots (14)$$

An oscillator, stabilised by a non-linearity characterised by $a_1 f(x_1) = cx_1^2 bx_1$, will now be considered in the light of the above general analysis. For such an oscillator three distinct cases are to be considered; these are discussed below :

Case I : ω_{20}/ω_{10} has a value other than 2/1 or 3/1. In this case,

$$\begin{aligned} (1-K_1K_2)a_{10} &= a_2A_1(\omega_1^2-\omega_{10}^2)\omega_{10}-a_1A_1(\omega_2^2-\omega_{10}^2)\omega_{10} \\ &\quad + \frac{c}{4} A_1(\omega_2^2-\omega_{10}^2)\omega_{10}(A_1^2+2A_2^2), \quad \dots (15a) \end{aligned}$$

$$\begin{aligned} (1-K_1K_2)a_{20} &= -a_2A_2(\omega_{20}^2-\omega_1^2)\omega_{20}+a_1A_2(\omega_{20}^2-\omega_2^2) \\ &\quad - \frac{c}{4} A_2(\omega_{20}^2-\omega_2^2)\omega_{20}(A_2^2+2A_1^2), \quad \dots (15b) \end{aligned}$$

$$b_{10} = b_{20} = 0 \quad \dots (15c)$$

Putting

$$\frac{\omega_1^2-\omega_{10}^2}{\omega_2^2-\omega_{10}^2} = \rho, \quad \frac{\omega_{20}^2-\omega_1^2}{\omega_{20}^2-\omega_2^2} = \sigma,$$

$$\frac{4}{c} (\rho a_2 - a_1) = -A_{10}^2,$$

$$\text{and} \quad \frac{4}{c} (\sigma a_2 - a_1) = -A_{20}^2,$$

Eqn. (15a) and (15b) may be written as

$$(1-K_1K_2)a_{10} = \frac{c}{4} (\omega_2^2-\omega_{10}^2)[-A_{10}^2+A_1^2+2A_2^2]A_1, \quad \dots (16a)$$

$$(1-K_1K_2)a_{20} = -\frac{c}{4} (\omega_{20}^2-\omega_2^2)[-A_{20}^2+A_2^2+2A_1^2]A_2 \quad \dots (16b)$$

Hence from Eqns. (10a) and (10b)

$$2(1-K_1K_2)\dot{A}_1 = -\frac{c}{4} \frac{(\omega_2^2 - \omega_{10}^2)}{(\omega_{20}^2 - \omega_{10}^2)} [-A_{10}^2 + A_1^2 + 2A_2^2]A_1, \quad \dots \quad (17a)$$

$$2(1-K_1K_2)\dot{A}_2 = -\frac{c}{4} \frac{(\omega_{20}^2 - \omega_2^2)}{(\omega_{20}^2 - \omega_{10}^2)} [-A_{20}^2 + A_2^2 + 2A_1^2]A_2 \quad \dots \quad (17b)$$

Conditions of equilibrium are given by

$$A_1(-A_{10}^2 + A_1^2 + 2A_2^2) = 0,$$

$$A_2(-A_{20}^2 + A_2^2 + 2A_1^2) = 0.$$

These conditions are satisfied by either of the following three possible combinations of A_1 and A_2 .

$$(1) \quad A_2 = 0, \quad A_1 = A_{10}. \quad \dots \quad (18a)$$

$$(2) \quad A_1 = 0, \quad A_2 = A_{20}. \quad \dots \quad (18b)$$

$$(3) \quad A_1^2 = \frac{2A_{20}^2 - A_{10}^2}{3}, \quad A_2^2 = \frac{2A_{10}^2 - A_{20}^2}{3}. \quad \dots \quad (18c)$$

The equilibrium corresponding to the combination $A_2 = 0$, $A_1 = A_{10}$ is stable if $\frac{A_{10}^2}{A_{20}^2} > \frac{1}{2}$ and that corresponding to the combination $A_1 = 0$, $A_2 = A_{20}$ is stable if $\frac{A_{10}^2}{A_{20}^2} < 2$. The third combination gives unstable equilibrium (Van Der Pol 1922).

Thus, the oscillator will oscillate at one frequency at a time. Further, if $\frac{1}{2} < \frac{A_{10}^2}{A_{20}^2} < 2$ the oscillator may choose any of the two frequencies, the choice being determined by the initial values of A_1 , A_2 and their derivatives.

$$\text{Case II :} \quad \omega_{20} : \omega_{10} = 3 : 1.$$

Here,

$$(1-K_1K_2)a_{10} = -[A_{10}^2 - (A_1^2 + 2A_2^2) - A_1A_2 \cos \phi] \frac{c}{4} \omega_{10}A_1(\omega_2^2 - \omega_{10}^2), \quad \dots \quad (19a)$$

$$(1-K_1K_2)a_{20} = \left[A_{20}^2 - (A_2^2 + 2A_1^2) - \frac{A_1^3}{3A_2} \cos \phi \right] \frac{c}{4} \omega_{20}A_2(\omega_{20}^2 - \omega_2^2), \quad \dots \quad (19b)$$

$$(1-K_1K_2)b_{10} = -\frac{c}{4} \omega_{10}(\omega_2^2 - \omega_{10}^2)A_1^2A_2 \sin \phi. \quad \dots \quad (19c)$$

$$(1-K_1K_2)b_{20} = -\frac{c}{4} \omega_{20}(\omega_{20}^2 - \omega_2^2) \frac{A_1^3}{3} \sin \phi. \quad \dots \quad (19d)$$

Thus, from Eqns. (10a), (10b), (10c) and (10d) and remembering Eqn. (12),

$$2(1-K_1K_2)\dot{A}_1 = \frac{c}{4} \frac{(\omega_{20}^2 - \omega_{10}^2)}{(\omega_{20}^2 - \omega_{10}^2)} \left[A_{10}^2 - (2A_2^2 + A_1^2) - A_1A_2 \cos \phi \right] A_1, \dots \quad (20a)$$

$$2(1-K_1K_2)\dot{A}_2 = \frac{c}{4} \frac{(\omega_{20}^2 - \omega_{10}^2)}{(\omega_{20}^2 - \omega_{10}^2)} \left[A_{20}^2 - (2A_1^2 + A_2^2) - \frac{A_1^3}{3A_2} \cos \phi \right] A_2 \dots \quad (20b)$$

$$2(1-K_1K_2)\dot{\phi} = \frac{c}{4} \left[\frac{3(\omega_{20}^2 - \omega_{10}^2)}{(\omega_{20}^2 - \omega_{10}^2)} A_2^2 + \frac{(\omega_{20}^2 - \omega_{10}^2)}{(\omega_{20}^2 - \omega_{10}^2)} \frac{A_1^2}{3} \right] \frac{A_1}{A_2} \sin \phi. \dots \quad (20c)$$

Equilibrium conditions are obtained for either of the two possible combinations:

$$(1) \quad A_1 = 0, \quad A_2 = A_{20}. \quad \dots \quad (21a)$$

$$(2) \quad A_{10}^2 = 2A_2^2 + A_1^2 + A_1A_2 \cos \phi \quad (\sin \phi = 0), \quad \dots \quad (21b)$$

$$A_{20}^2 = 2A_1^2 + A_2^2 + \frac{A_1^3}{3A_2} \cos \phi \quad (\sin \phi = 0). \quad \dots \quad (21c)$$

Of these the equilibrium given by the first combination will be stable if $\frac{A_{10}^2}{A_{20}^2} < 2$. The equilibrium corresponding to the second combination will be stable if $\cos \phi = -1$, i.e. $\phi = \pi$ and if A_1 and A_2 , given by equations (21b) and (21c) satisfy the condition

$$(2A_1^2 - A_1A_2) \left(2A_2^2 + \frac{A_1^3}{3A_2} \right) - (4A_1A_2 - A_1^2)^2 < 0.$$

Writing $A_2 = nA_1$, n being a positive real number, the above inequality reduces to

$$n^3 + 6n^2 + \frac{2}{3} - 4n - \frac{1}{3n} > 0,$$

$$\text{Whence,} \quad n < 0.54 \quad \dots \quad (22)$$

i.e. the combination 2 is stable if the ratio between the equilibrium values of A_2 and A_1 is less than 0.54.

Further from Eqns. (21b) and (21c), it is observed that n is related to $\frac{A_{10}^2}{A_{20}^2}$ by the relation

$$\frac{A_{10}^2}{A_{20}^2} = \frac{2n^2 + 1 - n}{2 + n^2 - \frac{1}{3n}} \quad \dots \quad (23)$$

When ω_{20} departs from $3\omega_{10}$ by a small amount $\Delta\omega$, i.e., $\omega_{20} = 3\omega_{10} \pm \frac{\Delta\omega}{2(1-K_1K_2)}$, equilibrium conditions are given by

$$\Delta\omega = -\frac{c}{4} \left[\frac{3(\omega_2^2 - \omega_{10}^2)}{(\omega_{20}^2 - \omega_{10}^2)} A_2^2 + \frac{(\omega_{20}^2 - \omega_2^2)}{(\omega_{20}^2 - \omega_{10}^2)} \frac{A_1^2}{3} \right] \frac{A_1}{A_2} \sin \phi. \quad \dots (24a)$$

$$A_{10}^2 = 2A_2^2 + A_1^2 + A_1A_2 \cos \phi, \quad \dots (24b)$$

$$A_{20}^2 = 2A_1^2 + A_2^2 + \frac{A_1^3}{3A_2} \cos \phi. \quad \dots (24c)$$

Case III : $\omega_{20} : \omega_{10} = 2 : 1$.

In this case, it may be seen that

$$2(1-K_1K_2)A_1 = \frac{c}{4} \frac{(\omega_2^2 - \omega_{10}^2)}{(\omega_{20}^2 - \omega_{10}^2)} \left[A_{10}^2 - (A_1^2 + 2A_2^2) - \frac{2b}{c} A_2 \cos \phi \right] A_1, \dots (25a)$$

$$2(1-K_1K_2)A_2 = \frac{c}{4} \frac{(\omega_{20}^2 - \omega_2^2)}{(\omega_{20}^2 - \omega_{10}^2)} \left[A_{20}^2 - (A_2^2 + 2A_1^2) - \frac{2b}{c} \frac{A_1^2}{2A_2} \cos \phi \right] A_2, \dots (25b)$$

$$2(1-K_1K_2)\dot{\phi} = \frac{b}{2} \left[\frac{2(\omega_2^2 - \omega_{10}^2)}{(\omega_{20}^2 - \omega_{10}^2)} A_2^2 + \frac{(\omega_{20}^2 - \omega_2^2)}{(\omega_{20}^2 - \omega_{10}^2)} \frac{A_1^2}{2} \right] \frac{\sin \phi}{A_2}. \quad \dots (25c)$$

Equilibrium conditions are given by either of the two possible combinations :

$$(1) \quad A_1 = 0, \quad A_2 = A_{20}. \quad \dots (26a)$$

$$(2) \quad A_{10}^2 = A_1^2 + 2A_2^2 + \frac{2b}{c} A_2 \cos \phi \quad (b \sin \phi = 0) \quad \dots (26b)$$

$$A_{20}^2 = A_2^2 + 2A_1^2 + \frac{2b}{c} \frac{A_1^2}{2A_2} \cos \phi \quad (b \sin \phi = 0) \quad \dots (26c)$$

For the first combination the equilibrium is stable when $\frac{A_{10}^2}{A_{20}^2} < 2$. For the second combination, the equilibrium is stable if $b \cos \phi$ is negative and

$$\frac{b}{c} A_1^2 + \frac{8b}{c} A_2^2 - 6A_2^3 - \frac{2b^2}{c^2} A_2 > 0, \quad \dots (27)$$

where A_1 and A_2 satisfy the equations (26b) and (26c).

It may be noted that Eqns. (26b) and (26c) may be solved directly to obtain the equilibrium values of A_1 and A_2 . Thus, on eliminating A_1 the following equation is obtained.

$$A_2^3 - \frac{2b}{c} A_2^2 + \frac{1}{3} \left[A_{20}^2 - 2A_{10}^2 + 2 \left(\frac{b}{c} \right)^2 \right] A_2 + \frac{1}{3} \frac{b}{c} A_{10}^2 = 0, \quad (28)$$

For a particular combination of the values of $\frac{b}{c}$, A_{10}^2 and A_{20}^2 there are three values of A_2 which satisfy Eqn. (28). However, only one of them satisfy the inequality (27).

When ω_{20} departs from $2\omega_{10}$ by a small amount $\Delta\omega$, i.e., $\omega_{20} = 2\omega_{10} \pm \frac{\Delta\omega}{2(1-K_1K_2)}$,

Eqn. (25c) is replaced by

$$\Delta\omega = -\frac{b}{2} \left[2 \frac{(\omega_2^2 - \omega_{10}^2)}{(\omega_{20}^2 - \omega_{10}^2)} A_2^2 + \frac{(\omega_{20}^2 - \omega_2^2)}{(\omega_{20}^2 - \omega_{10}^2)} \frac{A_1^2}{2} \right] \frac{\sin \phi}{A_2} \quad \dots (29)$$

It should be noted that in both Cases II and III oscillation at the lower frequency alone is not possible. The oscillator may either oscillate at the higher frequency alone or at both simultaneously.

EXPERIMENTAL VERIFICATION

The theoretical results presented in the above section have been verified on an electronic differential analyser. In the following paragraphs the application of the analyser for the verification of Eqns. (18a), (18b), (23), (24a) and (28) has been discussed.

The differential equations to be set on the computer are

$$\frac{d^2x_1}{dt^2} + \omega_1^2 x_1 + (-a_1 + bx_1 + cx_1^2) \frac{dx_1}{dt} + K_2 \frac{d^2x_2}{dt^2} = 0, \quad \dots (30a)$$

$$\frac{d^2x_2}{dt^2} + \omega_2^2 x_2 + a_2 \frac{dx_2}{dt} + K_1 \frac{d^2x_1}{dt^2} = 0. \quad \dots (30b)$$

Eqn. (30a) can also be written as

$$\frac{dx_1}{dt} + \omega_1^2 \left\{ x_1 dt + \left(-a_1 x_1 + \frac{b}{2} x_1^2 + \frac{c}{3} x_1^3 \right) \right\} + K_2 \frac{dx_2}{dt} = 0 \quad \dots (30c)$$

A set-up of the differential analyser for solving Eqns. (30c) and (30b) is shown in figure 3. The non-linear function generator for generating the function $f_1(x_1) =$

$\frac{b}{2} x_1^2 + \frac{c}{3} x_1^3$ is of the biased diode type (Burt and Lange, 1956, Meissinger, 1955).

The solution x_1 , x_2 and their derivatives appear at the points marked on the figure.

Eqs. (18a) and (18b) relate the losses at the two frequencies with the amplitudes of oscillations when the oscillations occur singly. For verification of these

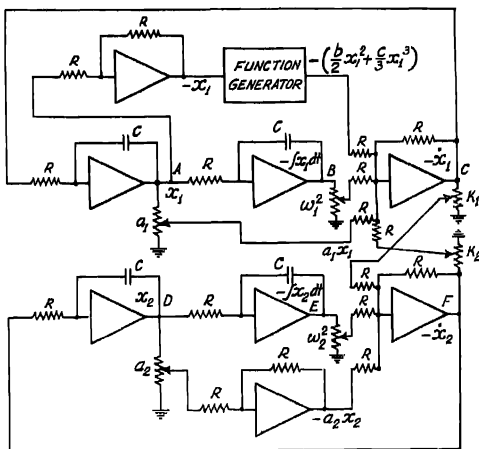


Fig. 3. Set-up of the differential analyser for solving the equations :

$$\ddot{x}_1 - a_1 x_1 + (bx_1 + cx_1^2)x_1 + \omega_1^2 x_1 + k_2 \ddot{x}_2 = 0.$$

$$\ddot{x}_2 + a_2 \ddot{x}_2 + \omega_2^2 x_2 + k_1 \ddot{x}_1 = 0.$$

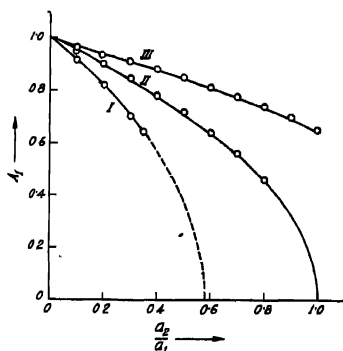
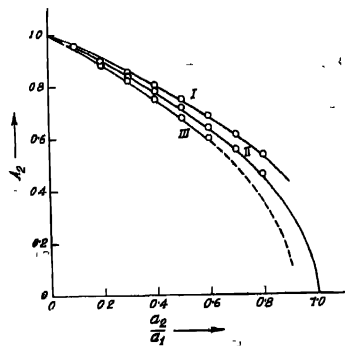


Fig. 4. (a) Plots of A_1 against a_2/a_1 .



(b) Plots of A_2 against a_2/a_1

— Theoretical plot for stable oscillations.

--- Theoretical plot for unstable oscillation.

○ Experimental points.

I — $\sigma = 0.012$, $\rho = 1.714$ II — $\sigma = 1$, $\rho = 1$ III — $\sigma = 1.096$, $\rho = 0.55$

equations oscillations at the two frequencies are excited individually and their amplitudes measured for selected values of the parameters ρ , σ and $\frac{4a_1}{c}$. In

figure 4 experimental plots relating A_1 and A_2 with $\frac{a_2}{a_1}$ are shown along with the

theoretically calculated curves for three sets of values of ρ and σ for $\frac{4a_1}{c} = 1$.

Eqn. (23) gives the ratio of the amplitudes of simultaneous oscillations at the two frequencies related by the ratio 3 : 1 for different values of $\frac{A_{10}^2}{A_{20}^2}$. Verification

of this equation would require determination of the ratio $\frac{A_2}{A_1}$ for different settings

of $\frac{A_{10}^2}{A_{20}^2}$. Different values of $\frac{A_{10}^2}{A_{20}^2}$ were set by varying $\frac{a_2}{a_1}$. Values of $\frac{A_{10}^2}{A_{20}^2}$ within

the range 0 to ∞ were obtained by making $\omega_1^2 = 1$ and $\omega_2^2 = 0.8$ and values within the range $-\infty$ to 0, by making $\omega_1^2 = 0.8$ and $\omega_2^2 = 1$. For determining the ratio of the amplitudes, oscillations at the two frequencies were first separated by combining the outputs at B and C . The output at A is given by

$$x_1 = A_1 \cos (\omega_{10} t + \phi_1) + A_2 \cos (\omega_{20} t + \phi_2)$$

The outputs at B and C are therefore given by respectively

$$E_B = - \int x_1 dt = - \frac{A_1}{\omega_{10}} \sin (\omega_{10} t + \phi_1) - \frac{A_2}{\omega_{20}} \sin (\omega_{20} t + \phi_2)$$

$$\text{and} \quad E_C = -\dot{x}_1 = \omega_{10} A_1 \sin (\omega_{10} t + \phi_1) + \omega_{20} A_2 \sin (\omega_{20} t + \phi_2)$$

Hence,

$$\frac{\omega_{10}^2 E_B + E_C}{\omega_{20} \left(1 - \frac{\omega_{10}^2}{\omega_{20}^2} \right)} = A_1 \sin (\omega_{20} t + \phi_2) \quad \dots (31a)$$

$$\frac{E_B + \frac{E_C}{\omega_{20}^2}}{\frac{1}{\omega_{10}} \left(\frac{\omega_{10}^2}{\omega_{20}^2} - 1 \right)} = A_1 \sin (\omega_{10} t + \phi_1) \quad \dots (31b)$$

Thus, the amplitudes of oscillation at the two frequencies can be determined using the Eqns. (31a) and (31b). Experimental values of $n = \frac{A_2}{A_1}$ for

different values of $\frac{A_{10}^2}{A_{20}^2}$ along with the theoretical values are given in figure 5.

Eqn. (24a) relates the phase difference between two approximately synchronous oscillations pulled into synchronism by the non-linearity, with $\Delta\omega$. Verification

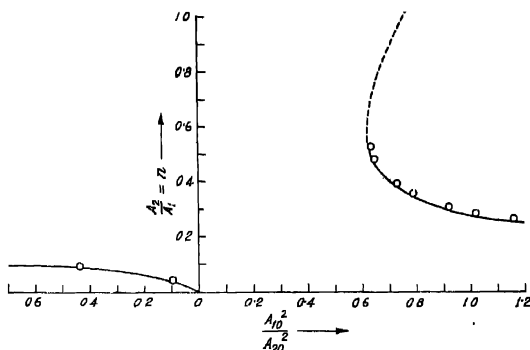


Fig. 5. Plot of $n = \frac{A_2}{A_1}$ against $\frac{A_{10}^2}{A_{20}^2}$ for $\omega_{20} = 3\omega_{10}$.

- — — Theoretical plot for stable oscillations
- - - - Theoretical plot for unstable oscillations
- o Experimental points.

of this equation requires determination of ϕ for different settings of $\Delta\omega$. This was set to different values by varying the value of K_1K_2 . The phase ϕ was measured by an oscilloscope. The arrangement used is shown in figure 6.

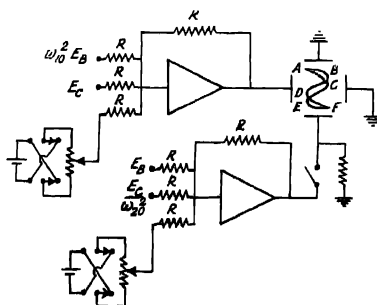


Fig. 6. Experimental arrangement for measuring ϕ when $\omega_{20} = 3\omega_{10} \pm \Delta\omega$.

Oscillations at the two frequencies were separated as described above. The sinusoidal voltage varying at the frequency ω_{20} was fed to the X-plate and that varying at the frequency ω_{10} was fed to the Y-plate. In general, the plot on the oscilloscope screen touches the vertical line at six points, marked A, B, C, D, E and F in figure 6. Let d_{AF} , d_{BE} and d_{CD} denote the distances between A and

F, B and E, C and D respectively. Then $\frac{d_{BE}}{d_{AF}} = \cos\left(\frac{\pi}{3} - \frac{\phi}{3}\right)$ and also $\frac{d_{CD}}{d_{AF}} = \cos\left(\frac{\pi}{3} + \frac{\phi}{3}\right)$. The distances d_{AF} , d_{BE} and d_{CD} were measured by shifting the

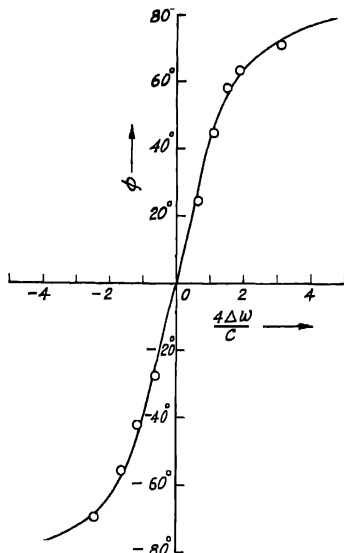


Fig. 7. Plot of ϕ against $\Delta\omega$ for $\omega_{20} = 3\omega_{10} \pm \Delta\omega$.

— Theoretical plot.
o Experimental points.

pattern vertically and noting the voltages required for bringing the different points on the zero line, which was put on the oscilloscope by opening a switch at intervals. The shifting voltage was obtained from a calibrated helipot which gives the distance directly. The experimental plot of ϕ against $\Delta\omega$, for $\omega_1^2 = \omega_2^2 = 1$ are shown in figure 7 together with the theoretical plot.

Data for verification of Eqns. (26b) and (26c) were obtained in the same manner as indicated in connection with Eqn. (23). The experimental plots of $\frac{A_2}{A_1}$ against $\frac{2b}{c}$ for three values of A_{20}^2 corresponding to $A_{10}^2 = .2$ is shown in figure 8 along with the theoretically calculated curves.

EXPERIMENTAL TRAJECTORIES IN THE A_1 - A_2 PLANE

In all the cases discussed above it is found that the oscillator has two possible modes of stable oscillation. The particular mode chosen by it depends on the

initial values of A_1 , A_2 and ϕ . The growth of a particular mode from the initial conditions is usually illustrated by drawing trajectories in the A_1 - A_2 plane

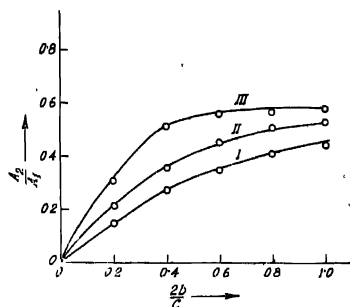


Fig. 8. Plots of A_2/A_1 against $\frac{2b}{c}$ for $\omega_{20} = 2\omega_{10}$.

— Theoretical plot

o Experimental points

- | | |
|------------------------|-------------------|
| I - $A_{10}^2 = 0.2$ | $A_{20}^2 = 0.1$ |
| II - $A_{10}^2 = 0.2$ | $A_{20}^2 = 0.2$ |
| III - $A_{10}^2 = 0.2$ | $A_{20}^2 = 0.26$ |

applying the method of isoclines. On the differential analyzer these trajectories may also be easily obtained by applying voltages proportional to A_1 and A_2 or some function of A_1 and A_2 to the X and Y plates. It has been described before how voltages proportional to $A_1 \sin(\omega_{10}t + \phi_1)$ and $A_2 \sin(\omega_{20}t + \phi_2)$ may be obtained by combining the outputs at B and C (figure 3) in the steady state. During the transient state also the combined voltages will have amplitudes very nearly proportional to A_1 and A_2 when a_1 and a_2 are small. Similarly by combining the outputs at A and D voltages proportional to $A_1 \cos(\omega_{10}t + \phi_1)$ and $A_2 \cos(\omega_{20}t + \phi_2)$ may be obtained. By squaring these Sine and Cosine voltages and adding them voltages representing A_1^2 and A_2^2 may be obtained.

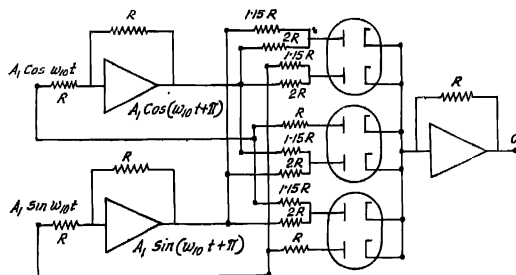


Fig. 9. Experimental arrangement for double three phase rectification.

For getting voltages proportional to A_1 and A_2 , one may subject the sine and cosine voltages to multiphase rectification. One arrangement for doing this is shown in figure 9.

It will be noted that the voltage output at O is proportional to A_1 but is mixed up with a certain amount of ripple, which is 3% in this case. The ripple content may be further reduced by quadruple three phase rectification in which case the ripple is only .6%. For obtaining the trajectories it was found advantageous to employ the voltages corresponding to A_1 and A_2 as obtained through the multiphase rectification circuit for it requires less components and is simpler than the squaring circuit.

The trajectories as obtained on the analyser are shown in figure 10. Figure 10(a) gives the trajectories for a particular combination of ω_{20} and ω_{10} , not integrally related. It is seen that in this case the two stable equilibrium points lie on the two axes. The third equilibrium point which is unstable is also clearly indicated.

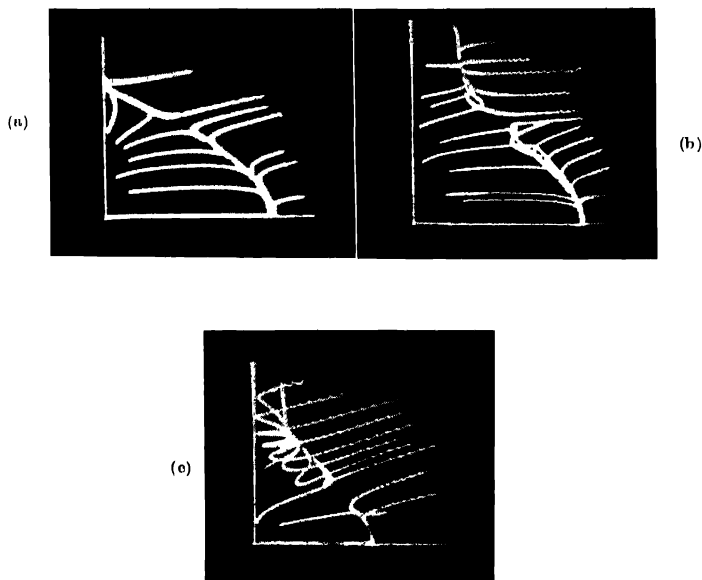


Fig. 10. Experimental trajectories in the A_1 - A_2 plane.

- (a) Trajectories for ω_{20} and ω_{10} non-integrally related.
- (b) Trajectories for $\omega_{20} = 3\omega_{10}$
- (c) Trajectories for $\omega_{20} = 2\omega_{10}$

Figure 10(b) gives the trajectories for $\omega_{20} = 3\omega_{10}$. In this case one of the stable equilibrium points lies on the A_2 axis, whereas the other one lies at a point for which both A_1 and A_2 have finite values. There is a third equilibrium point which is, however, unstable. In contrast to the previous case, trajectories in the A_1, A_2 plane are not unique in this case since they also depend on ϕ . This explains the crossing of some of the trajectories. Figure 10(c) gives the trajectories for $\omega_{20} = 2\omega_{10}$, the general characteristics of which are similar to those in figure 10(b).

CONCLUSIONS

An oscillator with two degrees of freedom and stabilised by a cubic non-linearity has two possible modes of oscillations. It may oscillate at one of the two possible frequencies at a time or at both simultaneously. The latter mode is stable only if the two frequencies are related approximately by the integral ratio 3:1 or 2:1. The order of approximation in the integral ratio permitting the simultaneous oscillation is determined by the magnitude of the non-linearity. The stable amplitudes of oscillation as also their conditions of stability as obtained theoretically by the variation of parameter method agree quite closely with those obtained experimentally with the help of a differential analyser. A differential analyser can also be used very usefully for obtaining trajectories in the A_1-A_2 plane which show clearly the growth of oscillations of a particular mode from the various initial conditions, as well as the different possible equilibrium points.

ACKNOWLEDGMENT

The author is deeply indebted to Professor J. N. Bhar for his constant guidance and valuable suggestions.

REFERENCES

- Burt, E. G. C. and Lange, O. H., 1956, *Proc. I.E.E.*, Part C, **103**, 51.
- Fontana, R. E., 1951, *Proc. I.R.E.*, **39**, 945.
- Meissinger, H. F., 1955, I.R.E. Convention Records, 150.
- N. Kryloff and N. Bogoliuboff, 1943, Introduction to Non-linear Mechanics, 73.
- N. Minorsky, 1947, Non-linear Mechanics, 148; 251.
- Schaffner, J. S., 1954, *Trans. I.R.E.*, **2**.
- Van der Pol., B., 1922, *Phil. Mag.*, **43**, 700.

LIGHT ABSORPTION IN PARAMAGNETIC IONS IN STATE OF SOLUTION. PART I—CUPRIC IONS

A. MOOKHERJI AND N. S. CHHONKAR

PHYSICS LABORATORIES, AGRA COLLEGE, AGRA

(Received, January 6, 1959)

ABSTRACT. The light absorption from 3900 Å to 10,000 Å for eighteen cupric salts in aqueous solution have been studied with a Hilger "UVISPEK" spectrophotometer with an accuracy of 2 Å to 10 Å in different regions.

It is observed that Cu^{++} ions in aqueous solution have sharp absorption bands lying between 8110 Å and 6180 Å for different salts. The results are discussed in relation to the observed magnetic moments and g -values. From a study of the calculated covalency factors it is concluded that the mean magnetic moments do not change from salt to salt amongst the sulphates, chlorides and nitrates but are appreciably different for acetate, amines etc. In state of aqueous solution the salts are more ionic than in crystalline state if ΔE is the same. In aminosalts, acetate and propionate the covalency factor is made up of two factors arising from the σ and π orbital overlap.

1. INTRODUCTION

Extensive magnetic measurements on single crystals of cupric sulphate pentahydrate (Krishnan and Mookherji, 1936 & 1938) and other salts (Krishnan and Mookherji, 1938 ; Mookherji, 1945 , Bose, 1948 and Bose *et al*, 1957) have revealed that magnetic behaviour of Cu^{++} ions in crystals may be explained in several details by assuming the Cu^{++} ions to be under the influence of a strong and asymmetric crystalline electric field arising out of an axially distorted octahedral cluster of water dipoles, surrounding the metal ion. The effect of such a field is to split the ground state of the ion into a Stark pattern. According to Bethe (1929, 1930) and others (Abragam & Pryce, 1951 and Owen, 1954) Stark splitting of the original ground state, $^2D_{5/2}$, of free Cu^{++} ion due to a crystalline electric field conforming to a potential

$$V = D(X^4 + Y^4 + Z^4) + A(X^2 + Y^2 - 2Z^2) + B(Z^4 + 6X^2Y^2) \quad (1)$$

is shown in figure 1, spin-orbit splitting being neglected. The first fourth degree terms in this expression represent a field of cubic symmetry the coefficient D of which is positive here (Gorter, 1932 and Van Vleck, 1932) and the remaining two terms represent the second and fourth degree components of the axial (tetragonal) field with symmetry about z -axis and both the coefficients are positive for the usual Cu^{++} salts (Bleaney, Bowers & Pryce, 1955; Abragam & Pryce, 1951 ; Bleaney, Bowers and Ingram, 1955 and Bose *et al*, 1957).

A numerical estimate in $\text{Cu}(\text{KSO}_4)_2 \cdot 6\text{H}_2\text{O}$ by Polder (1942) using a model $\text{Cu}^{++}(\text{H}_2\text{O})_6$ gives the tetragonal splitting of the same order of magnitude as due to the cubic field. Experimental observations do not support this (Abragam and Pryce, 1951 and others).

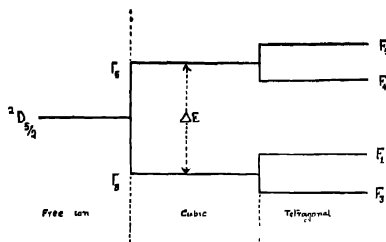


Fig. 1. Stark splitting of ground state of Cu^{++} ion.

According to these workers the cubic splitting may be taken as $\sim 10^4 \text{ cm}^{-1}$, and tetragonal splitting as $\sim 10^3 \text{ cm}^{-1}$. Hence the transitions between the levels so split will produce absorption spectra lying between ultraviolet and infra-red regions and as such will be capable of optical verification. Dreisch and Trommer (1937) working on the selective absorption for $\text{CuSO}_4 \cdot 5\text{H}_2\text{O}$ and $[\text{Cu}(\text{NH}_3)_4]\text{Cl}_2 \cdot \text{H}_2\text{O}$ in state of solution find that the absorption bands are roughly at $12,297 \text{ cm}^{-1}$ and $14,160 \text{ cm}^{-1}$ respectively.

In the state of solution of a given salt the lattice structure breaks down completely while the anisotropic ionic clusters retain their identities (Krishnan, 1939 and Chakravarty, 1942). But since they are oriented at random the medium will show no anisotropy of susceptibility. But optical absorption should reveal the fine structure in the Stark pattern arising from the anisotropic field splittings.

A systematic optical investigation of the consequences of the crystal field on the paramagnetic ions both in the crystalline state and in state of solution is under progress in this laboratory. The present communication deals with the absorption of light by a number of cupric salts in state of solution (aqueous) and are discussed in the light of the findings from magnetic measurements and paramagnetic absorption experiments.

2. EXPERIMENTAL

The selective absorption bands of paramagnetic salts of iron group of metals in state of solution show very broad absorption bands when photographed by a spectrograph; as such it is not possible to determine with any degree of accuracy, the position of the absorption maximum from an examination of the absorption

spectra of these salts with a spectrograph (Dreisich and Trommer, 1937). Consequently the measurements on light absorption were carried out by a Hilger's "UVISPEK" spectrophotometer.

The description of the instrument is available from the literature (H700.307/57887) supplied by the company. Interested readers may refer to it.

The image of the lamp was accurately focussed on the entrance slit. The wavelength drum was calibrated by a hydrogen discharge tube and a mercury discharge lamp. The absorption cells were cleansed thoroughly and their percentage of transmission checked. The wavelength drum was set to the desired wavelength and the absorption cell tray was set such that the reference medium was in the light beam. The test solutions were then brought one by one in the light beam and for each of them the percentage of transmission was directly noted from the scale for that wavelength. This was repeated for various wavelengths.

The absorption due to the solvent and the absorption cell was nullified by filling the absorption cell with the solvent and putting it in place of the reference medium. Chemicals used were of 'Merck's' analytical reagent quality.

The accuracy of the measurements in the region 10,000Å to 6500Å is approximately $10 \text{ Å} \pm 2\text{Å}$, from 6500Å to 5000Å is approximately $5\text{Å} \pm 1\text{Å}$ and from 5000Å to 3900Å is approximately $2\text{Å} \pm 1\text{Å}$. Measurements are centred round about 27°C but no observable change in the position of the absorption bands was noticed for small room temperature variations.

3. RESULTS

Results of the measurements are collected in Table I. The location of the absorption bands for various cupric salts in the state of solution are given both in wavelength and wavenumbers. In order to get prominent absorption peaks for the salts studied we had to use dilute solutions. Progressive dilution from that concentration at which prominent absorption peak is obtained does not change the position of the absorption peak.

The variation of absorption in different salt solutions are shown graphically in figures 2 to 19. No fine structure of the lines corresponding to tetragonal splitting could be observed.

4. DISCUSSION

(a) Crystal field and energy levels

According to the calculations of Polder (1942) the mean centres of the energy levels Γ_5 and Γ_3 (figure 1) are at $\frac{6}{21} D'$ and $-\frac{4}{21} D'$, where $D' = \frac{2}{5} e r^4 \cdot D$, D

TABLE I

S.No.	Salts	Concentration	Absorption (ΔE) at		$D' = 2.1\Delta E$	Remarks
			$\lambda \text{ \AA}$	Wave numbers cm^{-1}		
1.	CuSO_4	1.0	8060	12,405	26,055	Not sharp, lies between λ 8050 to λ 8075
2.	$\text{Cu}(\text{NH}_4.\text{SO}_4)_2$	1.0	8050	12,420	26,085	Not sharp, lies between λ 8050 to λ 8063
3.	$\text{Cu}(\text{K}.\text{SO}_4)_2$	1.0	8055	12,415	26,070	
4.	$\text{Cu}(\text{Rb}.\text{SO}_4)_2$	1.5	8085	12,370	25,977	
5.	$\text{Cu}(\text{Ti}.\text{SO}_4)_2$	1.0	8075	12,385	26,010	
6.	CuCl_2	1.0	8075	12,385	26,010	
7.	$2\text{NH}_4\text{Cl}.\text{CuCl}_2$	1.0	8075	12,385	26,010	
8.	$2\text{KCl}.\text{CuCl}_2$	1.0	8075	12,385	26,010	
9.	CuBr_2	1.1	8110	12,330	25,893	
10.	$\text{Cu}(\text{NO}_3)_2$	0.5	8060	12,405	26,055	
11.	$\text{Cu}_3\text{Bi}_2(\text{NO}_3)_{12}$	1.16	8075	12,385	26,010	
12.	$\text{Cu}(\text{CHOO})_2$	0.5	7775	12,860	27,005	
13.	$\text{Cu}(\text{CH}_3\text{COO})_2$	0.25	7675	13,030	27,360	
14.	$\text{Cu}(\text{CH}_3\text{CH}_2\text{COO})_2$	0.4	7710	12,970	27,237	
15.	$[\text{Cu}(\text{NH}_3)_4](\text{SO}_4)$	$\left. \begin{smallmatrix} .080 \\ 1:1 \end{smallmatrix} \right\} \text{NH}_4\text{OH}$	6250	16,000	33,600	Band head changes with conc. of NH_4OH
16.	$[\text{Cu}(\text{NH}_3)_4](\text{OH})_2$	$\left. \begin{smallmatrix} .120 \\ 1:1 \end{smallmatrix} \right\} \text{NH}_4\text{OH}$	6230	16,050	33,705	-do-
17.	$[\text{Cu}(\text{NH}_3)_4](\text{CH}_3\text{COO})_2$	$\left. \begin{smallmatrix} .150 \\ 1:1 \end{smallmatrix} \right\} \text{NH}_4\text{OH}$	6200	16,130	33,875	-do-
18.	$[\text{Cu}(\text{NH}_3)_4](\text{Cl})_2$	$\left. \begin{smallmatrix} .150 \\ 1:1 \end{smallmatrix} \right\} \text{NH}_4\text{OH}$	6180	16,180	33,980	-do-

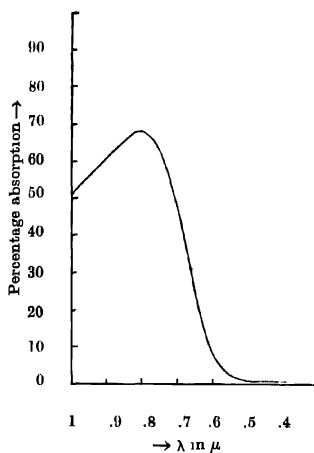


Fig. 2. Absorption curve of 1% CuSO_4 solution.

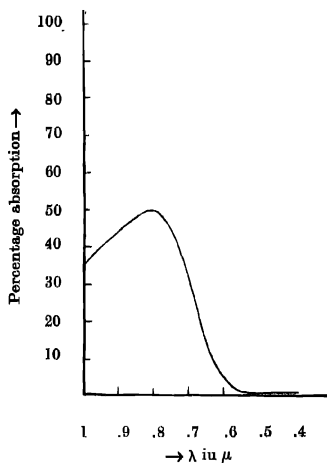


Fig. 3. Absorption curve of 1% $\text{Cu}(\text{NH}_4)_2\text{SO}_4$ solution.

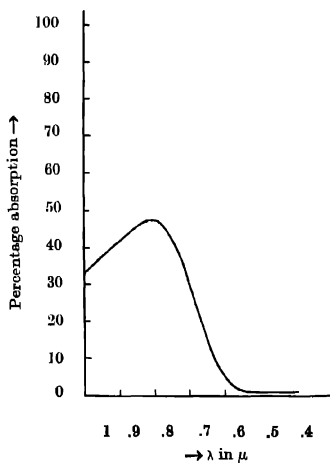


Fig. 4. Absorption curve of 1% $\text{Cu}(\text{K}_2\text{SO}_4)_2$ solution.

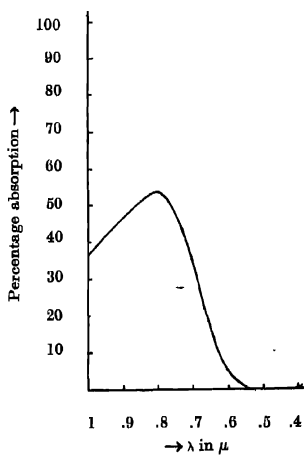


Fig. 5. Absorption curve of 1.5% $\text{Cu}(\text{Rb}_2\text{SO}_4)_2$ solution.

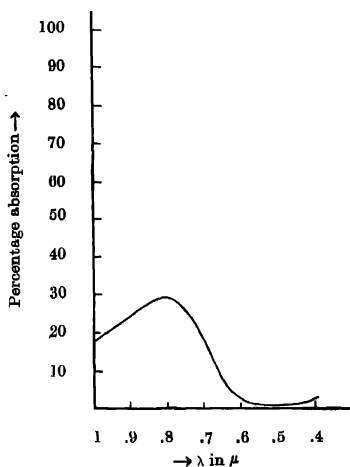


Fig. 6. Absorption curve of 1%
 $\text{Cu}(\text{Tl}.\text{SO}_4)_2$ solution.

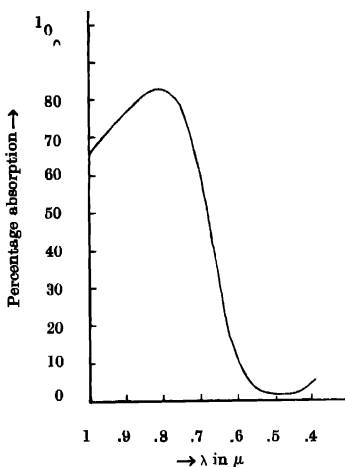


Fig. 7. Absorption curve of 1%
 CuCl_2 solution

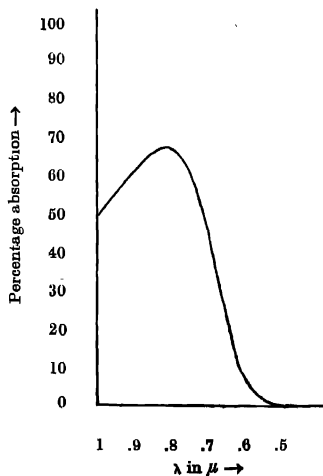


Fig. 8. Absorption curve of 1%
 $2\text{NH}_4\text{Cl}.\text{CuCl}_2$ solution.

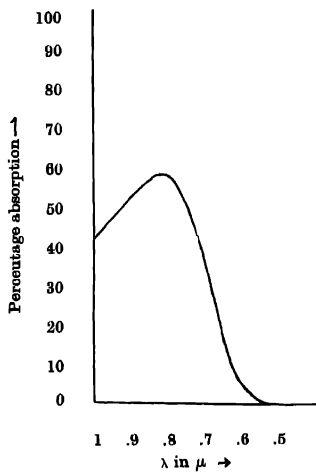


Fig. 9. Absorption curve of 1%
 $2\text{KCl}.\text{CuCl}_2$ solution.

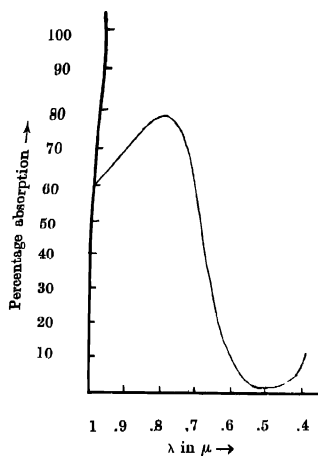


Fig. 10. Absorption curve of 1.1% CuBr_2 solution.

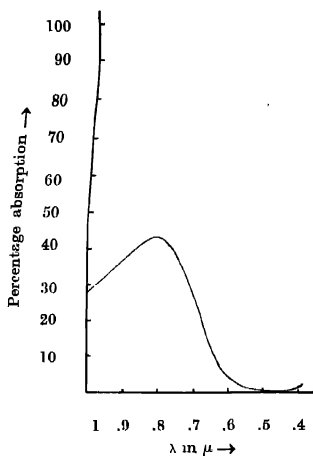


Fig. 11. Absorption curve of 0.5% $\text{Cu}(\text{NO}_3)_2$ solution.

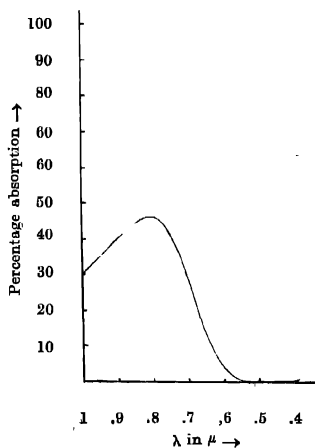


Fig. 12. Absorption curve of 1.10% $\text{Cu}_3\text{Bi}_2(\text{NO}_3)_{12}$ solution.

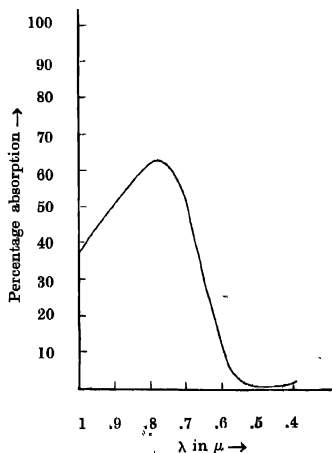


Fig. 13. Absorption curve of 0.5% $\text{Cu}(\text{CHOO})_2$ solution.

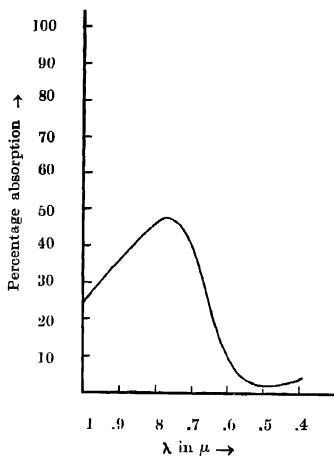


Fig. 14. Absorption curve of 0.25% $\text{Cu}(\text{CH}_3\text{COO})_2$ solution.

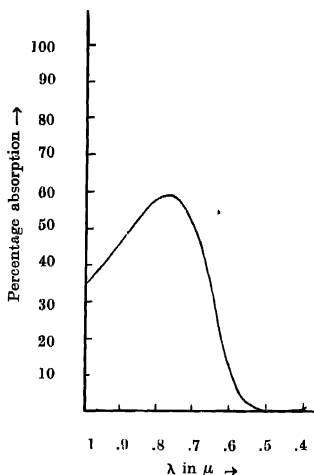


Fig. 15. Absorption curve of 0.4% $\text{Cu}(\text{C}_2\text{H}_3\text{O}_2)_2$ solution.

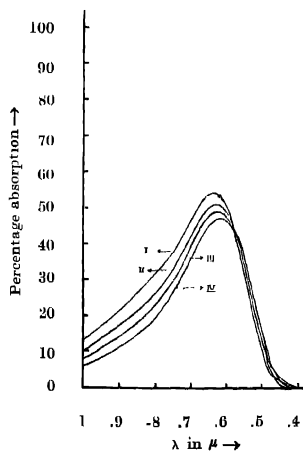


Fig. 16. Absorption curve of (all) .080% $\text{Cu}(\text{NH}_3)_4(\text{SO}_4)$ solution.

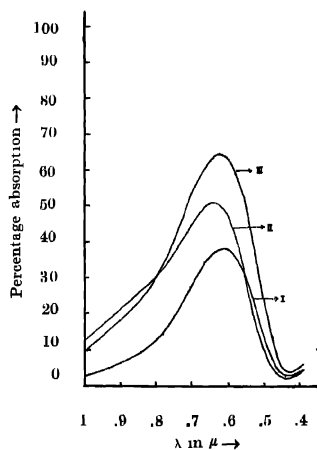


Fig. 17. Absorption curve of I, II°, III° .12%, .23% $\text{Cu}(\text{NH}_3)_4(\text{OH})_2$ solution.

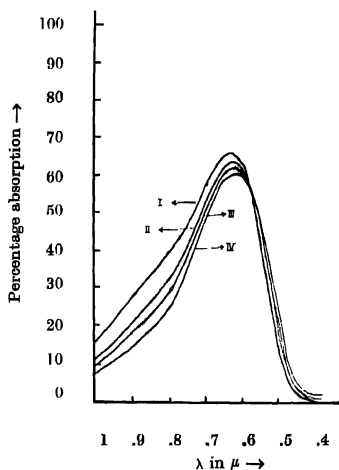


Fig. 18. Absorption curve of 0.15% $\text{Cu}(\text{NH}_3)_4(\text{CH}_3\text{COO})_2$ solution.

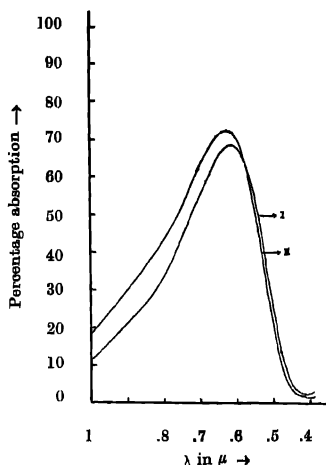


Fig. 19. Absorption curve of 0.15% $\text{Cu}(\text{NH}_3)_1(\text{Cl})_2$ solution.

being the cubic field coefficient (Eqn. 1) and r^4 is the average value of the fourth powers of the radii of $3d$ electrons. Thus ΔE , the cubic splitting is given by

$$\Delta E = \frac{10}{21} D' \quad \text{or} \quad D' = 2.1 \Delta E$$

Hence it will be interesting to calculate D' from the observed ΔE values which gives us an idea of the size of the octahedron of water molecules surrounding the Cu^{++} ion. This is given in Table I.

It will be seen from these values that the octahedral clusters about Cu^{++} ion are of nearly the same size in all the halides, $\text{Cu}(\text{TiSO}_4)_2$, $\text{Cu}(\text{RbSO}_4)_2$ and $\text{Cu}_3\text{Bi}_2(\text{NO}_3)_{12}$. Single sulphate, single nitrate and other double sulphates have also practically the same size of octahedron. This indicates further that in the solution state probably all the six members of the cluster are the same namely water molecules, though this was not the case in the solid state e.g. in the single sulphate and the halides. In copper formate, copper acetate and copper propionate solutions these octahedra are much smaller. Amino-salts have the smallest octahedra. Thus at least some of the coordination members in solution are very probably other than water molecules.

(b) Calculation of the covalency factor

Abragam and Pryce (1951) have calculated the "spectroscopic splitting factor" g in a tetragonal field for Cu^{++} ion in crystals. For directions parallel

and perpendicular to the tetragonal axis, neglecting square and product terms we have

$$\text{and } \left. \begin{aligned} g_{\parallel} &= 2 - \frac{8\lambda \cdot f^2}{F_4 - F_3} \approx 2 - \frac{8\lambda}{\Delta E'} \\ g_{\perp} &= 2 - \frac{2\lambda \cdot f^2}{F_5 - F_3} \approx 2 - \frac{2\lambda}{\Delta E'} \end{aligned} \right\} \dots (2)$$

in which f^2 is the covalency factor arising from the partial overlap of the $3d$ orbitals with σ and π orbitals of the surrounding atoms (Owen 1954) assumed isotropic for the present; and $F_4 - F_3 \approx F_5 - F_3 = \Delta E = \Delta E'$. f^2 , is valid since the tetragonal separation in state of solution will be even less than $\sim 10^3 \text{ cm}^{-1}$ owing to the absence of the effect of the long range field in solution state (Bose & Mitra, 1952; Bose, Mitra and Datta, 1957).

Using experimentally determined g -values from paramagnetic resonance both for solids and liquids we have calculated $1/\Delta E'$, for the various salts using relation (3) taking $\lambda = -828 \text{ cm}^{-1}$ (Shenstone and Wilets, 1951).

$$g = \sqrt{\frac{g_{\parallel}^2 + 2g_{\perp}^2}{3}} \approx 2 \left(1 - \frac{2\lambda}{\Delta E'} \right) \dots (3)$$

These are given in Table III. It is observed that $1/\Delta E'$ values of solutions differ considerably from those of the solid values, indicating the effect of long range field as mentioned above.

Now following Polder (1942), Bleaney *et al* (1949) and Owen (1954) the principal moments along and normal to the tetragonal axis of the paramagnetic units calculated from the susceptibilities of the crystalline salts are

$$\left. \begin{aligned} \frac{\mu_{\parallel}^2}{3} &= \left(1 - \frac{4\lambda \cdot f^2}{F_4 - F_3} \right)^2 + \frac{8kT \cdot f^2}{F_4 - F_3} \\ \frac{\mu_{\perp}^2}{3} &= \left(1 - \frac{\lambda \cdot f^2}{F_5 - F_3} \right)^2 + \frac{2kT \cdot f^2}{F_5 - F_3} \end{aligned} \right\} \dots (4)$$

Taking as before

$$F_4 - F_3 \approx F_5 - F_3 = \Delta E = \Delta E' \cdot f^2$$

we have

$$\bar{\mu}^2 = (\bar{\mu}_{\parallel}^2 + 2\bar{\mu}_{\perp}^2)/3 = \frac{3}{4}g^2 + \frac{12kT}{\Delta E'} = 3 \left[1 - \frac{4}{\Delta E'} (\lambda - kT) \right] \dots (5)$$

TABLE II

S.No.	Salts	g -values		μ — Values from g -Values		μ — Values from susceptibility	
		Crystal Solution		Crystal Solution		Crystal Solution	
1.	$\text{CuSO}_4 \cdot 5\text{H}_2\text{O}$	2.208 ¹	2.184 ²	1.952	1.9265	1.923 ³	1.97 ⁴
2.	$\text{Cu}(\text{NH}_4\text{SO}_4)_2 \cdot 6\text{H}_2\text{O}$	2.180 ²		1.922		1.938 ³	
3.	$\text{Cu}(\text{KSO}_4)_2 \cdot 6\text{H}_2\text{O}$	2.184 ²		1.926		1.920 ³	
4.	$\text{Cu}(\text{RbSO}_4)_2 \cdot 6\text{H}_2\text{O}$	2.204 ²		1.947		1.930 ¹⁰	
5.	$\text{Cu}(\text{TlSO}_4)_2 \cdot 6\text{H}_2\text{O}$	2.177 ²		1.918		1.970 ¹⁰	
6.	$\text{CuCl}_2 \cdot 2\text{H}_2\text{O}$	2.1605	2.184 ²	1.902	1.9265	1.932 ¹¹	1.985 ⁶
7.	$\text{CuCl}_2 \cdot 2\text{NH}_4\text{Cl}$	2.1603		1.901		1.880 ¹⁰	1.967 ⁶
8.	$\text{CuCl}_2 \cdot 2\text{KCl}$	2.167 ³		1.908		1.850 ¹⁰	
9.	CuBr_2		2.175 ³		1.9175		2.000 ⁶
10.	$\text{Cu}(\text{NO}_3)_2 \cdot 3\text{H}_2\text{O}$		2.184 ³		1.9265	1.922 ¹²	1.956 ⁶
11.	$\text{Cu}_3\text{Bi}_2(\text{NO}_3)_{12} \cdot 24\text{H}_2\text{O}$	2.184 ⁴		1.962			
12.	$\text{Cu}(\text{CHOO})_2 \cdot 4\text{H}_2\text{O}$	2.150 ⁵					1.740
13.	$\text{Cu}(\text{CH}_3\text{COO})_2 \cdot \text{H}_2\text{O}$	2.164 ⁵		1.45		1.410 ¹⁰	1.488
14.	$\text{Cu}(\text{C}_2\text{H}_3\text{CH}_2\text{COO})_2 \cdot \text{H}_2\text{O}$	2.184 ⁵					1.560
15.	$[\text{Cu}(\text{NH}_3)_4](\text{SO}_4)$	2.074 ⁷	2.100 ⁸	1.811	1.838	1.845 ¹³	
16.	$[\text{Cu}(\text{NH}_3)_4](\text{CH})_2$		2.100 ⁸		1.838		
17.	$[\text{Cu}(\text{NH}_3)_4](\text{CH}_3\text{COO})_2$		2.100 ⁸		1.838		
18.	$[\text{Cu}(\text{NH}_3)_4](\text{Cl})_2$ ⁹		2.100 ⁸		1.838		

1-Bauggley & Griffiths (1950), 2-Bleaney, Penrose and Plumpton (1949), 3-Abe, Ono, Hayashi, Shimada and Iwanaga (1954), 4-Trenam R. S. (1953), 5-Abe, (1953), 6-Mathur, S. C. (Unpublished), 7-Okamura and Dato (1954), 8-B.M. Kozyrev (1957), 9-Bose (1948), 10-Mookherji (1946), 11-Birch (1928), 12-Welo (1929), 13-Janes(1935).

TABLE III

S.No.	Salts	$1/\Delta E' \times 10^{-6}$				f^2			
		From g-values		From μ -values		From g-values		From μ -values	
		crystal solution	crystal solution	crystal solution	crystal solution	crystal solution	crystal solution	crystal solution	crystal solution
1.	$\text{CuSO}_4 \cdot 5\text{H}_2\text{O}$	62.8	55.6	54.7	68.9	.779	.689	.679	.855
2.	$\text{Cu}(\text{NH}_4\text{SO}_4)_2 \cdot 6\text{H}_2\text{O}$	54.4		51.0		.676		.633	
3.	$\text{Cu}(\text{KSO}_4)_2 \cdot 6\text{H}_2\text{O}$	55.6		53.5		.690		.664	
4.	$\text{Cu}(\text{RbSO}_4)_2 \cdot 6\text{H}_2\text{O}$	61.6		56.7		.762		.702	
5.	$\text{Cu}(\text{TlSO}_4)_2 \cdot 6\text{H}_2\text{O}$	53.5		68.2		.662		.844	
6.	$\text{CuCl}_2 \cdot 2\text{H}_2\text{O}$	48.5	55.6	57.6	72.9	.600	.688	.713	.903
7.	$\text{CuCl}_2 \cdot 2\text{NH}_4\text{Cl}$	48.3		42.0	67.45	.600		.520	.835
8.	$\text{CuCl}_2 \cdot 2\text{KCl}$	50.4		33.6		.624		.416	
9.	CuBr_2		52.84		94.85		.65		990
10.	$\text{Cu}(\text{NO}_3)_2 \cdot 3\text{H}_2\text{O}$		55.6	54.3	64.2		.689	.674	.795
11.	$\text{Cu}_3\text{Bi}_2(\text{NO}_3)_{12} \cdot 24\text{H}_2\text{O}$	66.0		54.3		.817		.672	
12.	$\text{Cu}(\text{CHOO})_2 \cdot 4\text{H}_2\text{O}$	45.3				.58		.028	.69
13.	$\text{Cu}(\text{CH}_3\text{COO})_2 \cdot \text{H}_2\text{O}$	49.4		48.8	51.4	.644		.636	.67
14.	$\text{Cu}(\text{CH}_7\text{CH}_2\text{COO})_2 \cdot \text{H}_2\text{O}$	55.6				.72			.68
15.	$[\text{Cu}(\text{NH}_3)_4](\text{SO}_4)$	22.3	30.19	32.0		.357	.483	.512	
16.	$[\text{Cu}(\text{NH}_3)_4](\text{OH})_2$		30.19				.485		
17.	$[\text{Cu}(\text{NH}_3)_4](\text{CH}_3\text{COO})_2$		30.19				.489		
18.	$[\text{Cu}(\text{NH}_3)_4](\text{Cl})_2$		30.19				.487		

We have calculated the values of $\bar{\mu}$ from the resonance values of 'g' using the above equation and have given them for comparison with experimental susceptibility values of $\bar{\mu}$ for both solids and solutions in Table II.

The experimentally determined values do not agree with the calculated values. So we have calculated $1/\Delta E'$ from experimentally determined $\bar{\mu}$ -values of solids and solutions. There also the two values are different. Hence we presume that we can not utilize our optically observed value of ΔE from solutions to calculate f^2 for crystals. To get the values of f^2 for crystals we need optical data in crystal state. However, taking the $\bar{\mu}$ -values of solutions and using our optical data in state of solution, we have calculated f^2 for various cupric ions in state of solution which are given in Table III. It is seen that the single sulphate, the chloride, bromide and the nitrate are predominantly ionic; f^2 values tend to be ~ 0.9 in state of solution.

In the case of copper acetate according to Bleaney and Bowers (1952) pairs of Cu^{++} ions in the crystal are coupled together by exchange forces. Thus they will form a triplet state with parallel spin and a singlet state with anti-parallel spin. The triplet state will show a resonance spectrum similar to nickel salts with effective spin unity. Here again g is given by the expression (3). Using this expression and taking g for copper acetate from table II, we have calculated f^2 which is 0.644.

Bleaney and Bowers (1952) have deduced expressions for the principal susceptibilities for copper acetate from which $\bar{\mu}^2$ is given by

$$\mu^2 = 4 \left(1 - \frac{4\lambda \cdot f^2}{\Delta E} \right) \left[\frac{1}{1 + \frac{1}{2} e^{-J/RT}} \right] + \frac{12kT \cdot f^2}{\Delta E} \quad \dots (6)$$

Taking $\bar{\mu}^2$ value for the crystal (Table II) using $J = -315 \text{ cm}^{-1}$ (Bleaney and Bowers, 1952) and our observed ΔE for solution we have calculated f^2 , which comes out as 0.636; now taking mean of these two values we have calculated J utilising $\bar{\mu}$ and ΔE values for solution which is found to be $\approx -270 \text{ cm}^{-1}$. If one calculates f^2 with $J = -315 \text{ cm}^{-1}$ as in crystal and $\bar{\mu}$ and ΔE for the solution f^2 comes out as 1.022 which is inadmissible. This anomaly may be attributed to the value of J which should be different in different states.

An examination of f^2 values in different states suggests that the most probable value of f^2 should be $\approx .67$, which gives the parameter $J = -275 \text{ cm}^{-1}$.

Anomalous resonance absorption spectra similar to copper acetate has been observed by Abe (1953) in case of copper propionate monohydrate. Our magnetic measurements on the moment of Cu^{++} ion in $\text{Cu}(\text{CH}_3\text{CH}_2\text{COO})_2 \cdot \text{H}_2\text{O}$ salt in state of solution shows that $\bar{\mu} = 1.56$. These findings point to the fact that the

behaviour of Cu^{++} ions in the propionate will be similar to that of Cu^{++} ions in the acetate. Hence expression (6) is applicable in this case also.

Supplying experimental g -value and our observed ΔE for copper propionate in expression (3) we have calculated f^2 which comes out to be 0.72 (table II). Now substituting this values of f^2 and using μ value for solution in the expression (6) we have calculated J the exchange integral which comes out to be -244 cm^{-1} . Since f^2 in solution is not the same as in solid state, hence this value of J will be slightly different in state of solution. Due to want of $\bar{\mu}$ value for the crystal it is not possible to suggest a most probable value for f^2 but a comparison of the solution $\bar{\mu}$ values of acetate and propionate suggests that f^2 should be almost like the acetate; hence taking f^2 as 0.68, J comes out $\approx -230 \text{ cm}^{-1}$.

The behaviour of Cu^{++} ion in formate from our observed ΔE value seems to be alike the acetate and propionate; but paramagnetic resonance spectrum as observed by Abe (1953) does not support this. The moment value as observed by us in state of solution goes to suggest that this is the limiting case between the Tutton salts with $\bar{\mu}$ values more than the spin-only value on one side and the acetate and propionate on the other with $\bar{\mu}$ values less than the spin-only value.

If Cu^{++} ions in formate behave like that in Tutton salts then f^2 from expression (5) comes out to be .028 which is inadmissible. This led us to presume that the behaviour of Cu^{++} ion in formate should be like those of the acetate and propionate.

On evaluating f^2 from the observed g -value in solid state and ΔE value from solution, it comes out as .58; but f^2 in state of solution should be different. A study of the f^2 values for propionate and acetate suggests that the probable value of $f^2 \approx .69$. This when substituted in (6) gives $J = -130 \text{ cm}^{-1}$, with $\bar{\mu} = 1.74$ as given in Table II. It is observed that the exchange integral in these three salts are in the right direction.

The acetate, propionate, formate and the amino-salts suggest that f^2 is really made up of two factors arising from the σ -orbital overlap and the other from π -orbital overlap eg., in the amino-salts f^2 may be, $f_{\sigma}^2 \sim .62$ and $f_{\pi}^2 \sim .85$ making $f^2 = f_{\sigma}^2 + f_{\pi}^2 = .53$ as observed (very nearly so), while for the acetate, propionate and formate $f_{\sigma}^2 \sim .75$ and $f_{\pi}^2 \sim .9$ giving $f^2 = .68$ which is very near the observed values.

ACKNOWLEDGMENTS

The work was carried out at the Physics laboratories of Agra College, Agra. We wish to express our sincere thanks to the Universities Grants Commission due to whose generous grant it was possible to purchase the 'UVISPEK' spectrophotometer which enabled us to carry out this piece of work.

Our sincere thanks are also due to Professor A. Bose, D.Sc., F.N.I., for his helpful criticisms and concrete suggestions.

REFERENCES

- Abragam, A. & Pryce, M. H. L., 1951, *Proc. Roy. Soc.*, **A206**, 165.
 Abe, H., 1953, *Phys. Rev.*, **92**, 1572.
 Abe, H., Ono, Hayashi, Shimada, Iwanaga, 1954, *J. Phys. Soc. Japan*, **9**, 814.
 Birch, J., 1928, *J. de Physique*, **9**, 137.
 Bothe, H., 1929, *Ann. Physik*, **3**, 133.
 ——— 1930, *Z-Physik*, **60**, 218.
 Bose, A., 1948, *Ind. Jour. Phys.*, **22**, 483.
 Bleaney, B., Penrose, R. P., & Plumptre, B. I., 1949, *Proc. Roy. Soc.*, **A198**, 406.
 Baugley, D. M. S. & Griffiths J. H. E., 1950, *Proc. Roy. Soc.* **201**, 366.
 Boso, A. & Mitra, S. K., 1952, *Ind. Jour. Phys.*, **26**, 393.
 Bleaney, B. & Bowers, K. D., 1952, *Proc. Roy. Soc.*, **214**, 454.
 Bleaney, B., Bowers, K. D. & Pryce, M. H. L., 1955, *Proc. Roy. Soc.* **228**, 166.
 Bleaney, B., Bowers, K. D. & Ingram, D. J. E., 1955, *Proc. Roy. Soc.*, **228**, 147.
 Boso, A., Mitra, S. K. & Dutta, S.K., 1957, *Proc. Roy. Soc.*, **239**, 165-183.
 Chakravarty, D. C., 1942, *Science & Culture*, **7-3**, 140.
 Dreisch & Trommer, 1937, *Z. Phys. Chem. B.*, **37**, 37.
 Gorter, C. J., 1932, *Phys. Rev.*, **42**, 437.
 Guha, B. C., 1951, *Proc. Roy. Soc.*, **A206**, 353.
 Janes, R. B., (1935), *Phys. Rev.*, **48**, 78.
 Krishnan, K. S. & Mookherji, A., 1936, *Phys. Rev.*, **50**, 860.
 ——— 1938, *Phys. Rev.*, **54**, 533-541.
 Krishnan, K. S., 1939, *Nature*, **143**, 600.
 Kozyrev, B. M., 1957, *Acad. Sciec of the USSR, Physical series No. 6*, **21**, 828-832.
 Mookherji, A., 1945, *Ind. Jour. Phys.*, **19**, 63.
 Okamura & Date, 1954, *Phys. Rev.* **92**, 314.
 Owen, J., 1954, *Proc. Roy. Soc.*, **A227**, 183.
 Polder, D., 1942, *Physica*, **9**, 713.
 Schenstone & Wilots, 1951, *Phys. Rev.*, **41**, 208.
 Van Vleck, J. H., 1932, *The theory of electric and magnetic susceptibilities*, Oxford Press,
 Wolo, L. A., 1929, *Nature*, **124**, 575-576.
 Tromam, R. S., 1953, *Proc. Roy. Soc.*, **66**, 118.

A TEST FOR HULBURT-HIRSCHFELDER POTENTIAL FUNCTION

N. R. TAWDE AND M. R. KATTI

DEPARTMENT OF PHYSICS, KARNATAK UNIVERSITY, DHARWAR

(Received, December 22, 1958)

ABSTRACT. Following up the modification recently reported of Hulburt-Hirschfelder potential function for the prediction of the molecular vibration-rotation constant α_e , it is shown that similar predictions of the anharmonicity constant $\omega_e x_e$ are possible by suitable substitutions. The comparison of the calculated data with the experimental data on $\omega_e x_e$ shows that in this case too, the H-H function works out much better than Morse's.

In a recent paper (Tawde and Katti, 1959), the efficacy of the original Hulburt-Hirschfelder (H. H., 1941) function was demonstrated by introducing in it suitable modifications. The test applied for the efficacy was the prediction of certain verifiable molecular constants. Although the original function contained all the five usual molecular constants, ω_e , $\omega_e x_e$, B_e , D_e and α_e , they were, in the ultimate analysis, reduced to four, leaving the vibration-rotation interaction constant α_e to be predicted from the knowledge of the four. Such transformation was brought about by the incorporation of Morse-Pekeris relation which made one of the constants of H-H relation independent of α_e . The modified expression proved highly successful in reproducing α_e data within $\pm 15.3\%$.

Such expressions are also possible to be tested for their capacity to predict the anharmonic constant $\omega_e x_e$. Although earlier we tried to explore this possibility in the case of H-H function in the above manner, we did not succeed. While pursuing this issue further, we could now succeed in suitably modifying the function to predict $\omega_e x_e$ in the same way as the constant α_e . This paper presents this study, as the results seemed very promising.

The development of modified *H-H* equation has been shown in full steps by (Tawde and Katti, 1959) for evaluation of α_e . Now for the purposes of deriving $\omega_e x_e$, we have their equations (3.2) and (3.3) as follows :

$$\begin{aligned} X &= 3a(c-1) \\ Y &= a^2[7+12c(b-1)] \end{aligned}$$

where the Morse constant $a = 1.2177 \times 10^7 \omega_e(D_e/\mu_A)^{1/2}$ and *H-H* constants $c = 1 + a_1(D/a_0)^{1/2}$, $b = 2 - [7/12 - Da_2/a_0]/c$ with $a_0 = \omega_e^2/4B_e$, $a_1 = -1 - \alpha_e\omega_e/6B_e^2$, $a_2 = 5/4a_1^2 - 2\omega_e x_e/3B_e$. Here X and Y need to be made independent of $\omega_e x_e$ so that by assuming the other constants ω_e , D_e , B_e and α_e , one could get

at the value of $\omega_e x_e$. The only empirical relation that we could think of was $D_e = \omega_e^2/4\omega_e x_e$. This is a quantity derived from Morse relation and since it is the basic part of H-H function, one could justify the use of this expression in the present set-up. Thus substituting $\omega_e x_e = \frac{\omega_e^2}{4D_e}$ in the expression for a_2 above, we get

$$a_2 = 5/4a_1^2 - \omega_e^2/6B_e D_e$$

This makes Y independent of $\omega_e x_e$ and X does not involve $\omega_e x_e$ at all.

This modified expression a_2 allows predictions to be made for $\omega_e x_e$. We have therefore calculated their values in the same set of 23 diatomic molecules,

TABLE I

Diatom	Morse % error (Varshni, 1957)	H-H % error (present paper)
H ₂	+ 7.0	+24.5
ZnH	+52.9	-14.6
CdH	+78.8	+ 0.6
HgH	+55.6	-15.2
CH	+ 8.2	+12.3
OH	+13.0	+13.9
HF	-11.3	+ 6.8
HCl	+15.3	+13.0
HBr	+22.8	+11.1
HI	+30.0	+19.0
Li ₂	+37.3	+ 3.3
Na ₂	+44.3	-13.2
K ₂	+44.6	-23.5
N ₂ ¹	(+58.0)	(+19.0)
N ₂ ²	+20.5	+13.4
P ₂	+32.5	+ 5.0
O ₂	+23.0	+11.4
SO	+57.2	+18.4
Cl ₂	- 1.7	-13.2
Br ₂	+41.8	-18.5
I ₂	+49.8	- 3.9
IOI	+43.4	+10.9
CO(1)	(+17.1)	(+ 7.6)
CO(2)	(+11.3)	(+ 6.6)
CO(3)	- 3.5	- 3.6
NO(1)	(+48.5)	(+14.2)
NO(2)	+21.9	+ 9.7
Average	±31.2	±12.1

which we have earlier used to prove the efficacy of the $H-H$ function in terms of α_e . The calculated results when compared with observed data give errors which are recorded as percentage errors in Table I. As Morse function is the most universally used function we are giving the percentage errors (cf. Varshni, 1957) produced by Morse function too, for comparison, in order to bring out the relative merits of the present results.

It may be noted from Table I that the average percentage error ± 12.1 obtained with $H-H$ function is significantly lower than that due to Morse, viz. ± 31.2 . The performance of $H-H$ function in relation to the other functions on the basis of percentage errors is shown in Table II. The figures for other functions are taken from Varshni. It may be noted that the only function which stands superior to $H-H$ function is the empirical one. Thus latter has also been found to be the best among the functions examined by Varshni

TABLE II

Function	% Error
Morse	± 31.2 (a)
Rydberg	± 23.1 (a)
First	± 18.2 (a)
Seventh	± 13.6 (a)
Lippincott	$+12.7$ (a)
Hulburt & Hirschfelder	± 12.1 (b)
Empirical	± 11.1 (a)

(a) Varshni, (b) the present paper.

Further the $H-H$ function which was shown to be superior in making the estimates of α_e with $\pm 15.3\%$ by (Tawde and Katti, 1959) has given a better accuracy for $\omega_e x_e$, viz. ± 12.1 on the lines of the development of $H-H$ expression indicated above. This observation fits in the general conclusion arrived at by Varshni that for any function, $\omega_e x_e$ can be estimated to a greater degree of accuracy than α_e .

REFERENCES

- Hulburt, H. M. and Hirschfelder, J. O. 1941, *J. Chem. Phys.* **9**, 61.
 Tawde, N. R. and Katti, M. R., 1959, *Ind. J. Phys.*, **33**, 18.
 Varshni, Y. P. 1957, *Rev. Mod. Phys.* **29**, 664.

RAMAN SPECTRA OF SOLUTIONS OF ETHYLENE DICHLORIDE, ETHYLENE DIBROMIDE AND ETHYLENE CHLORHYDRIN AT LOW TEMPERATURES*

MONOMOCHAN MAZUMDER

OPTICS DEPARTMENT, INDIAN ASSOCIATION FOR THE CULTIVATION
OF SCIENCE, CALCUTTA-32.

(Received, January 5, 1959)

ABSTRACT. The Raman spectra of 25% solutions in ethyl alcohol of ethylene dichloride at 30°C, -60°C and -180°C, of ethylene dibromide at 30°C and -5°C and of ethylene chlorhydrin at 30°C - 80°C, and -180°C have been studied and the ratio of intensities of the lines 654 cm^{-1} and 755 cm^{-1} in the first case, 551 cm^{-1} and 660 cm^{-1} in the second case and 662 cm^{-1} and 750 cm^{-1} in the third case has been determined quantitatively. It has been observed that in the case of solutions of ethylene dichloride and ethylene dibromide the number of gauche type of molecules tends to diminish at lower temperatures while in the case of the pure liquids the number diminishes with the rise of temperature. In the case of solution of ethylene chlorhydrin the change in the ratio of intensity of the lines mentioned above is smaller and the ratio increases at lower temperatures. It is pointed out that these results cannot be explained on Wada's (1954) theory and that the hypothesis of virtual linkages between the hydrogen atoms of the OH groups of neighbouring solvent molecules and the chlorine and bromine atoms of the molecules of the liquids can explain the results satisfactorily.

INTRODUCTION

The abrupt change in the ratio of intensity of the two Raman lines 654 cm^{-1} and 755 cm^{-1} of ethylene dichloride which takes place when the liquid at 25°C is transformed into vapour at 170°C was first demonstrated by Morino *et al* (1941). Watanabe *et al* (1942) explained the results by assuming that the energy-difference of the two rotational isomers, namely *trans* and *gauche*, of ethylene dichloride increases with the change from the liquid to the vapour state. The present author (1953), however, studied the Raman spectrum of gaseous ethylene dichloride at 135°C and measured the ratio of intensity of the lines 654 cm^{-1} and 755 cm^{-1} which was found to be 1 : 4.5, while the value obtained by Watanabe *et al* (1942) at 170°C is 1 : 5. This shows that the ratio does not change very much with the change of temperature of the vapour from 135°C to 170°C. Watanabe *et al* (1943) tried to explain the change in the energy-difference due to the change of state mentioned above by assuming that in the liquid state the gauche molecule acquires an excess of electrostatic energy which is equal

* Communicated by Professor S. C. Sirkar.

to $\mu^2(c-1)/(2e+1)a^3$, where c is the dielectric constant, μ the permanent electric moment of the gauche molecule and a is the radius of the cavity of the solute molecule. They showed that the influence of this electrostatic energy would diminish the energy-difference of the two types of molecules to a very small value in the liquid state.

If the liquid were dissolved in a solvent having non-polar molecules, the dielectric constant of the medium would be expected to be much lower than that of the pure liquid and the energy-difference of the trans and gauche molecules would be larger than that in the pure liquid. When, however, the solution is further diluted the dielectric constant of the medium is not likely to change appreciably and hence there should not be any appreciable change in the energy-difference of the two types of molecules. Banerjee (1954), however, observed that the ratio of intensity of the lines 654 cm^{-1} and 755 cm^{-1} of ethylene dichloride diminishes when the liquid is dissolved in heptane and cyclohexane to make a 65% solution and that the ratio diminishes further when the concentration is diminished to 35% in each case. Very recently, the present author (1958) studied the infra-red absorption spectra of solutions of ethylene dichloride in carbon tetrachloride, heptane and methyl cyclohexane of different concentrations and observed that the ratio of the integrated intensities of the absorption peaks 1297 cm^{-1} and 1236 cm^{-1} in the case of 20% solutions in heptane and methyl cyclohexane is less than that for the pure liquid and that the ratio diminishes further when the strength of the solution is diminished to 3%. In the case of solution in carbon tetrachloride the changes in the ratio mentioned above are much smaller. This indicates that probably the changes in the energy-difference brought about by the electrostatic field in the solution are not responsible for the observed change in the intensities of the two lines.

The hypothesis put forward by Watanabe *et al* (1943) mentioned above would, however, be tested more conclusively by changing the temperature of the solution and finding out whether the relative intensities of the two lines change in accordance with the energy-differences derived from their hypothesis. With this object in view the Raman spectra of solutions of ethylene dichloride, ethylene chlorhydrin and ethylene dibromide in ethyl alcohol at different temperatures below 30°C and also of the first two solutions at -180°C have been investigated and the relative intensities of the lines 654 cm^{-1} and 755 cm^{-1} in the case of ethylene dichloride, 662 cm^{-1} and 750 cm^{-1} in the case of ethylene chlorhydrin and 551 cm^{-1} and 660 cm^{-1} in the case of ethylene dibromide have been measured. These results have been discussed in the present paper in the light of the hypothesis put forward by Watanabe *et al* (1943).

EXPERIMENTAL

Dehydrated ethyl alcohol was chosen as the solvent and was distilled several times under reduced pressure before being used in the solutions. The experimental

arrangement used to record the Raman spectra of the solutions at low temperatures is shown in figure 1. The scattered light was reflected by the right angled prism, P, attached at the bottom of the Dewar vessel and was focussed on the slit of the spectrograph. The container of the liquid, C, was placed inside the Dewar vessel dipped in ethyl alcohol which was then gradually cooled by adding small quantities of liquid oxygen to it until the required temperature was attained. Liquid oxygen had to be added frequently to keep the temperature fairly constant. The temperature was read with the pentane thermometer, T.

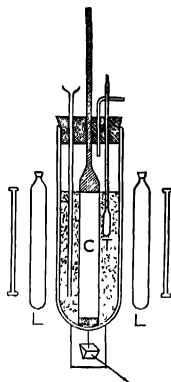


Fig. 1.

The Raman spectra of 25% solution of ethylene dichloride, ethylene dibromide and ethylene chlorhydrin at -60°C , -5°C and -80°C respectively were photographed using this arrangement. The Raman spectra of the last two solutions in the frozen state at -180°C were also photographed by keeping the sample tube immersed in liquid oxygen.

A Fuess glass spectrograph having a dispersion of about 11 A.U. per mm in the 4046 A.U. region was used to record the spectra. Microphotometric records of the lines were taken with a Kipp and Zonen type self-recording microphotometer. Using blackening log-intensity curves drawn with the help of intensity marks taken with known slit-widths and continuous radiation the intensities of the lines mentioned above of ethylene dichloride, ethylene dibromide and ethylene chlorhydrin in the pure state and in solutions at different temperatures, were measured quantitatively.

RESULTS AND DISCUSSION

Microphotometric records of the lines 654 cm^{-1} and 755 cm^{-1} due to pure ethylene dichloride at 30°C and its solution in ethyl alcohol at 30°C and -60°C ,

551 cm^{-1} and 660 cm^{-1} due to pure ethylene dibromide at 30°C and its solution at 30°C and -5°C, 662 cm^{-1} and 750 cm^{-1} due to pure ethylene chlorhydrin at 30°C and its solution at 30°C and -80°C are reproduced in figures 2, 3 and 4 respectively. The values of the ratio of intensities of the two lines observed in each case mentioned above are given in Tables I, II and III.

TABLE I

Raman spectra of ethylene dichloride
Value of I_{654}/I_{755}

Pure liquid		Solution in EtOH		
at 30°C (Watanabe <i>et al</i> 1942)	at -25°C	at 30°C	at -60°C	at -180°C
1 : 1.8	1 : 1.5	1 : 1.3	1 : 1.5	0 : 3

TABLE II

Raman spectra of ethylene dibromide
Value of I_{551}/I_{660}

Pure liquid at 30°C	Solution in EtOH	
	at 30°C	at -5°C
1 : 7	1 : 6	1 : 6.2

TABLE III

Raman spectra of ethylene chlorhydrin
Value of I_{662}/I_{750}

Pure liquid at 30°C	Solution in EtOH		
	at 30°C	at -80°C	at -180°C
2 : 1	2.2 : 1	2.5 : 1	4 : 1

(i) *Ethylene dichloride*

It can be seen from Table I and figure 2 that the ratio of the intensity of the lines 654 cm^{-1} and 755 cm^{-1} of ethylene dichloride changes from 1 : 1.8 to 1 : 1.3 when the liquid is dissolved in ethyl alcohol to make a 25% solution and that the ratio becomes 1 : 1.5 when the solution is cooled down to -60°C . Moreover, when the solution is solidified and cooled to -180°C the line 654 cm^{-1} disappears and the line 755 cm^{-1} appears with its intensity relative to that of the line 300 cm^{-1} increased to about double the value for the liquid state. These results, therefore, clearly show that if the line 654 cm^{-1} be assigned to the gauche configuration, the number of such molecules increases when the liquid is dissolved

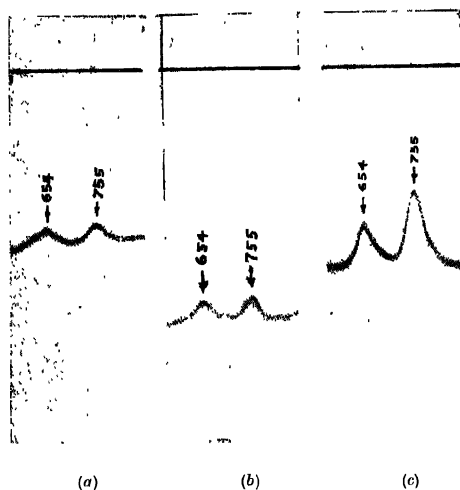


Fig. 2 Microphotometric records of the Raman spectra of ethylene dichloride.

(a) Solution at -60°C .

(b) Solution at 30°C .

(c) Pure liquid at 30°C .

in alcohol and that the number then diminishes when the temperature of the solution is lowered to -60°C . On the other hand Watanabe *et al* (1942) have shown that in the case of pure ethylene dichloride the ratio I_{654}/I_{768} increases from 1 : 2 to 1 : 1.5 when the temperature of the liquid is lowered from 150°C to -25°C . Wada (1954) suggested that the energy of the gauche molecule is lowered in the state of aggregation owing to the influence of the field due to the surrounding permanent dipoles on the permanent moment of the molecules. According to his calculations in the pure liquid both the gauche and the trans molecules are of the same energy, while in solution in methyl alcohol the energy

of the gauche molecule is lower than that of the trans molecule by 260 cal/mole. Hence the number of gauche molecules would increase at lower temperatures in solution in methyl alcohol and similar results would be expected in the case of solution in ethyl alcohol also. Actually, however, it is observed that in the case of solution in ethyl alcohol the number of gauche molecules increases with rise of temperature, while in the case of pure liquid the number diminishes with the rise of temperature. Thus the results for the solution and the liquid at low temperatures are not in agreement with the predictions of Wada's theory.

From the argument stated above, it is clear that the ratio of population of the two types of molecules is not determined by the energy-difference of the trans and gauche molecules in the liquid, as postulated by Watanabe *et al* (1942). On the other hand, it can be explained by arguing that the OH groups of the alcohol molecules are linked to one of the chlorine atoms of ethylene dichloride and the random distribution of the alcohol molecules and their restricted freedom of motion about the C-C bond produce the change from the trans to the gauche configuration. When, however, the solution is cooled to a very low temperature the freedom of movement of the solvent molecules decreases and both the chlorine atoms of the ethylene dichloride molecules form virtual linkage with hydrogen atoms of the neighbouring molecules and ultimately the two virtual linkages come in the same plane to produce the trans configuration in the solid state.

(ii) *Ethylene dibromide*

The results given in Table II and the microphotometric records reproduced in figure 3 show that the ratio of the intensity $I_{0.51}/I_{4.00}$ slightly increases when ethylene dibromide is dissolved in ethyl alcohol and the ratio tends to diminish slowly when the solution is cooled down to -5°C . So, the changes with lowering of temperature of the solution are similar to those observed in the case of ethylene dichloride.

According to the calculations made by Wada (1954) the decrease of energy-difference between gauche and trans configuration with liquefaction of the vapour and dissolution in methyl alcohol would be respectively 1270 and 1530 cal/mole in the case of ethylene dichloride but the values are 900 and 1170 cal/mole in the case of ethylene dibromide. So, the gauche molecules of ethylene dibromide should have energy higher than that of the trans molecules in the solution, but in the case of ethylene dichloride the reverse is true. The changes in the ratio of the numbers of the two types of molecules with change of temperature are, however, similar in both the cases. Hence the cause of this change is different from the energy-difference of the two types of molecules in solution and evidently the formation of virtual linkage mentioned above takes place in both the cases. The results of investigation on the infra-red absorption spectra of ethylene dichloride in different solvents reported earlier (Mazumder, 1958) support such a conclusion.

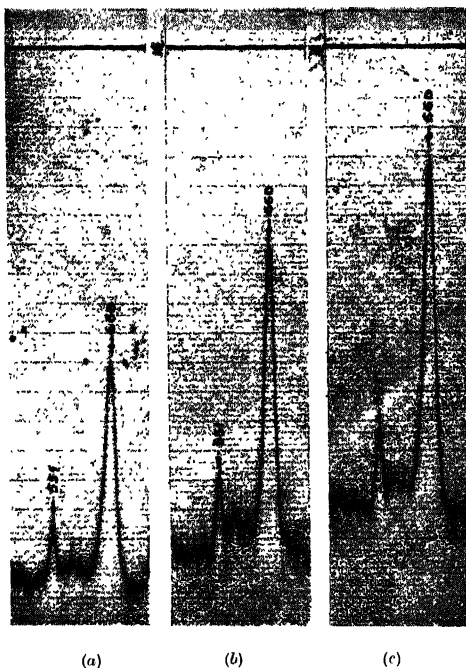


Fig. 3. Microphotometric records of the Raman spectra of ethylene dibromide.

- (a) Solution at -5°C .
- (b) Solution at 30°C .
- (c) Pure liquid at 30°C .

(iii) Ethylene chlorhydrin

It can be seen from Table III and figure 4 that the ratio of the lines 622 cm^{-1} and 750 cm^{-1} becomes 2.2 : 1 when ethylene chlorhydrin is dissolved in ethyl alcohol and the ratio increases slightly to 2.5 : 1 when the solution is cooled down to -80°C . In the case of pure liquid the ratio is 2 : 1. So the ratio increases very slightly when the liquid is dissolved in alcohol. Mizushima *et al* (1940), however, observed a larger change in the ratio of intensity of the two lines when they dissolved the liquid in water. Evidently, the greater number of OH groups around each molecule in the solution is responsible for the difference. Mizushima *et al* (1939) had earlier studied the infra-red absorption due to second harmonic

of the OH vibration and concluded that in the vapour there are two configurations of the molecules, one formed by weak attraction between the chlorine atoms and the hydrogen atoms of the OH group in the same molecule and the other the trans configuration. In the liquid they observed only the presence of the former configuration. In the Raman spectrum of the liquid also there is no line in the vicinity of 3350 cm^{-1} due to the OH valence oscillation. Hence it is evident that most of the molecules in the liquid are associated with each other through

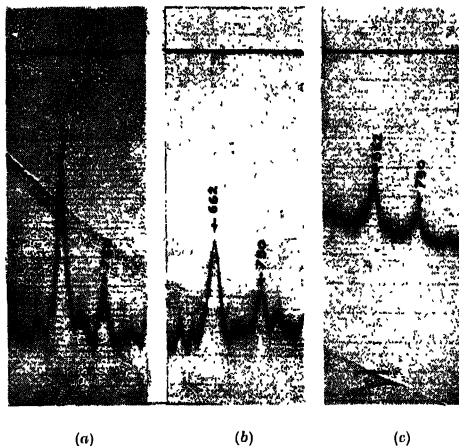


Fig. 4. Microphotometric records of the spectra of ethylene chlorhydrin.

- (a) Solution at -80°C .
- (b) Solution at 30°C .
- (c) Pure liquid at 30°C

hydrogen-chlorine virtual linkages and this is responsible for the larger intensity of the line 662 cm^{-1} in this case than in the case of ethylene dichloride and ethylene dibromide. In the vapour this line is very weak (Mazumder, 1955) and therefore most of the molecules are single. Calculation of frequencies of the modes of vibration of the molecules carried out by Mizushima *et al* (1951) shows that the line 750 cm^{-1} is due to the trans configuration. Hence the other configuration is formed by association of single molecules and has energy lower than that of the trans configuration as assumed by Mizushima *et al*. This explains the wide discrepancies between the values of energy-difference calculated by them and those reported by Zumwalt and Badger (1940). As the association is rather strong and most of the molecules are associated in the liquid, in the solution in alcohol not much change in the number of associated molecules occurs.

When, however, the solution is cooled to -80°C the number of such molecules increases and when the solution is frozen all the molecules become associated and the line 750 cm^{-1} disappears. When the pure liquid is frozen the line 750 cm^{-1} appears with a very feeble intensity (Bishui, 1948) which shows that only a few percentage of the molecules are of the trans configuration in the solid state.

ACKNOWLEDGMENT

The author is indebted to Professor S. C. Sirkar, D.Sc., F.N.I., for his kind interest and helpful guidance throughout the progress of the work.

REFERENCES

- Banerjee, S. B., 1954, *Ind. J. Phys.*, **28**, 205
Bishui, R. M., 1948, *Ind. J. Phys.*, **22**, 333.
Mazumder, M., 1953, *Ind. J. Phys.*, **27**, 406.
„ 1955, *Ind. J. Phys.*, **29**, 361.
„ 1958, *Ind. J. Phys.*, **32**, 451.
Mizushima, S., Kubota, A. and Morino, Y., 1939, *Bull. Chem. Soc., Japan*, **14**, 15.
Mizushima, S., Morino, Y. and Nakamura, S., 1940, *Sc. Papers I.P.C.R. (Tokyo)*, **37**, 205
Mizushima, S., Shimizuuchi, T., Miyazawa, T., Abe, K. and Yasuni, M., 1951, *J. Chem. Phys.*, **19**, 1477.
Morino, Y., Watanabe, I. and Mizushima, S., 1941, *Sc. Papers I.P.C.R. (Tokyo)*, **39**, 396.
Wada, A., 1954, *J. Chem. Phys.*, **22**, 198.
Watanabe, I., Mizushima, S. and Morino, Y., 1942, *Sc. Papers I.P.C.R. (Tokyo)*, **39**, 401.
Watanabe, I., Mizushima, S. and Masiko, Y., 1943, *Sc. Papers, I.P.C.R. (Tokyo)*, **40**, 425.
Zurwult, L. R. and Badger, R. M., 1940, *J. Am. Chem. Soc.*, **62**, 305.

Letters to the Editor

The Board of Editors will not hold itself responsible for opinions expressed in the letters published in this section. The notes containing reports of new work communicated for this section should not contain many figures and should not exceed 500 words in length. The contributions must reach the Assistant Editor not later than the 15th of the second month preceding that of the issue in which the letter is to appear. No proof will be sent to the authors.

1

STUDIES ON PHASE TRANSITION OF SYNTHETIC



S. RAY AND A. ROY

DEPARTMENT OF MAGNETISM, INDIAN ASSOCIATION FOR THE CULTIVATION OF SCIENCE,
CALCUTTA-32

(Received, January 10, 1959)

The X-ray powder diffraction study of the structural changes of synthetic $\gamma\text{-Fe}_2\text{O}_3 \cdot \text{H}_2\text{O}$ (lepidocrocite, orthorhombic) due to heat treatment by Williams and Thewlis (1931) appears to show that the substance starts being dehydrated to the ferromagnetic $\gamma\text{-Fe}_2\text{O}_3$ (maghaemite, cubic) at about 250°C . The formation of $\gamma\text{-Fe}_2\text{O}_3$ appears to be complete at 300°C . No further change in crystal structure is observed up to 450°C , but at 500°C lines of $\alpha\text{-Fe}_2\text{O}_3$ (haematite, anti-ferromagnetic, hexagonal) appear in the X-ray powder diagram. Presence of $\gamma\text{-Fe}_2\text{O}_3$ is observable at 550°C , but X-ray photographs of the sample heated to higher temperatures show only lines of $\alpha\text{-Fe}_2\text{O}_3$. Later works of Bernal, Dasgupta and Mackay (1957) show that precipitated lepidocrocite begins to lose water at 180°C , and is completely converted into maghaemite and some haematite at 200°C , all maghaemite being converted to haematite below 250°C . A natural crystal of lepidocrocite, according to them, seems to be more stable, and can be heated in air to 235°C without any change. Only at 250°C it is transformed to an oriented texture of a spinel phase and haematite. One half molecule of water begins to come off at about 240°C , and the entire water is lost at about 300°C . The presence of a magnetic phase was observed above 240°C .

Such controversial findings by earlier workers led the authors to undertake a thorough investigation on the subject. $\gamma\text{-Fe}_2\text{O}_3 \cdot \text{H}_2\text{O}$ was prepared by precipitation from dilute solution of ferrous chloride with barium hydroxide in the form of suspension in water, and subsequent slow oxidation at room temperature. The carefully washed final precipitate, dried at room temperature, showed the lines

of lepidocrocite in the X-ray powder diagram. The dehydration curve of this specimen shows that at about 130°C, the sample starts losing water at a rapid rate which continues upto about 160°C, total loss corresponding to about half a molecule of water. Then the rate of loss decreases, so that there is a kink in the curve at about 160°C, which is also corroborated from the X-ray powder photographs showing lines of maghaemite in this region. Magnetic test indicates that the product obtained above 160°C is ferromagnetic. Loss of water is complete above about 260°C. It is very possible that near about 160°C a distinct phase of the oxide, namely, $\text{Fe}_2\text{O}_3 \cdot \frac{1}{2} \text{H}_2\text{O}$ (turgite) (Mellor, 1934) exists, as indicated by the kink in the dehydration curve, the magnetic behaviour, and certain weak new lines in the diffraction pattern, though the existence of such a hydrate has been denied by some authors. The formation of maghaemite is complete above about 260°C.

The differential thermal curve also gives similar results. There is an endothermal peak extending from about 65°C to 145°C, indicating the removal of adsorbed water. Then there is a flat exothermal peak, extending from about 145°C to about 265°C, which shows the formation of maghaemite through the intermediate phase of turgite. A large endothermal peak follows, extending from about 265°C to 370°C, which is however not associated with any structural change as shown by diffraction patterns. This peak may be then due to an order-to-disorder transition of maghaemite associated with the ferromagnetic Curie temperature. Some ferromagnetism, however, still persists upto the middle of the next endothermal peak, extending from 370°C to 475°C, where the transition from maghaemite to haematite seems to be complete as seen from the diffraction pattern. The reason for this is not yet clear.

Detailed investigations comprising of magnetic and X-ray studies are being pursued, and the final results will be published in due course.

Authors express their sincerest gratitude to Prof. A. Bose, D.Sc., F.N.I., for his kind guidance and keen interest in the work, and are also thankful to Mr. A. K. Dutta and Dr. D. R. Dasgupta for helpful discussions.

REFERENCES

- Bernal, J. D., Dasgupta, D. R. and Mackay A. L. 1957, *Nature*, **180**, 645. —
Mellor, J. W., 1234, *A comprehensive Treatise on Inorganic and Theoretical Chemistry*, Vol. **13**, p. 874.
Williams, R. D. and Thewlis, J., 1931, *Trans. Farad. Soc.* **27**, 767.

CALCULATIONS OF THE NUCLEAR QUADRUPOLE COUPLING CONSTANT FOR I_2

D. V. G. L. NARASIMHA RAO

PHYSICS DEPARTMENT, ANDHRA UNIVERSITY, WALTAIR

(Received, February 16, 1959)

ABSTRACT. Certain theoretical studies on the quadrupole coupling constant of I^{127} in I_2 molecule are made following the general principles of Townes and Dailey (1949). The I-I bond is assumed to be one of a covalent type. Effects of sp -hybridization are considered and the results indicate the possibility of considerable amount of hybridization of the bonding orbitals.

INTRODUCTION

Though a number of values of the quadrupole coupling constant eqQ were accumulated for several nuclei in various molecules both from pure quadrupole spectra and also from a study of the hyperfine structure of rotational spectra in the microwave region, theoretical calculations were made only for a few molecules. The fundamental principles underlying the interpretation of the observed data and also some approximate methods for their theoretical evaluation were outlined by Townes and Dailey (1949). It is known that a knowledge of eqQ gives useful information about the pattern of chemical bonding in the molecules. In the description of Townes and Dailey, the charges which influence $q \left(= \frac{\partial^2 v}{\partial z^2} \right)$, the field gradient) at a particular nucleus in the molecule are divided as due to (i) the inner core electrons, (ii) valence electrons and (iii) the electrons and nuclei external to the atom under consideration. The contribution to q of the valence electrons which have a high probability of being found near the nucleus is shown to be larger by an order of magnitude than the contribution due to other charges.

A theoretical study of the ionic character and hybridization in HCl was made by Schatz (1954) in terms of an spd -hybrid valence bond function including an ionic term. The quadrupole coupling constant was found to depend principally on the ionic character and could not distinguish among the various possible sets of hybridization. Similar conclusions were drawn for Cl_2 (Schatz-1954a) and also for CH_3Cl by the same author (1954b).

Calculations of the quadrupole coupling constant of I^{127} in I_2 molecule are made by the present author using a simple model and the results of the investigation are given below.

CALCULATIONS AND RESULTS

Since the two atoms forming the bond are the same, the bond may be assumed to be one of a covalent type. The bonding wave function of I_2 may hence be written on the atomic orbital approximation as

$$\chi_b = A[\psi_{I_1}(1)\psi_{I_2}(2) + \psi_{I_1}(2)\psi_{I_2}(1)]$$

where ψ_{I_1} , ψ_{I_2} are the bonding wave functions of I_1 , I_2 atoms respectively and A is a normalisation factor given as $A = 1/(2+2S^2)^{1/2}$ with S as the overlap integral of ψ_{I_1} and ψ_{I_2} . Assuming only sp-hybridization, the ψ_I 's are

$$\psi_{I_1} = a\psi_I(5s) + b\psi_I(5p_z)$$

$$\psi_{I_2} = a\psi_I(5s) + b\psi_I(5p_z)$$

the z-axis being taken to represent the internuclear axis. The normalization condition gives $a^2 + b^2 = 1$. The wave function of the non-bonding s-electrons (the lone-pair) consequently becomes

$$\chi_{I_{nb}} = (1-a^2)^{1/2}\psi_I(5s) + a\psi_I(5p_z).$$

The iodine quadrupole coupling constant in I_2 may be regarded as due to (i) the electron pair forming the bond, (ii) the pairs of electrons $5p_x$ and $5p_y$ assumed to remain in non-bonding orbitals and (iii) the lone-pair electrons which make a non-zero contribution to eQq since ψ_I is a sp-hybrid function.

The contribution of the first factor is given as

$$2eQ \int \chi_b^2 \frac{(3 \cos^2 \phi - 1)}{r^3} d\tau$$

where Q is the nuclear quadrupole moment of I^{127} . χ_b^2 is the square of the bonding wave function integrated over electron (2) and ϕ , r are the polar co-ordinates of electron (1). Similarly for the contribution of the lonepair we may write

$$2eQ \int \chi_{I_{nb}}^2 \frac{(3 \cos^2 \phi - 1)}{r^3} d\tau$$

To evaluate the second factor we make use of the result that

$$2q_{px} + 2q_{py} + 2q_{pz} = 0$$

(i.e., when the p shell is completely filled, its contribution to q is zero) and hence its contribution is $-2eQq_{pz}$. Making use of the symmetry and orthogonal properties of the wave functions it can easily be seen that the quadrupole coupling constant of I^{127} in the I_2 molecule is given as

$$\begin{aligned} eQq &= \left[b^2/(1+S^2) - 2b^2 \right] eQ \int \psi_{5pz}^2 \frac{(3 \cos^2 \phi - 1)}{r^3} d\tau \\ &= (eQq)_{atomic} [b^2/(1+S^2) - 2b^2]. \end{aligned}$$

The results of the calculations are shown in the table below. Slater type wave functions are used and the required overlap integrals are read from Mulliken's (1949) Master tables. The value of the quadrupole coupling constant of a free I^{127} atom (eQq_{pz}) is assumed as 2500 Mc/s. as given by Townes and Dailey (*i.e.*

$$eQ \int \psi^2_{5p_z} (3 \cos^2 \phi - 1) \frac{\partial \tau}{r^3} d\tau = 2500 \text{ Mc/s })$$

TABLE 1

Percentage <i>s</i> -character	$\frac{eQq}{\text{Mc/s.}}$
0	2725
5	2689
10	2578
15	2450
20	2332
25	2187
26	2161
27	2130
30	2046

The observed value of the quadrupole coupling constant of I^{127} in I_2 is reported to be 2153 Mc/s. (Dehmelt, 1950) from a study of the pure quadrupole spectrum. It may be seen from the table that about 26 percent *s*-hybridization of the bonding orbital is necessary to account for this value. No investigation could be made on the microwave spectrum of I_2 molecule since it is homonuclear and hence the gas value of eQq is not available. The low value of eQq in the solid state as compared to the value assumed for the free atom has been attributed by Townes and Dailey (1952) to the formation of weak intermolecular bonds. The actual *s*-hybridization may be much less than the 26 percent assigned from data on the solid state. But it may be mentioned that even though it is assumed that the molecular eQq is near about the free atomic value of 2500 Mc/s., the bonding orbitals must involve about 10 per cent *s*-character. This happens because of the overlap S between the two bond wave functions. Similar conclusions were reached by Schatz (1954a) for Cl_2 .

The conclusions remain essentially the same also when the calculations are carried out based on the picture of Gordy (1951) with the value of 2153 Mc/s for the atomic eQq of I^{127} as assumed by him.

ACKNOWLEDGMENTS

The author is deeply indebted to Prof. K. R. Rao for his kind and invaluable guidance throughout the progress of work. His grateful thanks are also due to the Council of Scientific and Industrial Research for financial assistance.

REFERENCES

- Dehmelt, H. G., 1950, *Die Naturwissenschaften*, **37**, 398.
Gordy, W., 1951, *J. Chem. Phys.*, **19**, 792.
Schatz, Paul, N., 1954, *J. Chem. Phys.*, **22**, 695.
Schatz, Paul, N., 1954a, *J. Chem. Phys.*, **22**, 755.
Schatz, Paul, N., 1954b, *J. Chem. Phys.*, **22**, 1974.
Townes C. H. and Dailey, B. P., 1949, *J. Chem. Phys.* **17**, 782.
Townes C. H. and Dailey, B. P., 1952, *J. Chem. Phys.* **20**, 35.

CRYSTAL STRUCTURE OF 1,2-CYCLO-PENTENOPHENANTHRENE

B. S. BASAK

PRESIDENCY COLLEGE, CALCUTTA

AND

M. G. BASAK

JHARGRAM RAJ COLLEGE, JHARGRAM, WEST BENGAL

(Received, February 12, 1959)

ABSTRACT. The crystal structure of 1,2-cyclo-pentenophenanthrene has been determined by the Fourier-synthesis method. A qualitative suggestion about the structure was made by Iball (1935). Following are the crystal data: Molecular formula $C_{17}H_{14}$; Monoclinic system: $a = 18.38 \text{ \AA}$; $b = 5.83 \text{ \AA}$, $c = 23.61 \text{ \AA}$; $\beta = 114^\circ-18'$; space-group $B2_1/c$ (Real space-group $P2_1/c-C_{2h}^{11}$). density = 1.23 gm/c.c. at 20°C ; No. of molecules per unit cell ('h' face-centred cell) = 8.0.

Zero-layer and equi-inclination Weissenberg photographs were taken in a Unicam Weissenberg goniometer with copper radiation and the intensities estimated microphotometrically for stronger spots and visually for the weaker ones. The substance was kindly supplied by Dr. Devdas Mukherjee of Scottish Gas Board from Dr. Loudon of the Biochemistry Laboratory, Glasgow University.

In finding out the structure by trial, help was taken of the suggestion made by Iball (loc. cit). After a fairly satisfactory trial structure was arrived at, two projections were made about the a and b axes respectively. Because of the large values of a and c axial lengths, electron densities were calculated at intervals of 3° along them, using 3° strips of Lipson and Beevers. Values were calculated at 6° interval along b axis. Of the 17 carbon atoms, 13 were fairly well resolved in the b axis projection (figure 1). Only a very small number of atoms were resolved in the a axis projection, although the 'y' co-ordinates could be fixed to a fair degree of accuracy from the same. The considerations of the hydrogen atoms have been omitted for the present. Taking the new co-ordinates obtained from these projections, the values of structure factors were calculated when the reliability index R had the values 0.28 for both the $(o\ k\ l)$ and $(h\ o\ l)$ zones, where

$$R = \frac{\sum |F_{obs} - F_{calc}|}{\sum |F_{obs}|}$$

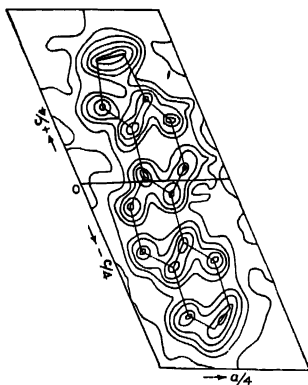


Fig. 1.

This high value of R is due most probably to the presence of a comparatively large number of very weak and absent reflections in these two zones. The coordinates of the carbon atoms of one asymmetric unit (one molecule) are given in Table I. The bond lengths and bond angles are all shown in figure 2. If χ_1, ψ_1, ω_1 be the angles made by the long axis of the molecule formed by joining atoms C_8 and C_{17} with the a, b and c axes respectively and χ_2, ψ_2 and ω_2 be the corresponding angles made by the short axis represented by the straight line joining C_{10} and C_{12} , then

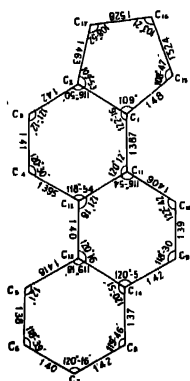


Fig. 2.

$$\begin{array}{ll} \chi_1 = 109^\circ & \chi_2 = 121^\circ - 12' \\ \psi_1 = 90^\circ & \psi_2 = 32^\circ - 22' \\ \omega_1 = 5^\circ - 18' & \omega_2 = 98^\circ - 23' \end{array}$$

The minimum distance of approach between two molecules comes out to be 3.98 Å.

TABLE I
Coordinates of the atoms of one molecule

Atom	$\frac{x}{a}$	$\frac{y}{b}$	$\frac{z}{c}$
C ₁	.1204	.0616	.0656
C ₂	.1629	-.1173	.1060
C ₃	.1948	-.2910	.0804
C ₄	.1827	-.2858	.0174
C ₅	.1656	-.2730	-.1063
C ₆	.1565	-.2701	-.1675
C ₇	.1130	-.0900	-.2060
C ₈	.0797	.0851	-.1824
C ₉	.0539	.2510	-.0991
C ₁₀	.0638	.2410	-.0375
C ₁₁	.1077	.0668	.0035
C ₁₂	.1403	-.1068	-.0212
C ₁₃	.1303	-.1016	-.0832
C ₁₄	.0895	.0773	-.1216
C ₁₅	.0884	.2177	.0993
C ₁₆	.1150	.1320	.1657
C ₁₇	.1596	-.0896	.1664

That the structure is substantially correct is confirmed from the following considerations; (i) The value of $\omega_1 = 5^\circ - 18'$ agrees very well with that of $\omega_1 =$ about 6° as predicted by Bernal (1935) from optical measurements, (ii) The 'b' axis projection of the molecule except the five-membered ring agrees very well with the corresponding electron density projection of phenanthrene crystal as obtained by Basak (1950). The structure obtained agrees with the suggestions put forward by Iball (loc.cit). The bond lengths, bond angles and intermolecular

distances all lie within the limits of values generally obtained in other organic compounds of similar chemical formulae. The structure is now being refined with the help of latest techniques and when completed will give informations about the finer details.

ACKNOWLEDGMENTS

The authors wish to record their gratefulness to Prof. K. Banerjee, D.Sc., F.N.I., Head of the Physics Department, Allahabad University, for his kind interest in the work and also to Dr. S. C. Chakravorty, of the same department for helping them in some of the experimental works.

REFERENCES

- Basak, B. S., 1950, *Ind. Journ. Phys.*, **24**, 309.
Bernal, J. D., 1935, *J. Chem. Soc. London*, pp. 93.
Hall, J., 1935, *Zeits. f. Kryst.* pp. 293.

A SIMPLE PHASE-METER FOR LABORATORY USE

B. CHATTERJEE

INDIAN INSTITUTE OF TECHNOLOGY, KHARAGPUR

(Received, January 27, 1959)

ABSTRACT. A simple phase-meter for ordinary use in a laboratory is described in this article. The construction of this equipment is very simple and the accuracy of measurement is much better than that available with an oscilloscope. It needs no calibration and can be used over a wide range of frequency.

INTRODUCTION

Measurement of phase is quite often needed in a radio engineering laboratory not only for research studies, but also for day-to-day practical work. In experiments on amplifiers, filters etc., it is often necessary to study their phase-response over the frequency range of interest. The ordinary method of phase measurement with an oscilloscope is inaccurate and inconvenient as it is basically a graphical method. Mainly for this reason phase-response of such systems is not always measured for ordinary purposes.

In the simple method of phase measurement described below, the accuracy of measurement is much higher than the ordinary oscilloscope method, and, in addition, it is a very convenient one. The accuracy is of course not as high as the other described earlier by the present author (1957), but it is sufficiently good for ordinary works. The equipment is very simple and can be readily constructed. The same instrument, without any modification, can be used for measuring phase changes in almost all types of electronic systems, covering a very wide range of frequency and signal amplitude. It is hoped to be found useful for measuring phase characteristics of different systems and their variations with frequency.

DESCRIPTION OF THE EQUIPMENT

The phase measuring equipment consists simply of two cathode-followers having a common cathode load as shown in figure 1. The two signals, whose phase difference is to be measured, are applied to the grids of the two tubes through switches as shown. The output of the cathode follower is measured with an a.c. vacuum tube voltmeter. Inputs are fed to both the grids through high resistance (of the order of megohms) potentiometers or some such device for adjusting the levels of input signals to the respective grids.

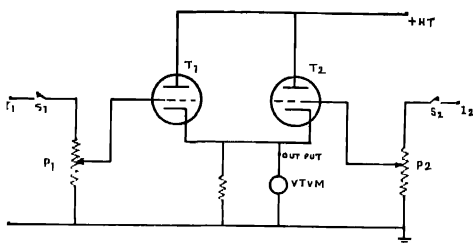


Fig. 1. A schematic circuit diagram of the phase-meter

In order to measure the phase difference between two signals, they are applied to the input terminals I_1 and I_2 (figure 1) respectively. Then the switch S_1 is closed, allowing the input at I_1 to be applied to the grid of the tube T_1 . S_2 is kept open. The potentiometer P_1 is next adjusted to get a convenient reading (V) across the cathode follower output. Then S_1 is opened and S_2 is closed, allowing the input at I_2 to be applied to the grid of T_2 . The potentiometer P_2 is adjusted to get the same voltage reading (V) across the output. Then S_1 is also closed and with both the inputs applied simultaneously, the output voltage (V_0) is measured. It is evident that this output (V_0) is the vector sum of the two inputs (V) which were made to be of equal magnitude.

Thus, $V_0 = 2V \cos \frac{\theta}{2}$ (from figure 2), where θ is the phase difference between the two inputs. [For θ approaching 180° , V_0 may be so small that it may not be possible to measure it in the same scale of the voltmeter as used for measuring V , and a lower voltage scale has to be used. In that case, it is advisable to compare the readings in these two scales and make necessary corrections for discrepancies if any].

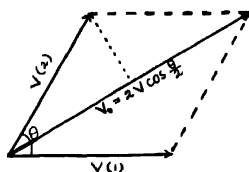


Fig. 2. Illustrating the vector addition of voltages at the output

As V and V_0 are known quantities, we can calculate $\cos \frac{\theta}{2}$ and hence θ . Also, as the same voltmeter (in the same range or in two ranges which are compared with each other and discrepancies corrected for) is used for measuring both V and V_0 and only their ratio is taken for calculating θ , any inaccuracy in the voltmeter itself is eliminated.

It is evident that V_0 will vary from $2V$ to 0 as $\cos \frac{\theta}{2}$ varies from 1 to 0 (the limits of its variations) i.e., θ varies from 0 to 180° —positive or negative. As the cosine of an angle is independent of its sign, no information is obtained regarding the sign of the phase angle. This is also not needed in most cases as the sign (i.e. relative lead or lag) of the phase angle is normally known beforehand.

RESULTS

To determine the accuracy of measurement of the instrument voltages having known phase shifts (introduced by standard circuit components) were applied to the two input terminals of the above meter and the phase measurements were made at different frequencies, as described in section 2. Known phase shifts were introduced by a combination of a standard condenser (of $0.01\mu F$) and a standard resistance (of $1K\Omega$) as shown in figure 3(a) and the voltages between terminals (1) and (2) were applied to the phase-meter for the measurement of phase shift produced. The measurements were carried out at different frequencies from 100 c/s to 20 Kc/s. The theoretically calculated values of phase-shifts produced by the above R - C combination of figure 3(a) at different frequencies were plotted and the curve in figure 3(b) shows this calculated variation of phase with frequency. The observed values of phase-shifts at different frequencies, as were experimentally measured by our phase-meter, were shown as circles on the same graph. A good agreement is observed between the calculated and measured values.

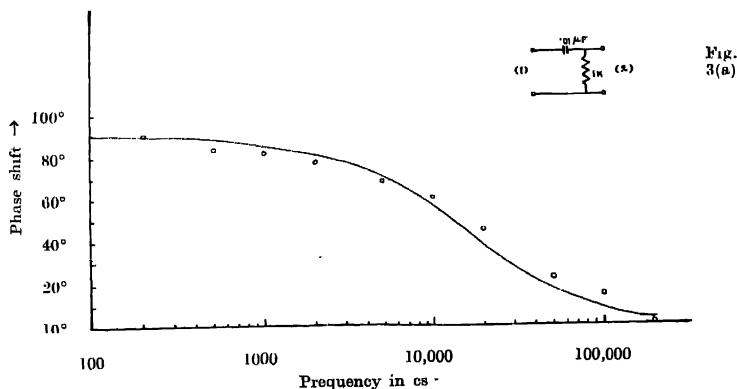


Fig. 3(a). R-C network with standard components for producing known phase-shifts.

Fig. 3(b). Variation of phase with frequency in the above network. The smooth line gives the calculated values and the circles indicated the values as measured with the given phase-meter.

Measurements were also carried out on phase-shifts produced by (1) a low frequency amplifier (untuned) and (2) a high frequency amplifier (tuned). The phase-shifts ϕ produced between the inputs and the output of an R - C coupled amplifier at different frequencies were measured and the relative phase-shift $\theta [|\theta| = 180^\circ - |\phi|]$ of the output voltage at different frequencies, with respect to the mid-frequency phase, are plotted in figure 4. The calculated values of phase-shifts at different frequencies are also shown dotted on the same graph. A good agreement is observed. But the agreement between the calculated and measured values in this case (as also in figure 5) is not as good as in figure 3.

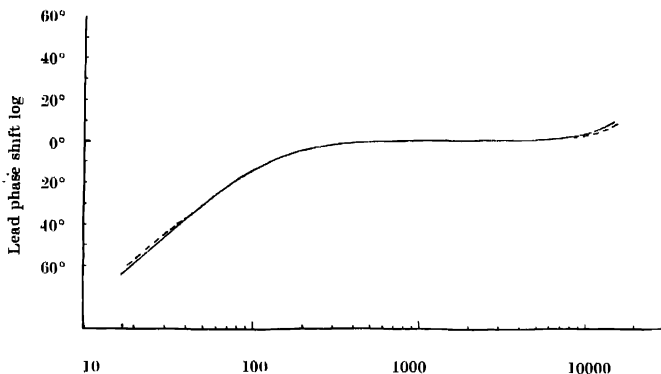


Fig. 4 Variation of phase with frequency of an R - C coupled amplifier, as measured with the given phase-meter. The dotted line shows the calculated values.

Figure 5 shows a similar measurement in a single-tuned amplifier with its tuning frequency at 440Kc/s. The observed results of phase-shifts with frequency are shown by the full line curve and the dotted line shows the calculated values. Here also, a more or less good agreement is observed. As the values of the components used in this (as also the R - C coupled amplifier) are not known with so high precision as that for the standard components (in figure 3), the calculated values of phase-shifts are themselves not accurate. Hence, a larger discrepancy between the calculated and observed values is also expected.

DISCUSSIONS

By selecting a proper range for the V.T.V.M. and adjusting the potentiometers, the output voltage V (for a single input) may be made equal to half the full-scale reading. In that case the V.T.V.M. reading will be proportional to $\cos \frac{\theta}{2}$. As the scale of a V.T.V.M. (like that of Philips type GM6017) meter has normally about 100 divisions or more the accuracy of measurement of $\cos \frac{\theta}{2}$ becomes of the order of 1 in 100. This makes the accuracy of phase measurement of an order of

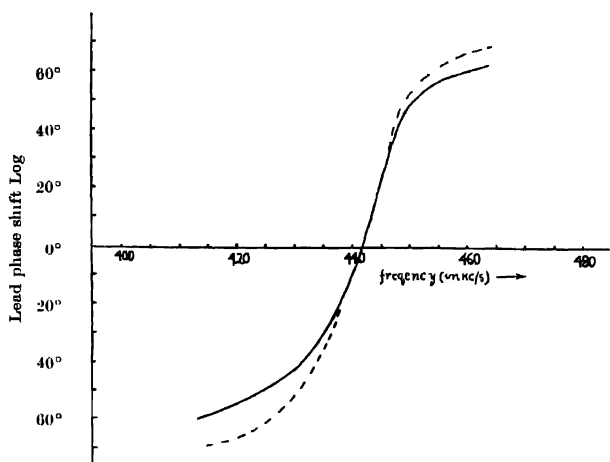


Fig. 5. Variation of phase with frequency of a single tuned voltage amplifier, as measured with the given phase-meter. The dotted line shows the calculated values.

about 2° and this is much better than that available with an oscilloscope. As $\cos \frac{\theta}{2}$ is not a linear function of θ , the accuracy of measurement will of course differ with different values of θ . But it is approximately about 2° except for very small values of θ . The accuracy will be somewhat less for θ approaching zero degree, as in that case $\cos (\theta/2)$ changes very little with θ .

As the instrument uses only cathode followers with resistive load, it can work satisfactorily over a wide range of frequency. With proper choice of tubes and circuitry, accurate results can be obtained from a few cycles per sec. up to a high frequency in the hundred megacycles range. The accuracy is not lowered even if the cathode follower gain falls somewhat at higher frequency. As the same V.T.V.M. is used to measure both V_0 and V , their ratio $\left(2\cos \frac{\theta}{2}\right)$ remains unaffected even if the cathode follower gain falls much below unity. It also gives linear operation over a large range of input voltage.

The major source of error at high frequency is the stray shunt capacitance across the input and output circuits of the cathode follower which cause undesirable (and unknown) phase changes. This is more important at the input end, where, to prevent loading of the circuit under test, a high resistance potentiometer is used. As the potentiometer settings for the two inputs generally differ, different amounts of phase-shifts will be introduced in the two signal inputs and the measurement will be in error. To prevent such errors caused by unequal

phase shifts introduced at the two input terminals, specially when the two signal intensities differ much in amplitude, an arrangement similar to that in figure 6 may be used. The signal having the larger amplitude is passed through a cathode follower having a variable load resistance (R_K) and its amplitude at the phase meter input terminal I_1 is made to be equal to that of the other signal by varying R_K . As R_K is small, the effect of shunt capacitance across R_K can be neglected. Also, as both the signals are fed to the same resistor R_g , the phase-shifts produced by them (R_g) are equal and the relative phase difference between the two signals remain unchanged at the phase meter tube grids. As such no error is introduced.

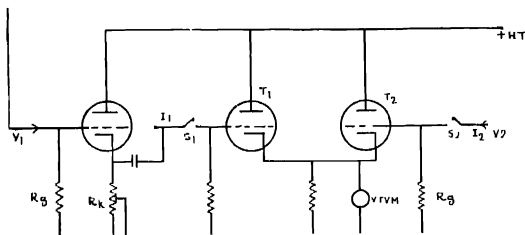


Fig. 6. A modified version of figure 1 for measuring phase at high frequencies.

As the measurement of phase needs a voltage measurement across the cathode follower output terminals (which is of low impedance), a voltmeter of ordinary design whose input impedance need not be high, may be used for this purpose.

In the ideal case, both the tubes T_1 and T_2 should be identical having the same values of r_p and g_m . For this purpose, it is preferable to use two triode tubes whose parameters have been found to be identical, as it is very difficult to find a twin-triode the two halves of which are identical. Of course, the condition of having identical parameters for both the tubes is not a stringent one, because the stage gain of a cathode follower is not much dependent on the tube parameters.

As mentioned earlier, the meter reading will be independent of the sign of phase change i.e. the meter will not indicate which voltage is leading or lagging. Thus, we should have a previous knowledge of the sign of phase change produced, which, of course, is known in most cases.

ACKNOWLEDGMENTS

The author is indebted to Prof. H. Rakshit, D.Sc., F.N.J., F.Inst.P., for his guidance, helpful suggestions and active interest in the work.

REFERENCES

Chatterjee, B., 1957, *Ind. Jour. Phys.*, **31**, 541.

INVESTIGATIONS ON THE PARAMAGNETIC RESONANCE IN COAL WITH A TRANSMISSION TYPE ELECTRON PARAMAGNETIC RESONANCE SPECTROMETER

G. N. SARKAR, A. MUKHERJI, R. N. CHATTERJEE AND
U. S. GHOSH,

SATA INSTITUTE OF NUCLEAR PHYSICS, CALCUTTA

(Received, January 20, 1959)

ABSTRACT. A simple transmission type electron paramagnetic resonance spectrograph operating at 3.2 cm wave length is briefly described. Preliminary investigations on the variation in the number of paramagnetic centres in coal samples with the temperature of carbonisation, are reported. The temperature variation results corroborate with those obtained by the British group of workers, but differ in certain respects from the observations of the Russian group. The samples from different depths in a mine have also been investigated, but they show a very small variation in the paramagnetic centre concentration.

INTRODUCTION

The electron paramagnetic resonance observed in coals has been studied recently by different groups of workers (Ingram *et al*, 1954; Ubersfeld, *et al*, 1954 and Garifyanov *et al*, 1957), but no conclusive theory of its origin has as yet been arrived at. Amongst the most interesting behaviours shown by coal are the variation in the absorption signal strength with carbonizing temperature (Ingram, Tapley and others, 1954), with the percentage of carbon present (Ingram, Tapley and others, 1954), and with the carbonization in presence and absence of Oxygen (Ingram and Tapley, 1955).

With a view to investigate and explain these phenomena we have studied the variations of the electron paramagnetic resonance signal strength with temperature of carbonization and also with the depths in a mine for naturally occurring coal samples. Section I of this paper describes briefly a simple transmission type spectrometer operating at 3.2 cm wave length. The results of the experiments are given in Section II and a discussion on them are incorporated in Section III.

SECTION I

THE ELECTRON PARAMAGNETIC RESONANCE SPECTROMETER

Figure 1 shows a block diagram of the Spectrometer. It employs a 723 A/B Klystron as the source of the microwave power. A resonant cylindrical

through a 10 db directional coupler. A proton resonance fluxmeter designed after Knoebel and Hahn (1951) is employed for the measurement of the steady magnetic field. With a superhet frequency meter, calibrated with reference to a primary frequency standard, type GR 1100-AP, the measurement of the magnetic field with an accuracy more than 1 part in 10^4 is very easily attained. Here the limitation to the accuracy in measuring the magnetic field is due to the inhomogeneity present in it. The present sensitivity of detection of the instrument is about $10\mu\text{gm.}$ of diphenyl picryl hydrazyl.

With the present arrangement signals having line widths upto 15 gauss can be observed on the oscilloscope screen. Derivatives of such and still broader lines can be recorded through phase-sensitive detector. Figures 2 and 3 show typical oscillogram and pen-recorder traces respectively for coal. In our experiments, the sharp absorption line of Diphenyl picryl hydrazyl is used as a standard of reference.

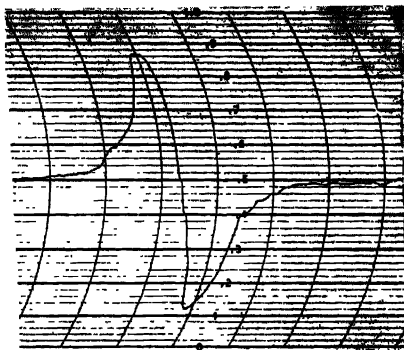


Fig 3 Derivative of the epr absorption signal in powdered lignite carbonised at 550°C .

SECTION II

INVESTIGATION ON COAL

A *Effect of the carbonizing temperature*

Briquetted samples of Lignite carbonized at different temperatures have been investigated. The temperature range runs from 250°C upto 750°C . Table 1 and figure 4 show the variation in the concentration of paramagnetic centres per gm of carbon as the carbonizing temperature is increased. No signal was observed for the sample carbonized at 750°C . A maximum in the concentration was shown for temperatures in between 550°C and 650°C . The line widths also increase with the increase in the temperature.

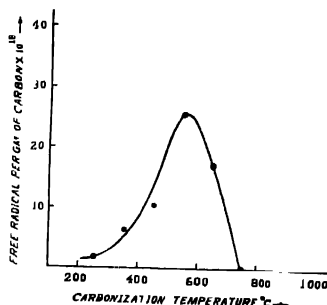


Fig. 4. Variation of paramagnetic centre concentration with carbonizing temperature in briquetted lignite

Similar behaviour is shown by powdered Lignite treated to different temperatures (Table II). The paramagnetic centre concentration is greater in briquettes as compared to the corresponding powdered samples.

The total number of paramagnetic centres in the coal samples were determined from a comparison of the areas under the absorption signals for these samples with that for a known mass of diphenyl-picryl-hydrazyl, under identical setting of the spectrometer. For the line-width measurement full width at half maximum of diphenyl-picryl-hydrazyl signal was taken to be 3 gauss.

B. Effect of depth :

To study the effect of depth on the concentration of paramagnetic centres produced, we have investigated samples obtained from different depths of a mine. Depths ranging from 760 ft. up to 2876 ft. have been covered. The line width and also the concentration of paramagnetic centres per gm of carbon for these samples are given in Table III.

TABLE I
Line width and paramagnetic center concentration in briquetted lignites
carbonized at different temperatures

Temperature	Line width in gauss	No. of paramagnetic centres per gm. of carbon
Not heated	3.4	1.0×10^{18}
250°C	4.2	1.5×10^{18}
350°C	4.4	6.4×10^{18}
450°C	4.7	10.4×10^{18}
550°C	4.8	25.8×10^{18}
650°C	6.3	17.4×10^{18}
750°C	×	×

TABLE II

Line width and paramagnetic centre concentration in powdered lignites carbonized at different temperatures

Temperature	Line width in gauss	No. of paramagnetic centres per gm. of carbon
250°C	3.8	2.2×10^{18}
350°C	3.8	2.2×10^{18}
450°C	4.2	8.7×10^{18}
550°C	4.6	10.3×10^{18}
650°C	5.5	10.1×10^{18}
750°C	x	x

TABLE III

Line width and paramagnetic centre concentration in coal samples from different depths of a mine

Depth from the surface	Line width in gauss	No. of paramagnetic centres per gm. of carbon
700'-7" to 765' 0"	4.7	1.9×10^{19}
1589'-7" to 1599'-5"	5.0	2.0×10^{19}
1944' 6" to 1951' 0"	4.9	2.2×10^{19}
2521' 6" to 2526' 10"	4.9	2.4×10^{19}
2866' 0" to 2876'-0"	4.9	2.0×10^{19}

SECTION III

DISCUSSION

Our results show that the concentration of paramagnetic centres increases steadily up to a carbonizing temperature of 550°C. This is in absolute agreement with the observations of the British group of workers (Ingram *et al*, 1954) and also with those of the Russian workers (Garifyanov *et al*, 1957). We find, for the maximum absorption at 550°C, for the powdered lignite, the number of paramagnetic centres per gm of carbon is 1.0×10^{19} and for briquettes it is 2.6×10^{19} , while from Ingram's (1954) report this figure comes out to be about 6×10^{19} . We assign the difference in the numerical values to be due to different types of specimens used in the experiments. However, our results cannot be compared quantitatively with those of the Russian group, for their data are given in relative terms.

There is, however, an important difference between our observations and those of the Russians. They observe that if the thermally treated samples are subjected to weathering in air, quite strong signals are observed for the samples heated to 750°C and to 900°C, while studies immediately after the heat treatment show no signal for those temperatures. But, in our case, all the samples after being carbonised at high temperatures were subjected to normal atmospheric condition for more than two months and no signal was observed for the sample treated up to 750°C. Also this behaviour observed by the Russians is found only in powdered samples and not in briquettes.

The data in Table 3 indicate only a very small variation of the paramagnetic centre concentration with depth. The line width is nearly constant. Ingram, Tapley and others (1954) observed large variation of signal strength with carbon percentages for samples having more than 80% carbon content, while for lower concentrations (as in our case) the absorption signal is expected to be nearly independent of carbon percentage. So the observed small variation in the signal cannot be attributed to the change in carbon percentage, specially since we are concerned only over a small range of its variation.

ACKNOWLEDGMENTS

The authors take the opportunity to express their indebtedness to late Prof. M. N. Saha under whose encouragement the work began and who provided the requisite funds for researches in Microwave Spectroscopy.

Thanks are also due to Prof. B. D. Nag Chaudhuri, for his helpful suggestions and discussions on the work, and to Prof. A. K. Saha for his keen interest during the progress of the work. We also thank Dr. S. S. Dharmatti of the Tata Institute of Fundamental Research for kindly giving us a quantity of diphenyl picryl hydrazyl and to Dr. M. S. Iyengar of the Central Fuel Research Institute for kindly providing us the coal samples for investigation.

The authors also express their appreciation to the Fuel Research Institute and also to Dr. C. Dutta of the Micro Chemical Laboratory of the Chemistry Department of the Calcutta University for the analysis of the coal samples.

REFERENCES

- Gaifuyanov, N. S., Kozyrev, B. M. and Kiyvoviyaz, I. M., 1957, *Chemistry and Technology of Fuel and Oils*, Issue No. 2.
Ingram, D. J. E. and Bennett, J. E., 1954, *Phil. Mag.*, **45**, 545.
Ingram, D. J. E., Tapley, J. G., Jackson, R., Bond, R. L. and Murnaghan, A. R., 1954, *Nature (Lond)*, **174**, 797.
Ingram, D. J. E. and Tapley, J. G., 1955, *Chemistry and Industry*, p. 568.
Knoebel, H. W. and Hahn, E. L., 1951, *Rev. Sci. Instr.*, **22**, 904.
Ubersfeld, J., Etienne, A. and Combrisson, J., 1954, *Nature, (Lond)*, **174**, 614.

RENNINGER EFFECT IN NAPHTHAZARIN

P. SRIVASTAVA

INDIAN ASSOCIATION FOR THE CULTIVATION OF SCIENCE, CALCUTTA-32

(Received, February 6, 1959)

ABSTRACT. While studying the space group of naphthazarin, Renninger Effect has been observed in highly exposed zero-layer [010] Weissenberg photograph. This has been completely verified by construction of reciprocal lattice, and by calculation, and the space group of the crystal has been definitely established.

INTRODUCTION

During investigation of space group of naphthazarin, $C_{10}H_4O_2(OH)_2$, a sharp reflection, different from the nature of the normal ones, was observed in the position ($\bar{4}05$). This presented difficulty in ascertaining the spacegroup of the crystal. The characteristics of this reflection, which is forbidden by the suspected space-group extinction rules, have been studied thoroughly and its origin is ascribed to double reflection from three pairs of strong planes.

DETECTION OF RENNINGER EFFECT

The forbidden reflection was very sharp and it was not accompanied by its usual CuK_{β} reflection (unfiltered CuK radiation was used) while equally intense normal spots were accompanied with their CuK_{β} reflections. A study of the reflecting conditions of the reciprocal lattice has been made which confirms the presence of Renninger (1937) reflection.

GRAPHICAL VERIFICATION

The verification of a case of double reflection in anthraquinone has been discussed by Murty (1954). The unit cell dimensions of naphthazarin have been determined from rotation photographs by standardising the camera diameter with aluminium powder, and from a consideration of the high angle spots of the Weissenberg picture (where $K_{\alpha_1\alpha_2}$ doublet is well resolved). These are $a = 7.90\text{\AA}$, $b = 7.30\text{\AA}$, $c = 16.91\text{\AA}$ and monoclinic angle $\beta = 124^{\circ}38'$. The reciprocal lattice has been constructed on the basis of these values and shown in figure 1.

The radius of the sphere of reflection has been taken as 5 cms. Various circles drawn in figure 1 are the projections, on the zero-layer of the reciprocal lattice, of the intersections of the first, third and fourth layers with the sphere of reflection.

tion, the incident direction of X-ray beam being normal to the axis of rotation. The equatorial circle (radius R_0) passes through the origin O of the reciprocal

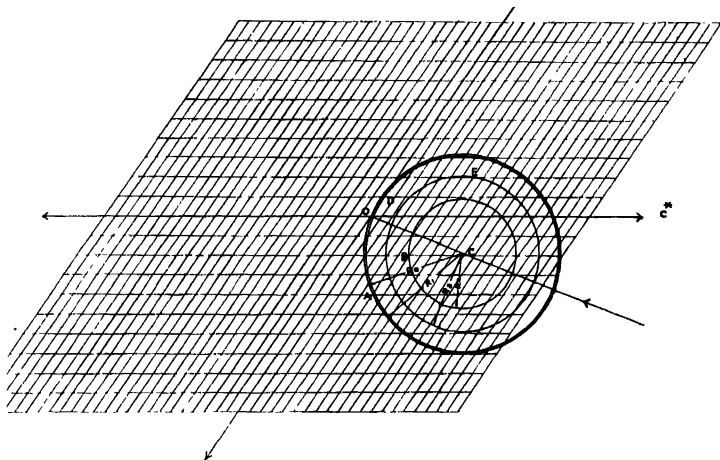


Fig 1

lattice, and the point $A(\bar{4}, 5)$. Then it is found that the first circle (radius R_1) passes through point $D(1, 0)$, third circle (radius R_3) passes through point $E(2, 7)$ and the fourth circle (radius R_4) passes through point $B(\bar{2}, 6)$. Thus it appears that reflection $(\bar{4}05)$ is caused by simultaneous reflections from three pairs of lattice planes, one plane of each pair being (110) , (237) and $(\bar{2}46)$ respectively. Since these three coincidences are rough and cannot be ascertained very accurately by graphical method, the accuracy was tested analytically.

ANALYTICAL VERIFICATION

Let the equation of the equatorial circle be, as shown in figure 2,

$$r/2 = \cos(\alpha - \theta) \quad \dots (1)$$

the co-ordinates of the centre C are $(1, \alpha)$. (taking the radius of the sphere of reflection to be unity). Polar co-ordinates of the points are calculated from the reciprocal lattice (figure 1). For the point $A(\bar{4}05)$, $r = 0.5064$ and $\theta = 34^\circ 38'$. Then from Eqn. (1) $\alpha = 101^\circ 41'$.

The radii of the circles produced by intersection of the reciprocal lattice layers with the sphere of reflection are calculated from BOC ,

$$R_n^2 = 1 + r_n^2 - 2r_n \cos(\alpha - \theta_n) \quad (2)$$

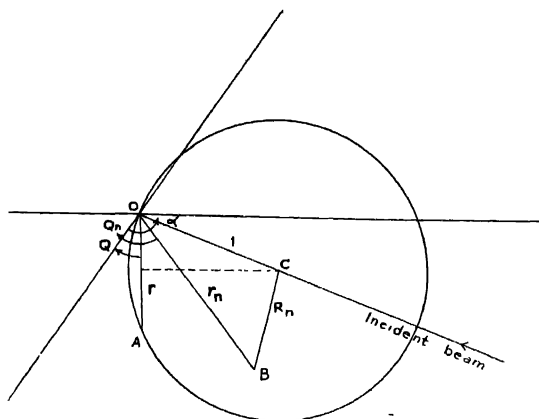


Fig. 2.

and compared with those obtained from the consideration of the ζ -co-ordinates, figure 3, given by the relation

$$R_n = \cos v_n = \cos (\sin^{-1} \zeta_n) \quad \dots \quad (3)$$

where

$$\xi_n = \frac{n\lambda}{b}$$

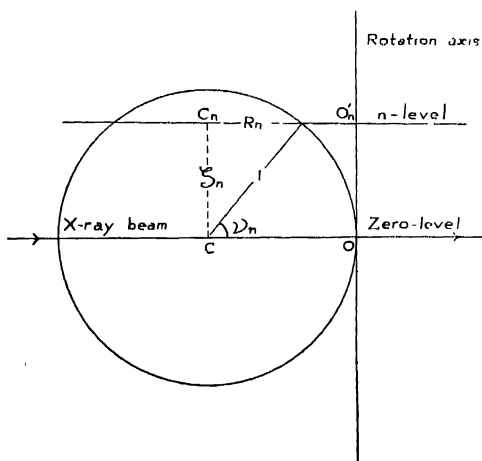


Fig. 3.

Both sets of values are given in Table I.

TABLE I

Points	Radii from Eqn. (2)	Radii from Eqn. (3)
(110) R_1	0.9775	0.9799
(237) R_3	0.7742	0.7799
(246) R_4	0.5363	0.5357

R -values obtained from Eqs. (2) and (3) are in good agreement.

Now the other lattice-planes of the three pairs can be easily found out (Lipson and Cochran, 1953). If $(h\ k\ l)$ are the indices of the forbidden reflection, and $(h_1k_1l_1)$ and $(h_2k_2l_2)$ those of a pair of lattice planes contributing to the formation of this reflection, then the following relations must be satisfied.

$$h = h_1 + h_2 ; \quad k = k_1 + k_2 \quad \text{and} \quad l = l_1 + l_2.$$

Hence the three pairs which must contribute to reflection $(\bar{4}\ 0\ 5)$ are (110), $(\bar{5}\ \bar{1}\ 5)$; (237), $(\bar{6}\ \bar{3}\ \bar{2})$ and $(\bar{2}46)$, $(\bar{2}\ \bar{4}\ \bar{1})$.

From the study of the Weissenberg photographs, it is found that each of these reflections are sufficiently strong to contribute to the formation of $(\bar{4}\ 0\ 5)$ reflection.

RESULTS

From the study of the indexed reflections of the Weissenberg photographs, it has been found that all $(h\ k\ l)$ reflections are present. The systematic absences are $(h\ 0\ l)$ with l odd and $(0\ k\ 0)$ with k odd. The forbidden reflection $(\bar{4}\ 0\ 5)$ is found due to double reflection. Hence the space-group No.14 — $P2_1/c$, for naphthazarin, is established beyond doubt.

ACKNOWLEDGMENTS

The author wishes to express his thanks to Prof. B.N. Srivastava for taking much interest and to Dr. B. V. Ramanamurty for suggesting the problem and guidance throughout the work.

REFERENCES

- Lipson, H. and Cochran, W., 1953, "The Crystalline State, Vol. III.", pp. 30.
 Murty, B. V. R., 1954, *Proc. Nat. Acad. Sc.* **23A**, 119.
 Renninger, M. Z., 1937, *Zeit. f. Kristallogr.*, **97**, 107.

A NOTE ON THE DEPENDENCE OF THE SPUTTERING PRODUCED BY BOMBARDMENT BY CANAL RAYS ON THEIR ANGLE OF IMPACT

V. T. CHIPLONKAR AND B. N. VARADRAJAN

INSTITUTE OF SCIENCE, BOMBAY

Received, January 21, 1951)

Plate II

ABSTRACT. The sputtering produced by bombardment of metal targets with canal rays has been observed to consist of two types I and II, appearing in the two characteristic angular regions of 0° – 20° and 30° – 90° respectively (with respect to the incident beam). There is evidence to show that the magnitude of sputtering as well as the angular intensity distribution in type I (which appears to be the significant one involved in the sputtering of wires) show a definite dependence on the angle of impact, thus indicating that it involves a momentum transfer mechanism.

INTRODUCTION

From the point of view of the elucidation of its mechanism, it is important to determine whether the sputtering produced by impacting positive ions, is a function of their angle of incidence. Experiments of Seeliger and Sommermeyer (1935) had shown that for sputtering produced by canal rays of Argon (5–10 kV energy) at oblique angles of impact (of not more than 45°), on plane targets of silver and gallium, the angular intensity distribution in the sputtered deposit showed a cosine variation, which was however not a function of the angle of impact. More indirect experiments by Fetz (1942) on the sputtering of molybdenum wires produced by positive ions of mercury (150 volts energy), in the plasma region of a discharge, indicated that the magnitude of sputtering depends on the angle of impact and increases with increasingly oblique incidence. This result has been confirmed by the experiments of Wehner and others (1954) on the sputtering of wires, observed under similar conditions. It may be pointed out that the angular intensity distribution in the sputtered deposit, as well as the magnitude of sputtering, would show a dependence on the angle of impact, if the sputtering occurs as a result of a momentum-transfer mechanism but would be independent of it, if the sputtering is produced as a result of the alternative mechanism of local vaporisation (Handbuch der Physik, 1956). In view of these conflicting observations a direct investigation of the effect was considered essential (Massey & Burhop, 1952).

EXPERIMENTAL

For this purpose, polished plane targets of brass, silver, gold and alluminium (2.7 mm \times 16 mm) were exposed to the canal rays of hydrogen and air, in the low energy range of 2-4 kV, in the observation chamber of a canal ray tube (pressure not more than 50-70 microns, dark space length = 30-45 mm) under conditions where the effects due to back diffusion can be considered as insignificant (Handbuch der Physik, 1956). For comparison observations were also taken on the sputtering of a silver wire (diameter = 0.4 mm) under similar conditions. The target was mounted in a ground-joint base, in such a manner that the angle of impact ϕ (taken to be the angle between the surface of the target and the normal to the incident beam) could be varied and measured. Observations have been taken for values of $\phi = 15^\circ, 30^\circ, 45^\circ, 60^\circ, 75^\circ$ (and also 0° in one case). The sputtered material was received on a transparent plastic film, mounted cylindrically (radius = 10 mm) about the target as the axis. A circular hole was punched in the film, to allow the canal rays to enter the target chamber. The angular intensity distribution in the deposit was determined with the help of a microphotometer. A preliminary experiment, in which a target covered with a small layer of copper-oxide, was exposed to the canal rays of hydrogen enabled the determi-

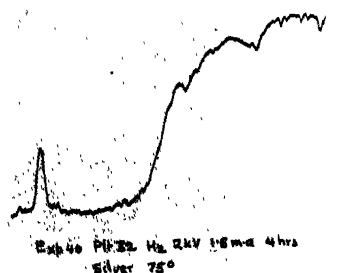


Fig. 1.

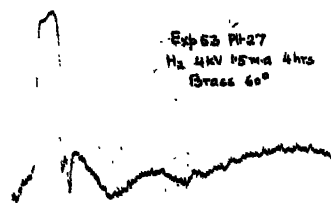


Fig. 2.

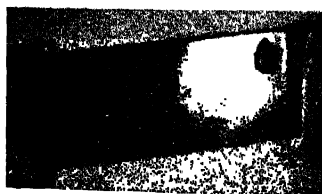


Fig. 4 Dep. 32, Silver
 $\phi = 75^\circ$

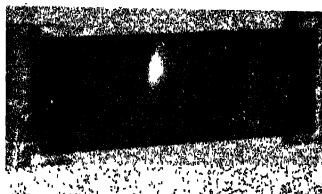


Fig. 5 Dep. 43, Gold
 $\phi = 75^\circ$



Fig. 6 Dep. 41, Gold
 $\phi = 60^\circ$

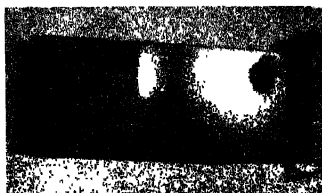


Fig. 7 Dep. 40, Gold
 $\phi = 45^\circ$

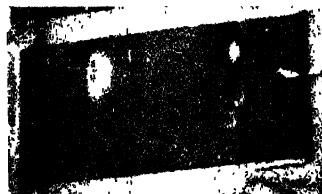


Fig. 8 Dep. 27, Brass
 $\phi = 60^\circ$

Photographs showing sputtered deposits.

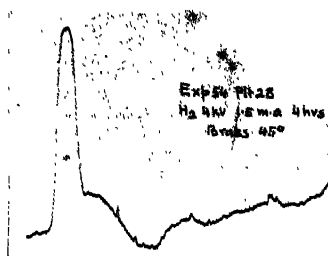


Fig. 3.

nation of the angular divergence of the beam, at the target surface, which was shown to be of the order of 3° . The observational data obtained have been shown in Tables 1-7. Some typical microphotometer records are given in figures 1-3 and the photographs of some of the actual deposits (in reflected light) are given in figures 4-8 (Plate II).

The observations show that sputtered deposits are obtained in two distinct and characteristic regions. Denoting by θ , the angular position of the deposit with respect to the incident beam, deposit I (Dep I hereafter) which is the more prominent one, appears in the region $\theta = 0^\circ$ - 20° whereas deposit II (Dep. II hereafter) covers a region between $\theta = 30^\circ$ - 90° . In a majority of the observations these two deposits are well demarcated from each other. The appearance of these two types of deposits appears to be interesting as we have not been able to find any reference to them, in the available literature.

In the table of observations V = discharge voltage in kV, i = discharge current in ma, t = time of exposure in hrs, ϕ = the impact angle (*i.e.*, the angle between the target surface and the normal to the incident beam), α = angular position in degrees, of the deposit with respect to the target surface, α_m = angular position in degrees, of the main maximum in intensity, in Dep I, w.r.t. the target surface. α_s = angular spread in degrees of Dep I, w.r.t. the target surface, $\alpha_m(\text{II})$ = angular position in degrees of the first intensity maximum in Dep II, w.r.t. the target surface, I_m = Intensity maximum in Dep I (corresponding to α_m) in arbitrary units as measured from the microphotometer records and A = area under the microphotometer curve for Dep I (corresponding to α_s) in arbitrary units.

I_m has been taken as a measure of the maximum sputtering in the deposit, whereas the value of A is taken to represent the magnitude of the sputtering. It may be pointed out that the intensity distribution for Dep I shows only one prominent maximum (corresponding to α_m) whereas that for Dep II shows, in general, a number of maxima which are however not as distinct and prominent, as the one in the case of Dep I. The position of the first maximum (nearest to Dep I), viz $\alpha_m(\text{II})$ only has been shown in the tables.

TABLE I

Canal rays of 'air, Target—Brass plate

 $V = 2kV$, $i = 1.5$ ma, $t = 4$ hrs.

Plt No.	ϕ	Im	A	Dep I		Dep II $\alpha_m(II)$	Relative intensities
				α_m	α_s		
20	75°	17	48	65°	25°	—	Dep II absent
21	60°	—	—	50°	51°	85	Dep I strongest
22	45°	17	33	37°	22°	—	Dep II absent
23	15°	13	15	9°	18°	—	„

TABLE II

Canal rays of air, Target—Brass plate

 $V = 4kV$, $i = 1.5$ ma. $t = 4$ hrs

Plt No.	ϕ	Im	A	Dep I		Dep II $\alpha_m(II)$	Relative intensities
				α_m	α_s		
10	75°	74	58	67°	37°	—	Dep I strongest
11	60°	74	46	57	38	75°	„
12	45°	72	47	41	40	78	„
13	30°	65	47	24	29	—	„
15	15°	71	67	10	38	38	„
16	0°	—	—	—	—	—	Dep II strongest Dep I negligible

TABLE III

Canal rays of hydrogen, Target—Brass plate.

 $V = 4kV$, $i = 1.5$ ma, $t = 4$ hours.

Plt No.	ϕ	Im	A	Dep I		Dep II $\alpha_m(II)$	Relative Intensities
				α_m	α_s		
26	75°	—	90°	61°	28°	87°	Dep I strongest
27	60°	—	58	52	36	8	„
28	45°	—	85	37	44	76	„
29	30°	—	63	24	48	—	„
30	15°	—	49	10	44	—	„

TABLE IV

Canal rays of air Target—Brass plate.

 $V = 4kV$, $i = 3.0$ ma, $t = 4$ hrs.

Plt No.	ϕ	Im	A	Dep I		Dep II $\alpha_m(II)$	Relative intensities
				α_m	α_s		
5	75°	57	107	65°	33°	19	Dep I strongest
4	60°	59	78	54	55	83	„
6	45°	59	95	37	55	6	„
7	30°	62	74	20	43	—	„
8	15°	50	—	7	49	—	„

TABLE V

Canal rays of hydrogen, Target—Silver plate

 $V = 2kV$, $i = 1.5$ ma, $t = 4$ hrs.

Plt No	ϕ	Im	A	Dep I		Dep II $\alpha_m(II)$	Relative intensities
				α_m	α_s		
32	75°	54	56	75°	62°	81°	Dep II strongest
33	60°	34	25	56	58	48	„
34	45°	43	—	—	66	39	„
35	30°	39	—	—	66	24	„
36	15°	36	—	—	—	11	„

TABLE VI

Canal rays of hydrogen, Target—Gold plate

 $V = 2kV$, $i = 1.5$ ma, $t = 4$ hrs.

Plt No.	ϕ	Im	A	Dep I		Dep II $\alpha_m(II)$	Relative intensities
				α_m	α_s		
43	75°	24	34	72°	46°	—	Dep I strongest
41	60°	5	32	54	26	—	„
40	45°	5	49	39	—	48	„
39	30°	32	16	22	29	53	Dep II strongest
38	15°	46	—	—	66	4	„

TABLE VII

Canal rays of hydrogen, Target—Silver wire

 $V = 2kV$, $i = 1.5$ ma, $t = 4$ hrs

Plt No	ϕ	I_m	A	Relative intensities
47		7	73	Dep II absent

DISCUSSION

Dep I appears to be quite similar to the one observed by Seeliger and Sommermeyer (1935). It appears as has been pointed out, in a characteristic angular region with respect to the incident beam. That this deposit occurs as a result of an interaction between the impacting ions and the target was shown by our observation that it appeared with negligible intensity when the target was of aluminium or of copper oxide ($\phi = 75^\circ$). From the observations given above, it is evident that the relative intensities of the two deposits are determined among other factors by the nature of the target surface. For example, with a brass target, Dep I was always stronger than Dep II (as a matter of fact in some observations it was absent). On the other hand in the case of a silver plate target, Dep II was always stronger than Dep I, for a silver wire only Dep I was present. (Dep II being absent). The intensity of Dep I showed in general a dependence on ϕ . Dep I sometimes showed a structure in the form of a sharp minimum (which can be seen in figure 2). Observations on sputtering obtained for large values of i ($i = 3.0$ ma and 6.0 ma) indicated that this structure is probably due to a redistribution of the deposit in this region, produced by a subsequent bombardment by the canal rays, as this structure was invariably obtained in the case of large value of i . As the inlet aperture in the film, covers a part of the region occupied by Dep II the available data in general give adequate information about Dep I only and the discussion in this paper is therefore mainly concerned with this deposit.

To assess the extent to which the sputtering observed in Dep I involves a momentum-transfer mechanism, one has the available data on the variation with ϕ of :

- (1) The amount of sputtering A ,
- (2) α_m —the angular position of the intensity maximum,
- (3) α_s —the angular spread of the deposit,
- (4) I_m —the maximum of intensity in the deposit,

The variation of A with ϕ in the various observations shows a fairly definite increase with ϕ although in the case of a few observations (c.f. Table VI) there are indications of a secondary maximum for $\phi = 45^\circ$.

The angular position of the intensity maximum shows a clear dependence on ϕ . It must be pointed here that the variation in the θ -positions of this maximum (*i.e.* with respect to the incident beam) with ϕ is not as significant. Another interesting observation in this connection is that the intensity distribution in this deposit was not found to show the cosine variation observed by Seeliger and Sommermeyer (1935). It was experimentally shown by them that this type of variation was obtained in a deposit formed as a result of a local thermal vapourisation.

From the point of view of the evaporation mechanism the angular spread α_s of the deposit should be independent of ϕ whereas in terms of the momentum-transfer mechanism, it should show a decrease on general grounds, with increase in ϕ . Many of the results obtained indicate in fact the occurrence of such a decrease but there are others in which this does not take place. The results obtained on this aspect of the problem cannot therefore be considered as conclusive. It is interesting to note that the angular spread for Dep II obtained in one case (Table VI) showed a constant value independent of ϕ (shown in Table VIII) which would be the case had this deposit resulted as a result of a local vapourisation mechanism.

TABLE VIII

Deposit II variation of angular spread with ϕ .

ϕ	75°	60°	45°	30°	15°
α_s	50°	50°	53°	53°	-

Unfortunately the values of α_s for other observations are not available.

The values of I_m show in general a variation with ϕ which can be considered as constant with the transfer mechanism although the data for gold (Table VI) show a further increase in I_m as ϕ decreases from 45° to 15°. The redistribution of the deposit on account of the bombardment by the canal rays could be partly responsible for the fact that I_m does not show a significant and simple dependence on ϕ .

In conclusion it can be said that there is evidence to show that a part of the sputtered deposit shows a dependence on the impact angle, suggesting that it involves a momentum-transfer mechanism. It appears likely that the sputtering arises not as a result of one simple mechanism but possibly involves a number of them (Wehner, 1954).

REFERENCES

- Retz, H., 1942, *Zeits. f. Phys.*, **119**, 590.
Handbuch Der Physik, 1956, vol. **22**, p. 159.
Massey and Burhop, *loc. cit.*, p. 588.
Seeligor, R. and Sommermeyer, K., 1935, *Zeits. f. Phys.*, **93**, 692.
Massey and Burhop, 1952, Electronic and Ionic impact phenomena, pp. 589.
Whener, G. and Medicus, G., 1954, *J. App. Phys.*, **25**, 698.
Wehner, G., 1954, *J. App. Phys.*, **27**, 271.

INTENSITY OF BRILLOUIN COMPONENTS IN LIGHT SCATTERED BY SOME LIQUIDS*

K. C. MEDHI

(OPTICS DEPARTMENT, INDIAN ASSOCIATION FOR THE CULTIVATION OF SCIENCE,

CALCUTTA-32

(Received, January 27, 1959)

Plate III

ABSTRACT. The Brillouin components in light scattered by water and acetone have been recorded using an experimental arrangement in which stray light was avoided very carefully. It is observed that the intensities of the Brillouin components relative to those of the central components are in agreement with those predicted by the theory of Landau and Placzek.

INTRODUCTION

After the Brillouin components in light scattered by liquids had been first discovered by Gross (1930), Landau and Placzek (1934) calculated the relative intensities of the Brillouin components and the undisplaced component of the Rayleigh line. According to this theory the ratio of the intensity of the undisplaced component and the total intensity of the Brillouin components is given by $(c_p - c_n) : c_n$ and Birus (1938) observed that the experimental results obtained by him in the case of toluene agreed with the theory mentioned above. He also pointed out that the validity of Landau and Placzek's theory could be tested more rigorously by studying the structure of Rayleigh line due to water, because the undisplaced component would be almost absent in this case. He therefore studied the Brillouin components due to water distilled very carefully and concluded that there was no undisplaced component.

Exhaustive investigations on the Brillouin scattering in a large number of liquids were carried out later by Venkateswaran (1942) who also measured the polarisation and intensity of the Brillouin components relative to that of the central component in each case. He used a Fabry-Perot interferometer and a zinc arc as source of monochromatic light. He found that in the case of many liquids including water and acetone the undisplaced central component was too strong to be explained by the Landau-Placzek theory.

The cause of this discrepancy between the experimental results and those predicted by Landau-Placzek theory was investigated later more carefully by

* Communicated by Professor S. C. Sikar.

Rank *et al* (1948) who used a Fabry-Perot etalon 10 cm in diameter and a three-prism spectrograph of high light gathering power. They investigated the intensities and polarisation of the Brillouin components due to ethyl alcohol, acetone and water. They concluded from the results obtained by them that the results were in agreement with those predicted by Landau-Placzek theory. They further pointed out that the discrepancy observed by previous workers was due to insufficient resolving power of the instrument used by them and to the presence of some percentage of stray light in the scattered light. More recently, Febelinskii (1956) found the central component to be too strong to be accounted for by Landau-Placzek theory in the case of a few liquids, but in the case of water it was almost absent.

It is, however, very difficult to eliminate stray light and it was therefore thought worthwhile to set up a suitable arrangement for the study of Brillouin effect in a large number of liquids eliminating stray light to find out whether Landau-Placzek theory can explain the observed facts. The preliminary results obtained in the case of acetone and water are discussed in the present paper.

EXPERIMENTAL

The liquids studied were distilled repeatedly under reduced pressure direct into the sample tube in order to eliminate dust particles. A pyrex tube 4 cm. in diameter and about 40 cm long with a Pyrex disc fused at one end served as the sample tube. Its horn-shaped tail was blackened with dull black paint and a long black tube of diameter 1 cm placed in front of the window allowed only the light scattered by a narrow cone of the liquid inside the tube to reach the focussing lens. Two mercury arcs each about 35 cm long, carrying 12 amperes of current and with the electrodes cooled by running water were placed horizontally on the two sides of the sample tube and two wide glass tubes filled with distilled water were used to focus the light on the axis of the sample tube. Two parabolic mirrors were also used to focus the mercury arcs on the tube. Two Soller slits were placed between the sample tube and the two cylindrical lenses to make the direction of incidence approximately perpendicular to the axis of the sample tube. The deviation was, however, about 12 degrees on each side.

A Fabry-Perot interferometer with a spacing of 5.71 mm was used in conjunction with a Hilger two-prism glass spectrograph provided with F/4.5 camera lens to photograph the interference patterns. The 4078 Å line of the Hg arc was used to find out the structure of the Rayleigh line. Ilford Special Rapid plates were used to record the spectra. In the case of acetone an exposure of 24 hours was required to record the pattern due to 4078 Å line with moderate density, but in the case of water the rings were very feeble even with an exposure of 18

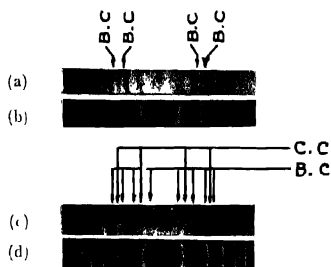


Fig. 1

- (a) Brillouin spectrum of water.
 (b) Incident λ 4047 Å. U. of Hg.
 (c) Brillouin spectrum of acetone.
 (d) Incident λ 4078 Å. U. of Hg.

B. C.—Brillouin component.

C. C.—Central component.

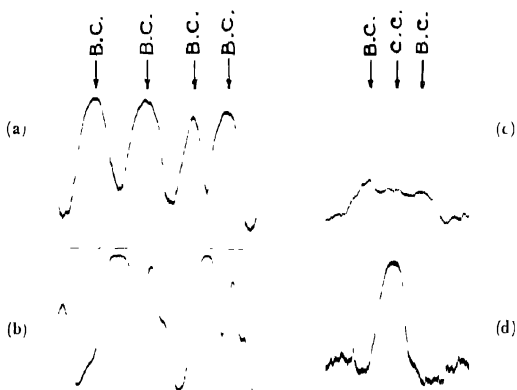


Fig. 2 Microphotometric records.

- (a) Brillouin spectrum of water
 (b) λ 4047 Å. U. of Hg.
 (c) Brillouin spectrum of acetone.
 (d) λ 4078 Å. U. of Hg.

hours. The structure, although not reproducible, was visible on such spectrograms, but a shorter exposure was used to record the rings due to the 4047 Å line with greater density. This line in the incident light showed one very strong component, a second component of about one fifth the intensity of the main component and another much weaker component. As discussed later, the presence of these components did not create much difficulty in interpreting the pattern.

RESULTS AND DISCUSSION

The interference patterns due to 4047 Å line of Hg scattered by water and 4078 Å line scattered by acetone are shown in figure 1 (Plate III) along with those due to these incident lines. The microphotometric records of the rings are reproduced in figure 2.

It can be seen from figure 1(a) that the main component of the 4047 Å line has been split up into two components in the pattern due to water, the intensity at the midpoint between these components being less than 10% of the main peak, and there being no indication of any maximum at this place. Further, the outer one of the two components of the doublet into which each main peak splits up is broader than the inner one, because the two components of the strong satellite fall on either side of this component. The curve thus demonstrates that the central undisplaced component in the case of water has an intensity less than 10% of the Brillouin components.

Figure 2(d) and 2(c) show that each ring due to the incident 4078 Å line is split up in the light scattered by acetone into three components all of which are of about the same intensity, the central component being slightly weaker. Thus the ratio of the intensity of the central component to the sum of the intensities of the two Brillouin components is about 0.45 in this case. This is in fair agreement with the ratio 0.42 reported by Rank *et al* (1948) and is much less than the value 0.79 reported by Venkateswaran (1942). The high intensity of the central component observed by Venkateswaran (1942) is probably due to presence of stray light. He studied the light scattered backwards and as the background was directly illuminated by the incident light probably the background was not perfectly black.

The results obtained in the present investigation show that it has been possible to eliminate the stray light almost completely. The investigation is therefore being extended to other liquids for which the central component has been found by Venkateswaran (1942) to be too strong to be accounted for by the Landau-Placzek theory in order to find out whether the discrepancy in those cases also is due to presence of stray light.

ACKNOWLEDGMENT

The author's thanks are due to Professor S. C. Sirkar, D.Sc. F.N.I., for his kind interest and guidance throughout the progress of the work.

REFERENCES

- Birus, K., 1938, *Physik. Zeit*, **39**, 80.
Fabelinski, I. L., 1956, *Doklady Akad. Nauk, S.S.S.R.*, **106**, 822.
Gross, E., 1930, *Naturwiss*, **1**, 718.
Landau, L. and Placzek, G., 1934, *Physik. Zeit. Sowjet Union*, **5**, 172.
Rank, D. H., McCartney, J. S. and Szasz, G. J., 1948, *J. Opt. Soc. of America*, **38**, 287.
Venkateswaran, C. S., 1942, *Proc. Ind. Acad. Sc.*, **15A**, 322.

A MAGNETIC SPECTROMETER FOR CHARGED PARTICLES

S B KARMOHAPATRO

SAHA INSTITUTE OF NUCLEAR PHYSICS, CALCUTTA

(Received February 25, 1959)

ABSTRACT. A Siegbahn-Svartholm type magnetic spectrometer, designed for focussing of ~ 1 Mev protons and developed in this laboratory is described with constructional details

Results of the measurement of the magnetic field and its gradient are given. Performance of the instrument in the low field region is tested with the conversion electron spectrum of Cs-137 source. Experiments showing the resolution, dispersion and the axial focussing properties of the spectrometer are presented.

INTRODUCTION

Since the use of a $\sqrt{2}\pi$ focussing inhomogeneous magnetic analyser for β -spectrometry for the first time by Siegbahn and Svartholm (1946), a number of such electromagnets has been constructed in different laboratories for spectrometry of high energy ions and β -particles

The theories on this type of two directional focussing magnetic analysers are fully developed by Siegbahn and Svartholm, Shull and Dennison (1947), Judd (1950), Resenblum (1950), Verster (1950) and others

Theories show that at any angle other than $\sqrt{2}\pi$, these magnetic analysers may also be used for focussing of charged particles. Based on this idea nuclear spectrometers have been constructed by Rubin and Snyder *et al* (1950), Rubin and Sachs (1955), Mileikowsky (1953) and others with a focussing angle π . In these cases, the transmission of the instrument fairly decreases, so as $\sqrt{2}\pi$ focussing angle is preferred for β -spectrometry work.

In this paper, we have described such a $\sqrt{2}\pi$ focussing magnetic spectrometer, designed for moderately high intensity mass spectrometry and may be useful for focussing energetic heavy ions with a limit upto ~ 1 Mev protons.

THEORETICAL CONSIDERATIONS

The idea of two-directional focussing of charged particles with an inhomogeneous magnetic analyser of the shape

$$H_z = H_0 \left(\frac{r_0}{r} \right)^n \quad \dots \quad (1)$$

where H_0 is the field at the mean radius r_0 , the field index $n = -\frac{r_0}{H_0} \frac{dH}{dr}$ of the radially varying field H , is due to Kerst and Serber (1941) in connection with the focussing of the synchrotron oscillations. Expanding eqn (1) we have

$$H_z = H_0(1 - \alpha\delta + \beta\delta^2) \quad \dots (2)$$

where
$$\alpha = n, \quad \beta = \frac{n^2 + n}{2}, \quad \delta = \frac{r - r_0}{r_0}$$

where $r = r_0 + \delta r$, r_0 , being the mean radius

For $n = \frac{1}{2}$, the charged particles are focussed in radial and axial directions at an angle $\sqrt{2}\pi$. The term β in equation (2) determines the order of focussing. For $\beta = \frac{3}{8}$ or $\frac{1}{8}$, the second order aberration in axial or radial direction respectively, can be eliminated. Rosenblum (1950) suggested the value of β equal to $\frac{1}{4}$ for an average first order focussing in both the directions. Higher order terms for improved resolution has been considered by Verster (1950) Stoker *et al* (1954) Lee-whiting and Taylor (1947) Lehr (1955) and others.

For $\beta = \frac{1}{4}$, the $\sqrt{2}\pi$ focussing magnetic analyser gives the spherical aberration

$$\delta_{ab} = \frac{2}{3} r_0 (\gamma_1^2 + \gamma_2^2) \quad (3)$$

where
$$\gamma_{1,2} = \frac{h_{1,2}}{r_0 \sqrt{2}}$$

h_1 and h_2 are the radial and axial apertures of the chamber of the spectrometer respectively.

For angles other than $\sqrt{2}\pi$, focussing of the charged particles has been considered by Judd (1950), Rosenblum (1950) and others for $n = \frac{1}{2}$. In these cases, unlike $\sqrt{2}\pi$ focussing angle, the source and the detector are to be placed outside the magnetic field. For other values of n , the possibilities of using these magnetic analysers have been considered by Sternheimer (1953) and others as Alsecevesky *et al* (1955). However, from the general expression for the solid angle

$$\Omega = \left[l^2 + \frac{1-l^2}{n(1-n)} \right]^{-\frac{1}{2}} \text{ sterad} \quad (4)$$

where $A r_0^2$ is the maximum available cross section area for the ion path, we see that for any focussing angle other than $\sqrt{2}\pi$, due to the finite distance l of the source from the field boundary, the solid angle factor is diminished. For a focussing angle $\sqrt{2}\pi$, $l = 0$ such as $\Omega = \frac{A}{2}$ sterad and is maximum compared to any other focussing angle with the field index $n = 0.5$.

DESIGN AND CONSTRUCTION OF THE MAGNET

Due considerations were given to the different types of inhomogeneous magnets before the present magnet was constructed. It was found that for high intensity ion-spectrometry with a moderate resolution a $\sqrt{2\pi}$ focussing magnetic analyser will be more efficient than any other type. A closed cylindrical type magnet has been used by Arbman and Svartholm (1955) for β -spectrometry and such types are better in respect of the stray field, however, we chose a central core type, so that the cost of magnetic materials is less for a bigger spectrometer as required for heavy ions.

The magnetic analyser has been constructed with a central core 406 mm dia, 254 mm height, two circular yokes 100 mm thick, 430 mm dia. Two annular pole pieces 430 mm O.D., 330 mm I.D., mean radius $r_0 = 381$ mm.

The magnet is cast by Messrs Bhartia Electric Steel Co. Private Limited, Calcutta, with a special iron with 0.08%–0.12% carbon content. The pole pieces are given a gardient, so that $\eta = 2^\circ$ where η is the angle of the surface to the symmetry plane and the gap width is slightly greater than 50 mm, so as $\beta = 1/4$, is satisfied at least in the region of $r_0 = 381$ mm

We should mention that the dimensions of the above described magnet is not optimum, and it would be better to use a core of larger diameter. But considering the space for the coil and the cost of the magnetic material, we have limited our design to the above dimensions

After preliminary measurements on the field gradient, two guard rings 430 mm I.D., 470 mm O.D., tapered at an angle 7° are inserted to the outside boundary of the pole faces to avoid the stray fringing fields

The exciting coils consist of five pancakes each having 4000 turns of 20 S.W.G. double glass served silicone bonded copper wire, wrapped with glass cloth and impregnated with silicone 996 varnish for attaining high insulation. One of the pancakes has 200 turns less for providing insulating materials, decided to be used after the design. The coils have total d.c. resistance of 800 Ω and are given power from a stabilised high voltage supply of 200V–1.5 kV and max. current 1.25 amp. In this circuit 6336 double triodes (Chatham) are used as series tubes, and 5651 for reference voltage, the power supply has a voltage stabilisation $\sim 0.1\%$. The weight of the magnet is 3000 lbs. and that of the coil 450 lbs.

MEASUREMENT OF THE MAGNETIC FIELD AND ITS GRADIENT

The magnetic field is measured with varying current at the mean radius r_0 with a fluxmeter (Norma). The field vs current curve (figure 1) shows that the magnet may be used for the spectrometry work with $H_0 r_0 \sim 144$ G gauss-cm.

For measuring the field gradient, of the above type of magnets, rotating search coil methods have been employed by Hedgran (1951), Lamb and Rother-

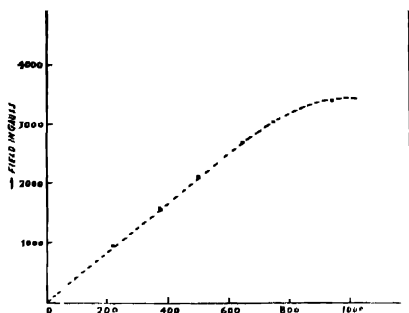


Fig. 1. Field vs current curve

ford (1951), Langer and Scott (1950). Null reading flip coil method has been used by Buechner *et al* (1948), Fletcher and Rubin (1955) for measuring the gradient of the inhomogeneous magnets. We followed the latter method because it required

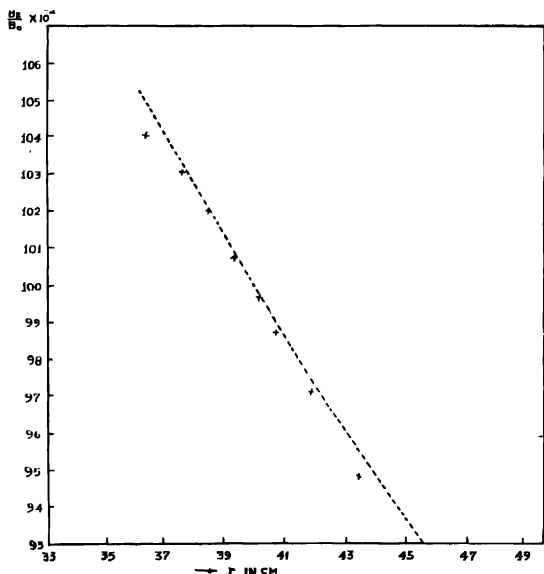


Fig. 2 $\frac{B_z}{B_0} - r$ curve, (Theo ---, expt x,)

less precision in mechanical construction. We used two search coils, mounted on a brass tube and driven by a 1/100 h.p. small motor coupled to the end of the tube. The rotation is limited to 180° by a switch which stops the motor when the 180° rotation is complete. One of the coils (2500 turns) is fixed at $r_0 = 381$ mm and the other one (850 turns) is movable. The circuit, which is employed for balancing the output voltages from the search coils using sensitive galvanometer as a null indicator is similar to Fletcher *et al* (1955). The resistance divider consists of a decade resistor (100 Ω per step) and a 100 Ω helipot. Null point is recorded for different points of the magnetic pole piece setting, the movable coil at those points with the fixed coil at $r_0 = 381$ mm with the different values of H_0 . The ratio was calculated from the resistance potentiometer for different values of r . Figure 2 shows the $\frac{B_z}{B_0} - r$ curve experimentally found with the finally shaped pole pieces. The accuracy of the measurement is not better than 0.2%, because of the broadening of the null point due to the phase shift in the search coils. The curve theoretically calculated with $\beta = 1/4$ in equation (2) is compared with the experimental points, so a small part of the pole faces seems to be available for a first order two-directional focussing of the charged particles.

VACUUM EQUIPMENTS

The annular shaped vacuum chamber is made of $\frac{3}{16}$ inch thick brass sheets and welded to fit the pole gap. It extends a few cms over the 270° extension of the pole pieces for facilitating the introduction of the source and the detector. The entrance and exit slit-holders for the charged particles are mounted within the chamber at an angle $\sqrt{2}\pi$ before welding it. Three baffles are inserted within the chamber at equidistant spacings between the slit-holders for avoiding scattering of the particles. The central one may also be used to place slits to reduce the radial and axial aperture of the spectrometer. The baffles and the slit holders have approaches from the outside through the openings. All the openings are made vacuum tight with flanges and O-rings.

The chamber is evacuated by a 6" diffusion pump backed by a mechanical pump. The speed of the diffusion pump is 180 litres per sec. at 10^{-4} mm. Hg. with a water cooled baffle. The limit of the vacuum attained is $\sim 1 \times 10^{-5}$ mm. Hg without the use of any low temperature cooling trap. The general view of the spectrometer with the vacuum equipments is given in figure 3.

PERFORMANCE

To test the performance of the spectrometer, a solution of chloride of Cs-137 was deposited on an aluminium plate, the width of the source being ~ 7 mm. The source was placed in the slit-holder of the spectrometer vacuum chamber and the conversion electron spectrum of 0.661 Mev γ is detected with a 1B85 (Victoreen)



Fig. 3. General view of the spectrometer.

counter through a 3.2 mm slit at an angle $\sqrt{2}\pi$ at the detector side. The magnet is excited with acid cells in the following experiments. Figure 4 shows the resolved spectra of *K* and *L* lines at a solid angle $\sim 0.4^\circ$ sterad, the resolution attained

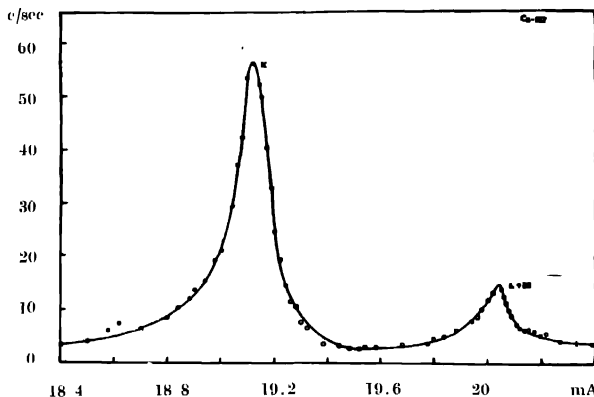


Fig. 4. Conversion electron spectrum *K* and *L* of Cs-137 , detected by counter.

is 0.54% at the half-width compared to the theoretical resolution 0.42% , calculated from the formula,

$$\text{Resolution at half peak} = \frac{a + b + \delta_{ab}}{8r_0} \quad (5)$$

The radial aperture, $h_1 = 44$ mm and the axial aperture, $h_2 = 22$ mm determine the aberration, δ_{ab} . By reducing the apertures and the width of the source 'a' and that of the detector slit 'b', the resolution can further be increased. The experimental resolution obtained above is worse than the theoretical value due to the secondary radiations from the chamber walls and the source target itself. Some improvement may be expected by using a more suitable source target so that back scattering and such radiations are avoided.

The dispersion of a two-directional focussing magnetic analyser with $n = 0.5$ is twice that of a homogeneous magnet. It can be represented as

$$D = \frac{\delta s}{r_0} \frac{\delta p}{p} \quad (6)$$

where r_0 is the mean radius, δs is the distance between the peaks of the particles having momentum p and a difference in momentum δp . The dispersion of the magnetic spectrometer is tested with a (Ilford) G-5 nuclear emulsion (100μ) plate, placed in the detector side and is exposed to the conversion lines L and M of a narrower Cs-137 source. Since with this method a less intense beam can be detected, resolved L and M spectra are recorded. Figure 5 shows the L and M conversion lines scanned from an exposed plate according to the method adopted by Anatov

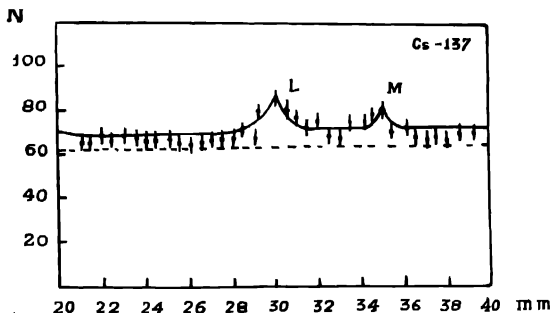


Fig. 5. L and M conversion lines of Cs-137 recorded by nuclear emulsion plates.

(1956) The number of electron tracks N plotted with the length of the plate in figure 5 includes the background counts determined from a plate without any exposure to the source. To attain accuracy in the estimation of the internal conversion coefficients from the spectra, with this method, it is better to attain an improved statistics from two or more plates exposed under the same conditions. However, from the scanning of a single plate with a Leitz Ortholux microscope

of magnification 1000, we have a distance of 5 ± 0.5 mm between the peaks of L and M lines having energy difference 4.304 keV. As the plate makes an angle 10° to the plane, perpendicular to the optic axis for facilitating the detection of electrons, δs is equal to 4.92 ± 0.5 mm. in that plane. Thus

$$D = 3.8 \pm 0.4$$

This is to be compared to the theoretical value of D , which is 4 for such two directional $\sqrt{2}\pi$ focussing magnetic analysers

The axial focussing property of the magnetic spectrometer is also tested with the same source deposited on a cotton thread and placed lengthwise in the radial direction of the spectrometer. The sharpness of its image in figure 6 shows the



Fig. 6. The image of a cotton thread soaked with Cs-137 source placed lengthwise in the radial direction

existence of the axial focussing, attainable with this type of magnetic analysers. The less intense luminous part near the image is due to the cotton fibres of the thread.

The present magnetic spectrometer shows the possibility of its use for high resolution β -spectrometry work. With the stabilised power supply for exciting the magnet, the spectrometer is expected to focus ~ 1 Mev protons as tested by the measurement of the field. Measurement of the gradient also shows that a comparable resolution may be attained with high energy ions.

Further works, to test this instrument with a high intensity ion source and high accelerating voltage, are in progress.

ACKNOWLEDGMENTS

The work was financially supported by the Department of Atomic Energy, Govt. of India, in connection with the development of a magnetic analyser for mass-spectrometry work.

The author is indebted to prof. B. D. Nag, Director of the Saha Institute of Nuclear Physics for his valuable guidance and encouragement in course of this work. I also thank prof. D. N. Kundu for some valuable discussions in the latter part of the work.

The author owes his warmest thanks to the members of the staff of the institute. who have contributed in various ways to this project. Among these special mention is to be given to Mr. S. K. Mukherjee for the design of the diffusion pump, to Miss Bani Sen for application of the nuclear emulsion plates to electron detection and to Mr. P. N. Mukherjee for the source targets. Thanks are also due to Mr. N. C. Sen for scanning nuclear plates.

The author is grateful to Prof. N. Svartholm, Chalmers Institute of Technology, Göteborg, Sweden for his private communication of the design of his mass spectrometer magnet, which was helpful in designing the above spectrometer.

REFERENCES

- Alseovsky, N. E., Prudokvsky, G. P., Kusuorov, G. I. and Filimov, S. I., 1955, *Proc. Acad. Sci. (U.S.S.R.)*, **100**, 229.
- Anatov, I. A., 1950, *Soviet physics*, **3**, 461.
- Arbman, E. and Svartholm, N., 1955, *Arkiv For Fysik*, **10**, 1.
- Buechner, Strait, Stergiopoulos and Sperduto, 1948, *Phys. Rev.*, **74**, 1569.
- Fecher, H. R. and Rubin, S., 1955, *Rev. Sci. Inst.*, **26**, 1108.
- Hodgran, A., 1951, *Manne Siegbahn (Almqvist and Wiksells, Uppsala, Sweden)* p. 269.
- Judd, D. L., 1950, *Rev. Sci. Inst.*, **21**, 213.
- Kerst, D. W. and Serber, R., 1941, *Phys. Rev.*, **63**, 60.
- Lamb, W. E., and Rotherford, R., 1951, *Phys. Rev.*, **81**, 222.
- Langer, L. M. and Scott, F. R., 1950, *Rev. Sci. Inst.*, **21**, 522.
- Lee-whiting, G. E. and Taylor E. A., 1957, *Canad. J. Physics*, **35**, 1.
- Lohr, G., 1955, *Monat. Sitzungsberichte.*, **78**, 47.
- Mileikowsky, C., 1953, *Arkiv For. Fysik*, **7**, 33, 57.
- Rosenblum, E. S., 1950, *Rev. Sci. Inst.*, **21**, 586.
- Rubin, S. and Sachs, D. C., 1955, *Rev. Sci. Inst.*, **26**, 1029.
- Shull, F. B., and Donnison, D. N., 1947, *Phys. Rev.*, **71**, 681.
- Snyder, C. W., Rubin, S., Fowler, W. A. and Lauritsen, C. C., 1950, *Rev. Sci. Inst.*, **21**, 852.
- Sternheimer, R. M., 1953, *Rev. Sci. Inst.*, **24**, 573.
- Stoker, P. H., Hok, Ong. ping, DeHaan, E. F. Sizoo, G. T., 1954, *Physica*, **20**, 337.
- Svartholm, N. and Siegbahn, K., 1946, *Arkiv for Mat. Astr. Fysik*, **33A** nr 21.
- Svartholm, N. 1946, *Arkiv. Mat. Astr. Fys*, **33A** nr 24.
- Verster, N. F., 1950, *Physica*, **19**, 195.

CONSTRUCTION OF A 14 MEV NEUTRON GENERATOR UTILIZING $T^3(d, n) He^4$ REACTION AND MEASUREMENT OF FAST NEUTRON FLUX*

BIMALENDU MITRA

BOSE INSTITUTE, CALCUTTA-9

(Received for publication, March 14, 1959)

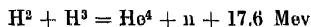
ABSTRACT. Construction of a low voltage accelerating machine for accelerating deuterons which is utilized as a source of production of 14 Mev neutrons, by $T^3(d, n) He^4$ reaction, has been described. Neutron counting has been done by counting recoil protons in a suitable scintillation counter. Neutron yield has also been measured indirectly from saturated activity of an irradiated thin silver foil. Increase in relative flux with increasing deuteron energy from 30 Kev to .1 Mev has been obtained.

1. INTRODUCTION

Banerjee (1955) reported previously the construction of a neutron generator in the Bose Institute. The machine was capable of focussing 2 microamperes of deuteron beam current accelerated to 52 kilovolts, on a Zr—T target placed at a distance of 34". The yield was also determined which was about 1×10^7 neutrons per second in the experimental condition. It was then proposed that a larger machine capable of a much greater and continuous yield of neutrons be built up in the laboratory in addition to the existing one. The present author has successfully built up such an apparatus in the Institute. The instrument is (i) more compact, almost portable, and (ii) has high efficiency with very large neutron yield.

2. CONSTRUCTION

The apparatus, like the previous one, is a low voltage deuteron accelerator which is utilized to produce 14 Mev neutrons by the following reaction :



Deuterium gas is obtained by electrolysis of heavy water and stored in an one-litre flask at nearly normal pressure. This gas is led into an ion-source made of pyrex glass through a fine needle valve. The ion-source is similar to that which has been described by Moak, Reese and Good (1951), but differing in a few details.

*Partly reported in Low Energy Nuclear Physics Symposium 1959, organised by the D.A.E

It is also of large volume, nearly 350 c.c., to minimize the space charge effect and the exposed metallic parts have been kept minimum. The electrodes are carefully concealed within projecting pyrex glass jackets. Figure 1. shows the schematic drawing of the ion-source.

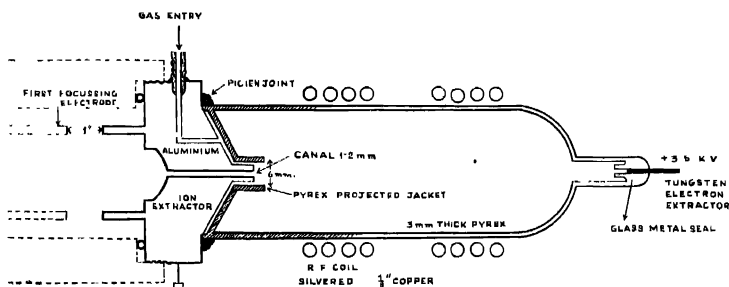


Fig. 1. Ion source.

A radio-frequency discharge is maintained in the ion-source by means of an oscillator of frequency 20-22 megacycles per second and capable of delivering nearly 200 watts of power (figure 2). Loss in the output of the oscillator is minimized by use of a parallel transmission line upto resonating coil round the discharge tube and matching the impedance by trials with dimension of the exciting coil. A second resonance circuit's coil is kept near the first coil, placed axially with the discharge tube and energy transferred to it by link coupling. Diameter of the coils is 2.3" and it is $\frac{1}{8}$ " thick silvered copper wire, having 6 turns. The variable condenser has vanes separated by 4 mms and immersed in oil.

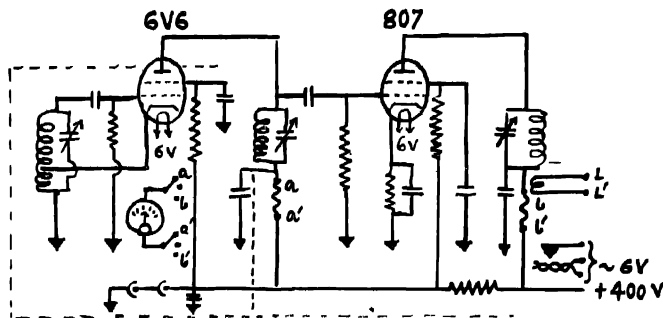


Fig. 2(a) Master oscillator and driver unit of R. F. oscillator, 15-30 Mc/s.

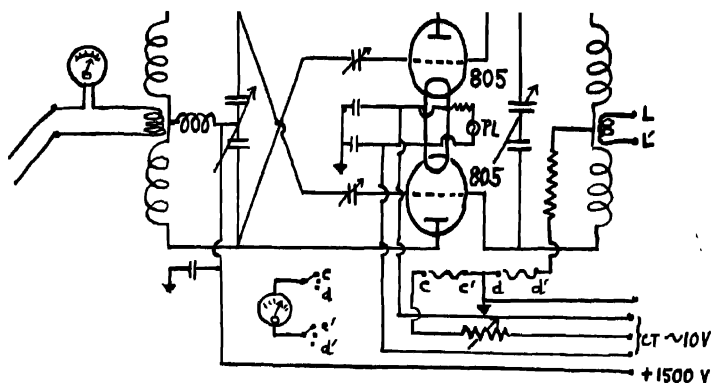


Fig. 2(b) Amplifier unit.

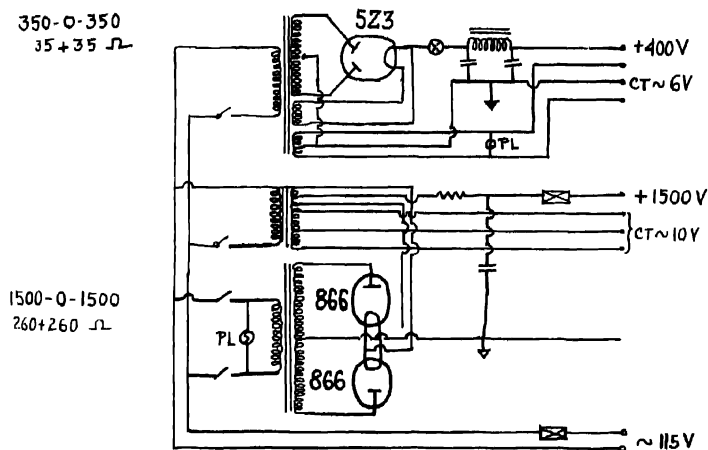


Fig 2(c) Power supply unit.

Under the experimental condition this frequency band of 20-22 megacycles has been seen to be most effective in producing maximum ion current. A magnetic analysis of ions produced in such an ion-source has been previously done by Banerjee (1953) under nearly the same experimental condition, which showed that more than 60% of the ions produced were atomic ions. The ions are drawn out of the discharge tube through an orifice in the aluminium probe in the discharge tube.

Figure 3 is the photographic record of the deuterium discharge, close to the probe canal. The discharge when viewed by a direct visions spectrograph shows three clear spectral lines, α , β , γ , corresponding to Balmer lines of hydrogen. The ions, drawn out of the discharge tube is focussed electrostatically by means of two 1/16" thick cylindrical aluminium electrodes. The lengths of the focussing and next accelerating electrodes are 18" and 4" respectively. The inner diameter is 2.8", but the first focussing electrode has a six-inch part of it of different diameter being 1.8". Information regarding the design has been greatly obtained from the pioneering works of Tuve *et al* (1935) who conducted detailed experiments with various kinds of such electrostatic lenses for focussing positive ions.



Fig. 3 Photograph of ion-source showing deuteron discharge close to probe-canal

The electrodes are held within 0.25" thick Index glass cylinders, specially made for this work by Messrs Sigco Ltd., Calcutta, having inner diameters 3.75" and lengths 6", 9" and 2" respectively. Each cylinder is flanged at either end having ground flat surfaces. The whole assembly forms a cylinder, whose different parts are made vacuum tight by greased O-rings and suitable clamps. The general arrangement is shown in the figure 4.

The target is fitted on a circular brass plate which is clamped at the end of the accelerating cylinder. The accelerator including the ion-source has an overall length of 24" only and rests in a horizontal position on two insulating perspex stands. The accelerator tube and the ion-source with the aluminium probe extractor are attached to the two shorter limbs of a T-shaped mild steel tube of inner diameter 4" — the longer end of the tube is connected to the vacuum system.

This T-tube has been bored from a solid block of steel to avoid any possible vacuum leakage.

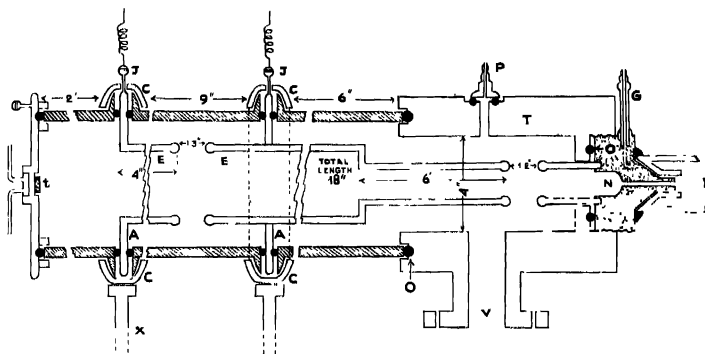


Fig. 4 I—Ion source. G—deuterium gas entry, K—probe-canal, P—Pirani gauge head, V—vacuum connection, T—T-shaped mild steel tube, E—aluminum electrodes for electrostatic focussing, A—aluminum rings for holding the electrodes in position, C—clamps, O—neoprene O-rings, t—target, J—high voltage leads, x—Perspex stands

The pumping system consists of Leybold's OT 100 and D 10 oil diffusion and backing pumps respectively, having pumping speed of 100-120 litres per sec. and reaching an ultimate vacuum of 10^{-6} mm of Hg. There is arrangement for inserting a Pirani gauge head close to the probe canal.

For typical operation, the ion-source probe attached to the T-tube is kept at zero potential while the tungsten electron-extractor at the other end of the ion-source kept at +3.5Kv, the first focussing electrode and the second accelerating electrode are given successively increasing negative potentials. The target is kept 500 volts negative with respect to the preceding electrode.

The targets have been procured from AERE, Harwell, and consist of Tritium gas adsorbed in Titanium metal, deposited on a copper disc. The target contains about 1.4 mg. of titanium in which .61 c.c. of 97% pure tritium gas is absorbed.

The high voltage apparatus consists of a rectifier-voltage doubler circuit capable of giving 125 Kv at 500 milliamps from 50 cycles A.C. supply (figure 5). For greater voltages, the existing R. F. Cockroft Walton type generator, capable of giving 400 μ amps of current at 240 Kv D.C. potential can be used. Output 10 Kv from the r.f. oscillator, at 100 kc/s is multiplied 24 times.

In a particular experimental condition, a total beam current of more than 500 μ amps has been obtained, focussed under 75 Kv., on the target within a

circular spot of nearly 1 cm in diameter. But for the experimental purposes current is now kept limited to only a few μ amps, because of two considerations

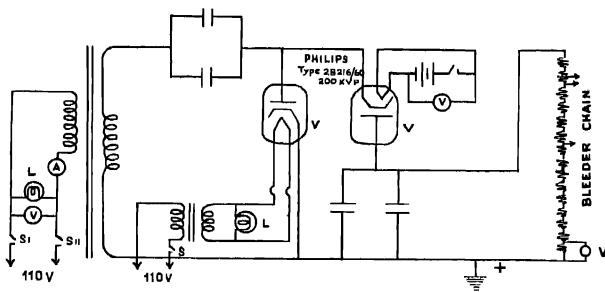


Fig. 5. 125 Kilovolts high tension unit

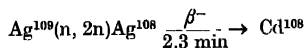
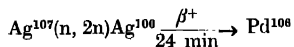
(1) Target requiring more efficient cooling arrangement (2) Neutron shielding of the apparatus requiring more elaborate arrangement. Cooling is now proposed to be done by refrigerated CCl_4 liquid circulating in a closed system through polythene tubes.

At present the apparatus is kept in a second storeyed room of the laboratory and the room is air-conditioned where humidity control is possible. As the neutron shielding is difficult in an upper storeyed room, the apparatus has been proposed to be shifted to an underground room, under construction for its own.

3. MEASUREMENT OF NEUTRON FLUX:

The neutrons have been detected by counting recoil protons with the help of a photomultiplier-scintillation detector employing ZnS in perspex as phosphor. The tube used is EMI type 6260. The measurement of neutron flux has been done in the following way

Fast neutron flux turns the silver nuclei, present in silver metal in normal isotopic forms Ag^{107} and Ag^{109} in the ratio 51.35% : 48.65%, to radioactive silver, Ag^{106} and Ag^{108} by mainly $(n, 2n)$ reaction. The decay scheme of them is the following :



The cross section of $(n, 2n)$ reaction in both the cases is fairly well known. Hence by irradiating a very thin silver foil long enough in the fast neutron flux to get the

2.3 min. saturated activity, and counting product β -particles we can know the equivalent activity. Then neutron flux is given by

$$(nv) = \text{no. of neutrons/sec. cm}^2 = \frac{A}{N\sigma} \quad \dots \quad (i)$$

A = equivalent activity

N = no of nuclei/cm² in sample foil

σ = $(n, 2n)$ reaction cross section.

The actual count in the β -counter is related to total disintegration rate by a formula :

$$\frac{c}{m} = \frac{d}{m} \cdot E \cdot f_t \cdot f_B \cdot f_w \cdot f_s \quad \dots \quad (ii)$$

where

$\frac{d}{m}$ = disintegration rate

$\frac{c}{m}$ = actual count rate

E = corrected efficiency of the counter

f_t = counter dead time correction factor

f_B = backscattering correction factor

f_w = factor for correction of absorption in window, air and counter wall etc.

f_s = self-absorption factor

In the investigation a very thin silver foil is attached to the atmospheric side of the target. It is circular, having diameter exactly 1", i.e. being equal to the tritium absorbed layer of the target. It is irradiated by fast neutron flux for 10 mins. During the irradiation, pressure inside the ion source is adjusted very cautiously by the needle valve so that the ion-current indicated by the microammeter in series with the target connection, remains strictly constant. The oscillator output remains constant, as shown by a r.f. ammeter in series with the coil.

The total accelerating voltage used is 62 kilovolts, total beam current kept fixed at 50 μ amps. The focus spot can easily be marked on the target by its deep bluish colouration and is less than one cm in diameter. The ion-source probe voltage is 3.5 Kv. The discharge current is 2.5 mA. The potential in the first focussing electrode is 37.5 Kv.

Waiting for 1½ minutes after irradiation, the thin foil, having a thin aluminium backing, is held under an end window β -counter (having 3mg/cm² window thick-

ness) in a fixed geometry. The decay curve is plotted as number of counts per minute (every half minute interval) against time and from this decay curve, initial activity is extrapolated, assuming that in 10 minutes, saturation is reached for 2.3 minute product.

In the formula (ii), E is the product of geometrical factor $\frac{\omega}{4\pi}$ and probability ϵ of counting a β particle which enters the counter, neglecting multiple pulses. The relative value of E has been determined by the help of a P^{32} standard source of known strength prepared from sodium phosphate of 2mc/ml strength. P^{32} beta particles have nearly the same energy as Ag^{108} betas. The other corrections are made after usual procedures. The correction f_B is taken from the backscattering curves obtained by Zumwalt (published in the U.S. AECU-567), for P^{32} radiation, with Al backing. f_s have been neglected because the foil is a very thin one. The value of σ has been obtained from Los Alamos results given in USAEC, -BNL325. Calculation from (1) shows in this experiment, 50 μ a of total beam accelerated upto 62 Kev, yield 1.4×10^9 neutrons/sec/cm² passing through the foil attached on the atmospheric side of the target.

4. VARIATION OF NEUTRON YIELD WITH INCREASE OF DEUTERON ENERGY

Bretscher and French (1948) studied the cross section of (d, t) reaction for projectile energy upto 125 Kev, and their works showed the presence of a resonance at nearly 100 Kev

Conner *et al* (1952) studied the (T, d) reaction in details, employing tritium adsorbed targets, and varying the deuteron energy from 10 Kev to 1732 Kev. They obtained the maximum value of cross section at 109 Kev, σ , being equal to 5.1 ± 1 barns. From their curve it has been determined that increase of (T, d) reaction cross section, i.e. increase of product neutron yield is nearly 5 times at 100 Kev than its value at 51 Kev.

In the present investigation, the scintillation counter reading in a fixed geometry from the source has been calibrated to read neutron flux directly. Keeping the beam current constant and varying the projectile energy from 30 Kev to 100 Kev (the focus-spot on the target is seen to remain on the target area inspite of a little variation in the dimension of focal spot), counts per minute in the scintillation-detector, which counts recoil protons, is plotted against deuteron energy and thus variation in neutron yield with increase of deuteron energy has been obtained (figure 6).

The curve fits with the curve of Conner *et al* (1952) in voltage region lower than 100 Kev.

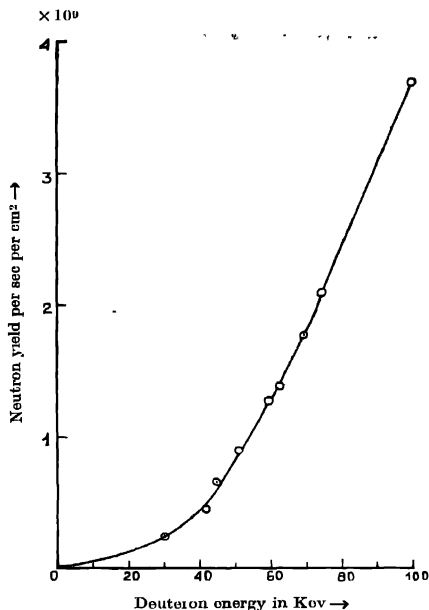


Fig. 6. Curve showing neutron yield with increase of deuteron energy.

ACKNOWLEDGMENT

The author is grateful to Prof. D. M. Bose, Director of the Bose Institute for his keen interest in the work.

REFERENCES

- Banerjee, A., 1953, *Ind. Jour. Phys.*, **57**,
 Banerjee, A., 1955, *Science and Culture*, 454.
 Broecker, E. and French, A. P., 1948, *Phys. Rev.*, **75**, 1154.
 Connor, J. P., Bonner, T. W., and Smith, J. R., 1952, *Phys. Rev.*, **88** 468.
 Moak, C. D., Reese, H. and Good, W. M., 1951, *Nucleonics*, **9**, 3.
 Tuve, M. A., Dahl, O. and Hafstad, L. R., 1935, *Phys. Rev.*, **48**, 241.

ENERGY DISTRIBUTION OF NEUTRONS FROM RA-D-BE SOURCE

B. SEN

SAHA INSTITUTE OF NUCLEAR PHYSICS, CALCUTTA-9

(Received for publication, March 19, 1959)

ABSTRACT. The energy distribution of neutrons from RaD-Be source has been studied with photographic plates. The effect of scattering of these neutrons in lead was investigated also. The neutron peaks in the energy distribution curve correspond to different levels of C^{12} . The discrepancies are discussed.

INTRODUCTION

The neutron energy spectra from Po-Be source has been investigated by various methods (Richards and Demers, year; Whitmore and Baker, 1950; Gursky *et al*, 1953, Elliot *et al*, 1954, Breen *et al*, 1945). Almost in each case the spectra obtained show two general characteristics.

(i) The presence of three peaks of neutrons near 3 Mev, 5 Mev and 7 Mev energies corresponding to the levels of residual nucleus C^{12} at 4.43, 2.5 Mev. and the ground state (Hornyak and Lauritsen, 1948) respectively and

(ii) an average energy of neutrons of about 4.6 Mev. The peak near 5 Mev. has been explained by Whitmore and Baker(1950) due to the presence of a level of C^{12} at 2.5 Mev; however the data from other experimental results show the level structure of C^{12} (Ajzenberg and Lauritsen, 1955) with the first excited level at 4.43 Mev. In view of these conflicting reports an attempt was made to check the energy spectra of the neutrons from Po-Be source. Instead of Po-Be source a RaD-Be neutron source was however used. It is well known from the decay scheme that there is no α emitting nuclide between RaD and Po and as such the α -particles taking part in the reaction producing neutrons from a (RaD+Be) source are those from the decay of Po^{214} . Hence the neutron energy distribution from a RaD-Be source should be identical with that from a Po-Be source. There are however a few low energy γ -rays in the decay of RaD and RaE. Lead absorber was used to cut off these γ 's which fogged the plate slightly which was exposed to this source directly. The spectra obtained in this experiment also show a prominent peak near 5 Mev. Possible reasons for the presence of this peak are discussed.

EXPERIMENTAL PROCEDURES

The RaD-Be source of 20 millicurie strength was used as the source of neutrons and photographic plates were used as detectors. Ilford C-2 plates of

100 microns thickness were mounted radially about the source with the plane of the emulsion horizontal, the distance of the centre of the plate being 10 centimeters from the source. Exposures were given once with the source only and once with lead of thickness nearly one inch surrounding the source. The plates were processed by the usual method of processing thin plates using Ilford ID-19 developing solution.

METHOD OF MEASUREMENT

The proton recoil method has been followed in the experiment described and since it is most extensively used in neutron energy measurements, no detailed descriptions are necessary here. All measurements were done according to the method given by Rosen (1953). The projected length to the emulsion surface of the available tracks were measured. The selection criteria were that only those recoil proton tracks were recorded which had horizontal angles of less than or equal to 15° with the central line and dip angles of less than or equal to 15° in the unprocessed emulsion, further only those tracks were accepted which started and ended within the emulsion.

With these criteria, the corresponding energy of the neutron was obtained using the following procedure. The projected length R_p of a recoil track is related to the absolute range L_p of the proton track in the unprocessed emulsion by the relation $L_p = R_p / \cos \bar{\psi}$ where $\cos \bar{\psi}$ is the average value of the cosine of the angle ψ between R_p and L_p and is a function of the angles θ_{max} and ϕ_{max} which are the maximum values of the half angles θ and ϕ respectively (each equal to 15° in the present case) of the rectangular pyramid formed by the recoil proton track.

The energy of the recoil protons is directly obtained from the range energy curve of Lattes *et al.* The neutron energy E_n corresponding to the recoil proton energy E_p is given by the relation $E_n = E_p / \cos^2 \rho$ where $\cos^2 \rho$ is the average value of the cosine squared of the angle ρ between the incident neutron and the recoil proton directions and is again given as the function of θ_{max} , γ_{max} and ϕ_{max} where γ_{max} is the maximum value of the angle γ that the incident neutron makes with the axis along which the projected lengths of the tracks are measured. This method leads to an error of less than one per cent in the neutron energy E_n for θ_{max} , ϕ_{max} and γ_{max} less than 15° . Finally in order to transform the measured proton energy distributions into the neutron energy distributions the variation of the n - p scattering cross section with neutron energy and the escape probability of the recoil protons from the emulsion surface ((Rosen, 1953) should be taken into account

About 1100 tracks were scanned in the case in which lead absorber was used and 750 tracks were observed for the case in which no absorber was used. A Leitz microscope with 8×100 magnification was used for the measurements,

No corrections were made for straggling effects. The shrinkage factor was taken to be 2.5.

RESULTS AND DISCUSSIONS

The energy distribution curves for both the cases were plotted at the energy interval of 0.5 Mev as shown in the figure 1. There is good agreement of our curves with that obtained by Whitmore and Baker (1950), Elliot *et al.* (1954) and others. The common features are the followings:

- (i) The spectra extend upto the maximum neutron energy of nearly 11 Mev.
- (ii) Neutron peaks are obtained near 3 Mev, 5 Mev, and 7 Mev.

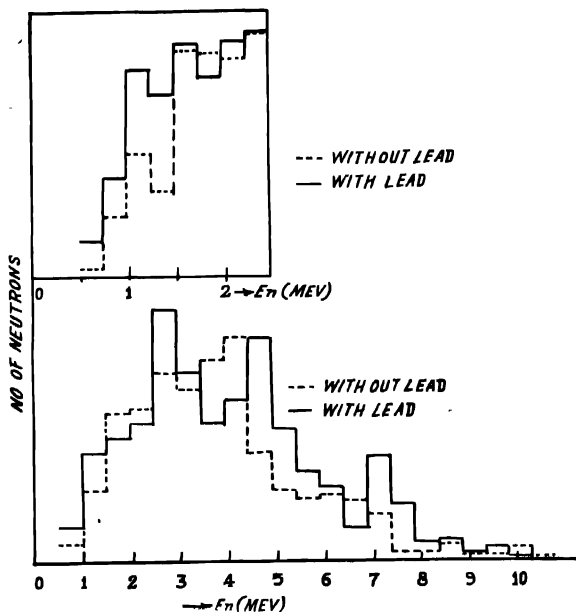


Fig. 1 (bellow) & Fig. 2 (above).

No peak was present near 1 Mev when the plot was at 0.5 Mev energy interval. When the histogram is drawn at an energy interval of 0.25 Mev a small peak is obtained near 1.5 Mev.

The low energy sides of both the spectra were plotted (figure 2) at an interval of 0.25 Mev neutron energy to study the effect of inelastic scattering of neutrons in lead. No sharp difference is observed between the two curves.

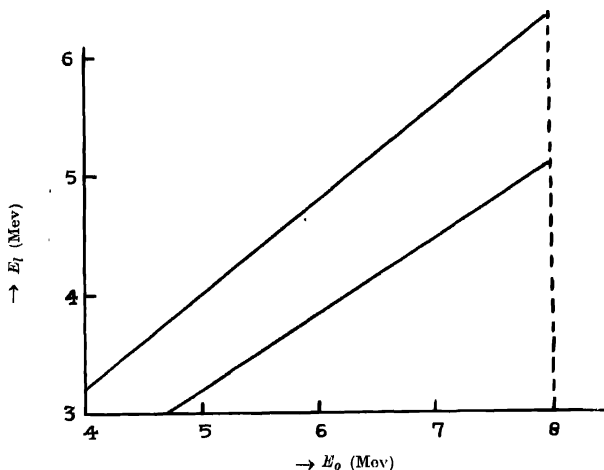


FIG. 3

A thorough discussion has been made by Whitmore and Baker (1950) to give proper explanation of the energy spectra of neutrons obtained from Po-Be source, examining all the possible discrepancies. In the curve obtained in this experiment almost all the characteristics noted by Whitmore are present. The peak near 5 Mev or the 2.5 Mev level of C^{12} is absent in many other experiments (Powell, 1943; Champion and Powell, 1944, Bradford and Bennett, 1950). Experiments detecting γ 's and γ - γ coincidences (Ajzenberg and Lauritsen, 1955) show the presence of 4.43 Mev level as the 1st excited state of C^{12} . These evidences indicate that the peak near 5 Mev is not due to excitation of any level of C^{12} . The comparison of the theoretical neutron spectra (Whitmore and Baker, 1950) considering only the ground state and first excited state with that of the experimentally obtained shows that the intensity of the higher energy sides i.e. from 6 Mev to 11 Mev is much reduced in the experimental curve. All these discrepancies may be due to the elastic scattering of the neutrons. The neutrons liberated in the source after $Be^9(\alpha, n)C^{12}$ reaction before coming out of it may be scattered elastically again in the beryllium nuclei within the source itself. The emerging neutrons then lose some energy which transfer to the recoil nuclei. The neutrons within the energy range 5.5 Mev to 8 Mev after elastic scattering attain the energy value near about 5 Mev. Whether a peak occurs or not can be checked in the following way. The energy of an elastically scattered neutron E_e for a given

energy of neutrons before scattering E_0 is again function of scattering angle $\bar{\phi}$ and is given by the relation

$$E_{el} = \frac{E_0}{(M+m)^2} \left[m \cos \bar{\phi} + (M^2 - m^2 \sin^2 \bar{\phi})^{\frac{1}{2}} \right]$$

where m = mass of the neutron and M = the mass of the nucleus under investigation (Be^9)

Again for a fixed neutron energy a uniform distribution in angle in centre-of-mass system corresponds to a uniform distribution in energy in the laboratory system. The maximum and minimum values of E_{el} corresponding to a fixed value of E_0 are calculated and plotted in figure 3 in the range from 6 Mev to 8 Mev. Now to determine the effect of varying neutron energies we need the excitation function of this. It is to be noted here regarding the result of this calculation that the assumption has been made that neutrons of fixed energy E_0 liberate neutrons with a uniform distribution of energy. Following the same type of calculation used by Whitmore and Baker (1950) the distributions of scattered neutrons may be obtained from the given range of energy of neutrons before scattering. If the number of neutrons having energies in the range dE_0 is proportional to dE_0 , and if each such particle after scattering gives $f(E_0)$ scattered neutrons and if these neutrons are spread uniformly over a range of energies ΔE_{el} then the number of such neutrons having energies between E_{el} and $(E_{el} + dE_{el})$ is proportional to $f(E_0) dE_0 \cdot dE_{el} / \Delta E_{el}$. The number of neutrons of this energy therefore may be calculated on this basis using the value of elastic scattering cross section at that energy to obtain $f(E_0)$. The elastic scattering cross section is taken equal to half of the total cross section σ_t at this energy. The σ_{el} was obtained from $\sigma_t^{(14)}$. The curve obtained is shown in figure 4. It shows the presence of a peak in the region of 4—5 Mev. There is however difficulty in interpreting the intensity of the peaks observed with the theoretical one.

The average energy of the continuous distribution of neutrons is 4.6 Mev. The effect of inelastic scattering in lead is mainly from the neutrons of this energy. But actually there is the contribution from neutrons of energies extending upto 11 Mev. This gives rise to a very complicated pattern. The effect of inelastic scattering of 4.6 Mev and also of 14 Mev neutrons has been studied in lead (Mandeville and Swann, 1951; Graves and Rosen, 1953; Whitmore, 1953). These results show an increase in number of neutrons in the low energy region and a peak near 1 Mev due to the excitation of the level near 3 Mev of naturally occurring lead. In our curve no sharp peak near 2 Mev was obtained using lead, and the increase of number of neutrons in the inelastic region is very small. Also the peak near 8 Mev is sharp using lead for which no proper explanation can be given.

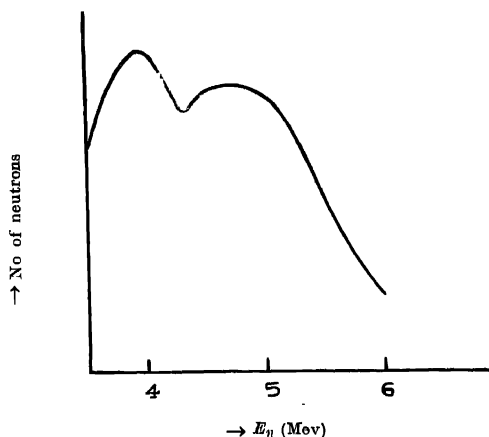


Fig. 4

No detail and precise analysis is possible because of the large statistical error and the complicated nature of the process because of the continuous energy distribution.

ACKNOWLEDGMENT

The author is grateful to Prof. B. D. Nag for his encouragement during the work and for providing all possible facilities to carry it out and to Dr. S. N. Ghoshal for initially suggesting the investigation. Acknowledgment is also due to the D.A.E. under whose auspices the scheme has been undertaken.

REFERENCES

- Ajzenberg, F. and Lauritsen, T. 1955, *Rev. Mod. Phys.*, **27**, 77.
- Allerik, J. C. and Armstrong, A. H. 1950. Laboratory handbook of nuclear microscopy; L.A.
- Bradford, C. F. and Bennett, W. E. 1950, *Phys. Rev.*, **77A**, 753.
- Breen, Hertz and Wight, 1956, *MLM*, **10**, 1054.
- Champion, F. C. and Powell, C. F. 1944, *Proc. Roy. Soc.*, **A183**, 64.
- Elliot, J. O., McGarry, W. I. and Faust, W. R. 1954, *Phys. Rev.*, **93**, 1348.
- Graves, E. R. and Rosen, L. 1953, *Phys. Rev.*, **89**, 343.
- Gursky, H., Winnemore, B. and Cowan, D. A. 1953, *Phys. Rev.*, **91**, 209.
- Hornyak, W. F. and Lauritsen, T. 1948, *Rev. Mod. Phys.*, **20**, 191.
- Lattes, Fowler and Cier, 1947, *Nature*, **159**, 301.
- Mandeville, G. E. and Swann, C. P. 1951, *Phys. Rev.*, **84**, 214.

Powell, C. F. 1943, *Proc. Roy Soc.*, **A181**, 344.

Richards and Demers, Anderson: Neutrons from alpha-Emitters Nuclear Science Series No. 3.

Rosen, L. 1953, *Nucleonics*, Vol. **11**, No. 7, 32, and No 8, 38.

Tables of Neutron cross sections A.E. C U. 2040

Whitmore, B. G. and Baker, W. B. 1950, *Phys. Rev.*, **78**, 799.

Whitmore, B. G. 1953, *Phys. Rev.* **92**, 654.

MAGNETIC STUDY OF IRON-CONTAINING GLASSES AT ROOM TEMPERATURE

BHUPATI KUMAR BANERJEE*

INDIAN ASSOCIATION FOR THE CULTIVATION OF SCIENCE, JADAVPUR, CALCUTTA-32

(Received for publication, January 30, 1959)

ABSTRACT. The well-known magnetic method of analysis is applied to elucidate the origin of colour in boric oxide, borate and high lead silicate glasses containing iron. It is observed that iron exists in glass in more than one form and the proportion of different forms of iron in glass changes with the (1) composition of the glass base, (2) the nature and concentration of iron compound and (3) the temperature and the time of heating. All these observations are discussed with reference to the existing theories about the origin of colour in iron glass. The above observations are also explained from the structural picture of each glass base. The colour of iron glass comprising solid phase colours and liquid phase colours is due to the resultant effect of two or more forms of iron of different valency states with the different types of electronic binding including the covalent and electrovalent linkages.

INTRODUCTION

The study of the origin of colour in iron glass has provided a fascinating problem from the early time onwards. Outstanding workers on this line are Jackson, Weyl, Moore, Jung, Stevels, Cole, Kreidl and few others. Though the published information is vast and voluminous yet our knowledge of the mechanism of coloration in iron glass is still elementary. An excellent summary of the different schools of thought has been compiled by Weyl (1950) in a monograph on coloured glasses. But from the results of several workers like Moore *et al* (1949 and 1950), Weyl (1943), Cole (1951a) Stevels (1950), Jong (1952, 1954) and Abou-El-Azm (1954), it is clear that there is no consensus of opinion regarding the chemical picture of different chromophores in iron glass. Their observations are summarised in Table I.

Perhaps the most distinctive property of different forms of iron is their magnetic behaviour. The nature of bondings of iron ion with its surrounding ions, its co-ordination number, valency etc. have a direct influence on the magnetic property of the element. Further it is known from the work of Cole (1951b) that the bondings with oxygen in the network forming position are more covalent than the bondings in the network modifying position. Naturally with the transition of the electronic bonding to the more covalent type of bonding the paramagnetic susceptibility will decrease by the quenching of the orbital

*Present address:—Central Fuel Research Institute, P.O. Jeolgora, Dhanbad

moments. In the Table II, the susceptibility values of iron are given in various states of valency and coordination which will be useful for comparison with our experimental findings.

As such, it will be interesting to study by magnetic method the state of existence of iron in glasses of varying compositions as well as in the specimens prepared under different melting conditions. There, too, the effect of concentration of colourant and the relationship between the colour and the state of existence of iron in 'neutral' *glasses and in some 'reduced' †glasses as well as in a few 'oxidised' glasses deserve careful attention

TABLE I

Description of colour	Name of different workers with their views given in the vertical column				
	Moore and Co-workers (1949, 1951 & 1951)	W.A.Weyl (1943)	H.Cole (1951)	J.M Stewels (1950)	J.De Jong (1952 & 1954)
Colourless (Absorption in ultraviolet)	FeO_4	Fe^{+3}		Fe^{+2}	Fe^{+3}
	Tetrahedral	N.W.M.*		N.W.M.	N.W.F.
Brown	Fe_2O_3	Fe^{+3}	Fe^{+3}	Fe^{+3}	
	Colloidal	N.W.F.*		N.W.F.	
Blue	Fe^{+2}	Presence of a group $\text{Fe}^{+2} - \text{O} - \text{Fe}^{+3}$	Fe^{+2}	Interaction of $\text{Fe}^{+2} - \text{Fe}^{+3}$ (probably not work forming)	
Colourless (Absorption in Infra-red)		Fe^{+2} N.W.M.		Fe^{+2} both N.W.F. and N.W.M.	Fe^{+2} N.W.F.
Grey	Fe_3O_4 Colloidal			Mixture of Fe^{+3} (N.W.F.) and $\text{Fe}^{+2} - \text{Fe}^{+3}$	

*Where N.W.M. means network modifying cation and N.W.F. means network forming cation

†Glasses are prepared in neutral or oxidising or reducing furnace atmosphere.

TABLE II

Magnetic property of some forms of iron

Description of iron ion with no electron pairing	χ of Fe $\times 10^6$ at 25°C	Description of iron ion with electron pairing	χ of Fe $\times 10^6$ at 25°C	Description of some oxides of iron	Magnetic behaviour
Fe ⁺² with orbital moment	225.4	Fe ⁺² in square configuration	59.68	FeO in solid aggregates	Feebly paramagnetic
Fe ⁺² spin only value	178.8	Fe ⁺² in Octahedron	Diamagnetic		
Fe ⁺³ spin only value	261.1	Fe ⁺³ in square	111.6	α -Fe ₂ O ₃ in solid aggregates	Feebly Ferromagnetic
Fe ⁺³ with orbital moment	225.4	Fe ⁺³ in Octahedron	22.29	α -Fe ₂ O ₃ in colloidal dispersion in glass	$\chi^* = 39.4 \times 10^{-6}$ at 20°C (after Abou-El-Azm, 1954)
Fe ⁺⁴ without orbital moment	178.8	Fe ⁺⁴ in square	178.8	γ -Fe ₂ O ₃ in solid aggregates	Ferromagnetic.
Fe ⁺⁶ with orbital moment	178.8	Fe ⁺⁴ in Octahedron	59.68		
Fe ⁺⁶ without orbital moment	59.68	Fe ⁺⁶ in square	59.68	Fe ₃ O ₄ in solid aggregate	Ferromagnetic
		Fe ⁺⁶ in Octahedron	59.68	Fe ₃ O ₄ in colloidal dispersion in glass	$\chi^* = 424 \times 10^{-6}$ at 20°C (after Abou-El-Azm, 1954)

*Different values are also found in the literature.

EXPERIMENTAL PROCEDURE

The present investigation covers several glass systems such as primary, binary and ternary iron glass where boric oxide is the main glass forming oxide. Glass series studied are as follows. B₂O₃, alkali-boric oxide and lithia-beryllium oxide boric oxide glass systems. The last named glass is usually known as Lindemann glass. A variety of high lead potash silica glass is also included.

All experimental specimens were prepared from extra pure materials such as borax, boric oxide, alkali carbonate, alkali nitrate, beryllium carbonate, red lead (Pb₃O₄), ferrous exalate, tartaric acid, precipitated silica etc. Boric oxide was prepared from pure boric acid by heating at 1260°C in an electric furnace for eight hours. The requisite proportions of different components of glass batch were thoroughly powdered, mixed and then heated at 1050°C for six hours in a platinum crucible, except in the case of lead glass where sillimanite crucible was used. All glass samples were prepared in a neutral furnace atmosphere with the

exception of few 'reduced' borate glasses and 'oxidised' lead silicate glasses. Special care was taken to prevent frothing in some high alkali glass batch by adding the batch compositions in small quantities to the melting pot till they melt. The melt of silicate glass was agitated several times during the course of melting so as to ensure complete homogeneity of the system. Further all glasses were annealed at 575°C for half an hour and then cooled to room temperature in the same way prior to any physical examination.

The total iron content of each specimen was determined chemically by the usual dichromate process after removing the boric oxide as methyl borate. In the case of lead glass and Lindemann glass (lithia beryllium oxide-boric oxide glass) necessary steps were taken for the removal of interfering elements like lead and silica in lead glass and beryllium in Lindemann glass respectively before determining the iron content in the system. The alkali content in each glass specimen was calculated from batch composition.

All magnetic measurements were carried out in an accurate and sensitive torsion type Curie balance which was developed and modified in our laboratory. The details of the balance with the method of calibration and the limit of accuracy have already been published by Dutta-Roy (1955).

The susceptibility at room temperature 300°K is calculated from the standard expression :

$$\chi_1 = \frac{m_2 \theta_1}{m_1 \theta_2} \left(\chi_2 - \frac{K_a}{P_2} \right) + \frac{K_a}{P_1} \quad \text{where the correction}$$

for air has been introduced.

χ_1 = mass susceptibility of the unknown substance at 300°K.

χ_2 = mass susceptibility of the standard substance at 300°K.

m_2 = mass of the standard substance.

m_1 = mass of the unknown substance.

θ_1 = rotation in degrees for the unknown substance of the torsion fibre to balance the magnetic force.

θ_2 = Corresponding rotation in degrees for the standard substance.

K_a = volume susceptibility of air at 300°K.

P_1 = density of the unknown substance at 300°K.

P_2 = density of the known standard substance at 300°K.

The standard substance used in the present investigation was chromium potassium alum. The value for the mean square of the effective moment of Cr^{+3} is 15.05 in Bohr unit [Dutta-Roy, (1955)] . For pure glass base which is diamagnetic, water was taken as a standard substance with mass susceptibility at 300°K = 0.7200×10^{-6} . Mean of three measurements of each specimen was taken.

In the vitreous system like iron-glass the magnetic property of iron is affected much by the diamagnetic property of the glass base, due to the small concentration of the colouring constituent. However, the mass susceptibility of iron can be determined from the following additivity relation :

$$\chi_g = \chi_o C_r + \chi_b(1-C_r)$$

where χ_g = mass susceptibility of glass

χ_o = mean mass susceptibility of iron

χ_b = mass susceptibility of the glass base

C_r = concentration of iron

Thus the mass susceptibilities obtained for the iron in different types of iron glasses were compared with one another amongst several glass series studied here

MAGNETIC PROPERTY OF IRON IN BORIC OXIDE GLASS

In the literature some valuable observations have been reported on the colour mechanism of borate and borosilicate glasses containing iron by Moore, Weyl, Abd-El-Moneim etc. but so far no such work has been done on pure B_2O_3 series possibly due to the difficulty of preparing boric-oxide iron glass where the colouring oxide Fe_2O_3 (in the pure form) does not satisfy the criteria of glass forming oxide. However, it is observed that iron oxide can be dispersed in pure dry boric oxide at a temperature of $1050^\circ C$ to the extent of 0.3 per cent iron (of the total glass content) and the resultant colour of the glass is yellow. Two such samples with varying iron content have been studied. It is observed that the colour of the glass deepens more with the increasing content of colouring constituent in glass.

The susceptibility value of iron in each sample is given in the following table :

TABLE III
Boric Oxide Glass

Glass sample No.	Iron content in weight percent	χ of glass $\times 10^6$ at $25^\circ C$	χ of glass base $\times 10^6$	χ of iron $\times 10^6$ at $25^\circ C$
1	0.1722	-0.2981	-0.4300	73.70
2	0.2712	-0.1983	-0.4300	84.98

It can be readily seen from Table III that the susceptibility of iron in B_2O_3 glass does not correspond with the value of any single form of iron. Again, from the consideration of the glass composition it is evident that Fe_2O_3 in itself or in combination with B_2O_3 cannot form network forming or network modifying

cations. All these indicate that iron exists in two or more forms as solid phase colours in the glassy matrix. The distribution of different forms of iron is very much dependent on the total iron content in the same glass base.

MAGNETIC PROPERTY OF IRON IN ALKALI-BORIC OXIDE SERIES

The present investigation of different binary borate systems is extended to various samples with increasing alkali content in lithia-boric-oxide, soda-boric oxide and potash-boric oxide glasses. The magnetic work on similar glass systems is already reported by Abd-El-Moneim (1954) and Bhatnagar (1945).

The experimental specimens comprise a number of samples of different compositions and each glass specimen was prepared in neutral furnace atmosphere. In all these cases, iron was introduced in the original glass base as Fe_2O_3 . The mass susceptibility of iron in different glass bases is given in the following table :

TABLE IV
Lithia-boric oxide series

Glass sample No.	Alkali oxide in wt. percent	Fe in weight percent	χ of glass $\times 10^6$ at 25°C	χ of glass base $\times 10^6$	χ of Fe $\times 10^6$ at 25°C
3	5.745	1.745	3.587	-0.3115	223.0
4	10.04	1.672	3.530	-0.4173	235.7
5	15.00	1.013	2.055	-0.4160	243.5
6	18.483	0.72	1.337	-0.4193	243.5
7	18.483	1.010	2.099	-0.4193	249.1
8	18.483	1.119	2.411	-0.4193	252.5
9	31.20	0.250	0.2150	-0.3971	244.4

Soda-boric oxide series

10	9.475	2.848	5.534	-0.4213	208.6
11	17.46	1.585	5.271	-0.4432	225.8
12	31.00	0.650	1.116	-0.4217	236.1
13	31.00	1.048	2.137	-0.4217	243.6
14	31.00	1.210	2.571	-0.4217	246.9
15	34.00	1.358	2.870	-0.3989	240.2

Potash-boric oxide series

16	4.615	1.621	2.629	-0.4580	190.0
17	14.22	1.673	3.120	-0.4186	211.1
18	41.44	0.830	1.556	-0.4155	237.1
19	41.44	1.221	2.528	-0.4155	240.6
20	41.44	1.310	2.789	-0.4155	244.2
21	58.55	0.421	0.790	-0.4213	243.1

It is evident from Table IV that the mass susceptibility value of iron changes with the change of glass composition, nature and the content of alkali ion. In the same weight for weight composition of different alkali-boric oxide glasses, the mass susceptibility value of iron decreases from lithia-boric oxide glass to potash-boric oxide glass. Further, the experimental susceptibility value of iron does not correspond with the theoretical value of any likely form of iron. Again, in comparison with the mass susceptibility value of iron in B_2O_3 glass, the mass susceptibility value of iron in the present binary system is quite high, which is due to the presence of more of high-mass-susceptibility form of iron like ferric ion in the system. Further, in all cases the mass susceptibility value of iron in binary system lies between the susceptibility value of ferrous and ferric ions.

It may be of interest to mention here that the present result is not in agreement with that of Abou-El-Azm or Bhatnagar. The value of mass susceptibility of iron in the above soda-boric oxide glass as well as in other lithia-boric oxide and potash-boric oxide glasses of composition similar to ours and of similar thermal history as obtained by Abou-El-Asm lies much below the Fe(ous) 'spin only' value of iron in each case. In contrast with that the value of mass susceptibility of iron in 'oxidised' borax (with 31% Na_2O) glass as obtained by Bhatnagar (who studied only few samples of soda-boric oxide glasses) is very close to the ferric 'spin only' value. Whereas our results of mass susceptibility of iron lie in between those of ferrous and ferric 'spin only' values.

MAGNETIC PROPERTY OF IRON IN TERNARY BORATE GLASS

The ternary borate system is represented by lithia-beryllium oxide-boric oxide glass (usually called Lindemann glass) of the following percentage composition: $Li_2O = 13.74$, $BeO = 5.54$ and $B_2O_3 = 80.72$. The colouring constituent is introduced in the glass as Fe_2O_3 . The choice of the above system has been made after due consideration of the structure of lithia-boric oxide glasses. In connection with the constitution of ternary borate glass, it is worthwhile to mention here that the above system contains small amount of Be^{+2} ion which has a small ionic radius ($r = .31 \text{ \AA}$) and high ionic potential (8.6).

The mass susceptibility of iron in Lindemann glass is given in the following table wherein the susceptibility value of iron in two binary lithia-boric oxide glasses with 10 and 15 per cent lithia content respectively is included for the sake of comparison.

It is seen from Table V that the susceptibility value of iron in Lindemann glass lies in between that of ferrous and ferric ions and this value is greater than the corresponding lithia-boric oxide glass (vide table II). This can be accounted for by the presence of Be^{+2} ion in Lindeman glass where Be^{+2} ion can also function as a network forming cation. Thus in the competition for occupying the network

TABLE V
Lindemann Glass

Glass sample No.	Type of glass	Lithia in wt per cent	Fe in weight per cent	χ of glass $\times 10^6$ at 25°C	χ of glass base $\times 10^6$	χ of Fe $\times 10^6$ at 25°C
22	Lindemann glass	13.74	2.004	4.515	-0.4425	247.0
23	"	13.74	1.100	2.246	-0.4425	244.0
4	Lithia-boric oxide	10.04	1.672	3.530	-0.4173	235.7
5	Lithia-boric oxide	15.00	1.013	2.055	-0.4160	243.5

forming position in the glass meshwork in both Lindemann glass and lithia-boric oxide glass, the number of ferric ion in network forming position will be usually smaller in lithia-boric oxide glass and still smaller in Lindemann glass. That is why the possibility of the greater proportion of ferric ion in network modifying position is more in Lindemann glass than in the corresponding lithia-boric oxide glass. So the susceptibility value of iron in Lindemann glass is more than the corresponding lithia-boric oxide glass.

MAGNETIC PROPERTY OF IRON IN POTASH-LEAD
OXIDE-SILICA 'OXIDISED' GLASS

The potash-lead oxide silica glass of percentage composition, $\text{PbO} = 60.0$, $\text{K}_2\text{O} = 10.0$ and $\text{SiO}_2 = 30.0$ stands quite in contrast with other glass systems studied in the present case. The major constituent in this case is lead ion Pb^{+2} with its high polarizability capacity with $(18+2)$ outer electrons. In this glass batch Fe_2O_3 was added as colouring oxide and potassium was introduced as KNO_3 so as to ensure oxidising condition during the period of melting. The colour of this glass is yellow and in such high-lead glasses, small amount of iron produces intensive colour [(Jackson, 1927) and Hampton, (1946)]. This type of glass has been described by Moore and co-workers as fully ferric glass where iron exists mainly as a colouring ferric ion. The susceptibility value of iron in high lead silica glass as obtained by us is given in the following table.

TABLE VI
Potash high lead silica glass

Glass sample No.	Iron in weight per cent	χ of glass $\times 10^6$ at 25°C	χ of glass base $\times 10^6$	χ of iron $\times 10^6$ at 25°C
24	0.78	1.614	-0.3259	242.2
25	4.01	10.110	-0.3259	259.9

It is quite evident from Table VI that the susceptibility value of iron in the above glass series with higher iron content shows a close similarity to that of the ferrous ion, although in the case of low iron content specimen the mass susceptibility of iron is somewhat lower than the corresponding ferric iron. It is to be noted here that Moore and Kumar (1951) and Abou-El-Azm (1954) studied the similar type of glass and their experimental data are discussed in this connection. Moore and Kumar did also record like us, the gradual increase of mass susceptibility value of iron in glass with the increase of iron content in the glass system but their experimental values stand quite high (χ of iron = 330×10^{-6} at 20°C) compared to those of ours. But Abou-El-Azm's data are too low (χ of iron = 133.8×10^{-6} at 20°C). Again when compared with other glass systems studied here, the susceptibility value of iron in this glass system is usually high, specially in a high iron content specimen (4.01%). Thus the composition and the oxidising condition of the above glass batch favour the formation of the higher mass susceptibility variety of iron like ferric ions in the system.

THE EFFECT OF IRON CONCENTRATION ON THE SUSCEPTIBILITY VALUE OF IRON IN GLASS

It is quite evident from the preceding tables (I to VI) that the mass susceptibility value of iron in the same glass base increases with the rise of iron content. This observation opens a number of speculations about the relationship between the concentration and proportion of different forms of iron including the ferromagnetic form of iron.

In order to identify the ferromagnetic component in the glassy matrix, if there be any, the magnetic measurements of almost all samples of preceding tables were extended to different fields strength (3500 gauss and 2500 gauss) and in each case the same result was obtained. The above observation rules out any possibility of the existence of any discrete ferromagnetic substance in the glassy matrix.

It is to be noted here that the influence of concentration of iron on the colour of iron-glass has been studied by some workers like Che Andresen Kraft (1931), Fuwa (1935-38), Densem and Turner (1938), Wang and Turner (1942), Abou-El-Azm and a few others. Besides the spectro-optical absorption study, Abou-El-Azm studied the relationship between the concentration of iron and the mass susceptibility of iron in the same glass of alkali-silicate series. He observed that with the increase of iron concentration, there is a corresponding increase in the susceptibility value of iron.

THE STATE OF IRON IN GLASS PREPARED UNDER REDUCING CONDITION

Hitherto, all the work has been done in the glass systems wherein iron was introduced in the form of Fe_2O_3 and the colour of the glass was yellow in general.

But a variety of blue or bluish green coloured iron glass can be prepared by adjusting the composition of the glass base and having a reducing atmosphere in the furnace. This condition is nearly fulfilled by using iron-oxalate in place of Fe_2O_3 and the partial replacement of alkali oxide by alkali tartarate or alkali oxide with tartaric acid in the glass batch composition. Some typical alkali-boric oxide glasses have been prepared under these conditions and the colour of these glasses is bluish green. Abou-El-Azm (1954) and Bhatnagar (1954) had studied some such borate glasses. It is observed that the reduction of iron in potassium borate is easier than that in sodium borate glass. The mass susceptibility value of iron in 'reduced' sodium diborate and potassium diborate glasses are given in the following table along with the corresponding values of 'yellow' (neutral) glasses with the same iron content.

TABLE VII

Glass sample No	Description of glass	Alkali oxide in wt. per cent	Fe in weight per cent	χ of glass $\times 10^6$ at 25°C	χ of glass base $\times 10^6$	χ of Fe $\times 10^6$ at 25°C
26	Soda borix oxide reduced	31.00	1.210	2.389	-0.4217	238.9
14	Soda borix oxide neutral	31.00	1.210	2.574	-0.4217	246.9
27	Potash-boric oxide reduced	41.40	1.221	2.086	0.4155	204.5
19	Potash-boric oxide neutral	41.40	1.221	2.528	-0.4155	240.6

It is quite evident from Table VII that the mass susceptibility value of iron in so-called ferrous glass is less than that of the corresponding yellow ferric glass but this observation is not in agreement with the results of Abou-El-Azm who found that the mass susceptibility of Fe in reduced alkali borate glass is more than the corresponding neutral glass. Bhatnagar (1945) however observed that the mass susceptibility value of iron in reduced glass was lower than the corresponding oxidised or neutral glass. That is quite clear from the consideration of the fact that the mass susceptibility value of the ferrous ion is less than that of the ferric ion. Again the overall mass susceptibility value of iron in ferrous glass is greater than the mass susceptibility value of pure ferrous ion and that indicates the presence of ferric ion in the system. As a matter of fact it is almost impossible to have all the iron in divalent state as is evident from the work of Baneroff and Cunningham (1930) and Weyl (1943).

MAGNETIC STUDY OF SOME GLASS SAMPLES OF DIFFERENT THERMAL HISTORY

In the course of the present investigation, the influence of temperature and time of heating on the susceptibility of some iron glasses have been studied.

Some glass specimens have been thermally treated at various temperatures without, of course, devitrifying the glass as a whole, with a view to studying the change in the magnetic property of those samples. It is well known that the glass as a class is very much susceptible to temperature treatment. As a matter of fact all its physical and thermodynamic properties are dependent on its thermal history. So in the same iron glass, it is quite expected that the relative proportion of ferrous and ferric state of iron in the glassy matrix will be affected very much due to the varying way of temperature treatment. With the increasing of time and temperature of melting, the colour of the same glass undergoes a change. As, for example, the colour of the ferric glass changes from yellow to grey through some intermediate stages during the process of long heating. Similar is the case with ferrous glass where the colour changes from blue to green and finally to grey through some intermediate states. The change of colour at different colouring stages is associated with the change of different forms of iron already present in the glass. Consequently along with that, the overall susceptibility value of iron in glass changes with the change of colour. Thus the different forms of iron undergo oxidation, reduction as the case may be, with the tempera-

TABLE VIII

Glass sample No	Description of glass*	Alkali oxide in wt per cent	Fe in weight per cent	Thermal history Temp. in °C	Time in hours	χ of glass $\times 10^6$ at 25°C	χ of Fe $\times 10^6$ at 25°C
28	Soda-boric oxide	9.475	2.848	900	3	5.272	199.5
29	—do—	9.475	2.848	1050	3	5.525	208.4
10	—do—	9.475	2.848	1050	6	5.534	208.6
30	—do—	9.475	2.848	1200	3	6.120	230.0
31	—do—	9.475	2.848	1350	3	7.509	278.1
32	—do—	31.00	1.048	1050	3	2.005	231.2
13	—do—	31.00	1.048	1050	6	2.137	243.6
33	Potash-boric oxide	41.40	1.221	825	2	2.276	219.7
34	—do—	41.40	1.221	825	4	2.314	222.8
35	—do—	41.40	1.221	1050	1½	2.470	235.6
36	—do—	41.40	1.221	1050	3	2.496	237.8
19	—do—	41.40	1.221	1050	6	2.528	240.6
1	Boric oxide	0	0.172	1050	6	—0.298	73.7
37	—do—	0	0.172	1050	16	—0.052	218.7

*Glasses prepared in neutral furnace atmosphere.

ture of melting, duration of heating and the furnace atmosphere. Ferrous glass in the absence of reducing furnace atmosphere gets oxidised to ferric state on prolonged heating. In ferric glass there is a possibility of formation of a ferrate and ferroso-ferric oxide at a reasonably high temperature (about 1300°C). Thus it is quite expected that in glass system the thermal treatment affects the magnetic property of the glass. The magnetic data of some such glasses along with their thermal history are given in the following table.

It is thus seen from Table VIII that the susceptibility value of iron in glass increases with the increase of temperature of melting and the duration of heating and that the increase of susceptibility value of iron is due to the increase in and formation of some forms of iron with high mass susceptibility as well as the simultaneous growth of colloidal dispersoid like Fe_2O_3 if there be any, in the vitreous matrix. In this context the absence of ferromagnetic solid phase colours is shown by making the susceptibility measurements of the above samples at different field strengths of 3500 gauss and 2500 gauss respectively

ACKNOWLEDGMENT

Thanks are due to Prof. K. Banerjee, Prof. A. Bose and Mr. S. Dutta Roy for their keen interest in the work.

REFERENCES

- Abou-El-Azm Abd-El-Moneim, 1954, *J. Soc. Glas. Technol.*, **38**, 101, 146, 197, 241, 271.
 Androsen-Kraft Cho, 1931, *Glas. Tech. Ber.*, **9**, 577.
 Baneroff, W. D. and Cunningham, G. E., 1930, *J. Phys. Chem.*, **34**, 1.
 Bhatnagar, S. S., 1954, *J. Sci. Indus. Res.*, **14**, 151.
 Cole, H., 1951a, *J. Soc. Glas. Technol.*, **35**, 40.
 Cole, H., 1951b, *J. Soc. Glas. Technol.*, **35**, 5.
 Densom, N. E. and Turner, W. E. S., 1938, *J. Soc. Glas. Technol.*, **22**, 372.
 Dutta Roy, S., 1955, *Ind. J. Phys.*, **38**, 429.
 Fuwa, K., 1935-38, *J. Jap. Ceram. Asso.*, **43**, **44**, **45**, **46**.
 Hampton, W. M., 1946, *Nature*, **158**, 582.
 Jackson, H., 1927, *Nature*, **120**, 264, 301.
 Jong, J. de, 1952, Thesis Delft.
 „ „ 1954, *J. Soc. Glas. Technol.*, **38**, 57.
 Moore, H. and Prasad, S. N., 1949, *J. Soc. Glass. Technol.*, **34**, 336.
 Moore, H. and Prasad, S. N., 1950, *J. Soc. Glas. Technol.*, **35**, 173, 193.
 Moore, H. and Kumar, S., 1951, *J. Soc. Glas. Technol.*, **35**, 58.
 Stovels, J. M., 1950, *Verres et Ref.*, **4**, 293.
 Wang, T. H. and Turner, W. E. S., 1942, *J. Soc. Glas. Technol.*, **26**, 272.
 Woyl, W. A., 1950, 'Monograph of Coloured Glass' published by the Society of Glass Technology.
 Woyl, W. A., 1943, *J. Soc. Glas. Technol.*, **22**, 265.

PROTON-NUCLEUS SCATTERING AT 96 MEV

ARUNDHATI GHOSE

DEPARTMENT OF THEORETICAL PHYSICS,

INDIAN ASSOCIATION FOR THE CULTIVATION OF SCIENCE, JADAVPUR, CALCUTTA-32

(Received for publication, March 5, 1959)

ABSTRACT. In this paper the cross section for the proton-nucleus scattering at 96 Mev has been calculated in the Born approximation with a diffuse surface optical model potential

INTRODUCTION

The analysis of elastic scattering of protons by nuclei in the low and medium energy region has been done by Woods and Saxon and others. In earlier studies it has been found that for large angles a square well potential predicts larger values of scattering cross section than what are observed experimentally. With a view to obtaining a better fit of the theory with the experimental values, a rounding of the edge of the nuclear well was first introduced by Woods and Saxon (1954) who had obtained good agreement for scattering of 20 Mev protons by medium and heavy nuclei. Other workers have obtained similar agreements for different energy values of proton.

In the present paper using an optical model potential the proton-nucleus scattering cross section is calculated in the Born approximation for 96 Mev protons.

MATHEMATICAL FORMULATION

The scattering of proton by a nucleus is treated as scattering by point source generating an average potential. This potential consists of a nuclear optical model part plus a coulomb part arising from the uniform charge distribution of the nucleus. Thus

$$\begin{aligned} V &= V_N + V_C \\ V_N &= (V + iW) / [1 + \exp(r - R)/a] \\ V_C &= \frac{ze^2}{2R} \left(3 - \frac{r^2}{R^2} \right) \text{ for } r \leq R \\ &= \frac{ze^2}{r} \text{ for } r \geq R \end{aligned}$$

where R and a are known as the half way radius and the diffuseness parameter respectively. R is expressed as

$$R = r_0 A^{1/3} \times 10^{-13} \text{ cm},$$

V and W are the parameters that determine the strength of the nuclear potential. In addition to the nuclear potential, we have the coulomb potential similar to that of uniformly charged sphere. The idea is to see how well such a velocity independent and central potential can explain the angular variation of the scattering cross section at high energies.

The scattering amplitude according to Born approximation is

$$f(\theta) = - \frac{8\pi^2 m}{h^2} \int_0^\infty \frac{\sin kr}{kr} V(r) r^2 dr$$

when

$$K = \frac{2mv}{\hbar} \sin (\theta/2)$$

The nuclear potential extends from zero to infinity and the coulomb potential is split into two parts,

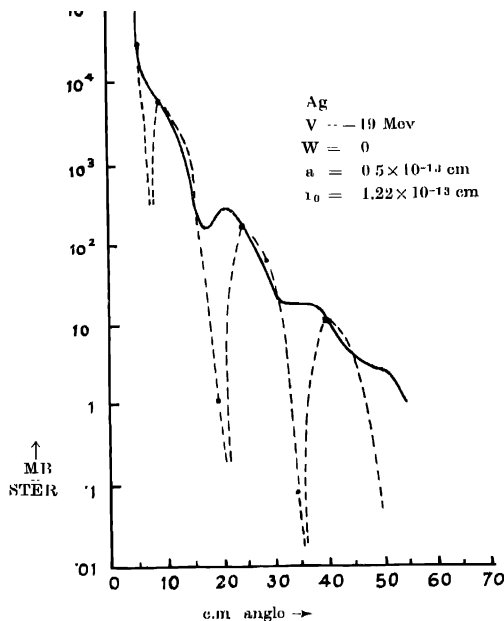
$$\begin{aligned} f(\theta) = & - \frac{8\pi^2 m}{h^2} \left[\int_0^\infty \frac{\sin kr}{kr} \frac{V+iW}{1+e^{(r-R)/a}} r^2 dr + \int_0^R \frac{\sin kr}{kr} \right. \\ & \left. + \frac{Ze^2}{2R} \left(3 - \frac{r^2}{R^2} \right) r^2 dr + \int_R^\infty \frac{\sin kr}{kr} \frac{Ze^2}{r} r^2 dr \right] \\ = & - \frac{8\pi^2 m}{h^2} \left[\frac{V+iW}{k} \left\{ \frac{a\pi R \cos kR}{\sinh a\pi} - \frac{a^2 \pi^2 \sin kR}{\sin h^2 a K \pi} \cdot \cosh a k \pi \right. \right. \\ & \left. \left. + 2Ka^3 \sum_{n=1}^\infty \left(\frac{-}{n^2 + K^2 a^2} \right)^n \cdot \frac{n \cdot e^{-\frac{nR}{a}}}{(n^2 + K^2 a^2)^2} \right\} + \frac{3Ze^2}{R^3 K^5} \sin KR - \frac{3Ze^2}{R^2 K^4} \cos KR \right] \end{aligned}$$

The scattering cross section is given by

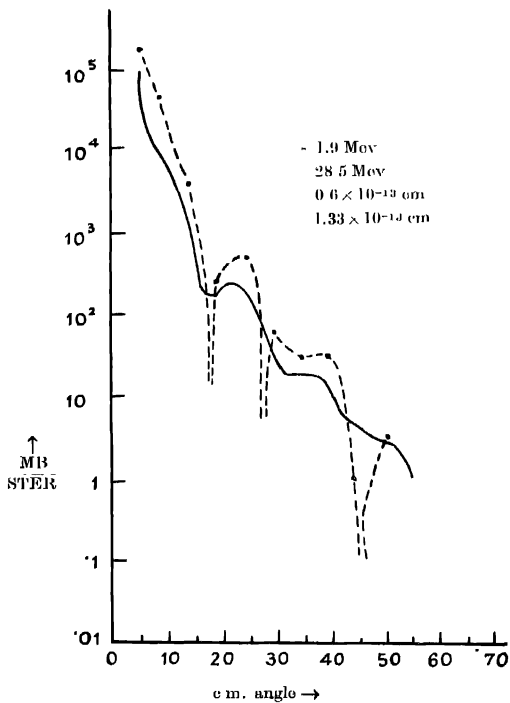
$$\sigma(\theta) = |f_V(\theta) + f_C(\theta)|^2 + |f_W(\theta)|^2$$

where $f_V(\theta)$, $f_W(\theta)$ and $f_C(\theta)$ are the scattering amplitudes due to nuclear and coulomb potentials.

The contribution of coulomb scattering predominates only at the forward scattering angles and sharply decreases with the increase of the angle. The interference due to the nuclear and coulomb potentials arises only from the real part of the nuclear potential and not from the imaginary part. The minima in the scattering cross section appear because of the sine and cosine terms present in the scattering amplitude arising from both the coulomb and nuclear potentials. It may be mentioned here that the positions of minima are almost entirely determined by r_0 , the influence of a is very little. The values of the parameters in the interaction potential are so fixed as will give the best fit with experimental results. As energy of the proton increases, it has been found necessary to decrease V and increase W . Finally at 300 Mev proton-nucleus scattering, Bjorklund and others (1957) have taken V to be zero and W equal to -16 Mev. We have tried to adjust the parameters such that the theoretical findings agree with the experimental results of Gerstein *et al* (1957). For silver we take $V = -19$ Mev, $W = 0$, $a = 0.5 \times 10^{-13}$ cm and $r_0 = 1.22 \times 10^{-13}$ cm. We find that there is a minimum at 5° which is not borne out from observational data (figure 1). Moreover



the positions of the minima are a little away from where they should be on the large angle side. In order to eliminate both the above anomalies for silver we propose to take $V = -1.9$ Mev., $W = -28.5$ Mev., $a = 0.6 \times 10^{-13}$ cm and $r_0 = 1.33 \times 10^{-13}$ cm. It is noticed (figure 2) that the theoretical values of the minimal points are still very much less than the experimental points. The values of the scattering cross section at large scattering angles are appreciably affected by the variation of the parameter W of the nuclear potential.



For lead we choose: $V = 0$, $W = -28$ Mev, $a = 0.6 \times 10^{-13}$ cm and $r_0 = 1.33 \times 10^{-13}$ cm. It is noticed (figure 3) that the positions of the minimum values of the cross section agree with the theory.

It may be mentioned here that in all the above cases, in the positions of minima the theoretical values drop to zero for the cross section whereas the experimental

values are not as low as that. Since the Born approximation is not strictly valid in this energy region, the agreement between theoretical calculations and experi-

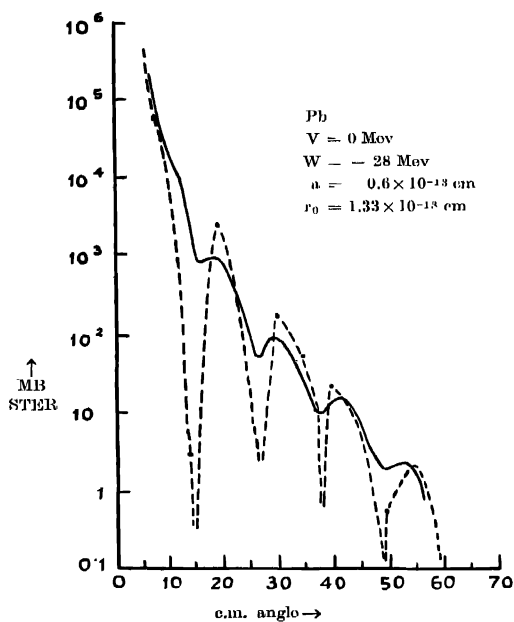


Fig. 3.

- - - Theoretical curve
 ——— Experimental Curve

mental values is not expected to be very close. We propose to improve the agreement by extending the calculations to higher energies and by modifying the potential.

ACKNOWLEDGMENT

My grateful thanks are due to Prof. D. Basu for his suggesting the problem and for helpful discussions.

APPENDIX

With the substitution $\frac{r-R}{a} = x$ the integral

$$I = \int_0^{\infty} \frac{\sin kr}{kr} \frac{V}{1 + e^{(r-R)/a}} r^2 dr$$

becomes

$$I = \frac{aV}{K} \left[\int_{-R/a}^0 \frac{R+ax}{1+e^x} \sin K(R+ax) dx + \int_0^{R/a} \frac{R+ax}{1+e^x} \sin K(R+ax) dx \right]$$

Now
$$\frac{1}{1+e^x} = \sum_{n=0}^{\infty} e^{-nx} (-)^n \quad \text{for } x < 0$$

and
$$\frac{1}{1+e^x} = \sum_{n=1}^{\infty} e^{-nx} (-)^{n+1} \quad \text{for } x > 0$$

The infinite series occurring in the expression for $f(\theta)$ can be summed up (c.f. Bromwich, 1947) as shown below.

Using
$$\frac{1}{1+2a^2 \sum_{n=1}^{\infty} \frac{(-)^n}{n^2 + a^2}} = \frac{a\pi}{\sinh a\pi}$$

we get
$$\sum_{n=1}^{\infty} \frac{(-)^n}{n^2 + k^2 a^2} = \frac{1}{2a^2 k^2} \left[\frac{ak\pi}{\sinh ak\pi} - 1 \right] \quad \dots (a)$$

Differentiating (a) with respect to a , we have

$$\begin{aligned} \sum_{n=1}^{\infty} (-)^n \frac{1}{(n^2 + k^2 a^2)^2} &= \frac{1}{2a^4 k^4} \left[\frac{a\pi k}{\sinh ak\pi} - 1 \right] \\ &= \frac{1}{4a^3 k^3} \left[\frac{\pi \sinh ak\pi - ka\pi^2 \cosh ak\pi}{\sinh^2 ak\pi} \right] \quad \dots (b) \end{aligned}$$

Combining (a) and (b) we get

$$\sum_{n=1}^{\infty} (-)^n \frac{n^2}{(n^2 + k^2 a^2)^2} = \frac{1}{4ak} \frac{\pi \sinh ak\pi - ak\pi^2 \cosh ak\pi}{\sinh^2 ak\pi} -$$

REFERENCES

- Bjorklund, Blandford and Fernbach, 1957, *Phys. Rev.*, **108**, 795.
 Bromwich, 1947, Introduction to the theory of Infinite Series, 2nd Edition
 Gerstein, Niederer and Strauch, 1957, *Phys. Rev.*, **108**, 427.
 Woods and Saxon, 1954, *Phys. Rev.*, **95**, 577.

SOME STUDIES ON THE EFFECTS OF LIMITING IN A POSITION CONTROL SERVO CONTAINING BACKLASH

A. K. MAHALANABIS

INSTITUTE OF RADIO PHYSICS AND ELECTRONICS, CALCUTTA 9

(Received for publication, March 20, 1959)

ABSTRACT. Effects of limiting on the stability of a second order position control servomechanism containing backlash in the output coupling have been studied. Two cases have been considered, the signal being limited (i), in the first case, θ_m , the motor speed, and in the second case $\dot{\theta}_m \leq a\theta_m$, a being a constant. Describing function method was applied for theoretical analyses and experimental studies were made with the help of a simulator.

1 INTRODUCTION

All servo systems are in practice nonlinear--the nonlinearities arising from limitations of the different components. The most common and important forms of nonlinearities encountered arise from (i) saturation or limiting of the response, (ii) dead-zone, (iii) backlash in different linkages and (iv) nonlinear load frictions, such as, static and coulomb frictions. The individual effects of these nonlinearities on the performance of a servo system have been fairly widely studied. Results indicate that from the point of view of system stability backlash may be one of the most disquieting factors.

Tustin (1947) and Liversidge (1952) have made detailed studies of systems containing backlash in output couplings and have suggested means for countering the adverse effects of backlash on system stability. In these studies presence of other nonlinearities were not considered, i.e. the entire system was assumed to behave linearly except for the backlash element. As is well known such ideal conditions seldom occur in practice. It is therefore important to study the effects of simultaneous occurrence of more than one nonlinearity in the system. The present paper describes results of some preliminary studies made on the performance of a servomechanism effected by limiting and backlash in the output coupling, with particular reference to the question of stability. A second order position control system has been considered.

There is no readily applicable method of analysis suitable for systems with multiple nonlinearities. A modification of the describing function method (Johnson, 1952) has here been utilised for theoretical analysis aimed at qualitative results. The experimental part of the analysis involved studies with the help of an analog simulator.

2 THE BASIC SYSTEM

The basic system under consideration is shown in figure 1 in the form of a block diagram. The output of the error detector is amplified by an amplifier of gain K' . The amplifier output is the control signal of the motor. The motor is assumed

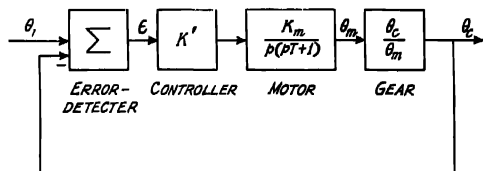


Fig. 1. The basic system under consideration.

to be adequately representable by two time constants as indicated in figure 1, viz., T and ∞ , the latter being the integrating one. The motor shaft is coupled to the load shaft by means of a backlash element; θ_m and θ_c are respectively the motor and load positions. The backlash characteristic assumed is shown in figure 2. The load inertia is neglected and it is also assumed that the load is sufficiently damped so as to prevent any overcoasting during reversals.

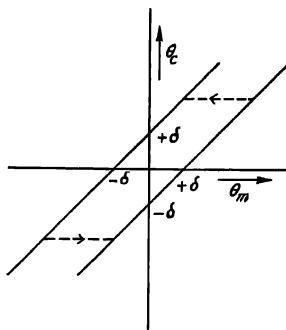


Fig. 2. Assumed backlash characteristic of the coupling gear.

This system was studied in some details by Nichols (1953). It has been shown that the effect of backlash on system stability depends on the value of the amplifier gain K' . For small values of K' backlash merely deteriorates the relative stability of the system. If K' is larger than a certain critical value backlash produces absolute instability and causes the system to sustain oscillations of definite amplitude and frequency. We shall here extend the study of Nichols to examine the effects of limiting which may be inherently present or may be introduced intentionally in the system of figure 1.

For convenience we shall assume that the motor time constants are separable. This assumption may appear to be somewhat impracticable but will be shown later to be justified on analytical grounds. Two different cases studied are shown in figures 3(a) and 3(h). In case of figure 3(a) it is easily verified that the signal

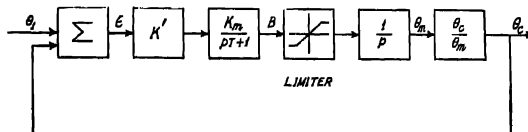


Fig. 3(a). Schematic diagram of the system with simple velocity limiting.

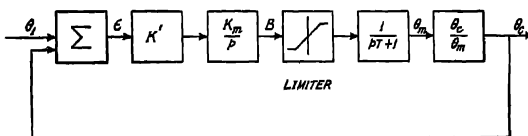


Fig. 3(b). Schematic diagram of the system with modified velocity limiting

which is limited is $\dot{\theta}_m$, whereas in the case of figure 3(b) the corresponding signal is $\dot{\theta}_m + \alpha \theta_m$ where $\dot{\theta}_m = \frac{d\theta_m}{dt}$ and α is a constant. We shall refer to the case of figure 3(a) as simple velocity limiting and to that of figure 3(b) as modified velocity limiting.

3. SIMPLE VELOCITY LIMITING

The system is shown in figure 3(a). The limiter characteristic assumed is shown in figure 4. The describing function of the limiter is given by (Johnson, 1952)

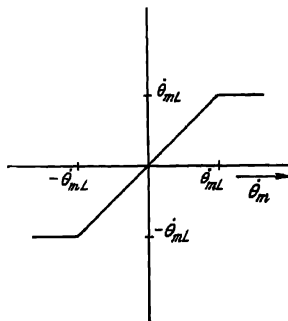


Fig. 4. Limiter characteristic assumed in figure 3(a).

If we consider a point Q on the $-G_B$ locus corresponding to a definite input signal amplitude, it is possible to find a point P on the G^{-1} locus corresponding to the same signal amplitude, which is nearest to Q . Then

$$\frac{OQ}{QP} = \frac{G_B}{[G^{-1} + G_B]_{\min}} = \left(\frac{\theta_c}{\theta_1} \right)_P$$

where, from relation (6) $(\theta_c/\theta_1)_P$ is the maximum value of the ratio (θ_c/θ_1) , which is analogous to the closed-loop frequency response peak (M_P) (Brown, 1955) of the linear theory. The value of $(\theta_c/\theta_1)_P$ gives an estimate of the damping present in the system, larger value corresponding to lesser damping and vice versa. Also the frequency ω_P corresponding to P gives an idea of the speed of response, larger values of ω_P corresponding to greater speed of response.

It can be seen from figure 6 that if we move on to another point Q' corresponding to a signal amplitude larger than that at Q , the magnitude of this ratio decreases. That is, the system damping increases as the signal amplitude increases. Also the frequency ω_P decreases with signal amplitude and so the system becomes more sluggish.

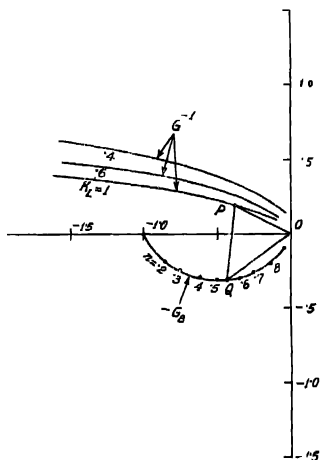


Fig. 6. Complex plots of G^{-1} and $-G_B$ for the system in figure 5(a) with $K = 10$ and $T = 1$ sec.

Records of responses to step inputs of the system in figure 3(a) obtained with the help of the simulator are shown in figure 7. Here for convenience of

comparison, the magnitude of the input step was kept constant and the limiting amplitude ($\dot{\theta}_{mL}$ in figure 3) was changed. The three curves correspond to values of $\frac{\theta_1}{\dot{\theta}_{mL}} = 1, 2.0$ and 10.0 . It is seen that as the extent of limiting increases the response becomes more and more sluggish corresponding to more damping and less speed of response.



Fig. 7. Experimental step responses of the system in figure 3(a) obtained with the simulator for $\theta_{mL}/\theta_1 = 1.0$ (Top), $= 2.0$ (middle) and, $= 10.0$ (bottom).

(b) *Large amplifier gain :*

In this case the system has absolute instability and produces sustained oscillations. In the absence of any velocity limiting, amplitude and frequency of these oscillations are determined by the value of the amplifier gain K and the backlash width. We shall examine the effects of simple velocity limiting on the amplitude and frequency of these oscillations. For this purpose it is most expedient to make use of the gain-phase shift plots. Eqn. (7) is the starting relation. We plot G as a family of amplitude dependent loci on the gain-phase shift diagram. The gain is expressed in db and phase shift in degrees. Plot of $-G_B^{-1}$ as an amplitude locus is also superposed on the same diagram. These plots are shown in figure 8 for an assumed value of $T = 1$ and $K = 10$ for the system shown in figure 5(a).

As is evident from Eqn. (7) sustained oscillations of amplitude θ_{ma} (say) are possible only if for this value of signal amplitude $G = -G_B^{-1}$. This condition, if satisfied by the system, can be easily detected from the plots of figure 8. Thus in figure 8 some of the G -loci intersect with the $-G_B^{-1}$ locus. Sustained oscillations will be produced only if and when at the points of intersection the amplitude marked on one of these G -loci is equal to that marked on $-G_B^{-1}$

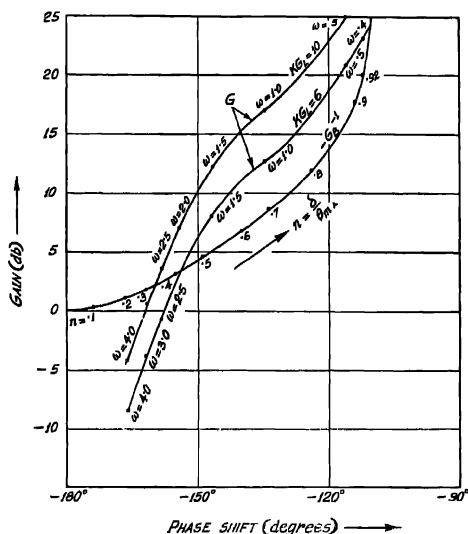


Fig. 8. Gain-phase shift plots of G and $-G_B^{-1}$ for the system in figure 3(a) with $K = 10$ and $T = 1$ sec.

locus. This is then the amplitude of the resultant sustained oscillations. The frequency of these oscillations is equal to the frequency marked on the relevant G -locus at the point of intersection.

Figure 8 predicts two sets of possible oscillations. It can be shown (Johnson, 1952), however, that oscillations of lower amplitude and frequency correspond to an unstable limit-cycle and no sustained oscillations at this amplitude and frequency are possible.

To see the effect of simple velocity limiting on the amplitude and frequency of oscillations let us assume first that there is no limiting. The amplitude dependence of G -loci then vanishes and all the G -loci converge to a single frequency-locus. Sustained oscillations are produced whenever this locus intersects with the $-G_B^{-1}$ locus. The amplitude of oscillations is that marked on the $-G_B^{-1}$ locus at the point of intersection. Thus in absence of simple velocity limiting the amplitude of oscillation is solely determined by the backlash characteristic. Presence of simple velocity limiting transforms plots of G into a family of amplitude dependent loci and the amplitude of any sustained oscillations are now determined by both the limiter and the backlash characteristics. Suppose the limiting amplitude is set to a certain value and oscillation of some amplitude and frequency is present. If the limiting amplitude is reduced the effective

system gain also reduces and from figure 6 it is evident that equilibrium oscillations are now possible only at lower amplitudes. If the limiting amplitude is further reduced oscillation amplitudes also fall but oscillation never ceases, for in absence of oscillation the limiter does not reduce the gain. Thus oscillation amplitudes can be controlled to some extent by imposing simple velocity limiting but can not be stopped altogether.

4. MODIFIED VELOCITY LIMITING

The arrangement is shown in figure 3(b). The corresponding quasilinearized model is shown in figure 5(b). The effects of the limiter in this case also can be studied under the two conditions, viz., small amplifier gain and large amplifier gain. In both the cases similar conclusions as in Sec. 3(a) and 3(b) are arrived at. In the second case, however, an additional remarkable result is obtained.

Thus in the set up shown in figure 3(b) if a step signal is applied at the input the limiter characteristic becomes unsymmetrical as indicated in figure 11. This can be easily verified if we compute the transfer function between the points θ_1 and B which shows a finite d.c. gain. Thus any step of amplitude θ_1 applied at the input will also be present at the input of the limiter (assuming the d.c. gain between θ_1 and B to be unity which is true for $\theta_1 \leq L$, L being the limiting amplitude, as shown in figure 11). This will cause the reference lines of the limiter characteristic to be shifted from the position shown by dotted lines to that shown by solid lines. As a result any sustained oscillations that may be present in the system will be subjected to this unsymmetrical characteristics.

Relation (7) is still applicable but now G is dependent not only upon oscillation amplitude but also on the magnitude of any step signal applied at the input. The describing function (G_L') of the unsymmetrical limiter characteristic is derived in Appendix. This is plotted in figure 12 with the amplitude of step input as a parameter. It is seen that for a fixed value of assumed sinusoidal signal amplitude the value of the describing function decreases as the magnitude of the step input is increased.

The effect of input steps on the amplitude and frequency of sustained oscillation in the system of figure 3(b) can be determined by redrawing the curves of figure 8 for a number of assumed input step amplitudes. Thus if we first assume zero input step, we have the curves of figure 8 and the amplitude and frequency of oscillations are found out as outlined in Sec. 3(b). If the step input is increased to a finite value, the describing function gain for the oscillations of amplitude determined above will be reduced and the G -locus for this amplitude shifts towards right in figure 8. Thus new equilibrium oscillations will occur at lower amplitude and frequency.

Results obtained with the help of the simulator are presented in figure 9 in the form of graphs. For convenience, results obtained by applying the

describing function method as outlined in the foregoing paragraphs, are also shown in the figure.

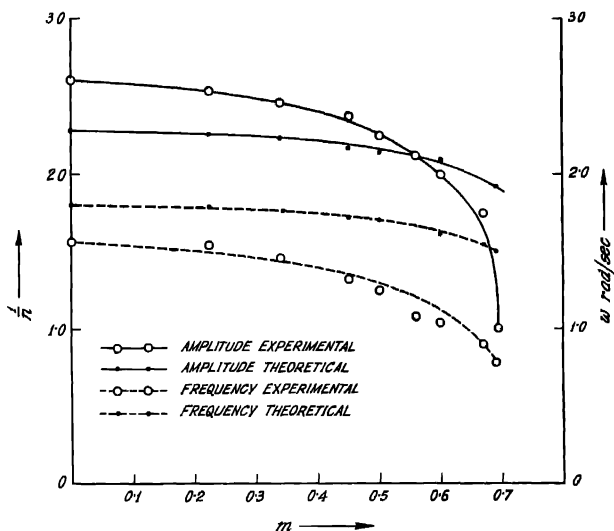


Fig. 9 Plots of dimensionless amplitude ($\theta_m/8$) and frequency (rad./sec.) of sustained oscillations vs. the dimensionless d.c. input (θ_1/L) for the system in figure 3(b), obtained with the help of the simulator. L is the limiting amplitude in absence of d.c. input.

It is seen that the discrepancy between experimental and theoretical results changes sign and then increases as the amplitude of the input step increases. The increased discrepancies in the results for larger input steps are to be expected, for with increase of the input step amplitude the limiter characteristic becomes more unsymmetrical and the percentage of harmonics produced goes on increasing. Further, oscillation amplitude falls off more rapidly with input step amplitude than indicated by the describing function analysis.

5. ON THE POSSIBILITY OF REALISING THE EFFECTS OF MODIFIED VELOCITY LIMITING

In practice the most common method of limiting the velocity of a servo motor is to place a limiter ahead of it. This has the effect of limiting $\dot{\theta}_m$ and corresponds in effect to the case represented in figure 3(a). It has been shown that a desirable effect from the point of view of system stability can be achieved by incorporating a somewhat different scheme for limiting the motor speed. This case has been referred to as modified velocity limiting and is schematically represented in figure 3(b).

It will be clear from Sec. 4 that the desirable effect of the modified velocity limiting limiting stems from the fact that in this case any d.c. input to the system makes the nonlinearity asymmetrical. The same effect is produced if the nonlinearity is placed in the feedback path as shown in figure 10. It is then possible to achieve the effects of modified velocity limiting by the system of figure 10.

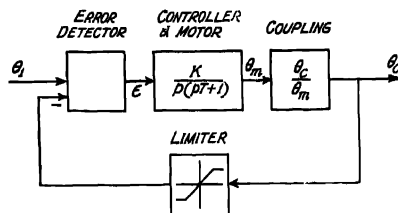


Fig. 10 Alternative configuration for realising the effects of modified velocity limiting system stability.

It is to be noted that in figure 10 the two nonlinearities are no longer separated by low-pass units and the describing function method does not apply. That is why in the foregoing analyses the system of figure 3(b) was chosen instead of that of figure 10.

6. CONCLUSION

It is evident from the above studies that effect of the presence of simple velocity limiting in a servomechanism containing backlash is to improve the relative stability of the system for larger signals. It is thus possible to reduce, for large signals, the derogatory effects of backlash by inclusion of simple velocity limiting. This has however the severe drawback, viz., that this improvement in damping constant as a result of velocity limiting is associated with a comparatively large reduction in speed of response.

It has also been found that simple velocity limiting has no stabilising effect on a system caused to have absolute instability in the sense that it can not stop oscillations but can be used to control the amplitude of oscillations present. A remarkable result is obtained in this case by introduction of modified velocity limiting. It is seen that amplitude of oscillation is in this case dependent on magnitude of any d.c. input signal, and that oscillation ceases entirely as the d.c. input signal amplitude increases above certain value. This result is of some importance because in practice inputs to servo systems are in most cases random time functions and signals of certain amplitudes are more likely to occur than others. Since the oscillations due to backlash effect are essentially of small amplitudes superimposed on the comparatively large displacements due to signals

it is evident that it is possible to adjust the limiter characteristic in the case of modified velocity limiting so as to make any oscillation negligible.

ACKNOWLEDGMENT

The author is indebted to Professor J. N. Bhar, for his constant guidance and keen interest in the work. He is also grateful to Dr A. K. Choudhury for some helpful suggestions and discussions.

The award of a Senior Research Training Scholarship by the Ministry of Education, Government of India, is also thankfully acknowledged.

REFERENCES

- Brown, G. S. and Campbell, D. P., 1955, *Principles of Servomechanism*, pp. 106.
Johnson, E. C. (Jr.), 1952, *Trans. A.I.E.E.*, **71**, 169.
Koehnburger, R. J., 1953, *Trans. A.I.E.E.*, **72**, 180.
Laversidge, J. H., 1952, *Automatic and Manual Control*, pp. 343.
Nichols, N. B., 1953, *Trans. A.I.E.E.*, **72**, 462.
Tustin, A., 1947, *Journal of I.E.E.*, Part 11A, **94**, 143.

APPENDIX

Describing Function of the Unsymmetrical Limiter Characteristics

The limiter characteristic assumed is shown in figure 11. If L is the limiting amplitude for the symmetrical case as shown in dotted lines in figure 11 and θ_1 is the value of the positive d.c. input to the limiter, the new limiting values are $L - \theta_1$ and $-(L + \theta_1)$ on the positive and negative sides respectively.

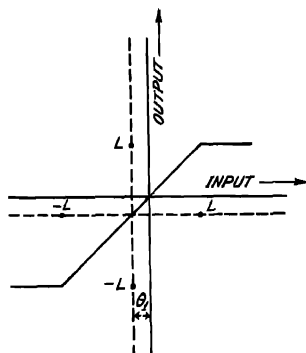


Fig. 11. Unsymmetrical characteristic of the limiter in figure 3(b) resulting from d.c. input θ_1 . Dotted lines show the positions of the reference lines in absence of any d.c. input.

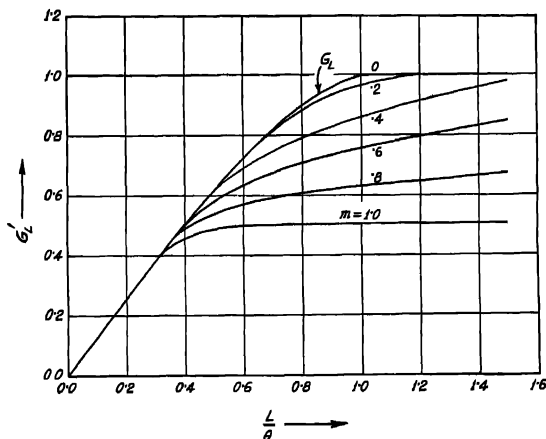


Fig. 12. Describing functions of the unsymmetrical limiter of figure 10. $m = \theta_1/L$, the non-dimensional d.c. input, θ_1 is the amplitude of assumed sine wave input to the limiter.

As usual we assume the input to be a sinusoidal function of the form

$$\theta_{in} = \theta_a \sin \omega t.$$

The output of the limiter is then defined by

$$\begin{aligned}\theta_{out} &= \theta_a \sin \omega t ; 0 \leq \omega t \leq \sin^{-1} \frac{L-\theta_1}{\theta_a} \\ &= L-\theta_1 \quad ; \sin^{-1} \frac{L-\theta_1}{\theta_a} \leq \omega t \leq \pi - \sin^{-1} \frac{L-\theta_1}{\theta_a} \\ &= \theta_a \sin \omega t ; \pi - \sin^{-1} \frac{L-\theta_1}{\theta_a} \leq \omega t \leq \pi.\end{aligned}$$

for the positive half period of θ_{in} and

$$\begin{aligned}\theta_{out} &= \theta_a \sin \omega t ; \pi \leq \omega t \leq \pi + \sin^{-1} \frac{-(L+\theta_1)}{\theta_a} \\ &= -(L+\theta_1) ; \pi + \sin^{-1} \frac{-(L+\theta_1)}{\theta_a} \leq \omega t \leq 2\pi - \sin^{-1} \frac{-(L+\theta_1)}{\theta_a} \\ &= \theta_a \sin \omega t ; 2\pi - \sin^{-1} \frac{-(L+\theta_1)}{\theta_a} \leq \omega t \leq 2\pi,\end{aligned}$$

for the negative half period of θ_{in} .

By applying Fourier's expansion to θ_{out} we can find the value of the fundamental components for the two halves. This gives

$$\begin{aligned}[\theta_{out}]_f &= \frac{\theta_a}{\pi} \left[\sin^{-1} \frac{L-\theta_1}{\theta_a} + \frac{L-\theta_1}{\theta_a} \cos \sin^{-1} \frac{L-\theta_1}{\theta_a} \right] \sin \omega t \\ &+ \frac{\theta_a}{\pi} \left[\sin^{-1} \frac{L+\theta_1}{\theta_a} + \frac{L+\theta_1}{\theta_a} \cos \sin^{-1} \frac{L+\theta_1}{\theta_a} \right] \sin \omega t\end{aligned}$$

the describing function

$$\begin{aligned}G'_L &= \frac{1}{\pi} \left\{ \left[\sin^{-1} \frac{L-\theta_1}{\theta_a} + \frac{L-\theta_1}{\theta_a} \cos \sin^{-1} \frac{L-\theta_1}{\theta_a} \right] \right. \\ &\quad \left. + \sin^{-1} \frac{L+\theta_1}{\theta_a} + \frac{L+\theta_1}{\theta_a} \cos \sin^{-1} \frac{L+\theta_1}{\theta_a} \right\} \\ &= \frac{1}{\pi} \left\{ \left[\sin^{-1} \frac{L}{\theta_a} (1-m) + \frac{L}{\theta_a} (1-m) \cos \sin^{-1} \frac{L}{\theta_a} (1-m) \right] \right. \\ &\quad \left. + \left[\sin^{-1} \frac{L}{\theta_a} (1+m) + \frac{L}{\theta_a} (1+m) \cos \sin^{-1} \frac{L}{\theta_a} (1+m) \right] \right\},\end{aligned}$$

where

$$m = \theta_1/L.$$

This is plotted in figure 12 as a function of (L/θ_a) with m as a parameter.

ELASTIC SCATTERING AND POLARIZATION OF 300 MEV PROTONS

ARUNDHATI GHOSH

DEPARTMENT OF THEORETICAL PHYSICS,
INDIAN ASSOCIATION FOR THE CULTIVATION OF SCIENCE, JADAVPUR, CALCUTTA-32.

(Received, March 30, 1959)

ABSTRACT. Analysis of elastic scattering and polarization of 300 Mev energy protons is made in Born approximation for Woods-Saxon type of nucleon-nuclear potential with spin-orbit coupling.

It has been felt by Sternheimer (1955) and Bjorklund and others (1957) that to account for the polarization of elastically scattered beam of protons in the high energy region there should be a spin orbit coupling along with the central part of the nucleon-nuclear potential. In this paper we take the potential to be of the form :

$$V = [V_{CR} + iV_{CI}] \rho(r) + [V_{SR} + iV_{SI}] \left(\frac{\hbar}{\mu c} \right)^2 \frac{1}{r} \cdot \frac{d\rho(r)}{dr} \vec{\sigma} \cdot \vec{\sigma}.$$

$$\rho(r) = \frac{1}{1 + e^{(r-R)/a}}; R = r_0 A^{1/3}$$

The Born approximation analysis gives the matrix element for the central part of the potential as

$$\begin{aligned} \langle f | V_C | i \rangle &= - \frac{2M}{\hbar^2} \left[\frac{V_{CR} + iV_{CI}}{K} \left\{ \frac{a^2 \pi^2 \sin KR \cosh a K \pi}{\sin \hbar^2 a K \pi} \right. \right. \\ &\quad \left. \left. - \frac{a \pi R \cos KR}{\sin \hbar a K \pi} - 2K a^3 \sum_{n=1}^{\infty} \frac{(-)^n \cdot e^{-\frac{nR}{a}} \cdot n}{(n^2 + K^2 a^2)^2} \right\} \right] \end{aligned} \quad (1)$$

where $K = \frac{2p}{\hbar} \sin \theta/2$

The matrix element of the spin-orbit part of the potential is given by

$$\begin{aligned} \langle f | V_S | i \rangle &= - \frac{2M}{\hbar^2} (V_{SR} + iV_{SI}) \left(\frac{\hbar}{\mu c} \right)^2 i \cos \theta/2 \sin \phi \frac{p}{\hbar} \cdot \\ &\quad \left[\frac{a^2 \pi^2 \sin KR \cosh a K \pi}{\sin \hbar^2 a K \pi} - \frac{a \pi R \cos KR}{\sin \hbar a K \pi} - 2K a^3 \sum_{n=1}^{\infty} \frac{(-)^n \cdot e^{-\frac{nR}{a}} \cdot n}{(n^2 + K^2 a^2)^2} \right] \dots \quad (2) \end{aligned}$$

Here we have considered the initial state a plane wave parallel to z axis with spin parallel to x axis. We are interested in the scattering in YZ plane. The differential scattering cross section $d\sigma/d\omega$ is given by

$$\frac{d\sigma}{d\omega} = \frac{4M^2}{\hbar^4} \left[\frac{a^2 \pi^2 \sin KR \cosh a K \pi}{\sinh^2 a K \pi} - \frac{a \pi R \cos KR}{\sin h a K \pi} - 2Ka^3 \sum_{n=1}^{\infty} \frac{(-)^n \cdot e^{-\frac{nR}{a}} \cdot n}{(n^2 + K^2 a^2)^2} \right]^2$$

$$\left[\left\{ \frac{V_{CR}}{K} - V_{SI} \left(\frac{\hbar}{\mu c} \right)^2 \cos \theta/2 \sin \phi \frac{p}{\hbar} \right\}^2 + \left\{ \frac{V_{CI}}{K} + V_{SR} \left(\frac{\hbar}{\mu c} \right)^2 \cos \theta/2 \sin \phi \frac{p}{\hbar} \right\}^2 \right] \dots \quad (3)$$

The square well limit for the scattering cross section as given by Fermi (1954) is obtained by making a tend to zero. Of course Fermi has taken $V_{SI} = 0$ and $V_{CR} = V_{SR}$. The intensity of polarization is as usual expressed by

$$e(\theta) = \frac{I \left(\phi = \frac{\pi}{2} \right) - I \left(\phi = \frac{3\pi}{2} \right)}{I \left(\phi = \frac{\pi}{2} \right) + I \left(\phi = \frac{3\pi}{2} \right)}$$

From formula (3) we obtain

$$e(\theta) = \frac{\frac{2}{K} \left(\frac{\hbar}{\mu c} \right)^2 \cos \theta/2 \frac{p}{\hbar} [V_{CI} V_{SR} - V_{CR} V_{SI}]}{\frac{1}{K^2} [V_{CR}^2 + V_{CI}^2] + \left[\left(\frac{\hbar}{\mu c} \right)^2 \cos \theta/2 \frac{p}{\hbar} \right]^2 [V_{SI}^2 + V_{SR}^2]}$$

This expression is independent of the diffusivity parameter a and thus, as expected, we find that the polarization depends only upon the magnitudes of the potentials and not on their radial shapes. So, for the polarization, no better agreement with experiment is obtained from the diffuse well shape than from the square well potential as shown by Fermi (1954). For the scattering cross section we have taken

average of $d\sigma/d\omega$ which is given by $\bar{d\sigma} = \frac{1}{2} \left[I \left(\phi = \frac{\pi}{2} \right) + I \left(\phi = \frac{3\pi}{2} \right) \right]$. The

real part of the central potential will be somewhat modified in forward scattering angles if the coulomb potential is taken into account. This we have neglected because in the 300 Mev region coulomb cross section drops off very rapidly with angle for the elements considered here.

We present here the result (figure 1) of our calculation of the differential scattering cross sections of 340 Mev protons scattered by lead and 313 Mev protons

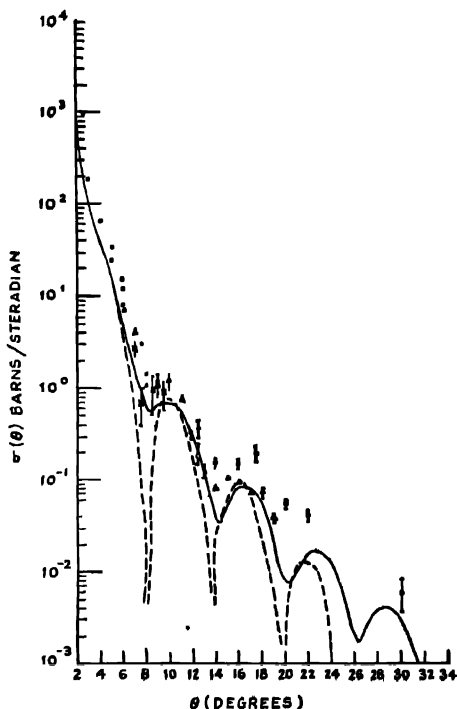


Fig. 1. — Exact phase-shift analysis (1957).
 - - - Born approximation analysis.

scattered by carbon (figure 2) along with the results of exact phase shift analysis of Bjorklund, Blandford and Fernbach (1957). As regards parameters, we have chosen $r_0 = 1.25 \times 10^{-13}$ cm, $a = 0.65 \times 10^{-13}$, $V_{CR} = 0$ Mev, $V_{CI} = 16$ Mev, $V_{SR} = 1.08$ Mev, and $V_{SI} = -2.28$ Mev. For small angles the scattering cross section is not affected by the spin orbit coupling term which predominates as the scattering angle increases. At 30° angle of scattering the contribution of spin-orbit coupling term to the scattering cross section is 10 times greater than that of the central potential. The effect of increasing the magnitude of the spin-orbit coupling term is to raise the scattering cross section at larger angles. It appears from the figures that the calculations in Born approximation for 300 Mev protons agree closely with those of the exact phase shift analysis.

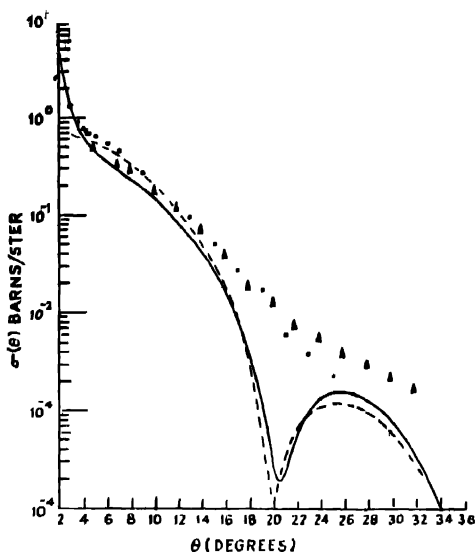


Fig. 2. — Exact phase shift analysis (1957).
 - - - Born approximation analysis.

ACKNOWLEDGMENT

I am greatly indebted to Prof. D. Basu for his suggesting the problem and for his kind interest in the work.

REFERENCES

- Bjorklund, F. E., Blandford, I., and Fernbach, S., 1957, *Phys. Rev.* **108**, 711.
 Fermi, E., 1954, *Nuovo Cimento*, **11**, 407.
 Sternheimer, R. M., 1955, *Phys. Rev.*, **97**, 1314 ; **110** 886

MAGNETIC STUDY OF IRON-CONTAINING GLASSES AT LOW TEMPERATURE

BHUPATI KUMAR BANERJEE*

INDIAN ASSOCIATION FOR THE CULTIVATION OF SCIENCE, CALCUTTA 32

(Received, January 30, 1959)

ABSTRACT. This paper deals with the low temperature magnetic property of several iron glasses. The value of the square of the magnetic moment of iron at different temperatures in the liquid oxygen range has been determined. In almost all cases this value is found to decrease with decreasing temperature. The variation of the moments with temperature is dependent on the composition of the glass. These findings have been discussed from the point of view of the glass structure.

INTRODUCTION

In a previous paper by the author (1959) on the magnetic study of iron glasses at room temperature, it was suggested that the electrovalent and covalent forms of iron can both exist simultaneously along with the colloidal oxides of iron in the same glass system. In the course of the investigation on the magnetic property of iron glass at room temperature, the evidence for the presence of ferromagnetic component in any glass system has not been observed. It was however expected that similar studies at low temperature may yield more fruitful results.

EXPERIMENTAL

Iron glasses of boric oxide, soda-boric oxide, potash-boric oxide, lithia-boric oxide and high lead-silica glass bases respectively were selected for the present study. Details of the method of preparation and analysis are given in the previous paper by the author (1959).

In the case of low temperature measurement at any desired temperature in the liquid oxygen range, a cryostatic arrangement of the gas-flow type originally designed by Bose (1947) and recently modified by Dutta Roy (1955) was used. The cryostatic chamber is cooled by the flow of cold air through it obtained by the evaporation of liquid oxygen at the bottom of the chamber. The efficiency of cooling and the steadiness of the temperature is ensured by packing the chamber with copper gauze which furnishes heat exchange in the system. An automatic relay system controlled by a constant volume air thermometer drives a suction pump and regulates the flow of cold air.

* Present address :—Central Fuel Research Institute, P.O.—Jeaigora, Dhanbad.

The experimental glass specimens consisted of a number of samples of different compositions prepared under neutral, reducing or oxidising conditions including one set of high potash content ($K_2O = 41.40\%$) potash-boric oxide glass prepared in both neutral and reduced conditions. The colour of the oxidised and neutral glasses were yellow, while that of the reduced glass was bluish green. The variation of the square of the effective moment value (p_{eff}^2) of each specimen from room temperature to $100^\circ K$ is given in the Figure 1, where ordinate on the

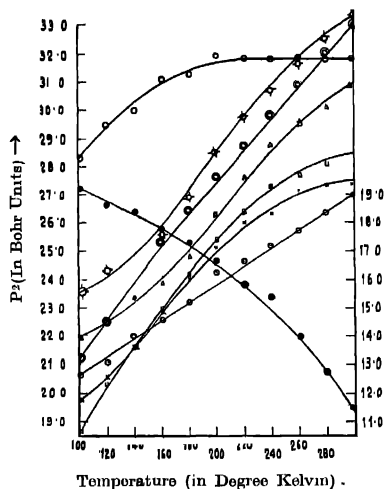


Fig. 1.

- | | |
|--|---|
| ○ Soda-Boric oxide (neutral)
$Na_2O = 9.475\%$; $Fe = 2.8$ | × Potash-Boric oxide (reduced)
$K_2O = 41.4\%$; $Fe = 1.221\%$ |
| △ Soda-Boric oxide (reduced)
$Na_2O = 31.0\%$; $Fe = 1.210\%$ | @ Lithin-Boric oxide (neutral)
$Li_2O = 31.2\%$; $Fe = 0.25\%$ |
| □ Potash-Boric oxide (neutral)
$K_2O = 14.2\%$; $Fe = 1.673\%$ | ★ Lead Oxide-Potash Silica (oxidised)
$PbO = 60\%$; $K_2O = 10\%$; $Fe = 0.78\%$ |
| ○ Potash-Boric oxide (neutral)
$K_2O = 41.4\%$; $Fe = 1.221\%$ | ● Boric oxide
$Fe = 0.2712\%$ |

left represents the effective mean square moments p_{eff}^2 , in Bohr units for alkali-boric oxide and lead oxide-potash silica glasses, while the ordinate on the right is p_{eff}^2 for boric oxide glass; the abscissa represents the temperature on Kelvin scale.

DISCUSSION

From a critical analysis of the experimental results it is quite evident that though in most cases the room temperature values of p_{eff}^2 lie between the ferrio

and ferrous ion values (with the exception of the boric oxide glass which has been dealt with separately later on), they decrease with decreasing temperature and even drop down below the ferrous 'spin-only' value. The comparative values of p^2_{eff} at several temperatures between 300°K and 100°K of each glass are shown in the following table.

TABLE I

Description of glass	Composition in weight percent	Iron in weight percent	P^2_{eff} values at				
			300°K	240°K	200°K	160°K	100°K
Soda-boric oxide (neutral)	Na ₂ O = 9.475	2.848	27.00	25.15	23.75	22.65	20.65
Soda-boric oxide (reduced)	Na ₂ O = 31.0	1.210	31.45	28.65	26.40	24.10	22.00
Potash-boric oxide (neutral)	K ₂ O = 14.2	1.673	28.50	27.40	25.50	23.00	18.65
Potash-boric oxide (neutral)	K ₂ O = 41.4	1.221	31.85	31.85	32.00	31.40	28.25
Potash-boric oxide (reduced)	K ₂ O = 41.4	1.221	27.39	26.79	25.21	22.92	19.84
Lithia-boric oxide (neutral)	Li ₂ O = 31.2	0.2500	33.00	29.76	27.58	25.56	21.12
High lead-potash-silica (oxidised)	K ₂ O = 10.0 PbO = 60.0	0.780	33.35	30.78	28.42	25.85	23.43

The deviation in each case from the standard Fe⁺³ and Fe⁺² (spin-only) value can be readily observed if we consider the theoretical p^2 values of these two ions: p^2 for Fe⁺³ = 35.04; p^2 for Fe⁺² (spin-only) = 24.01 in terms of the Bohr unit.

For the sake of comparison the p^2_{eff} -T data for two typical ionic salts of iron are quoted below :

TABLE II

Fe ₂ (SO ₄) ₃ , (NH ₄) ₂ SO ₄ , 24H ₂ O (Dutta-Ray ² , 1955)		FeSO ₄ , (NH ₄) ₂ SO ₄ , 6H ₂ O (Bose ⁴ , 1948)	
Temp.°K	p^2_{eff}	Temp.°K	p^2_{eff}
300.5	35.08	296.8	28.49
278.8	35.06	182.5	28.57
242.0	35.07	84.8	27.13
222.1	35.05		
195.5	34.84		
179.2	34.81		
171.2	34.74		
147.8	34.83		
133.2	34.92		
121.0	35.00		
99.0	34.91		

It is quite evident from the preceding p^2_{eff} data for the electrovalent iron compounds that the variation of the p^2_{eff} values with lowering temperature is small. In contrast with this the decreasing trend of the p^2_{eff} values at low temperatures in the case of glass specimens is quite prominent.

In the multicomponent paramagnetic carriers of iron glass the mean moment of iron in the glass is due to the contribution of the moment values of the several magnetic carriers. The effective moment value of iron in glass and its behaviour towards low temperature will depend on the state of existence and proportion of the different forms of iron which again are interrelated with the glass composition, the method of preparation and working conditions. In the present set of samples, the deviation from the straight line nature of the p^2_{eff} -T curves with respect to T axis at the low temperature region increases in the following order :

$K_2O(41.4)-B_2O_3(N)$, $K_2O(41.4)-B_2O_3(R)$, $K_2O(14.2)-B_2O_3(N)$, $Na_2O(9.475)-B_2O_3(N)$, $Na_2O(31.0)-B_2O_3(R)$, $Li_2O(31.2)-B_2O_3(N)$, $PbO(60.0)-K_2O(10.0)-SiO_2(O)$

Where (N) = Neutral glass

(R) = Reduced glass

and

(O) = Oxidised glass

It is thus clear that there is no simple relation between the abnormally low p^2_{eff} values at low temperatures and those at room temperature of iron in the glass. For example, at room temperature the p^2_{eff} value of iron in high lead silica glass ($p^2_{eff} = 33.35$) is greater than iron in high potash ($p^2_{eff} = 31.85$; 41.4% K_2O) boric oxide glass but deviation from the straight line relation of p^2_{eff} -T curve is much greater in high lead silica glass than in the above potash

The decreasing trend of the p^2_{eff} values with the lowering of temperature may be due to the single or combined effects of the following factors : (1) the covalent nature of the linkage of some forms of liquid phase colouring iron complexes; (2) anomalous low temperature behaviour of some solid phase iron colouring centres, if there be any in the glassy matrix; and (3) a gradual change of the glass structure with the lowering of temperature, in which case a change in the distribution and nature of the electronic linkage in some forms of iron, particularly of the liquid phase colours, takes place.

It is well known that the nature of the chemical bonding, valency, etc. of a paramagnetic substance is directly related to its paramagnetic moment value. Mention has been made by Guha (1951) of some compounds of iron where the moment value (μ) of iron decreases considerably with the lowering of temperature,

e.g. $K_3Fe_3(CN)_6$, $FeSO_4 \cdot 7H_2O$ (Guha, 1951), etc. The p^2_{eff} -T values of these substances are quoted in the following table

TABLE III

$K_3Fe_3(CN)_6$		$FeSO_4 \cdot 7H_2O$	
Temp. °K	p^2_{eff}	Temp. °K	p^2_{eff}
304.9	5.077	303.1	26.76
254.9	4.871	241.9	26.42
226.0	4.656	186.3	25.41
193.9	4.546	139.6	24.58
156.9	4.216	107.4	23.60
123.6	3.962	82.0	22.90
81.1	3.631		

It is quite evident from the above table that in $K_3Fe_3(CN)_6$ (the covalent compound) ferric iron has a moment of 2.25 B.M. at room temperature, a little higher than the 'spin only' value for one unpaired electron. Moreover, the moment square value of iron in that compound decreases to about 1.9 B.M. at 81.1°K with the lowering of temperature. Similar is the case with $FeSO_4 \cdot 7H_2O$ (though to a smaller extent) where the room temperature value corresponds satisfactorily to the 'spin only' value with some orbital contribution for the Fe (ous) ion in the ionic compound, but the value decreases with the decrease of temperature even below the 'spin only' value. Thus from the consideration of the above results of the covalent ferric compound and of the ionic ferrous salt, it is suggested that some of the paramagnetic carriers of iron glass may behave similarly towards low temperature, especially those (iron complexes) with covalent linkage. Again, the rate of decrease of the p^2_{eff} value with temperature is connected with the glass composition, for the rate of fall in lithia-boric oxide and high lead-silica glasses is higher than in the potash-boric oxide glasses.

Thus it is observed that the decrease with temperature of the p^2_{eff} value in almost all the glasses resembles very much the behaviour of Fe^{+3} ion in the covalent compound of ferricyanide, but the moment square values of iron at room temperature remain always very high, although somewhat lower than the ferric 'spin only' value. The resultant behaviour of iron glass depends on the percentage composition of different forms of Fe^{+2} and Fe^{+3} in different stages of bonding.

It has been stated before that some other factors, such as the low temperature magnetic property of some solid phase colours, e.g. oxides of iron and low temperature glass structure are worth considering for the peculiar low temperature behaviour of iron glass.

Among the possible forms of solid phase colours, the presence of $\alpha\text{-Fe}_2\text{O}_3$ and Fe_3O_4 has been suggested by Moore and his coworkers (1949 and 1951). The absence of any ferromagnetic component like Fe_3O_4 in the glass is shown in the previous paper by the author (1959). Consequently, if at all any ferromagnetic component is present, its particle size must be lower than the magnetic domain size, in which case it can exhibit only strong paramagnetism with complicated dependence on temperature. The Moore school of workers assigns susceptibility values $\chi_m = 39.4 \times 10^{-6}$ for $\alpha\text{-Fe}_2\text{O}_3$ and $\chi_m = 424 \times 10^{-6}$ for Fe_3O_4 at 20°C [Abou-El-Azin (1954)]. The change in the magnetic behaviour of those oxides in a finely divided state of varying particle size with the lowering of temperature promises to be an interesting problem of study. In the massive form, χ_m for $\alpha\text{-Fe}_2\text{O}_3$ is independent of temperature and again the moment value of $\alpha\text{-Fe}_2\text{O}_3$ is related to the particle size [Chevallier *et al* (1937)].

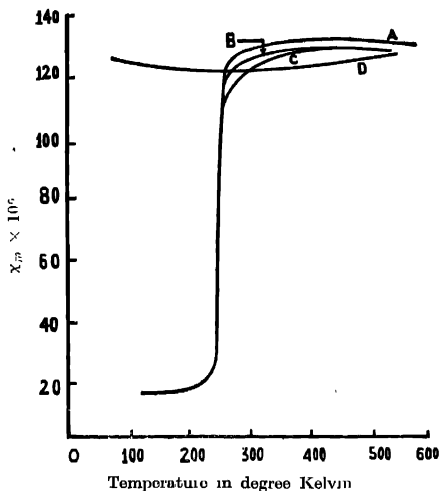


Fig. 2.

- A \rightarrow Puro $\alpha\text{-Fe}_2\text{O}_3$
 B $\rightarrow \alpha\text{-Fe}_2\text{O}_3 + 0.2 T_i$
 C $\rightarrow \alpha\text{-Fe}_2\text{O}_3 + 0.5 T_i$
 D $\rightarrow \alpha\text{-Fe}_2\text{O}_3 + 1.0 T_i$

However, in this connection it is important to refer here to the observation of Morin (1950) who found the mass susceptibility of $\alpha\text{-Fe}_2\text{O}_3$ abruptly falls down from 130×10^{-6} to 19.0×10^{-6} at below 240°K (figure 2).

It is well known that the structure of glass is sensitive to temperature. It is not unlikely that at low temperature a modified structure of each glass may

also set in with an altered atomic arrangement in glass structure, where the structure of the liquid phase colours (which are part and parcel of the glass structure), also change. It is likely in the case of low temperature glass structure that the mean moment values of some of these covalent types of iron groupings are smaller than the corresponding room temperature mean moment values. Consequently, there will be an overall decrease in the moment value with decreasing temperature.

Thus a number of probable causes for the decreasing trend of moment value of iron with lowering of temperature, for each glass, have been discussed. The resultant effect may be due to one or more of the above causes. In the light of these reasonings the peculiar low temperature behaviour of iron glasses like lithia-boric oxide and high lead potash-silica glass (vide Table II) can be accounted for, particularly for the anomalous low temperature behaviour of 'solid phase' paramagnetic carriers, apart from the relative decrease due to covalent iron groupings in those iron glasses which are likely to be small from the consideration of their glass composition.

It is of interest to mention here that there is an indication of sharp fall in p^2_{eff} values of iron in all experimental samples around 240°K (figure 1). This bears a similarity with the low temperature behaviour of $\alpha\text{-Fe}_2\text{O}_3$ (Morin, 1950; figure 2).

In contrast with the results on the borate and potash-lead-silica glasses, the behaviour of the boric oxide-iron glass is interesting in the sense that (1) the moment value of iron in the boric oxide glass at room temperature is very low, much lower than the moment value of Fe(ous) 'spin only' value and (2) the moment value of iron increases very slightly with the lowering of temperature. The p^2_{eff} -T values of boric oxide glasses are given in figure 1.

The low moment value of iron in the B_2O_3 glasses is due to the presence in large proportion of one or more forms of iron with a small moment value, such as $\alpha\text{-Fe}_2\text{O}_3$ or covalent Fe^{+2} or Fe^{+3} ion complexes, chances of the presence of any ionic groupings of iron are very remote as is evident from the consideration of the above glass. In a corresponding iron glass system like B_2O_3 -- SiO_2 with 80% B_2O_3 there is no singly bonded oxygen ion and the solid phase colours like $\alpha\text{-Fe}_2\text{O}_3$ is the major phase (Abd-El-Moneim Abou-El-Azm). It is likely that the small moment value of iron in the B_2O_3 system is due to the presence of a large proportion of $\alpha\text{-Fe}_2\text{O}_3$. Gradual rise in the moment value of iron with the lowering of temperature may be due to the single or cumulative effect of (i) the formation or increase in particle size of a form of iron with comparatively high moment value like paramagnetic Fe_3O_4 , though the overall content of such form will be small in the glass composition; or (ii) the gradual increase in size of the $\alpha\text{-Fe}_2\text{O}_3$ particle with the lowering of temperature which at the same time overrides the

negative effect of the temperature independent behaviour of $\alpha\text{-Fe}_2\text{O}_3$. R. R. Chevallier and Mathieu(1937) have shown that the moment value of $\alpha\text{-Fe}_2\text{O}_3$ increases with the size of particle. It will be interesting to mention here that the low temperature behaviour of $\text{Fe}_2\text{O}_3\text{--B}_2\text{O}_3$ samples bear a close similarity to a system of $\alpha\text{-Fe}_2\text{O}_3$ contaminated with TiO_2 as impurity to the extent of 1.00% Ti of the total metal atoms present, studied by Morin (1950) where the transition at 240°K disappears totally and there is a tendency for the rise of mass susceptibility value of $\alpha\text{-Fe}_2\text{O}_3$ with the lowering of temperature.

ACKNOWLEDGMENT

Thanks are due to Prof. K. Banerjee, Prof. A. Bose and Mr. S. Dutta Roy for their keen interest in the work.

REFERENCES

- Abd-El-Moneim Abou-El-Azm, 1954, *J. Soc. Glas. Technol.*, **38**, 101.
 Banerjee, B. K., 1959, *Ind. J. Phys.*, **33**, 165.
 Bose, A., 1947, *Ind. J. Phys.*, **47**, 247.
 Bose, A., 1948, *Ind. J. Phys.*, **22**, 483.
 Chevallier, R. and Mathieu, S., 1937, *Comp. Rend.*, **204**, 854.
 Chevallier, R. and Begui, Z. E., 1937, *Bull. Soc. Chim. men.*, **4**, 1935.
 Dutta Roy, S., 1955, *Ind. J. Phys.*, **38**, 429.
 Gubin, B. C., 1951, *Proc. Roy. Soc.*, **206**, 353.
 Moore, H. and Prasad, S. N., 1949, *J. Soc. Glas. Technol.*, **33**, 336.
 Moore, H. and Kumar, S., 1951, *J. Soc. Glas. Technol.*, **35**, 58.
 Morin F. J., 1950, *Phys. Rev.*, **78**, 819

SINGLET \rightarrow TRIPLET TRANSITION IN PARA-CHLOROTOLUENE

J. K. ROY*

OPTICS DEPARTMENT, INDIAN ASSOCIATION FOR THE CULTIVATION OF SCIENCE,
JADAVPUR, CALCUTTA 32

(Received, March 20, 1959)

Plate IV

ABSTRACT. The luminescence spectra excited in para-chlorotoluene have been studied using monochromatic radiations of different wavelengths. It has been observed that such a radiation of wavelength as large as 3750 Å excites the luminescence bands. As the near ultraviolet absorption band due to singlet \rightarrow singlet* transition in this case is at 2760 Å it has been concluded that the observed luminescence is produced by absorption of the radiation due to the singlet \rightarrow triplet transition and that the selection rule is violated in this case owing to the particular type of substitution.

INTRODUCTION

It was first observed by Sanyal (1953) while studying the Raman spectra of ortho- and para-chlorotoluene at low temperatures, that either of these two substances exhibits strong luminescence in the visible region in the solid state at -180°C . Later, Biswas (1954, 1955a, 1955b) observed that many disubstituted benzene compounds irradiated with 3650 Å group of Hg lines at -180°C give rise to similar luminescence in the visible region. It has also been observed (Sirkar and Biswas, 1956 and Biswas, 1956 a) that the intensity of this luminescence increases rapidly with lowering of temperature of the solidified mass and the relative intensities of the bands in the band system are altered considerably when the substance is dissolved in different solvents such as benzene, *n*-heptane, cyclohexane, methyl alcohol, etc. Using suitable light filters, Biswas (1956b) has also observed that the group of Hg lines at 3650 Å and other lines of shorter wavelengths upto 3000 Å are responsible for the production of this luminescence. The 0,0 band in the absorption spectrum due to solid *p*-chlorotoluene at -180°C had been observed by Swamy (1952) to be at 2760 Å and therefore it was surprising that radiation of wavelengths much longer than 2760 Å could excite the strong luminescence without absorbing light in the process of singlet-singlet* transition. The excitation of luminescence in *p*-chlorotoluene by the 3650 Å group of Hg-lines indicates that the *p*-chlorotoluene molecule in the solid state at -180°C absorbs radiation of wavelengths as long as 3650 Å. Such absorption could not

* Communicated by Prof. S. C. Sirkar.

be detected by Biswas (unpublished results). He, however, (Biswas 1958) observed that part of the luminescence is produced by delayed emission. Biswas did not use monochromatic radiation of different wavelengths to excite the luminescence. It was, therefore, not known whether any monochromatic radiation of wavelength longer than 3650\AA could excite the luminescence. It was, therefore thought worthwhile to study the luminescence spectra of these substances using different monochromatic exciting radiations in the region from 3500\AA — 4000\AA eliminating all radiations of shorter wavelengths in order to understand the process which gives rise to this luminescence.

EXPERIMENTAL

In order to get the monochromatic radiations of large intensity, light from a carbon arc running at 5 amps was focussed with the help of a large glass condenser on the entrance slit of a plane grating monochromator in which a large schlieren concave mirror was used both as a collimator and as the camera lens. The glass condenser cut off all wavelengths below 3000\AA . Radiations of different wavelengths could be taken out from the exit slit of the monochromator by turning the plane grating about a vertical axis. The light coming out through the exit slit of the monochromator was allowed to irradiate the sample contained in a sealed tube of Pyrex glass. The tube was immersed in liquid oxygen in a Dewar vessel in order to lower the temperature of the substance. The scattered light at right angles to the incident beam was focussed on the slit of a Fuess glass spectrograph having a dispersion of about $11\text{\AA}/\text{mm}$ in the 4046\AA region and the spectrum was photographed on Ilford HP3 films. Such spectrograms were taken using exciting radiations of wavelengths 3650\AA , 3750\AA and 3800\AA . Iron arc spectrum was superposed on each spectrogram using Hartmann diaphragm for comparison.

As the luminescence bands are broad, the widths of the slit of the spectrograph was increased to about 0.7 mm to reduce the time of exposure. Even with such a wide slit the time of exposure varied from 7 hours to 14 hours. The substance was of pure quality and was distilled in vacuum to remove dissolved impurities.

RESULTS AND DISCUSSION

The three spectrograms mentioned above are reproduced in Plate IV. The positions, approximate widths and the estimated relative intensities of the luminescence bands exhibited by pure *p*-chlorotoluene in the solid state at -180°C excited by the 3650\AA and 3750\AA respectively are given in Table I. The relative intensities are indicated as very strong (vs), strong(s) etc. in the table. The radiation of wavelength 3800\AA did not excite any luminescence.

It will be seen from figure 1 (Plate IV) that the bands excited by 3650\AA radiation photographed with an exposure of 7 hours is many times more intense than the bands due to 3750\AA although the exposure in the latter case is 11 hours.

RG.

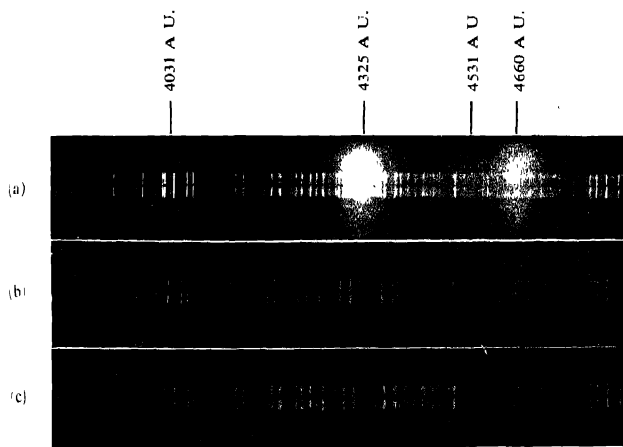


Fig. 1. Luminescence spectra of *p*-chlorotoluene at -180°C
 (a) Excited by 3650 Å U. (b) Excited by 3750 Å U. (c) Excited by 3800 Å U.

It is evident from these spectrograms that the radiation of wavelength as large as 3750Å excites the luminescence in this case, and therefore, the radiation

TABLE I
Luminescence spectra of *p*-chlorotoluene at -180°C

Exciting wavelength in A.U.	Wavelengths of the bands in A.U. (present author)	Wavelengths of the bands in A.U (Biswas, 1956a)	Width of the band in A.U. (present author)
3650Å	4031 (s)	4038 (s)	66
	4219 (w)	4219 (m)	75
	4325 (vs)	4325 (vs)	113
	4531 (s)	4529 (s)	80
	4660 (vs)	4660 (vs)	105
	—	4807 (vw)	
	—	4900 (w)	
3750Å	—	5031 (vw)	
	4325 (s)		91
	4531 (w)		74
3800Å	4660 (s)		89
	No band		

is first absorbed in the process of singlet-triplet transition and then re-emitted. As shown by Biswas (1958) part of the luminescence consists of phosphorescence and therefore the triplet-singlet transition is responsible for the origin of this phosphorescence.

As the intensity of luminescence is fairly large the initial absorption is also large. The failure in detecting this large absorption in the region from 3600Å – 3800Å by Biswas is evidently due to the fact that the triplet state has a large lifetime and therefore once some molecules are excited they do not return to the ground state for sometime and the incident radiation during this time is transmitted without any further absorption.

The violation of the selection rule regarding the transition from the singlet to triplet state in this particular case seems to be due to the particular substitution in the benzene ring, because neither dichlorobenzenes nor xylenes exhibit such a strong luminescence in this region in the solid state at low temperatures. The violation of the selection rules in this case is thus definitely established by the results of the present investigation.

ACKNOWLEDGMENT

The author's thanks are due to Prof. S. C. Sirkar, D.Sc., F.N.I, for his kind interest and constant guidance during the progress of the work.

REFERENCES

- Biswas, D. C., 1954, *Ind. J. Phys.*, **28**, 423
,, 1955a, *Ind. J. Phys.*, **29**, 257.
,, 1955b, *Ind. J. Phys.*, **29**, 503.
,, 1956a, *Ind. J. Phys.*, **30**, 143.
,, 1956b, *Ind. J. Phys.*, **30**, 255.
,, 1958, *Ind. J. Phys.*, **32**, 301
Sanyal, S. B., 1953, *Ind. J. Phys.*, **27**, 447.
Sirkar, S. C. and Biswas, D. C., 1956, *J. Chem. Phys.*, **24**, 470.
Swamy, H. N., 1952, *Ind. J. Phys.*, **26**, 445.

POLARISATION OF NUCLEONS DUE TO ANOMALOUS MAGNETIC MOMENT IN HIGHER BORN APPROXIMATION

S. SARKAR

DEPARTMENT OF THEORETICAL PHYSICS,

INDIAN ASSOCIATION FOR THE CULTIVATION OF SCIENCE, JADAVPUR, CALCUTTA-32.

(Received, March 14, 1959)

ABSTRACT. (1) We have extended Schwinger's calculation on polarisation of neutrons up to the second Born approximation taking non-relativistic form of the interaction of spin orbit coupling. (2) Considering the corresponding invariant interaction of the form $F_{\mu\nu} \gamma_\mu \gamma_\nu$ we have calculated the expression for the polarisation of the scattered particles in first order relativistic Born approximation. This result agrees with Wollenstein's expression except for the characteristic Coulomb phase factor. (3) We have also made an attempt to calculate the corresponding second order relativistic Born approximation.

Mott (1929) has shown from Dirac's electron theory that electrons are polarised when they are scattered by a Coulomb field. A non-relativistic reduction of Dirac's theory shows that this polarisation is due to the spin orbit coupling in Coulomb field. Recently Schwinger (1948) has suggested a method for polarising neutrons by making use of the spin-orbit interaction of the magnetic moment of neutron with the Coulomb field of the scattering nucleus. The spin-orbit interaction of neutron moving in nuclear Coulomb field V is given by the following contribution to neutron Hamiltonian

$$H' = \mu(e\hbar/2m^2c^2)(\sigma \cdot c \times \vec{p})$$

where the electric field $\epsilon = -\Delta V$

and μ is the neutron magnetic moment in units of $(e\hbar/2mc)$, σ is the Pauli spin vector, and \vec{p} is the momentum of the neutron. Schwinger has made the non-relativistic calculations in the first Born approximation, we have here extended his result to second Born approximation.

Later Wollenstein (1949) has investigated the polarisation of proton scattered by nuclear Coulomb field. He has introduced a term representing the interaction of the anomalous magnetic moment with the electromagnetic field of the invariant form proportional to $F_{\mu\nu} \gamma_\mu \gamma_\nu$ as first proposed by Pauli.

Wollenstein has given an approximate expression for the scattered wave which is valid only when $v^2/c^2 \ll 1$ and $\alpha^2 = (Z/137)^2 \ll 1$ where Z is the charge of target. He states that this expression can be obtained from Mott's expansion of the solution of the second order equation arising from the Dirac's

linear equation modified by the addition of the Pauli term. Wolfenstein's formula is identical with that obtained in first Born's approximation taking the non-relativistic interaction term $\mu(c\hbar/2m^2c^2)\sigma \cdot \epsilon \times \vec{p}$.

In this paper we propose to set up an integral equation corresponding to the modified Dirac's equation. Iterating the integral equation only once the scattered wave obtained by this method agrees with that obtained by Wolfenstein's method except for the characteristic Coulomb phase factor. Next we have made an attempt to extend the calculation by iterating the above mentioned integral equation twice which corresponds to second relativistic Born's approximation.

First we give the non-relativistic calculation of the scattered wave due to spin orbit interaction. We can write

$$\psi = \psi_0 + \psi_1 + \psi_2 + \dots \quad (1)$$

ψ_0 is the incident wave $e^{ip_1 \cdot r} \chi$ where χ is the spin wave function. ψ_1 and ψ_2 are respectively the first and second Born's approximations of the scattered wave. The calculation of ψ_1 is due to Schwinger and it is given by (taking $\hbar = 1$ and $c = 1$).

$$\begin{aligned} \psi_1 &= \frac{1}{4\pi} \frac{e^{ipr}}{r} \left[\int e^{-ip_2 \cdot r'} 2mH'(r') e^{ip_1 \cdot r'} d^3r' \right] \chi(p_1) \\ &= + \frac{e^{ipr}}{r} \cdot \frac{iZe^2\mu}{m} \cdot \frac{\sigma \cdot p_2 \times p_1}{|p_2 - p_1|^2} \quad \dots \quad (2) \end{aligned}$$

where \vec{p}_1 and \vec{p}_2 are respectively the momentum of initial and final states. The expression for the second Born's approximation of the scattered wave is given by

$$\begin{aligned} \psi_2 &= \frac{1}{4\pi} \frac{e^{ipr}}{r} \left[(2\pi)^{-3} \int \frac{d^3q}{q^2 - (p^2 + i\epsilon)} \int e^{ip_2 \cdot r'} 2mH'(r') e^{iq \cdot r'} d^3r' \right. \\ &\quad \left. \times \int e^{-iq \cdot r''} 2mH'(r'') e^{ip_1 \cdot r''} d^3r'' \right] \chi(p_1) \\ &= - \frac{e^{ipr}}{r} \frac{1}{2\pi^2} \left(\frac{Ze^2\mu}{m} \right)^2 \int \frac{(\sigma \cdot p_2 \times q)(\sigma \cdot q \times p_1) d^3q}{|p_2 - q|^2 |q - p_1|^2 (q^2 - (p^2 + i\epsilon))} \chi(p_1) \\ &= - \frac{e^{ipr}}{r} \frac{1}{2\pi^2} \left(\frac{Ze^2\mu}{m} \right)^2 \left[i \int \frac{(\sigma \cdot q)(q \cdot p_1 \times p_2) d^3q}{|p_2 - q|^2 |q - p_1|^2 (q^2 - (p^2 + i\epsilon))} \right. \\ &\quad \left. + \int \frac{(q \cdot p_2)(p_1 \cdot q) - q^2(p_1 \cdot p_2)}{|p_2 - q|^2 |q - p_1|^2 (q^2 - (p^2 + i\epsilon))} \chi(p_1) \right] \end{aligned}$$

The letters occurring in the scalar product, vector product and within modulus sign denote vector quantities. The rest are scalar quantities.

$$\begin{aligned}
 &= \frac{e^{ipr}}{r} - \frac{Z^2 e^4 \mu^2}{2m^2} p \sigma \cdot \vec{n} \left(-\tan \theta/2 \ln \sin^2 \theta/2 - i\pi \tan \theta/2 + i\pi \frac{\sin^2 \theta/2}{\cos^2 \theta/2} \chi(p_1) \right) \\
 &+ \frac{e^{ipr}}{r} \left(\frac{Z e^2 \mu}{m} \right)^2 \left[p \frac{\sin^2 \theta}{8} \left\{ \frac{i}{\sin^2 \theta/2 \cos^2 \theta/2} \right. \right. \\
 &+ \left. \left(-\frac{1}{\cos^2 \theta/2} + \frac{2}{\cos^4 \theta/2} \right) \frac{1}{\sin \theta/2} \pi/2 + \frac{2i}{\cos^4 \theta/2} (\ln \sin \theta/2 + i\pi/2) \right\} \\
 &+ \left. \frac{p \cos \theta}{2} \left(\frac{2i}{\cos^2 \theta/2} \ln \sin \theta + \pi \frac{\sin \theta/2}{\cos^2 \theta/2} - \frac{\pi}{\cos^2 \theta/2} \right) \right] \chi(p_1) \quad \dots \quad (3)
 \end{aligned}$$

where $p_2 \times p_1 = \vec{n} p^2 \sin \theta$

For the case of electron the first Born's approximation does not give any polarisation effect since σ dependent part is imaginary and σ independent part is real. Here polarisation is in second Born's approximation where part of the σ dependent term is real. If we put $\mu = \frac{1}{2}$ real part of σ dependent term of the above calculation agrees with that obtained by Mott

We now give the relativistic calculation for the Scattered wave due to the interaction of the anomalous magnetic moment of the scattered particle in the field of the target nucleus. The covariant form of modified Dirac's equation in the case where the vector potential is zero is given by

$$\left(\sum_{k=1}^3 \gamma_k p_k - \gamma_4 E + m \right) \psi = -\gamma_4 e V \psi + (e/2m)(\mu/i)\gamma_4 \gamma_k i F_{4k} \psi \quad \dots \quad (4)$$

Multiplying the above equation from the left by the operator $\gamma_4 \alpha \cdot p - \gamma_4 E - m$ we get

$$(\nabla^2 + p^2) \psi = (\gamma_4 \alpha \cdot p - \gamma_4 E - m) \left\{ (-\gamma_4 e V + \frac{e}{2m} (\mu/i) \alpha \cdot \epsilon) \psi \right\} \quad \dots \quad (5)$$

Knowing the Green's function of the above differential equation we obtain an integral equation the first approximation of which is the following :

$$\begin{aligned}
 \psi &= e^{ip_1 \cdot r} u(p_1) + \frac{e^{ipr}}{4\pi r} \int e^{-ip_2 \cdot r'} (\gamma_4 \alpha \cdot p - \gamma_4 E - m) \left\{ \left(-\gamma_4 e V + \frac{e}{2m} (\mu/i) \alpha \cdot \epsilon \right) \right. \\
 &\quad \left. e^{ip_1 \cdot r'} u(p_1) \right\} d^3 r'
 \end{aligned}$$

Now,

$$\begin{aligned} \epsilon \cdot p \left(\frac{\alpha \cdot r'}{r'^3} e^{ip_1 \cdot r'} \right) &= -i\alpha \cdot \nabla \left(\frac{\alpha \cdot r'}{r'^3} e^{ip_1 \cdot r'} \right) = \frac{p_1 \cdot r' + i\sigma \cdot p_1 \times r'}{r'^3} e^{ip_1 \cdot r'} \\ &= \frac{\alpha \cdot r' \alpha \cdot p_1 + 2i\sigma \cdot p_1 \times r'}{r'^3} e^{ip_1 \cdot r'} \quad \dots (6) \end{aligned}$$

$$\begin{aligned} (\gamma_4 \alpha \cdot p - \gamma_4 E - m) \left\{ \frac{\alpha \cdot r}{r^3} e^{ip_1 \cdot ru(p_1)} \right\} &= \frac{\alpha \cdot r}{r^3} (-\gamma_4 \alpha \cdot p_1 + \gamma_4 E - m) e^{ip_1 \cdot ru(p_1)} \\ &+ \frac{2i\gamma_4 \sigma \cdot p_1 \times r}{r^3} e^{ip_1 \cdot ru(p_1)} = \frac{2i\gamma_4 \sigma \cdot p_1 \times r}{r^3} e^{ip_1 \cdot ru(p_1)} \quad \dots (7) \end{aligned}$$

also

$$\begin{aligned} -(\gamma_4 \alpha \cdot p - \gamma_4 E - m) \left\{ \gamma_4 \frac{e}{r} e^{ip_1 \cdot ru(p_1)} \right\} &= -\gamma_4 \frac{e}{r} (-\gamma_4 \alpha \cdot p_1 - \gamma_4 E - m) e^{ip_1 \cdot ru(p_1)} \\ -i\alpha \cdot \left(\text{grad} \frac{e}{r} \right) e^{ip_1 \cdot ru(p_1)} &= 2E \frac{e}{r} e^{ip_1 \cdot ru(p_1)} - i\alpha \cdot \left(\text{grad} \frac{e}{r} \right) e^{ip_1 \cdot ru(p_1)} \quad \dots (8) \end{aligned}$$

Remembering the above relations we have

$$\begin{aligned} \psi = e^{ip_1 \cdot ru(p_1)} + \frac{e^{ipr} Ze}{4\pi r} \left[\frac{e}{2m} (\mu/i) \frac{8\pi\gamma_4 \sigma \cdot p_1 \times p_2}{|p_2 - p_1|^2} + \frac{4\pi e}{|p_2 - p_1|^2} \alpha \cdot (p_2 - p_1) \right. \\ \left. + \frac{2Ee \cdot 4\pi}{|p_2 - p_1|^2} \right] u(p_1) \quad \dots (9) \end{aligned}$$

If the incident beam is in the z direction we have

$$\alpha \cdot (p_2 - p_1) u(p_1) = \alpha \cdot (p_2 - p_1) \begin{pmatrix} \frac{A}{B} \\ -\frac{p_{1z}}{E+m} \frac{A}{B} \\ +\frac{p_{1z}}{E+m} \frac{B}{A} \end{pmatrix} = \begin{pmatrix} -\frac{\sigma \cdot (p_2 - p_1) \sigma \cdot p_1 \chi}{E+m} \\ \sigma \cdot (p_2 - p_1) \chi \end{pmatrix} \quad \dots (10)$$

In determining polarisation we are interested in the large component of the spinor represented by χ and rewriting the expression for ψ in terms of the large component of the spinor we have

$$\begin{aligned} \psi = e^{ip_1 \cdot r} \chi(p_1) + \frac{e^{ipr} Ze}{r} \left[-\frac{i\mu e}{2m} \sigma \cdot n \cot \theta/2 \right. \\ \left. - \frac{e}{E+m} \cdot \frac{1}{4p^2 \sin^2 \theta/2} \left((p_2 - p_1) \cdot p_1 + i\sigma \cdot (p_2 \times p_1) \right) + \frac{Ee}{2p^2 \sin^2 \theta/2} \right] \chi(p_1) \end{aligned}$$

$$= e^{i\mathbf{p}_1 \cdot \mathbf{r}} \chi(p_1) + \frac{e^{i\mathbf{p} \cdot \mathbf{r}} Ze}{r} \left[-i\sigma \cdot \mathbf{n} \left(\frac{\mu e}{2m} + \frac{1}{2} \frac{e}{E+m} \right) \cot \theta/2 + \frac{e}{2(E+m)} \right. \\ \left. + \frac{Ee}{2p^2 \sin^2 \theta/2} \right] \chi(p_1) \quad \dots \quad (11)$$

The spin dependent amplitude of the scattered wave agrees with that obtained by Wolfenstein if we put $E = m$ in our formula except for the characteristic Coulomb phase factor.

The contribution of anomalous magnetic moment to spin dependent part of the scattered wave is twice that due to the intrinsic spin of the nucleon.

For the case of electron the above expression for the scattered wave reduces to that obtained by Mott and is given by

$$\psi_{sc} = \frac{e^{i\mathbf{p} \cdot \mathbf{r}}}{r} \frac{Ze^2 E}{2p^2} \left[\left(\operatorname{cosec}^2 \theta/2 + \frac{m-E}{E} \right) + \frac{m-E}{E} \begin{pmatrix} 0 & e^{-i\varphi} \\ e^{i\varphi} & 0 \end{pmatrix} \right] \chi(p_1) \quad \dots \quad (12)$$

where we have put

$$\sigma \cdot \mathbf{n} = \sigma \cdot \frac{\mathbf{p}_2 \times \mathbf{p}_1}{p^2 \sin \theta} = i \begin{pmatrix} 0 & e^{-i\varphi} \\ e^{i\varphi} & 0 \end{pmatrix}, \varphi \text{ being the azimuthal angle.}$$

Iterating twice the integral equation corresponding to equation (5) the second Born approximation of the scattered wave is given by

$$\psi_2 = \frac{e^{i\mathbf{p} \cdot \mathbf{r}}}{4\pi r} \left(\frac{Ze^2 \mu/i}{2m} \right)^2 \frac{1}{(2\pi)^3} \left[\int \frac{d^3 q}{q^2 - (p^2 + i\epsilon)} \int e^{i\mathbf{p}_2 \cdot \mathbf{r}'} \left\{ (-i\gamma \cdot \Delta - \gamma_4 E - m) \right. \right. \\ \left. \left. - \frac{\alpha \cdot \mathbf{r}'}{r'^3} e^{i\mathbf{q} \cdot \mathbf{r}'} \right\} d^3 r' \right. \\ \left. \times \int e^{-i\mathbf{q} \cdot \mathbf{r}''} \left\{ (-i\gamma \cdot \Delta - \gamma_4 E - m) - \frac{\alpha \cdot \mathbf{r}''}{r''^3} e^{i\mathbf{p}_1 \cdot \mathbf{r}''} \right\} d^3 r'' \right] u(p_1) \quad \dots \quad (13)$$

We insert the unit matrix $u(q)\bar{u}(q) = \sum_{r=1}^4 u_r(q)\bar{u}_r(q) = I$ after $e^{i\mathbf{q} \cdot \mathbf{r}'}$ where spinor $u_r(q)$'s are the four solutions of the equation. $(\gamma \cdot q - \gamma_4 E(q) + m) = 0$. Hence

$$\psi_2 = \frac{e^{i\mathbf{p} \cdot \mathbf{r}}}{4\pi r} \left(\frac{Ze^2 \mu/i}{2m} \right)^2 \frac{1}{(2\pi)^3} \left[\int \frac{d^3 q}{q^2 - (p^2 + i\epsilon)} \cdot \frac{8\pi\gamma_4 \sigma \cdot \mathbf{p}_2 \times (\mathbf{p}_2 - \mathbf{q})}{|\mathbf{p}_2 - \mathbf{q}|^2} \cdot \right. \\ \left. \frac{8\pi\gamma_4 \sigma \cdot \mathbf{q} \times (\mathbf{q} - \mathbf{p}_1)}{|\mathbf{q} - \mathbf{p}_1|^2} u(p_1) \right] \\ + \int \frac{d^3 q}{q^2 - (p^2 + i\epsilon)} \cdot \frac{\gamma_4 E(q) - \gamma_4 E}{1} \cdot \frac{-i4\pi\alpha \cdot (\mathbf{p}_2 - \mathbf{q})}{|\mathbf{p}_2 - \mathbf{q}|^2} \cdot \frac{8\pi\gamma_4 \sigma \cdot \mathbf{p}_1 \times (\mathbf{p}_1 - \mathbf{q})}{|\mathbf{q} - \mathbf{p}_1|^2} u(p_1) \\ \dots \quad (14)$$

Here the first part of the wave ' ψ_2 ' called ' ψ_2' ' agrees with ψ_2 of equation (3) calculated in non-relativistic Born approximation. In the second part of ψ_2 called ' ψ_2'' ' the integral involving $E(q)$ is zero since $E(q)$ will have both $+ve$ and $-ve$ signs. Then ψ_2'' is given by

$$\psi_2'' = + \frac{e^{ipr}}{4\pi r} \left(\frac{Ze^2\mu/i}{2m} \right)^2 \frac{1}{(2\pi)^3} \frac{32\pi^2 i E}{E+m} \int \frac{d^3q}{q^2 - (p^2 + i\epsilon)} \times \frac{q \cdot p_2 \times p_1 + i\sigma \cdot \{p_1(p_2 \cdot q) - q(p_1 \cdot p_2)\} - i\sigma \cdot \{p_1 q^2 - q(p_1 \cdot q)\}}{|p_2 - q|^2 |q - p_1|^2} \rho_1 u(p_1) \quad \dots (15)$$

Expressing again ψ_2'' in terms of the large component of spinor using the relation (10) we have

$$\begin{aligned} \psi_2'' &= - \frac{e^{ipr}}{4\pi r} \left(\frac{Ze^2\mu/i}{2m} \right)^2 \frac{1}{(2\pi)^3} \frac{32\pi^2 E}{E+m} \int \frac{d^3q}{(q^2 - (p^2 + i\epsilon))} \frac{1}{|p_2 - q|^2 |q - p_1|^2} \\ &\times [p_1^2(p_2 \cdot q) - (p_1 \cdot q)(p_1 \cdot p_2) - p_1^2 q^2 + (p_1 \cdot q)(p_1 \cdot q) - i\sigma \cdot (q \times p_1)(p_1 \cdot p_2) \\ &\quad + i\sigma \cdot (q \times p_1)(p_1 \cdot q)] \chi(p_1) \\ &= - \frac{e^{ipr}}{4\pi r} \left(\frac{Ze^2\mu/i}{2m} \right)^2 \frac{1}{(2\pi)^3} \frac{32\pi^2 E p}{E+m} \left[\frac{\pi^2 \sin^2 \theta}{8} \left\{ 4i \left(\frac{1}{\cos^2 \theta/2} + \frac{1}{\cos^4 \theta/2} \right) \right. \right. \\ &\quad \left. \left. (\ln \sin \theta/2 + i\pi/2) \right. \right. \\ &\quad \left. \left. + \left(\frac{2}{\cos^4 \theta/2} + \frac{1}{\cos^2 \theta/2} \right) \frac{\pi}{\sin \theta/2} \right. \right. \\ &\quad \left. \left. - \frac{\pi}{\cos^2 \theta/2} (\operatorname{cosec} \theta/2 - 1) - \frac{i}{\cos^2 \theta/2} \ln \sin^2 \theta/2 \right\} - \pi^2 \left(\frac{2i}{\cos^2 \theta/2} \ln \sin \theta/2 \right. \right. \\ &\quad \left. \left. + \frac{\pi \sin \theta/2}{\cos^2 \theta/2} - \frac{\pi}{\cos^2 \theta/2} \right) \right] \chi(p_1) \\ &- \frac{e^{ipr}}{4\pi r} \left(\frac{Ze^2\mu/i}{2m} \right)^2 \frac{1}{(2\pi)^3} \cdot \frac{32\pi^2 E p}{E+m} \sigma \cdot n \left[- \frac{i}{2} \sin \theta \cos \theta \right. \\ &\quad \left. \left\{ - \frac{\pi^3}{4 \cos^2 \theta/2} (\operatorname{cosec} \theta/2 - 1) \right. \right. \\ &\quad \left. \left. - \frac{\pi^2 i}{4 \cos^2 \theta/2} \ln \sin^2 \theta/2 \right\} - \frac{i\pi^2}{4} \cdot 2 \sin \theta \cos \theta \left\{ i \left(\frac{2}{\cos^4 \theta/2} + \frac{1}{\cos^2 \theta/2} \right) \right. \right. \\ &\quad \left. \left. (\ln \sin \theta/2 + i\pi/2) \right. \right. \\ &\quad \left. \left. + \left(\frac{i}{\cos^4 \theta/2} + \frac{\pi}{\cos^4 \theta/2 \sin \theta/2} \right) \right\} - \frac{i\pi^2}{4} \sin \theta (1 - \cos \theta) \left\{ \frac{2i}{\cos^4 \theta/2} \right. \right. \\ &\quad \left. \left. (\ln \sin \theta/2 + i \frac{\pi}{2}) \right) \right] \end{aligned}$$

$$+ \frac{1}{\cos^2 \theta/2 \sin^2 \theta/2} + \left(-\frac{1}{\cos^2 \theta/2} + \frac{2}{\cos^4 \theta/2} \right) \frac{\pi/2}{\sin \theta/2} \} \times \chi(p_1) \quad \dots \quad (16)$$

The amplitude of the scattered wave is of the form

$$\psi_{sc} = \frac{e^{i p r}}{r} f(\theta) \chi(p_1) \quad \dots \quad (17)$$

We split up $f(\theta)$ into σ -independent and σ dependent components and write

$$f(\theta) = f_1(\theta) + \sigma \cdot n f_2(\theta) \quad \dots \quad (18)$$

$f_1(\theta)$ accounts for the amplitude of the wave scattered by nuclear forces and other types of forces independent of spin term.

The intensity of scattered wave is given by

$$r^2(\psi_{sc}, \psi_{sc}) = |f_1(\theta)|^2 + |f_2(\theta)|^2 + 2 \operatorname{Re}[f_1(\theta) f_2(\theta)] n \cdot P_{inc} \quad \dots \quad (19)$$

where

$$P_{inc} = (\chi \sigma \chi)$$

Following the notation of Schwinger the vector P represents the polarisation state of the beam. For an initially unpolarised beam for which $P_{inc} = (\chi \sigma \chi) = 0$, polarisation state of scattered wave is given by

$$P_{sc} = \frac{\vec{n} \cdot 2 \operatorname{Re}[f_1(\theta) f_2(\theta)]}{|f_1(\theta)|^2 + |f_2(\theta)|^2} = n \cdot P(\theta) \quad \dots \quad (20)$$

The polarisation of the scattered beam can be observed by subjecting once scattered polarised beam to a second scattering process. It has been shown that the left hand and right hand asymmetry of double scatterings is

$$R = \frac{1 + P(\theta_1) + P(\theta_2)}{1 - P(\theta_1)P(\theta_2)} \quad \dots \quad (21)$$

Of the integrals occurring in the paper, the first two have been evaluated by Dalitz and the third one is straight forward, though tedious. Their values are as follow :

$$\begin{aligned} \int \frac{d^3 q}{|p_2 - q|^2 |q - p_1|^2 (p^2 - q^2 + i\epsilon)} &= \int_{-1}^1 \int \frac{d^3 q}{[|q - P|^2 + \Lambda^2]^2} \frac{dZ}{(p^2 - q^2 + i\epsilon)} \\ &\quad \lambda \rightarrow 0 \\ &= I \\ \int \frac{q_r d^3 q}{|p_2 - q|^2 |q - p_1|^2 (p^2 - q^2 + i\epsilon)} &= \int_{-1}^1 \int \frac{q_r}{[|q - P|^2 + \Lambda^2]^2} \frac{dZ}{(p^2 - q^2 + i\epsilon)} \\ &\quad \lambda \rightarrow 0 \end{aligned}$$

$$\begin{aligned}
&= \frac{(p_1 + p_2)r}{2} \left\{ -\frac{\pi^2}{4p^3 \cos^2 \theta/2} (\operatorname{cosec} \theta/2 - 1) - \frac{\pi^2 i}{4p^3 \cos^2 \theta/2} \ln \sin^2 \theta/2 + I \right\} \\
&\int \frac{q_r q_s d^3 q}{|p_2 - q|^2 |q - p_1|^2 (p^2 - q^2 + i\epsilon)} = \int \int_{-1}^1 \frac{q_r q_s d^3 q dZ}{[|q - P|^2 + \Lambda^2]^2 (p^2 - q^2 + i\epsilon)} \\
&\lambda \rightarrow 0 \\
&= \int_{-1}^1 \left[\frac{\pi^2 \delta_{rs}}{2P} \left(\frac{\Lambda + ip}{P} + i \frac{p^2 + P^2 + \Lambda^2}{2P^2} \ln \frac{p - P + i\Lambda}{p + P + i\Lambda} \right) \right. \\
&\quad - \frac{\pi^2 p^2}{8} \left\{ (p_1 + p_2)_r (p_1 + p_2)_s + (p_1 - p_2)_r (p_1 - p_2)_s + (Z^2 - 1)(p_1 - p_2)_r (p_1 - p_2)_s \right\} \\
&\quad \times \left\{ \frac{3i}{2} \left(\frac{P^2 + p^2 + \Lambda^2}{P^3} \right) \ln \frac{p - P + i\Lambda}{p + P + i\Lambda} + \frac{2(\Lambda + ip)}{P^4} - \frac{2}{\Lambda(p + P + i\Lambda)(p - P + i\Lambda)} \right. \\
&\quad \left. \left. + \frac{i(p^2 + 3P^2 + \Lambda^2)}{2P^4} \left(\frac{1}{p - P + iV} + \frac{1}{p + P + i\Lambda} \right) \right\} \right] dZ \\
&= \frac{\pi^2 \delta_{rs}}{2} \left(\frac{2i}{p \cos^2 \theta/2} \ln \sin \theta/2 + \frac{\pi}{p \cos^2 \theta/2} - \frac{\pi}{p \cos^2 \theta/2} \right) \\
&- \frac{\pi^2}{8} \left\{ (p_1 + p_2)_r (p_1 + p_2)_s + (p_1 - p_2)_r (p_1 - p_2)_s \right\} \frac{2}{p^3} \left[i \left(\frac{2}{\cos^4 \theta/2} + \frac{1}{\cos^2 \theta/2} \right) \right. \\
&\quad \left. (\ln \sin \theta/2 + i\pi/2) + \frac{i}{\cos^2 \theta/2} + \frac{2}{\cos^4 \theta/2 \sin \theta/2} \cdot \frac{\pi}{2} - \frac{I}{\pi^2} \right] \\
&+ \frac{\pi^2}{8p^3} (p_1 - p_2)_r (p_1 - p_2)_s 2 \left[\frac{2i}{\cos^4 \theta/2} \left(\ln \sin \theta/2 + \frac{i\pi}{2} \right) + \frac{i}{\sin^2 \theta/2 \cos^2 \theta/2} \right. \\
&\quad \left. + \left(-\frac{1}{\cos^2 \theta/2} + \frac{2}{\cos^4 \theta/2} \right) \frac{\pi/2}{\sin \theta/2} \right]
\end{aligned}$$

where $\vec{P} = \frac{1}{2}[(1 + Z)\vec{p}_1 + (1 - Z)\vec{p}_2]$, so that $P^2 = p^2(\cos^2 \theta/2 + Z^2 \sin^2 \theta/2)$ and $\Lambda^2 = \lambda^2 + p^2 \sin^2 \theta/2 (1 - Z^2)$

ACKNOWLEDGMENTS

The author is grateful to Prof. D. Basu for his constant guidance throughout the progress of this work.

REFERENCES

- Dalitz, A. H., 1951, *Proc. Roy. Soc., A*, **206**, 509.
Mott, N. F., 1929, *Proc. Roy. Soc., A*, **124**, 425.
Schwinger, Julian, 1948, *Phys. Rev.*, **73**, 407.
Wolfenstein, Lincoln, 1949, *Phys.*, **75**, 1664.

UNLIKE MOLECULAR INTERACTIONS FROM VISCOSITY AND INTER-DIFFUSION

A. K. BARUA

INDIAN ASSOCIATION FOR THE CULTIVATION OF SCIENCE
CALCUTTA-32

(Received for publication, April 20, 1959).

ABSTRACT. Force constants for unlike molecular interactions for the systems H_2-CH_4 , H_2-CO_2 , H_2-N_2 , H_2-He , $N_2-C_2H_4$ for the Lennard-Jones (12 : 6), model have been determined by combining the data on inter-diffusion coefficient and viscosity of gas mixtures. To test the appropriateness of the force constants thus determined, the available experimental data have been compared with the values of the viscosity, inter-diffusion and thermal diffusion calculated by utilising these force constants and satisfactory agreement has been obtained. From the available data it appears that the force constants, herein determined, give better agreement than those obtained from the usual combination rules.

INTRODUCTION

Considerable amount of information has been obtained for the like molecular interactions on the Lennard-Jones (12 : 6) and the exp-six potentials from the experimental viscosity and second virial coefficient data. Some other properties such as, self-diffusion (Srivastava and Madan, 1952); thermal diffusion (Srivastava and Madan, 1953); thermal conductivity (Saxena, 1955a; Srivastava 1957a) have also been utilised. Unfortunately, information regarding the unlike molecular interactions has so far been very meagre. This is mainly due to the non-availability of suitable experimental data having sufficient accuracy and temperature range.

The most suitable property for determining unlike interactions is the inter-diffusion coefficient D_{12} for, it depends, to a first approximation, only on the unlike interactions. Usually the range of temperature for these measurements is small so that it is not possible in practice to determine accurately the unlike interactions solely from inter-diffusion data. This lead Srivastava and Madan (1953) to utilise the extensive thermal diffusion data for this purpose and the method has been subsequently employed by several workers (Saxena, 1955b; Srivastava and Srivastava, 1957; Srivastava 1957b). Recently several workers (Strehlow, 1953; Bunde, 1955c; Rumpel, 1955, Srivastava and Srivastava, 1959; Srivastava, 1959) have tried to extend the temperature range of measurement of D_{12} and have utilised their data to determine unlike interactions on the Lennard-Jones (12 : 6) model. Srivastava and Srivastava (1959) have suggested a method in which the data on inter-diffusion coefficient and the viscosity of gas mixtures are

combined to determine the force parameters for the unlike interactions. The advantage of this method is that it can be used even when the inter-diffusion coefficient is known at a single temperature provided it is sufficiently accurate. In this paper the accurate inter-diffusion data available in the literature have been combined with the data on viscosity of gas mixtures to determine unlike interactions on the Lennard-Jones (12 : 6) model.

DETERMINATION OF THE PARAMETERS

The Lennard-Jones (12 : 6) potential may be written as

$$\phi(r) = 4\epsilon \left[\left(\frac{\sigma}{r} \right)^{12} - \left(\frac{\sigma}{r} \right)^6 \right] \quad \dots (1)$$

where $\phi(r)$ is the potential energy between two molecules separated by a distance r , σ is the value of r for which $\phi(r) = 0$, ϵ is the depth of the potential well. Unfortunately, the theory is not sufficiently developed to give the unlike interaction parameters in terms of like ones and it is usual to employ some empirical combination rules for this purpose. The set of rules, hitherto most successful, is the following :—

$$\sigma_{12} = 1/2(\sigma_1 + \sigma_2) \quad \dots (2)$$

$$\epsilon_{12} = (\epsilon_1 \cdot \epsilon_2)^{1/2} \quad \dots (3)$$

Relations (2) and (3) are semi-empirical and at best only approximate; it is therefore always desirable to determine σ_{12} and ϵ_{12} from the experimental data by suitable methods.

The coefficient of inter-diffusion of two gases 1 and 2 may be written, to the first approximation, in the form

$$[D_{12}]_1 = \frac{0.002628 [T^3(M_1 + M_2)/2M_1M_2]^{1/2}}{p\sigma_{12}^2\Omega_{12}^{(1,1)*}(T_{12}^*)} \quad \dots (4)$$

where D_{12} is the mutual diffusion coefficient in cm^2/sec , p the pressure in atmosphere, $\Omega_{12}^{(1,1)*}$ is a reduced collision integral tabulated by Hirschfelder, Curtiss and Bird (1954), and $T_{12}^* = kT/\epsilon_{12}$. M_1 , M_2 are the molecular weights and T is the temperature in $^\circ\text{K}$.

The viscosity of a binary gas mixture, η_{mix} , to a first approximation is given by

$$[\eta_{mix}]_1 = \frac{1 + Z_\eta}{X_\eta + Y_\eta} \quad \dots (5)$$

$$\text{where } X_\eta = \frac{x_1^2}{\eta_1} + \frac{2x_1x_2}{\eta_{12}} + \frac{x_2^2}{\eta_2}$$

$$\begin{aligned}
 Y_\eta &= \frac{3}{5} A_{12}^* \left\{ \frac{x_1^2}{\eta_1} \left(\frac{M_1}{M_2} \right) + \frac{2x_1x_2}{\eta_{12}} \left(\frac{(M_1+M_2)^2}{4M_1M_2} \right) \frac{(\eta_{12})^3}{\eta_1\eta_2} \right. \\
 &\quad \left. + \frac{x_2^2}{\eta_2} \left(\frac{M_2}{M_1} \right) \right\} \\
 Z_\eta &= \frac{3}{5} A_{12}^* \left\{ \frac{x_1^2 M_1}{M_2} + 2x_1x_2 \left[\left(\frac{(M_1+M_2)^2}{4M_1M_2} \right) \left(\frac{\eta_{12}}{\eta_1} + \frac{\eta_{12}}{\eta_2} \right) - 1 \right] \right. \\
 &\quad \left. + x_2^2 \frac{M_2}{M_1} \right\}
 \end{aligned}$$

x_1, x_2 are the mole fractions, η_1, η_2 are the viscosities and M_1, M_2 the molecular weights of the components 1 and 2 respectively. η_{12} is the viscosity of a hypothetical gas having the molecular weight $2M_1M_2/(M_1+M_2)$. A_{12}^* is a function of the collision integrals and is temperature dependent. It has been tabulated by Hirschfelder, Curtiss and Bird (1954). Solving Eq.(4) and (5) to eliminate σ_{12} we obtain.

$$\begin{aligned}
 A_{12}^* = & \frac{1 - \eta_{mix} \left[\frac{x_1^2}{\eta_1} + \frac{x_2^2}{\eta_2} \right] + \frac{3}{10} \frac{x_1x_2}{\eta_{12}} \left(\frac{M_1+M_2}{M_1M_2} \right) \eta_0[\eta_1 + \eta_2 - \eta_{mix}]}{2x_1x_2 \left(\frac{\eta_{mix}}{\eta_0} \right) + \frac{3}{5} \frac{x_1^2}{\eta_1} \left(\frac{M_1}{M_2} \right) [\eta_{mix} - \eta_1] + \frac{3}{5} \frac{x_2^2}{\eta_2} \left(\frac{M_2}{M_1} \right) [\eta_{mix} - \eta_2] + \frac{9}{5} x_1x_2} \\
 & \dots \quad (6)
 \end{aligned}$$

$$\text{with } \eta_0 = \frac{266.93}{0.002628} \times \frac{2M_1M_2}{M_1+M_2} \times \frac{D_{12}}{T} \times 10^{-7}$$

Thus by knowing D_{12} , η_{mix} , η_1 and η_2 at the same temperature $T^\circ K$, A_{12}^* may be determined. From the tables the value of T_{12}^* corresponding to this value of A_{12}^* can be read and hence $c_{12/k}$ may be calculated from the relation $T_{12}^* = kT/\epsilon_{12}$. Once the value $c_{12/k}$ is fixed, σ_{12} can be determined from Eq. (4). If D_{12} data are available at several temperatures, the corresponding values of σ_{12} are determined and the mean taken.

The force parameters σ_{12} , ϵ_{12}/k obtained for the systems H_2-CH_4 , H_2-CO_2 , H_2-N_2 , H_2-He and $N_2-C_2H_4$ have been recorded in table I. In the table are also given for the sake of comparison the values calculated from the combination rules. It will be seen from Table I that the values of σ_{12} determined from the experimental data are always lower than those given by the combination rule. This is to be expected as the combination rule given by Eqn. (2) is expected to hold for rigid spheres only. It may also be observed that except in the case of $N_2-C_2H_4$, the values obtained for ϵ_{12}/k are always higher than those obtained from the combination rule.

TABLE I
Force Parameters on the Lennard-Jones (12 : 6) Model

Gas Pair	From D_{12} and η_{mix}		From combination rules		Ref. for data	
	σ_{12} Å	$\epsilon_{12}/k^\circ K$	σ_{12} Å	$\epsilon_{12}/k^\circ K$	D_{12}	η_{mix}
H ₂ —CH ₄	3.346	71.31	3.425	67.54	(Boyd, 1951)	(Hirschfelder, 1949)
H ₂ —CO ₂	3.420	83.37	3.482	79.54	„	„
N ₂ —C ₂ H ₄	3.883	135.60	3.957	137.00	„	„
H ₂ —N ₂	3.283	58.41	3.325	55.20	(Bunde, 1955)	(Iitterbeek, <i>et al</i> , 1947)
H ₂ —He	2.747	21.31	2.772	20.70	(Rumpel, 1955)	(Hirschfelder, 1949)

COMPARISON WITH EXPERIMENT

In order to test the reliability of the force parameters thus determined it is necessary to see how far they reproduce the experimental data over a wide range of temperature. In table II are shown the experimental and the calculated values of D_{12} for the systems for which data are available at more than one temperature. D_{12} values have also been calculated from the combination rules. It will be seen from table II, that the force parameters determined in the present paper represent the experimental D_{12} data better than the combination rules, and this is very marked in the case of H₂—He.

TABLE II
Experimental and the calculated values of D_{12} for H₂—N₂ and H₂—He

Gas Pair	T°K	D_{12} in cm ² /sec.		
		Expt.	Calc. from force parameters obtained	Calc. from combination rules
H ₂ —N ₂	298.2	0.7385	0.7714	0.7803
	328.2	0.9079	0.9074	0.8956
	358.2	1.052	1.053	1.016
H ₂ —He	298.2	1.550	1.539	1.665
	328.2	1.843	1.805	1.940
	358.2	2.080	2.092	2.232

In table III are shown the experimental and the calculated values of the viscosity of gas mixtures, η_{mix} , for different gas pairs.

In table IV are shown the calculated and the experimental values of the thermal diffusion factor k_T for the gas pairs for which data are available

TABLE III

Experimental and calculated values of $\eta_{mix} \times 10^7$ (in gm/cm.sec)

Gas Pair	T°K	% of lighter constituent	$\eta_{mix} \times 10^7$		
			Expt.	Calc. from force parameters obtained	Calc. from combination rules
H_2-CH_4	293	28.08	1099	1107	1093
		48.55	1098	1108	1092
		60.22	1086	1092	1081
		92.23	955	960	944
	373	28.08	1337	1339	1330
		48.55	1328	1327	1320
		60.22	1306	1307	1296
		92.23	1132	1130	1121
	473	28.08	1602	1601	1591
		48.55	1587	1574	1576
		60.22	1551	1551	1540
		92.23	1338	1329	1321
	523	28.08	1718	1722	1705
		48.55	1699	1695	1683
		60.22	1662	1663	1650
		92.23	1423	1413	1411
H_2-CO_2	300	19.93	1501	1504	1502
		41.29	1506	1510	1512
		78.50	1370	1372	1374
	400	19.93	1945	1953	1945
		41.29	1933	1938	1936
		78.50	1713	1721	1718
	500	19.93	2358	2350	2346
		41.29	2321	2318	2307
		78.50	2026	2023	2011
	550	19.93	2542	2549	2528
		41.29	2506	2515	2481
		78.50	2173	2175	2160

TABLE III (contd.)

Gas Pair	T°K	% of lighter constituent	$\eta_{mix} \times 10^7$		
			Expt.	Calc. from force parameters obtained	Calc. from combination rules
H ₂ —N ₂	291.1	84.0	1251	1254	1256
		55.9	1560	1563	1567
		38.0	1660	1661	1665
		24.1	1677	1675	1679
		13.4	1742	1745	1752
H ₂ —He	293	55.20	1317	1319	1322
		60.69	1252	1258	1265
		69.18	1166	1172	1176
	373	55.20	1551	1550	1550
		60.69	1478	1481	1486
		69.18	1383	1379	1388
	473	55.20	1817	1818	1793
		60.69	1728	1737	1714
		69.18	1619	1617	1598
	523	55.20	1939	1942	1895
		60.69	1852	1857	1819
		69.18	1732	1735	1694
	300	23.79	1169	1174	1172
		43.05	1308	1312	1302
		75.95	1574	1576	1573
	400	23.79	1491	1496	1490
		43.05	1655	1658	1651
		75.95	1956	1954	1950
N ₂ —C ₂ H ₄	500	23.79	1786	1788	1778
		43.05	1963	1974	1962
		75.95	2292	2297	2285
	550	23.79	1921	1927	1908
		43.05	2108	2117	2092
		75.95	2453	2459	2439

A glance at the Table III shows that the agreement between the experimental and the calculated values of η_{mix} is very satisfactory. In general the same degree of agreement is obtained with the force parameters determined in the paper and with those determined from combination rules. But at least in some cases the former gives better agreement.

Agreement in the case of thermal diffusion factor is only approximate. However, generally the agreement is better than that obtained with the usual combination rules. A part of the disagreement between the experimental and the calculated values of k_T may be attributed to comparatively large inaccuracy in the experimental determination of k_T .

TABLE IV

Experimental and calculated values of thermal diffusion factor k_T

Gas Pair	% of lighter constituent	T°K	$k_T \times 10^2$			Ref. for data
			Expt.	Calc. from force parameters obtained	Calc. from combination rules	
H ₂ —CO ₂	53	300	6.89	8.13	8.39	(Bastick <i>et al.</i> , 1939)
		370	8.99	8.89	9.60	
	29.4		3.95	4.07	3.97	
	42.0	143	5.21	5.23	5.01	
H ₂ —N ₂	77.5		4.84	4.92	4.44	
	29.4		5.48	5.74	5.90	(Ibbs <i>et al.</i> , 1926)
	42.0	264	7.49	7.39	7.37	
	77.5		6.63	7.04	6.36	
	81	358	1.79	2.05	2.31	(Murphey, 1947)
H ₂ —He	50		4.81	3.94	3.74	
	60		4.42	3.88	3.56	
	70	330	3.50	3.38	3.08	(Heath, 1941)
	80		2.84	2.62	2.31	
	90		1.32	1.44	1.29	

ACKNOWLEDGMENTS

The author is grateful to Prof. B. N. Srivastava, D.Sc., F.N.I., for suggesting the problem and for his valuable guidance throughout the progress of the work.

REFERENCES

- Bastick, R. E., Heath, H. R. and Ibbs, T. L., 1939, *Proc. Roy. Soc. (Lond)*, **A173**, 543.
 Boyd, C. A. *et al.*, 1951, *J. Chem. Phys.* **19**, 548.
 Bunde, R. E., 1955, Univ. of Wisconsin, CM-850, 8 Aug.

- Heath, H. R., Ibbas T. L. and Wild, N. E., 1941, *Proc. Roy. Soc. (Lond)*, **A178**, 380.
- Hirschfelder, J. O., Bird R. B. and Spotz, E. L., 1949, *Chem. Rev.* **44**, 205.
- Hirschfelder, J. O., Curtiss, C. F. and Bird, R. B., 1954, *Molecular Theory of Gases and Liquids*, John Wiley & Sons, Inc., New York.
- Ibbas, T. L., Grew, K. E. and Hirst, A. A., 1926, *Proc. Roy. Soc. (Lond)*, **A41**, 456.
- Itterbeck, A. van, Pacmel, O. van, Lierde, Miss I. Van, 1947, *Physica* **13**, 88.
- Murphuy, B. F., 1947, *Phys. Rev.* **72**, 834.
- Rumpel, W. F., 1955, Univ. of Wisconsin, CM—851, 1 Aug.
- Saxena, S. C., 1955a, *Ind. J. Phys.*, **29**, 587.
- Saxena, S. C., 1955b, *Ind. J. Phys.*, **29**, 131.
- Srivastava, B. N. and Madan, M. P., 1952, *Phil. Mag.* **63**, 968.
- Srivastava, B. N. and Madan M. P., 1953, *J. Chem. Phys.*, **21**, 807.
- Srivastava, B. N. and Srivastava, K. P., 1957, *Physica*, **23**, 103.
- Srivastava, B. N. and Srivastava, K. P., 1959, *J. Chem. Phys.*, (in press)
- Srivastava, K. P., 1957a, *Ind. J. Phys.*, **31**, 404.
- Srivastava, K. P., 1957b, *J. Chem. Phys.*, **26**, 579.
- Srivastava, K. P., 1959, *Physical* (in press)
- Strohlow, R. A., 1953, *J. Chem. Phys.*, **21**, 2101.

THE TEMPERATURE DEPENDENCE OF INTER-DIFFUSION COEFFICIENT FOR SOME PAIRS OF RARE GASES

K. P. SRIVASTAVA AND A. K. BARUA

DEPARTMENT OF GENERAL PHYSICS, INDIAN ASSOCIATION FOR THE CULTIVATION OF SCIENCE, CALCUTTA-32

(Received for publication, April 30, 1959)

ABSTRACT. The inter-diffusion coefficients for the three gas pairs He-Ne, He-Kr and Ne-Xe have been determined at 0°, 15°, 30° and 45°C. The diffusion takes place between two bulbs separated by a precision capillary tube. Samples of the gas are withdrawn from one bulb at different intervals of time and analysed by a differential conductivity analyser. These experimentally determined diffusion coefficients have been utilised for calculating the unlike potential parameters ϵ_{12} and σ_{12} on the Lennard-Jones (12:6) model and compared with the values determined from the usual combination rules. The agreement is found to be satisfactory. The experimentally determined values of ϵ_{12} and σ_{12} reproduce the experimental data on inter-diffusion quite satisfactorily. By utilising Kelvin's method, self-diffusion coefficients have been calculated from inter-diffusion coefficient data and the results have been compared with the experimental data when they are available.

INTRODUCTION

The influence of intermolecular forces on gaseous transport properties has long been recognised and a great deal of information concerning like molecular interactions has been obtained from the determinations of the coefficient of viscosity of pure gases as a function of temperature, but corresponding information on forces between unlike molecules obtained directly from measurements on gaseous mixtures is very meagre. The most suitable transport property for studying unlike molecular interactions is inter-diffusion coefficient, for it depends in the first approximation only on the force fields of the unlike diffusing molecules and is independent of the like interactions. Thus ϵ_{12} and σ_{12} can best be determined from the experimental data on inter-diffusion but unfortunately little work has been done so far in this field. Further, the available data are usually confined to one or two temperatures only and hence no reliable information can be obtained from them. Recently, Srivastava and Srivastava (1959) and Srivastava (1959) have determined the coefficients of inter-diffusion for the gas pairs Ne-A, Ne-Kr, A-Kr and A-He, A-Xe, He-Xe. In the present investigation the inter-diffusion coefficients for the gas pairs He-Ne, He-Kr, Ne-Xe at 0°, 15°, 30° and 45°C, have been measured.

APPARATUS

The diffusion apparatus consists of two bulbs connected by a specially designed brass capillary tube and stop-cock. The bulbs are immersed in a thermostat bath which is maintained at temperatures 0° , 15° , 30° , and 45°C to $\pm 0.01^{\circ}\text{C}$. A detailed account of the diffusion apparatus used has been given by Srivastava and Srivastava (1959).

For analysing the gas mixture a differential conductivity analyser essentially similar to the one employed by Grew (1954) was designed and constructed as shown in figure 1. A precision conductivity cell of stainless steel of the type described by Srivastava and Saxena (1957) is constructed with a platinum wire 0.075 mm. in diameter mounted axially and insulated at one end with Perspex cap. A compression unit capable of compressing the gas upto twenty times, together with a sensitive manometer, is permanently sealed to the above cell by cold setting Araldite adhesive. Two such units form the two arms of a Wheatstone bridge, one of the cells containing a suitable standard gas (heavier) while the other a sample of the gas to be analysed. Two fixed manganin resistors of S.W.G.

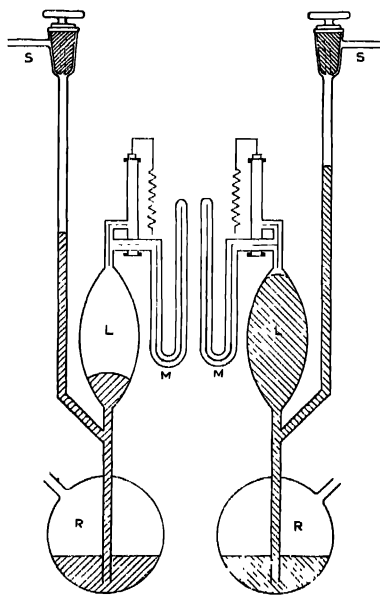


Fig. 1

20 of about 3 ohms resistance forming the other two arms of the bridge are mounted close to the conductivity cells.

It was observed that at a pressure of 6 cm. of Hg or more, the wire resistance is insensitive to the change of pressure and therefore all the samples were compressed to 6 cm. of Hg, and this was kept the same for calibration and also for analysis. For greater accuracy and stability the conductivity analyser as well as the two resistances in the other arms of the bridge circuit are immersed in an oil thermostat controlled at $35^{\circ}\text{C} \pm 0.05^{\circ}\text{C}$ by efficient stirring in conjunction with a spiral type mercury-ether thermal regulator and electronic relay. The analyser takes only 0.3 cc. of gas at N.T.P. for analysis and therefore the pressure of the gas in the two diffusion bulbs is not disturbed.

The two conductivity cells, each of about 1.3 ohms resistance and the two fixed resistors are placed close to each other in the same thermostat to obtain steady and reproducible conditions. A variable resistance of W. G. Pye (accurate to 0.02%) adjustable to 0.01 ohm resistance is placed in parallel to one of the fixed resistors and serves to balance the bridge. The bridge is fed by a constant current of about 0.3 ampere from a high capacity battery with a standard resistance and fine rheostat included in the circuit, the rheostat being adjusted to keep the e.m.f. across the standard resistance constant as read on a vernier potentiometer reading upto $1\mu\text{V}$ with an accuracy of $\pm 0.004\%$. The value of the parallel

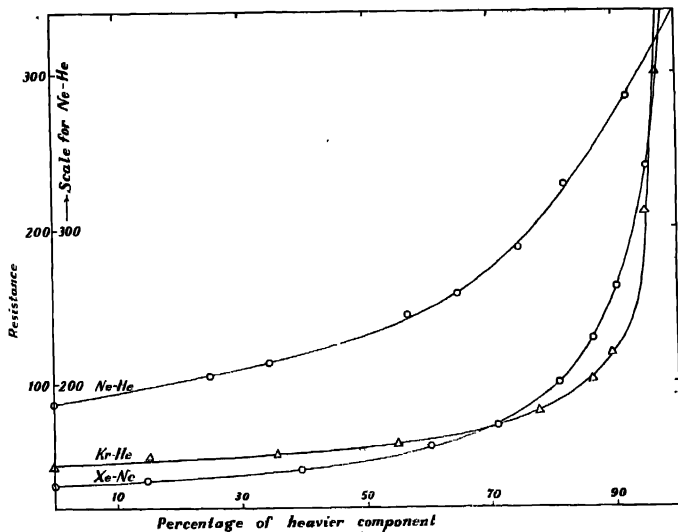


Fig. 2

resistance is adjusted to be about 500 ohms when both the cells of the analyser are filled with the heavier gas at the same pressure. When a mixture of unknown composition is introduced in one of the cells, the bridge balance is disturbed and the parallel resistance is carefully adjusted to restore the balance as read on a voltage sensitive galvanometer (Cat. No. 7940) of W. G. Pye.

For each gas mixture values of the parallel resistance required to balance the bridge for different compositions of the gas mixture are observed and a calibration curve plotted (figure 2) giving the composition of the mixture for any value of the parallel resistance. Considering the accuracy of the electrical circuit and the error involved in making a mixture of known composition it is believed that the error in the composition of the mixture as determined from the calibration curve is about $\pm 0.05\%$

EXPERIMENTAL PROCEDURE

The dimensions of the diffusion capillary are first determined and then it is fitted vacuum tight to the two diffusion bulbs. The two bulbs are then evacuated to about 10^{-3} mm. of Hg. by a two stage rotary pump. The heavier gas is first allowed to fill both the diffusion bulbs at the desired pressure which is read on a manometer with help of a cathetometer. One of the gas filled bulbs is cut off from the vacuum circuit by operating the stop-cock connecting the two bulbs and then the other bulb is evacuated. The other gas is then filled in the evacuated bulb and the pressure adjusted to be the same in both the bulbs. After allowing sufficient time to the bulbs to attain the temperature of the bath, diffusion is started by opening the stop-cock connecting the two bulbs. Samples of the gas are drawn through the capillary leak at suitable intervals. The analyser is highly evacuated by an oil diffusion pump and the order of vacuum attained is read on a Pirani gauge. Gas from one of the diffusion bulbs is allowed to leak into the analyser for one minute and then compressed to the desired pressure and the value of the resistance required to balance the bridge is determined. The middle of the interval of one minute is taken as the time at which the composition is determined.

THEORY AND FORMULAE

The theory of this method has been fully discussed by Ney and Armistead (1947) who showed that the relaxation time $1/\alpha$ of the system defined by the relation

$$\frac{C_1^t - C_1^\infty}{C_1^0 - C_1^\infty} = \exp(-\alpha t) \quad \dots (1)$$

is given by

$$\alpha = \frac{D_p A}{l} \left(\frac{V_0}{V_1 V_2} \right) \quad \dots (2)$$

where C_1^0 , C_1^t and C_1^∞ are respectively the concentrations of the heavier gas initially, at time 't' seconds, and after complete mixing, V_1 and V_2 are the volumes of the two bulbs in cc. and $V_0 = V_1 + V_2$. D_p is the coefficient of diffusion in cm^2/sec at the pressure of p cm. of mercury. A and l are respectively the effective cross-sectional area and effective length of the diffusion path.

A graph connecting $\log_e(C_1^t - C_1^\infty)$ and t is plotted which gives a straight line the slope of which determines $-\alpha$. This is substituted in Eq. (2) to give D_p at the pressure p of the gas. In the actual experiment the diffusion path consists of several sectors of varying l/A , the volume of the diffusion path being negligible as compared to the volume of the diffusion bulbs. Eq. (2) is then written

$$\alpha = D_p \sum \frac{A_j}{l_j} \left(\frac{V_0}{V_1 V_2} \right) \quad \dots (3)$$

where A_j and l_j refer to the various sectors of the diffusion path.

EXPERIMENTAL RESULTS

The gases used in the present investigation were supplied by the British Oxygen Co., England; helium was quoted as spectroscopically pure while krypton and xenon contained some traces of impurities.

TABLE I

Observed concentration of the heavier components at different times for He-Ne, He-Kr, Ne-Xe at 0°C for all gas pairs $C_1^\infty = 0.373$

Gas Pair	Time in mins	Resistance in ohms	C_1^t	$\log_{10} (C_1^t - C_1^\infty)$
He-Ne	0	..	1.0	1.7913
	20	326.0	0.820	.6500
	34	281.5	0.721	.5422
	55	250.3	0.612	.3787
	90	231.8	0.499	.1000
He-Kr	0	..	1.0	.7973
	23	152.0	0.870	.6964
	50	113.4	0.745	.5700
	82	87.8	0.636	.4200
	118	76.0	0.559	.2701
Ne-Xe	0	..	1.0	.7973
	50	152.0	0.893	.7160
	80	113.4	0.839	.6680
	120	87.8	0.771	.6001
	160	76.0	0.721	.5420

After a careful flushing of the leak tubes, the gas from one of the diffusion bulbs was allowed to leak into the analysis cell of the differential conductivity analyser. This was done at four different intervals of time and the gas was analysed to give C_1^t . Tables I-IV show the observations for all gas pairs at 0°, 15°, 30° and 45°C. $\log_{10} (C_1^t - C_1^\infty)$ versus t were plotted and found to be straight lines whose slope determined α . C_1^∞ is calculated from the initial concentrations of the two bulbs and later on checked experimentally by determining the concentration after a time interval greater than several multiples of the relaxation time.

TABLE II

Observed concentration of the heavier components at different times for He-Ne, He-Kr, Ne-Xe at 15°C. For all gas pairs $C_1^\infty = 0.373$

Gas Pair	Time in mins	Resistance in ohms	C_1^t	$\log_{10} (C_1^t - C_1^\infty)$
He-Ne	0	..	1.0	1.7973
	20	311.0	0.790	.6205
	30	280.3	0.720	.5400
	45	252.4	0.625	.4005
	70	235.3	0.525	.1810
He-Kr	0	..	1.0	.7973
	18	102.0	0.863	.6900
	50	70.0	0.697	.5100
	70	64.3	0.621	.3950
	106	60.0	0.527	.1883
Ne-Xe	0	..	1.0	.7973
	40	157.0	0.898	.7204
	80	99.3	0.808	.6381
	120	78.8	0.734	.5580
	160	68.0	0.675	.4804

The quantity D/α which is a constant independent of the mixture used is determined previously from the measured geometric constants of the apparatus with the help of Eq. (3). Thus knowing α , the value of D_p for the gas pair is determined at the pressure of the gas. It is then converted into the diffusion coefficient at atmospheric pressure by the relation

$$D_{atm} = \frac{D_p \cdot p}{760} \quad (4)$$

where p is the pressure of the gas in *mm.* of Hg. The experimental values of D_{12} thus obtained are collected in table V for all the gas pairs, the last column

TABLE III

Observed concentration of the heavier components at different times for He-Ne, He-Kr, Ne-Xe at 30°C. For all gas pairs $C_1^\infty = 0.373$

Gas Pair	Time in mins	Resistance in ohms	C_1^t	$\log^{10} (C_1^t - C_1^\infty)$
He-Ne	0	.	1.0	1.7973
	15	330.5	0.832	.0620
	24	284.0	0.730	.5531
	41	250.6	0.616	.3857
	61	235.2	0.528	.1900
He-Kr	0	..	1.0	.7973
	20	95.5	0.841	.6701
	46	69.8	0.689	.5003
	71	63.0	0.682	.3430
	113	58.8	0.491	.0701
Ne-Xe	0	..	1.0	.7973
	38	95.5	0.886	.7100
	90	69.8	0.771	.6002
	135	63.0	0.682	.4000
	168	58.8	0.636	.4203

giving the value of D_{12} at atmospheric pressure. The various sources of error in this method have been fully discussed by Ney and Armistead (1941) and Srivastava and Srivastava (1959). The values of D_{12} obtained in the present paper are believed to be accurate to within 1%.

DETERMINATION OF FORCE CONSTANTS

Srivastava and Srivastava (1959), Bunde (1958) and Strehlow (1953) have discussed the various methods employed for determining force constants from the diffusion data. These methods are : (1) The ratio method, (2) the translational method of Keesom (1912) and Lennard-Jones (1924), (3) the intersection method of Buckingham (1938), (4) Combination method utilising binary viscosity or conductivity in addition. Srivastava and Srivastava (1959) have discussed the limitations and difficulties of methods (1) and (2). These fail to give any suitable force

TABLE IV

Observed concentration of the heavier components at different times for He-Ne, He-Kr, Ne-Xe at 45°C. For all gas pairs $C_1^\infty = 0.373$

Gas Pair	Time in mins	Resistance in ohms	C_1^t	$\log^{10} (C_1^t - C_1^\infty)$
He-Ne	0	..	1.0	1.7973
	20	274.2	0.704	.5203
	40	239.1	0.552	.2519
	60	228.0	0.470	2.9851
He-Kr	0		1.0	1.7973
	21	94.8	0.84	.6702
	42	72.2	0.724	.5449
	58	66.6	0.665	.4498
	85	62.0	0.568	.2903
Ne-Xe	0		1.0	.7973
	36	135.5	0.874	.7000
	88	84.0	0.758	.5850
	120	69.1	0.682	.4902
	176	59.7	0.607	.3703

TABLE V

Observed values of the Diffusion Coefficient.

Gas Pair	Temp °K	Pressure (mm. of Hg.)	D_p (cm ² /sec)	D_{atm} (cm ² /sec)
He-Ne	273	89.26	7.715	0.906
	288	84.84	8.833	0.986
	303	82.02	9.868	1.065
	318	71.16	12.37	1.158
He-Kr	273	92.64	4.561	0.556
	288	79.98	5.749	0.605
	303	77.56	6.458	0.650
	318	89.32	6.127	0.720
Ne-Xe	273	85.08	1.662	0.186
	288	78.32	1.960	0.202
	303	78.54	2.139	0.221
	318	74.58	2.481	0.244

constants in the present case. Methods (3) and (4) have been carried out quite successfully and are given below:

Method 3. The method can yield the force constants even if the experimental data are limited to only two temperatures, not far apart, provided the data are highly accurate. The diffusion equation is solved for the collision diameter σ_{12} , as

$$\sigma_{12} = \frac{0.002628[T^3(M_1 + M_2)/2M_1M_2]^{\frac{1}{2}}}{D_{12}p\Omega_{12}(1,1)^*(T_{12}^*)} \quad (5)$$

where D_{12} is the mutual diffusion coefficient in cm^2/sec , p is the pressure in atmospheres, σ_{12} in Angstroms, and $\Omega_{12}(1,1)^*$ is a reduced collision integral tabulated by Hirschfelder, Curtiss and Bird (1954). The higher approximation term coming through the factor $f_{D_{12}}^{(m)}$ is always close to unity and has therefore been neglected. For arbitrarily selected values of ϵ_{12} a series of mutually consistent values of ϵ_{12} and σ_{12} are determined from Eqn.(5) and a graph plotted with ϵ_{12} as abscissa and σ_{12} as ordinate. Such a graph is drawn for each experimental value of D_{12} and the best value of the intersection point fixes up ϵ_{12} and σ_{12} . In practice it is difficult to obtain one unique point of intersection for all the curves due inherently to the fact that the D_{12} data are not very accurate. Different intersection points yield a range of values of ϵ_{12} and σ_{12} and these are averaged to give a mean value. The values are collected in Table VI column 3.

Method 4. The diffusion equation and the expression for the binary viscosity, η_{mix} , are solved together to eliminate σ_{12} . The solution involves the only temperature dependent factor A_{12}^* which can be put in the convenient form

$$A_{12}^* = \frac{1 - \eta_{mix} \left[\frac{x_1^2}{\eta_1} + \frac{x_2^2}{\eta_2} \right] + \frac{3}{10} \frac{x_1 x_2}{\eta_1 \eta_2} \frac{(M_1 + M_2)^2}{M_1 M_2} \eta_0 [\eta_1 + \eta_2 - \eta_{mix}]}{2x_1 x_2 \left(\frac{\eta_{mix}}{\eta_0} \right) + \frac{3}{5} \frac{x_1^2}{\eta_1} \left(\frac{M_1}{M_2} \right) [\eta_{mix} - \eta_1] + \frac{3}{5} \frac{x_2^2}{\eta_2} \left(\frac{M_2}{M_1} \right) [\eta_{mix} - \eta_2] + \frac{6}{5} x_1 x_2 \dots} \quad (6)$$

where η_1 , η_2 are the viscosities of the pure components and M_1 , M_2 and x_1 , x_2 are respectively their molecular weights and molar fractions η_0 is given by the expression

$$\eta_0 = \frac{266.93}{0.002628} \left[\frac{2M_1 M_2}{M_1 + M_2} \right] \times \frac{D_{12}}{T} \times 10^{-7} \quad \dots \quad (7)$$

From a knowledge of η_{mix} , η_1 , η_2 , D_{12} , the quantity A_{12}^* may be obtained with the help of Eqn. (6). The corresponding value of T_{12}^* is read from the table given by Hirschfelder, Curtiss and Bird (1954), which ultimately determines ϵ_{12}/k from the relation $T_{12}^* = kT/\epsilon_{12}$. Eqn. (5) is then used to fix up the value of σ_{12} .

This is repeated for each temperature and the values of σ_{12} thus obtained are averaged. The values of $\epsilon_{12/k}$ and σ_{12} are listed in column 4 of table VI. These may be compared with the values obtained previously from thermal diffusion data by Saxena (1955) and also those obtained with the usual combination rules viz. $\epsilon_{12} = (c_1 \times c_2)^{1/2}$ and $\sigma_{12} = \frac{1}{2}(\sigma_1 + \sigma_2)$. These are respectively given in columns 5 and 6 of table VI.

The values of the force constants given in column 4 are believed to be more accurate than those recorded in column 3. They have, therefore, been used to calculate the mutual diffusion coefficient of the different gas pairs on the Lennard-Jones (12 : 6) model and the calculated values compared with the experimentally observed values in table VII. The agreement between calculated and experimental values of D_{12} is found to be very close which shows that the force constants derived by us are quite reliable and can be used to calculate other transport properties.

SELF-DIFFUSION

It is possible to calculate self-diffusion coefficient of gases on the rigid sphere model by combining inter-diffusion coefficient data for different triads of gases which give the self-diffusion coefficient for each of the gases forming the triad.

TABLE VI

Potential parameters on the Lennard-Jones (12 : 6) model from experimental data

Gas Pair	Force Parameters	Intersection method	From combination of D_{12} and η_{mix}	From thermal diffusion	From combination rules
He-Ne	ϵ_{12}/k	18.6	20.19	19.11
	σ_{12}	2.681	2.662	2.683
He-Kr	ϵ_{12}/k	46.0	44.07
	σ_{12}	3.084	3.093
Ne-Xe	ϵ_{12}/k	91.5	71.99	90.42
	σ_{12}	3.377	.. .	3.460	3.422

The method of calculation of self-diffusion coefficient which is due to Kelvins is as follows :—

For rigid elastic spheres the first approximation to the coefficient of inter-diffusion of two gases 1 and 2 is

$$[D_{12}]_1 = \frac{3}{8(n_1 + n_2)\sigma_{12}^2} \left[\frac{kT(m_1 + m_2)}{2\pi m_1 m_2} \right]^{1/2} \quad \dots (8)$$

TABLE VII

Comparison of observed values of the mutual diffusion coefficient with those calculated from the force parameters derived from the experimental data. Values of D_{12} are expressed in cm^2/sec .

Temp °K	273	288	303	318
Gas Pair				
He-Ne				
Expt.	0.996	0.986	1.065	1.158
Calc.	0.901	0.984	1.070	1.160
He-Kr				
Expt.	0.556	0.605	0.659	0.720
Calc.	0.554	0.604	0.660	0.718
Ne-Xe				
Expt.	0.186	0.202	0.221	0.244
Calc.†	0.185	0.203	0.222	0.242

*All data at one atmosphere.

† Calculated from the force parameters given in Column 4 of table VI.

where m_1, m_2 are the masses of the molecules 1 and 2, n_1 and n_2 their number densities and σ_{12} the collision diameter for the pair of gases.

σ_{12} may be calculated from Eqn.(8) by utilising the experimental value of D_{12} . From the triad of gases 1-2-3 we can determine $\sigma_{12}, \sigma_{23}, \sigma_{13}$ and since $\sigma_{12} = \frac{1}{2}(\sigma_1 + \sigma_3)$ with similar expressions for σ_{23} and σ_{13} we can find $\sigma_{11}, \sigma_{22}, \sigma_{33}$. Then the self-diffusion coefficient for the same temperature may be determined from the relation

$$[D_{11}]_1 = \frac{3}{8n\sigma_{11}^2} \left[\frac{kT}{\pi m} \right]^{\frac{1}{2}} \quad \dots (9)$$

Recently Srivastava and Srivastava (1959) and Srivastava (1959) have given the data on inter-diffusion for the gas pairs Ne-A, A-Kr, Ne-Kr, A-He, A-Xe, He-Xe at 0°, 15° 30° and 45°C. By utilising Kelvin's method, they have also calculated self-diffusion coefficients for He, Ne, A, Kr, Xe on the rigid sphere model. The values thus obtained have been compared with the experimental values. We have combined the inter-diffusion coefficients at N.T.P. for all the gas pairs reported in this paper and those reported by Srivastava and Srivastava (1959) and Srivastava (1959) to yield the values of the self-diffusion coefficient. The results of calculation are shown in Table VIII. Only for Ne, A, experimental data are available at N.T.P. The calculated values of D_{11} for Ne, A, are found to be in fair agreement with the experimental values.

TABLE VIII
Coefficient of self-diffusion (at N.T.P.)

Combination of gases used	Coefficients of self-diffusion cm ² /sec.				
	He	Ne	A	Kr	Xe
Ne-A-Kr	..	0.520	0.152	0.087	..
A-He-Xe	2.548	..	0.136	...	0.055
He-Ne-Kr	1.052	0.589	...	0.084	...
He-Ne-Xe	1.086	0.482	0.059
A-He-Kr	1.892	..	0.150	0.090	...
A-Ne-Xe	..	0.565	0.142	..	0.047
Mean	1.945	0.540	0.148	0.087	0.053
Expt	..	0.452	0.156

ACKNOWLEDGMENTS

The authors wish to acknowledge their deep indebtedness to Prof. B. N. Srivastava, D.Sc., F.N.I., for his valuable guidance throughout the progress of the work presented here. They are thankful to the Council of Scientific and Industrial Research, New Delhi, for the award of a research scholarship to one of them (K.P.S.).

REFERENCES

- Buckingham, R. A., 1938, *Proc. Roy. Soc.*, **A168**, 264.
 Bunde, R. E., 1955, University of Wisconsin, CM-850, Aug.
 Chapman, S, and Cowling, T. G., 1952, *The Mathematical Theory of non-Uniform Gases*, Cambridge University Press, England.
 Hirschfelder, Curtiss & Bird, 1954, *The Molecular Theory of Gases and Liquids* (John Wiley and Sons, Inc., New York)
 Keeson, W. H., 1912, Leiden. Comm. Suppl. No. 25.
 Lennard-Jones, J. E., 1924, *Proc. Roy. Soc.* **A106**, 463.
 Ney, E. P. and Armistead, F. C., 1947, *Phys. Rev.* **71**, 14.
 Saxena, S. C., 1955, *Ind. J. Phys.*, **29**, 131.
 Srivastava, B. N. and Srivastava, K. P., 1959, *J. Chem. Phys.*, (in press).
 Srivastava, K. P., 1959 *Physica*, (in press).
 Strahlow, R. A. 1953, *J. Chem. Phys.* **21** 2101.

Letters to the Editor

The Board of Editors will not hold itself responsible for opinions expressed in the letters published in this section. The notes containing reports of new work communicated for this section should not contain many figures and should not exceed 500 words in length. The contributions must reach the Assistant Editor not later than the 15th of the second month preceding that of the issue in which the letter is to appear. No proof will be sent to the authors.

2

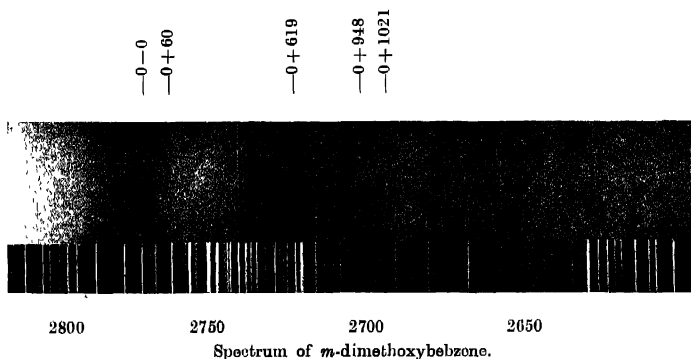
SPECTRA OF DIMETHOXYBENZENES. PART I— META DIMETHOXYBENZENE

K. SRERAMAMURTY

SPECTROSCOPY LABORATORY, PHYSICS DEPARTMENT, S. V. UNIVERSITY, TIRUPATI

(Received, April 6, 1959)

Dimethoxybenzenes have the constitution $C_6H_4(OCH_3)_2$ with the radical OCH_3 substituting the H atoms in the three isomeric positions. The present study is on the meta substituted compound. A 100 cms absorption column is used for photographing the spectrum under different pressure conditions of the vapour. The spectrum is reproduced in figure 1. Measurements on 15 bands are presented in the table along with their probable assignments.



Three distinct regions of absorption are found. In each region the band is broad with a fairly sharp edge towards the violet. The 0,0 band is located at ν 36117 and is accompanied by a structure consisting of a number of very close

bands. On the violet side is a band of medium intensity at a wavenumber separation of 60 units. It does not conform to the usual difference frequency found in these spectra. If this frequency is genuine, it is expected to represent the

Wavenumber	Int	Assignment	Wavenumber	Int	Assignment
36020	m	0-2 41	36781	w	
059	vw		793	mw	0+619+60
076	m	0-41	891	mw	
103	m		945	mw	
117	st	0, 0	37027	mw	0+948-41
177	m	0+60	065	mw	0+948
736	mst	0+619	138	w	0+1021
752	mw				

difference between a smaller ground state and a larger upper state frequency—a feature found in paracresol and phenetole. On the long wavelength side of the 0,0, band a band at an interval of 41cm^{-1} corresponds to the usual $v-v$ transition. This recurs in combination with other frequencies. Prominent bands on the violet side led to three distinct frequencies 619, 948 and 1021 only 948 is obviously a totally symmetric carbon vibration. 1021 can either be another carbon vibration or more probably a O-CH_3 vibration.

Study of the spectra of the other isomers is in progress.

AN INVESTIGATION INTO THE MOMENTUM DISTRIBUTION IN LIGHT NUCLEI

C. M. PUJARA AND K. M. GATHA

DEPARTMENT OF PHYSICS, INSTITUTE OF SCIENCE, BOMBAY

(Received, March 3, 1959)

ABSTRACT. The characteristic nuclear density distribution for light elements has been obtained by Gatha and Shah. Using this density distribution, the nucleonic momentum distributions have been obtained on the basis of the Thomas-Fermi-Weizsäcker method for carbon and oxygen. Using these momentum distributions the proton energy spectra, resulting from the inelastic scattering at 30° and 40° of 340 Mev protons by these elements, have been calculated. Using the momentum distribution for carbon, the production efficiencies and the meson energy spectra at 45° , 90° and 135° , resulting from the photo-production of mesons on carbon, have also been calculated.

I. INTRODUCTION

According to the commonly accepted nuclear model, a nucleus is regarded as composed of nucleons. These nucleons are confined within the nuclear volume. The linear dimensions of such a nuclear region are of the order of 10^{-13} cm. For a nucleon confined in such a region there would be a corresponding uncertainty in its momentum according to the uncertainty principle. The corresponding uncertainty in the kinetic energy of a nucleon can be estimated to be of the order of several million electron volts.

If the exact nuclear wave function is known for the ground state of the nucleus, the corresponding nuclear momentum distribution can be determined through the transformation of the same to momentum space. However, such a nuclear wave function cannot be obtained at present for any complex nucleus. Therefore, it is necessary to obtain the nucleon momentum distribution by some appropriate approximation.

An approximate relation between the nuclear density distribution and nuclear momentum distribution is provided by the Thomas-Fermi method, as discussed by Coulson and March (1950). Some improvements of this method have been suggested by Plaskett (1953) as well as by Weizsäcker (1935). An attempt has been made in this investigation to provide an approximate three-dimensional form to the Plaskett method on the basis of certain assumptions. The Thomas-Fermi method, the Thomas-Fermi-Weizsäcker method and the modified Plaskett method have been tested for the determination of the nuclear momentum distribution assuming an isotropic harmonic oscillator potential. It has been found that the Thomas-Fermi-Weizsäcker method provides the best

results. The Thomas-Fermi-Weizsäcker method has been used in the present investigation for determining the nuclear momentum distributions.

Using the characteristic nuclear density distribution for light elements, determined by Gatha and Shah, the corresponding nuclear density distributions for carbon and oxygen have been calculated and used in this investigation to determine their respective nuclear momentum distributions.

The nuclear momentum distribution can be expected to affect significantly those nuclear reactions where the interaction energy is comparable to the kinetic energy of the nucleon within the nucleus. Cladis, Hess and Moyer (1952) have observed the proton energy spectra for the nuclear inelastic scattering of 340 Mev protons at 30° by carbon and at 40° by carbon and oxygen. At the same time, McMillan, Peterson and White (1949), Steinberger and Bishop (1952), Peterson, Gilbert and White (1951) as well as Sargent Janes and Kraushaar (1954) have observed the pion energy spectra at fixed angles for carbon for the photo-production by bremsstrahlung photons. Some estimates of pion production efficiency have also been reported by some of the above workers. Jenkins, Luckey, Palfrey and Wilson (1954) as well as Luckey (1955) have reported some observations on the pion production efficiency during the photo-production by carbon at certain photon energies.

The above experimental data have been so far correlated on the basis of some assumed nuclear momentum distributions. Cladis *et al* (1952) have used the Gaussian as well as the Chew-Goldberger distributions. They find that the latter distribution is inappropriate while the former distribution, with a kinetic energy half-width of 14 to 19 Mev, is quite suitable for this purpose. Wolff (1952) has correlated the same data on the basis of Chew-Goldberger (1950), Fermi, (1936) as well as Gaussian nuclear momentum distributions. He concludes that the Gaussian nuclear momentum distributions, with a kinetic energy half-width of 12 to 20 Mev, appear appropriate for this purpose. Lax and Feshbach (1951), on the other hand, claim to have reasonably correlated some experimental data on the photo-production of positive pions on carbon by using the Chew-Goldberger distribution.

The purpose of the present investigation has been to correlate the above experimental data on the basis of the nuclear momentum distributions determined from the characteristic nuclear density distribution of Gatha and Shah through the Thomas-Fermi-Weizsäcker method. For this purpose, the theoretical methods developed by Wolff (1952) as well as Lax and Feshbach (1951) have been employed for correlating the respective experimental data with these nuclear momentum distributions.

Therefore, it is concluded that the characteristic nuclear density distribution for light elements, determined by Gatha and Shah, provides at least approximate nuclear momentum distributions for such elements.

II. NUCLEAR MOMENTUM DISTRIBUTIONS

A. Characteristic nuclear density distribution

A characteristic nuclear density distribution can be defined by $\rho(r) = \rho(\bar{r})$, where $\rho(r)$ is the nucl ar density distribution for any particular element, while $\rho(\bar{r})$ is the nuclear density distribution for all elements, with r representing the radial distance from the nuclear centre and $\bar{r} = rA^{-1/3}$. Gatha and Shah have determined an improved characteristic nuclear density distribution by eliminating the effects of the higher Born approximations on the nuclear scattering of 340 Mev protons. This characteristic nuclear density distribution is given by

$$\rho(\bar{r}) = \alpha_1 \rho^{-\beta_1 \bar{r}^2} + \alpha_2 \rho^{-\beta_2 \bar{r}^2} \{1 - \beta_3 \bar{r}^2 + \beta_4 \bar{r}^4\} \quad \dots (1)$$

where

$\alpha_1 = 0.12 \times 10^{39} \text{cm}^{-3};$	$\alpha_2 = 0.25 \times 10^{39} \text{cm}^{-3};$
$\beta_1 = 8.62 \times 10^{26} \text{cm}^{-2};$	$\beta_2 = 1.09 \times 10^{26} \text{cm}^{-2};$
$\beta_3 = 0.44 \times 10^{26} \text{cm}^{-2};$	$\beta_4 = 0.13 \times 10^{52} \text{cm}^{-4}.$

This $\rho(\bar{r})$ for light elements, shown in figure 1, has been used in the present investigation.

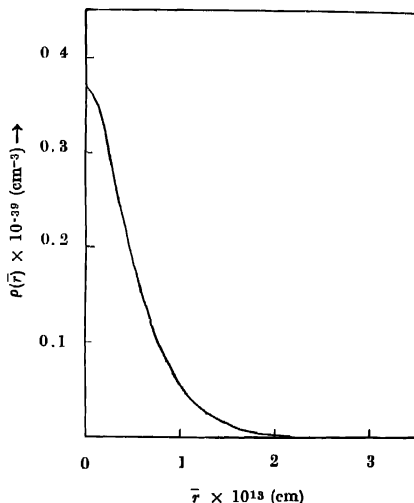


Fig. 1. Characteristic nuclear density distribution for light nuclei.

B. Thomas-fermi method

A simple relation between the spherically symmetric nuclear density distribution $\rho(r)$ for proton or neutron, normalised to the number of particles N , and

the corresponding nuclear maximum momentum distribution $p_m(r)$ within the nucleus is given by Coulson and March (1950) as

$$\rho(r) = \frac{1}{3\pi^2\hbar^3} p_m^3(r) \quad \dots (2)$$

Defining $I(p)dp$ as the probability of one nucleon having its absolute momentum between p and $p+dp$, one can write

$$I(p)dp = \int_0^{r(p)} \frac{I_r(p)dp\rho(r)}{N} \cdot 4\pi r^2 dr \quad \dots (3)$$

where $I_r(p)dp$ is the probability of the nucleon at r having its absolute magnitude of momentum between p and $p+dp$, and $r(p)$ has to be determined from the function $p_m(r)$. Substituting $I_r(p)dp$ and $\rho(r)$ in equation (II, 3), one finds

$$I(p) = \frac{4}{3\pi\hbar^3} \cdot \frac{r^3(p)}{N} \cdot p^2 \quad \dots (4)$$

March (1954) has tested the validity of the Thomas-Fermi method for the nuclear problem by assuming an isotropic harmonic oscillator nuclear potential. He finds that there is a close agreement for medium and heavy nuclei, while the method needs some improvement for light nuclei. He further points out that $I(p)$, obtained by this method, is particularly unreliable for very small and very large momenta.

It may be noted that, for a characteristic nuclear density distribution, one can rewrite equation (II, 4) to have

$$I(p) = \frac{4\pi^3(p)p^2}{3\pi\hbar^3} \quad \dots (5)$$

C. Thomas-Fermi-Weizsäcker method

Weizsäcker's method, for a single type of particle without spin, can be derived from the variation principle

$$\delta \int \left(\frac{\pi^2\hbar^2}{6M} \rho^3 + \rho V + \frac{\hbar^2}{8M} \frac{\rho'^2}{\rho} \right) dx = 0 \quad \dots (6)$$

where ρ is the particle density and V is the potential energy. It may be noted that the last term alone represents the correction introduced by Weizsäcker. The corresponding Euler equation gives

$$\frac{\pi^2\hbar^2}{2M} \rho^2 + V - \frac{\hbar^2}{4M} \frac{\rho''}{\rho} + \frac{\hbar^2}{8M} \frac{\rho'^2}{\rho^2} = E \quad \dots (7)$$

where E is the Lagrange multiplier of the dimensions of energy.

Plaskett (1953), using a more fundamental analysis, obtains

$$\frac{\pi^2\hbar^2}{2M} \rho^2 + V + \frac{\hbar^2}{4M} \frac{\rho''}{\rho} - \frac{3\hbar^2}{8M} \frac{\rho'^2}{\rho^2} = E \quad \dots (8)$$

Ballinger and March (1954) have tested both these methods by comparing the particle density given by them for an oscillator potential with the exact density for the same. They indicate that the Weizsäcker method provides the appropriate behaviour for the density for small as well as large distances. It may, therefore, be expected that the Weizsäcker method may provide an appropriate behaviour for $I(p)$ for small as well as large momenta. Therefore the Thomas-Fermi-Weizsäcker method has been used in the present investigation for determining the nuclear momentum distributions from the nuclear density distributions.

The Thomas-Fermi-Weizsäcker method for the nuclear problem, in three dimensions, can be derived from the variation principle

$$\delta \int \left[\frac{\pi^2 \hbar^2}{10M} \left(\frac{3}{\pi} \right)^{5/3} (\rho_P^{5/3} + \rho_N^{5/3}) + (\rho_P + \rho_N) V + \frac{\hbar^2}{8M} \left\{ \frac{(\nabla \rho_P)^2}{\rho_P} + \frac{(\nabla \rho_N)^2}{\rho_N} \right\} \right] d\vec{r} = 0 \quad \dots (9)$$

where ρ_P and ρ_N are the proton and neutron densities. Following Gombas (1952), it will be assumed that $\rho_P = \rho_N = \rho/2$. Thus one has

$$\delta \int \left[\frac{\pi^2 \hbar^2}{5M} \left(\frac{3}{2\pi} \right)^{5/3} \rho^{5/3} + \rho V + \frac{\hbar^2}{8M} \frac{(\nabla \rho)^2}{\rho} \right] d\vec{r} = 0 \quad \dots (10)$$

Thus the above equation can be written as

$$\delta \int F(\rho, \rho') d\vec{r} = 0 \quad \dots (11)$$

where,

$$F(\rho, \rho') = \frac{\pi^2 \hbar^2}{5M} \left(\frac{3}{2\pi} \right)^{5/3} \rho^{5/3} + \rho V + \frac{\hbar^2}{8M} \frac{(\nabla \rho)^2}{\rho}.$$

The Euler equation for such a variation principle can be written as

$$\frac{\partial F}{\partial \rho} - \nabla \cdot \left\{ \frac{\partial F}{\partial (\nabla \rho)} \right\} = E \quad \dots (12)$$

where E appears as the Lagrange multiplier of the dimensions of energy. In the Thomas-Fermi-Weizsäcker formalism, E can be regarded as the maximum effective nucleonic energy within the nucleus. This assumption, which has no clear theoretical justification, has been empirically found to improve upon the Thomas-Fermi method in respect of the nuclear momentum distribution. Assuming V to be independent of any small variation of ρ , as well as considering ρ and V spherically symmetrical, one can write

$$p_m = \left[(3\pi^2)^{2/3} \hbar^2 \rho^{2/3} + \frac{\hbar^2}{4} \left(\frac{\rho'}{\rho} \right)^2 - \frac{\hbar^2}{2} \frac{\rho''}{\rho} - \frac{\hbar^2}{r} \frac{\rho'}{\rho} \right]^{1/2} \quad \dots (13)$$

The above $p_m(r)$ may be used, along with equation (II, 3) to determine the shapes of the nuclear momentum distributions. Such nuclear momentum distributions require suitable renormalization, as $p_m(r)$ is no longer connected with $\rho(r)$ through the equation (II, 2).

D. Plaskett method

The Thomas-Fermi method, in one dimension, has been sought to be replaced by Plaskett (1953). It has not been possible for him to obtain a three dimensional form. In analogy with Plaskett's method in one dimension, an approximate relation in three dimensions has been set up in this investigation.

The Schrödinger equation in three dimensions is given by

$$\left[-\frac{\hbar^2}{2M} \nabla^2 - g(\bar{r}) \right] \psi(\bar{r}) = 0 \quad \dots (14)$$

where $g(\bar{r}) = E - V(\bar{r})$. One may now require that the solution of the above equation has the form

$$\psi(\bar{r}) = A(\bar{r}) \rho^{(i/\hbar)} \int_{\bar{r}}^{\bar{r}} \bar{P}(\bar{\xi}) \cdot d\bar{\xi} \quad \dots (15)$$

Substituting the solution given in equation (II, 15) into equation (II, 14) and separating the real and the imaginary parts, one obtains the simultaneous equations

$$A \bar{\nabla} \cdot \bar{P} + 2 \bar{P} \cdot \bar{\nabla} A = 0 \quad \dots (16)$$

$$2Mg = P^2 - \hbar^2 \Delta A / A \quad \dots (17)$$

One may note that

$$\frac{\bar{\nabla} A}{A} = \left(\frac{\bar{\nabla} A}{A} \right)^2 + \bar{\nabla} \cdot \left(\frac{\bar{\nabla} A}{A} \right) \quad \dots (18)$$

which by equation (II, 16) leads to

$$\frac{\bar{\nabla} A}{A} = \frac{1}{4} \left(\frac{\bar{\nabla} \cdot \bar{P}}{\bar{P}} \right)^2 - \frac{1}{2} \bar{\nabla} \cdot \left(\frac{\bar{\nabla} \cdot \bar{P}}{\bar{P}^2} \bar{P} \right) \quad \dots (19)$$

Substituting equation (II, 19) into equation (II, 17) one has

$$2Mg = P^2 - \frac{\hbar^2}{4} \left(\frac{\bar{\nabla} \cdot \bar{P}}{\bar{P}} \right)^2 + \frac{\hbar^2}{2} \bar{\nabla} \cdot \left(\frac{\bar{\nabla} \cdot \bar{P}}{\bar{P}^2} \bar{P} \right) \quad \dots (20)$$

Applying the above equation to the motion of the nucleon with the highest energy, one may require that it should revert to the Thomas-Fermi relation when \bar{P} is a slowly varying function of \bar{r} . By using equation (II, 2), one has

$$P^2 = (3\pi^2 \hbar^3)^{2/3} \rho^{2/3} \quad \dots (21)$$

Thus a connection can be established between the magnitude of \bar{P} and ρ . However, this does not give any information regarding the directional properties of \bar{P} . Therefore, it is not possible to make use of equation (II, 20) directly.

One may make a simplifying assumption that \bar{P} varies slowly in direction. To introduce this assumption one can rewrite (II, 16) as

$$\bar{\nabla} \cdot (A^2 \bar{P}) = 0 \quad \dots (22)$$

One may also note that

$$\bar{\nabla} \cdot \left(\frac{\bar{P}}{\bar{P}} \right) = \bar{\nabla} \cdot \bar{n} = 0 \quad \dots (23)$$

where \bar{n} is a unit vector in the direction of \bar{P} , provided the directional variation of \bar{n} is slow as assumed. Comparing equation (II, 22) with equation (II, 23), one can write $A = CP^{-1}$ where C is an undetermined constant.

Substituting the value of A and P^2 into equation (II, 17) and replacing $2Mg$ by p_m^2 , one obtains

$$p_m^2 = P^2 - \hbar^2 P^4 \Delta(P^{-1}) \quad \dots (24)$$

Substituting into equation (II, 24) from equation (II, 21) and considering ρ and P spherically symmetrical, one obtains

$$p_m = \left[(3\pi^2 \hbar^3)^{2/3} \rho^{2/3} + \frac{\hbar^2}{3r} \frac{\rho'}{\rho} - \frac{7\hbar^2}{36} \left(\frac{\rho'}{\rho} \right)^2 + \frac{\hbar^2}{6} \frac{\rho''}{\rho} \right]^{1/2} \quad \dots (25)$$

where ρ' and ρ'' are the first and the second radial derivatives of ρ respectively.

The above $p_m(r)$ may be used along with the equation (II, 3) to determine the nuclear momentum distributions. Such nuclear momentum distributions would also require renormalization as mentioned before.

17. Application to isotropic harmonic oscillator

The nuclear density distribution, used in the present investigation, is similar in form to the particle density distribution in an isotropic harmonic oscillator potential. Therefore it is advisable to test the applicability of the various methods for determining the nuclear momentum distributions by considering such an isotropic harmonic oscillator. Such tests can be carried out because it is possible to calculate the particle density distribution as well as the corresponding particle momentum distribution exactly in this instance,

March (1954) has carried out such tests for the Thomas-Fermi method by considering 20, 58 and 92 protons or neutrons. Since only carbon and oxygen nuclei have been tested in the present investigation, only 6 or 8 protons or neutrons need be considered in this connection. Since the case of 8 protons or neutrons would provide completed shells, only such a case has been treated here for simpli-

city. The Thomas-Fermi method, the Thomas-Fermi-Weizsäcker method and the modified Plaskett method have also been tested.

Morse and Feshbach (1953) have given, for an isotropic harmonic oscillator, the expression for $\psi_{nlm}(r, \theta, \phi)$. Similarly Morse and Feshbach (1953) have also given the corresponding expression for $\chi_{nlm}(p, \theta, \phi)$. Both these expressions needed some small corrections for proper normalization. Using such corrected expressions and taking $\rho_{nlm}(r, \theta, \phi) = |\psi_{nlm}(r, \theta, \phi)|^2$ and $I_{nlm}(p, \theta, \phi) = 4\pi p^2 |\chi_{nlm}(p, \theta, \phi)|^2$, one has in terms of dimensionless quantities,

$$\xi_{nlm}(t, \theta, \phi) = \frac{\pi^{\frac{1}{2}}}{2} (2l+1) \frac{(l-|m|)!}{(l+|m|)!} \frac{\left(\frac{n}{2} - \frac{l}{2} - \frac{1}{2}\right)!}{\left[\Gamma\left(\frac{n}{2} + \frac{l}{2} + 1\right)\right]^3} t^{2l} e^{-t^2} \\ \times \left[L_{\frac{n}{2} - \frac{l}{2} - \frac{1}{2}}^{l+\frac{1}{2}}(t^2) \right]^2 \{P_l^m(u)\}^2 \dots \quad (26)$$

$$\eta_{nlm}(s, \theta, \phi) = \frac{\pi^{\frac{1}{2}}}{2} (2l+1) \frac{(l-|m|)!}{(l+|m|)!} \frac{\left(\frac{n}{2} - \frac{l}{2} - \frac{1}{2}\right)!}{\left[\Gamma\left(\frac{n}{2} + \frac{l}{2} + 1\right)\right]^3} s^{2l+2} e^{-s^2} \\ \times \left[L_{\frac{n}{2} - \frac{l}{2} - \frac{1}{2}}^{l+\frac{1}{2}}(s^2) \right]^2 \{P_l^m(u)\}^2 \dots \quad (27)$$

where $t = \beta^{\frac{1}{2}} r$, $s = p/\hbar\beta^{\frac{1}{2}}$, with $\beta = M\omega/\hbar$ where M the nucleon mass and ω the classical frequency for the oscillator potential. Also $\xi_{nlm}(t, \theta, \phi) = (\pi/\beta)^{3/2} \rho_{nlm}(r, \theta, \phi)$ and $\eta_{nlm}(s, \theta, \phi) = (\hbar/4) (\pi\beta)^{\frac{1}{2}} \times I_{nlm}(p, \theta, \phi)$, where $n = \cos \theta$. Further, L represents the Laguerre function of the corresponding orders as discussed by Morse and Feshbach. In order to obtain purely radial expressions, it is necessary to average over angular variations. Allowing for two spin orientations, this leads to

$$\bar{\xi}_{nl}(t) = \pi^{\frac{1}{2}} \frac{\left(\frac{n}{2} - \frac{l}{2} - \frac{1}{2}\right)!}{\left[\Gamma\left(\frac{n}{2} + \frac{l}{2} + 1\right)\right]^3} t^{2l} \rho^{-t^2} \left[L_{\frac{n}{2} - \frac{l}{2} - \frac{1}{2}}^{l+\frac{1}{2}}(t^2) \right]^2 \dots \quad (28)$$

$$\bar{\eta}_{nl}(s) = \pi^{\frac{1}{2}} \frac{\left(\frac{n}{2} - \frac{l}{2} - \frac{1}{2}\right)!}{\left[\Gamma\left(\frac{n}{2} + \frac{l}{2} + 1\right)\right]^3} s^{2l+2} \rho^{-s^2} \left[L_{\frac{n}{2} - \frac{l}{2} - \frac{1}{2}}^{l+\frac{1}{2}}(s^2) \right]^2 \dots \quad (29)$$

In case of 8 particles only the terms for $n = 1, l = 0$ and $n = 2, l = 1$ are necessary. For both cases, one gets $L_0^1 = \pi^1/2$ and $L_0^{3/2} = 3\pi^1/4$. Substituting the above values into equations (II, 28) and (II, 29) and allowing for $(2l+1)$ degeneracy for values of m , one has for all the 8 particles.

$$\bar{\xi}(t) = \rho^{-t^2}(2+4t^2) \quad (30)$$

$$\bar{\eta}(s) = \rho^{-s^2}s^2(2+4s^2) \quad (31)$$

The dimensionless total density $\bar{\xi}(t)$ for 8 particles, shown in figure 2, roughly similar in form to the characteristic nuclear density of Gatha and Shah as shown

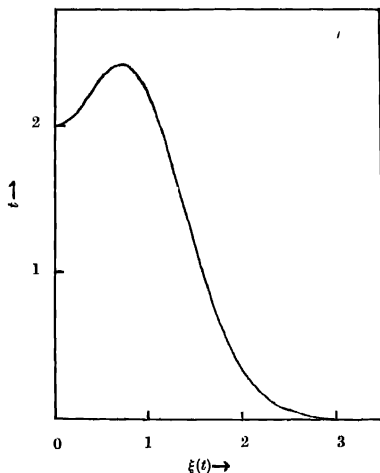


Fig. 2. Dimensionless nuclear density distribution for eight particles in an isotropic harmonic oscillator potential.

in figure 1. This similarity makes the case of the isotropic harmonic oscillator potential useful for testing the applicability of the various methods for the determination of the of the nuclear momentum distributions.

Using Thomas-Fermi method, one has from equation (II, 4) for all the 8 particles

$$\eta_{T.F.}(s) = \frac{s^2}{3\pi^1} t^3(s) \quad (32)$$

One has to determine $t(s)$ by using equation (II, 1) in the form

$$s_{T.F.} = [3\pi^1 \bar{\xi}(t)]^{1/3} \quad (33)$$

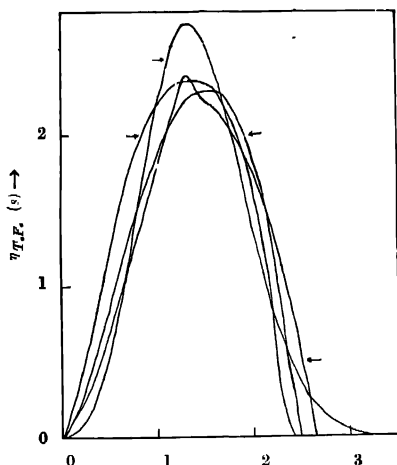


Fig. 3. Dimensionless nuclear momentum distribution for eight particles in an isotropic harmonic oscillator potential.

Top arrow η : By exact method.

Middle left arrow : η_{TF} : By Thomas-Fermi method.

Middle right arrow η_P : By Plaskett method

Bottom arrow : η_{TFW} : By Thomas-Fermi-Weizsacker method.

Substituting for $\xi(t)$ from equation (II, 30) into equation (II, 33) $t(s)$ has been obtained graphically. Using this $t(s)$, $\eta_{TF}(s)$ has been determined from equation (II, 32). This $\eta_{TF}(s)$ has been shown in figure 3 for comparison with the exact $\eta(s)$.

Using Thomas-Fermi-Weizsacker method, one has from equation (II, 3) for all the 8 particles

$$\eta_{TFW}(s) = 3s^2 \int_0^{t(s)} \frac{\xi(t)}{\{s_{TFW}(t)\}^3} t^2 dt \quad \dots (34)$$

where from equation (II, 13), one has

$$s_{TFW} = \left[\left\{ 3\pi^4 \xi(t) \right\}^{2/3} + \frac{1}{4} \left\{ \frac{\xi'(t)}{\xi(t)} \right\}^2 - \frac{1}{2} \left\{ \frac{\xi''(t)}{\xi(t)} \right\} - \frac{1}{t} \left\{ \frac{\xi'(t)}{\xi(t)} \right\} \right]^{1/2} \dots (35)$$

Similarly using Plaskett method, one has again from equation (II, 3) for all the 8 particles

$$\eta_P(s) = 3s^2 \int_0^{t(s)} \frac{\xi(t)}{\{s_P(t)\}^3} t^2 dt \quad \dots (36)$$

where from equation (II, 25), one has

$$s_P = \left[\left\{ 3\pi^{\frac{1}{2}} \bar{\xi}(t) \right\}^{\frac{2}{3}} - \frac{7}{36} \left\{ \frac{\bar{\xi}'(t)}{\bar{\xi}(t)} \right\}^2 + \frac{1}{6} \left\{ \frac{\bar{\xi}''(t)}{\bar{\xi}(t)} \right\} + \frac{1}{3t} \left\{ \frac{\bar{\xi}'(t)}{\bar{\xi}(t)} \right\} \right]^{\frac{1}{2}} \quad \dots (37)$$

From these equations $s_{TF, W}(t)$ and $s_P(t)$ were determined by substituting for $\bar{\xi}(t)$ from equation (II, 30). The limits $t'(s)$ for both cases were determined graphically from the corresponding implicit equations (II, 35) and (II, 37). The determination of $\eta_{TF, W}(s)$ and $\eta_P(s)$ were determined graphically from equation (II, 34) and (II, 36) respectively and the same were renormalized as indicated before. Both $\eta_{TF, W}(s)$ and $\eta_P(s)$ have been shown in figure 3 along with $\eta_{TF}(s)$ for comparison with the exact $\bar{\eta}(s)$ determined before.

It is clear from figure 3 that $\eta_{TF}(s)$ is not a very good approximation to $\bar{\eta}(s)$. The deviations are particularly apparent both for small and large values of s as can be expected. It is also clear that $\eta_P(s)$ deviates even more from $\bar{\eta}(s)$ at such values of s . On the other hand, $\eta_{TF, W}(s)$ is closer to $\bar{\eta}(s)$ for such value of s . For other values of s , however it is rather difficult to prefer any one approximation over others. Therefore the behaviour of these approximations for large and small values of s has been used as a criterion for selection. The Thomas-Fermi-Weizsacker method is regarded a somewhat superior to others for determining the momentum distribution from the density distribution, of an isotropic harmonic oscillator. Since the nuclear density distribution of Gatha and Shah is of a similar form as the density distribution for the isotropic harmonic oscillator, the Thomas-Fermi-Weizsacker method has been used, in the present investigation for determining the nuclear momentum distributions.

F. Nuclear momentum distributions for carbon and oxygen.

The nuclear momentum distributions for carbon and oxygen have been determined, by using the Thomas-Fermi-Weizsacker method, from the corresponding nuclear density distributions obtained from the characteristic nuclear density distribution given in equation (II, 1). Since such density distributions pertain to nucleons, one has to modify the expression for the maximum momentum distribution $p_m(r)$ of equation (II, 13), so as to account for the two isotopic spin states of the nucleons. The expression for $p_m(r)$ now becomes

$$p_m(\bar{r}) = \left[\left(\frac{3\pi^2}{2} \right)^{\frac{2}{3}} \bar{\hbar}^2 \rho^{\frac{2}{3}} + \frac{1}{A^{\frac{2}{3}}} \left\{ \frac{\bar{\hbar}^2}{4} \left(\frac{\rho'}{\rho} \right)^2 - \frac{\bar{\hbar}^2}{2} \frac{\rho''}{\rho} - \frac{\bar{\hbar}^2}{r} \frac{\rho'}{\rho} \right\} \right]^{\frac{1}{2}} \quad \dots (38)$$

It may be noted that, in this method, $p_m(\bar{r})$ is not characteristic although $\rho(\bar{r})$ is characteristic. Substituting for $\rho(\bar{r})$ from equation (II, 1), $p_m(\bar{r})$ was explicitly calculated for carbon as well as oxygen.

In the above notation one can rewrite the expression for nuclear momentum distribution $I(p)$ from equation (II, 3) as

$$I(p) = 12\pi p^2 \int_0^{\bar{r}(p)} \frac{\rho(\bar{r})}{\{p_m(\bar{r})\}^3} \bar{r}^2 d\bar{r} \quad \dots (39)$$

Using $\rho(\bar{r})$ of equation (II, 1) and $p_m(\bar{r})$ as determined before, the momentum distributions $I_o(p)$ and $I_c(p)$ for carbon and oxygen respectively were calculated by performing the necessary integrations graphically. It may be noted that these nuclear momentum distributions have to be normalized to unity. Suitable re-normalisations, to this effect, were carried out by multiplying with appropriate normalization constants. Both $I_o(p)$ and $I_c(p)$ have been shown in figure 4.

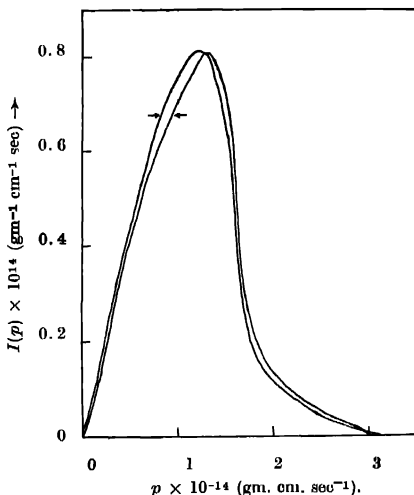


Fig. 4. Nuclear momentum distributions for carbon and oxygen.
 \rightarrow : I_o : For oxygen. \leftarrow : I_c : For carbon.

These $p_m(\bar{r})$ have been used in the present investigation to correlate the experimental data, for carbon and oxygen, on the nuclear inelastic scattering of high energy protons and the photo-production of positive pions.

III. NUCLEAR INELASTIC SCATTERING OF HIGH ENERGY PROTONS

The proton energy spectra at 30° for carbon and at 40° for carbon and oxygen¹¹ resulting from the nuclear inelastic scattering of 340 Mev protons from these elements, have been observed by Cladis *et al* (1952). Serber (1947) has proposed a model for the nuclear interactions of high energy nucleons, wherein such

en counters are treated as a series of nucleon-nucleon interactions. For treating such problems, Fermi (1936) first proposed the impulse approximation. Chew (1950) has later elaborated the concepts behind this approximation. On the basis of the above approximation Wolf (1952) has developed an expression for the scattering cross-section $\sigma(T, \theta)$ for the nuclear scattering of high energy protons. Following Cladis *et al* (1952) this can be simply written as

$$\sigma(T, \theta) = \frac{MA}{2\pi} \int_{P-Q}^{\infty} \frac{I(p)}{P-Q} \sigma_E(\theta) \frac{dp}{p} \quad \dots (3.1)$$

where M = nucleon mass,

A = nuclear mass number,

$I(p) = 4\pi p^2 N(p)$ = nuclear momentum distribution,

P = incident nucleon momentum,

Q = scattered nucleon momentum,

$\sigma_E(\theta)$ = average free nucleon-nucleon scattering cross section at the angle θ for the incident energy E ,

T = scattered nucleon kinetic energy.

The lower limit K for the above integral has been given by Wolff (1952) as

$$K = [2(P^2 - PQ \cos \theta) - 2\{(P^2 - Q^2)(P^2 + Q^2 - 2PQ \cos \theta)\}^{1/2}]^{1/2} \quad \dots (3.2)$$

The nuclear momentum distributions, determined above, have been used to correlate the experimental data of Cladis *et al* (1952) on the proton energy spectra resulting from the nuclear inelastic scattering of 340 Mev protons by carbon and oxygen. Inserting the values of $I_o(p)$ and $I_o(p)$ in equation (II, 39), taking $\sigma_E(\theta)$ as per Wolff (1952) and calculating K from equation (11, 38), $\sigma_e(T, 30^\circ)$, $\sigma_e(T, 40^\circ)$ and $\sigma_o(T, 40^\circ)$, for carbon and oxygen as indicated, have been calculated through graphical integration procedures. The observed proton energy spectrum at 30° for carbon is shown in figure 5, while the observed proton energy spectra at 40° for carbon and oxygen are shown in figure 6. The theoretical curve for $\sigma_e(T, 30^\circ)$ has also been shown in figure 5. Similarly, the theoretical curves for $\sigma_e(T, 40^\circ)$ and $\sigma_o(T, 40^\circ)$, have been shown in figure 6. All the theoretical energy spectra have been shifted along both scales to give the best agreement with the corresponding experimental energy spectra.

It can be seen from figures 5 and 6 that the agreement between the theoretical and the experimental proton energy spectra is about as reasonable as that given by the Gaussian distribution used by Wolff (1952) as well as by Cladis *et al* (1952). However, the peaks in the theoretical spectra, determined in this investigation, are somewhat narrower than those given by the Gaussian distribution. The shapes of such peaks are determined by the nature of the nuclear momentum distributions for very low momenta. At the same time the theoretical spectra, determined in this investigation, deviate slightly more from the experimental spectra than in the case of the Gaussian distribution for very small and very

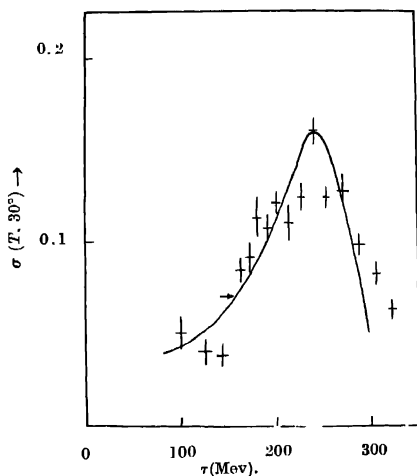


Fig. 5. Relative proton energy spectra at 30° scattering angles from 343 Mev protons on carbon.

$\rightarrow \cdot \sigma_c$ Theoretical energy spectrum. $+$ Experimental energy spectrum.

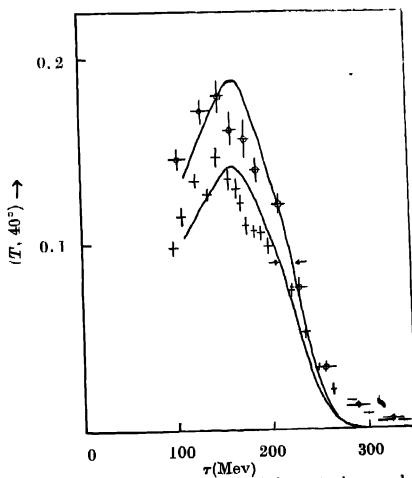


Fig. 6. Relative proton energy spectra at 40° scattering angle from 340 Mev protons on carbon and oxygen.

\rightarrow : σ_c : Theoretical energy spectrum for carbon.
 \leftarrow : σ_o : Theoretical energy spectrum for oxygen.
 $+$: Experimental energy spectrum for carbon.
 $+$: Experimental energy spectrum for oxygen.

large T . The shapes of the theoretical spectra, for such extremal regions, are determined by the nature of the nuclear momentum distributions for very large momenta. It may be noted that all approximate statistical methods, including the Thomas-Fermi-Weizsacker method, for determining the nuclear distribution from the nuclear density distribution are somewhat unreliable for very low and very high momenta. These deviations can, therefore, be presumably ascribed to the failure of the statistical methods for determining the nuclear momentum distributions. Hence, it is reasonable to conclude that the characteristic nuclear density distributions, determined by Gatha and Shah, provides reasonable nuclear momentum distributions from the point of view of the proton energy spectra resulting from the nuclear inelastic scattering of 340 Mev protons by light elements.

IV. NUCLEAR PHOTO-PRODUCTION OF HIGH ENERGY PIONS

McMillan *et al* (1949), Steinberger and Bishop (1952), Peterson *et al* (1951) as well as Sargent Janes and Kraushaar (1954) have observed the pion energy spectra at certain definite angles for carbon for the photo-production by bremsstrahlung photons. Attention has been concentrated, in this investigation on the pion energy spectra and pion production efficiency for the photo-production of high energy positive pions by carbon. Some estimates of pion production efficiency have also been reported by some of the above workers. Jenkins *et al* (1954) as well as Luckey (1955) have reported some observations on the pion production efficiency during the photo-production by carbon at certain photon energies. These observed nuclear reactions can be expected to depend on the nuclear momentum distributions of the elements concerned. Comparing the corrected charged pion energy spectrum at 90° for carbon due to Peterson *et al*. with the positive pion energy spectrum at 90° for carbon due to Sargent Janes and Kraushaar, one finds that the two spectra are considerably inconsistent. In this circumstance, it is natural to place more reliance on the results of electrical measurements than on the results of photographic measurements. Therefore, the pion energy spectra, due to McMillan *et al* and Peterson *et al*, have been disregarded in this investigation. Consequently, the positive pion energy spectrum at 90° for carbon, due to Sargent Janes and Kraushaar has been considered for theoretical interpretation in this investigation. This energy spectrum, as pointed out by Sargent Janes and Kraushaar, give practically no pions below about 8 Mev pion kinetic energy. It is suspected that this may be due to some systematic error of this magnitude in their energy determination. Therefore, this energy spectrum has been shifted towards lower pion kinetic energies by about 8 Mev before comparing the same with the corresponding theoretical energy spectrum in figure 7. Observations have been made for 200 Mev, 235 Mev and 265 Mev

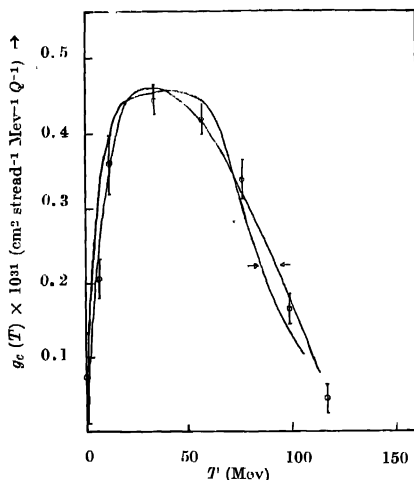


Fig. 7. Positive pion energy spectra at 90° for the photo-production on carbon by 326 Mev Bremsstrahlung photons.

→ : G_c (Lax) : Theoretical energy spectrum of Lax and Feshbach.

← : G_c : Present theoretical energy spectrum.

○ : Experimental energy spectrum.

photons by Jenkins *et al* as well as Luckey for the production efficiencies for the photo-production of positive pions by carbon. From these observations, the differential photo-production cross section $\sigma_H(\theta)$ for hydrogen, the integrated photo-production cross section σ_H for the same and the angular photo-production efficiency $\epsilon(\theta)$ for carbon are considered relevant. The differential photo-production cross section $\sigma_c(\theta)$ per proton for carbon was calculated at various angles by multiplying $\sigma_H(\theta)$ with the corresponding $\epsilon(\theta)$. The probable errors on $\sigma_c(\theta)$ have been estimated by taking the same fractional errors as shown on their direct measurements of $\sigma_c(T', \theta)$. The probable errors on θ have also been given by them. Then $\sigma_c(\theta)$, obtained above, were graphically integrated after drawing smooth curves through their plots against $\cos(\theta)$ in the centre of mass system. Finally, the production efficiencies ϵ for positive pions for carbon were calculated at these energies by dividing σ_c by the corresponding values of σ_H . These values of ϵ at 200 Mev, 235 Mev, and 265 Mev, together with their probable errors, are shown in figure 8 for comparison with the theoretical expression for ϵ at such energies.

The theoretical analysis for the nuclear photo-production of positive pions by Hayakawa (1951) as well as Lax and Feshbach (1951) has been based only on formal expressions for the nuclear photo-production of pions by hydrogen, independent of any specific form for the same. Consequently, the theoretical

analysis by Hayakawa has been based on certain assumptions regarding the initial and final nuclear states. He has used the Fermi nuclear momentum distribution only. Lax and Feshbach have carried out their analysis by using the

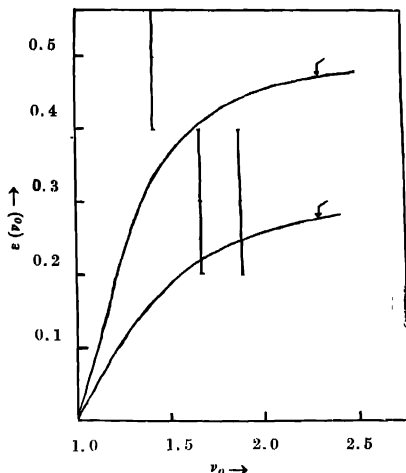


Fig. 8. Positive pion photo-production efficiencies for carbon.

Upper arrow : ε : Present theoretical efficiency.

Lower arrow : ε : (Lax) : Theoretical efficiency of Lax and Feshbach.

Φ : Experimental efficiency.

closure approximation. The theoretical considerations of Hayakawa as well as Lax and Feshbach lead to similar results, except for the differences pointed out by Marshak (1952). However, the theoretical analysis due to Lax and Feshbach can be applied to any nuclear momentum distribution as illustrated by them. Consequently, the theoretical analysis of Lax and Feshbach has been used in the present investigation.

Lax and Feshbach (1951) have expressed the relative differential cross section as a function of photon and pion energies, for the nuclear photo-production of positive pions, in the dimensionless form

$$g(v_0, \mu_0) = (\mu_0^2 - 1)^{1/2} I(v_0, \mu_0) / v_0 \quad \dots (4.1)$$

where the expression $I(v_0, \mu_0)$ is given by

$$I(v_0, \mu_0) = 2\pi \frac{M + v_0 - \mu_0}{a} \int_a^{a+b} \frac{\rho(k)k dk}{(b-a) \text{ or } (a^2 - b^2)^{1/2}} \quad \dots$$

In these expressions they have taken $\hbar = C = 1$ and also the pion rest mass

$\mu = 1$. In these units M represents the nucleon rest energy, while ν_0 and μ_0 represent the photon and the pion energies respectively. At the same time, $\bar{\nu}$ and $\bar{\mu}$ represent the photon and the pion momenta respectively. Further, $\rho(k)$ represents the nuclear momentum distribution. When the incident radiation is a bremsstrahlung spectrum $f(\nu_0)$ one can obtain the relative differential cross section, as a function of pion energy, by integrating over such a spectrum. Thus one has

$$g(\mu_0) = \int^{\nu_{max}} g(\nu_0, \mu_0) f(\nu_0) d\nu_0 \quad \dots (4.3)$$

where ν_{max} is the maximum photon energy for the bremsstrahlung spectrum. According to Marshak (1952), one can use the simple expression, $f(\nu_0) = 1/\nu_0$. Since only the relative values of $g(\mu_0)$ are calculated from equation (IV, 3), normalization of $f(\nu_0)$ becomes unnecessary.

Using such a bremsstrahlung spectrum with $\nu_{max} = 2.35$, Lax and Feshbach (1951) have calculated $g(\mu_0)$ at 90° for carbon on the basis of the Chew-Goldberger nuclear momentum distribution. Since this theoretical $g(\mu_0)$ is only relative, it was suitably normalized and compared with the corresponding experimental positive pion energy spectrum of Steinberger and Bishop (1952). A reasonable agreement was obtained between the theoretical and the experimental pion energy spectra. This theoretical pion kinetic energy $T = \mu c^2(\mu_0 - 1)$ expressed in Mev, has been shown in figure 7. Lax and Feshbach have expressed the positive pion production efficiency, as a function of photon energy, in the form

$$c(\nu_0) = \int \rho(\bar{k}) d\bar{k} \quad \dots (4.4)$$

$$|\bar{\nu} - \bar{k}| \leq [2M(\nu_0 - 1)]^{\frac{1}{2}}$$

where \bar{k} represents the nucleonic momentum within the nucleus in this units. The production efficiency can be expressed by

$$\epsilon = \frac{\int^{\nu_{max}} \sigma(\nu_0) \epsilon(\nu_0) f(\nu_0) d\nu_0}{\int^{\nu_{max}} \sigma_H(\nu_0) f(\nu_0) d\nu_0} \quad \dots (4.5)$$

where $\sigma_H(\nu_0)$ is the cross section, per unit photon energy interval at ν_0 , for the photo-production of positive pions by hydrogen. The monochromatic positive pion production efficiency $\epsilon(\nu_0)$, due to Lax and Feshbach, has been shown in figure 8, after reducing the same to half as required by Steinberger and Bishop.

The theoretical positive pion energy spectrum at 90° and the positive pion production efficiency, for the photo-production by carbon, have been obtained in this investigation on the basis of $I_c(p)$, determined before, from the theoretical expressions for the same given by Lax and Feshbach. $N_c(p)$ has been obtained for carbon from $I_c(p)$ by using the relation $N_c(p) = I_c(p)/4\pi p^2$. Using a transformation $p = \mu ck$, where μ is the pion rest mass, $\rho_c(k)$ has been obtained from the relation $\rho_c(k) = (\mu c)^3 N_c(p)$.

Substituting $\rho_c(k)$ into equation (IV, 2) and introducing the result into equation (IV, 1) and performing the necessary integration graphically, $g_c(v_o, \mu_o)$ have been determined, for various values of μ_o , for each of a set of values of v_o . Next with the bremsstrahlung spectrum defined by $f(v_o) = 1/v_o$ and $v_{max} = 2.32$, $g_c(\mu_o)$ has been calculated as a function of v_o . Next, $g_c(T)$ was obtained by taking pion kinetic energy $T = \mu c^2(\mu_o - 1)$ and converting T to Mev. Since this $g_c(T)$ is only relative, it has been suitably renormalized and shown in figure 7. It can be seen from figure 7 that the theoretical positive pion energy spectrum, based on the present nuclear momentum distribution, reasonably agrees with the corresponding experimental positive pion energy spectrum. Further, $g_c(T)$ have also been determined for carbon, at 45° and 135° . These have been shown in figure 9 on an arbitrary scale.

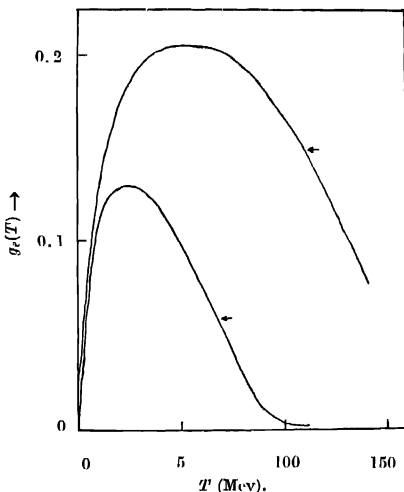


Fig. 9. Theoretical positive pion energy spectra at 45° and 135° for the photo-production on carbon by 326 Mev Bremsstrahlung photons.
Upper arrow : $g_c(45^\circ)$. Lower arrow : $g_c(135^\circ)$.

Substituting $\rho_c(k)$ into equation (IV,4) and performing the necessary integration graphically, the positive pion production efficiency $\epsilon_c(v_o)$ for carbon has been calculated as a function of v_o . This $\epsilon_p(v_o)$, after reducing the same to half as per the prescription of Steinberger and Bishop, has been shown in figure 8 with the experimental values derived before. It can be seen from figure 8 that the theoretical pion production efficiency for carbon, based upon the present nuclear momentum distribution, roughly agrees with the experimental pion production efficiency.

CONCLUSION

The nuclear momentum distributions for light elements can be obtained from the characteristic nuclear density distribution on the basis of an empirically reasonable method. Such nuclear momentum distributions can be used for reasonable correlations of the available experimental data on the inelastic nuclear scattering of high energy protons as well as the nuclear photo-production of positive pions by such light elements. Since the theoretical analysis, in each case, has been based on several plausible assumptions and the experimental data contain large errors, it is not possible to discriminate unambiguously between the present momentum distributions and the other proposed nuclear momentum distributions. However, it can be safely concluded that the theoretical deductions, provide at least as good agreement with experimental results as given by any of the proposed nuclear momentum distributions. These conclusions, therefore, further justify the validity of the characteristic nuclear density distribution for light elements employed in the present investigation.

REFERENCES

- Ballinger, R. A., and March, N. H., 1954, *Proc. Phys. Soc. (London)*, **67**, 378.
 Chew, G. F. and Goldberger, M. L., 1950, *Phys. Rev.*, **77**, 470.
 Chew, G. F., 1950, *Phys. Rev.*, **80**, 196.
 Chudis, J. B., Hess, W. N. and Moyer, B. J., 1952, *Phys. Rev.*, **87**, 425.
 Coulson, C. A. and March, N. H., 1950, *Proc. Phys. Soc. (London)*, **A63**, 367.
 Formi, E., 1936, *Ricerca Sci.* VII-11, 13.
 Gatha, K. M. and Shah, G. Z., (Private Communication)
 Gombas, P., 1952, *Acta Phys. Hung.*, **1** 329.
 Hayakawa, S., 1951, *Phys. Rev.*, **82**, 836.
 Jenkins, J. L., Luckey, D., Palfrey, T. R. and Wilson, R. R., 1954, *Phys. Rev.*, **95**, 179
 Lax, M. and Feshbach, H., 1951, *Phys. Rev.*, **81**, 189.
 Luckey, D., 1955, *Phys. Rev.*, **97**, 469.
 Marshak, R. E., 1952, *Meson Physics* (McGraw-Hill, New York.)
 March, N. H., 1954, *Proc. Phys. Soc. (London)*, **67**, 288.
 McMillan, E. N., Peterson, V. Z., and White, R. S., 1949, *Science*, **110**, 579.
 Morse, P. M., and Feshbach, H., 1953, *Methods of Theoretical Physics*, (McGraw-Hill), New York, P. 1663.
 Morse, P. M. and Feshbach, H., *op. cit.* P. 1679.
 Morse, P. M. and Feshbach, H., *op. cit.* P. 785.
 Peterson, J. M., Gilbert, W. S., and White, R. S., 1951, *Phys. Rev.*, **81**, 1003.
 Plaskett, J. S., 1953, *Proc. Phys. Soc. (London)*, **A66**, 178.
 Sargent Jones, G., and Kruusgaard, W. L., 1954, *Phys. Rev.*, **93**, 900.
 Serber, R., 1947, *Phys. Rev.*, **72**, 1114.
 Steinberger, J., and Bishop, A. S., 1952, *Phys. Rev.*, **86**, 171.
 Weizsäcker Van C. F. V., 1935, *Z. Phys.*, **96**, 431.
 Wolff, P. A., 1952, *Phys. Rev.*, **87**, 434.

DESIGN OF PULSE AMPLIFIER

R. C. GANGULI,

INDIAN INSTITUTE OF TECHNOLOGY, Kharagpur

(Received for publication, April 20, 1959)

ABSTRACT. This paper describes a new approach to the design of pulse amplifier based on its transient response characteristics. A pulse amplifier is characterised by its gain, risetime and overshoot and its design is dependent upon the relation between these parameters and the circuit constants. Analytical relation between overshoot and risetime (defined as the time for 10% to 90% of the final value) cannot be obtained. Relation between gain, overshoot and the time to rise from zero to peak value has, however, been obtained, and the method of designing an actual pulse amplifier from a knowledge of these parameters shown. Results are compared with an actual pulse amplifier designed from the data obtained theoretically

INTRODUCTION

It is known that the unwanted shunt capacitance sets a limit to the high frequency response and hence the sharp risetime of R-C coupled pulse amplifiers. Since it is not possible to reduce its value indefinitely one aims at reducing its detrimental effects and thus improving the high frequency response with the help of some complicated circuitry. The simplest method is shunt compensation.

The degree of h.f. compensation may be ascertained from the transient response characteristics. A short risetime for a step function input corresponds to a high upper 3 db point, and hence large bandwidth. In this paper a brief review is made of the effect of pole-zero location on the transient response characteristics and the process of designing parameters of a shunt compensated R-C coupled amplifier, which gives the best possible combination of gain, overshoot and risetime, is discussed. (Gupta Sharma, 1954 and Martin, 1955).

2. DESIGN ANALYSIS

If the mutual impedance function of a network is given by $g(p)$ the voltage output for a unit current step input is given by

$$v(t) = \frac{1}{2\pi j} \int_{c-j\infty}^{c+j\infty} \frac{g(p)}{p} e^{pt} dp,$$

where the contour has to be chosen in such a way that all the singularities of $g(p)$ are to the left of the path of integration. Thus

$$\begin{aligned} v(t) &= \frac{1}{2\pi j} \times 2\pi j \sum \text{Residues } \frac{g(p)}{p} e^{pt} \text{ at the poles of } g(p) \\ &= \sum \text{Residues } \frac{g(p)}{p} e^{pt} \text{ at the poles of } g(p), \end{aligned}$$

where $g(p)$ can be expressed as

$$H \cdot \frac{(p - \alpha_1)(p - \alpha_3) \dots}{(p - \alpha_2)(p - \alpha_4) \dots} e^{pt}$$

In the above expression H is a constant, $\alpha_1, \alpha_3, \dots$ are zeros and $\alpha_2, \alpha_4, \dots$ poles of the network function in the complex frequency plane.

Hence we can write

$$v(t) = H \sum \text{Residue } \frac{1}{p} \frac{(p - \alpha_1)(p - \alpha_3) \dots}{(p - \alpha_2)(p - \alpha_4) \dots} e^{pt}$$

It may be mentioned here that pentode tubes are normally used for such amplifiers with relatively low values of plate load. So that equivalent generator for the output circuit is ideally a constant current generator and the output voltage is proportional to the output current which, in turn, is proportional to the input voltage. Hence, in calculating $v(t)$ we have taken a step current input function.

The conventional shunt compensated amplifier and its high frequency equivalent circuit are given in figures 1(a) and (b) respectively where C denotes the output capacitance of the first stage together with the input capacitance of the second stage.

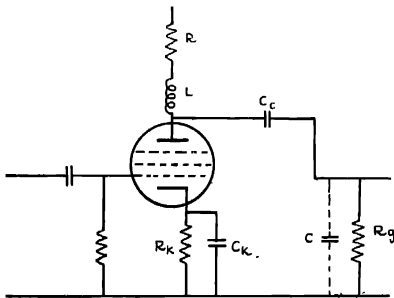


Fig. 1 (a)

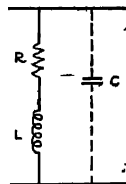


Fig. 1 (b) High frequency equivalent circuit.

For this equivalent circuit

$$g(p) = \frac{Z_1 \cdot Z_2}{Z_1 + Z_2 + Z_3}$$

where

$$Z_1 = R + pL$$

$$Z_2 = \frac{1}{pC}$$

$$Z_3 = 0$$

$$\begin{aligned} \therefore g(p) &= \frac{1}{C} \cdot \frac{p + \frac{R}{L}}{p^2 + p \cdot \frac{R}{L} + \frac{1}{LC}} \\ &= H \cdot \frac{p + a}{(p - b)(p - c)} \end{aligned}$$

Where

$$H = \frac{1}{C}; \quad a = R/L$$

$$b = -\frac{R}{2L} + j \sqrt{\frac{1}{LC} - \frac{R^2}{4L^2}} = -\alpha + j\beta \text{ (say)}$$

and

$$c = -\frac{R}{2L} - j \sqrt{\frac{1}{LC} - \frac{R^2}{4L^2}} = -\alpha - j\beta \text{ (say)}$$

$$\text{Hence } v(t) = H \sum \text{Residue } \frac{1}{p} \frac{p + a}{(p - b)(p - c)} e^{pt}$$

for unit step current input.

$$\begin{aligned} &= H \cdot \frac{a}{\alpha^2 + \beta^2} \left[1 + \frac{e^{-\alpha t}}{\sin \phi} \sin (\beta t - \phi) \right] \\ &= H \cdot \frac{2\alpha}{\alpha^2 + \beta^2} \left[1 + \frac{e^{-\alpha t}}{\sin \phi} \sin (\beta t - \phi) \right] \end{aligned}$$

where

$$\phi = \tan^{-1} \frac{a\beta}{\alpha^2 + \beta^2 - a\alpha}$$

The nature of the solution clearly indicates that the response is non-monotonic (oscillatory) and some overshoot is present which is always the case as long as poles of the network functions are complex conjugates. For real poles the response is monotonic (damped), but the risetime is large. In order to minimise the risetime the parameters have therefore to be so adjusted that the roots are complex conjugates and in such a case some overshoot has to be

tolerated. To obtain such a condition the relation $\frac{L}{R^2} > \frac{C}{4}$ has to be satisfied.

Now locating the poles and zero's in the complex frequency plane (figure 2) we obtain

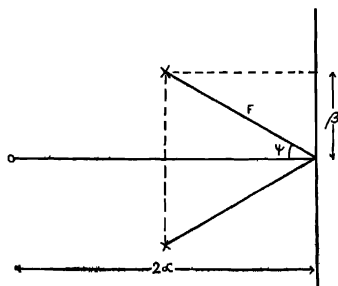


Fig. 2.

$$v(t) = H \cdot \frac{2 \cos \psi}{F} \left[1 - e^{-\alpha t} \frac{\sin(\beta t + 2\psi)}{\sin 2\psi} \right]$$

where

$$\alpha = F \cos \psi$$

$$\beta = F \sin \psi$$

$$\psi = \tan^{-1} \frac{\beta}{\alpha} = \tan^{-1} \sqrt{\frac{4L}{CR^2} - 1}$$

$$F = \sqrt{\alpha^2 + \beta^2} = \sqrt{\frac{1}{LC}}$$

The plot of $v(t)$ against t as given in figure 3 reveals that $v(t)$ passes through alternate maxima and minima, before it reaches the steady state value given by $H \frac{2 \cos \psi}{F}$.

T_m is the risetime at which the first maximum is obtained and can be found out by satisfying the following two conditions simultaneously $\frac{d}{dt} v(t) = 0$

$$\text{and} \quad \frac{d^2}{dt^2} v(t) = \text{negative.}$$

We thus have

$$\beta T_m = \pi - \psi$$

or

$$T_m = \frac{\pi - \psi}{\beta} = \frac{\pi - \psi}{F \sin \psi}$$

for the first maximum.

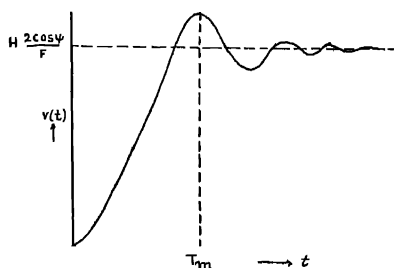


Fig. 3.

Substituting the value of T_m in the expression of $v(t)$ we get

$$v(t)_{max} = H \cdot \frac{2 \cos \psi}{F} \left(1 + \frac{e^{-\alpha T_m}}{2 \cos \psi} \right)$$

The percentage overshoot is therefore given by

$$\frac{v(t)_{max} - v(t)_{\infty}}{v(t)_{\infty}} \times 100$$

$$= \frac{e - (\pi - \psi) \cot \psi}{2 \cos \psi} \times 100$$

From the expressions for overshoot, T_m and steady state value it is clear that overshoot is a function of ψ alone whereas the steady state value and T_m are functions of both ψ and F . It is therefore expected that by properly adjusting F and ψ , it is possible to obtain favourable combination of overshoot, risetime and gain to suit a particular purpose.

Now in any case C is fixed by the choice of the tube. So to vary ψ and F , we have to adjust L and R , but the limit of variation is decided by the relation $\frac{4L}{CR^2} > 1$.

Or, we can write

$$\frac{L}{R^2} = K \frac{C}{4}$$

where $K > 1$

Let us now find for what value of K one can obtain an optimum combination of gain, overshoot and risetime. Expressing them in terms of C and K we get

$$\text{Overshoot } S = \frac{\sqrt{K}}{2} e^{-\frac{\pi - \tan^{-1} \sqrt{k-1}}{\sqrt{k-1}}}$$

$$T_m = \frac{CR}{2} \frac{K}{\sqrt{k-1}} (\pi - \tan^{-1} \sqrt{k-1})$$

Steady state gain $G = g_m R$. (midfrequency gain)

$$\therefore \frac{T_m}{G} = \frac{C}{2g_m} \cdot \frac{K}{\sqrt{k-1}} (\pi - \tan^{-1}\sqrt{k-1})$$

The plot of S vs K and T_m/G vs K are shown respectively in figures 4 and 5.

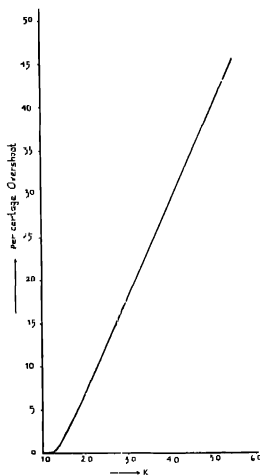


Fig. 4.

The above sets of curves can be taken as a guide to the design process. To start with one fixes up the amount of overshoot that can be tolerated. From the knowledge of tolerated overshoot, one knows the value of K which automatically fixes up T_m/g ratio. Then knowing the value of G , T_m is automatically fixed or from the knowledge of T_m , G is fixed up. In fact one has to make a compromise between T_m and G . For the same permissible overshoot, if a large gain is desired T_m will also have to be large and if, on the other hand, a small T_m is required one has to sacrifice gain. G decides the value of R in the circuit. Thus knowing R and K , L can be known from a knowledge of C .

It will be noted from figure 5 showing the plot of T_m/G against K , that the curve passes through a minimum i.e., the gain-risetime ratio is maximum for a particular value of $K = 2.55$. The percentage overshoot for this value of K is 13%. If this can be tolerated, the combination of gain, overshoot and risetime as defined by this value of K should be taken as a guide to the design procedure.

It may further be noted that the minimum of the curve is not very sharp, it is rather flat for values of K greater than that for minimum. This means

that beyond a certain value of K (≈ 2) although T_m/G does not vary appreciably, the overshoot rises rapidly with increase of K .

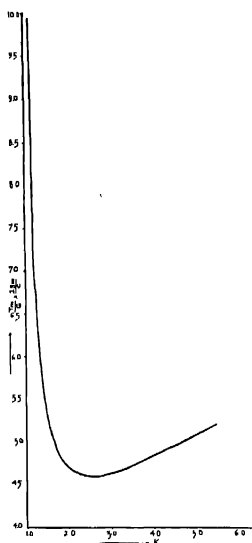


Fig. 5

From the expressions of T_m and G we have seen that both include R as the multiplier, but T_m/G becomes solely a function of K without having any multiplier R . Further, since $K = 4L/CR^2$, any change in K by varying R and L will modify the individual values of T_m and G . The specified gain will fix up the value of R and any modification of K required will be done only by changing L . The following observations were carried out on an R - C coupled amplifier with an inductance connected in series with the plate load resistance having the following circuit parameters, with a view to study its behaviour for different values of K involving changes in L and also R as discussed above.

Tube : 6AK5

Plate load R : $2K\Omega$

Inductance : $20\mu H$

HT supply : 200V.

The equivalent shunt capacity with the measuring aids connected to the corresponding points was approximately equal to $30pF$ of which the input capacitance of the measuring probe was $8pF$. The input rectangular pulses were fed from Marconi Video Oscillator (TF885 A/1). The parameter K ($= \frac{4L}{CR^2}$) was

varied by varying L alone and the output waveform was examined on the calibrated pulse oscilloscope, Tektronix type 541. It was observed that with increase in the value of K from zero to unity (monotonic condition), effected by varying L from zero to $30\mu H (= CR^2/4)$ the risetime improved i.e. decreased uniformly, the steady state gain remaining constant; with further increase in the value of K risetime was still reduced but overshoot appeared.

When the inductance was further increased to $60\mu H$, keeping $R = 2K \Omega$ i. e. $K (= \frac{4L}{CR^2}) = 2$, the observed overshoot was approximately 6% whereas from the graph it was 6.7%. Now K was increased by decreasing R in steps. It was found that the risetime was reduced and the steady state gain began to fall. For large values of K with small values of R the output approximated a damped oscillation and the steady state gain approached zero. Under this condition the risetime, which is the time for a quarter cycle of oscillation is given by $\pi/2\sqrt{LC}$. Upto a value of $K=2.5$ there is a rapid improvement in the risetime with very little loss in steady state gain, thus resulting in a minimum value of T_m/G for this value of K . This value of K corresponds to about 13% overshoot and if that is tolerable (which is normally the case), pulse amplifiers can be conveniently designed with $K = 2.5$. With further increase in the value of K , loss of gain becomes more rapid than improvement in risetime, thus resulting in increased values of T_m/G (figure 5).

DESIGN EXAMPLE

Suppose we want to design a single stage pulse amplifier with a vacuum tube type 6Ak5 having $gm = 5 \text{ mA/V}$. The unavoidable shunt capacity C at the under practical conditions is, say, $30pF$. Let the tolerable overshoot (S) in the amplifier be 12.5%. Referring to figure 4, we find $K = 2.5$ for this value of S . From figure 5 we then have, for $K = 2.5$,

$$\frac{T_m}{G} \times \frac{2g_m}{C} = 4.6$$

Thus we see that the value of K automatically fixes up the T_m/G ratio, for a given value of g_m/C .

For the operating conditions specified above we get

$$\frac{T_m}{G} = 1.38 \times 10^{-8}$$

Now if we specify G , T_m will be fixed up and vice versa. If the desired gain is 10, the risetime becomes

$$T_m = 1.38 \times 10^{-7}$$

If permissible risetime is less than $0.138 \mu \text{ sec.}$, the value of G will be correspondingly reduced, keeping $T_m/G = 1.38 \times 10^{-8}$.

For $G = 10$ we have $R = 2000$ ohms. Substituting this value of R in the eqn. $\frac{L}{R^2} = K \cdot \frac{C}{4}$, we get $L = 75\mu H$. If, on the other hand, the permissible value of T_m is $0.1\mu\text{sec}$, G comes to be 7.24 and $R = 1488$ ohms, which in turn gives $L = 41.43\mu H$.

Experiments were carried out with a shunt compensated amplifier as discussed above, the input rectangular pulse being obtained from a pulse generator. The output was observed on a calibrated pulse oscilloscope.

Observations carried out with $R = 2000$ ohms, $L = 75\mu H$ and $C = 30 pF$ gave $T_m = 0.15\mu\text{ sec}$, gain 9.2 and $S = 12\%$ approximately.

The experiment was further varied by connecting a $10pF$ condenser between anode and ground of the 6Ak5 tube in the amplifier and thereby making the total shunt capacity $40 pF$. With the same overshoot and gain i.e. $K = 2.5$ and $G = 10$, since $\frac{T_m}{G} \times \frac{2g_m}{C} = 4.6$, we have for the operating conditions specified above $\frac{T_m}{G} = 1.84 \times 10^{-8}$ or $T_m = 1.84 \times 10^{-7}$ sec. with $G = 10$. Actual observations carried out with $R = 2000$ ohms, $L = 100\mu H$ and $C = 40pF$ gave $T_m = 0.2 \mu\text{sec}$, gain 9.4 and $S = 12\%$ approximately.

The above design example refers to a single stage pulse amplifier. If the desired gain for a given overshoot is higher than that obtainable with a single tube the number of stages must have to be increased.

From the expression deduced above we have $\frac{T_m}{G} = \frac{C}{2g_m} \times \text{some factor specified by the overshoot}$. Hence for same overshoot using same tube, higher gain will automatically increase T_m to keep $\frac{T_m}{G}$ a constant. Now if T_m is to be reduced $\frac{g_m}{C}$ should be increased, which can be done by arranging the tubes in such a way that only the g_m of individual tubes are added and not their shunt capacitances. This again can be done by arranging the tubes to form a distributed amplifier.

APPENDIX: A

It is shown before that the mutual impedance of the high frequency equivalent circuit of the shunt compensated amplifier is given by

$$Z_m = \frac{(R + pL) \times \frac{1}{pC}}{R + pL + \frac{1}{pC}}$$

$$\text{or } |Z_m| = R \sqrt{\frac{1 + \frac{\omega^2 L^2}{R^2}}{(1 - \omega^2 LC)^2 + \omega^2 C^2 R^2}}$$

A_H (high frequency amplification)

$$\begin{aligned} &= g_m \cdot |Z_m| = g_m R \sqrt{\frac{1 + \frac{\omega^2 L^2}{R^2}}{(1 - \omega^2 LC)^2 + \omega^2 C^2 R^2}} \\ &= A_r \sqrt{\frac{1 + \frac{\omega^2 L^2}{R^2}}{(1 - \omega^2 LC)^2 + \omega^2 C^2 R^2}} \\ &= A_r \cdot f(\omega) \end{aligned}$$

Where A_r = the mid. frequency gain.

Now to get the peak in the frequency response curve i.e. the maximum value of $|Z_m|$ we are to satisfy the conditions

$$\frac{d}{d\omega} f(\omega) = 0$$

and

$$\frac{d^2}{d^2\omega^2} f(\omega) = \text{negative}$$

Satisfying the above two conditions we get

$$\omega^2 = \frac{\sqrt{2LCR^2 + L^2}}{L^2C} - \frac{R^2}{L^2}$$

Expressing ω^2 in terms of K , we have

$$\omega^2 = \frac{2}{LC} \left[\sqrt{\frac{2}{K} + \frac{1}{4}} - \frac{2}{K} \right]$$

From this expression we get for ω to be real and positive

$$\text{Or } K^2 + 8K - 16 > 0$$

$$\text{Or } K > 4 \cdot (\sqrt{2} - 1)$$

That is, the frequency response characteristic will show a peak only for values of $K > 4(\sqrt{2}-1)$. Thus, it is seen that although the transient response shows a peak (overshoot) as soon as the amplifier load circuit becomes underdamped ($K > 1$), the steady state response (frequency response) shows a peak only when $|Z_m|$ exceeds R . i.e. $K > 1.656$.

In order that $|Z_m| > R$ at some values of f , K must be greater than $[4(\sqrt{2}-1)]$. For value of K lying between unity and $[4(\sqrt{2}-1)]$, there will be no peak in the

frequency response characteristic although overshoots will occur for pulse amplification. Thus we see that to construct a pulse amplifier, a knowledge of transient response is more important than its steady state response. As such a design procedure directly based on the transient response, as done here, will be of much use.

APPENDIX : B

The above discussions are all valid if the Power Supply impedance is zero. But practical power supplies are not perfectly regulated and hence, the resulting internal impedance will modify the load impedance of the amplifier. The shift in the pole-zero location depends upon the nature and magnitude of the impedance. The equivalent circuit of the amplifier with the power supply impedance is shown and its effects on the response are discussed. It may be mentioned that if the power supply has a resistive impedance then its effect can be minimised by connecting a large condenser across the power supply. In any case the power supply source can be made to behave as a source of practically zero impedance by using an R - C filter consisting of a resistance in series with and a condenser across the supply. The power supply with its internal impedance Z_{bb} is shown in figure 6. If the source impedance is reactive the shunt condenser across the source has some peculiar effects on the load impedance characteristics and hence on pulse response, as discussed below :

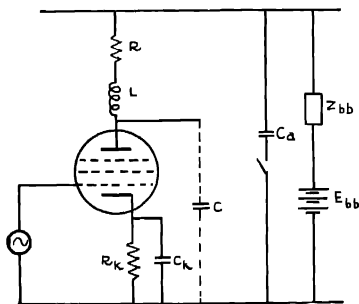


Fig. 6.

(1) *Internal impedance is capacitive.*

When the condenser is connected across the power supply, the effective inductance is reduced,

$\therefore K$ is reduced, and hence overshoot is decreased and risetime is increased.

(2) *Internal impedance is inductive:*

We know if the power supply impedance is zero, the load impedance approaches $\frac{1}{\omega C}$ (C = the total shunt capacity), but when the power supply impedance is inductive, it can be shown that as the power supply is shorted by a condenser, magnitude of the load impedance passes alternately through a maximum followed by a minimum and a maximum before the impedance approaches $\frac{1}{\omega C}$ at the high frequency. This is obvious from the equivalent circuit of the load impedance together with the inductive internal impedance of the power supply,

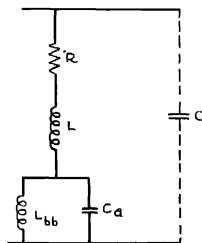


Fig. 7 The equivalent circuit with inductive internal impedance of the power supply.

figure 7. Since it is a minimum phase-shift type of network, the imaginary part of the complex impedance also changes from inductive to capacitive nature along with the impedance variation. Thus the zero-pole location changes and hence overshoot, risetime etc., are also modified accordingly.

Experimental observations revealed the fact that the power supply had inductive impedance, and hence the response was modified when a condenser was connected across the power supply, as explained above. Now, since, in the case of inductive internal impedance if the capacitance across the power supply

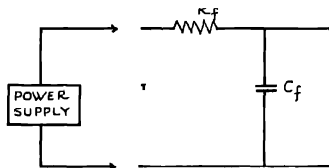


Fig. 8. R - C filter

is not very large, the internal impedance of power supply instead of being zero becomes more complicated. It is found that an *R-C* filter as shown in figure 8 will give better performance.

CONCLUSION

In this article we have defined risetime to be equal to the time required to reach the peak and not as time required to reach 10% to 90% of the final value. Hence in actual practice the risetime according to the conventional definition will be less than the calculated value.

ACKNOWLEDGMENTS

I am grateful to Prof. H. Rakshit, D.Sc., F.N.I., Head of the Department of Electronics and Electrical Communication Engineering, Indian Institute of Technology, Kharagpur, for his constant guidance and to Prof. B. Chatterjee for his helpful suggestions.

REFERENCES

- Gupta Sarma, D., 1954, *Wireless Engineer*, **31**, 327.
Martin, T. L. Jr., 1955, *Electronic Circuits*, Prentice Hall, Inc.

ON POLARISED ELECTRONIC SPECTRUM OF SINGLE CRYSTAL OF PARADIBROMOBENZENE AT -180°C^*

T. N. MISRA

OPTICS DEPARTMENT, INDIAN ASSOCIATION FOR THE CULTIVATION OF
SCIENCE, CALCUTTA 32.

(Received for publication, March 14, 1959)

PLATE V

ABSTRACT. The polarisation of the ultraviolet absorption spectra of very thin single crystals of paradibromobenzene at -180°C has been studied by photographing simultaneously the two components with the light vector parallel to *b*- and *c*-axes respectively. It has been observed that although the bands due to $0 \rightarrow v$ transitions are sharp in both the components, the 0, 0 band is sharp only in the *c*-axis spectrum, but in the *b*-axis spectrum it has a triplet structure. The two new bands adjacent to the central 0, 0 band have been assigned to an intermolecular vibration of frequency about 48 cm^{-1} which is coupled to the electronic transition only in the *b*-axis spectrum.

The intensity ratio of the *b*-axis and *c*-axis spectra calculated from the crystallographic data given by Croatto *et al* on the assumption that the transition is a short-axis one, agrees with the observed value. Hence the orientations of the molecules in the lattice as given by Croatto *et al* are correct. The expected Davydov-splitting has been calculated and found to be 15 cm^{-1} , but the poor dispersion of the spectrograph used did not allow the detection of such a small splitting.

INTRODUCTION

The polarised electronic spectrum of single crystal of paradichlorobenzene was recently studied by Sirkar and Misra (1959) and the nature of the spectrum was found to be different from that observed by Craig and Hobbins (1955) in the case of anthracene. It was observed that absorption is much stronger when the light vector is along the *b*-axis of the crystal than that observed with the light vector parallel to the *c*-axis of the crystal. An intermolecular vibration of frequency 53 cm^{-1} is found to be coupled with the 0,0 band in the former spectrum, hereinafter called the *b*-axis spectrum, but no such coupling takes place when the light vector is almost perpendicular to the molecular plane in the latter spectrum. It was further observed that some $0 \rightarrow v$ transitions observed in vapour are absent in the *c*-axis spectrum but they are present in the *b*-axis spectrum. It was also pointed out that the splitting of the two components calculated on

* Communicated by Prof. S. C. Sirkar.

Davydov's theory (1948) was found to be 22 cm^{-1} , but such a splitting could not be observed.

The crystal of paradibromobenzene belongs to the monoclinic system with two molecules per unit cell and according to Croatto *et al* (1954) it has a structure identical with that of paradichlorobenzene. Also, the crystal structure remains unchanged at -180°C (Krishnamurti, 1959, unpublished work.). So in this case also splitting on Davydov's theory could be easily calculated and verified experimentally.

The study of polarised spectrum of single crystal of paradibromobenzene would be helpful in ascertaining the orientation of the molecules in the lattice and also in finding out the influence of intermolecular forces on the electronic transitions in molecules fixed in crystal lattice. So, the study of polarised electronic spectra of single crystals of *p*-dibromobenzene was undertaken and the results are discussed in this paper.

EXPERIMENTAL

Very thin single crystals of *p*-dibromobenzene were prepared from solution in distilled acetone at room temperature. Larger surface area of the crystallizing basin and very slow rate of evaporation gave crystals of larger size. X-ray rotation photographs were taken for some of the crystals and in all cases, they were found to be developed as thin plates with the *bc*-plane elongated along *c*-axis, the *b*-axis lying along the width of the crystal plate. The primitive translation along *c*-axis was found to be 4.11\AA . According to Croatto *et al* (1949) the long axis of the molecule is nearly in the *ab*-plane taking the same general direction as the *a*-axis. The plane of the molecule is tilted with respect to the axial planes to a degree that gives the usual intermolecular separations. The experimental set up was the same as used in an earlier investigation (Sirkar and Misra, 1959). The crystal was mounted with its *c*-axis vertical and the *bc*-face normal to the incident light between two fused silica discs in a brass frame the lower portion of which was immersed in liquid oxygen contained in a Dewar vessel of fused silica.

Spectrograms were taken on Ilford HP3 films with Hilger E1 quartz spectrograph having a dispersion 3\AA per mm in the region 2600\AA .

Microphotometric records of the spectra were taken with a Kipp and Zonen type self-recording microphotometer. The wavelength of the bands were measured by the method discussed in the earlier paper (Sirkar and Misra, 1959). The dispersion in the record was about 2\AA or 24 cm^{-1} per mm in the region 2800\AA .

RESULTS

Assignment of bands :

The vertical and the horizontal components of the polarised electronic absorption spectrum of *p*-dibromobenzene are reproduced in figure 1 and the

microphotometric records of the bands are shown in figure 2, Plate V. The frequencies of the bands in the two components and their intensities are given in Table I.

The frequencies of the bands due to vapour reported by earlier workers are also included in the table.

TABLE I

Polarised absorption bands of *p*-dibromobenzene at -180°C

Vapour (Sroerama-murty, 1951)		Light vector parallel to c-axis		Light vector parallel to b-axis	
ν in cm^{-1}	Assignment	ν in cm^{-1}	Assignment	ν in cm^{-1}	Assignment
				35391 w	$\nu_0 - 48$
35643 s	0, 0 (ν_0)	35438 vs	0, 0 (ν_0)	35438 vs	0, 0 (ν_0)
				35486 w	$\nu_0 + 47$
				35639 m	$\nu_0 + 201$
		35768 m	$\nu_0 + 330$	35770 ms	$\nu_0 + 332$
36113 ms	$\nu_0 + 470$	36022 ms	$\nu_0 + 584$	36024 ms	$\nu_0 + 586$
36320 ms	$\nu_0 + 677$	36157 m	$\nu_0 + 719$	36158 ms	$\nu_0 + 720$
36657 m	$\nu_0 + 1014$	36458 s	$\nu_0 + 1020$	36458 m	$\nu_0 + 1020$
36787 w	$\nu_0 + 677 + 470$	36679 m	$\nu_0 + 1241$	36679 m	$\nu_0 + 1241$
37071 m	$\nu_0 + 1449 - 21$	36922 m	$\nu_0 + 1484$		
37092 m	$\nu_0 + 1449$	37039 w	$\nu_0 + 1020 + 581$		
		37177 w	$\nu_0 + 1020 + 719$		
37660 w	$\nu_0 + 2 \times 1014$	37478 s	$\nu_0 + 2 \times 1020$		
37761 vw	$\nu_0 + 1449 + 677$	37700 m	$\nu_0 + 1020 + 1242$		
38106 w	$\nu_0 + 1449 + 1014$	37942 ms	$\nu_0 + 1020 + 1484$		
38299 vw	$\nu_0 + 1449 + 1014 + 200$	38500 s	$\nu_0 + 3 \times 1020$		
		38959 m	$\nu_0 + 2 \times 1019 + 1483$		

It can be seen from figure 2(b) that the 0, 0 band in the horizontal component is broad, but it is sharp in the vertical component; the $0 \rightarrow \nu$ transitions are sharp in both the components.

It is seen from Table I that the bands in two components are approximately in the same position and there is no appreciable shift of any of the components.

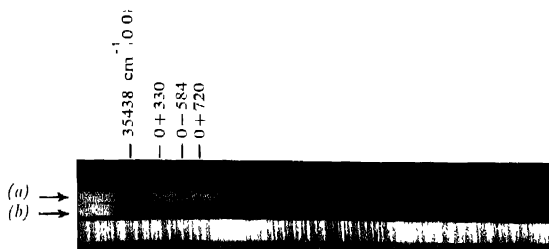


Fig. 1 Polarised electronic spectrum of single crystal of *p*-dibromobenzene at -180°C , with light vector (a) parallel to *c*-axis, (b) parallel to *b*-axis.

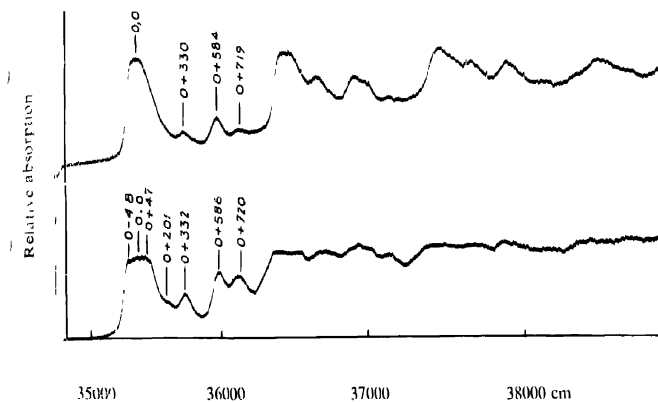


Fig. 2 Microphotometric records of the polarised electronic spectrum of single crystal of *p*-dibromobenzene at -180°C (a) Light vector parallel to *c*-axis (b) Light vector parallel to *b*-axis.

DISCUSSION

It can be seen from figure 2(h) that the structure of the 0,0 band is similar to that observed in the case of paradichlorobenzene with light vector parallel to *b*-axis (*b*-axis spectrum). In this component the 0,0 band has a triplet structure, the distance of the two outer components from the central one being 48 cm^{-1} . These two components can be explained on the assumption that they are due to some intermolecular vibration of frequency 48 cm^{-1} which are coupled with the electronic transition when the light vector is along the *b*-axis of the crystal, but no such coupling takes place when the light vector is along the *c*-axis. The other bands in the *b*-axis spectrum are about three times as strong as the corresponding bands in the *c*-axis spectrum. These bands can be attributed to excited state frequencies 201 cm^{-1} , 332 cm^{-1} , 586 cm^{-1} , 720 cm^{-1} , 1020 cm^{-1} , 1241 cm^{-1} and 1484 cm^{-1} respectively. It was pointed out earlier (Sirkar and Misra, 1959) that this intermolecular vibration is coupled to the electronic transition only when the light vector is almost parallel to the plane of the molecule. So, in the present case also the light vector should be nearly parallel to the molecule when it is parallel to the *b*-axis of the crystal. According to the data reported by Croatto *et al* (1949) the molecular plane is almost parallel to the *ab*-plane. Hence the results of present investigation corroborate the data reported by Croatto *et al* (1949). Incidentally, it may be pointed out here that the study of the polarised electronic spectra is helpful in finding out the orientation of the benzene ring in the crystals of substituted benzenes.

The excited state frequencies 201 cm^{-1} , 330 cm^{-1} , 584 cm^{-1} and 720 cm^{-1} were not observed in the spectrum due to the vapour by Sreeramamurty (1951), but he observed two frequencies 470 cm^{-1} and 677 cm^{-1} in this region. These frequencies do not agree with any of the frequencies mentioned above but the frequency 470 cm^{-1} is approximately the mean of 332 cm^{-1} and 586 cm^{-1} and the other one of 586 cm^{-1} and 720 cm^{-1} . If the latter two bands become a little broader in the spectrum due to the vapour they can merge into one another to form a broad band of mean frequency, but the absence of the band 332 cm^{-1} in the spectrum due to the vapour is difficult to understand.

In the case of paradibromobenzene all the $0 \rightarrow v$ transitions in the *b*-axis spectrum are also present in the *c*-axis spectrum although with much smaller intensity. In the case of paradichlorobenzene, however, some of the bands absent in the vertical component appear in the horizontal component, *i.e.*, when the light vector is almost parallel to the short axis of the molecules (Sirkar and Misra, 1959).

According to Croatto *et al* (1952) paradichlorobenzene and paradibromobenzene are isostructural, but the orientations of the molecules with respect to the crystallographic axes are slightly different in the two cases. Attempts have been made to find out whether the difference in the relative intensities of the two

components of the spectra due to the two crystals is accounted for by this difference in orientation. It was assumed by Sponer (1942) that the electronic transition giving this band system is a short-axis one. The intensity ratios of the *b*-axis and the *c*-axis spectrum were calculated from the crystallographic data of Croatto *et al* (1949) for a short axis transition and it was found to be 3 : 1 for paradibromobenzene and 6 : 1 for paradichlorobenzene. The intensity ratio of the *b*-axis spectrum and *c*-axis spectrum for *p*-dibromobenzene as reproduced in figures 1 and 2 and for *p*-dichlorobenzene as in the previous paper (Sirkar and Misra, 1959) are qualitatively in good agreement with the calculated ratio and Sponer's assignment is shown to be correct.

The agreement between the calculated and the observed intensity ratios for the two spectra supports the crystal structure of the substances and the molecular orientation in the lattice as given by Croatto *et al* (1952).

Davydov Splitting

Using the atomic parameters in the *p*-dibromobenzene crystal lattice given by Croatto *et al* (1949), the angles made by the short and long axes of the molecules with the three crystallographic axes are found to be 62°11', 49°24' and 68° for the short axis and 35°48', 125°45' and 109°40' for the long axis respectively and the values of $A/|M|^2$, $B/|M|^2$, $C/|M|^2$ (A , B , C having significances as before) were found out from the relation

$$J_{lk}/|M|^2 = -\frac{e^2}{(r_{lk})^3} [2 \cos \theta_{l1} \cos \theta_{k1} - \cos \theta_{l2} \cos \theta_{k2} - \cos \theta_{l3} \cos \theta_{k3}]$$

where M is the molecular transition moment in Å unit and r_{lk} is the distance between the centres of the two molecules, θ_{l1} , θ_{l2} , θ_{l3} are the angles made by the transition moment of the l th molecule with a set of rectangular axes erected at its centre; θ_{l1} refers to an axis along the line of the centre of the l th and k th molecule. The values of A , B and C for *p*-dibromobenzene are given in Table II.

TABLE II

Neighbour intermolecular integrals for crystalline *p*-dibromobenzene.

Integral	Long axis transition cm ⁻¹ Å ⁻²	Short axis transition cm ⁻¹ Å ⁻²
$A/ M ^2$	- 62	+ 22
$B/ M ^2$	- 29	-328
$C/ M ^2$	-539	-111

The splitting between the b and c components will be $8C$ and for the short axis transition it comes out to be $-888 |M|^2$ and for long axis transition it will be $-4312 |M|^2$. The negative sign means that the bands in the b -axis spectrum should be shifted towards red relative to those in the c -axis spectrum.

The value of $|M|^2$ was found from the relation (Sklar, 1942)

$$|M|^2 = \frac{3hf}{8\pi^2 m c \nu}$$

where f , the oscillator strength is given by

$$f = 2.3 \times \frac{nc^2 m}{N\pi e^2} \cdot 10^3 \int \epsilon d\nu$$

the notations having usual significances.

The value of $\int \epsilon d\nu$ for the solution of p -dibromobenzene and benzene were reported by Klingstedt (1933). The value of oscillator strength for the migration in the ring in para dibromobenzene molecule was 5.8×10^{-3} and the migrational transition moment $|M|^2$ was calculated and found to be $15.38 \times 10^{-3} \text{Å}^{-2}$.

Hence the splitting expected from Davydov's theory in this case for short axis transition comes out to be 15 cm^{-1} and for long axis transition this value should be 66 cm^{-1} . As in the case of p -dichlorobenzene this band system is due to short axis transition.

From the spectrogram and the microphotometric record it is seen that there is no appreciable shift of the band in the b -axis spectrum from the corresponding bands in the c -axis spectrum. Hence the splitting of 15 cm^{-1} is not observed probably because the dispersion of the spectrograph is too small to allow detection of such a small splitting.

ACKNOWLEDGMENT

The author is indebted to Professor S. C. Sirkar, D.Sc., F.N.I., for his kind interest and constant guidance throughout the progress of the work.

REFERENCES

- Craig, D. P. and Hobbins, P. C., 1955, *J. Chem. Soc.*, 539.
 Croutto, U. and Bezzi, S., 1949, *Gazz. Chim. Ital.*, **79**, 240.
 Croatto, U., Bezzi, S. and Bus, E., 1952, *Acta. Cryst.*, **5**, 825.
 Davydov, A. S., 1948, *Zhur ekspl'ti teor Fiz.*, **18**, 210.
 Klingstedt, F. W., 1933, *Ziet. Physik Chemie.*, **B20**, 133.
 Sirkar, S. C. and Misra, T. N., 1959, *Ind. J. Phys.*, **33**, 45.
 Sklar, A. L., 1942, *Rev. Mod. Phys.*, **14**, 232.
 Sponer, H., 1942, *Rev. Mod. Phys.*, **14**, 229.
 Sreeramamurty, C., 1951, *Current Science*, **20**, 176.

Letters to the Editor

The Board of Editors will not hold itself responsible for opinions expressed in the letters published in this section. The notes containing reports of new work communicated for this section should not contain many figures and should not exceed 500 words in length. The contributions must reach the Assistant Editor not later than the 15th of the second month preceding that of the issue in which the paper is to appear. No proof will be sent to the authors.

2

EFFECT OF CHEMICAL TREATMENT ON THE STRUCTURE AND PROPERTIES OF GRAPHITE

S. RAY

DEPARTMENT OF MAGNETISM INDIAN ASSOCIATION FOR THE CULTIVATION OF
SCIENCE, CALCUTTA 32

(Received for publication, May 10, 1959)

Plate VI

In view of the looseness of binding between the different layers of the crystals of graphite, the usual practice (Primak and Fuchs, 1954, Soule, 1958) of purifying the natural crystals of graphite by treating them with hydrofluoric and hydrochloric acids and drying them by heating before measuring their electrical properties may naturally be expected to cause a certain amount of disturbance in the structure and possibly in the electrical resistivities along the hexagonal axis also (as in the case of magnetic properties of graphite after treatment with H_2SO_4 , HNO_3 , $KClO_3$; Ganguly, 1936). Such purificatory treatments may therefore be objectionable from the point of view of studying the properties of single crystals of graphite. We, in consequence, undertook to detect the presence, if any, of such structural changes by means of X-rays.

Rotation photographs about a binary axis of naturally occurring crystals of graphite were taken using filtered copper radiation. The crystals were then treated with strong hydrofluoric acid, washed with water, then treated with strong hydrochloric acid, again washed in running water for a long time, and finally dried in a vacuum oven. Rotation photographs were then taken again as before. (Figures 1(a) & (b) (Plate VI) show the effect of these treatments on a particular crystal of graphite. In the case of untreated crystal it is seen that the spots corresponding to the reflections from the basal planes (0002 and 0004) appear, as is usual with naturally occurring graphite, a little drawn out, due evidently to the presence of a small amount of randomness in the arrangement of the crystal

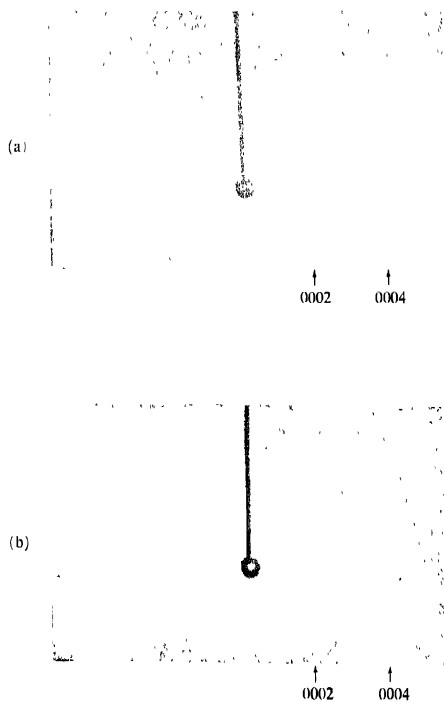


Fig. 1.—Rotation photographs about a -axis of a natural crystal of graphite
(a) Before chemical treatment. (b) After chemical treatment.
(The superposed Debye-Scherrer pattern is due to aluminium powder sprinkled on the crystal).

counter which detects the positrons, then assuming that all the positrons are counted we can write for the beta-1.28 coincidences

$$N_{\beta^+, 1.28} = N_0 f_+ \sigma_{1.28} = a$$

and for the gamma ray

$$N_{1.28} = N_0 \sigma_{1.28} = b$$

where N_0 is the transition rate,

f_+ = the fraction of decays by positron emission

and $\sigma_{1.28}$ = the efficiency for detecting the 1.28 MeV gamma ray. The ratio of a to b then yields f_+ , from which the e/β^+ ratio can be computed. This is possible provided the entire positron spectrum can be measured.

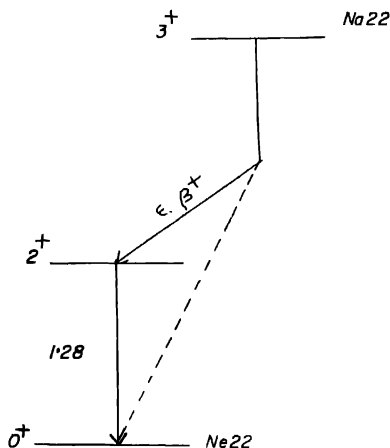


Fig. 1. Decay Scheme of Na-22

We have employed a 4π plastic scintillation counter for detecting the positrons and a NaI(Tl) counter for the 1.28 MeV gamma ray. The gamma counter is biased to accept only the photopeak. The effectiveness of the 4π plastic scintillation counter for measuring the shapes of beta spectra has been demonstrated by the work of Johnson *et al* (1956) and more recently by Robinson and Langer (1958), and is substantiated by the present experiments.

A Na-22 source from a HCl solution was evaporated on a 0.0001" mylar foil and covered with a similar foil. The 4π counter was formed in the following way. Two plastic cylinders, each 3mm thick and 1 cm in diameter were chosen. One of the cylinders had a depression 1/2 mm deep and 1/2 cm in diameter. The Na-22 sandwich was placed in the depression. The two cylinders were pressed

together to form the 4π counter. A cone-shaped light pipe 1-1/2" long having a well at the apex was mounted on a DuMont 6292 phototube. To the bottom of the well the 4π plastic scintillation crystal was cemented by means of Canada balsam. The sides of the well had been painted white to ensure good light collection. The top of the well had a thin aluminium foil whitened inside. The gamma counter was a 2" cube NaI(Tl) crystal which had a resolution of 11% for 0.661 MeV gamma ray of Cs-137. The 4π counter had a resolution of 16% for the 0.624 MeV *K*-conversion line of Cs-137. The entire assembly of crystal and counters was surrounded by 2" of lead at 4".

EXPERIMENTAL

The general features of the 4π counter were investigated by a P-32 source using plastic cylinders, each 5mm thick and 1 cm in diameter. A Fermi plot of

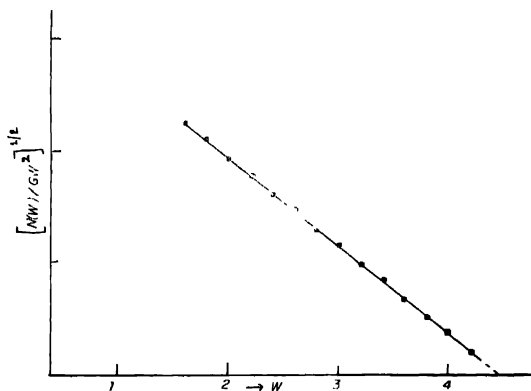


Fig. 2. Fermi plot of P-32 spectrum taken with a 4π plastic scintillation spectrometer. Note the end-point at 1.72 MeV.

the spectrum is shown in figure 2. An end-point of 1.72 MeV is indicated, in good agreement with the value in the literature (King, 1954). Experiments on Na-22 were started with plastics of dimensions described in the Introduction. The gamma counter was set on the photopeak of the 1.28 MeV gamma ray. The peak had a width of 3.5 volts at 35 volts. This was used to gate the 20-channel analyzer. The positron spectrum coincident with the 1.28 MeV gamma ray is shown in figure 3. Energy calibration of the spectrometer was obtained by using external gamma rays of Na-22 (0.511 MeV), and Cs-137 (0.661 MeV). The Compton edges located at 3/4 of the maximum were used. The calibration is also shown in figure 3(c). The calibration curve intercepted the axis corresponding to zero pulse height at 18 KeV in agreement with similar observations by Johnson *et al* (1956).

Because of the fact that the plastic chosen had dimensions somewhat greater than the range of positrons, one would expect that the observed beta spectrum

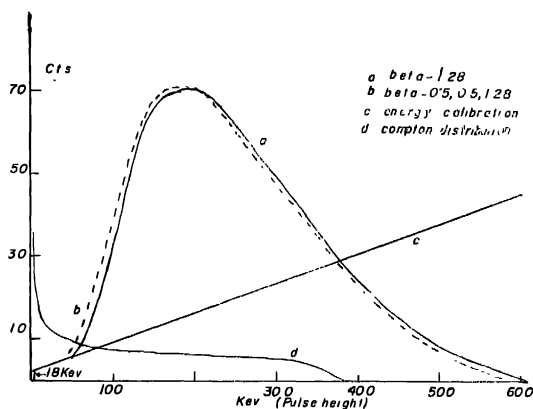


Fig. 3.

- (a) Continuous curve—beta spectrum of Na-22 in 4π plastic counter coincident with the 1.28 MeV gamma ray.
- (b) Dotted curve—beta spectrum of Na-22 in triple coincidence with the 1.28 MeV gamma ray and the two annihilation quanta. The spectrum is normalized to the doubles spectrum (beta-1.28*) above 50 KeV to 1/10%.
- (c) Energy calibration of the 4π plastic counter using Compton edges of 0.511 (Na-22) and 0.661 (Cs-137) MeV.
- (d) Compton distribution of Na-22 gamma rays in 4π plastic counter (with positrons completely stopped by lucite) coincident with the annihilation radiation and the 1.28 MeV gamma ray.

may not be the correct one, but somewhat distorted by the simultaneous detection of a beta particle and its associated Compton electron. Thus the effect would be qualitatively to shift the spectrum towards higher energy, without changing the area under the spectrum.

In order, therefore, to obtain the undistorted spectrum, the beta spectrum was measured in triple coincidence with the 1.28 MeV gamma ray and the two annihilation quanta. The experimental arrangement and a functional diagram of the electronic circuitry are shown in figure 4. Pulses from the two 0.511 MeV counters and the 1.28 MeV counter were fed to a triple coincidence circuit, whose output was used to gate the 20-channel analyzer. The positron spectrum gated by the triples is shown also in figure 3, normalized to the doubles spectrum beyond 50 KeV. The statistical error for each point on the triples spectrum varied from 2 to 4%. The doubles and the triples spectra are indeed displaced as expected. To obtain a quantitative justification for the spectral displacement, the positrons

were completely stopped in just enough lucite and the Compton distribution was obtained in coincidence with the annihilation radiation and the 1.28 MeV gamma ray. The spectrum thus obtained is shown as curve *d* in figure 3 and is seen to be similar to the one that is obtained using an external source except for the absence of edge effects.

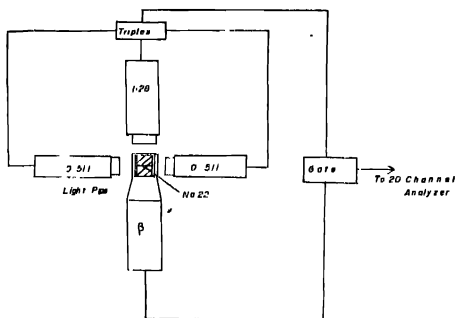


Fig. 4. Block diagram of experimental set-up for Na-22 studies.

If the assertion that the effect of the Compton distribution due to annihilation radiation is simply to shift the doubles spectrum is indeed correct, then it must be possible to express the doubles spectrum $d(h)$ in terms of the triples spectrum $t(h')$, and the Compton distribution $C(h-h')$. In other words, we should be able to write

$$d(h) = \sum^n t(h') C(h-h')h.$$

A numerical calculation was carried out to test this assumption. For an assumed Compton of 6% the agreement from point to point was 3-4%. The assumption of 6% is not inconsistent with the dimensions of the plastic and the Compton cross-section (the choice of 6% is not critical, since the triples spectrum itself was known to 2-4%). The agreement thus obtained provides quantitative justification for the assertion made earlier. It must be pointed out in this connection that the effect of the inner bremsstrahlung is to displace the true spectrum in a direction opposite to that due to the Compton distribution but because of the weakness of the effect, the Compton effect predominates. The preservation of areas under the doubles and triples spectra is indicated by the fact that the two areas could be normalized to within 1/10%.

Since the lowest energy observed was around 40 KeV, an extrapolation of the spectrum to zero energy has to be made in order to obtain the area under the whole beta spectrum. To do this, the following procedure was adopted. The ideal

Fermi spectrum corrected for screening was plotted. The spectrum was distorted for finite resolution at various points of the spectrum by folding in a gaussian of the proper width. The assumption was made that the half-width varied as the square root of the energy over the entire energy range. Choosing various energies (designated as h_{min}), the area to the right of h_{min} was obtained. It was determined that below 50 KeV the area under the beta-spectrum with and without resolution correction differed only by 1/10% and amounted to 5.3% of the area under the beta-spectrum beyond 50 KeV. Thus the area under the ideal Fermi distribution was taken as the correct area. This when added to the area due to the remaining portion of the doubles spectrum (which had been corrected by the Compton distribution to get the undisplaced spectrum) would give the total area.

In order to test for any possible systematic errors the ratio of area to the right of h_{min} and the entire area from 50 KeV upto the maximum energy was plotted as a function of h_{min} both for the ideal Fermi spectrum corrected for finite resolution, and the actual doubles beta spectrum corrected to the triples spectrum. The result is displayed in figure 5. It is observed that the data of three different runs

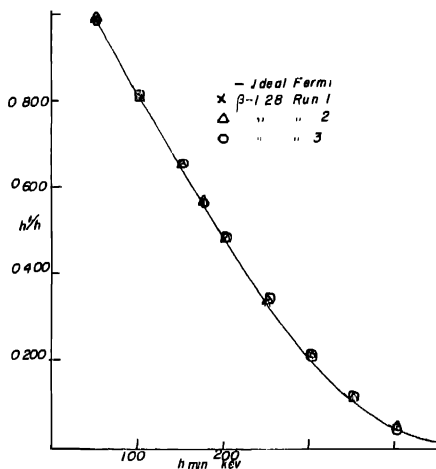


Fig. 5. Study of systematic errors in the Na-22 experiment.

are consistent within themselves to 1-1/2% and with the theoretical plot to within 1%. This may be taken as evidence for the absence of any systematic errors.

The experiments were repeated with and without shielding. The effect of channel width on the gamma ray side was next studied. A different source was

made and the experiments repeated. In each case consistent results were obtained. Throughout the course of the experiments the counters were periodically checked. The energy calibration of the beta spectrometer was carried out before and after each run. The overall statistical error in the double run was 1/10 to 2/10%. Altogether seven runs were made.

RESULTS

The data from six of the runs are assembled in Table I together with explanation. The average value of f_+ is calculated to be 0.899 ± 0.003 . This yields an average ϵ/β^+ ratio of 0.112 ± 0.004 .

Apart from statistical error, the other uncertainty is due to the folding of the Compton distribution, and in the estimation of the areas under the beta and gamma spectrum. A calculation was made to see how much error would be introduced if the half-width of the gaussian curve deviated from obeying the \sqrt{E} law. Dependences proportional to $E^{0.4}$ and $E^{0.6}$ were investigated. From this it was concluded that the error introduced is less than 1/10% in the final result.

Finally an error in the determination of the end-point of the positron spectrum would introduce an error in the value of h_{mn} . Because of the assumed linearity in energy scale, this would tend to introduce a linear systematic error (as distinguished from any due to the apparatus itself). In Table 2 the end-points are tabulated for various runs together with uncertainties. From this table the systematic error introduced in this way is estimated to be less than 1.2%. Thus allowing for this our ϵ/β^+ ratio would at worst become

$$\epsilon/\beta^+ = 0.112 \pm 0.005$$

resulting in the Fierz term (see Discussion)

$$b_G = -0.004 \pm 0.013.$$

DISCUSSION

The computed value of ϵ/β^+ is somewhat better than that of Sherr and Miller. The theoretical value of ϵ/β^+ is 0.1135 ± 0.0020 , when corrected for screening and 6.5% L-capture (Rose and Jackson, 1949). The value of $\langle W^{-1} \rangle$ for $W = 2.061$ for Na-22 is 0.7. The Fierz term is computed from the expression

$$b_{GT} = \frac{R/R_0 - 1}{2[1 + R/R_0 \langle W^{-1} \rangle]} = -0.004 \pm 0.012.$$

Na-22 is perhaps the ideal case for determining the Fierz term because of the low Z involved. It is very unfortunate that the end-point of the positron spectrum is not known well enough to attempt any further refinement in experimental

TABLE I

 Na^{22} (Data)

Run No.	Conditions	(a)	(b)	(c)	(d)
		$\beta +,$ 1.28 (> 50 kev)	$\beta +,$ 1.28 (> 0 kev)	$N_{1.28}$ cps	$f_+ = (h)/(c)$
Source No. 1	1. 2" of Pb shield at 4". γ -ray ch. width=3.5 volts	64.08 \pm 0.18	67.48 \pm 0.19	75.21 \pm 0.11	0.898 \pm 0.003
	2. No shield. ch. width=3.5 volts	64.23 \pm 0.19	67.63 \pm 0.20	75.24 \pm 0.15	0.900 \pm 0.003
	3. No shield ch. width=3 volts	57.82 \pm 0.22	60.88 \pm 0.23	67.76 \pm 0.15	0.899 \pm 0.004
	4. 2" of Pb shield at 4". γ -ray ch. width=3.5 volts	48.31 \pm 0.14	50.87 \pm 0.15	56.52 \pm 0.10	0.900 \pm 0.003
No. 2	5. No shield ch. width=3.5 volts	48.07 \pm 0.17	50.62 \pm 0.18	56.31 \pm 0.11	0.899 \pm 0.004
	6. No shield ch. width=3 volts	42.78 \pm 0.13	45.05 \pm 0.14	50.11 \pm 0.10	0.899 \pm 0.003
$\epsilon = 1 - f_+ = 0.101 \pm 0.003$				Average value of	
$\therefore \epsilon/\beta^+ = \frac{0.101 \pm 0.003}{8/899 \pm 0.003} = 0.112 \pm 0.004$				$f_+ = 0.899 \pm 0.003$	

TABLE II

End-point energies of positron spectrum

Run No	End-point (keV)
1	546 \pm 11
2	541 \pm 10
3	548 \pm 11
4	539 \pm 10
5	540 \pm 10
6	544 \pm 11

TABLE III

Summary of results on Fierz term

Nucleus	Transition	W_0	b_{GT}	Reference
Ga-68	$1^+ \rightarrow 2^+$	4.70	-0.03 ± 0.02	Ramaswamy, 1959
Co-58	$2^+ \rightarrow 2^+$	1.024	-0.004 ± 0.014	„, 1958
Na-22	$3^+ \rightarrow 2^+$	2.061	-0.004 ± 0.012	present work

techniques to measure ϵ/β^+ ratio. In any case it has been demonstrated that the plastic scintillation counter can be effectively used in the study of beta spectra and precision results obtained if analyzed with caution.

CONCLUSIONS

A reinvestigation of the electron capture to positron branching ratio in the decay of Na-22 has been made with somewhat greater precision than has been possible before, using a 4π plastic scintillator and a gamma counter in conjunction with double and triple coincidence techniques. The result for ϵ/β^+ ratio is 0.112 ± 0.004 . It is suggested that the beta spectrum end-point be measured with greater precision to make much more meaningful estimates of the Fierz term. It would be further of interest to measure K/β^+ ratios in unique forbidden transitions allowed only by Gamow-Teller selection rules.

ACKNOWLEDGMENTS

The author wishes to thank Professor L. Madansky for valuable suggestions and illuminating discussions.

APPENDIX

SUMMARY OF FIERZ INTERFERENCE IN BETA DECAY

In this section the conclusions regarding the status of Fierz interference in Gamow-Teller transitions as indicated by our measurements reported here and elsewhere are summarised (Table III).

Gerhart (Gerhart, 1958) has made an excellent analysis of Fierz interference in Fermi transitions and concludes $b_F = 0.00 \pm 0.12$. A brief review of Fierz interference in beta-decay has been recently given by the author (Ramaswamy, 1959). From Table 3 one sees that the best evidence for the smallness of the Fierz term in G-T interaction comes from Na-22. Konijn *et al* have summarized data regarding the Fierz term as determined by the K/β^+ ratio technique. They conclude that $b_{GT} = -0.007 \pm 0.010$.

From evidence presented above and from Gerhart's analysis one can conclude that the Fierz term in allowed transitions is practically zero. Before parity nonconservation was discovered the Fierz term in G-T transition could be expressed as

$$b_{GT} = -\frac{C_A^* C_T}{|C_A|^2 + |C_T|^2}$$

The smallness of b could be interpreted as implying that C_A/C_T or C_T/C_A was small. With the discovery that parity is not conserved in beta-decay, the definition of b has acquired the extended form

$$b_T = \frac{\text{Re}(C_A C_T^* + C_A' C_T'^*)}{|C_A|^2 + |C_T|^2 + |C_A'|^2 + |C_T'|^2}$$

where

C_A, C_T are the parity conserving and

C_A', C_T' are the parity non-conserving coupling constants.

The *s denote complex conjugation resulting from a possible violation of time reversal invariance.

With the new definition of b , the smallness of b means

$$\text{Re}(C_A C_T^* + C_A' C_T'^*) = 0.$$

This implies that

$$\frac{C_A'}{C_A} = - \frac{C_T'^*}{C_T^*}$$

Nothing more can be said concerning the coupling constants unless the relation between the parity conserving and non-conserving coupling constants is known. It is now established from electron polarization measurements on pure Gamow-Teller transitions that $C_A/C_A' \simeq -1$

Thus the parity conserving and non-conserving coupling constants seem to have about the same strength. The loss of definitiveness of the Fierz term is one of the consequences of the discovery of parity non-conservation.

REFERENCES

- Gerhart, J. B., 1958, *Phys. Rev.*, **110**, 897.
 Gertrude Goldhaber, 1953, **90**, 587.
 Johnson, Johnson and Langer, 1956, *Phys. Rev.*, **102**, 1142.
 King, R. W., 1954, *Revs. Mod. Phys.*, **26**, 327.
 Konijn, van Nooijen, Hagedoorn and Wapstra, 1959, *Nuclear Phys.*, **9**, 296.
 Mack, J. E., 1950, *Revs. Mod. Phys.*, **22** 64.
 Ramaswamy, M. K., 1959, *Nuclear Physics* **10**, 205.
 Ramaswamy, M. K., 1958, *Bull. Am. Phys. Soc.*, **2**, 3, 357.
 Ph.D. Dissertation, Johns Hopkins University, 1959 (unpublished).
 Ramaswamy, M. K., 1959, submitted to *Current Science*.
 Robinson, R. L., and Langer, L. M., 1958, *Phys. Rev.*, **109**, 1255.
 Rose, M. E. and Jackson, J., 1949, *Phys. Rev.*, **76**, 1540.
 Sherr, R. and Miller, R. H., 1954, **93**, 1076.

THE INFRARED SPECTRA OF ORTHO META AND PARA THIOCREOLS

R. N. BAPAT

PHYSICS DEPARTMENT, COLLEGE OF SCIENCE, NAGPUR.

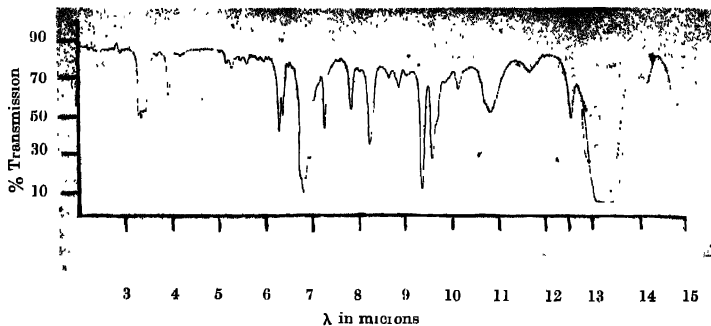
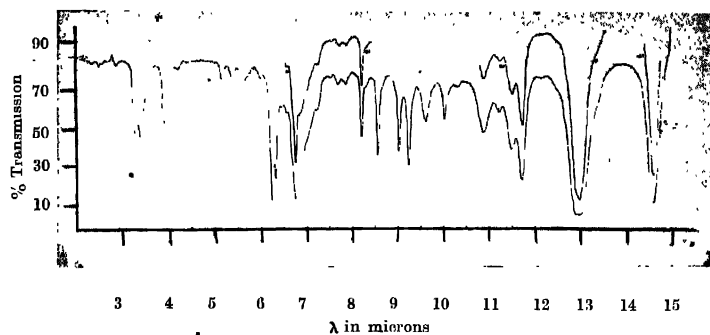
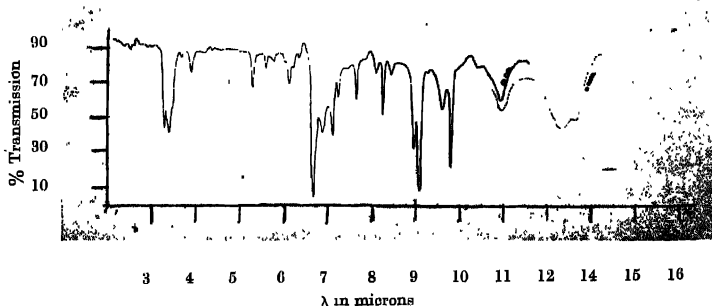
ABSTRACT. The infrared spectra of the *o*-, *m*-, and *p*- thiocresols were taken on the Perkin Elmer infrared spectrophotometer between the region 2 to 15 microns. The S-H stretching frequency is reported to be near about 2580 cm^{-1} . This characteristic frequency was observed to be present in all the three molecules the values being 2577, 2577 and 2571 cm^{-1} in ortho, meta and para thiocresols respectively. The frequencies arising out of phenyl and methyl parts have been assigned to their respective modes of vibration.

INTRODUCTION

The ultraviolet vapour absorption of these molecules was undertaken and to assign frequencies to definite modes of vibration, it was thought necessary to take the infrared spectra of these molecules as the data were not available. The samples were supplied by Eastman Kodak Company. The infrared spectra of toluene, thiophenol and cresols are known and a comparative study in a tabular form is carried out to bring out the broad features in the spectra of these molecules with the substitution of SH in thiocresols in place of OH in cresols.

EXPERIMENTAL

The infrared spectra of all the three molecules were recorded on the Perkin Elmer infrared spectrophotometer using sodium chloride optics. In case of para thiocresol the substance was dissolved in carbon tetrachloride and then introduced in between the plates of sodium chloride and the thickness was 0.1 mm and kept in the absorption path. The other pair of plates contained only carbon tetrachloride and was kept in the absorption path in front of the second aperture. The light source is divided in two beams and one passes through the solution and the other through the solvent. In the case of meta and ortho thiocresols the substances were introduced directly in between the plates having the film thickness of 0.025 mm and kept in front of one of the apertures. In front of the second aperture only one plate of sodium chloride having the same thickness as the total thickness of these two plates was kept. In case of broad bands, in order to define them further the strength of the solution was made less in case of para thiocresol while in case of meta and ortho thiocresols the film was made thin by introducing a drop between the plates and pressing them together. In figures 1, 2 and 3 the infrared spectra of the three molecules ortho, meta and para thiocresols respectively are given.

Fig. 1. Infrared absorption spectrum of *o*-thiocresol.Fig. 2. Infrared absorption spectrum of *m*-thiocresol.Fig. 3. Infrared absorption spectrum of *p*-thiocresol.

RESULTS

All these three molecules show an absorption band near about 2580 cm^{-1} , and another absorption band between 1200 and 1210 cm^{-1} . All the bands observed in the case of the three molecules are given in Table I together with the infrared absorption bands for toluene, thiophenol, ortho, meta and para cresols for comparing them with the absorption bands in ortho, meta and para thiocresols with the intensities for the same.

DISCUSSION

Of the three cresols, *p*-thiocresol belongs to the C_{2v} symmetry and the other two to C_s symmetry. Para-thiocresol has 15 A_1 , 3 A_2 , 14 B_1 , and 10 B_2 vibrations whereas ortho and meta thiocresols have 29 A' and 13 A'' vibrations. Except for the 3 A_2 vibrations in case of para thiocresol all others are active both in Raman and infrared. The assignment of these vibrations is proposed on the basis of comparison with thiophenol on one hand and toluene on the other. These are also compared with the corresponding cresols.

The phenyl vibrations :

Table II gives the correlation of the phenyl vibrations¹ (Herzfeld *et al*, 1946) with those of thio- cresols. The six C-C stretching vibrations including ring breathing vibration are assigned to the frequencies as indicated in table. The e_g vibration 1596 of benzene gives rise to two bands around 1600 corresponding to a_1 and b_1 in C_{2v} , and a' in C_s . It is important to observe that the corresponding bands are rather weak in para thiocresol. In paracresol there are two strong bands at 1600 and 1616 . In *p*-thiocresol there is only one strong maximum near 1631 with shoulders at 1575 and 1608 . The bands 1631 and 1608 are assigned to these two modes in *p*-thiocresol. Two bands are also expected corresponding to $1485\ e_u$ of benzene. This region is, however, complicated by the fact that there are also bands corresponding to symmetric and asymmetric C-CH₃ bending vibrations in this region. Two bands one near 1480 and other near 1400 are assigned to these. The breathing vibration $992\ a_{1g}$ of benzene drops to between 772 to 789 in thiocresols.

The C-H stretching region near 3000 cm^{-1} is not well resolved and only a tentative assignment is proposed. The C-H in plane and deformation vibration lying between 1280 and 1600 cm^{-1} have been assigned. It is observed that the spectrum of the meta compound usually gives rise to a number of strong bands in this region. From the correlation of other benzene derivatives the assignments given in the table are proposed. The out of plane deformation vibrations are assigned by comparison with other disubstituted benzenes.

Toluene cm ⁻¹ Int.	Thiophenol cm ⁻¹ Int.	<i>o</i> -Cresol cm ⁻¹ Int.	<i>o</i> -Thiocresol cm ⁻¹ Int.	<i>m</i> -Cresol cm ⁻¹ Int.	<i>m</i> -Thiocresol cm ⁻¹ Int.	<i>p</i> -Cresol cm ⁻¹ Int.	<i>p</i> -Thiocresol cm ⁻¹ Int.
	4785 (w)						
4651 (mw)			4545 (vw)		4545 (vw)		
4405 (sh)	4444 (vw)			4386 (vw)		4367 (w)	4444 (vw)
4292 (mw)					4310 (vw)		4255 (vw)
4049 (m)	4098 (m)					4098 (w)	4098 (w)
	4032 (sh)			4016 (vw)	4032 (vw)		4000 (vw)
3861 (sh)	3788 (w)		3846 (vw)				
3676 (w)	3731 (w)						
3460 (w)	3484 (m)		3484 (vw)		3484 (vw)		3472 (vw)
		3344 (ms)		3289 (m)		3322 (s)	
3040 (s)	3086 (s)	3049 (ms)	3067 (m)	3021 (m)	3067 (m)	3021 (m)	3030 (m)
2924 (s)		2933 (ms)	3021 (m)	2907 (m)	2941 (m)	2915 (m)	2924 (m)
2874 (s)	2899 (sh)	2874 (m)	2976 (m)				
		2747 (w)	2941	2833 (m)		2874 (sh)	
2747 (m)			2747 (vw)	2732 (m)	2747 (vw)	2725 (w)	2725 (vw)
				2681 (m)		2688 (w)	
2597 (mw)	2584 (s)	2590 (w)	2577 (m)			2611 (w)	
		2518 (w)		2564 (m)	2577 (m)		2571 (w)
2551 (sh)							

TABLE I (contd.)

Toluene cm ⁻¹ Int.	Thiophenol cm ⁻¹ Int.	<i>o</i> -Cresol cm ⁻¹ Int.	<i>o</i> -Thiocresol cm ⁻¹ Int.	<i>m</i> -Cresol cm ⁻¹ Int.	<i>m</i> -Thiocresol cm ⁻¹ Int.	<i>p</i> -Cresol cm ⁻¹ Int.	<i>p</i> -Thiocresol cm ⁻¹ Int.
2415 (w)	2451 (sh)	2444 (w)	2415 (vw)	2475 (w)	2410 (vw)	2475 (w)	
2364 (sh)				2439 (w)	2381 (vw)		
2336 (w)	2358 (ms)					2347 (w)	
2315 (sh)	2294 (w)						2299 (vw)
2257 (w)	2273 (w)						
2203 (w)	2232 (w)						
2165 (w)	2183 (w)	2092 (w)		2208 (w)			
2110 (w)	2105 (w)	2053 (vw)					
2070 (w)	2058 (w)	1996 (w)	2000 (vw)	2088 (w)		2073 (w)	
1984 (sh)		1934 (m)	1949 (vw)	2016 (w)		1988 (w)	
1946 (s)	1953 (s)		1908 (w)		1942 (w)		
				1919 (w)			
1859 (s)	1866 (s)	1883 (m)	1838 (vw)	1880 (w)	1862 (w)	1869 (mw)	1890 (m)
				1842 (w)			
1802 (s)	1799 (s)		1795 (vw)	1812 (w)			
1776 (sh)		1769 (m)	1761 (vw)		1770 (w)	1757 (w)	1786 (w)
					1748 (sh)		
1736 (m)	1736 (s)		1745 (vw)	1733 (w)	1730 (sh)		1730 (vw)
			1730 (vw)				
			1712 (vw)		1712 (vw)		
1675 (w)	1706 (sh)	1680 (m)	1695 (vw)	1698 (w)	1698 (sh)		
			1684 (vw)				

TABLE I (contd.).

Toluene cm ⁻¹ Int.	Thiophenol cm ⁻¹ Int.	<i>o</i> -Cresol cm ⁻¹ Int.	<i>o</i> -Thiocresol cm ⁻¹ Int.	<i>m</i> -Cresol cm ⁻¹ Int.	<i>m</i> -Thiocresol cm ⁻¹ Int.	<i>p</i> -Cresol cm ⁻¹ Int.	<i>p</i> -Thiocresol cm ⁻¹ Int.
1653 (sh)	1695 (sh)		1658 (vw)		1664 (w)		1658 (sh)
			1645 (vw)				
1603 (s)	1639 (sh)		1595 (m)	1616 (s)	1603 (s)	1616 (s)	1631 (m)
1575 (m)	1582 (s)	1592 (ms)	1577 (m)	1585 (s)	1582 (s)	1600 (s)	1608 (vw)
			1548 (vw)		1550 (w)		
1524 (m)	1522 (sh)		1527 (sh)		1522 (sh)		1575 (vw)
1495 (s)	1479 (s)	1490 (ms)	1484 (sh)	1488 (s)	1479 (s)	1511 (s)	1497 (s)
			1475 (s)				
1462 (s)		1461 (ms)	1462 (s)		1462 (sh)	1456 (s)	1451 (ms)
	1445 (s)		1443 (s)	1433 (ms)	1453 (sh)	1435 (s)	1403 (ms)
			1408 (sh)		1429 (sh)		
					1401 (sh)		
1377 (ms)	1383 (s)	1375 (ms)	1381 (m)	1399 (m)	1383 (w)	1380 (sh)	1379 (m)
	1370 (sh)			1364 (m)			
1333 (sh)	1330 (s)	1344 (ms)		1344 (ms)	1330 (vw)	1335 (sh)	1343 (w)
1315 (m)	1305 (s)	1321 (ms)				1351 (s)	1305 (m)
				1324 (ms)	1302 (w)		
				1304 (m)			
1282 (sh)	1276 (m)	1295 (m)	1280 (m)	1279 (s)	1282 (vw)	1292 (m)	1271 (sh)
				1266 (s)	1272 (vw)		
1247 (m)	1236 (m)	1256 (ms)	1250 (vw)	1233 (s)		1236 (s)	1232 (w)
1209 (ms)	1202 (sh)	1219 (ms)	1217 (ms)		1218 (m)	1214 (s)	1211 (m)
			1209 (sh)		1205 (sh)		
1178 (s)	1185 (s)	1207 (ms)				1172 (s)	1182 (w)

TABLE I (contd.)

Toluene cm ⁻¹ Int.	Thiophenol cm ⁻¹ Int.	o-Cresol cm ⁻¹ Int.	o-Thiocresol cm ⁻¹ Int.	m-Cresol cm ⁻¹ Int.	m-Thiocresol cm ⁻¹ Int.	p-Cresol cm ⁻¹ Int.	p-Thiocresol cm ⁻¹ Int.
1157 (s)	1159 (ms)	1169 (ms)	1159 (w) 1139 (sh)	1156 (ms)	1168 (ms)		
1107 (s)	1120 (s)	1106 (ms)	1131 (w) 1111 (vw)		1109 (ms)	1117 (m)	1115 (ms)
1081 (s)	1094 (s)		1070 (s)	1088 (m)	1083 (ms)	1106 (s)	1099 (s)
1043 (sh)	1072 (s)	1043 (ms)	1046 (s)	1042 (m)	1041 (m)	1044 (mw)	1041 (m)
1031 (s)	1027 (s)		1035 (ms)				
1001 (sh)	1003 (s)		1016 (vw)	1011 (m)		1016 (mw)	1019 (s)
980 (w)	981 (m)	987 (ms)	988 (w)	1001 (m)	982 (m)	987 (w)	1002 (vw)
967 (sh)	960 (m)			966 (w)	971 (w)	952 (w)	956 (sh)
930 (w)	915 (s)	933 (m)	924 (m)	928 (ms)	919 (m)	927 (w)	913 (m)
896 (s)	898 (s)				891 (w)		
873 (w)	872 (sh)			892 (m)	870 (m)		
843 (m)	833 (ms)	844 (m) 818 (m)	856 (w)	852 (m)	853 (s)	842 (ms)	
					824 (vw)	816 (s)	827 (m)
					803 (sh)	805 (sh)	810 (m)
					772 (vs)		789 (m)
				776 (s)			
				769 (s)			
				735 (m)		740 (ms)	751 (sh)
728 (s)	735 (s)	751 (ms)	744 (s)			703 (w)	725 (w)
693 (s)	699 (s)	710 (ms)	705 (w)				
	689 (s)			689 (m)			
	668 (s)		676 (w)		686 (s)		

N.B.—The infrared frequencies for toluene, thiophenol, o-cresol, m-cresol and p-cresol are taken from the A.P.I. Catalogue giving the infrared data.

TABLE II
Vibrations from benzene ring

	Benzene D _{6h}	<i>p</i> -thiocresol C _{2v}	<i>o</i> -thiocresol C _s	<i>m</i> -thiocresol C _s
C-C stretching }	<i>a</i> _{1g} 992	789 <i>a</i> ₁	772 <i>a'</i>	772 <i>a'</i>
	<i>b</i> _{2u} 1310	1232 <i>b</i> ₁	1250 <i>a'</i>	1272 <i>a'</i>
	<i>e</i> _{1u} 1485	1497 <i>a</i> ₁	1475 <i>a'</i>	1479 <i>a'</i>
	<i>e</i> _{1u} 1485	1403 <i>b</i> ₁	1408 <i>a'</i>	1401 <i>a'</i>
	<i>e</i> _{2g} 1596	1631 <i>a</i> ₁	1595 <i>a'</i>	1603 <i>a'</i>
	<i>e</i> _{2g} 1596	1608 <i>b</i> ₁	1577 <i>a'</i>	1582 <i>a'</i>
C-H stretching }	<i>e</i> _{2g} 3047	Raman 3136 <i>b</i> ₁	— <i>a'</i>	Raman 3117 <i>a'</i>
	<i>b</i> _{1u} 3060	Raman 3061 <i>a</i> ₁	— <i>a'</i>	Raman 3055 <i>a'</i>
	<i>e</i> _{1u} 3080	— <i>a</i> ₁	3067 <i>a'</i>	3067 <i>a'</i>
	<i>a</i> _{1g} 3062	3030 <i>a</i> ₁	3021 <i>a'</i>	Raman 3176 <i>a'</i>
C-H inplane deformation }	<i>e</i> _{2g} 1178	1182 <i>a</i> ₁	1159 <i>a'</i>	1168 <i>a'</i>
	<i>e</i> _{1u} 1033	1019 <i>a</i> ₁	1035 <i>a'</i>	1019 <i>a'</i>
	<i>b</i> _{2u} 1110	1115 <i>b</i> ₁	1111 <i>a'</i>	1109 <i>a'</i>
	<i>a</i> _{2g} 1326	1271 <i>b</i> ₁	1280 <i>a'</i>	1282 <i>a'</i>
C-H out of plane deformation }	<i>e</i> _{1g} 850	810 <i>b</i> ₂	797 <i>a''</i>	803 <i>a''</i>
	<i>e</i> _{2u} 970	956 <i>a</i> ₂	988 <i>a''</i>	982 <i>a''</i>
	<i>e</i> _{2u} 970	827 <i>b</i> ₂	856 <i>a''</i>	853 <i>a''</i>
	<i>b</i> _{2g} 985	913 <i>b</i> ₂	924 <i>a''</i>	919 <i>a''</i>
C-C inplane bending }	<i>b</i> _{1u} 1010	1099 <i>a</i> ₁	1070 <i>a'</i>	1083 <i>a'</i>
	<i>e</i> _{1g} 606	639 <i>a</i> ₁	661 <i>a'</i>	685 <i>a'</i>
	<i>e</i> _{2g} 606	— <i>b</i> ₁	552 <i>a'</i>	523 <i>a'</i>
C-C out of plane bending }	<i>b</i> _{2g} 703	(—) <i>b</i> ₂	676 <i>a''</i>	676 <i>a''</i>
	<i>e</i> _{2u} 404	(—) <i>a</i> ₂	432 <i>a''</i>	410 <i>a''</i>
	<i>e</i> _{2u} 404	(—) <i>b</i> ₂	146 <i>a''</i>	147 <i>a''</i>
C-X stretching }	<i>e</i> _{1u} 3080	(—) <i>b</i> ₁	686 <i>a'</i>	686 <i>a'</i>
	<i>e</i> _{2g} 3047	1211 <i>a</i> ₁	1217 <i>a'</i>	1218 <i>a'</i>

TABLE II (contd.)

		Benzene D_{6h}	<i>p</i> -thiocresol C_{2v}	<i>o</i> -thiocresol C_s	<i>m</i> -thiocresol C_s
C-X inplane bonding]	e_{1u}	1033	(—) b_1	(—) a'	(—) a'
	e_{2g}	1178	(—) b_1	(—) a'	(—) a'
C-X out of plane bending]	a_{2u}	671	(—) b_2	(—) a''	(—) a''
	e_{1g}	850	(—) a_2	(—) a''	(—) a''

TABLE III

Methyl vibrations in the three cresols, toluene and the three thio cresols

	Toluene	Cresols			Thiocresols		
		<i>o</i> -	<i>m</i> -	<i>p</i> -	<i>o</i> -	<i>m</i> -	<i>p</i> -
Asymmetric Stretching	2920	2933	2907	2915	2941	2941	2924
Symmetric Stretching	2870	2874	2833	2874	Expected (2870)	Raman (2870)	Expected (2870)
Symmetric bonding	1377	1375	1399 or 1364	1380	1381	1383	1379
Asymmetric bending	1460	1461	1488	1456	1462	1462	1451
	1436	1440	1433	1435	1443	1429	14037
Rocking	1081	—	—	—	—	—	—
	1041	1043	1042	1044	1046	1041	1041

The inplane ring vibrations corresponding to e_g + 606 of benzene give rise to two bands usually one above 606 cm^{-1} and other below this value. The assignments of 552 and 553 cm^{-1} in case of ortho and meta-thiocresols of one of the components is given by the Raman data. Out of plane ring vibrations corresponding to 703 b_{2g} of benzene is assigned to a weak band at 676 cm^{-1} in ortho and meta thiocresols. The others are discussed in Raman effect. The substituent sensitive vibrations from the phenyl part are tabulated. In this stretching vibration one should correspond to C-CH₃ stretching (Pitzer and Scott, 1943) which is usually found near 1210 cm^{-1} and the other C-S stretching. The latter vibration is known to occur near 680 cm^{-1} as in other mercaptans (Sheppard, 1950). No definite assignment can however be made. The position of these and the corresponding C-S in-plane and out of plane bending is not satisfactory.

Methyl group gives rise to three C-H stretching and three C-H bending and two rocking vibrations. The general trend in these vibrations has been shown by various workers (Shappard, 1953). The assignment of CH_3 modes is shown in table III. •

The S-H stretching frequency is observed to be present at 2577, 2577 and 2571 cm^{-1} in ortho, meta and parathiocresols respectively.

ACKNOWLEDGEMENTS

The author is indebted to Dr. R. K. Asundi and Dr. M R. Padhye for their keen interest in the work.

REFERENCES

- Horzfeld, N., Ingold, C. K. and Poole, H. G., 1946. *Jour. Chem. Soc.*, **316**,
Pitzor, K. S and Scott, D. W., 1943, *Jour. Amer. Chem. Soc.*, **65**, 803
Sheppard, N., 1950, *Trans. Farad. Soc.*, **46**, 429.
Sheppard, N., 1953, *Quart. Revs.*, **7**, 19.
Trotter, I. F. and Thompson, H. W., 1946, *Jour. Chem. Soc.*, **481**.

THE SPACE GROUP OF META TOLUIC ACID

R. C. SRIVASTAVA

DEPARTMENT OF PHYSICS, UNIVERSITY OF ALLAHABAD, ALLAHABAD

(Received for publication, May 8, 1959)

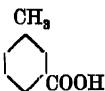
Plate VII

ABSTRACT. Goniometric and X-ray study of single crystals of *m*-toluic acid shows that it belongs to monoclinic class. Crystallographic data resulting from the above study is given by

$$a=10.51 \text{ \AA}, \quad b=8.01 \text{ \AA}, \quad c=16.49 \text{ \AA}, \quad \beta=92^\circ 46.5'.$$

Number of molecules per unit cell=8

Weissenberg photographs about crystallographic axes showed that (*h*0*l*) planes are present when *l* is even and (*o**k*0) planes are present when *k* is even. The crystal belongs to the space group $C_{2h}^2-P_{21}/c$, and so each one of the four asymmetric units is composed of two molecules.

m-Toluic acid or *m*-methylbenzoic acid has structural formula 

No goniometric or X-ray data are available for it. Single crystals of *m*-Toluic acid of suitable size were prepared by slow evaporation of the solution of the substance in ethyl alcohol. It gave prismatic crystals with six faces in one zone and having a tendency of elongation along this zone axis.

Goniometric measurement of the zone containing faces parallel to needle axis was made. Rotation photograph about four selected zone axes were taken (Plate VII). Axial parameters thus got were further refined with the help of (00.12), (10.00), (00.14) reflections from Weissenberg goniometer photographs and are given below

$$a = 10.51 \text{ \AA}$$

$$b = 8.01 \text{ \AA}$$

$$c = 16.49 \text{ \AA}$$

$$\beta = 92^\circ 46.5'$$

The interfacial angles measured and as calculated with the help of above axial parameters are given in Table I

The density of the crystals was determined by the flotation method. The lighter liquid used was kerosene oil and the heavier carbon tetrachloride. Density

thus determined is 1.239 gm./cm³. Thus the number of molecules comes out to be 8 per unit cell.

TABLE I

Indices of the faces	Measured interfacial angles	Calculated angles
100 : 00 $\bar{1}$	92° 45'	β
00 $\bar{1}$: 10 $\bar{2}$	34° 4'	37° 3.5'
10 $\bar{2}$: $\bar{1}$ 00	50° 18"	50° 10.5'
$\bar{1}$ 00 : 001	92° 48'	β
001 : 102	37° 7'	37° 3.5'
102 : 100	49° 58'	50° 10.5'

Zero layer line Weissenberg photographs along a and b axis and 1st layer line equi-inclination Weissenberg photograph about b axis were taken. On indexing them the following extinctions were observed.

($h0l$) planes absent for l odd.

(oko) planes absent for k odd.

No systematic absence in the general planes (hkl).

The space group of the crystal is therefore $C^5_{2h}-P_{21/c}$. The number of asymmetric units per unit cell necessary for this space group is four, so two molecules form one asymmetric unit.

ACKNOWLEDGMENTS

The author is thankful to Prof. K. Banerji for his guidance and to Dr. S. C. Chakraborty for his valuable help. The author is also thankful to C.S.I.R. for financial assistance.

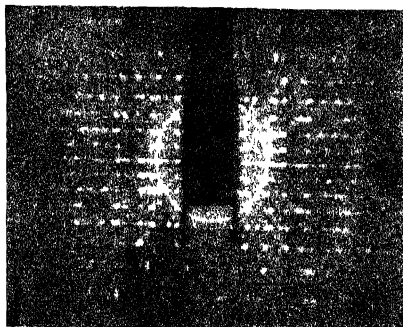


Fig 1.
About c -axis



Fig 2.
About b -axis

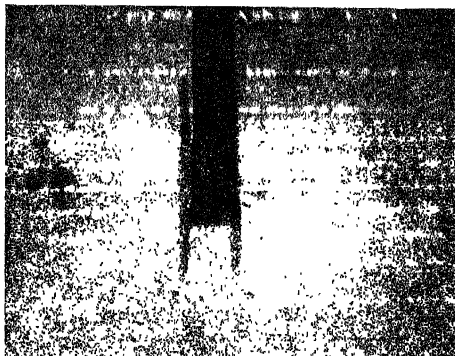


Fig 3.
About a -axis

Rotation photographs of m -toluc acid.

ON WAVE SOLUTION OF FIELD EQUATIONS IN EINSTEIN'S UNIFIED FIELD THEORY*

N. N. GHOSH

SANTINIKETAN, WEST BENGAL, INDIA

(Received for publication May 25, 1959)

ABSTRACT. A static non-symmetric tensor field $g_{\mu\nu}$ with 4 symmetric components $S_{kk}, S_{mm}, S_{nn}, S_{ll}$ ($k, m, n, l = 1, 2, 3, 4$) and one anti-symmetric component a_{mn} (the rest being all zeros), involving either the coordinate x_k or the coordinates x_k, x_m is made non-static by changing x_k into $x_k + \epsilon x_l$ where ϵ is a constant. On solving the relevant field equations in the 'strong' form it is found that such a wave solution is generally spurious, being transformable into corresponding static solution. It is, however, observed that if the field is not spherically symmetric non-trivial solutions in wave form may be constructed.

1. INTRODUCTION

In a recent paper (Ghosh, 1957) a type of non-static solution of Einstein's field equations in 'strong' form was studied with respect to the tensor field $g_{\mu\nu}$ having the following structure :

$$g_{\mu\nu} = \begin{pmatrix} S_{kk} & 0 & 0 & a_{kl} \\ 0 & S_{mm} & a_{mn} & 0 \\ 0 & -a_{mn} & S_{nn} & 0 \\ -a_{kl} & 0 & 0 & S_{ll} \end{pmatrix} \begin{pmatrix} k, m, n, l \\ (= 1, 2, 3, 4) \end{pmatrix}, \quad \dots \quad (1.1)$$

where S_{kk}, S_{ll}, a_{kl} are functions of $(x_k + \epsilon x_l)$, ϵ being a constant and S_{mm}, S_{nn}, a_{mn} are each expressible as the product of a function of $x_k + \epsilon x_l$ and a function of x_m of the type

$$\begin{aligned} S_{mm} &= \phi_{mm}(x_k + \epsilon x_l) \psi_{mm}(x_m), \\ S_{nn} &= \phi_{nn}(x_k + \epsilon x_l) \psi_{nn}(x_m), \\ a_{mn} &= \phi_{mn}(x_k + \epsilon x_l) \sqrt{\psi_{mm} \psi_{nn}}. \end{aligned} \quad \dots \quad (1.2)$$

On completing the solution of the relevant field equations we were led to make the following observations :

(a) The ψ 's in (1.2) satisfy an auxiliary differential equation involving a parameter λ which can take negative, positive or zero values. When λ is negative the equation gives $\psi_{mm} = 1$, and $\psi_{nn} = \sin^2 x_m$, which corresponds to a spherically symmetric field. When λ is positive we get $\psi_{mm} = 1$, $\psi_{nn} = \sinh^2 x_m$ and for $\lambda = 0$ the ψ 's are transformable into constants.

*An abstract of this paper was read at the forty-sixth session of the Indian Science Congress, 1959.

(b) A solution of ϕ 's with $\lambda \neq 0$ in the above wave form is generally spurious as it is transformable into the corresponding solution for the static field.

(c) When $\lambda = 0$ new static solutions are obtained, but with further restrictions, non-trivial solutions in wave form can be constructed, where the field components are functions of the argument $x_k + \epsilon x_l$ only.

The object of the present paper is to consider a special case of the above in which the tensor field (1.1) has only a single non-zero anti-symmetric element a_{mn} (the other one being zero) and to show that the above statements are in general maintained.

2. SYSTEM OF FIELD EQUATIONS WITH $a_{kl} = 0$, $a_{mn} \neq 0$.

To obtain the field equations in terms of non-vanishing Γ 's we make use of the general formulae given in one of my earlier papers (Ghosh, 1955). The relevant equations are $R_{kk} = 0$, $R_{ll} = 0$, $R_{kl} = 0$, $R_{mn} = 0$, $R_{mn}^v = 0$ of which the first three are linearly connected. Without going into details of the computation which is similar to that contained in my previous paper (Ghosh, 1957) we at once start with the following simplified set of 4 mutually independent field equations :

$$-A_{k,k} + \frac{1}{2}A_k(\gamma_{kkk} + \gamma_{llk}) - \frac{1}{2}(A_k^2 + \bar{B}_k^2) = 0, \quad \dots (2.1)$$

$$\gamma_{llk,k} + \gamma_{lk}(A_k - \frac{1}{2}\gamma_{kkk} + \frac{1}{2}\gamma_{llk})$$

$$+ \epsilon^2 \frac{S_{kk}}{S_{ll}} [\gamma_{kkk,k} + \gamma_{kk}(A_k - \frac{1}{2}\gamma_{llk} + \frac{1}{2}\gamma_{kkk})] = 0, \quad \dots (2.2)$$

$$B_{l,k} + B_k(A_k - \frac{1}{2}\gamma_{kll} + \frac{1}{2}\gamma_{llk})$$

$$+ \epsilon^2 \frac{S_{kk}}{S_{ll}} [\bar{B}_{l,k} + B_k(A_k - \frac{1}{2}\gamma_{llk} + \frac{1}{2}\gamma_{kll})] = \frac{2S_{kk}\phi_{mn}f(x_m)}{(\phi_{mn}^2 + \phi_{mn}^2)\psi_{mn}}, \dots (2.3)$$

$$A_{k,k} + A_k(A_k - \frac{1}{2}\gamma_{kkk} + \frac{1}{2}\gamma_{llk})$$

$$+ \epsilon^2 \frac{S_{kk}}{S_{ll}} [A_{k,k} + A_k(A_k - \frac{1}{2}\gamma_{llk} + \frac{1}{2}\gamma_{kkk})] = \frac{-2S_{kk}\phi_{mn}f(x_m)}{(\phi_{mn}^2 + \phi_{mn}^2)\psi_{mn}} \dots (2.4)$$

In the above

$$A_k = (\phi_{mn}\phi_{mn,k} + \phi_{mn}\phi_{mn,k})/(\phi_{mn}^2 + \phi_{mn}^2),$$

$$B_k = (\phi_{mn}\phi_{mn,k} - \phi_{mn}\phi_{mn,k})/(\phi_{mn}^2 + \phi_{mn}^2). \quad \dots (2.5)$$

$$f(x_m) = \frac{1}{2}[\gamma_{nnm,m} - \frac{1}{2}\gamma_{nnm}(\gamma_{mmm} - \gamma_{nnm})],$$

the symbols like γ_{lkk} , γ_{nnm} denoting respectively $S_{kk,k}/S_{kk}$ and $S_{nn,m}/S_{nn}$. Further, we have the condition

$$(\phi_{mn}^2 + \phi_{mn}^2)(\phi_{mn}^2 - \phi_{mn}^2) \neq 0, \quad \dots (2.6)$$

which ensures uniqueness in the solution of Γ 's.

The system of equation $\Gamma^\nu_{\mu\nu} = 0$ are identically satisfied and does not contribute any additional equation.

In the equations (2.3) and (2.4), there is a part $f(x_m)/\psi_{mm}$ which is a function of x_m only, while the rest involves only $x_k + \epsilon x_l$ and therefore, for consistency, we must have the auxiliary equation

$$4f(x_m) = \lambda \cdot \psi_{mm}(\lambda, \text{constant}) \quad (2.7)$$

This equation has been discussed in an earlier paper (Ghosh, 1956), leading to the statement (a).

3. SOLUTION OF FIELD EQUATIONS WHEN $\lambda \neq 0$

To solve equations (2.1–4) we adopt the procedure similar to that followed in my previous paper (Ghosh, 1957).

Introduce two new variables P, Q , functions of $x_k + \epsilon x_l$, defined by

$$S_{kk} = \frac{A_k^2(\phi_{mm}^2 + \phi_{nn}^2)^{\frac{1}{2}}}{P}, \quad S_{ll} = \frac{\epsilon^2 A_k^2(\phi_{mm}^2 + \phi_{nn}^2)^{\frac{1}{2}}}{Q} \quad (3.1)$$

$$\text{then} \quad \epsilon^2 S_{ll}/S_{ll} = Q/P \quad (3.2)$$

and

$$\begin{aligned} \gamma_{kkk} &= 2A_{k,k}/A_k + A_k - P_k/P, \\ \gamma_{lll} &= 2A_{k,k}/A_k + A_k - Q_k/Q. \end{aligned} \quad (3.3)$$

Substituting from (3.3) in (2.1) we get

$$A_{k,k} - \frac{1}{2} A_k \left(\frac{P_k}{P} + \frac{Q_k}{Q} \right) + \frac{1}{2} (A_k^2 - \bar{B}_k^2) = 0. \quad (3.4)$$

Using (3.4) let us rewrite (3.3) as

$$\gamma_{kkk} = \frac{Q_k}{Q} + \frac{\bar{B}_k^2}{A_k}, \quad (3.5)$$

$$\gamma_{lll} = \frac{P_k}{P} + \frac{\bar{B}_k^2}{A_k}.$$

If we insert (3.2) and (3.5) in (2.2), it takes the form

$$\left(\frac{\partial}{\partial x_k} + \frac{1}{2} \frac{P_k}{P} - \frac{1}{2} \frac{Q_k}{Q} + A_k \right) \left[M_k \left(1 + \frac{Q}{P} \right) \right] = 0, \quad \dots \quad (3.6)$$

where

$$M_k = \frac{\partial M}{\partial x_k} = \frac{P_k + Q_k}{P + Q} + \frac{\bar{B}_k^2}{A_k}. \quad \dots \quad (3.7)$$

where h is a complex constant of integration, $h = h_0 + ih_1$. The general solution of (3.20) may be presented in the well-known form

$$e^{M+is} = h \operatorname{sech}^2(h^2 M + k)/(-ib), \quad \dots \quad (3.22)$$

where k is an arbitrary complex constant.

It may now be proved that the real part h_0 of h in (3.22) must be $\frac{1}{2}$.

From (3.21) reverting to the variable $x_k + cx_l$ we get

$$(M_k + A_k + i\bar{B}_k)^2 = M_k^2[4ib e^M (\phi_{mn} + i\phi_{mn}) + 4(h_0 + ih_1)].$$

Equating the real parts in the above, we have

$$A_k^2 - \bar{B}_k^2 + 2A_k M_k = -4b\phi_{mn} M_k^2 e^M + (4h_0 - 1)M_k^2, \quad \dots \quad (3.23)$$

which, in view of (3.14) and (3.18), gives $h_0 = \frac{1}{2}$.

For the final solution with $\lambda \neq 0$ we have to consider the equations (3.22), (3.12) and (3.10). Thus

$$\phi_{mn} + i\phi_{mn} = e^{-M} [h \operatorname{sech}^2(h^2 M + k)/(-ib)], \quad \dots \quad (3.24)$$

$$S_{ll} S_{kk} = \frac{e^2}{C_1^2} \left(\frac{\partial}{\partial x_k} e^M \right)^2 (\phi_{mn}^2 + \phi_{mn}^2), \quad \dots \quad (3.25)$$

$$S_{ll} + e^2 S_{kl} = \frac{1}{C'} e^M, \quad \dots \quad (3.26)$$

where M is an arbitrary function of $x_k + cx_l$, k is an arbitrary complex constant, h is a complex constant of the form $\frac{1}{2} + ih_1$ and b, c_1, C' are real arbitrary constants.

The three equations written above give the solution of the field components apparently as functions of $x_k + cx_l$. Consider now the transformation

$$x'_k = x_k + cx_l, \quad x'_l = \phi(x_k, x_l), \quad (3.27)$$

where

$$\frac{\partial \phi}{\partial x_k} = \frac{-e S_{kk}}{e^2 S_{kk} + S_{ll}}, \quad \frac{\partial \phi}{\partial x_l} = \frac{S_{ll}}{e^2 S_{kk} + S_{ll}},$$

then the above solutions may be presented as involving one variable x'_k and are of the same form as obtained by Bonnor (1951) for the static field.

4. SOLUTION FOR A SPECIAL CASE WITH $\lambda \neq 0$

Returning to the equation (3.6) we notice that it is automatically satisfied if M_k , as defined in (3.7), identically vanishes. Let us consider now the special

case with $M_k = 0$. Referring to (3.4) and (3.1) this condition is seen to be equivalent to

$$\frac{\partial}{\partial x_k} \log (S_{ll} + \epsilon^2 S_{kk}) = 0 \quad \dots \quad (4.1)$$

whence $S_{ll} + \epsilon^2 S_{kk} = \alpha$ (a constant).

Again, from (3.1) we have

$$\frac{1}{S_{kk}} + \frac{\epsilon^2}{S_{ll}} = \frac{P + Q}{A_k^2 (\phi_{mm}^2 + \phi_{nn}^2)^{\frac{1}{2}}}$$

Therefore
$$S_{kk} S_{ll} = \frac{\alpha \cdot A_k^2 (\phi_{mm}^2 + \phi_{nn}^2)^{\frac{1}{2}}}{P + Q} \quad \dots \quad (4.2)$$

Consider now the equations (3.15) and (3.16). We note, first of all, that if L denotes the expression

$$\frac{(S_{kk} S_{ll})^{\frac{1}{2}}}{(\phi_{mm}^2 + \phi_{nn}^2)^{\frac{1}{2}}} \quad \dots \quad (4.3)$$

then
$$-\frac{\partial}{\partial x_k} \log L = \frac{P_k + Q_k}{P + Q} - \frac{1}{2} \frac{P_k}{P} - \frac{1}{2} \frac{Q_k}{Q} + A_k.$$

Inserting this and (4.2) in the equations (3.15) and (3.16) we get

$$B_{k,k} - B_k \frac{L_k}{L} = 2\beta \phi_{mn} L^2, \quad \dots \quad (4.4)$$

$$A_{k,k} - A_k \frac{L_k}{L} = -2\beta \phi_{mn} L^2, \quad \dots \quad (4.5)$$

where

$$\beta = \frac{1}{2} \frac{\lambda}{\alpha}.$$

We also find that the equation (2.1) gives

$$A_{k,k} - A_k \frac{L_k}{L} = \frac{1}{2} (A_k^2 - B_k^2) \quad \dots \quad (4.6)$$

Adopting the method of Wyman (1950) to solve the equations (4.4) and (4.5) in conjunction with (4.6) the solution may be presented in the form

$$\phi_{mn} + i\phi_{nm} = \hbar \operatorname{sech}^2 (\hbar^{\frac{1}{2}} x + k) / (-i\beta),$$

$$\frac{\partial x}{\partial x_k} = L, \quad (4.7)$$

where x is an arbitrary function of $x_k + cx_l$, k is a complex constant, h is a pure imaginary constant. Further from (4.1) and (4.3) we have

$$S_{ll} + e^2 S_{kk} = \alpha,$$

$$S_{kk} S_{ll} = \left(\frac{\partial x}{\partial x_k} \right)^2 (\phi_{mm}^2 + \phi_{nn}^2). \quad \dots (4.8)$$

The transformation (3.27) applies to this case also and the solutions are found to involve one variable x'_k and thus belong to a static field. Omitting the primes we write the solutions as follows :

$$\phi_{mn} + i\phi_{mm} = h \operatorname{sech}^2(h^2 x + k) / (-i\beta),$$

$$S_{ll} = \alpha,$$

$$S_{kk} = \frac{1}{\alpha} \left(\frac{dx}{dx_k} \right)^2 (\phi_{mm}^2 + \phi_{nn}^2), \quad \dots (4.9)$$

where x is an arbitrary function of x_k , h, k, β, α being constants as before. The solutions (4.9) for a static field have been discussed by Bonnor (1951).

5. SOLUTIONS FOR THE CASE $\lambda = 0$

When $\lambda = 0$ the field components are all functions of $x_k + cx_l$ and do not involve x_m (Ghosh, 1956). We shall consider now two cases, (i) $P+Q \neq 0$, (ii) $P+Q = 0$. Referring to (3.17) and (3.18) we have for the first case the equations

$$B_{k,k} - \bar{B}_k \frac{M_{k,k}}{\bar{M}_k} = 0, \quad \dots (5.1)$$

$$A_{k,k} - A_k \frac{M_{k,k}}{\bar{M}_k} = 0. \quad \dots (5.2)$$

Using (5.2) in (3.14) we have also

$$A^2_k - \bar{B}^2_k + 2A_k \bar{M}_k = 0. \quad \dots (5.3)$$

Making use of (3.19) in conjunction with (5.3) we can integrate the equations (5.1,2) and obtain as solution

$$\phi_{mn} + i\phi_{mm} = k e^{(\alpha_1 + i\alpha_2)M}, \quad \dots (5.4)$$

where M is an arbitrary function of $x_k + cx_l$, k is an arbitrary complex constant and α_1 and α_2 are two constants connected by the relation

$$\alpha_1^2 - \alpha_2^2 + 2\alpha_1 = 0. \quad \dots (5.5)$$

The components S_{kk} , S_{ll} are given by (3.25) and (3.26). If we now apply the transformation (3.27) the solutions are all transformed into the static form involving one variable x'_k .

In the special case with $M_k = 0$ considered in § 4, we also get a static solution. The equations (4.4, 5) become, when $\lambda = 0$,

$$\bar{B}_{k,k} - \bar{B}_k \frac{L_k}{L} = 0, \quad \dots \quad (5.6)$$

$$A_{k,k} - A_k \frac{L_k}{L} = 0 \quad \dots \quad (5.7)$$

with

$$A^2_k - \bar{B}^2_k = 0. \quad \dots \quad (5.8)$$

These equations in conjunction with (3.19) will give the solutions for ϕ_{mn} and ϕ_{mn} , while the set of equations (4.8) gives S_{kk} , S_{ll} . If we now apply the transformation (3.27), the first set of solutions is transformed into the static form considered in one of my earlier papers (Ghosh, 1956) and the second set gives the solutions for S_{kk} , S_{ll} as in (4.9).

In the second case, since $P+Q=0$ we have $S_{ll} + \epsilon^2 S_{kk} = 0$ and consequently $\gamma_{kkk} = \gamma_{llk}$. Substituting these in the original system of equations (2.1—4) and remembering $f(x_m) = 0$ we notice that the last three are automatically satisfied and we are left with the equation (2.1) expressed as

$$-A_{k,k} + A_k \gamma_{kkk} - \frac{1}{2}(A^2_k + \bar{B}^2_k) = 0. \quad \dots \quad (5.9)$$

This furnishes typical wave solutions. Setting

$$(\phi^2_{mm} + \phi^2_{nn})^{\frac{1}{2}} = u^2, \quad \phi_{mn}/\phi_{nn} = v,$$

u, v being arbitrary functions of $x_k + \epsilon x_l$ and introducing a function w defined by the equation $\bar{B}^2_k/A_k = 2w_{,k}/w$

that is, $(v_{,k})^2 u w = 4(1 + v^2)^2 u_{,k} w_{,k}$

the solutions may be presented as follows :

$$S_{kk} = C' u_{,k} w, \quad S_{ll} = -\epsilon^2 S_{kk}, \quad \dots \quad (5.10)$$

$$S_{mn} = S_{nn} = \frac{u^2 v}{\sqrt{1+v^2}}, \quad a_{mn} = \frac{u^2}{\sqrt{1+v^2}}, \quad \dots \quad (5.10)$$

The exact wave solutions as obtained above relate to a tensor field having plane symmetry (Taub, 1951). A field with spherical symmetry is found not to admit such wave solutions.

REFERENCES

- Bonnor, W, 1951, *Proc. Roy. Soc. A.*, **209**, 353.
 Ghosh, N. N, 1957, *Prog. Theor. Phys.*, **17**, 131.
 „ „ 1956, *Prog. Theor. Phys.*, **16**, 421.
 „ „ 1955, *Prog. Theor. Phys.*, **13**, 587.
 Taub, M., 1951, *Annals of Math.*, **53**, 472.
 Wyman, M., 1950, *Canad. J. Math.*, **2**, 427.

GYRO-FREQUENCY IN THE IONOSPHERIC REGIONS

S. DATTA AND R. N. DATTA

INSTITUTE OF RADIOPHYSICS AND ELECTRONICS, 92, UPPER CIRCULAR ROAD,
CALCUTTA-9

(Received for publication, June 29, 1959)

ABSTRACT. Gyro-frequencies in the E, F1 and F2 regions of the ionosphere over Haringhata (Geographic lat. 22.9°N, Geomag. lat. 12.5°N) have been calculated from the measurements of ordinary (f_o) and extraordinary (f_x) critical frequencies. It is found that the magnetic fields calculated therefrom are higher than those expected from extrapolation of the magnetic field at ground-level to the heights of the regions by inverse cube law. Further, the E region gyro-frequency has a marked semi-diurnal variation with a minimum near midday. This result is similar to that obtained by Scott at high latitudes. No diurnal variation is found in the F1 and F2 regions, though, the values near midday in the F1 region are lower. Possible causes of the E-region gyro-frequency variation are discussed. No satisfactory explanation is, however, obtainable.

In the F2 region, the average winter value of the gyro-frequency is found to be about 9% greater than the summer value. Seasonal variation, though of a larger magnitude (20%), has also been obtained by Scott at high latitudes.

The frequency difference ($f_x - f_o$) is found to be dependent on the ordinary critical frequency (f_o), the values at high frequency being lower than those at lower frequency. This is as may be expected for the case of quasi-transverse propagation.

INTRODUCTION

Appleton and Builder (1933) were the first to show how the difference of the critical frequencies ($f_x - f_o$) is related to the intensity of the magnetic field in the ionosphere and hence to the so-called gyro-frequency (f_H). Many estimations of the magnetic field and of the gyro-frequency have been made in different parts of the world from the measured values of $f_x - f_o$, both for the E and the F region. However, as the brief accounts of the experiments given below show there are many unexpected anomalous results. These have not all been fully explained.

Gyro-frequency in the F region at Slough was determined by Appleton by the above method in 1934. The value of the magnetic field in the F region was found to be 0.42 Gauss. This was consistent with that obtained from extrapolation by inverse cube law of the ground level field. Scott in 1950 estimated the magnetic field in the F region at arctic stations by the same method. The results, however, showed that the calculated field from the gyro-frequency is higher than the extrapolated value. Scott also found large diurnal, seasonal and other irregular variations in the calculated field. The field obtained from the longitudinal mode was usually found to be lower than that from the transverse mode. These pheno-

mena are ascribed by Scott as due to the ray path deflections (figure 2) coupled with normal latitude gradients of ionization.

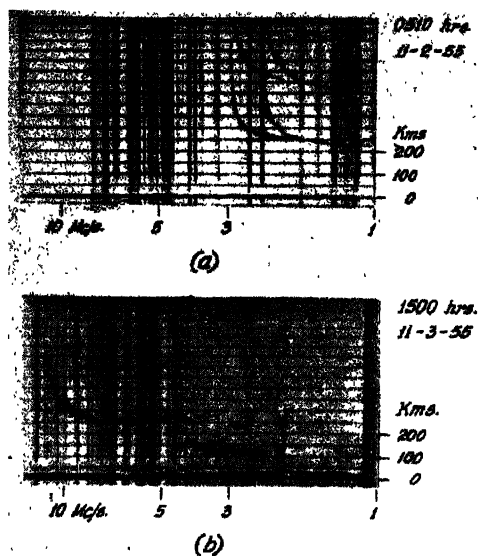


Fig. 1. Typical $h'-f$ records obtained at Haringhata.

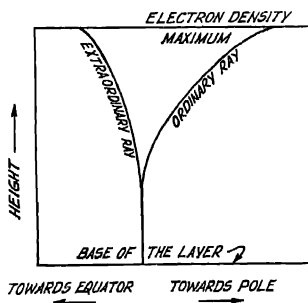


Fig. 2. Diagram illustrating the deviations of the ordinary and extraordinary rays in the Ionosphere.

Scott (1951) has also estimated the magnetic field in the E regions at high latitude arctic stations by the same method. His results show that the calculated

magnetic field was lower than the extrapolated value. At one of the stations, a large semi-diurnal variation of the gyro-frequency was found. Scott has suggested that this may be due to a variable concentration of heavy ions rising over 4,000 times the density of free electrons.

THEORETICAL CONSIDERATION

In the case of free-electron ionosphere the gyro-frequency f_H is given by

$$f_H = \frac{H \cdot e_e}{2\pi m_e} \quad \dots (1)$$

where H = magnetic field in the ionosphere

e_e = charge of an electron

and m_e = mass of an electron.

It can be shown that in such an ionosphere when critical frequency is greater than the gyro-frequency and the mode of propagation for the frequency is quasi-transverse.

$$f_H = \frac{f_x^2 - f_0^2}{f_x} = 2\Delta f - \frac{\Delta^2 f}{f_x} \quad \dots (2)$$

where $\Delta f = f_x - f_0$

From above, the value of H in terms of f_x and f_0 is given by

$$H = \frac{2\pi m_e}{e_e} \left\{ 2\Delta f - \frac{\Delta^2 f}{f_x} \right\} \quad \dots (3)$$

We can make an independent estimation of H at the height (h) of the ionospheric regions from the intensity of the magnetic field (H_0) at the surface of the earth by the inverse cube law :

$$H = H_0 \left(\frac{R}{R+h} \right)^3 \quad \dots (4)$$

where R is the radius of the earth.

Eq. (2) is for the case of free electron ionosphere i.e. when heavy ions are absent. In the presence of heavy-ions, Scott (1951) has shown that

$$\frac{\lambda}{\mu} = \frac{f_x [f_H \cdot f_x - (f_x^2 - f_0^2)]}{(f_x - f_H)(f_x^2 - f_0^2)} \quad \dots (5)$$

where

$$\lambda = \frac{e_i}{e_e} \cdot \frac{N_i}{N_e}$$

$$\mu = \frac{e_e \cdot m_i}{e_i m_e}$$

e_i = charge of ion

m_i = mass of ion

N_i = density of ion

and

N_e = density of electron

The above equation may be utilised to find the values of λ from the measured values of f_x and f_o for assumed values of μ and f_H . For this purpose, the value of f_H obtained by extrapolation of the ground level magnetic field by inverse cube law may be substituted.

Eq. (2), which is valid for quasi-transverse propagation can also be written as

$$f_x^2 - f_H f_x - f_o^2 = 0 \quad \dots (6)$$

When solved for f_x , we get

$$f_x = \frac{1}{2} \left\{ f_H + 2f_o \sqrt{1 + \left(\frac{f_H}{2f_o} \right)^2} \right\} \quad \dots (7)$$

If $f_H < 2f_o$, we get from Eq. (7)

$$\Delta f = f_x - f_o = \frac{f_H}{2} + \frac{f_H}{8} \cdot \frac{f_H}{f_o} - \frac{f_H}{128} \left(\frac{f_H}{f_o} \right)^3 + \dots \quad \dots (8)$$

Hence approximately,

$$\Delta f = \frac{f_H}{2} + \frac{f_H}{8} \cdot \frac{f_H}{f_o} \quad \dots (9)$$

The critical frequency difference between the O and X components for the Q.T. mode of propagation is thus found to be dependent on f_o . If the value of f_H obtained from extrapolation of magnetic field at ground level is substituted in Eq. (9), Δf will be lower for higher values of f_o and vice versa.

EXPERIMENTAL RESULTS

To find the gyro-frequency and its diurnal variations, if any, in the E, F1 and F2 regions, $h'-f$ records for the months of February to December 1955 (year of low sunspot activity) were examined. For the E and F1 regions, the records at intervals of 30 minutes were considered. Only the records in which simultaneous measurements of the ordinary and extraordinary critical frequencies could be measured accurately were considered. The critical frequencies (f_x , f_o) of E, F1 and, of the F regions at night, could be measured accurately upto ± 0.05 Mc/s. This is because the logarithmic frequency scale in the $h'-f$ records permits higher accuracy at lower frequencies. Measurements for the higher values for the F2 region during day time were less accurate.

The average diurnal variations for the equinoctial months (March, April, Sept. and October) of f_H , as calculated from f_x and f_0 for the E, F1 and F2 region

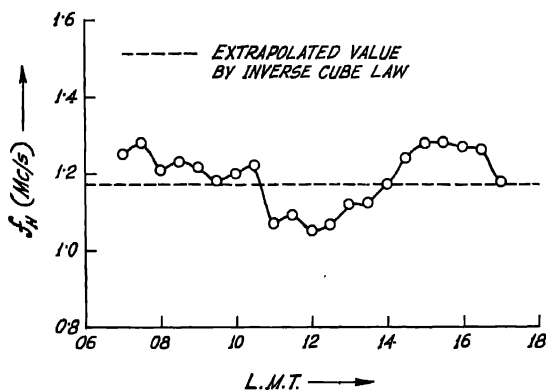


Fig. 3. Diurnal variation of the gyro-frequency (measured from f_x and f_0) in the E region

are shown in figures 3, 4 and 5 respectively. It is to be noted that in all the regions, the f_H values (average of all values) calculated from f_x and f_0 are higher than the

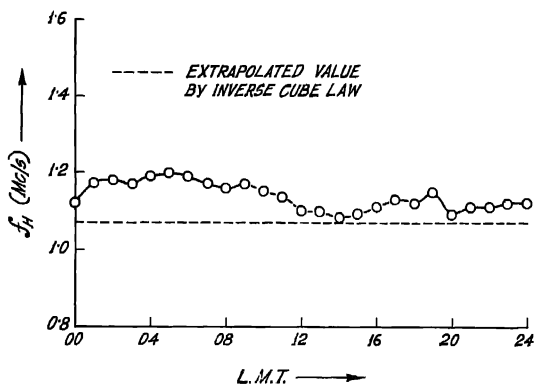


Fig. 4. Diurnal variation of the gyro-frequency (measured from f_x and f_0) in the F1 region.

values expected by extrapolation of the magnetic field at ground-level. In the E region, f_H has a marked semi-diurnal variation with a midday dip while in the F1 and F2 regions no such regular semi-diurnal variation is found except that the midday values in the F1 region are lower.

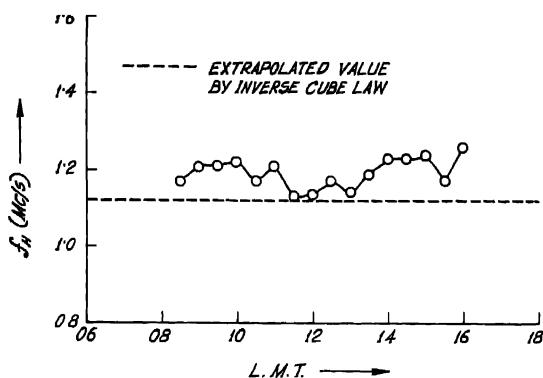


Fig. 5. Diurnal variation of the gyro-frequency (measured from f_x and f_0) in the F2 region.

Due to the high absorption of the extraordinary rays reflected from the F2 region during daytime, the number of records giving extraordinary critical frequencies during daytime was low. The diurnal variation curve of f_H for the F2 region between 0900 hr. and 1800 hr. (L.M.T.) is therefore shown by broken line.

Table I shows the average values (average of all values) of the gyro-frequency and the magnetic field calculated from f_x , f_0 for the equinoctial months in the E, F1 and F2 region and, the theoretical values of the same from the extrapolated magnetic field at ground-level by inverse cube law.

TABLE I

Region	f_H (from f_x, f_0) Mc/s	f_H (from inverse cube law) Mc/s	Magnetic field (from f_x, f_0) Gauss	Magnetic field (from inverse cube law) Gauss
E	1.20	1.17	0.43	0.42
F1	1.18	1.12	0.42	0.40
F2	1.14	1.07	0.41	0.38

Assuming the presence of heavy-ions in the E region, mean hourly values of the ratio (λ) have been calculated with the help of Eq. (5) from the measured values of f_x and f_0 . For this purpose, the value of μ used was 4.33×10^4 which corresponds to an ion mass of 24. (This value of μ was also used by Scott in calculating the values of λ). Theoretical value of f_H used was 1.17 Mc/s (from inverse cube law). The mean hourly values of λ so calculated for the E region are shown in Table II.

TABLE II

Hour (L.M.T.)	f_o Mc/s	f_x Mc/s	λ
07	2.30	3.00	-3830
08	2.70	3.37	-2120
09	3.13	3.80	-2560
10	3.20	3.85	-1090
11	3.52	4.09	6440
12	3.52	4.07	8760
13	3.60	4.20	2950
14	3.20	3.84	-277
15	3.10	3.80	-4910
16	2.82	3.52	-4680
17	2.40	3.06	-390

The calculated values of λ in Table II show that most of the hourly values (except near midday) of heavy-ion concentration are negative. This, in other words, means that assumption of the presence of heavy-ions leads to impossible results.

In the F region, the average nighttime value of the gyro-frequency is found to be 1.19 Mc/s in winter (Nov.-Dec.) and 1.09 Mc/s in summer (June- July). In this connection, it may be noted that when the f_H values in the F2 region for the equinoxial months are plotted with the height of maximum electron density, the plotted points do not show the expected variation (f_H decreasing with increasing height).

To find the dependence of Δf on f_o , only nighttime $h' - f$ records for the F region were examined when the F region critical frequency is low since these records permit greater accuracy of measurement. The values of Δf were found in three frequency ranges of f_o lying between 1.5 Mc/s to 2.5 Mc/s, 3.5 Mc/s to 4.5 Mc/s and 5.5 Mc/s to 6.5 Mc/s with the centre f_o values at 2.0 Mc/s, 4.0 Mc/s and 6.0 Mc/s respectively. The experimental results and the corresponding theoretical values expected according to Eq.(9) with the extrapolated value of $f_H = 1.07$ Mc/s at 300 km height are shown in Table III.

DISCUSSION

The gyro-frequency in the E region at Haringhata as obtained from the measurements of f_x and f_o shows a marked semi-diurnal variation (figure 3) with a dip near midday. Similar semi-diurnal variations have also been found by Scott at Resolute Bay (Lat. 74.7°N) and Baker Lake (Lat. 64.3°N). The value of the magnetic field, corresponding to the dip in the gyro-frequency near midday at Haringhata is about 5000 gammas lower than the extrapolated value obtained from inverse cube law. The corresponding values as obtained by Scott are about 13000 and 7000 gammas at Resolute Bay and Baker Lake respectively. No

satisfactory explanation of this diurnal variation of the deduced magnetic field has yet been offered. As shown before, calculation based on the assumption of heavy ions leads to impossible results. It may also be thought that as $(f_x - f_0)$ depends upon f_0 and as f_0 has a diurnal variation, the origin of the diurnal variation may be traced to the f_0 variation. But, the f_0 variation, even in extreme cases, amounts to only 55%, and this is insufficient to explain the magnitude of the variation.

TABLE III

Frequency range	$(f_x - f_0)$ (Experimental) Mc/s	$(f_x - f_0)$ (Theoretical) Mc/s
1.5 Mc/s to 2.5 Mc/s	0.63	0.61
3.5 Mc/s to 4.5 Mc/s	0.60	0.57
5.5 Mc/s to 6.5 Mc/s	0.55	0.56

One may also be tempted to ascribe the variation to the superposition of the magnetic field due to the wide-world upper atmospheric Sq current system on the magnetic field of the earth. Rocket measurements of the magnetic field at high altitudes [Maple *et al*, 1951; Singer *et al*, 1951 and Singer *et al*, 1952] have established the location of the current system near E region. If the current system is assumed to be an infinite horizontal plane current-sheet then the field due to it in the E region will be of the same order as that near ground, namely, about 30 gammas near midday. The observed diurnal variation of the gyro-frequency cannot, therefore, be an effect of the Sq. current system.

F region observations show a seasonal variation in the magnetic field. Thus, Baral and Mitra (1950) from observations of the critical frequencies over Calcutta had found the value of the magnetic field in Winter to be higher than in Summer. Scott has reported a large seasonal variation of 20%. Our observations show that Winter values are only 9% greater than the summer values. No explanation of this seasonal variation is yet available.

Scott has also obtained diurnal and other irregular variations of the apparent magnetic field (from f_x and f_0) in the F region. Our observations, however, do not show such variations. The reason of this may be understood from the explanation of these variations as given by Scott. According to Scott the variations are due to the deflections of the ray paths from the vertical in conjunction with normal latitude gradients of ionization. He shows that the ordinary and extraordinary rays in the ionosphere follow curved paths, as a result of which they are reflected from areas which are displaced north and south of the transmitter. In the absence of electronic collision, the ordinary ray is deflected towards the pole while the extraordinary ray is deflected towards equator in the

vertical plane of the earth's field. In the presence of collisions deflections of the ordinary and extraordinary rays have a small westward component. The horizontal separation of the ordinary and extraordinary reflection points affects the measured values of the critical frequency difference $f_x - f_0$. It is increased due to the separation of the reflection points for the usual variation of ionization with latitude (negative gradient of ionization density). As a result, the gyro-frequency, and hence the earth's magnetic field, calculated from $f_x - f_0$ is larger. Separation of the reflection points depends on the layer semi-thickness, the wave frequency, the magnetic field strength and the dip. It is negligible in the thin E and F1 region but is of considerable magnitude in the F2 region. Variation in the layer thickness (as is present in the F region) will produce a proportional change in the separation of the reflection points. Diurnal variations of the layer thickness, if any, will thus affect the values of f_H and of the magnetic field calculated from $f_x - f_0$. Scott (1950b) has calculated the separation of the reflection points for different values of the magnetic dip angles for a parabolic region. At Haringhata (Magnetic Dip $32^\circ N$) the separation of the reflection points in the F region should be small. It is about 20 kms only at a wave frequency of 10 Mc/s (when electronic collisions are neglected) for normal values of F layer semi-thickness (≈ 50 km). The latitude gradient of ionization density is also small compared to that in the polar latitudes. Thus, the effect of ray-path deflections on the values of f_H and its diurnal variation in the F region over Haringhata calculated from $f_x - f_0$ is small.

ACKNOWLEDGMENT

This work forms part of the programme of the Radio Research Committee of the Council of Scientific and Industrial Research, Government of India, and the authors wish to express their thanks to the Council for financial assistance.

The authors are indebted to Professor S. K. Mitra, F.R.S., for his interest throughout the progress of the work. They are also grateful to Professor J. N. Bhar, D.Sc., F.N.I., for the encouragement given. Thanks are due to Dr. A. K. Saha for helpful suggestions.

REFERENCES

- Appleton, E. V., and Builder, G., 1933, *Proc. Phys. Soc.*, **45**, 208.
 Appleton, E. V., 1934, *Nature, Lond.*, **133**, 793.
 Haral, S. S. and Mitra, A. P., 1950, *J. Atmos. Terr. Phys.*, **1**, 95.
 Maple, E., Bowen, W. A., and Singer, S. F., 1950, *J. Geophys. Res.*, **55**, 115.
 Nakata, Y., 1954, *J. Rad. Res. Lab.*, **1**, 55.
 Scott, J. C. W., 1948, *Terr. Mag. Atmos. Elect.*, **53**, 109.
 Scott, J. C. W., 1950a, *J. Geophys. Res.*, **55**, 65.
 Scott, J. C. W., 1950b, *Proc. I.R.E.*, **38**, 1057.
 Scott, J. C. W., 1951, *J. Geophys. Res.*, **56**, 1.
 Singer, S. F., Maple, E., and Bowen, W. A., 1951, *J. Geophys. Res.*, **56**, 265.
 Singer, S. F., Maple, E., and Bowen, W. A., 1952, *Nature, London*, **170**, 1093.

THE MAGNETIC BEHAVIOURS OF TITANIUM CAESIUM SULPHATE ALUM

A. BOSE, A. S. CHAKRAVARTY AND R. CHATTERJEE

DEPARTMENT OF MAGNETISM, INDIAN ASSOCIATION FOR THE CULTIVATION OF SCIENCE,
CALCUTTA-32

(Received for publication, June 20, 1959)

ABSTRACT. A preliminary short account of a new theory for titanium caesium alum is given. The crystalline field in this alum is treated on the molecular orbital method of Stevens and others, as the usual electrostatic field theory is found to fail to explain the magnetic behaviours. It is proposed that the spin-lattice relaxation follows a "Raman Process" at all temperatures between 300°K to 1.2°K. Experimental susceptibility data between 300°K and 100°K as well as the paramagnetic resonance data at 2.5°K can all be accounted satisfactorily by assuming that the trigonal field splitting changes from -800 cm^{-1} to -165 cm^{-1} , with temperature, which is also indicated by the large observed increase in the spin-lattice relaxation time from 300°K to 1.2°K.

1. INTRODUCTION

A satisfactory theory of vanadium ammonium alum to explain its magnetic and optical behaviours has been given in a recent paper (1959). The magnetic behaviour of the Ti^{3+} ion in crystals of caesium titanium alum shows certain anomalies, which have not been satisfactorily explained so far. Under the usual cubic and trigonal fields existing in the Ti^{3+} alum (Van Vleck, 1939), the ${}^2\text{D}$ ground state of the original free Ti^{3+} ion is split up into an orbital triplet and an orbital doublet lying above it with a cubic separation of about $20,000\text{ cm}^{-1}$ (Hartmann and Schlafer, 1951). The triplet is split by the trigonal field into a lowest lying singlet with a doublet above it (Van Vleck, 1939), but the upper doublet (cubic) is not split by the trigonal field and is thus non-magnetic (Bethe, 1929). Each orbital level has a two-fold Kramers spin degeneracy which is removed only by an external magnetic field or by the spin-spin and exchange interactions. As may be expected for such a highly diluted salt, the last two interactions show a spin splitting of only $\sim 0.002\text{ cm}^{-1}$ from the adiabatic demagnetisation experiments (Kurti and Simon, 1935). We should thus expect the magnetic susceptibility to obey a Curie law very strictly above $\sim 0.003^\circ\text{K}$ upto a temperature at which kT becomes comparable to the trigonal separation Δ , between the lowest orbital singlet and the doublet above it. Unfortunately, the susceptibility data on four different samples of Ti^{3+} alum obtained by Van den Handel (Thesis, 1940) show deviations from Curie law even in the liquid helium range and from one another so wide as to render them quite useless for a theoretical interpretation. The only explanation of the deviations appears to lie in possible

impurities in the samples or chemical decomposition or dehydration of the samples.

The masterly discussions of Van Vleck (1940) show that one has to assume mainly the 'Raman process' as the mechanism of the electron spinlattice relaxation in Ti^{3+} alum at *all* temperatures and that the separation Δ should be of the order of -1000 cm^{-1} , to explain the very short relaxation time $\approx 10^{-7}$ sec. in the liquid air range (Gorter *et al.*, 1938). But at the liquid helium range in order to explain the relaxation time of $\approx 10^{-3}$ sec. (de Haas *et al.*, 1938) Δ has to be taken $\approx -100\text{ cm}^{-1}$. With high magnetic fields in the liquid helium range the 'Direct process' may gain in importance but even that would require Δ to be $\approx -100\text{ cm}^{-1}$.

On the other hand, the experiments on paramagnetic resonance on Ti^{3+} alum, which could be performed only at the helium temperature range, because of the extremely short relaxation times at higher temperatures, yield the values $g_{\parallel} = 1.25$ and $g_{\perp} = 1.14$ for the spectroscopic splitting-factors along and perpendicular to the trigonal axis (Bleaney *et al.*, 1955). These g -values could not be fitted on Abragam and Pryces' theory (1951) with any reasonable value of the splitting Δ and the spin-orbit coupling coefficient ζ in the crystal, consistent with the optical absorption value of the cubic splitting $\approx 20,000\text{ cm}^{-1}$. Assuming a $p-d$ charge cloud overlap factor $k = 0.7$ following Steven's method (1953), a value of $\Delta \approx -50\text{ cm}^{-1}$ is obtained by Bleaney *et al.*, fitting the experimental g -values at helium temperatures, as against Van Vleck's estimate of -100 cm^{-1} .

We have, however, extended Steven's method by assuming anisotropic overlap factors k_z and k_x along and perpendicular to the trigonal axis and obtained the mean susceptibilities fitting to within 2% of the excellent experimental measurements in the range 300° to 100°K of Dutta-Roy (Thesis, 1958), of this laboratory, assuming the following values of the parameters:

$$\begin{aligned} k_z &= 0.800, & k_x &= 0.637 & \text{and } \Delta &\approx -800\text{ cm}^{-1} \\ \zeta_z &= 142.6, & \zeta_x &= 151 \end{aligned}$$

which give $g_z = g_{\parallel} = 1.919$; $g_x = g_y = g_{\perp} = 1.756$.

These g values and Δ are very different from the resonance values. But it is very interesting to note that with the same values of k 's and ζ 's the resonance g values can be made to give a good fit (within experimental errors) with $\Delta \approx -165\text{ cm}^{-1}$.

It is interesting to note that the above method of calculation becomes identical with Abragam and Pryce's method in the limit when $k_x = k_z = 1$, and ζ is the same as the free ion value $+154\text{ cm}^{-1}$ and in the range 100°K to 300°K agrees with the experimental susceptibility values to within 5% assuming $\Delta =$

-1000 cm^{-1} . This latter theory, however, cannot give fit with experimental g values at helium temperatures with any reasonable value of Δ and ζ .

It may be remarked that the decrease in spin-lattice relaxation time from $\sim 10^{-7}$ sec. to $\sim 10^{-3}$ sec. with temperature is dependent on the trigonal component of the field which couples the spins of the ground state (though apparently quite free by virtue of the Kramers degeneracy) to the lattice through the spin-orbit interaction, and clearly shows that the trigonal field has considerably decreased at low temperatures. Our two values of Δ at liquid air and liquid helium range are in very satisfactory agreement with the values estimated roughly by Van Vleck from paramagnetic relaxation data.

It is obvious from the above discussions that the trigonal field splitting in Ti^{3+} alum changes drastically from room to liquid helium temperature. The reduction of g -values with temperature indicated above (owing to increase of the negative orbital contributions) shows that the field has become much more symmetric at helium temperature, and also definitely more covalent as shown by the failure of A. & P.'s theory. From the discussions by Van Vleck on the effect of long range fields (1939) we know that in the Ti^{3+} alum the induced distortional effect of the distant atoms on the Jahn-Teller cluster $\text{Ti}^{3+}6\text{H}_2\text{O}$ may be as important as the J.-T. distortional effect itself. Moreover, the above changes in Δ might be easily brought about by changes in the disposition of the H_2O molecules by as small distances as $\sim 10^{-9}$ cm. In the absence of detailed reliable measurements on susceptibility in the range $100^\circ\text{K}-1^\circ\text{K}$ we are not able to say whether the change in dispositions takes place continuously as a function of the thermal expansion of the lattice or by a transition of crystal phase of some sort occurring at some intermediate temperatures, either of which might explain the experimental observations on Δ . The effect of thermal expansion is certainly observable from the 2% deviation of the theory from the experimental values even in the liquid air range.

The details will be published shortly elsewhere.

ACKNOWLEDGMENTS

Thanks are due to Mr. S. K. Dutta-Roy of this laboratory for his excellent susceptibility values of Ti^{3+} alum and to Mr. S. Roy for his help in calculations.

REFERENCES

- Abragam, A. and Pryce, M. H. L., 1951, *Proc. Roy. Soc.*, **A206**, 173.
Bethel, H. 1929, *Ann. der. Physik*, **3**, 133.
Bleaney, B., Bogle, G. S., Cooke, A. H., Duffus, R. J., O'Brian, M. C. M., Stevens, K. W. H., 1955, *Proc. Phys. Soc.*, **A68**, 57.
Chakravarty, A. S., 1959, *Proc. Phys. Soc.* (In Press).

- de Haas, W. J., 1938, *Physica*, **5**, 969.
Dutta-Roy, S. K., 1958, D. Phil. Thesis, Calcutta University.
Gorter, G. J., 1938, *Physica*, **5**, 969.
Hartmann, H. von. and Schlafer, H. L., 1951, *Z. Naturf.*, **6a**, 760.
Kurtz, N. and Simon, F., 1935, *Proc. Roy. Soc.*, **A149**, 152; **A152**, 21.
Stevens, K. W. H., 1953, *Proc. Roy. Soc. A* **219**, 542.
Van Vleck, J. H., 1939, *J. Chem. Phys.*, **7**, 61
Van Vleck, J. H., 1940, *Phys. Rev.*, **57**, 426.
Van den Handel, 1940, Thesis. Leiden University.

THE RAMAN SPECTRA OF ORTHO-, META-AND PARA-THIOCRESOLS

R. N. BAPAT

(PHYSICS DEPARTMENT, COLLEGE OF SCIENCE, NAGPUR)

(Received for publication April 16, 1950)

Plate VIII

ABSTRACT. The Raman spectra of ortho-, meta- and para-thiocresols have been studied in the present investigation. About twenty Raman lines have been recorded in the case of ortho, twelve in the case of para and about twentyfive in the case of meta- thiocresol respectively. The C-S frequency in thiocresols between 639 cm^{-1} and 685 cm^{-1} is compared with that for other mercaptans. All the three thiocresols show a strong Raman line between $1209\text{--}1222\text{ cm}^{-1}$ which is assigned to C-CH₃ stretching mode. The S H stretching frequency lies between 2566 cm^{-1} and 2577 cm^{-1} in thiocresols. A comparison between Raman spectra of the thiocresols, phenol and thiophenol, is given in a tabular form.

INTRODUCTION

The study of the absorption spectrum of ortho-, meta- and para-thiocresols in the vapour state was undertaken to find the effect of the substitution of SH in place of OH in the three cresols, ortho, meta and para. The infrared spectra of the three thiocresols have been studied in detail. As the Raman frequencies for the three thiocresols were not reported so far, the Raman spectra of these three molecules have been studied in the present investigation.

EXPERIMENTAL

The Raman spectra of the three thiocresols were photographed on a three-prism Steinheil spectrograph. The Raman source of Steinheil consists of a horizontal mercury arc placed in a chamber cooled by circulating water through the tubes in the chamber. The light from the arc was focussed by two common paraboloid reflectors on a tube kept horizontally at their focus, the tube containing the substance under investigation. The length of the tube is about 20 cm. In between the tube and the arc was kept a filter transmitting only the 4358\AA group of radiations of mercury. Carbon tetrachloride was first distilled and collected in the tube itself and the Raman spectrum of carbon tetrachloride was first recorded (figure 1) in order to eliminate the Raman lines from this substance. Parathiocresol was next dissolved in carbon tetrachloride. The substance is very soluble and a large quantity of the substance was dissolved and the solution put in the experimental tube. It was observed that the intensity

of the Raman lines improved with higher concentrations. An exposure of three hours with this source was necessary to bring out the details in the spectrum (figure 2). Ilford HP3 Hypersensitive panchromatic plates were used to record the spectra. An iron arc spectrum was superposed in the centre, and the wavelengths of the Raman lines were calculated by Hartmann's dispersion formula using iron lines as standard. In the case of the ortho and meta thiocresols the liquids were directly distilled in the experimental tube and the Raman spectra recorded in the same manner as explained above. The wavelengths tabulated in Table I are the mean of the three readings and are accurate to $\pm 6 \text{ cm}^{-1}$. The Raman spectra of meta thiocresol and ortho thiocresol are given in figures 3 and 4 respectively.

The wavelengths of the Raman lines are given in Table I with the intensities visually estimated and having the following meaning, *v.s.* -very strong, *s.*-strong, *ms.*-medium strong, *mw.*-medium weak, *w.*-weak, *vw.*-very weak and *vvw.*-very very weak.

TABLE I
Comparison of Raman frequencies of phenol, thiophenol
and thiocresols

Present work		Present work		Present work		Phenol (Ananth- krishnan 1936)	Thiophenol (Venkate- swaran 1930)
Ortho-thiocresol Raman	Infrared	Meta-thiocresol Raman	Infrared	Para-thiocresol Raman	Infrared	Raman	Raman
1	2	3	4	5	6	7	8
		121 vvw					
147 vw		146 vw					
233 m		177 vw				243 (-)	194 (5d)
334 w		223 mw					282 (2d)
432 m		410 w					415 (3)
500 w						—	
552 m		523 m				507 (3)	
						532 (4)	
						590 (0)	596 (0)
						620 (4)	618 (3)
661 m	676 m	685 ms	686 (s)	639 w	—	655 (00d)	695 (3)
723 w						756 (3)	730 (0b)
	772 s						
795 ms	797 m		772 vs		789 m	787 (0b)	
						812 (8)	
882 w		855 mw	853 s			830 (3)	

TABLE I (contd.)
Comparison of Raman frequencies of phenol, thiophenol
and thiocresols.

Present work		Present work		Present		Phenol (Ananth- krishnan 1936)	Thiophenol (Venkate- swaran 1930)
Ortho-thiocresol Raman	Infrared	Meta-thiocresol Raman	Infrared	Para-thiocresol Raman	Infrared	Raman	Raman
1	2	3	4		6	7	8
919 m	924 m	918 vvw 942 vw	919 m		913 m		918 (4d)
968 m						991 (0)	
		1001 vs	982 m	985 m	1002 vw	1001 (10)	1000 (10)
1047 s	1046 s		1041 m	1036 w	1041 m	1027 (8s)	1024 (4)
		1084 m	1083 ms			1072 (1)	1071 (0) 1092 (3)
	1111 m	1111 m	1109 ms	1102 vs	1115 ms	1113(0)	1118 (3)
						1155 (3s)	1157 (2)
		1172 m	1168 ms			1170 (4s)	
1209 ms	1217 ms	1221 ms	1218 m	1222 m	1211 m		
	1250 vw	1276 vw	1272 vw		1232 w	1253 (2h)	
1369 i	1381 m	1383 mw	1383 w	1386 w	1379 m		1361 (1d)
						1425 (00) 1464 (0)	1432 (0d)
	1408 sh 1475 s 1577 m		1401 sh 1479 s 1582 s		1403 ms 1497 s	1498 (½) 1595 (5)	1502 (0b) 1584 (5)
1611 i	1595 m	1597 m	1603 s	1597 s	1608 vw	1605 (5)	
					1631 m		
				2492 vw			
2566 w	2577 m	2575 vw 2870 vw	2577 m	—	2571 w		2573 (7d)
2913 m	2941 m	2927 m	2941 m	2914 m	2924 m		2945 (1b)
						3017 (½h)	
						3051 (5)	
3051 m	3067 m	3055 ms 3117 vvw 3176 vvw	3067 m	3051 m	3030 m	3064 (8)	3059 (8d)
				3136 w		3085 (½) 3150 (00d)	
						3200 (0bd)	
						3524 (00d)	

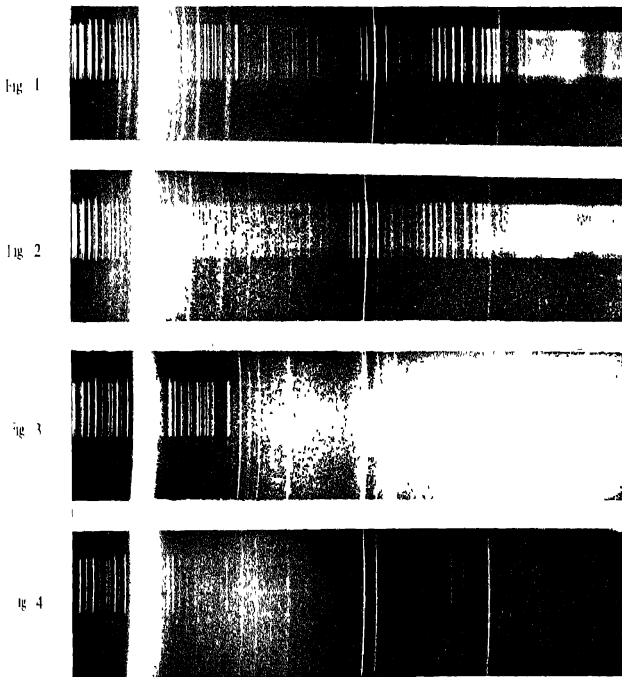
DISCUSSION

All the three isomers have certain features common in their Raman spectra. These will be discussed first. All the three thiocresols give a strong Raman line between 639 cm^{-1} and 685 cm^{-1} . The corresponding line in thiophenol is at 695 cm^{-1} . In the case of mercaptans (Sheppard, 1950) it is shown that the C-S frequency usually falls in this range. In analogy in the present case these frequencies have been assigned to C-S stretching mode. Comparison shows that there is no corresponding frequency either in toluene or phenol and hence such an assignment is justified. It may be observed that the corresponding frequencies are very strong in ortho and meta-isomers but rather weak in para-isomer. One would expect two lower frequencies arising out of the two split frequencies corresponding to 606 cm^{-1} of benzene. In thiophenol these presumably are 596 cm^{-1} and 618 cm^{-1} . In the thiocresols, however, the bands at 552 and 523 cm^{-1} in ortho and meta thiocresols respectively may be one of these, the other component being obscured by the strong C-S band.

In ortho-thiocresol there is a strong Raman line at 795 cm^{-1} which has no corresponding line in meta- and para-thiocresols. The comparison with infrared spectrum shows that there are strong infrared bands at 772 cm^{-1} and 789 cm^{-1} in the meta and para isomers. These have been assigned as corresponding to 992 a_{1g} breathing benzene vibration. The frequencies corresponding to this mode in the Raman spectra of toluene and phenol are $786, 812\text{ cm}^{-1}$. In thiophenol, however, there is no strong line corresponding to this frequency. The assignment of this frequency has been recently reviewed and it seems to be more justifiable to choose a value less than 992 according to Wilmshurst (1957) and Bernstein rather than about 1000 cm^{-1} as was done by Pitzer and Scott (1943). It, however, does not explain why this line particularly should not appear in the Raman spectra of meta and para thiocresols and phenol though there are strong bands in infrared in about the same region.

In the region around 1000 cm^{-1} there are two strong lines in toluene at 1004 cm^{-1} and 1030 cm^{-1} . Such lines in thiocresols are at 1046 cm^{-1} in *o*-thiocresol, 1001 cm^{-1} and 1084 cm^{-1} in *m*-thiocresol and 985 and 1036 cm^{-1} in *p*-thiocresol. At least three lines are expected in this region and following Wilmshurst and Bernstein, the line corresponding to 1004 cm^{-1} of toluene is assigned to 1010 b_{1u} of benzene. The other lines near 1040 and 1080 cm^{-1} are in the region where CH_3 rocking vibrations are expected. These lines are assigned as such in the Raman spectra of thiocresols.

The next strong Raman line in all the spectra of thiocresols is the strong one between 1209 and 1222 cm^{-1} . This apparently corresponds to the strong line at 1208 cm^{-1} of toluene and following the assignment in toluene it has been assigned



Raman spectra

- Fig. 1. Raman spectrum of CCl_4
 Fig. 2. " " " *p*-thiocresol (in CCl_4 solution)
 Fig. 3. " " " *m*-thiocresol
 Fig. 4. " " " *o*-thiocresol

to C-CH₃ stretching mode. That there is no corresponding line in phenol or thiophenol substantiates such a conclusion.

All the thiocresols show a line near 1369—1386 cm⁻¹ and toluene shows a corresponding strong line at 1379 cm⁻¹. In the case of toluene it has been assigned to an internal mode arising out of methyl group corresponding to CH₃ symmetric bending. The intensity of this line is however much weaker in meta and para-thiocresols and is stronger in *o*-thiocresol.

Ortho and meta-thiocresol show Raman lines near 1570 cm⁻¹ and 1600 cm⁻¹ which correspond to two lines in toluene at 1585 and 1604 cm⁻¹. These in the case of toluene correspond to the two components of the 1596 ν_6^+ frequency of benzene. The values corresponding to these are as shown in Table II. The question of assignment of the frequencies in *p*-thiocresol is, however, doubtful. The Raman spectrum of *p*-thiocresol shows a single strong line near 1597 cm⁻¹ and the infrared spectrum two bands, a weaker one at 1608 cm⁻¹ and a stronger one 1631 cm⁻¹. It is rather difficult to choose the two bands. The most obvious choice is 1597 and 1631 cm⁻¹, but the latter frequency however seems too large as compared to that in other disubstituted benzenes. This value however seems to be in line for a trisubstituted benzene. This is however true also of *p*-xylene and this observation about the relation of split frequency as a function of position of substitution has yet to be verified.

The next strong line obviously corresponds to S—H stretching frequency and is common to all the isomers. It lies between 2566–2577 cm⁻¹ in all the cases. Here again the line is missing in the case of para-thiocresol. The infrared band corresponding to this in infrared is also weak in case of para-isomer as compared to ortho- and meta-isomers. The two other bands on the higher frequency side, one near 2900 and the other near 3050 cm⁻¹ correspond to CH stretching of the methyl group and the aromatic CH stretching vibrations respectively.

It is thus observed that there are some interesting individualities in the Raman spectra of these isomers corresponding to position of substitution. It would be interesting to compare these in the corresponding cresols.

In the molecules as under discussion, a large number of vibrations are expected below 500 cm⁻¹ arising out of different bending modes specially due to substituents. In the present case about five frequencies are observed in the case of both *o*- and *m*-thiocresols. In the case of *p*-thiocresol the observations have not been extended to that region. It is rather difficult to give an unequivocal assignment of these bands, since the correlation with either the thiophenol or toluene spectrum is not possible. These low frequency vibrations in all these compounds possibly offer a fruitful subject for further investigation.

ACKNOWLEDGMENT

The author is indebted to Dr. R. K. Asundi and Dr. M. R. Padhye for their keen interest during the progress of the work.

REFERENCES

- Ananthkrishnan, R. 1936, *Proc. Ind. Acad. Sci.*, **3A**, 52.
Pitzer, K. S. and Scott, D. W. 1943 *Journ. Amer. Chem. Soc.* **65**, 803
Shoppard, N. 1950, *Trans. Far. Soc.* **46**, 429.
Venkateswaran, S. 1930 *Ind. J. Phys.* **5**, 219.
Wilmslust, J. K. and Bernstein, H. J., 1957, *Canad. Journ. Chem.*, **35**, 226

LOW ENERGY SPECTRUM OF THE SEA LEVEL ELECTRONS AND MUONS AT 12°N

NILIMA MISHRA (BASU)* AND M. S. SINHA

BOSE INSTITUTE, CALCUTTA

(Received, June 30, 1959)

ABSTRACT. The slow electron and muon components of cosmic rays at sea level and 12°N geomagnetic latitude have been studied with a multiplate cloud chamber triggered by a coincidence-anti-coincidence system. The differential energy spectra of these electrons have been obtained for energies between (5–300) Mev. The electron spectrum is found to be represented by a simple power law of the form $15 \cdot 1 \cdot 2$. In the range interval (7.60) g/cm² of air equivalent the differential range spectrum of muons has also been determined. The spectrum is found to be flat with a mean intensity $(5.89 \pm 0.15) \times 10^{-9}$ /g sec. varied in the range interval (15–60) g/cm² of air equivalent. Below this range the muon intensity falls off gradually. A comparison of the total intensities of muons and electrons has also been given.

1. INTRODUCTION

This paper contains the final and detailed results of previous investigations on the muon spectrum at Calcutta reported earlier by Basu and Sinha (1956–57). A multiplate cloud chamber was triggered by means of a narrow angle three-fold coincidence system placed above the chamber together with an anticoincidence tray placed just below, in order to photograph all particles which stopped inside the cloud chamber. There were seven $\frac{1}{4}$ " (5.6 g/cm²) of Cu plates inside the chamber and the total amount of material above the chamber was 6.5 g/cm² of air equivalent. Any muon stopping inside the chamber showed more than twice minimum ionisation in the last gap while electrons stopped with minimum ionisation. Fast electrons produced small soft showers all the secondaries of which had to stop inside the chamber.

Thus an estimate could be made of the number of low energy muons and electrons crossing our apparatus in a definite interval of time. The following information were obtained. (1) A fine structure of the differential range spectrum of muons within the range interval 6.5–61.3 g/cm² of air equivalent, (2) The differential energy distribution of electrons in the energy interval (5–300) Mev.

2. EXPERIMENTAL

The main body of the cloud chamber consisted of a glass cylinder with illuminated cylindrical volume of 30 cm diameter and 8 cm deep. It was filled with argon to a pressure of 96 cm of Hg and illuminated by Xenon flash tubes

* Now at Bethune College, Calcutta.

placed behind pairs of condensing lenses. The triggering arrangement $C_1C_2C_3-A$ is shown in figure 1. During this part of the investigation, there were seven $1\frac{1}{4}$ " Cu-plates inside the chamber. The solid angle times area of the three-fold counter

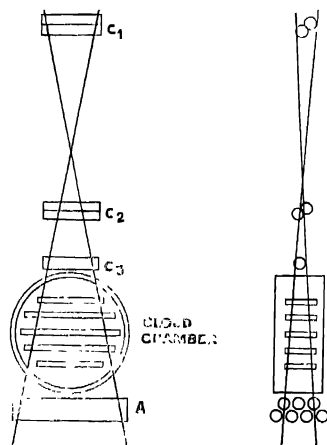


Fig. 1. The experimental arrangement of the various counter trays and the cloud chamber fitted with Cu-plates. In the present experiment there were seven Cu-plates instead of five as shown in the figure.

arrangement was $0.677 \text{ cm}^2\text{--Steradian}$. This solid angle was completely covered by the anticoincidence counters placed below the chamber. Stereoscopic photographs were taken and the ionisation and scattering angles of particles (where necessary) were evaluated from both the views.

The apparatus was covered by a thin roof consisting of 0.075 cm thick iron and 3.7 cm celotex. Other materials in the solid angle of the counter system were only the counter walls and counter trays. All these added together gave a total thickness of 6.5 gm/cm^2 of air equivalent.

The particles stopping in any one of the seven plates were identified from their ionisation characteristics only. The tracks of stopping electrons were nowhere dense, those of stopping muons were dense in the last compartment and in some cases slightly dense in the previous one and those of stopping protons were dense in all the compartments.

3. ENERGY CALIBRATION OF THE ELECTRONS

The energies of electrons which appeared singly inside the chamber were estimated from their ranges R inside the chamber. The values of R were calculated

by numerically integrating the curves of the total rate of energy loss, both radiation and ionisation as a function of energy. The average range of an electron as a function of its energy is given by

$$R = \int_0^{E_0} dE/(-dE/dx)$$

where E_0 is the energy of the stopping electron.

Fast electrons almost always give rise to showers and their energies can be estimated from the size of the shower. The equation (12) of Rossi (1952) gives the expression for the total number of electrons $\pi(E_0, 0, t)$ as function of thickness t . For electron initiated shower, the maximum value of the function $\pi(E_0, 0, t)$ is given by

$$\Pi_{max}(E_0, 0) = \frac{0.31}{|\ln(E_0/\epsilon_0) - 0.37|^{\frac{1}{2}}} \cdot \frac{E_0}{\epsilon_0}$$

where,

ϵ_0 = critical energy of the electron in the particular absorber

E_0 = energy of the initiating electron

Π_{max} = number of electrons at shower maximum

Thus from the number of particles at shower maximum, the initial energy of the initiating electron can be estimated, without making any use of information which might be derived from observations at points other than the maxima. This method is not very satisfactory for energies where the maximum number of electrons is small and therefore subject to large fluctuations. Hence an equation given by Bridge, Courant, DeStaebler and Rossi (1954) has been used to estimate the shower energy E_0 . According to this equation

$$E_0 = hNt \quad \dots (2)$$

where,

h = a constant which depends upon the cut-off energy

N = total number of electron tracks appearing in the separate sections of the chamber through which the shower develops

t = thickness of the plates measured in the direction of the shower axis

Thus Nt is an approximate value for the track length of the observable shower electrons which, according to shower theory, is proportional to the energy of the initiating particle.

The proportionality constant h was calculated after studying a few well-developed showers with at least 4 secondary electrons at the shower maximum

and for which the total number N of electrons at different sections of the cloud chamber was also known. These were consistent with the general theoretical expression for $\pi(E_0, 0, t)$, the maximum of which is given by equation (1). Thus for a number of showers E_0 was found out from equation (1) and for these N and t were also known. In this way a number of values of h was found out and the mean value of $h = 4.2$ Mev/gm of Cu was taken to calculate the initial energy of other shower-initiating electrons from the equation (2).

4. CORRECTIONS OF THE OBSERVED DATA FOR SCATTERING

The most serious error encountered in the measurement of the intensity of the soft component is the multiple scattering of low energy electrons both in air as well as in the apparatus, before the electron enters the cloud chamber. Barker (1955), however, pointed out that the scattering in the roof, the chamber wall, top counters and bottom counters can be neglected even for low energy (> 10 Mev) electrons as the number scattered out and scattered in will be approximately the same; but the scattering in the central counters is the main source of error. The electrons which scatter in the top counters in such a way that they go out of the solid angle of the counter system are compensated by those which enter the solid angle only because of the scattering in the top counters, and the third counter tray is so near the chamber that it may be assumed that all the electrons that excite this tray will enter the chamber. But the electrons which scatter in the central counters in such a way that they miss the bottom counter will be completely eliminated and the compensation by others scattered in, will be very small because these are required to pass through the top counters.

Following Barker, we assume that the average path length through two walls of a counter for particles uniformly distributed in space and moving perpendicular to the axis of the counter is equal to πd where d is the thickness of a counter wall. Then assuming the Gaussian angular distribution as given by Rossi and Greisen, (1941) the fraction F of electrons of energy E which are missed on account of scattering will be given by

$$F = 2(\lambda E)^{-2}(2\pi)^{-\frac{1}{2}}[h_2(0) - 2h_2(\lambda E) + h_2(2\lambda E)] \quad \dots (3)$$

where,

$$\lambda = 4a(2\pi d)^{-\frac{1}{2}}(21L)^{-1}$$

$$a = \text{diameter of a counter wall} = 2.7 \text{ cms}$$

$$L = \text{distance between the top and bottom counters} = 60 \text{ cms.}$$

$$d = \text{thickness of a counter wall in radiation lengths} = .015 \text{ cm Cu} = .011 \text{ radiation length}$$

Substituting these values we get $\lambda = 0.0345 \text{ Mev}^{-1}$

$h_0(x)$ are calculated from the tabulated functions

$$h_0(x) = \int_x^{\infty} \exp(-y^2/2) dy$$

$$h_1(x) = \int_x^{\infty} h_0(y) dy$$

$$h_2(x) = \int_x^{\infty} h_1(y) dy$$

The values of F are calculated for all the seven energy intervals assuming a mean energy for each energy interval. The corrected number is then obtained by multiplying the observed number of electrons by the factor $(1-F)^{-1}$.

5. ENERGY DISTRIBUTION OF ELECTRONS

Table I shows the distribution of electrons in different energy intervals. One of the characteristic features revealed from this table is that as the electron energy has increased the number of single electrons has decreased and the number of shower initiating electrons has increased. This is in qualitative agreement with shower theory. In column 5 the corrected total number of electrons within the different energy regions has been given. Since the energy interval has gradually increased with the increase of energy, the total number of electrons for each energy interval was divided by the corresponding energy interval in order to obtain the energy distribution per Mev in that energy interval.

TABLE I
Energy distribution of electrons

Energy interval Mev	Observed number of electrons Single	shower initiating	Total	Corrected number of electrons	Total number of electrons per Mev
5- 16	108		108	360	32.66 ± 1.09
16- 32	69		69	121	7.55 ± 0.44
32- 56	56	5	61	77	3.20 ± 0.24
56- 87	51	9	60	65	2.11 ± 0.17
87-132	37	7	44	46	1.03 ± 0.09
132-203	29	10	39	40	0.56 ± 0.06
203-310	14	25	39	39	0.37 ± 0.04

This distribution has been plotted in a double log scale in figure 2. It is found that within the energy band (5-300) Mev, the differential energy distribution is well represented by a simple power law of the form $E^{-1.2}$. Barker obtained a distribution of slope -1 between 30-400 Mev at 45°N , and for energy band above 400 Mev the slope was -1.5 .

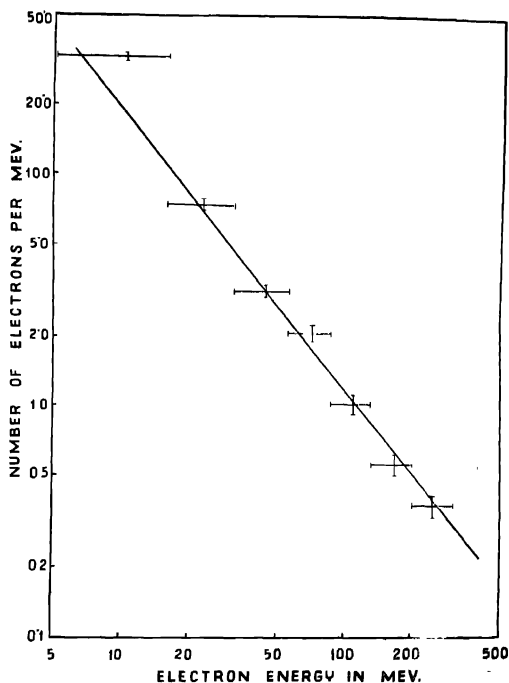


Fig. 2. The differential energy distribution of electrons.

6. RANGE DISTRIBUTION OF MUONS

A differential range spectrum of muons has been obtained previously by the authors, Basu and Sinha (1956-57) in the range interval $6.5\text{--}140\text{ g/cm}^2$ of air equivalent. It was pointed out there, that this range spectrum could not be evaluated accurately at the lowest range interval as the electron contribution in this region cannot be calculated from shower theory. Hence the Cu-plates were split into halves and the muons were experimentally separated from the electrons by ionisation characteristics alone. Furthermore, the splitting of the Cu-plates led to a determination of the fine structure of the muon spectrum in the lowest range interval.

The experiment was divided into two parts. The first part was carried out with no absorber above the chamber and during the second part a 4.5 cm lead absorber was placed above the chamber. The correction for the loss of particles due to scattering in this absorber and in the plates inside the chamber was taken into account exactly in the same manner as explained in the previous paper Basu and Sinha (1956-57). Table II shows the values of the muon intensity I_μ . The small gap between (32-36) g/cm² of air is due to the fact that the muons stopping in the last plate were not taken into account because of the inefficiency of the system in photographing these particles due to the emission of decay electrons in the downward direction so as to trip the anti counters.

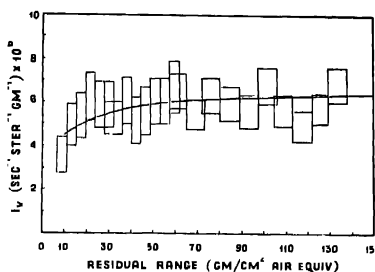


Fig. 3. The differential range spectrum of mu-mesons. The solid curve shown along is Sand's computed sea-level spectrum for mu-mesons.

In figure 3 the combined differential range spectra as found in this experiment and the previous one have been plotted as a histogram. The solid curve shown along the experimental histograms is Sand's (1949) computed sea level range spectrum of muons. The two curves are found to agree satisfactorily within experimental errors. The data below 20 g/cm² of air equivalent have been obtained for the first time in this experiment. It is clear from the histogram that the decrease in the muon intensity when we go below 20 g/cm² as predicted by Sand's computations is real.

7.8. The ratio of electrons to muons for different kinetic energy intervals

From the foregoing data on the intensity of low energy electrons and low energy mu-mesons we can construct a comparative data on the ratio of the intensities of these two kinds of particles at different energy intervals. Hence the whole muon distribution obtained during this and the previous experiments was converted into corresponding kinetic energy intervals from the curves of Rossi (1948). The mu-meson spectrum thus obtained covered the kinetic energy interval (35-304) Mev. In Table III the range as well as the K.E. distribution of mu-mesons have been shown.

TABLE II

Absolute differential range spectrum of muons at 12°N (Fine Structure)

Range interval (g/cm ² of air equivalent) R	Observed number of muons N	Total sensi- tive time in hours T	Vertical differ- ential muon- intensity I_0 gm ⁻¹ sec ⁻¹ sterad ⁻¹ × 10 ⁶
6.50-10 75	8	215	3.59 ± 0.84
10 75-15 00	11	215	4.94 ± 0.97
15.00-19.25	12	215	5.39 ± 1.03
19.25-23 50	14	215	6.28 ± 1.10
23 50-27 75	13	215	5.83 ± 1.08
27 75-32.00	13	215	5.83 ± 1.08
35 80-40 05	13.7	215	6.05 ± 1.09
40.05 44 30	11.7	215	5.15 ± 1.02
44.30-48.55	12.7	215	5.60 ± 1.07
48.55-52 80	13.7	215	6.05 ± 1.09
52 80-57 05	13.7	215	6.05 ± 1.09
57 05-61 30	14.2	215	6.72 ± 1.21

TABLE III

Range and kinetic energy distribution of mu-mesons

Range interval (g/cm ² of air equivalent)	Kinetic energy interval (Mev)	Number of muons	Number of muons per Mev in 215 hours
6.50- 10.75	35- 48	8	0.62 ± 0.15
10.75- 19 25	48- 69	23	1.07 ± 0.15
19.25- 32.00	69- 98	40	1.38 ± 0.13
35.80- 48 55	107-132	37	1.45 ± 0.16
48.55- 61.03	132-158	42	1.63 ± 0.16
72.00- 89.50	181-214	54	1.70 ± 0.15
89.50-106.50	214-246	55	1.70 ± 0.16
104.65-137.70	240-304	102	1.60 ± 0.11

In figure 4 both mu-mesons and electron distributions have been plotted in a bilogarithmic scale where the abscissa are the kinetic energies in Mev and the ordinates the corresponding numbers of particles per Mev. The error has been

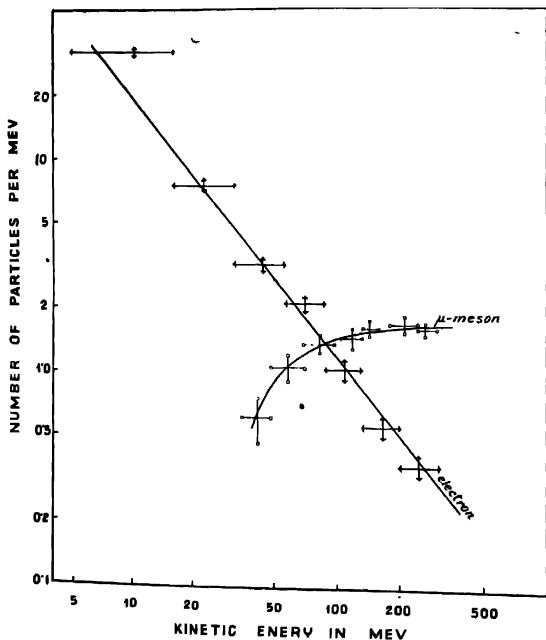


Fig. 4. The differential energy distribution of electrons and muons as function of their kinetic energies.

calculated from the probable statistical error ($0.67\sqrt{n}$) where n is the number of particles. These curves give directly the ratio of electrons to muons within different kinetic energy intervals ranging from 35 to 300 Mev at sea level.

It is interesting to note that the two curves intersect at 95 Mev and therefore electrons and muons of kinetic energy 95 Mev are almost equally abundant at this place.

8. TOTAL VERTICAL INTENSITIES OF THE PENETRATING PARTICLES AND THE LOW ENERGY ELECTRONS

The three-fold counting rate with 10 cm pb above the cloud chamber was found to be 0.317 min^{-1} . A large number of photographs triggered by a three-fold coincidence only, was taken and finally the corrected vertical intensity of the

penetrating particles was obtained from the observed rate of acceptable pictures, after excluding blanks, showers and heavy particles. This was found to be $(0.0073 \pm 0.00026) \text{ cm}^{-2} \text{ sterad}^{-1} \text{ sec}^{-1}$. Chandrasekharan *et al* (1950) measured the verticle intensity of penetrating cosmic rays (with 10 cmPb) at Poona (9°N) which is 555 meters above sea level, in terms of counts per minute. From the given geometry of the quadruple coincidence counter telescope used in this experiment, the vertical intensity of penetrating particles at Poona has been found to be $0.0076 \text{ cm}^{-2} \text{ sterad}^{-1} \text{ sec}^{-1}$. This is in good agreement with our observations at 12°N at sea-level. The value quoted by Rossi (1948) at 45°N as determined with counter telescope was 0.0083 at sea level.

The vertical intensity of electrons I_e with energy between 5–310 Mev was found to be $(0.00143 \pm 0.00021) \text{ cm}^{-2} \text{ sec}^{-1} \text{ sterad}^{-1}$ after correcting for scattering. Combining this value with the total intensity I_v of penetrating particles (0.0073 ± 0.00026) , we get a ratio $I_e/I_v = 0.020 \pm 0.03$ for electrons of energy below 300 Mev. at 12°N .

From the data of Hazen (1945) and more recently of Barker (1955) we find that, for latitude $>45^\circ$ the ratio I_e/I_v when I_e expresses electron intensity of energy >300 Mev is nearly 3%. Taking for granted that this ratio remains the same at low latitudes we find $I_e/I_v = 0.23 \pm 0.04$ when I_e expresses the intensity of all electrons of energy >5 Mev. This gives the vertical intensity of electrons at Calcutta (sea-level, 12°N) as (0.00167 ± 0.00029) compared with the value of 0.0022 obtained by Barker after extrapolating Rossi's curve. The ratio I_e/I_v as obtained by Barker (1955) for Ann Arbor (45°N) is 0.311 ± 0.028 with $E > 10$ Mev. Conversely, if we accept that the ratio I_e/I_v remains the same for all latitudes our results would then indicate that the percentage of high energy electrons (>300 Mev) in the sea level electron spectrum at 12°N is higher than that at 45°N by a factor of about three. An independent measurement of the intensity of electrons of energy >300 Mev at this station is needed to decide between the two alternatives.

ACKNOWLEDGMENT

The authors wish to acknowledge with thanks the financial help from A.E.C., Government of India, and are grateful to Dr. D. M. Bose, Director, Bose Institute, for his kind advice and encouragement during the progress of the work.

REFERENCES

- Barker, P. R., 1955, *Phys. Rev.*, **100**, 860.
 Basu, N. and Sinha, M. S., 1956-57, *Trans Bose Res. Inst.*, **21**, 67.
 Bridge, H. S., Courant, H., Destuehler, H. and Rossi, B., 1954, *Phys. Rev*, **95**, 1101.
 Chandrasekharan, K. S., Gokhale, G. S. and Rao, A. S., 1950, *Proc. Ind. Acad. Sci.*, **32**, 95.

- Hazen, W. E. and Lombardo, B., 1945, *Phys. Rev.* **68**, 74.
Mathematical Tables Vol. (British Association for the Advancement of Science, London, 1931).
Rossi, B., 1952, High Energy Particles 257.
Rossi, B. and Greison, K., 1941, *Rev. Mod. Phys.*, **13**, 240.
Rossi, B., 1948, *Rev. Mod. Phys.* **20**, 537.
Sands, M. Technical Report No. 28, Laboratory for Nuclear Science M.I.T. (unpublished) 1949.

INFRARED ABSORPTION SPECTRA OF ETHYLENE CHLORHYDRIN IN THE VAPOUR STATE AND IN SOLUTION IN DIFFERENT SOLVENTS*

MONOMOCHAN MAZUMDER

OPTICS DEPARTMENT, INDIAN ASSOCIATION FOR THE CULTIVATION OF SCIENCE,
CALCUTTA-32

(Received for publication June 25, 1959)

ABSTRACT The infrared absorption spectra of pure ethylene chlorhydrin in the vapour state at 28°C and 70°C and of its solutions in CCl_4 , C_2Cl_4 and heptane have been recorded with a Perkin Elmer Model 21 spectrophotometer. It is observed that the ratio of the integrated absorption at the bands 662 cm^{-1} and 750 cm^{-1} remains almost the same when the liquid at 28°C is converted into vapour, while the ratio diminishes considerably when the vapour is heated to 70°C. In the case of solutions in CCl_4 and C_2Cl_4 the band 750 cm^{-1} disappears, while in the case of solution in heptane no such change takes place. These results have been explained on the assumption that in the liquid state almost all the molecules are in the associated state forming two types of dimers one through the OH...Cl bond and the other through the H-O...H bond.

INTRODUCTION

Mizushima *et al* (1939) had earlier studied the infrared absorption spectrum of ethylene chlorhydrin in the vapour state and observed three absorption maxima due to the second harmonic of the OH vibration. They assigned two of them to one molecular form and the remaining one of much lower frequency to the other. In the latter form the hydroxyl hydrogen was assumed to be coupled with the chlorine atom to form the cis configuration and the alternative form, in which the hydroxyl group was free, was considered to be the trans configuration. In the liquid state they observed only one absorption maxima and assigned it to the cis configuration. The absence of the trans configuration in the liquid state was explained by them on the assumption that the molecules of such configuration form intermolecular hydrogen bond so that the absorption due to the OH group is depressed. Later, by studying the Raman spectrum of ethylene chlorhydrin in the liquid and solid states Mizushima *et al* (1940) assigned the line 662 cm^{-1} to the trans configuration and the line 751 cm^{-1} to the gauche configuration of the molecule. In the liquid state the ratio of intensities of the lines 751 cm^{-1} and 662 cm^{-1} was found to be about 0.7. Again, Mizushima *et al* (1951) studied the infrared absorption spectrum of this compound in the vapour state at different

*Communicated by Prof. S. C. Sarkar

temperatures ranging from 82°C to 250°C and found the ratio of intensities of the absorption bands 760 cm^{-1} and 669 cm^{-1} to change from 0.551 to 0.848 with the change of temperatures mentioned above.

The Raman spectrum of the vapour of the substance at 130°C and 180°C studied by Mazumder (1955) showed that the intensity-ratio of the two lines 750 cm^{-1} and 662 cm^{-1} is about 1 : 1 at 130°C and 5 : 1 at 180°C. These results are not in agreement with those for the infrared spectra reported by Mizushima *et al* (1951). In order to understand the cause of this discrepancy and also to find out the influence of intermolecular forces on the ratio of population of the two configurations of the molecule, the infrared absorption spectra of ethylene chlorhydrin in the vapour state at 28°C and about 70°C, liquid state at 28°C and also of its solution in different solvents have been investigated and the results have been compared with those reported by previous authors.

EXPERIMENTAL

The infrared absorption spectra were recorded with a Perkin-Elmer Model 21 spectrophotometer. Compensation cells containing pure solvents were used in the reference beam to balance the absorption due to the solvents in each case while the spectra due to the solutions were recorded.

Chemically pure ethylene chlorhydrin obtained from B.D.H. was dehydrated and fractionated. The solvents were also of purest quality. The absorption spectra of the pure liquid were recorded by using very thin films of the liquid enclosed between two NaCl discs. The thickness of the sample cell containing solutions was about 2% larger than that of the compensating cell used in the reference beam.

A 10-cm cell containing a few drops of ethylene chlorhydrin in a side tube was used to record the absorption spectrum of the vapour. In this case also a compensating cell was used. The apparatus was balanced very carefully till the CO_2 bands due to atmospheric carbon dioxide were absent in the record. The C-Cl bands due to the solvents were also absent in the test records when only either CCl_4 or C_2Cl_4 was introduced in the cells in both the beams.

RESULTS AND DISCUSSION

The absorption curves due to ethylene chlorhydrin in the liquid state, in the vapour state at 28°C and about 70°C and those of the solutions in CCl_4 , C_2Cl_4 and heptane are reproduced in figures 1-5 and 7 respectively. The frequencies of the bands in the spectra are given in Table I.

It can be seen from Table I as well as figure 1(b) that in the liquid state the band due to OH valence oscillation is many times stronger than the two bands at 2960 cm^{-1} and 2880 cm^{-1} due to CH valence oscillations and it extends from 3100 cm^{-1} to 3650 cm^{-1} with the broad maximum at 3360 cm^{-1} and a low inflexion

TABLE I

Frequencies of the absorption bands in the spectra in cm^{-1}

Pure ethylene chlorhydrin		Solution of ethylene chlorhydrin		
Liquid	Vapour	in CCl_4	in C_2Cl_4	in heptane
662 (3)	662 (2)	662 (5)	660 (5)	660 (3)
740 (2)	750 (1)			750 (2)
840 (2)	840 ($\frac{1}{2}$)	842 (1)	840 (1)	840 ($\frac{1}{2}$)
930 (5)	920 (2)	925 (4)	920 (1)	920 (2)
1025 (12)	1035 (10)	1030 (8)	1030 (8)	1025 (12)
1065 (15)	1060 (15)	1065 (16)	1065 (20)	1065 (15)
1160 (1)	1180 (2)	1160 (0)		1180 (1)
1240 (1)		1190 (0)	1195 (1)	
1295 (4)	1285 (2)	1295 (3)	1290 (4)	1280 (2)
1380 (0)	1380 (3)	1380 (1)	1385 (2)	1380 (1)
1430 (3)	1430 (0)	1430 (3)	1430 (3)	1430 (1)
2800 (3)	2800 (4)			
2950 (5)	2950 (6)			
3350 (15b)	3400(1b)			
3600 (3)	3640 (2)			

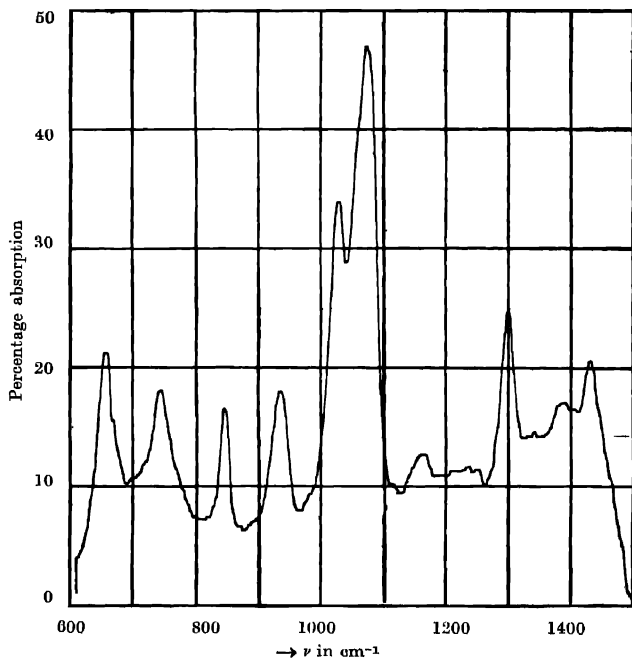


Fig. 1(a). Infrared absorption curve of thin film of pure ethylene chlorhydrin formed between two NaCl discs.

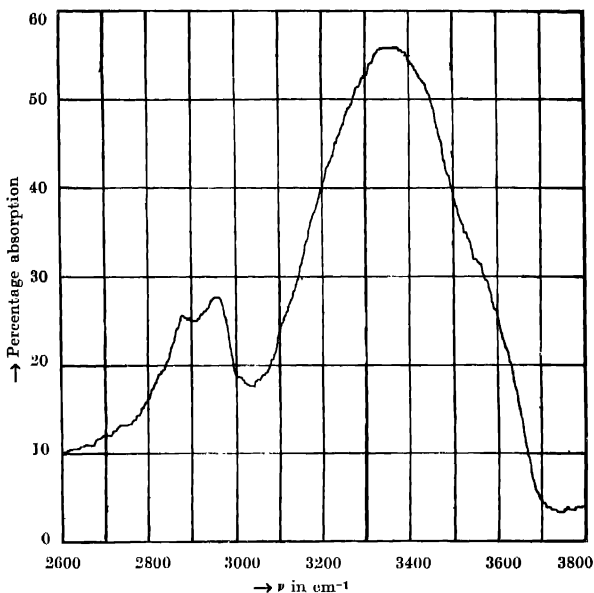


Fig. 1(b). Infrared absorption curve of thin film of pure ethylene chlorhydrin formed between two NaCl discs.

at 3550 cm^{-1} . On the other hand, in the spectrum due to the vapour [figure 2(b)] the OH band is very weak compared to the CH_2 bands, but it consists of one sharp peak at 3640 cm^{-1} and a weaker but broader band extending from 3200 cm^{-1} to 3500 cm^{-1} . Thus it is evident that the OH band with its maximum at 3360 cm^{-1} observed in the spectrum due to pure liquid is almost absent in that due to the vapour. This conclusion is not in agreement with that drawn by Mizushima *et al.*, (1939) from the results of investigation of the second harmonic of the OH bands in the near infrared region.

Table I also shows that the 1430 cm^{-1} band due to CH_2 deformation oscillations in the liquid becomes remarkably weaker, whereas the band at 1380 cm^{-1} becomes stronger in the vapour state. The ratio of the integrated absorption at the two bands 662 cm^{-1} and 750 cm^{-1} due to the vapour at 28°C is, however, almost the same as that in the case of the pure liquid. The values of the ratio observed in the absorption curves due to the three solutions given in Table I are of great help in determining the causes of these changes.

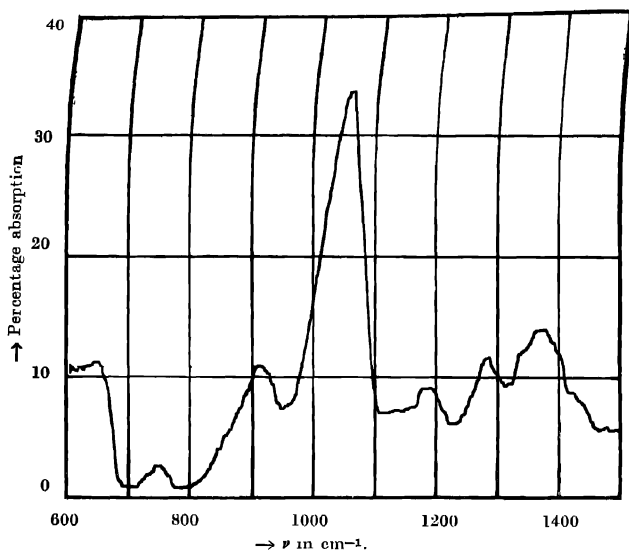


Fig. 2(a) Infrared absorption curve of ethylene chlorhydrin in the vapour state at 28°C (cell 10 cm).

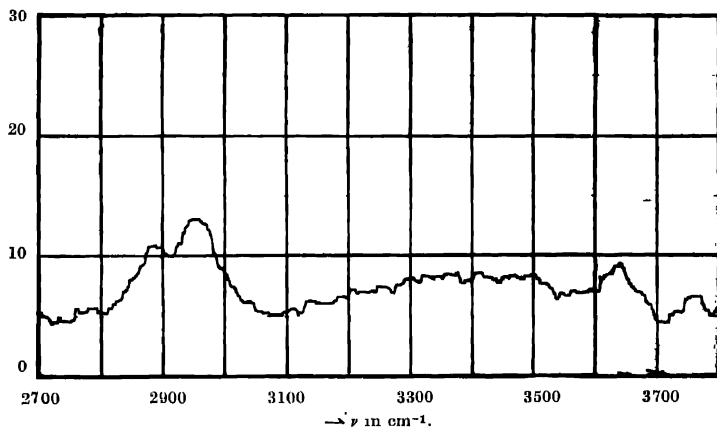


Fig. 2(b). Infrared absorption curve of ethylene chlorhydrin in the vapour state at 28°C (cell 10 cm).

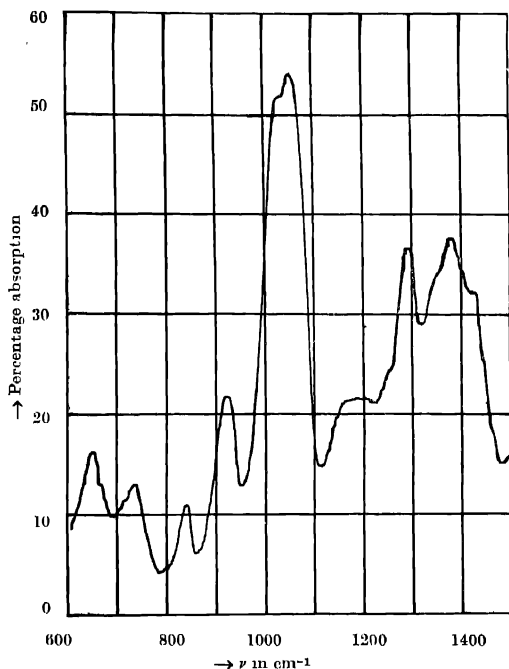


Fig. 3. Infrared absorption curve of ethylene chlorhydrin in the vapour state at about 70°C (cell 10 cm).

A comparison of the curves in figures 1, 4 and 5 show that when the pure liquid is dissolved either in CCl_4 or in the C_2Cl_4 the band 750 cm^{-1} disappears and the bands 842 cm^{-1} and 1030 cm^{-1} become weaker, while the bands 662 cm^{-1} , 1065 cm^{-1} and 1380 cm^{-1} become stronger. Thus the latter three bands are to be assigned to one configuration of the molecule. The frequencies 662 cm^{-1} , 845 cm^{-1} and 1035 cm^{-1} were, however, assigned by Mizushima *et al* (1951) to the *ganche* configuration and the frequencies 750 cm^{-1} and 1065 cm^{-1} to the *trans* configuration. It is quite evident from figures 1 and 4 that the frequencies 750 cm^{-1} and 1065 cm^{-1} cannot be assigned to the same configuration of the molecule. On the other hand, if it is assumed that the band 1065 cm^{-1} is produced by the *trans* configuration, the band 662 cm^{-1} is also to be assigned to the same configuration.

In the solution in CCl_4 or C_2Cl_4 the formation of $\text{OH} \cdots \text{Cl}$ bond between the OH group of ethylene chlorhydrin molecule and the chlorine atom of the solvent molecules is highly probable. In that case the frequency 662 cm^{-1} is to be

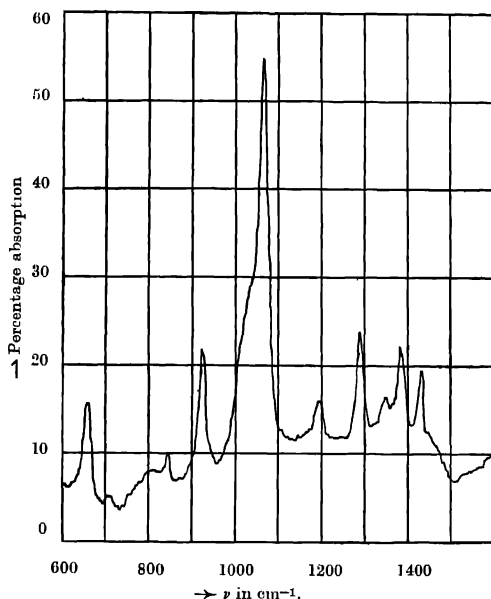


Fig. 4. Infrared absorption curve of 2% solution of ethylene chlorhydrin in CCl_4 (cell 0.1 mm).

assigned to such associated molecules. The disappearance of the Raman line 750 cm^{-1} in the spectrum due to the solid state of ethylene chlorhydrin (Mizushima *et al*, 1940) indicates that the molecules in the associated state yields the frequency 662 cm^{-1} , while the weakening of the Raman line 662 cm^{-1} in the vapour state (Mazumder, 1955) shows that the single molecules produce the frequency 750 cm^{-1} , because single molecules are expected to predominate in the vapour. In the liquid state we can expect the formation of dimers through OH...Cl bond between two neighbouring molecules [figure 6(a)]. Also some of the molecules may become associated through H-O...H bond [figure 6(b)] as pointed out by Pauling (1945) in the case of *o*-chlorophenol. The nature of the OH band at 3360 cm^{-1} given by the liquid in the present investigation appears to be similar to that of the OH band exhibited by *o*-chlorophenol (Sirkar *et al*, 1958) and this may confirm the assumption made regarding the formation of dimers through H-O...H bond.

Table I shows further that in the liquid state the ratio of the integrated absorption at the bands 662 cm^{-1} and 750 cm^{-1} is about 3:2 and in the vapour state at 28°C this ratio remains practically unchanged. To explain the results

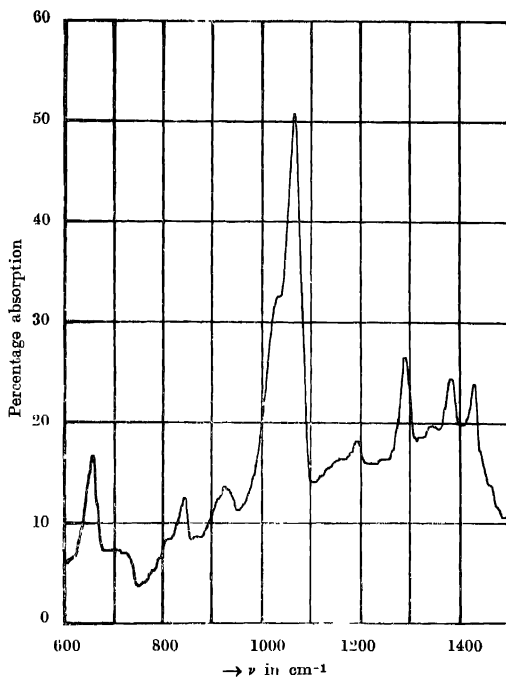


Fig. Infrared absorption curve of 2% solution of ethylene chlorhydrin in C_2Cl_4 (cell 0.1 mm)

described above it may be assumed that the dimers formed through $OH \cdots Cl$ bond predominate in the liquid state and the frequency 662 cm^{-1} is assigned to the $C-Cl$ vibration in these dimers. On the other hand, the frequency 750 cm^{-1} of $C-Cl$ vibration in single molecules may not be affected by the formation of dimers through $H-O \cdots H$ bond and the frequency 750 cm^{-1} may be assigned to the $C-Cl$ vibration in such dimers. In the vapour state at $28^\circ C$ most of the latter type of dimers may break up, while those formed through $O-H \cdots Cl$ bond may persist because of greater strength of the virtual bond in this case. Thus the breaking up of the dimers formed through $H-O \cdots H$ bond mentioned above is not expected to affect the ratio of the integrated absorption at the bands 662 cm^{-1} and 750 cm^{-1} . On the other hand, as the intense band at 3400 cm^{-1} due to the liquid is due to $H-O \cdots H$ group, this band disappears as the group breaks up in the vapour state. This may explain the absence of the band at 3400 cm^{-1} in the spectrum due to the vapour. The weak band at 3640 cm^{-1} is the OH band due to the free single molecules.

When the temperature of the vapour is raised to 70°C, however, the height of both the peaks at 750 cm^{-1} and 1035 cm^{-1} increases relative to those of 662 cm^{-1}

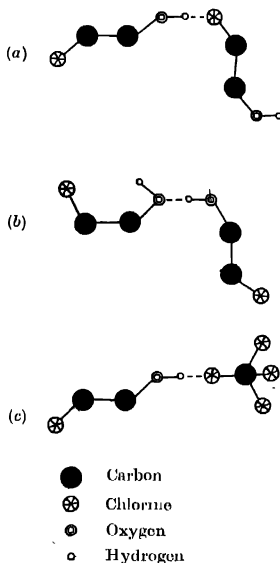


Fig. 6

and 1060 cm^{-1} respectively. This shows that the number of single molecules increases rapidly due to the dissociation of the dimers formed through O-H...Cl bond. The results of investigation on the Raman spectra of ethylene chlorhydrin in the vapour state at 130°C and 180°C (Mazumder, 1955) show that the ratio of the intensities of the lines 662 cm^{-1} and 750 cm^{-1} becomes about 1 : 1 at 130°C and it diminishes to about 1 : 5 at 180°C. So, the latter results are in agreement with those obtained in the present investigation. It is to be pointed out, however, that the results of investigation of the dependence on temperature of the relative heights of the absorption peaks at 669 cm^{-1} and 760 cm^{-1} reported by Mizushima *et al* (1951) are not in agreement with the facts observed in the present investigation. A comparison of the curves reproduced in figures 1 and 3 shows definitely that the latter curve is due to the vapour, because the band at 1430 cm^{-1} is very weak in this curve, whereas it is very strong in the curve due to the liquid. It is also found from figure 3 that the band at 750 cm^{-1} becomes much stronger at higher temperature of the vapour relative to that of the band at 662 cm^{-1} .

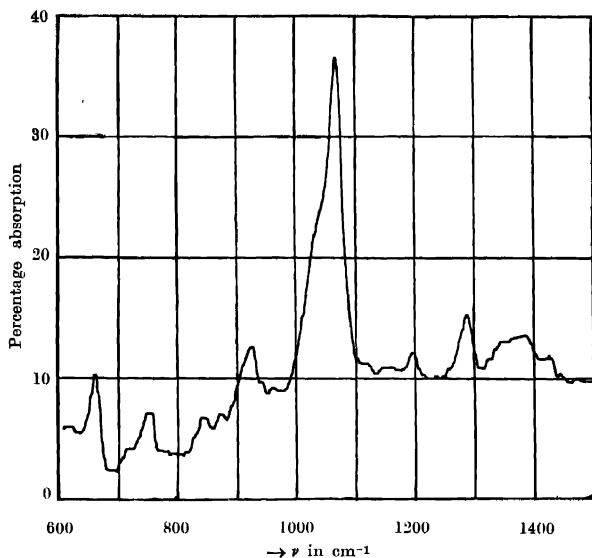


Fig. 7. Infrared absorption curve of 2% solution of ethylene chlorhydrin in heptane (cell 0.1 mm).

Figure 7 shows that the relative heights of the absorption peaks at 660 cm^{-1} and 750 cm^{-1} and also at 1025 cm^{-1} and 1065 cm^{-1} due to the solution of ethylene chlorhydrin in heptane remain almost the same as in those due to the pure liquid. This result is quite in good agreement with the assumption made in the above discussions, because the hydrogen atoms of the solvent molecules cannot break up the dimers formed through OH .Cl bond

It is thus evident from the above discussions that the assignment of the frequencies 662 cm^{-1} and 750 cm^{-1} to two different configurations of ethylene chlorhydrin molecules cannot explain satisfactorily the results obtained in this investigation and that the formation of dimers in the liquid is to be postulated to explain the observed changes in the relative strengths of the two absorption bands.

ACKNOWLEDGMENT

The author is indebted to Professor S. C. Sirkar, D.Sc., F.N.I., for kindly suggesting the problem and for his constant guidance throughout the progress of the work.

REFERENCES

- Mazumder, M., 1955, *Ind. J. Phys*, **29**, 361
- Mizushima, S., Kutoba, A. and Morino, Y., 1939, *Bull. Chem. Soc., Japan*, **14**, 15.
- Mizushima, S., Morino, Y. and Nakamura, S., 1940, *Sci. Papers I.I' C.R. (Tokyo)*, **37**, 205.
- Mizushima, S., Shimanouchi, T., Miyazawa, T., Abe, K. and Yasuno, M., 1951, *J. Chem. Phys.*, **19**, 1477
- Pauling, L., 1945, *Nature of the Chemical Bond.*, p. 324.
- Sirkar, S. C., Deb, A. R. and Banerjee, S. B., 1958, *Ind. J. Phys.*, **32**, 345.

A SIMPLE METHOD FOR THE ENERGY ESTIMATION OF ELECTRON PAIRS

P. K. ADITYA*

PHYSICS HONOURS SCHOOL, PANJAB UNIVERSITY, CHANDIGARH

(Received for publication July 2, 1959)

ABSTRACT. A simple and practical method is described by which electron pair energies from 2×10^7 ev to 10^{12} ev can be estimated with sufficient reliability. The initial divergence is allowed modification by the multiple coulomb scattering of the electrons, and the energy of the primary photon derived from the observed opening, which is directly measurable. This method when applied to a considerable number of pairs obtained from electromagnetic cascades has been shown to yield meaningful results. The advantages and limitations of the method are discussed.

During the course of an investigation (Kumar, 1956; 1957-a, b; Aditya, 1959a, b) on the phenomena of electromagnetic cascades at high energies, a simple method has been used for estimating energy of electron pairs, and found to yield reliable results. In principle, the initial divergence of the pair and the subsequent multiple scattering of the two partners are both taken account of, so that the energy of the materialising photon can be derived directly from the observed opening of the pair. The influence of multiple scattering on the true opening of a pair has been considered independently also by Lohrmann (1955) who concluded that the observed divergence for pairs of energy ≥ 1 Bev., is essentially determined by the multiple scattering. Koshiba *et al.*, (1954) had also proposed to discuss such an influence of the multiple scattering.

Using the method of energy estimation described below, some results on the mean free path for trident production have been recently published (I), where a brief outline of the method was given. In the present article we propose to discuss the principle alongwith the many approximations and assumptions involved and enumerate the merits, demerits and limitations of the method. The reliability has already been checked (I) by comparing the energies so estimated with those expected from using other methods.

When a photon materialises into a negaton-positon pair, the intermediate angle between the two partners is a function of the energy of the photon and of the ratio of the shared energies. This angle is minimum when the two electrons share the energy equally and increases with the disparity of the pair, the disparity being defined as the ratio of the energy of the low energy electron to the energy

* At present at the Institute for Theoretical Physics, University of Copenhagen, Denmark.

of the photon. This opening of the pair may be called its true opening and at a certain distance from the origin of the pair, the separation due to it be denoted as d_T .

It is well known that during passage through condensed matter, charged particles undergo multiple coulomb scattering the magnitude of which is a function of the particle momenta. Since the true opening is usually small ($\sim 10^{-3}$ radians for an energy \sim a few Bev.) the multiple scattering is expected to lead almost always to an increase of the true angle. For example, according to Baroni *et al* (1953) the probability that the angle is increased is $\sim \frac{4\pi - \Omega}{4\pi}$ where Ω is the solid angle defined by the aperture of the pair. Let us denote this increase in the separation of the pair by d_S .

Consequently, the observed separation is a resultant of the true opening d_T , and the subsequent separation due to scattering d_S . We shall estimate d_T and d_S in order to find their relative magnitude at various distances from the pair origin.

Stearns (1949) has derived the root mean square value of the angle ω_e between the electron and the direction of the photon, so that in the case of equipartition of energy between the negaton and the positon, the r.m.s. value of the true opening angle of the pair is given as :

$$\omega_p = 2 \frac{mc^2}{E} \ln \frac{E}{mc^2} \quad \dots (1)$$

For the electron rest mass, $m = 0.5 \text{ Mev.}$, and photon energy expressed also in Mev., eq., (1) gives

$$\omega_p \simeq 10/E \quad \dots (2)$$

for photons of energy from 1 Bev., to 100 Bev. Following similar arguments, Borsellino (1953) has derived the most probable value of the opening angle, given as

$$\omega_p = \frac{4mc^2}{E} \cdot \phi \quad \dots (3)$$

where $\phi = 1$ for energy equipartition and ~ 1 even when the energy of one of the electrons is twice than the other. Substitution for m , and for the photon energy in Mev., gives

$$\omega_p \simeq 2/E \quad \dots (4)$$

The energy found from Stearns' relation (eq. 2) is seen to be about five times that found by using Borsellino's relation (eq. 4). Since the latter gives the most probable value, and that in the energy region upto $\sim 200 \text{ Mev.}$, the results of

Hinterman (1954) suggest better accordance with Borsellino's relation, we have amongst many other workers, preferred to use this relation. Thus

$$d_T \simeq \frac{2}{E} \cdot t \quad \dots (5)$$

where t is the distance measured from the pair origin, and has the same units as d_T , say microns.

From the theory of multiple scattering, it is known that when two electrons of equal energy are involved, the mean relative scattering in $t \mu$, is given as

$$\bar{\alpha}_{t\mu}^0 = \bar{\alpha}_{100\mu}^0 \cdot \left(\frac{t}{100} \right)^{\frac{1}{2}} \cdot 2^{\frac{1}{2}} \quad \dots (6)$$

where $\bar{\alpha}_{100\mu}$ denotes in degrees the mean scattering angle per 100μ , while $2^{\frac{1}{2}}$ arises on account of the assumed equal scattering of the two electrons. For a photon of energy E (in Mev.) and equipartition as above,

$$\alpha_{100\mu} = \frac{K}{E/2} = \frac{52}{E} \quad \dots (7)$$

where K , the scattering constant is taken = 26 for the units of $\bar{\alpha}$ and E mentioned above. In view of the approximations involved in the method, much purpose is not served by taking into account the variation of the scattering constant with coll size. So that eqs. (6) and (7), with

$$\bar{\alpha}_{t\mu}^0 = \frac{ds}{t} \cdot \frac{180}{\pi} \quad \dots (8)$$

lead to

$$d_s = \frac{0.128}{E} \cdot t^{3/2} \quad \dots (9)$$

where d_s and t , are as usual in microns.

Equating d_T from eq.(5) with d_s from eq. (9), it is seen that the contribution due to scattering is as much as that due to initial divergence at a distance of $\sim 250 \mu$ from the pair origin, while for all larger distances, d_s predominates over d_T . As an illustration let us consider the combined effect of d_T and d_s on a pair of 10 Bev. In figure 1., are plotted the curves between the expected separation against distance from origin. In addition to the curves for the original and scattering corrected separations according to Borsellino's and Stearns' relation, are included two curves, one showing the contribution of multiple scattering alone (curve 3) and another showing the separation expected according to Borsellino's relation for a pair of energy 1 Bev., (curve 6). The close proximity of curve 6, with the other curves for 10 Bev., indicates that without a suitable correction for scattering, the opening angle relations would lead invariably to

an underestimation of energy. It is also evident, that as higher energies are approached, it makes little difference as to which one of the Borsellino's or Stearns'

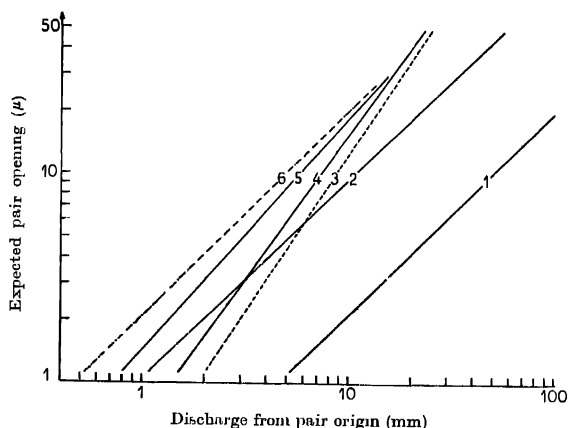


Fig. 1. Expected separation for a pair has been plotted against the distance from pair origin. For a 10 Bev. pair, curves 1 and 2 show the separation according to the relations of Borsellino and Stearns, while curve 3 indicates the root mean square value of the separation due to multiple scattering alone. Consequently, 4 and 5 are the respective modified curves. Curve 6, which gives Borsellino's separation for a 1 Bev. pair is included for comparison.

relation is used or may be that none of the two is essential, as has been concluded by Lohrmann (1955). However, since no sharp cut off can be defined above or below which either of the two contributions due to initial divergence or scattering may be neglected, it appears advantageous to consider at all energies the combined effect of initial divergence and scattering, so that none of the two is deprived of its true importance at various stages of energy and distance from origin.

For various energies from 100 Mev., to 1000 Bev., curves between expected separation and distance from pair origin were drawn in figure 1, of $\bar{r}(I)$. These curves can, in short, be expressed in the form of an equation as :

$$E = 6 \cdot d^{-1} \cdot t^{1.4} \quad \dots (10)$$

where E is in Bev., t in mm and d in μ .

It had been formerly felt that in those cases, when the energy is so high as to allow no measurement of the separation made within a few mm from the origin, the measurements made at larger distances involved uncertainty due to radiation losses, large single scatters and the presence of increasing number of secondary phenomena. At the present stage, most of this difficulty can be overcome by making use of the arguments described very recently by Weill (1959), according

to whom the variation of ionisation along the combined track can be used to derive the separation between the two partners.

The energies of 20 pairs initiating soft cascades, a number of associated pairs in the vicinity of a high energy interaction (Kumar, 1958, Aditya, 1959-c) and the secondary pairs of all these showers have been estimated by this method. Results in the very high region (Table 1, Aditya, 1959a) and the energy spectrum of the secondary electrons (figure 2, Aditya, 1959a) install confidence in the reliability of the energies estimated by this method. In the energy range, where the multiple scattering measurements are meaningful, both these methods yield identical results. There are however two factors that may point out the inaccuracy of the assumptions. Firstly, because of the separation due to relative scattering having an r.m.s., distribution, the most probable value shall not be as much as the r.m.s., separation, so that the method would lead to an overestimation of the pair energy. Secondly, since energy equipartition has been assumed, whenever one of the electrons has an energy much different from that of the other, the application of this method is likely to underestimate the energy. It is expected that in most of the cases these two factors might compensate for each other but it cannot be so for all pairs. That is why, for an individual pair the method is not likely to give in all cases the most representative value for the energy. The probability considerations mentioned by Lohrmann (1955) would apply to the distribution of the pair separation as a result of which large discrepancies have to be allowed for in some cases. In spite of these limitations, the method has a few outstanding advantages. It is perhaps the most simple method and can be applied even to those events which occur in the stack under unfavourable geometrical conditions such as steepness. Unless one needs to go very far from the pair origin, which is not essential in most of the cases, the influence of radiation losses is known to be small. Provided the pair separation is not directly measurable in the vicinity of the origin, it may be derived from the change of ionisation (Weill 1959).

ACKNOWLEDGMENTS

The basic idea of this method has been derived from Professor B. M. Anand to whom it is a great pleasure to thank also for encouragement and keen interest. This investigation was carried out while the author had a Research Fellowship from the Govt. of India, Department of Atomic Energy, to which thanks are due. The author is indebted to Professor B. Peters for allowing the use of emulsion stacks exposed by the Tata Institute of Fundamental Research, Bombay.

REFERENCES

- Aditya, P. K., 1959a, *Nuovo Cimento*, **11**, 546.
- Aditya, P. K., 1959b, *Nuovo Cimento*, under publication.
- Aditya, P. K., 1959c, *Nuovo Cimento*, **13**, 219.

- Baroni, G., Borsellino, A., Scarsi, L. and Vanderhaughe, G., 1953, *Nuovo Cimento*, **10**, 1653.
- Borsellino, A., 1953, *Phys. Rev.*, **76**, 1023.
- Hinterman, K., 1954, *Phys. Rev.*, **93**, 890.
- Koshiha M., and Kaplan, M. P., 1954, *Phys. Rev.*, **100**, 327.
- Kumar, P., 1956, *Proc. 43rd. Ind. Sci. Cong.*, III-3, Abs. 18.
- Kumar, P., 1957a., *Proc. 44th. Ind. Sci. Cong.*, III-3, Abs. 61.
- Kumar, P., 1957b, *Proceedings of the Cosmic Ray Symposium, Bombay, March 1957*, (Unpublished).
- Kumar, P., 1958, *Proc. 45th. Ind. Sci. Cong.*, III-3, Abs. 9.
- Lohrmann, E., 1955, *Nuovo Cimento*, **2**, 1029.
- Stearns, M., 1949, *Phys. Rev.*, **76**, 836.
- Weill, R., 1959, *Nuovo Cimento*, **11**, 781.

POWDER DATA, UNIT CELL AND SPACE GROUP FOR FERROUS SULPHATE*

C. W. F. T. PISTORIUS

INSTITUTE OF GEOPHYSICS, UNIVERSITY OF CALIFORNIA,

LOS ANGELES 24 CALIFORNIA, U.S.A.

(Received for publication, July 6, 1959)

ABSTRACT. Anhydrous ferrous sulfate crystallizes in the orthorhombic system. The dimensions of the unit cell are $a_0 = 5.261\text{\AA}$, $b_0 = 8.013\text{\AA}$, $c_0 = 6.454\text{\AA}$. The most probable space group is D_{2h}^{17} -Cmcm. The unit cell contains $(\text{FeSO}_4)_1$.

INTRODUCTION

Among compounds of the general formula MRO_4 there are some whose crystal properties, in spite of their simple composition, are still unknown. Such compounds are, for example, the anhydrous sulphates of the bivalent metals copper, iron, manganese and cobalt.

Our present inadequate knowledge of the crystallographic properties of these compounds is mostly due to the fact that they either form unstable, very hygroscopic crystals which are difficult to handle for x-ray analysis, or else do not form single crystals of satisfactory dimensions, but only a fine microcrystalline powder. FeSO_4 is one of the latter.

Recently, however, Dimaras (1957) succeeded in growing single crystals of NiSO_4 which possessed a sufficient size to enable him to determine the unit cell and space group. The present investigation was undertaken in the expectation that FeSO_4 would be isostructural with NiSO_4 , and that an unambiguous assignment of the powder pattern of FeSO_4 could be made in analogy to the known pattern of NiSO_4 .

EXPERIMENTAL

Fresh reagent grade $\text{FeSO}_4 \cdot 7\text{H}_2\text{O}$ was obtained from Merck. The company's analysis of the purity of the compound was as follows: Insoluble substances 0.010%, chloride (as Cl) 0.001%, phosphate (as PO_4) 0.003%, alkalis and earths 0.05%, copper (as Cu) 0.005%, ferric iron (as Fe) 0.010% and zinc (as Zn) 0.005%.

A weighed quantity of $\text{FeSO}_4 \cdot 7\text{H}_2\text{O}$ was heated to 150°C in vacuum for a period of three hours to drive off $6\text{H}_2\text{O}$. The product was then heated to 350°C

* Publication no. 155 of the Institute of Geophysics.

in a nitrogen atmosphere for one hour (Hedvall and Heubeger 1923). The weight loss agreed with the expected value.

The x-ray powder diffraction pattern of the resulting FeSO_4 , ground into a paste with petroleum jelly, was obtained at 26°C in a Norelco high angle recording diffractometer, using FeK_α radiation ($\lambda = 1.9373\text{\AA}$) and a Mn filter. The scanning speed was $1/8^\circ(2\theta)$ per minute. High-purity sodium chloride was used as an internal standard.

TABLE I
Spacings of anhydrous ferrous sulphate

observed <i>d</i> -spacing in \AA	calculated <i>d</i> -spacing in \AA	hkl	relative intensity in \AA
4.373	4.398	110	27
3.982	4.006	020	16
3.045	3.634	111	84
3.408	3.404	021	36
2.618	2.631, 2.602	200, 112	100
2.371	2.382	130	29
2.051	2.039	202	17
1.993	2.003	040	10
1.919	1.913, 1.916	041, 132	7
1.825	1.817	222	23
1.706	1.702	042	30
1.609	1.613	004	6
1.589	1.594, 1.596	240, 133	5
1.546	1.547	241	5
1.520	1.515, 1.513	114, 312	10
1.462	1.466, 1.466	043, 330	8
1.431	1.429	242	30
1.385	1.385	152	5
1.314	1.315	400	5
1.284	1.281	243	4
1.251	1.250	420	4
1.094	1.099	440	7

RESULTS

The powder pattern obtained was almost exactly identical to that of NiSO_4 , of which the powder pattern is listed in the ASTM powder data card file. However, it was totally different from the unassigned ASTM card for FeSO_4 . Presumably the former measurements were made on oxidized or incompletely hydrated material.

All the observed diffraction peaks—which were rather broad, due to poor crystallization—could be satisfactorily assigned as due to an orthorhombic lattice with the following unit-cell dimensions, as obtained from a least-squares treatment:

$$a_0 = 5.261 \pm .010 \text{ \AA.}$$

$$b_0 = 8.013 \pm .005 \text{ \AA.}$$

$$c_0 = 6.454 \pm .005 \text{ \AA.}$$

The axial ratios are

$$a_0 : b_0 : c_0 = 0.6566 : 1 : 0.8054.$$

The calculated density of FeSO_4 at 26°C , assuming 4 molecules per unit cell, is 3.707 gm/cm^3 . The experimental value is 3.346 gm/cm^3 (Thorpe and Watts 1880). It is probable that, as Dimaras (1957) found in the case of NiSO_4 , the crystallites have an incomplete internal development due to cavities, consequently causing a spuriously low macroscopic density.

The observed and calculated d -spacings, assigned indices and observed relative intensities are listed in Table I. The pattern is completely analogous to that of NiSO_4 , and it consequently seems safe to assume that the space group is also the same, viz. D^{17}_{2h} —Cmcm.

As the unit cell contains four molecules FeSO_4 , it is necessary to arrange in it four Fe, four S and sixteen O atoms. The space-group symmetry Cmcm possesses three four-fold positions. Two of these, position (a) $(0, 0, 0; 0, 0, \frac{1}{2}; \frac{1}{2}, \frac{1}{2}, 0; \frac{1}{2}, \frac{1}{2})$ and position (b) $(0, \frac{1}{2}, 0; 0, \frac{1}{2}, \frac{1}{2}; \frac{1}{2}, 0, 0; \frac{1}{2}, 0, \frac{1}{2})$ coincide with symmetry centers, while the third position (c) $(0, y, \frac{1}{4}; 0, \bar{y}, \frac{3}{4}; \frac{1}{2}, \frac{1}{2} + y, \frac{1}{4}; \frac{1}{2}, \frac{1}{2} - y, \frac{3}{4})$, with one degree of freedom, lies on a two-fold axis. Because of the presumed tetrahedral arrangement of the O atoms around the S atoms, the only possible positions of the S atoms are (c). The SO_4 tetrahedron is further oriented by the symmetry in such a way that its two-fold axis coincides with the $(0, y, \frac{1}{4})$ axis.

In this way the O atoms occupy eight-fold positions, and, in particular, the O atoms of one pair lie on the $(0, y, z)$ plane while those of the other pair lie on the $(x, y, \frac{1}{4})$ plane. The Fe atoms must necessarily occupy one of the four-fold positions (a) or (b).

ACKNOWLEDGMENTS

The author wishes to thank Mr. Edwin Sharp for his assistance, and Mr. Lawrence Knight for technical aid in connection with the X-ray equipment.

REFERENCES

- Dimmius, P. I., 1957, *Acta cryst.*, **10**, 313.
Hedvall, J. A. and Heuberger, J., 1923, *Z. anorg. Chem.*, **128**, 2.
Thorpe, T. F. and Watts, J. I., 1880, *J. Chem. soc.*, **37**, 116.

Letters to the Editor

The Board of Editors will not hold itself responsible for opinions expressed in the letters published in this section. The notes containing reports of new work communicated for this section should not contain many figures and should not exceed 500 words in length. The contributions must reach the Assistant Editor not later than the 15th of the second month preceding that of the issue in which the paper is to appear. No proof will be sent to the authors.

5

ABSORPTION OF 8-MILLIMETRE WAVES IN ETHYL BROMIDE

G. P. SRIVASTAVA

INSTITUTE OF APPLIED PHYSICS, UNIVERSITY OF ALLAHABAD, ALLAHABAD, INDIA

(Received for publication September 1, 1958)

The absorption of 8 mm electromagnetic waves has been studied in ethyl bromide at various pressures and two temperatures. The technique of measurement has already been reported. Klystron QK292 was used to generate power. Constant temperature chamber was used to maintain temperature. In the present equipment a five foot absorption cell has been used.

The pressure variation of the absorption has been studied and it has been found that pressure absorption curves do not follow exactly the general pattern $\alpha(\nu) \propto p^2$, indicating that study is being made in the region of rotational lines of ethyl bromide.

Table I gives the absorption coefficient values in ethyl bromide at two temperatures.

TABLE I

Absorption coefficient of ethyl bromide at various pressures and two temperatures
Wavelength 8 mm

No.	Temperature °K	Pressure (cm of Hg)	Absorption Coefficient 10 ⁻⁴ /cm
1.	283	5	10.6
		10	20.7
		15	25.6
		20	34.2
2.	303	5	7.6
		10	15.8
		15	20.2
		20	28.1

Ethyl bromide is nearly a prolate rotor ($K = -0.98$). The constants A, B and C have been determined by Wagner, Solimene and Dailey (1955). The constants for $C_2H_5Br^{79}$ are $B = 3804.82$ Mc and $C = 3522.21$ Mc and for $C_2H_5Br^{81}$ are $B = 3781.92$ Mc and $C = 3502.50$ Mc. They have observed lines for the transitions $2_{1,2} \rightarrow 3_{1,3}$, $2_{2,1} \rightarrow 3_{2,2}$ and $2_{2,0} \rightarrow 3_{2,1}$.

The absorption observed at 20 cm is very high. The total microwave absorption at a given frequency is the sum of (i) α_1 —resonance absorption i.e. absorption due to transitions taking place at the frequency of the measurement. (ii) α_2 —absorption due to transitions taking place at frequencies (not zero) far removed from the frequency of measurement. (iii) α_3 —absorption due to transitions taking place at zero frequency which are broadened by collision (Debye type). Therefore, the absorption observed is the sum of absorption due to Q branch transitions ($\Delta J = +D$) and R branch ($\Delta J = +1$) transitions. The majority of transitions which have high intensity, belong to Q branch and the most of them are at zero wavenumber. It seems that the absorption due to lines at the frequency of measurement (belonging to transitions $4 \rightarrow 5$) is heavy. Contribution of R branch transitions removed from the frequency of measurement to the absorption is also considerable.

The absorption due to transition at the frequency of measurement is independent of pressure and absorption due to lines removed from the frequency varies as p^2 . Therefore, the observed absorption is neither independent of pressure nor, follow the law $\alpha(\nu) \propto p^2$.

As far as the temperature variation is concerned, as the observations are only at two temperatures nothing definite can be said.

Attempt is being made to calculate the absorption theoretically and to determine the value of $\Delta\nu$.

Author is thankful to Prof. Krishnaji under whose supervision the present investigations were made. Author is also thankful to Prof. K. Banerji, Head of the Physics Department, for his interest in the work and the facilities provided.

REFERENCES

- Krishnaji and G. P. Srivastava, 1957, *Jour. Sc. & Ind. Res. (India)* **16**, 289.
 Krishnaji and G. P. Srivastava, 1957, *Phys. Rev.*, **106**, 1186.
 Krishnaji and G. P. Srivastava, 1958, *Phys. Rev.*, March 1.
 Wagner, R. S., N. Solimene and B. P. Dailey, 1955, *J. Chem. Phys.* **23**, 599.

SPACE GROUP OF 1, 3, 5-TRICHLOROBENZENE

S. G. BISWAS

OPTICS DEPARTMENT, INDIAN ASSOCIATION FOR THE CULTIVATION
OF SCIENCE, CALCUTTA-32.*(Received, August 31, 1959)*

Plate IX

ABSTRACT. Debye-Scherrer patterns of pure 1, 3, 5-trichlorobenzene at 30°C as well as at -180°C have been photographed and analysed. Analysis of the patterns shows that the crystals of the substance belong to orthorhombic system with $a=14.15\text{\AA}$, $b=9.90\text{\AA}$, $c=6.32\text{\AA}$ and at -180°C only a very small amount of contraction takes place. An electron diffraction pattern of a microcrystal resembling that due to a fibre has also been photographed with the fibre axis along the c -axis of the crystal. The unit cell dimensions mentioned above could explain all the reflections in the electron diffraction pattern.

Considering the dimensions of the unit cell and the approximate density of the crystal the number of molecules in the unit cell was found to be four, the accurate value of the density being 1.34 gm cm^{-3} . The space group D_{12}^2 has been assigned to the crystal.

INTRODUCTION

The molecules of 1, 3, 5-trichlorobenzene in the vapour state have a three-fold axis of rotation which makes the 0, 0 transition forbidden, and this has been confirmed by the results of the study of ultraviolet absorption spectrum of the vapour (Sponer and Hall, 1948). The 0, 0 band was, however, observed in the absorption spectra of the crystals of the compound at -180°C (Banerjee, 1957) and of its solutions in certain solvents (Roy, 1957). It was pointed out by Banerjee (1957) that the appearance of the 0, 0 band in the spectrum due to the crystals of 1, 3, 5-trichlorobenzene might indicate disappearance of the three-fold symmetry of the molecule in the solid state. More recently the polarisation of the absorption spectra of single crystals of the substance has been studied by Schnepf (1959) and he has observed that the spectrum consists of two parts which are polarised differently and has concluded that the new portion of the spectrum is induced by the crystal field and not by the deterioration of the three-fold symmetry of the molecule. He has also drawn some conclusion regarding the orientation of molecular planes in the crystal. As the crystal structure of the molecule was not known and it is difficult to grow single crystals attempt was made to determine its space group by studying the Debye-Scherrer pattern of the crystal and the results are reported here.

EXPERIMENTAL

To photograph the Debye-Scherrer pattern of 1,3,5-trichlorobenzene the substance was purified by repeated crystallisation from solutions in benzene and ether and only very fine needles were obtained by this method. Different solvents and different processes of crystallisation did not produce any well-defined single crystal. The needles were powdered and packed within a Lindemann glass capillary tube of bore 0.3 mm, and the Debye-Scherrer pattern was photographed at 30°C with a cylindrical camera of radius 4.50 cm. The same pattern was also photographed with the sample at -180°C in the same camera with a special arrangement for producing low temperature (Biswas, 1958). Cu-radiation filtered through nickel foil from a Seifert X-ray tube running at 32KV and 26mA was used to photograph the patterns with an exposure of 3½ hours.

The patterns are reproduced in figure 1(a) and figure 1(b) respectively. As well defined single crystals could not be prepared to photograph rotation diagram and to calculate the unit cell dimensions precisely, the habits of the single microcrystals were studied under electron microscope. The microcrystals were found to be of fibrous structure and actually an electron diffraction pattern was successfully photographed which closely resembles that due to a fibre (figure 2).

RESULTS AND DISCUSSION

Apart from the difficulty of preparing single crystals the determination of the unit cell dimensions from the powder pattern of 1, 3, 5-trichlorobenzene was found to be very difficult since ordinarily rings due to spacings higher than 4.25 Å could not be observed and therefore rings due to simpler planes from the indices of which the axial lengths of the unit cell could be determined were not recorded. In one of the well exposed photographs, however, very faint rings due to longer spacings were observed. These were extremely helpful in the determination of the unit cell of the crystal.

In the determination of the axial lengths of the unit cell Lipson's (1949) method was applied. First, attempts were made to index the Debye-Scherrer rings in terms of tetragonal and hexagonal systems, but the data did not fit in either of these systems. The unit cell dimensions calculated for the orthorhombic system from the three constants $\lambda^2/4a^2 (= .00296)$, $\lambda^2/4b^2 (= .00605)$, $\lambda^2/4c^2 (= .01482)$ are 14.15, 9.90 and 6.32 Å respectively. The spacings observed and the values of $\sin^2\theta$ observed and calculated from the above unit cell dimensions are given in Table I. It can be easily seen from Table I that all the observed spacings of the Debye-Scherrer photograph can be uniquely explained with these unit cell dimensions. It can also be seen from figure 2 that the electron diffraction pattern resembles single crystal rotation photograph. The primitive translation along the fibre axis calculated from the electron diffraction pattern was found to be 6.32 Å. This value exactly coincides with the primitive translation along the

TABLE I
Indexing of powder photograph

Observed spacings	Intensity	Values of $\sin^2\theta$		Indices (<i>hkl</i>)
		Observed	calculated	
14.150	(vw)	00300	.00296	(100)
9.900	(vw)	.00605	.00605	(010)
7.071	(vw)	.01186	.01184	(200)
5.327	(vw)	.02086	.02087	(011)
4.963	(vw)	02407	.02383	(111)
			.02420	(020)
4.244	(w)	.03306	.03259	(310)
3.904	(m)	.03890	.03902	(021)
3.769	(vs)	.04175	.04198	(121)
3.531	(vs)	04755	.04736	(400)
			.04741	(311)
3.402	(m)		.05086	(221)
			.05074	(320)
3.288	(m)	.05484	.05445	(030)
3.093	(w)	06195	.06224	(102)
			.06218	(401)
3.004	(m)	.06569	.06556	(321)
2.780	(m)	.07670	.07717	(212)
2.726	(w)	.07980	.08005	(510)
2.670	(m)	08320	.08348	(022)
2.545	(m)	.09150	.09187	(312)
2.490	(m)	09560	.09532	(222)
2.362	(w)	.1063	.1065	(600)
			.1066	(402)
2.300	(m)	.1120	.11162	(041)
			.11269	(412)
2.214	(w)	.1210	.12138	(601)
2.156	(w)	.1276	.12743	(611)
2.105	(w)	.1339	.13328	(502)
2.040	(w)	.1424	.14239	(113)
1.959	(m)	.1545	.15421	(150)
1.915	(m)	.1615	.16109	(431)
1.871	(w)	.1695	.16942	(223)
1.768	(w)	.1879	.18944	(800)
1.740	(w)	.1958	.19549	(810)
1.660	(w)	2153	.24137	(333)
1.603	(w)	.2308	.23018	(043)
			.22964	(260)
1.353	(w)	.3238	.32299	(370)
1.332	(w)	.3342	.33392	(044)

TABLE II

Interpretation of electron diffraction photograph

	Observed spacings (\AA) and Intensity	Calculated spacings (\AA)	Indices (hkl)
Zero layer line	1.915 (s) 1.413 (m) 1.155 (m) 0.981 (s)	1.917 1.414 1.155 0.9806	(630) (750) (770) (2,10,0)
First layer line	3.091 (s) 2.156 (s) 1.570 (m) 1.254 (s) 1.055 (m)	3.086 2.156 1.570 1.252 1.055	(401) (611) (551) (761) (391)
Second layer line	2.167 (m) 1.631 (vs) 1.311 (m) 1.095 (m) 0.936 (m)	2.172 1.631 1.309 1.095 0.9365	(232) (252) (841) (482) (2,10,2)
Third layer line	1.889 (vs) 1.564 (m) 1.293 (m) 1.107 (vs) 0.955 (w)	1.889 1.564 1.293 1.107 0.9548	(313) (243) (163) (10,33) (193)
Fourth layer line	1.230 (s) 1.065 (m) 0.955 (m)	1.230 1.065 0.9548	(154) (844) (384) (11,34)
Fifth layer line	1.235 (s) 1.060 (w) 1.016 (w) 0.899 (s)	1.235 1.060 1.016 0.8995	(215) (525) (645) (765)

c-axis obtained from the Debye-Scherrer pattern by applying Lipson's method. Using the values of a , b and c mentioned above all the reflections observed in the electron diffraction pattern could be successfully indexed. The observed spacings and those calculated from the values of a , b , c as well as the indices are given in Table II. As the agreement is satisfactory it can be concluded that the crystal of 1, 3, 5-trichlorobenzene belongs to orthorhombic system with the unit cell dimensions

$$a = 14.15 \text{\AA}$$

$$b = 9.90 \text{\AA}$$

$$c = 6.32 \text{\AA}$$

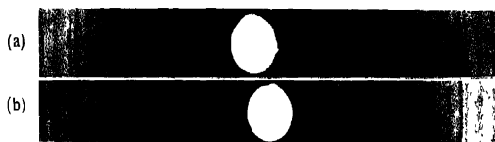


Fig 1 (a) Debye-Scherrer pattern of 1,3,5-trichlorobenzene at 30°C
(b) " " " " " " at -180°C

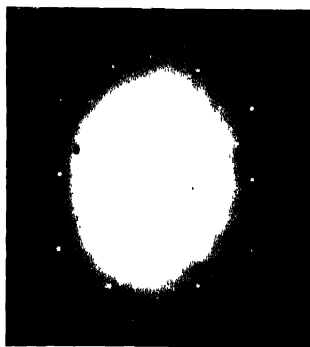


Fig. 2 Electron-diffraction pattern of 1,3,5-trichlorobenzene at 30°C

NUMBER OF MOLECULES PER UNIT CELL

The density of the substance was not found in the existing literature. Attempt was made to measure it and the value found was 1.28 gm cm^{-3} . This does not give any whole number of molecules in the unit cell. If, however, the density is taken as 1.34 gm cm^{-3} the number of molecules per unit cell becomes 4.

the condition of reflection. Since the crystal belongs to orthorhombic system and contains four molecules per unit cell the probable space group is either P_{222} , P_{222_1} or P_{mmm} .

Consideration of the dimensions of the unit cell, the size of the molecule and number of molecules in the unit cell led to the conclusion that the molecules cannot be parallel to any of the axial planes. Hence, the space group P_{222_1} and P_{mmm} are to be excluded.

UNIT CELL DIMENSIONS AT -180°C

The Debye-Scherrer pattern of 1,3,5-trichlorobenzene at -180°C is reproduced in figure 1(b). From the calculation of the spacings of the powder rings it can be easily seen that only very small amount of contraction of the unit cell dimensions takes place at -180°C .

ACKNOWLEDGMENT

The work has been carried out under a scheme financed by the Council of Scientific and Industrial Research. The author's thanks are due to the Council for the Award of a Fellowship. The author is also indebted to Professor S. C. Sirkar, D.Sc., F.N.I., for his kind interest and guidance during the progress of the work.

The author's grateful thanks are also due to Prof. N. N. Das Gupta, Ph.D., of Saha Institute of Nuclear Physics for his kindness in supplying the electron diffraction photograph.

REFERENCES

- Banerjee, S. B., 1957, *Ind. J. Phys.*, **31**, 483.
Biswas, S. G., 1958, *Ind. J. Phys.*, **32**, 13.
Lipson, H., 1949, *Acta, Cryst.*, **2**, 43.
Roy, S. B., 1957, *Ind. J. Phys.*, **31**, 588.
Schnepp, O., 1959, *J. Chem., Phys.*, **30**, 863.
Sponer, H. and Hall, M. B., 1948, *Contribution à l'Etude de la Structure Moléculaire*, (Deosor, liege), p. 211.

VISIBLE ABSORPTION SPECTRUM OF BENZOQUINONE*

RAMA SHANKAR SINGH

DEPARTMENT OF SPECTROSCOPY, BANARAS HINDU UNIVERSITY, BANARAS

(Received, August 8, 1959)

Plate X A & B and XI

ABSTRACT. The visible absorption spectrum of *p*-benzoquinone was studied in the vapour state. The bands which lie in the region of 4100-5000 Å consist of eight main groups developed at 100°C in a 50 cm cell. About 175 bands are measured in this region. These bands are very sharp, many of them having double and triple heads. One marked feature is the appearance of companion bands with separations of 36 cm⁻¹ lying on the shorter wave-length side. An analysis has been proposed assigning the bands as due to $n-\pi$ (Au \leftarrow Ag) transition.

INTRODUCTION

Benzoquinone (C₆H₄O₂) is an important organic compound. It is a fore-runner of many dyes as well as anti-biotics. The spectra of its solution enabled Braude (1945) to recognise three different band systems, two in the ultra-violet and one in the visible region.

Benzoquinone molecule which belongs to symmetry group D_{2h} is to be distinguished from other para-substituted benzene molecules in an important way. In the former the π -electrons are no longer mobile over the entire framework of the molecule with the result that bonds become localised. With a view to understand the bearing of this structural difference on the spectra of the molecule, the absorption spectra of benzoquinone in its vapour state were investigated in detail. The spectrum of the vapour consists of the three band systems (Asundi and Singh, 1955), two in the ultraviolet region and one in the visible region as already recognised by Braude in its absorption spectrum of the solution. The two ultraviolet systems are reported elsewhere. In general, they do not correspond to the band systems of di-substituted benzenes in the same region. The present paper deals with the analysis and discussion of the visible system of bands.

EXPERIMENTAL

The spectrograms were obtained with a quartz Hilger E492 spectrograph and a three prism 'Steinheil' glass spectrograph was used for the visible region. The dispersion of the former is about 17 Å/mm in this region, whereas that of the latter is about 11 Å/mm.. The previous work was done on the 'Hilger' E492

* This paper is a part of the author's thesis accepted for the Ph.D. degree of the Banaras Hindu University, 1955.

spectrograph and, therefore, the use of the Steinheil as the dispersing apparatus proved successful in resolving the multiple heads of many bands. However, a comparison of the spectra obtained from both the apparatus with regard to intensity of the bands and their grouping was found useful. The major portion of the work was, however, completed on the Steinheil glass spectrograph.

Various absorption cells were tried, but those supplied for the present investigation according to the requirements by the Andhra Scientific Company, Musli-patani, India, were found useful. These cells were 5 cm, 10 cm, and 50 cms in length with fused plane glass end-windows. However, the final spectrograms were photographed with a 100 cm cell with sealed plane windows, the furnace in this case being shorter than the length of the cell. The rest of the procedure was exactly the same as for part II of the series, except for the source of continuous radiation. For this, an automobile head lamp of 25 ? running on a regulated constant voltage (8 volts) from a battery was used. A reflector was used to intensity the radiation which was made into a parallel beam with the help of a lens before entering the cell. Another lens was used to condense the emergent beam on the slit of the collimator. The temperature was then raised in successive steps of 10°C as spectra were photographed from room temperature upto 105°C. Exposures of 1 minute to 2 minutes were generally needed for the various bands. The weak longer wave-length bands were measured in the spectrograms obtained 105°C with two minutes exposure whereas those obtained at 85°C with two minutes exposure were measured for the shorter wave length bands. However, one very weak shorter wavelength group was measured from a spectrogram obtained at 105°C with four minutes exposure.

RESULTS

The substance is a solid at room temperature and sublimates at 115°C. The absorption spectrum of the vapour was studied from room temperature upto 105°C with the different cell-lengths (Asundi and Singh, 1955). The absorption being very weak in the visible region, longer cells were found suitable. With 50 cm. cell there were no absorption bands in the visible region upto 70°C. At temperature of about 80°C seven main groups of the bands are observed. Of these groups, those at 20974 cm^{-1} , 22032 cm^{-1} and 23157 cm^{-1} are strong, the band at 22032 cm^{-1} being the strongest band of the system. Besides these three groups, the weak band groups are located at 22476 cm^{-1} , 22837 cm^{-1} and 23955 cm^{-1} . When the temperature is gradually increased, it is observed that these seven band groups become more intense, and most of the bands develop double and triple heads. At the same time, additional weak band groups appear at 19673 cm^{-1} , 20160 cm^{-1} , 20352 cm^{-1} , 20683 cm^{-1} , 21410 cm^{-1} and 21771 cm^{-1} filling the whole space between the first two main bands at 20974 cm^{-1} and 22032 cm^{-1} and extending considerably on the longer wave-length side of the first band

group at 20974 cm^{-1} . At the same temperature, very weak bands also develop on the longer wave-length side of all the seven main bands and an additional extremely weak band group develops at 24280 cm^{-1} . Thus, the spectrum becomes more complex at temperatures between 100° and 105°C .

About 175 bands are measured in the visible region including the twenty-eight bands reported by Seshan (1936). Many of the bands are sharp and have double and triple heads having frequency differences of 7 cm^{-1} to 12 cm^{-1} between them. Some of the bands are very sharp and line-like in appearance. Within the eight main groups seven developed at about 80°C and one developed at about 100°C . There are companion bands lying on the shorter wavelength side of the first band of each group and having a separation of 36 cm^{-1} . However, at temperatures between 100°C and 105°C , the companion bands also develop on the longer wavelength side of the main bands with recurring frequency differences of 37 cm^{-1} , 64 cm^{-1} and 92 cm^{-1} . Many of the bands are too weak to be measured.

TABLE I

Wave-length in Å	Wave-numbers in cm^{-1}	Intensity	Separation from (0 0)	Assignment	Remarks
5081.8	19673	ow, s	-1839	$0-3 \times 613$	The bands from 19673 cm^{-1} to 20097 cm^{-1} were measured and their intensities estimated from a spectrogram taken at a temperature of 105°C with an exposure of 2 minutes
5068.4	19725	ew, s	-1787	$0-538-1176-2 \times 37$	
5059.2	19760	cw, s	-1752	$0-538-1176-37$	
5049.7	19798	cw, v	-1714	$0-538-1176$	
5030.4	19874	ow, s	-1638	$0-3 \times 538-37$	
5020.6	19912	ew, s	-1600	$0-3 \times 538$	
5009.7	19956	w, d	-1556	$0-538-814-90-3 \times 37$	
4998.2	20002	vw, d	-1510	$0-538-814-90-2 \times 37$	
4989.5	20037	vw, d	-1475	$0-538-814-90-37$	
4980.9	20071	vw, d	-1441	$0-538-814-90$	
4974.5	20097	vw, d	-1415	$0-538-814-64$	
4958.9	20160	m, s	1352	$0-538-814$ or $0-538-613-5 \times 37-12$	The bands from 20160 cm^{-1} to 20910 cm^{-1} were measured and their intensities estimated from spectrograms at a temperature of 105°C with an exposure of one minute.
4956.2		w, s	-1341	$0-538-613-5 \times 37$ or $0-520-1680-3 \times 37$	
4949.5	20198	w, s	1314	$0-538-613-4 \times 37-12$	
4949.2		w, s	1304	$0-538-613-4 \times 37$ or $0-520-1680-4 \times 37$	
4940.8	20234	w, s	-1278	$0-538-613-3 \times 37-12$	
4938.3	20244	w, s	-1268	$0-538-613-3 \times 37$ or $0-520-1680-3 \times 37$	
4931.6	20272	w, s	1240	$0-538-613-2 \times 37-12$	
4929.7	20280	w, s	1232	$0-538-613-2 \times 37$ or $0-510-1680-2 \times 37$	

TABLE I (Contd.)

Wave-length in Å	Wave- numbers in cm ⁻¹	Intensity	Separation from (0,0)	Assignment	Remarks
4923.3	20306	w, sd	-1206	0-538-613-12	
4919.2	20323	w, sd	-1189	0-538-613-37 or 0+520-1680-37	
4914.8	20341	w, sd	-1171	0-538-613-12 or 0+520-1680	
4912.2	20352	w, sd	-1160	0-538-613 or 0+520-1674	
4904.4	20384	vw, sd	-1128	0+520-1680+36	
4902.7	20391	vw, sd	-1121		
4894.2	20427	w, vs	-1085	0+520-1680+2×36	
4889.4	20447	vw, sd	-1065		
4883.6	20471	vw, sd	-1041	0+520-1680+3×36	
4882.2	20477	vw, sd	-1035		
4868.0	20537	w, vs	-975	0-538-291-4×37	
4864.6	20551	vw, sd	-961		
4860.2	20570	vw, sd	-912	0-538-291-3×37	
4855.9	20588	vw, sd	-924		
4852.2	20603	vw, sd	-909	0-538-291-2×37	
4847.2	20625	vw, sd	-887		
4839.4	20658	vw, sd	-854	0-538-291-37	
4833.6	20683	ms, sd	-829	0-538-291	
4824.3	20723	ms, sd	-789	0-538-291+36	
4822.5	20730	m, sd	-782	0-538-291+36+7	
4820.8	20738	w, sd	-774		
4817.2	20753	w, sd	-759	0-538-291+2×36	
4814.4	20765	w, sd	-747		
4809.7	20786	w, sd	-726	0-538-5×37 or 0+520+40-1680 or 0+520-2×613	
4807.6	20794	w, sd	718	0-538-2×90 or 0+520+440-1669	
4801.3	20822	w, sd	690		
4800.4	20826	hw, sd	686	0-538-4×37	
4793.6	20855	vw, sd	657	0-538-3×37 or 0+520-1176	
4790.9	20867	m, s	645	0-538-37-64	
4784.9	20893	ms, s	619	0-538-90 or 0+520-1148	
4783.5	20899	m, s	613	0-613 or 0-538-2×37	
4781.1	20910	m, s	602	0-538-64	

TABLE I (Contd.)

Wave-length in Å	Wave-numbers in cm ⁻¹	Intensity	Separation from (0,0)	Assignment	Remarks
4774.8	20937	vw, d		0-538-37	The bands from 20937 cm ⁻¹ to 21222 cm ⁻¹ develop even at 80°C. They are however measured and their intensities estimated from spectrograms taken at 105°C with ex- posure of two minutes.
4768.4	20966	w, vd	546	0-538-7	
4766.6	20974	vs, vs	538	0-538	
4760.4	21001	w, d	511	0-538+36-7	0-520+1122-1149
4758.7	21008	vs, vs	504	0-538+36	
4755.9	21021	vw, d	491	0-538+36-7	
4750.2	21046	vs, vs	466	0-538+2×36	0-538+2×36+7
4748.7	21053	m, s	459	0-538+2×36+7	
4747.5	21058	m, s	454	0-538+2×37+12	
4742.7	21079	m, s	433		0-538+3×36
4741.1	21086	vs, vs	426	0-538+3×36	
4738.9	21096	m, s	416	0-538+3×36+12	
4733.6	21120		392	0-538-4×36	0-538-4×36+12
4731.4	21130		382	0-538-4×36+12	
4726.5	21151		361	0-538-5×36 or 0+520-806-1680	
	21170		342	0-538-613+806 or 0+520+806-1667	0-538+6×36
4718.5	21187	ms, s	325	0-538+6×36	
4710.9	21222	vw, s	290	0-520-814 or 0-291	
4707.3	21238	w, s	274	0+520-814	The bands from 21238 cm ⁻¹ to 22029 cm ⁻¹ are developed at 105°C. They are measured from spectrograms taken at 105°C with 1 minute exposure
4705.8	21245	w, s	267	0-520-814+7	
4704.9	21249	w, s	263	0+520-814+12	
4699.9	21271	vw, s	241	0+520-814+36	0+520-814+36+7
4698.4	21278	vw, s	234	0+520-814+36+7	
4691.6	21309	vw, s	203	0+520-814+2×36	
4690.2	21315	vw, s	197	0+520-814+2+36+7	0-538+440
4687.7	21327	vw, s	185	0-538+440+36	
4683.8	21344	vw, s	168	0-520-814+3×36	
4682.4	21351	vw, s	161	0-520-814+3×36+7	0-538+440+36
4679.9	21362	vw, s	150	0-520-814+3×36+12	
4669.4	21410	ms, s		0-538+440	
4668.5	21414	w, s	98		0+520+1122-1667
4667.8	21417	w, s	95	0-613+520	
4660.8	21450	vw, d	82	0-538+440+36	
4653.1	21485	m, s		0+520+1122-1667	0, 0
4651.1	21494	w, s	18		
4644.9	21524	m, d	12		
—	(21512)	—	0	0, 0	(Calculated)
4636.6	21562	w, d	50	0+520-470	0+520-470+36
4630.3	21591	m, d	79	0+520-470+36	
4628.4	21599	w, ds			
4620.4	21637	w, sd	125	0+520-470+2×36	

TABLE I (contd.)

Wave-length in Å	Wave-numbers in cm ⁻¹	Intensity	Separation from (0, 0)	Assignment	Remarks
4614 1	21607	vw, sd	155	0 + 520 - 4 × 90	
4611.5	21678	vw, sd	166	0 + 520 - 470 + 3 × 36 or 0 + 520 + 440 - 794	
4602.9	21719	vw, sd	207		
4591 9	21771	ms, s	259	0 - 538 + 806	
4583.1	21813	w, s	301	0 - 538 + 806 + 36	
4575 8	21848	vw, d	336	0 - 538 + 806 + 36 0 + 520 - 2 × 90	
4571 9}	21867	vw, d	355		
4568 8}	21881	vw, d	369	0 - 538 + 806 + 3 × 36 - 7	
4567.7}	21887	vw, d	375	0 - 538 + 806 + 3 × 36	
4562 9}	21991	vw, sd	399		
4561.7}	21916	vw, sd	404		
4560 5}	21921	vw, sd	409	0 - 538 + 806 + 4 × 36 or 0 + 520 - 3 × 37	
4557.7}	21935	w, d	423	0 + 520 - 90	The 21935 cm ⁻¹ band also develops at 80°C
4556.8}	21039	ew, d	427		
4555 4}	21945	wc, s	433		
4552 7}	21959	we, s	447	0 + 520 - 2 × 37	The 21980 cm ⁻¹ band also develops at 80°C
4550.1}	21971	ew, s	459		
5448 3}	21980	ms, s	468	0 + 520 - 04	
4546.1}	21991	ew, s	479	0 + 520 - 3 × 18	
4543.3}	22004	ms, s	492	0 + 520 - 37 or 0 + 520 - 2 × 18	
4541.4}	22014	ms, s	502	0 + 520 - 18	
4539.2	22024	ms, s	512	0 + 520 - 7	
4538.3	22029	cw, s	517	0 + 520 - 3	
4537 6}	22032	vs, vs	520	0 + 520	
4535 0}	22042	vs, vs	530	0 + 520 + 12	
4533.4}	22052	w, sd	540		
4530 7}	22066	w, s	554	0 + 520 + 36 - 7	
4529 7}	22070	s, s,	558	0 + 520 + 36	
4527.9}	22079	vs, s	567	0 + 520 + 36 + 12	
4525 8	22089	w, s	577	0 + 574	
4523 1}	22103	ms, s	591	0 - 538 + 1122	
4520 7}	22114	s, s	602	0 + 520 + 2 × 36	
4518 7}	22124	ms, s	612	0 + 520 + 2 × 36 + 12	
4515.7	22139	ow, s	627		
4513 4}	22150	ms, s	638	0 + 520 + 3 × 36	
4511.0}	22162	ms, s	650	0 + 520 + 3 × 36 + 12	
4508.2	22176	w, s	664		
4506.4	22185	ms, s	673	0 + 520 + 4 × 36	

The bands from 22032 cm⁻¹ to 22185 cm⁻¹ develop even at 80°C. They are measured and then intensities estimated from plates taken at 85°C with 2 minute exposure.

TABLE I (Contd.)

Wave-length in Å	Wave-numbers in cm ⁻¹	Intensity	Separation from (0,0)	Assignment	Remarks
4503.8	22197	vw, s	685	0 520 5 > 36	The bands from 22197 cm ⁻¹ to 22458 cm ⁻¹ develop at 105°C. They are measured and their intensities estimated from spectrograms taken at 105°C with 3 minutes exposure
4501.4	22209	vw, s	697		
4499.2	22220	vw, s	708		
4495.5	22238	vw, s	726		
4491.8	22257	vw, s	745	0 + 520 + 227	0 + 520 + 1122 806 - 1688
4490.3	22264	vw, s	752		
4487.2	22279	vw, s	767		
4481.9	22291	vw, ms	779		
4483.8	22290	vw, s	784	0 520 + 440 - 3 × 37	
4480.3	22314	vw, s	802		
4477.1	22330	vw, s	818		
4470.4	22363	vw, ms	851		
4465.3	22389	vw, s	877	0 520 440 - 90	0 + 520 + 440 - 2 × 37
4461.9	22406	vw, vs	894		
4459.5	22418	vw, d	906		
4456.3	22431	vw, ms	922		
4451.5	22458	vw, ms	946	0 520 1122 - 470	0 + 520 + 440 - 18
4447.9	22476	ms, d	961		
4441.8	22507	w, d	995		
4433.3	22550	w, d	1038		
4422.6	22605	vw, d	1094	0 + 520 + 1122 + 2 × 36	The bands from 22476 cm ⁻¹ to 22550 cm ⁻¹ develop at 80°C. The band at 22605 and 22700 cm ⁻¹ develop at 105°C
4404.0	22700	w, sd	1188		
4377.7	22837	ms, ms	1325		
4370.9	22872	ms, ms	1360		
4363.8	22909	ms, ms	1397	0 + 520 + 806 2 × 36 or 0 + 520 + 806 3 × 36	The bands from 22837 to 22945 cm ⁻¹ develop even at 80°C.
4357.0	22045	ms, ms	1433		
4329.8	23089	w, sd	1577		
4317.1	23157	s, sd	1645		
4309.7	23196	m, sd	1684	0 + 520 + 1122 - 35	The band at 23089 cm ⁻¹ develops at 105°C. The bands from 23157 to 23269 cm ⁻¹ develop at 80°C. The bands from 23304 to 23528 cm ⁻¹ develop at 105°C.
4303.2	23232	w, sd	1720		
4296.3	23269	w, sd	1757		
4290.0	23304	vw, sd	1792		
4282.4	23345	vw, sd	1833	0 + 520 + 1122 + 4 × 36	0 + 520 + 1122 + 440 - 90
4251.4	23515	m, sd	2003		
4243.7	23528	w, sd	2016		
4237.3	23593	ms, sd	2081		
4231.2	23627	m, sd	2115	0 + 520 + 1122 + 440 + 36 or 0 + 520 + 2 × 806	The bands from 23593 to 23761 cm ⁻¹ develop even at 80°C
4223.9	23668	m, sd	2156		
4218.6	23708	w, sd	2196		
4209.0	23761	vw sd	2259		

TABLE I (Contd)

Wave-length, in Å	Wave-numbers in cm ⁻¹	Intensity	Separation from (0, 0)	Assignment	Remarks
4178.4	23926	m, sd	2414	0 + 520 + 1122 + 37	The bands at 23926 and from 24067 to 24520 cm ⁻¹ develop at 105°C. The bands from 23955 to 24028 cm ⁻¹ develop even at 80°C.
4173.4	23955	ms, sd	2443	0 + 520 + 1122 + 806	
4167.1	23991	m, sd	2479	0 + 520 + 1122 + 806 + 36	
4160.7	24028	m, sd	2516	0 + 520 + 1122 + 806 + 2 × 36	The bands from 22476 to 24520 cm ⁻¹ are measured from spectograms taken at 85°C as well as 105°C.
4153.9	24067	w, sd	2556	0 + 520 + 1122 + 806 + 3 × 36	
4147.1	24106	vw, sd	2594	0 + 520 + 1122 + 806 + 4 × 36	
4117.4	24280	vw, ms	2768	0 + 520 + 2 × 1122	The bands from 22476 to 24520 cm ⁻¹ are measured from spectograms taken at 85°C as well as 105°C.
4111.3	24316	vw, sd	2794	0 + 520 + 2 × 1122 + 36	
4099.9	24384	vw, sd	2872	0 + 520 + 2 × 1122 + 3 × 36	
4087.7	24456	vw, sd	2944	0 + 520 + 2 × 1122 + 5 × 36	
4077.2	24520	ow, sd	3008		

The experimental data are presented in Table I. Here the wavelengths in air are listed in column 1 and the corresponding wavenumbers in vacuo converted by means of Keyser's Schwingungszahlen in column 2. The values are believed to be accurate to within 2 cm⁻¹ for the sharper bands and 5 cm⁻¹ for the broad bands. Visually estimated intensities and the degree of diffuseness of band-heads are given in column 3. The notations used in this column have the same meanings as in part II of the series (Singh, 1957-58). Column 4 is used to record the wavenumber differences between each band and the calculated (0, 0) band at 21512 cm⁻¹. Assignments are given in column 5 and 6, and the conditions under which the bands reported here were measured, are given.

PRELIMINARY AND GENERAL ANALYSIS

It is assumed that the para-benzoquinone molecule has a symmetry represented by D_{2h}(Vh). In case the visible system of benzoquinone is identified with the 4900 Å system of benzene, it has to be assigned to a symmetry allowed transition (Kasha, 1947) resulting from the reduction of symmetry from D_{6h} to D_{2h}. However, an attempt to analyse the bands as due to an allowed transition is met with two serious difficulties, namely, the unaccountability of an interval of 1058 cm⁻¹ between the strongest groups of the band system and the anomaly in the intensity distribution. Thus, it is not possible to assign unambiguously the (0,0) band of the system either at 20974 cm⁻¹ or at 22032 cm⁻¹ which are the two strongest bands. On the other hand, both these difficulties disappear if the analysis is made on the assumption of a forbidden transition made allowed by excitation of a suitable non-totally symmetric vibration. Under this assumption, the (0,0) band should have negligible intensity while the (0,1) and (1,0) bands of a non-totally symmetric vibration should show up strongly.

An inspection of the gross-structure of the spectrum shows that the strong bands at 22032 cm^{-1} and 20974 cm^{-1} can be assigned to the excited and the ground state vibration respectively superimposed upon the forbidden (0,0) band. The fact that the band at 20974 cm^{-1} is weaker in intensity in comparison to that at 22032 cm^{-1} and that it gains in intensity as the temperature is increased also lends support to this assignment. The interval 1058 cm^{-1} between these two bands should then correspond to the sum of the excited state and ground state frequencies of some non-totally symmetric vibration which makes the transition allowed. In the Raman spectrum (Kohlrausch *et al*, 1913 and Stammereich *et al*, 1952) there is a frequency 538 cm^{-1} (K.P.S.) reported as 540 cm^{-1} by Stammereich and Forneris and this is depolarised. By choosing 538 cm^{-1} as the frequency of this vibration which makes the transition allowed, the excited state frequency will then be 520 cm^{-1} , so that sum of the two frequencies may be equal to 1058 cm^{-1} . With those assumptions, the general analysis of the main bands is given in Table II.

TABLE II.

General analysis of the main groups

Group No.	Wave-numbers in cm^{-1}	Intensity	Separation from (0, 0)	Assignments
I	20974 21512	(6) —	-538 0	0—538 (0, 0) (Calculated)
II	22032	(10)	520	0+520
III	22476	(5)	964	0+520+440
IV	22837	(5)	1325	0+520+806
V	23157	(8)	1645	0+520+1122
VI	23593	(3)	2081	0+520+1440
VII	23955	(3)	2443	0+520+1122+806

The detailed analysis of the band (vide Table I) on the basis of a forbidden transition will now be given.

DETAILED ANALYSIS AND DISCUSSION

The transition is made allowed by a non-totally symmetric vibration of 538 cm^{-1} and is in many respects similar to the 2600A bands of benzene in its gross-structure. Just as in the 2600 A system of benzene the benzoquinone visible system should not have a (0,0) band, but instead a (0,1) band of a non-totally symmetric vibration. A (1, 0) band of the same vibration should occur with much

weaker intensity. For reasons discussed later, it seems probable that any of the b_{1g} , b_{2g} or b_{3g} vibrations may be instrumental in making the transitions allowed. Of these vibrations, there is one belonging to b_{1g} class, there are three belonging to b_{3g} class. As in benzene, carbon vibrations are expected to be more effective. There is difficulty, however, in establishing these vibrations, because the vibrational frequencies in the ground state of benzoquinone and their assignments to various modes of vibrations are not definitely known. As is well-known, the 606 cm^{-1} frequency of benzene splits into an (a_g) and a (b_{2g}) vibration (Sponer, 1942). The 444 cm^{-1} frequency found in the Raman spectrum is identified with the (a_g) part of this split vibration whereas 540 cm^{-1} may be identified as the b_{2g} part of the same vibration.

Another totally symmetric vibration has a frequency of 806 cm^{-1} in the excited state, and is associated with some kind of ring vibration. It is identified with the 794 cm^{-1} frequency found in the Raman spectrum (Stammreich and Forneris, 1952) though in that case, it will be observed that excited state frequency is slightly more than the ground state frequency. It is interesting to note that the same ground state 794 cm^{-1} vibration is found here loaded on various other suitable vibrations and is thus corroborated.

The 1122 cm^{-1} frequency found in the excited state corresponds to the ground state frequency of 1149 cm^{-1} found in the Raman spectrum (Stammreich and Forneris, 1952). The same Raman frequency has been reported as 1178 cm^{-1} by Kohlrausch *et al* (1913). The present work confirms this frequency as 1149 cm^{-1} and not as 1178 cm^{-1} . There is progression of this vibration which also appears in combination with 440 cm^{-1} and 806 cm^{-1} in the excited state. The intensity of the band with 1122 cm^{-1} frequency superimposed upon the (0, 1) band at 22032 cm^{-1} is greater than the intensity of bands resulting from the superposition of 440 cm^{-1} and 806 cm^{-1} on the same (0, 1) band. Further, the frequencies of 440 cm^{-1} and 806 cm^{-1} are loaded with one quantum on this 1122 cm^{-1} frequency already superimposed on the (0, 1) band. Thus, the successive groups are assigned as $0+520$, $0+520+440$, $0+520+806$, $0+520+1122$, $0+520+1122+440$ and $0+520+1122+806$. There is a very weak band group developed at a temperature of 105°C which is assigned as $0+520+2\times 1122$. It is to be marked that at higher temperatures, bands develop when the ground state vibration of frequency 1149 cm^{-1} corresponding to this excited state vibration of frequency 1122 cm^{-1} is excited in combination with various frequencies. This indicates a preferential excitement of this vibration both in the ground and excited states of the molecule.

There is a totally symmetric vibration of 90 cm^{-1} frequency reported in the Raman spectrum by Kohlrausch *et al* (1913) but not confirmed by Stammreich and Forneris (1952). It is curious enough that there are bands in the visible spectrum which may be interpreted with this vibration of 90 cm^{-1} but for which there is always an alternative interpretation which appears to be more reasonable.

Thus, the band assigned as 0—538—90 may be assigned as 0—520—1149. As bands develop invariably at higher temperatures where the ground state frequency of 1149 cm^{-1} is probably excited it is assumed that the latter assignment is correct. This is further supported by the excitation of this vibration at these temperatures in combination with other vibrations.

Another totally symmetric vibration reported in the Raman spectrum is 1674 cm^{-1} which has been reported as a doublet having frequencies 1667 and 1688 cm^{-1} (Strammereich and Forneris, 1952). In the vapour spectrum, there are bands which are assigned as due to the ground state vibrations of 1667 cm^{-1} and 1688 cm^{-1} . The excited state frequencies corresponding to these vibrations are found to be 1676 cm^{-1} and 1630 cm^{-1} , but as they fall within other band groups where interactions may take place, it is not possible to assign these values unambiguously. The other vibrations are 241 cm^{-1} and 613 cm^{-1} corresponding to the Raman frequencies of 243 cm^{-1} and 610 cm^{-1} .

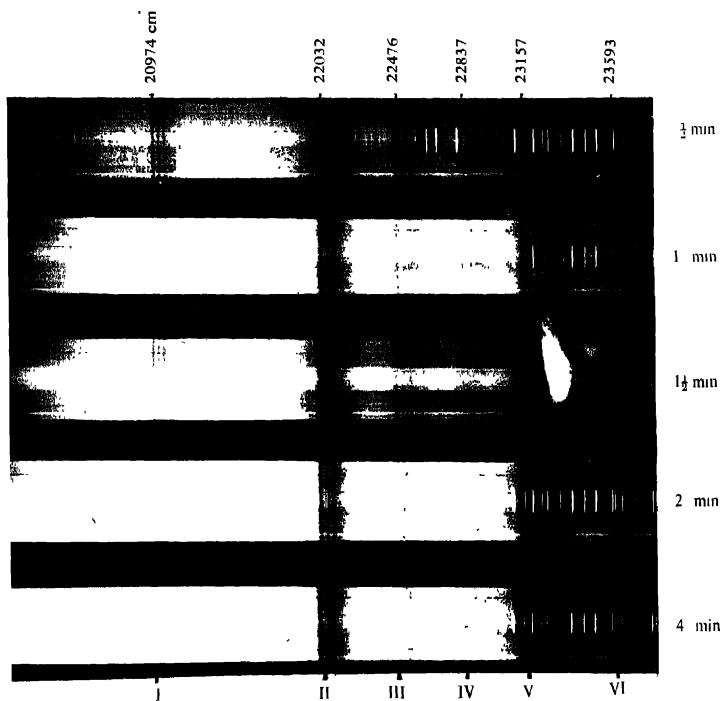
SYMMETRY TYPE OF THE EXCITED ELECTRONIC STATE

The ground electronic level of benzoquinone may be taken as A_g level. In order that it may be forbidden transition as it appears to be, the excited state should be either A_g or A_u or B_{1g} or B_{2g} or B_{3g} . From the proposed analysis, this forbidden transition is made allowed by a Raman active 'g' vibration of frequency 538 cm^{-1} . Therefore, if a forbidden transition in D_{2h} symmetry is made allowed by a 'g' type of vibration, the excited electronic level must belong to 'u' type, as only this contains a translation. Thus, out of the five probable classes A_g , A_u , B_{1g} , B_{2g} and B_{3g} , the excited level must be (A_u). Therefore, this transition may be assigned as $A_u \leftarrow A_g$ on the basis of this analysis. This is in agreement with a theoretical calculation made by Sidman (1957).

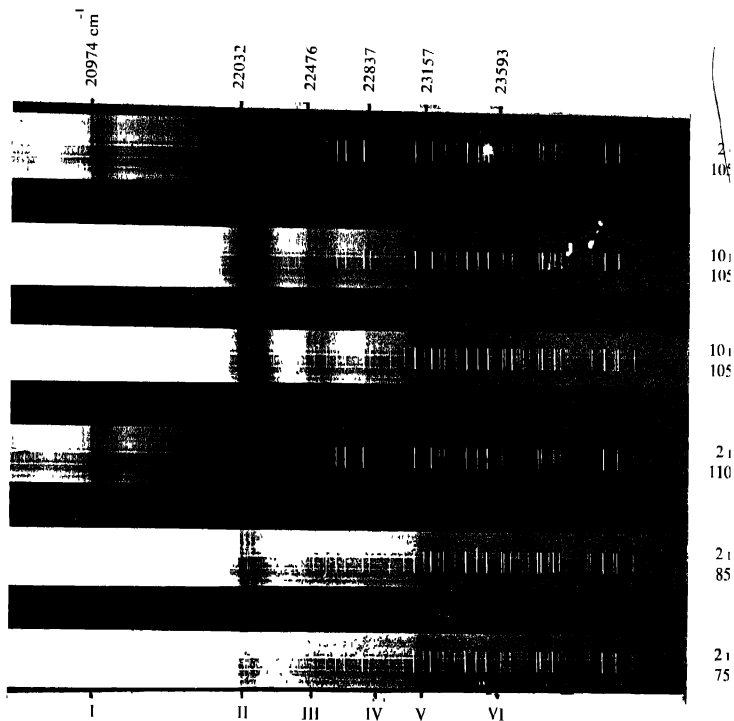
It is interesting to note in this connection that the characteristic long wavelength absorption of carbonyl compounds has been interpreted by Mc. Murry as corresponding to a transition in which a loosely bound electron occupying a non-bonding orbital lying in the molecular plane and across CO direction is excited to an excited molecular orbital with a node in the plane. On the basis of this, it was suggested that the visible absorption band of benzoquinone may also be of the same nature. Thus, this transition is assigned as $n-\pi(A_u \leftarrow A_g)$ transition. As suggested by Kasha (1947), a decision as to the cause of prohibition in carbonyl bands would be of great interest. The present analysis reveals that the cause of prohibition is the 'forbiddenness' of the electronic transition rather than the intercombination.

OTHER FEATURES OF THE SPECTRUM

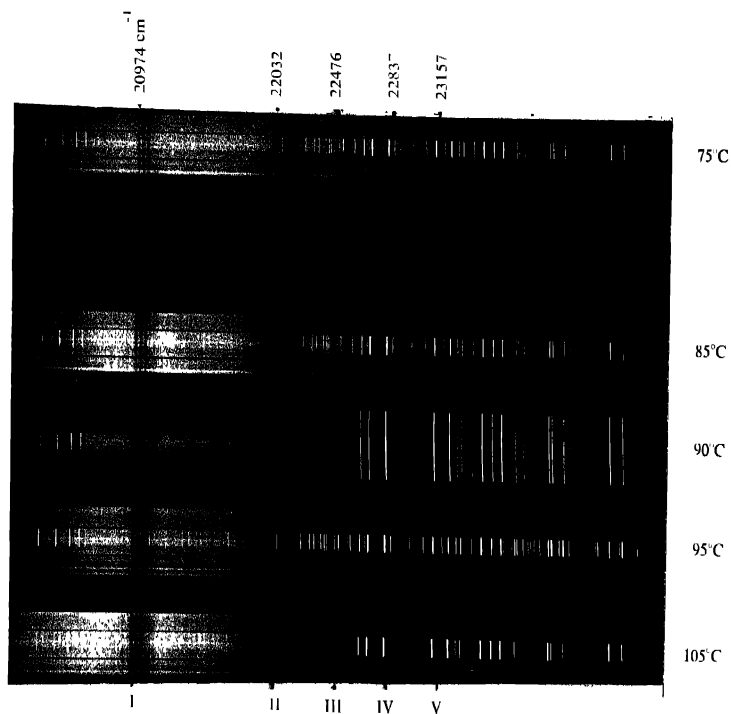
The 36 cm^{-1} recurring difference frequency lying on the shorter wavelength of each group may be interpreted as $v-v$ transitions of two different vibrations



The visible absorption spectrum of benzoquinone at 100°C with different exposure times on a 3 prism Steinheil glass spectrograph



The visible absorption spectrum of benzoquinone with different exposures
and at different temperatures.



The visible absorption spectrum at different temperatures and with the same exposure on the Steinheil glass spectrograph

possibly 538 cm^{-1} in the ground state and 574 cm^{-1} in the excited state, the latter corresponding to 613 cm^{-1} frequency in the ground state. Similarly, the v, v transitions of these two very vibrations with frequencies 520 cm^{-1} and 613 cm^{-1} , the former corresponding to 538 cm^{-1} in the ground state may be responsible for a recurring pattern of 90 cm^{-1} . The recurring pattern of 37 cm^{-1} on the longer wavelength side may likewise be assumed to be due to v, v transitions. Most of the bands are very sharp and have no degradations. However, there appears to be slight degradations towards violet in some of the bands. Many bands are double and triple headed, the common separations being 7 cm^{-1} and 5 cm^{-1} between triple-headed bands and 12 cm^{-1} between the double headed bands. The multiple heads may be due to rotational structure.

ACKNOWLEDGMENT

The author wishes to express his great indebtedness to Prof. R. K. Asundi for his inspiring guidance and helpful suggestions during the course of the present work.

REFERENCES

- Asundi, R. K. and Singh, R. S., 1955, *Nature*, **176**, 1223.
- Bruade, E. A., 1945, *J. Chem. Soc.*, **44**, 490.
- Seshan, P. K., 1936, *Proc. Ind. Acad. Sci.*, **3**, 172.
- Singh, R. S., 1955-56, *J. Sc. R. (B.H.U.)* **VI**(2), 286.
- Sidman, J. W., 1957, *J. Chem. Phys.*, **27**, 429.
- Singh, R. S., 1957-58, *J. Sc. R. (B.H.U.)*, **VIII**(2), 261.
- Kasha, M., 1947, *Chem. Rev.*, **41**, 405.
- Kohlrausch, K. W. F. et al., 1913, *Sitzber. Akad. Wiss. Wein. Abt. II*, **146**, 213.
- Stammreich, H. and Forneris, R., 1952, *Zeit. Natur.*, **79**, 756.
- Sponer, H., 1942, *Rev. Mod. Phys.*, **14**, 224.
- Mc. Murry, H. L., 1941, *J. Chem. Phys.*, **9**, 231, 241.

LEVEL SCHEME OF Pr^{144} A. K. SENGUPTA, R. BHATTACHARYYA, J. LAHIRI AND
P. N. MUKHERJEE

SAHA INSTITUTE OF NUCLEAR PHYSICS, CALCUTTA

(Received August, 27, 1959)

ABSTRACT. The level scheme of Pr^{144} following β -decay of Ce^{144} has been studied with a Siegbahn-Slatis β -ray spectrometer and scintillation spectrometers. Three β -groups have been observed with end-point energies and relative intensities as 184 Kev (26%), 240 Kev (8%) and 312 Kev (66%). Corresponding gamma-rays of energies 53 Kev, 81 Kev and 134 Kev have also been detected. Internal conversion lines of these transitions along with those of some other γ -lines of energies 33 Kev, 38 Kev, 42 Kev, 59 Kev and 95 Kev have been observed. K/L ratio and half-time measurement of the 134 Kev γ -line indicate an M1 multipolarity for this transition. Coincidence studies have also been made and a tentative decay scheme is proposed.

INTRODUCTION

The disintegration scheme of Ce^{144} has been studied by several investigators (Emmerich *et al*, 1951; Keller *et al*, 1951; Cook *et al*, 1951; Lin-Sheng *et al*, 1952; Hollander *et al*, 1953; Emmerich *et al*, 1954; Kregar *et al*, 1954; Cork *et al*, 1954; Pullman *et al*, 1956; Hickok *et al*, 1958). Though the decay scheme of Pr^{144} is well established, there remain considerable controversies about the decay of Ce^{144} , particularly about the energy of the highest excited state in Pr^{144} , the number of β -groups and excited states, the conversion co-efficients and multiplicities of the transitions. The highest energy gamma ray is reported to be of energy 175 Kev, 145 Kev and 134 Kev by different workers. Experimental K -conversion co-efficients of 81 Kev γ -ray appear to be in disagreement with theoretical values (Rose, 1958). The assignment of multiplicities to the observed gamma-rays does not seem to be unambiguous and the observed weaker lines are also not uniquely fitted to the disintegration scheme. The present investigation was undertaken to resolve some of the existing uncertainties.

EXPERIMENTAL METHODS AND MEASUREMENTS

The source was obtained carrier-free in the form of CeCl_3 in HCl solution from the Radiochemical Centre, Amersham. Sources were prepared by evaporation of the solution on a thin mylar foil (0.5 mg/cm²).

The β -spectrum was taken with a Siegbahn-Slatis β -ray spectrometer with a momentum resolution of 1.9% at a transmission of 5%. The detector was a G. M. counter with a window of mylar foil which transmitted electrons upto an

energy of about 20 Kev. Kurie plots in this set up were linear upto 50 Kev (Mukherjee *et al*, 1959). The γ -ray spectrum was taken with a single channel pulso height analyser in two different phosphor-photomultiplier combinations; one with a $1\frac{1}{2} \times 1\frac{1}{2}$ " NaI (Tl) crystal mounted on Dumont 6292 photomultiplier, and the other with a 4×4 " NaI (Tl) with a $3/16 \times 2$ " well crystal and a Dumont 6364 photomultiplier. The resolution in both the cases was about 9% for 661 Kev.

γ - γ coincidences were recorded with two thin NaI (Tl) phosphors and 6810A tubes. The thin phosphors were chosen in order to improve the detection efficiency for the lower energy γ -rays. The β - γ coincidences were recorded by means of scintillation spectrometers. 6810A photomultiplier tubes with anthracene and NAI (Tl) crystals were used in the β - and γ -channels respectively. The slow fast technique with Garwin's modified coincidence circuit was utilised for these measurements and the coincidence resolving time was kept around 2×10^{-8} sec.

RESULTS

Beta-spectrum

The β -spectrum of Ce^{144} is shown in figure 1. Table I shows the conversion electron lines. Kurie plots (after subtracting the high energy β -groups of Pr^{144})

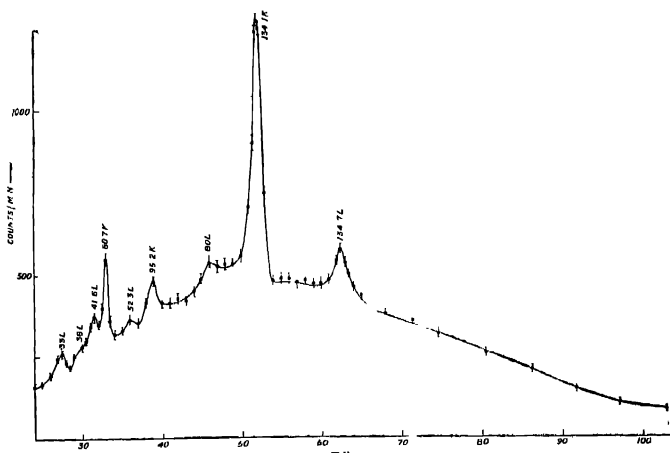


Fig. 1. Low energy β -spectrum of Ce^{144} .

yielded three β -groups (Table II). The spectrum taken with a better resolution (1%) around the electron energy of 73 to 90 Kev indicated the presence of a broad peak which was assigned to be the L-conversion line of 96 Kev. Table III gives the $K/(L+M)$ -ratios of stronger conversion lines.

Gamma-spectrum

The γ -spectrum taken with the external phosphor is shown in figure 2. There are two strong lines at 134 Kev and 36 Kev, and a rather broad peak around 81

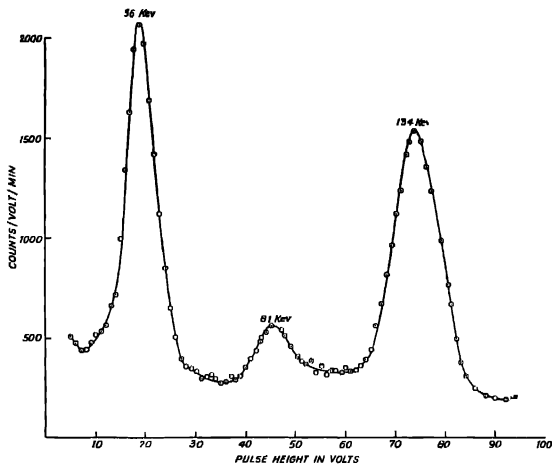


Fig. 2(a) Low energy γ -spectrum of Ce^{144}
(Source external to phosphor).

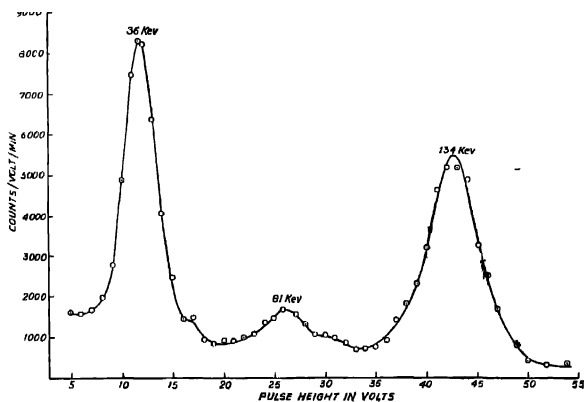


Fig 2(b). Low energy γ -spectrum of Ce^{144}
(Source within the well-type phosphor)

Kev perhaps indicates presence of weak unresolved transitions. The unconverted intensities of the gamma rays are given in Table IV; corrections for crystal efficiency, absorption in Al foil (β -absorber) and Iodine X-ray escape were made.

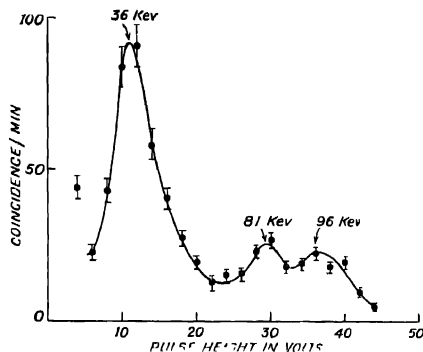


Fig. 3. γ - γ - coincidence spectrum with 36 Kev.

Gamma-Gamma coincidences

Figure 3 shows the γ -spectrum in coincidence with 36 Kev. A strong 36 Kev line with weaker lines at 54 Kev, 81 Kev and 96 Kev were seen. The γ -spectrum coincident with 81 Kev transition yielded a peak at 36 Kev with a broadening around 52 Kev on the high energy side.

Beta-Gamma coincidences

β - γ coincidences were performed to measure the life times of 134 Kev and 80 Kev states by delayed coincidence technique. β - γ coincidence with Hg^{203} provided the prompt resolution curve. The β -channel was made to accept all β 's above 120 Kev and delayed coincidences with 134 Kev and 81 Kev photopeaks were recorded. Comparison of the measured and normalised delayed-coincidence curves with that of Hg^{203} showed that the life times of both 134 Kev and 81 Kev states were less than 10^{-9} secs.

DISCUSSIONS

We have observed no γ - γ coincidence between 134 Kev and other γ -line down to 20 Kev. This and the absence of any β -group of energy < 184 Kev shows that 134 Kev level is fed by the lowest energy β -group and is the highest state excited in Pr^{144} . From the $(K/L+M)$ ratio and observed life-time limit, 134 Kev transition is most probably an M1 transition. Assuming the theoretical M1 conversion co-efficient for 134 Kev γ -ray (Rose, 1958), we find that about 34% of this level de-excites by cascade transitions,

A comparison of relative intensities of 134 Kev and 81 Kev γ -lines and their K-conversion lines yields a value of 0.55 ± 0.15 for the K-conversion co-efficient of 81 Kev γ -ray. This is, however, feared to be rather uncertain due to the presence of unresolved γ -lines in the 81 Kev photopeak and the error in the measurement

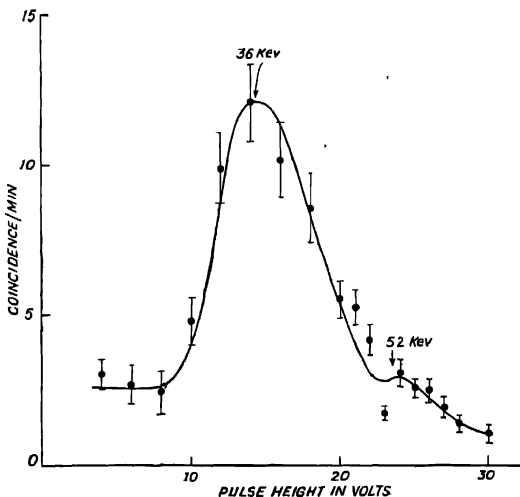


Fig. 4. γ -spectrum in coincidence with 81 Kev.

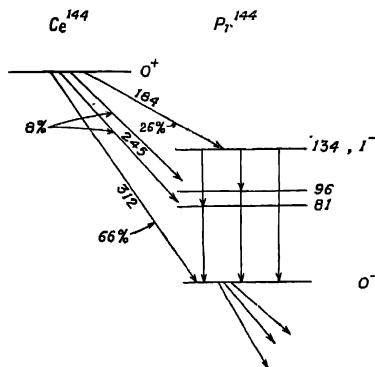


Fig. 5. Proposed decay scheme of Ce^{144}

of 81 Kev K-conversion peak area due to corrections for window absorption. From the conversion co-efficient of 134 and 81 Kev gammas and their relative intensities,

one can conclude that the 245 Kev β -group may partly feed the 96 Kev level. The existence of a 38-96 Kev cascade is also required to explain the observed coincidences and the high 36 Kev peak intensity in the gamma-spectrum. Also, the relative intensity of 81 and 134 Kev γ -rays ($\sim 100 : 30$) measured with the well-spectrometer when compared to that of Table IV indicates that 53-81 Kev cascade cannot be very strong.

TABLE I
Conversion lines observed in Ce^{144} decay

Electron energy (kev)	Assignment
128 3^a	134.7 (L+M)
92.1 a	134 1 K
73 0^a	80 (L+M)
53.2 a	95 2 K
	96.6 L
45 8^b	52 3 L
38.7 a	80 7 K
35 2^b	41 6 L
31 6	38 L
26 6^b	33 L

(a) energies correct upto 1%

(b) energies correct upto 2%

TABLE II
Continuous β -spectra of Ce^{144}

End-point Energy (kev)	Relative intensity	log fl.
312 \pm 7	66 \pm 8	7.5
240 \pm 15	8 \pm 3	7.4
184 \pm 4	26 \pm 6	7.1

TABLE III
K/(L+M) ratios of 134 and 81 Kev γ -rays

Energy (kev)	$K/(L+M)$ ratios				
	Observed	Theoretical (Rose)			
		E1	M1	E2	M2
134	5.1 ± 4	7.50	5.53	1.10	3.03
81	3.9 ± 1	5.10	5.50	0.19	2.62

TABLE IV

Relative intensities of unconverted γ rays
(Source external to phosphor)

Energy (Kev)	Relative Intensity
36+2	144 \pm 10
81 \pm 4	24 \pm 5
134 \pm 4	100 \pm 6

The three β -groups are characterised by rather high log ft values and probably all these are first forbidden transitions. The ground state of Ce^{144} is a 0^+ one. So, the states in Pr^{144} most probably have odd parity and spins 0, 1 or 2. The ground state of Pr^{144} has been assigned to be a 0^- one (Bromley, 1957) and shell-model considerations also predict the same. So, the highest excited state is 1^- . It is difficult to assign spins and parities to the 81 Kev and 96 Kev states conclusively from the present measurements.

The decay-scheme as proposed by Hickok *et al* is perhaps a simplified one. Particularly, we think that determination of the conversion co-efficients from 36 Kev X-ray intensity is liable to error. However, some discrepancies, e.g. the K-conversion co-efficient of 81 Kev and presence of weaker conversion lines, still remain to be explained. We hope further studies of this isotope with high resolution spectrometers will reveal a more consistent picture.

ACKNOWLEDGMENTS

The authors wish to thank Prof. A. K. Saha for his interest in this work. They are also grateful to Shri A. P. Patro for some valuable discussions and particularly for the help received from him in the design of the coincidence arrangement and in making his X-ray phosphors available for the work. The help of Sm. I. Dutt in the β -spectrometer measurements is also acknowledged with pleasure.

REFERENCES

- Bromley, D. A., 1957, *Proc. Rohovoth Conf. on Nuclear Structure*, 457.
 Cheng Lin-Sheng; John, G. and Kurbatov, J. D., 1952, *Phys. Rev.*, **85**, 487.
 Cook, C. S. and Porter, F. T., 1951, *Phys. Rev.*, **85**, 733.
 Cork, J. M.; Brice, M. K. and Schmidt, L. C., 1954, *Phys. Rev.*, **96**, 1295.
 Emmerich, W. S.; John, G. and Kurbatov, J. D., 1951, *Phys. Rev.*, **82**, 968.
 Emmerich, W. S.; Auth, W. J. and Kurbatov, J. D., 1954, *Phys. Rev.*, **94**, 110.
 Hickok, R. L., McKinley, W. A. and Fultz, S. C., 1958, *Phys. Rev.*, **109**, 113.
 Keller, H. B. and Cork, J. M., 1951, *Phys. Rev.*, **84**, 1079.
 Kröger, W. E. and Cook, C. S., 1954, *Phys. Rev.*, **96**, 1276.
 Mukherjee, P. N.; Dutt, I.; Sen Gupta, A. K. and Bhattacharyya, R. 1959, To be published.
 Pullman, I. and Axel, P. 1956, *Phys. Rev.*, **102**, 1366.
 Rose, M. E.: 1958, *Internal Conversion Co-efficients*, North-Holland Publishing Co.

NEUTRON STRENGTH FUNCTION $\bar{\Gamma}_n^0/D$ WITH COMPLEX DIFFUSE BOUNDARY POTENTIAL

ARUNDHATI GHOSH

DEPARTMENT OF THEORETICAL PHYSICS, INDIAN ASSOCIATION FOR THE CULTIVATION OF
SCIENCE, JADAVPUR, CALCUTTA 32

(Received, July 16, 1959)

ABSTRACT. The strength function $\bar{\Gamma}_n^0/D$ which is the average value of neutron width to level spacing and the effective radius R' are calculated with a complex spherical well having a diffuse boundary. The values of the parameters involved in the potential function are fixed by comparing our curves for the strength function with the same as given by Weisskopf. The S-state energy eigen-values calculated with the above parameters are in agreement with similar calculations of Green and Lee.

INTRODUCTION

The simple (square well) optical model potential as suggested by Feshbach, Porter and Weisskopf (1954) for nuclear reactions with neutrons provides a qualitative understanding of the scattering of neutrons by nucleus and also of the cross section for the formation of the compound nucleus. This model explains the irregular trend of the average neutron scattering cross section as function of the nuclear mass; the ratio of nuclear level width to level spacing for neutrons which is related to the scattering cross section, shows sharp increases near mass numbers $A = 55$ and $A = 155$. It is seen that the theory with this model predicts more pronounced maxima and minima of $\bar{\Gamma}_n^0/D$ with the variation of mass number than what is experimentally observed. Later Feshbach *et al* (1958) has studied the variation of strength function by taking Woods-Saxon type of potential, they find that a diffuse potential of this type gives much less pronounced maxima and minima of $\bar{\Gamma}_n^0/D$ than that given by the square well, thereby bringing the theory in better agreement with experimental findings than the previous one. If the theoretical points are made to agree with experimental ones at the maximum positions, then the theoretical curve lies above the experimental one at the minimum positions. At the peak at $A = 155$, the experimental points are much broader, lower and generally more irregular than the theoretical curve.

In this paper we have taken a complex spherical well with a diffuse boundary which may be said to be intermediate between the square well and the Woods-Saxon type; this potential has nearly the same nature as that of Woods-Saxon and at the same time allows easier solution than the latter. It is found that with proper adjustments of the depth of the potential, the nature of the curve for the

$\bar{\Gamma}_n^0/D$ is the same as that of Woods—Saxon potential. For the bound state problem, the imaginary part of the potential is zero, it is found that our S -state energy eigen values agree with similar calculations of Green and Lee (1955).

THEORY AND RESULTS

We choose the nucleon-nuclear potential to be of the form

$$V = -V_0(1+i\zeta) \text{ for } r < R$$

$$= -V_0(1+i\zeta)e^{-\frac{r-R}{a}} \text{ for } r > R$$

For the value of the nuclear radius R , we take the empirical relation of Feshbach *et al* (1958).

$$R = (1.15A^{1/3} + 0.4)10^{-13} \text{ cm.}$$

In the region $r > R$, we take the radial solution as a combination of incoming and outgoing waves for $l = 0$

$$u_0(r) = B[u_0^{(-)}(r) - \bar{\eta}_0 u_0^{(+)}(r)] \quad \dots (1)$$

At low enough energies, $\bar{\eta}_0$ is considered as the average value of the scattering amplitude over the neutron resonance energy and its value according to Feshbach, Porter and Weisskopf (1954) is given by

$$\bar{\eta}_0 = e^{-2ikR'}(1 - \pi\bar{\Gamma}_n/D), \quad \dots (2)$$

where k is the wave number of the incident neutrons, R' is a length of the order of nuclear dimensions, D is the average level distances, and $\bar{\Gamma}_n$ is the average value of the level widths for neutrons. It follows that for $kR' \ll 1$,

$$\bar{\Gamma}_n/D = (1/\pi)Re(1 - \bar{\eta}_0), \quad \dots (3)$$

$$kR' = \frac{1}{2} I_n(1 - \bar{\eta}_0) \quad \dots (4)$$

The experimental cross sections of scattering and absorption are related to $\bar{\Gamma}_n/D$ and R'/R by the relations

$$\sigma_{sc} = \frac{\pi}{k^2} |1 - \bar{\eta}_0|^2 \simeq 4\pi R^2, \quad \dots (5a)$$

$$\sigma_a = \frac{\pi}{k^2} (1 - |\bar{\eta}_0|^2) \simeq \frac{2\pi^2}{k^2} \frac{\bar{\Gamma}_n}{D} \quad \dots (5b)$$

Now the whole problem reduces to the determination of η_0 which is evaluated by matching the logarithmic derivative of the inner and outer solution at $r = R$.

For our potential the solution of Schrodinger equation for $l = 0$ in the region $r < R$ (cf. Weisskopf, 1954) is given by

$$\psi = C \frac{\sin \alpha r}{\alpha r} \text{ for } r < R, \quad \dots (6)$$

where
$$\alpha = \left[\frac{2M}{\hbar^2} \{V_0(1+i\xi) + |B|\} \right]^{1/2}$$

At the boundary eqn. (6) becomes $\psi = \frac{\sin X}{X}$

where
$$X = X_1 + iX_2 = \left[k^2 R^2 + \frac{2M}{\hbar^2} V_0 R^2 (1+i\xi) \right]^{1/2}$$

In the region $r > R$, the solution of Schrodinger equation for $l = 0$ (cf. Morse and Feshbach, 1953) comes out of the form

$$\psi = \frac{B}{r} [J_n(z) - \eta_0 J_{-n}(z)] \text{ for } r > R, \quad \dots (7)$$

when
$$n = 2ika; \quad Z = 2a \sqrt{\frac{2M}{\hbar^2} V_0 (1+i\xi)} e^{-\frac{1}{2}} \frac{r-R}{a}$$

Comparing with eqn. (1), the Bessel functions of eqn. (7) are related as

$$u_0^{(-)}(r) = J_n(z) \text{ and } u_0^{(+)}(r) = J_{-n}(z).$$

We expand $u_0^{(+)}(r)$ and $u_0^{(-)}(r)$ and the constants of the solutions are chosen in such a way that the first term of the series for $u_0^{(+)}(r)$ gives e^{ikr} and that for $u_0^{(-)}(r)$ gives e^{-ikr} for large values of r . The rest of the terms in the series gives the deviation of the wave function from that obtained with square well potential. The series is evaluated only upto fourth term and this will give us sufficiently reasonable results for the parameters chosen and the different nuclear radii considered. Thus we take

$$u_0^{(+)}(r) = J_{-n}(z) = e^{ikr} \left[1 - \frac{z^2}{2^2 \cdot 1 \cdot (1-n)} + \frac{z^4}{2^4 \cdot 1 \cdot 2 \cdot (1-n)(2-n)} - \dots \right] \dots (8)$$

$$u_0^{(-)}(r) = J_n(z) = e^{-ikr} \left[1 - \frac{z^2}{2^2 \cdot 1 \cdot (n+1)} + \frac{z^4}{2^4 \cdot 1 \cdot 2 \cdot (n+1)(n+2)} - \dots \right] \dots (9)$$

If we put

$$Z|_{r=R} = Pe^{ikr}$$

We obtain

$$u_0^{(+)}(r)|_{r=R} = e^{ikR} \left[\left\{ 1 - \frac{P^2 \cos 2\phi}{2^2} + \dots \right\} - i \left\{ \frac{P^2 \sin 2\phi}{2^2} + \frac{2kaP^2 \cos 2\phi}{2^2} - \dots \right\} \right] \quad \dots (10)$$

$$u_0^{(-)}(r)|_{r=R} = e^{-ikR} \left[\left\{ 1 - \frac{P^2 \cos 2\phi}{2^2} + \dots \right\} - i \left\{ \frac{P^2 \sin 2\phi}{2^2} - \frac{2kaP^2 \cos 2\phi}{2^2} - \dots \right\} \right] \quad \dots (11)$$

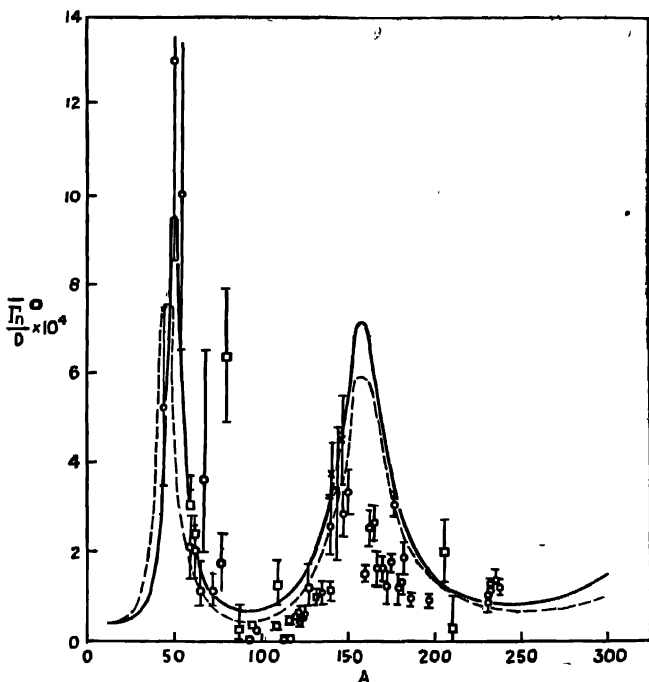


Fig. 1. Ratio of $\bar{\Gamma}_n^o/D$ of neutron width to level spacing. Here $\bar{\Gamma}_n^o/D$ is normalized to 1 ev. The solid curve is taken from Feshbach *et al.*, (1958). The dotted curve corresponds to our calculation with the parameters given in the figure.

$$V_0 = 48 \text{ Mev}$$

$$\xi = .06$$

$$a = 0.57 \times 10^{-13} \text{ cm}$$

$$r_R = (1.15A^{1/3} + 0.4) 10^{-13} \text{ cm}$$

assuming $ka \ll 1$. With the above notations and approximations $r \frac{du_0^{(+)}(r)}{dr} \Big|_{r=R}$

and $r \frac{du_0^{(-)}(r)}{dr} \Big|_{r=R}$ are calculated. We evaluate η_0 by matching the inside and out

side solutions and their derivatives at $r = R$. As regards parameters we choose $\zeta = .06$, $R = (1.15A^{1/3} + 0.4)10^{-13}$ cm, $a = 0.57 \times 10^{-13}$ cm, $V_0 = 48$ Mev. Except for V_0 , the values of other parameters are same as taken by Feshbach *et al* (1958) with Woods-Saxon potential. The results of our calculations are shown in figure 1 and figure 2. The nature of the curves is almost same as obtained by Feshbach, Porter and Weisskopf (1958) with one peak at $A = 50$ and another at $A = 155$ in Γ_n^0/D curve. We may point out that the height of the peaks in our Γ_n^0/D curve is less than that of Feshbach *et al*, this makes our curve agree more closely with the experimental points at $A = 155$, because of large errors at the other peak it is not possible to assert the same agreement at $A = 50$.

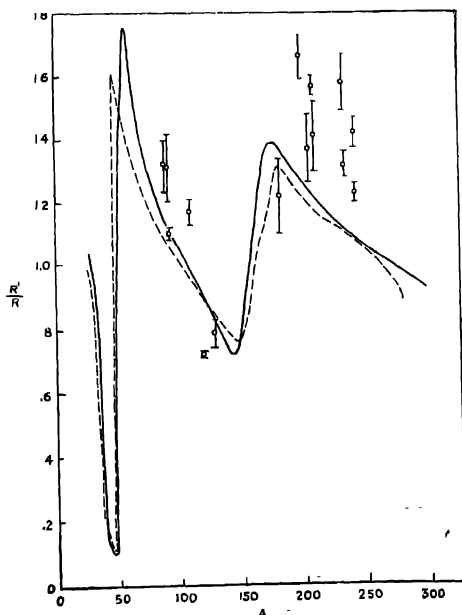


Fig. 2. Ratio of potential scattering length R' to nuclear radius R . The solid curve is taken from Feshbach *et al*, (1958). The dotted curve corresponds to our calculation with the parameters given in the figure.

$V_0 = 48$ Mev $\zeta = .06$
 $a = 0.57 \times 10^{-13}$ cm $R = (1.15A^{1/3} + 0.4) 10^{-13}$ cm

With the same parametric values (of course with $\zeta = 0$) we calculate (figure 3) the S -state energy eigen values for $A = 200$. The matching of the logarithmic derivatives of the inner and outer solutions at the nuclear boundary gives

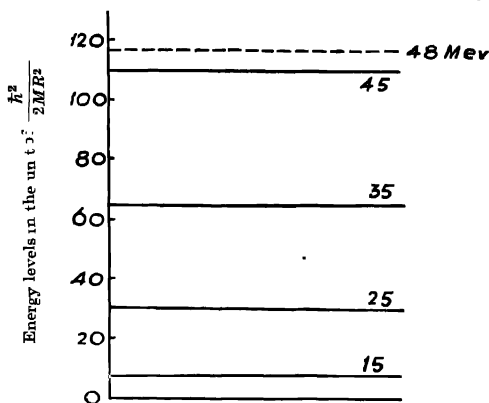


Fig. 2. Energy level diagram for $A = 200$

$$\alpha R \cot \alpha R = \frac{R}{2a} \left[\frac{z J_{n+1}(z)}{J_n(z)} - n \right] \quad \dots (12)$$

$$\text{when } \alpha = \left[\frac{2M}{\hbar^2} \{V_0 - |E|\} \right]^{\frac{1}{2}},$$

$$Z|_{r=R} = 2a \sqrt{\frac{2M}{\hbar^2}} V_0 \text{ and } n = 2ka.$$

The equation (12) is solved graphically and within the limitations of accuracy the results agree with those calculated by Green and Lee (1955).

In conclusion, it may be mentioned that so far as the interaction of slow neutrons with nuclei is concerned, our potential gives the same values as the Woods Saxon one which, though admits of solution (Lawson, 1956) for the Schrödinger equation, yet is not easy for evaluation.

I wish to thank Prof. D. Basu for his helpful guidance during the progress of this work.

REFERENCES

- Feshbach, H., Porter, C., and Weisskopf, V. F., 1954, *Phys. Rev.* **96**, 448.
 Feshbach, H., 1958, in *Annual Rev. of Nuclear Science*, Vol. 8.
 Green, A. F. S., and Leo, K., 1955, *Phys. Rev.*, **99**, 772.
 Lawson, R. D., 1956, *Phys. Rev.*, **101**, 311.
 Morse, P. M., and Feshbach, H., *Methods of Theoretical Physics. Part II* (McGraw-Hill Book Company, Inc. 1953), Chap. XII.

SPACE GROUP OF CYCLOHEXANONE AT -180°C

G. S. R. KRISHNA MURTI

OPTICS DEPARTMENT, INDIAN ASSOCIATION FOR THE CULTIVATION OF SCIENCE,
CALCUTTA-32*(Received, August 25, 1959)*

ABSTRACT. The Debye-Scherrer pattern of frozen cyclohexanone at -180°C has been photographed and analysed. It has been found that the crystal is orthorhombic with the unit cell dimensions $a = 10.38$ A.U., $b = 7.34$ A.U. and $c = 15.09$ A.U. The density of cyclohexanone at -180°C has been measured and it has been found that there are 8 asymmetric molecules in the unit cell. The space group Q_h is assigned to the crystal.

INTRODUCTION

Hassel and Sommerfeldt (1938) studied the habits of crystals of cyclohexane and its monosubstituted compounds like cyclohexanone, cyclohexanol, chloro-cyclohexane with a polarising microscope and reported that the crystals of all the substances mentioned above belong to the cubic system at a temperature just below their respective melting points. They found the lattice constant of cubic crystal of cyclohexanone at -55°C to be 8.61 A.U. by photographing the Debye-Scherrer pattern. It was, however, pointed out by them that the measurement of the lattice constant is subject to much uncertainty due to limited number of reflections observed and also because of the large width of the rings in the pattern. They further reported that in the case of cyclohexanone the cubic lattice of the crystals found at temperature of -55°C does not retain its physical shape at temperatures lower than -55°C . But they did not study the Debye-Scherrer pattern of the crystal at lower temperatures. An attempt has, therefore, been made to study the space group of the crystals of cyclohexanone at -180°C by photographing the Debye-Scherrer pattern of the crystals at that temperature and the results obtained are discussed below.

EXPERIMENTAL

Pure cyclohexanone, distilled under reduced pressure, was used for studying the Debye-Scherrer pattern of the substance at -180°C . The pattern of the crystals at -180°C was photographed by the method described earlier (Krishna Murti and Sen, 1956), using a camera of special design (Biswas, 1958).

A Seifert X-ray tube running at 32 KV, 26 mA was used to photograph the pattern. The X-ray tube was provided with a copper target and a nickel filter was used to cut off the $K\beta$ radiation. An exposure of about 3 hours was sufficient to record the pattern with moderate densities. The radius of the camera

was measured by photographing the Debye-Scherrer pattern of aluminium powder and was found to be 4.5 cms.

RESULTS AND DISCUSSION

The Debye-Scherrer pattern obtained for the crystal at -180°C is reproduced in Figure 1. The spacings and the values of $\sin^2\theta$ calculated from the rings of the Debye-Scherrer pattern for the crystal at -180°C are given in Table I, in which the spacings observed by Hassel and Sommerfeldt (1938) for the crystal at -55°C are also included for comparison.

It can be seen from Table I that the structure of crystals of cyclohexanone at -180°C is different from that of the substance at -55°C and also the pattern for the crystal at -180°C does not fit in with a cubic lattice.



Fig. 1 Debye-Scherrer pattern of cyclohexanone at -180°C

Lapson's method (1949) was applied to analyse the pattern and to find out whether the lattice was orthorhombic and it has been found that the crystal actually belongs to orthorhombic system. The values of $\lambda^2/4a^2$, $\lambda^2/4b^2$ and $\lambda^2/4c^2$ deduced from the values of $\sin^2\theta$ are 0.0055, 0.0110 and 0.002605 respectively. The unit cell dimensions of the crystal at -180°C calculated from the above constants are :

$$a = 10.38 \text{ A.U.}$$

$$b = 7.34 \text{ A.U.}$$

and

$$c = 15.09 \text{ A.U.}$$

It can be seen from the Table I that the values of $\sin^2\theta$ calculated from these unit cell dimensions agree well with those observed for the crystal at -180°C .

The density of frozen cyclohexanone at -180°C has been measured by the method used earlier in this laboratory (Biswas and Sirkar, 1957) and found to be 1.136. The number of molecules in the unit cell calculated with this value of density is 8. It can be seen from Table I that there is no restriction for the occurrence of reflections from the planes. The want of restriction leads to the conclusion that the space group is Q_h^1 and as the number of asymmetric molecules in the unit cell of this space group is 8, it appears that the molecule of cyclohexanone at -180°C is asymmetric. The structure of the molecule is not known and it can have only a plane of symmetry containing the HCCO group, but the results, mentioned above, show that no such symmetry is utilised by the molecules in forming the crystals

TABLE I

Debye-Scherrer rings of cyclohexanone at -180°C

Spacings in A.U.		Indices	Values of $\sin^2\theta$ at -180°C	
From Hassel & Sommerfeldt (1938) at -55°C	Observed at -180°C		Observed	Calculated
—	7.54 (w)	002	0.01042	0.01042
—	6.435 (m)	011	0.01410	0.01360
4.98 (vs)	5.15 (s)	200	0.02230	0.02200
4.305 (s)	4.30 (m)	202	0.03200	0.03243
—	4.13 (m)	013	0.03475	0.03444
—	3.77 (m)	004	0.04170	0.04170
—	3.68 (m)	$\begin{Bmatrix} 212 \\ 020 \end{Bmatrix}$	0.04370	$\begin{Bmatrix} 0.04342 \\ 0.04400 \end{Bmatrix}$
—	3.56 (w)	$\begin{Bmatrix} 021 \\ 104 \end{Bmatrix}$	0.04670	$\begin{Bmatrix} 0.04660 \\ 0.04720 \end{Bmatrix}$
—	3.45 (w)	300, 120	0.04970	0.04950
—	3.26 (vw)	213	0.05590	0.05640
—	3.12 (m)	310	0.06090	0.06050
—	2.905 (m)	105	0.07020	0.07060
2.84 (vw)	2.80 (vw)	$\begin{Bmatrix} 015 \\ 222 \end{Bmatrix}$	0.07580	$\begin{Bmatrix} 0.07610 \\ 0.07642 \end{Bmatrix}$
—	2.59 (s)	400	0.08850	0.08800
2.49 (w)	2.26 (w)	206	0.11590	0.11580
—	2.16 (w)	216	0.12650	0.12680
—	2.095 (w)	324	0.13560	0.13520
—	2.00 (w)	$\begin{Bmatrix} 330 \\ 520 \end{Bmatrix}$	0.14800	$\begin{Bmatrix} 0.14850 \\ 0.14790 \end{Bmatrix}$
—	1.885 (w)	008	0.16670	0.16670
—	1.755 (m)	142, 522	0.19240	0.19190
—	1.73 (m)	036, 416	0.19800	0.19280
—	1.685 (w)	600, 240	0.20880	0.19800
—	1.608 (w)	242	0.22900	0.20840
—	—	610	—	0.20900
—	—	434	—	0.22870

Hence it can be concluded that the crystal which is cubic at -55°C (Hassel and Sommerfeldt, 1938) has a low temperature modification of lower symmetry at -180°C .

ACKNOWLEDGMENT

The author is indebted to Professor S. C. Sirkar, D.Sc., F.N.I. for his kind interest and guidance during the progress of the work.

REFERENCES

- Biswas, S. G., 1958, *Ind. J. Phys.*, **32**, 13.
Biswas, S. G. and Sirkar, S. C., 1957, *Ind. J. Phys.*, **31**, 141.
Hassel, O. and Sommerfeldt, A. M., 1938, *Zeit. f. Phys. Chemic.*, **B40**, 391.
Krishna Murti, G. S. R. and Sen, S. N., 1956, *Ind. J. Phys.*, **30**, 242.
Lipson, H., 1949, *Acta Cryst.*, **2**, 43.

Letters to the Editor

The Board of Editors will not hold itself responsible for opinions expressed in the letters published in this section. The notes containing reports of new work communicated for this section should not contain many figures and should not exceed 500 words in length. The contributions must reach the Assistant Editor not later than the 15th of the second month preceding that of the issue in which the paper is to appear. No proof will be sent to the authors.

6

INCREASE IN BREAKDOWN POTENTIAL OF A GAS IN ELECTRODELESS DISCHARGE IN THE PRESENCE OF A TRANSVERSE MAGNETIC FIELD AND THE CONCEPT OF EQUIVALENT PRESSURE

S. N. GOSWAMI

CENTRAL CALCUTTA COLLEGE, CALCUTTA.

(Received, September 1, 1959)

The properties of electrical discharge in the presence of a uniform transverse magnetic field has been investigated by a large number of workers (Wehrli 1922, Somerville 1952, Blevin and Hydon 1958, Huxley, 1957). It has been shown that for a weakly ionised gas, a large variety of phenomena can be explained if, instead of the actual pressure p , use is made of an equivalent pressure p' defined by (Blevin and Haydon, 1958)

$$p' = p \sqrt{1 + C \left(\frac{H}{p} \right)^2} \quad \dots (1)$$

where p' , p are pressure in mm. of Hg, H = magnetic field, $C = \left(\frac{l}{m} \cdot \frac{L}{u} \right)^2 L$ being the mean free path at 1mm. Hg and u the mean electron velocity.

Experimental results can, however, be explained equally satisfactorily from other points of view. Thus, Dev and the author (Deb and Goswami, 1956) in course of study of the low frequency electrodeless discharge in a tube in the presence of a transverse static magnetic field has shown from an elementary consideration that the break-down potential in a gas should increase on application of the magnetic field. It was further shown that to a first approximation the increased breakdown potential V' is given by

$$\frac{V' - V}{V'} = 1 - \cos \theta \quad \dots (2)$$

where \bar{V}' , V are the breakdown potentials with and without the magnetic field respectively and θ is the angular deflection of the electronic path due to the magnetic field given by

$$\theta = \frac{He\lambda}{m\bar{v}} = \frac{HeL}{m\bar{v}p} \quad \dots (3)$$

The purpose of this note is to point out that the concepts of equivalent pressure and of increased breakdown potential are fundamentally the same and that Eq.(1) may be driven from (2) if certain plausible assumptions are made. Thus for a high pressure discharge tube, at least, it is reasonable to assume that the breakdown potential is proportional to the pressure (Loeb, 1939). Further, for such pressure and moderate values of H the angular deflection θ is small enough to justify the assumption $\tan \theta = \theta$. Hence, under these conditions, one can obtain from Eq. (2)

$$\frac{p' - p}{p'} = 1 - \cos \theta$$

or

$$p'/p = \sec \theta \sim \sqrt{1 + \theta^2}$$

or

$$p' = p \sqrt{1 + C \left(\frac{H}{p} \right)^2} \quad \text{where } C = \left(\frac{e}{m} \cdot \frac{L}{u} \right)^2,$$

which is Eq (1).

ACKNOWLEDGMENT

The work was carried out in the Department of Radio Physics and Electronics. The author is very much indebted to Professor J. N. Bhar for his kind permission to work in the laboratory and to Dr. S. Deb for constant guidance. He is also grateful to Professor S. K. Mitra for encouragement and interest in the work.

REFERENCES

- Blevin, H. A. and Haydon, S. C., 1958, *Aust. J. Phys.*, **11**, 18
- Blevin, H. A. and Haydon, S. C., 1958, *Z. Phys.*, **151**, 340.
- Deb, S. and Goswami, S. N., 1956, *Sci. and Cult.*, **22**, 283.
- Huxlov, I. G. H., 1957, *Aust. J. Phys.*, **10**, 240
- Loeb, L. B., 1939, *Fundamental Processes of Electrical Discharge in Gases*, Chap. X.
- Somerville, J. M., 1952, *Proc. Phys. Soc. (Lond.)*, **B65**, 620.

EFFECT OF CHEMICAL TREATMENT ON THE ELECTRICAL CONDUCTIVITY OF GRAPHITE

R. BHATTACHARYYA

DEPARTMENT OF MAGNETISM, INDIAN ASSOCIATION FOR THE CULTIVATION OF
SCIENCE, CALCUTTA-32

(Received, September 15, 1959)

Recently it has been shown by Ray (1959) that the usual purificatory treatments of the naturally occurring crystals of graphite for measuring their different properties, cause an easily detectable enhancement of the small amount of misalignment originally present between the basal planes of the different crystal blocks. It is also observed that most of the earlier measurements on the electrical conductivities of graphite (Krishnan and Ganguly, 1939; Dutta, 1953; Primak and Fuchs 1954) were with crystals which had been purified in the usual way. Investigations have therefore been undertaken to study the effect, if any, of such treatments on the electrical conductivities of graphite. Results of measurements on three different samples of Ceylon graphite are shown in the table below.

TABLE I

Crystal	Before Treatment			After Treatment			$\frac{\Delta\sigma_{ }}{\sigma_{ }} \times 100$	$\frac{\Delta\sigma_{\perp}}{\sigma_{\perp}} \times 100$
	$\sigma_{ }$ Conductivity to c-axis	σ_{\perp} Conductivity \perp to c-axis	$\frac{\sigma_{\perp}}{\sigma_{ }}$	$\sigma_{ }'$ Conductivity to c-axis	σ_{\perp}' Conductivity \perp to c-axis	$\frac{\sigma_{\perp}'}{\sigma_{ }'}$		
1	.068	$.805 \times 10^4$	11.84×10^4	.216	581×10^4	2.69×10^4	182.8	-38.4
2	.077	$.529 \times 10^4$	6.91×10^4	.217	$.327 \times 10^4$	1.51×10^4	183.0	-38.2
3	.089	$.371 \times 10^4$	4.14×10^4	.254	$.232 \times 10^4$	0.91×10^4	183.2	-37.6

It is observed that the conductivity perpendicular to the c-axis (along the basal plane) decreases appreciably while that along the c-axis increases considerably. This is easily explained on the basis of the findings of Ray (l.c.), who showed, as stated above, that the basal plane of the different crystal blocks orient due to such treatments randomly about directions in the basal plane. As a result, the observed conductivities in the two directions will be the resultants of the

components in these directions of the actual conductivities along and perpendicular to the c -axis corresponding to any oriented crystal block summed up for all such blocks. The conductivity along directions perpendicular to the c -axis being very much greater than that along the c -axis (Krishnan and Ganguly, 1939; Dutta, 1953; Primak and Fuchs, 1954), the decrease and increase of conductivities perpendicular and along the c -axis respectively, as observed experimentally (table above), is therefore quite obvious. It is to be noted in consequence that neither the earlier measurements (l.c.) on the electrical conductivities of graphite nor the present ones with untreated crystals represent the true conductivities of ideal graphite due respectively to the defects created and to defects originally present (Ray, l.c.). Therefore the observed difference between the results of the present measurements and the earlier ones* as also between the values of the conductivities of the different crystals of the present investigation are now easily understood. Evidently the X-ray tests of perfectness of the crystals as employed by earlier workers (l.c.) do not appear to be so carefully done as by Ray (l.c.).

Now in view of what has been stated above, the temperature variation of the conductivities, magneto-resistance effect, Hall effect, magnetic properties, etc. many of which are for treated samples (Dutta, 1953; Krishnan, 1953, Berlincourt *et al.*, 1955; Soule, 1956) also do not represent the true behaviour of ideal graphite crystals. Large number of theoretical attempts (McClure, 1956, 1957, Haering and Wallace, 1957; Lifshitz *et al.*, 1956; Lomer, 1955; Johnston, 1955, 1956; Nozières, 1958; Mase, 1958, etc.) have also recently been made to obtain a reasonable electronic picture of graphite based on the above experimental results. In order, therefore, to reassess these theories in view of the present findings, it is necessary to undertake to remeasure the above properties first with untreated natural crystals of graphite and then by producing defects artificially in them by the usual purificatory and other treatments, so as to be able to arrive at the true properties of ideal graphite crystals.

Details of some of these investigations will be published elsewhere shortly.

The author wishes to express his best thanks to Prof. A. Bose for his kind interest in the work and to Sri A. K. Dutta for suggesting the problem and guidance throughout the course of the work.

REFERENCES

- Berlincourt, T. G. and Steele, M. G., 1955, *Phys. Rev.*, **98**, 815.
Dutta, A. K., 1953, *Phys. Rev.*, **90**, 187.
Haering, R. R. and Wallace, P. R., 1957, *J. Phys. Chem. Solids*, **8**, 253.

*These differences in the values of σ_{\parallel} of the present and earlier measurements might be also due to differences in the methods of measuring the c -axis conductivity. Investigations to decide this point are in progress.

- Johnston, D. F., 1955, *Proc. Roy. Soc.*, **A227**, 349 and 359.
 " " 1956, *Proc. Roy. Soc.*, **A237**, 48.
Kinchin, G. H., 1953, *Proc. Roy. Soc.*, **A217**, 9.
Krishnan, K. S. and Ganguly N. 1939, *Nature*, **144**, 667.
Lifshitz, I. M. and Kosevitch, A. M. 1956, *J. Exp. Theor. Phys.* **2**, 636.
Lomer, W. M., 1955, *Proc. Roy. Soc.* **A227**, 330.
Mase, S., 1958, *Jr. Phys. Soc. Jap.*, **13**, 563.
McClure, J. W., 1956, *Phys. Rev.*, **104**, 666.
 " " 1958, *Phys. Rev.*, **108**, 612.
Nozières, P., 1958, *Phys. Rev.*, **109**, 1510.
Primak, W. and Fuchs, L. H., 1954, *Phys. Rev.*, **95**, 22.
Ray, S., 1959, *Ind. Jr. Phys.*, **33**, 282.
Soule, D. F , 1958, *Phys. Rev.*, **112**, 698.

MAGNETIC ANISOTROPY OF Fe^{++} ION IN SIDERITE

A. MOOKHERJI AND S. C. MATHUR

PHYSICS LABORATORY, AGRA COLLEGE, AGRA

(Received for publication, April 27, 1959)

Cu^{++} and Fe^{++} are in ${}^3D_{5/2}$ and 5D_4 states respectively. According to Bethe (1929) in an electric field of cubic symmetry the D -states split into a doublet and a triplet; a rhombic field separates the components of the doublet and triplet by amounts much smaller than doublet and triplet separation but large compared to kT in the case of Cu^+ and in Fe^{2+} . In case of Cu^{++} ion with positive cubic field coefficients the doublet is lowest while in Fe^{++} ion the triplet is lowest. Now this doublet is orbitally nonmagnetic. As a result the remains of the orbital moment should be larger in Fe^{++} ion than in Cu^{++} ion provided all other things are similar, and hence the magnetic anisotropy should be much more accentuated in Fe^{++} ion than in Cu^{++} ion. But a survey of the experimental results (Mookherji, 1945 and Krishnan and Mookherji 1938), ($\Delta K/\bar{K} = 41\%$ for Cu^{++} ion and 36% for Fe^{++} ion where ΔK is the average ionic anisotropy and K is the mean ionic susceptibility) shows that the reverse is the case. Apart from the explanation that the ratio of the orbital contribution to the spin contribution is of the same order in the two salts, there seems to be another reason for the above observation; that is, in all the cupric salts studied so far the crystal field has very nearly tetragonal symmetry whereas the ferrous salts mentioned above most probably have a large departure from axial symmetry. Hence in Fe^{++} ion the orbital contribution is distributed in different direction, whereas in Cu^{++} ion it is confined along the symmetry axis. Therefore, the calculation of the magnetic anisotropy on the tetragonal assumption makes ΔK lower for Fe^{++} ion than for Cu^{++} ion. Hence if one could study a ferrous salt where the crystal field has an axial symmetry, the magnetic anisotropy of Fe^{++} ion might be found to be more than for Cu^{++} ion. This seems to be the case with the naturally occurring trigonal crystal of siderite (Wyckoff 1920) which contains 66% ferrous carbonate. We have, therefore, measured its magnetic anisotropy ($\Delta K/\bar{K}$) which is 47% and more than for Cu^{++} ion. This is fairly satisfactory considering the fact that the internal symmetry of the paramagnetic unit in siderite may not be as good as in cupric salts.

Details of the measurements will be published later on.

REFERENCES

- Bethe, H., 1929, *Ann. der Phys.*, **3**, 133.
 Mookherji, A., 1945, *Ind. Jour. Phys.*, **19**, 63.
 Krishnan, K. S. & Mookherji, A., 1938, *Phil. Trans.*, **A237**, 135.
 Wyckoff, R. W. G., 1920, *Am. J. Sc.*, **50**, 317.

THE QUESTION OF THE EXISTENCE OF $(\Lambda^0 P)$, $(\Sigma^+ P)$ AND $(\Sigma^- n)$ HYPERFRAGMENTS

R. C. KUMAR

PHYSICS DEPARTMENT, UNIVERSITY COLLEGE, LONDON

(Received, March 9, 1959)

ABSTRACT. The question of the existence of $(\Lambda^0 P)$, $(\Sigma^+ P)$ and $(\Sigma^- n)$ hyperfragments has been discussed.

It is not known experimentally whether or not the $(\Lambda^0 P)$, $(\Sigma^+ P)$ and $(\Sigma^- n)$ hyperfragments exist in the bound state. One possible example each of $(\Lambda^0 P)$ and $(\Sigma^+ P)$ has been reported (George *et al.*, 1956 and Baldo-Ceolin *et al.*, 1957). If such fragments exist, they are expected to be produced in the interactions of K^- mesons in matter. The possibility of production of $(\Lambda^0 P)$ and $(\Sigma^- n)$ fragments from K^- interactions with deuterium has been examined in detail by Pais and Treiman (1957). The collinearity of the tracks produced in the reactions

$$\begin{aligned} K^- + D &\rightarrow (\Lambda^0 P) + \pi^- \\ &\rightarrow (\Sigma^- n) + \pi^+ \end{aligned}$$

and their unique ranges would almost certainly identify the $(\Lambda^0 P)$ and $(\Sigma^- n)$ fragments if produced. Bubble chamber studies of K^- interactions with deuterium have been made (Tripp, 1958); no example of such fragments has been found. In the interactions of K^- mesons with the more complex nuclei of emulsion, however, identification of these fragments, if produced, is not easy and would need measurements of mass to be made on all tracks produced in K^- stars including the short and black ones. Such measurements are not generally carried out mainly due to the fact that, in most cases, mass measurements on short black tracks are not very reliable. Identification of such tracks from K^- stars in emulsion is often based on the characteristics of the end of the track. We should examine, therefore, the possible end characteristics of the $(\Lambda^0 P)$, $(\Sigma^+ P)$, $(\Sigma^- n)$ fragments to see if they could be confused with other known particles.

$\Lambda^0 P$:—The $(\Lambda^0 P)$ can decay according to the following modes :

$$(\Lambda^0 P) \rightarrow P + P + \pi^- + 37.0 \text{ MeV}^* \quad \dots (1)$$

$$\rightarrow P + n + \pi^0 + 40.3 \text{ ,,} \quad \dots (2)$$

* In calculating the Q -values, the values of the masses have been taken from Cohen *et al.* (1957) and the unknown binding energies have been ignored.

$$\rightarrow D + \pi^0 \quad + 42.5 \text{ MeV} \quad \dots (3)$$

$$\rightarrow P + n \quad + 175.3 \text{ ,,} \quad \dots (4)$$

In (1), the ($\Lambda^0 P$) can be confused with H^3 hyperfragment decaying according to the process $\Lambda H^3 \rightarrow D + P + \pi^-$. It was pointed out by Telegdi (1957) in his survey of hyperfragments that certain examples of ΛH^3 hyperfragment in his sample could also well be ($\Lambda^0 P$). In (2), the energy of the charged product, the proton, could lie anywhere between 0 and 40 MeV. In this case the ($\Lambda^0 P$) might be classed as a Σ^- hyperon producing a one prong capture star from rest. The same is true with the decay-mode (3) where the charged product, the deuteron, will have an energy of approximately 1.5 MeV and a range in emulsion of 20μ . In (4), the proton will have an energy of approximately 88 MeV. This may be erroneously classified as an example of Σ^- capture star in which the Λ^0 has been trapped and decayed inside the nucleus (Goldsack and Lock, 1956) or as a heavy hyperfragment decaying non-mesonically.

$\Sigma^+ P$:— The ($\Sigma^+ P$) can decay according to the following modes :

$$(\Sigma^+ P) \rightarrow P + n + \pi^+ + 110.6 \text{ MeV} \quad \dots (5)$$

$$\rightarrow P + P + \pi^0 + 116.5 \text{ ,,} \quad \dots (6)$$

$$\rightarrow D + \pi^+ + 112.8 \text{ ,,} \quad \dots (7)$$

$$\rightarrow P + P + 251.5 \text{ ,,} \quad \dots (8)$$

In (5), the appearance of the ($\Sigma^+ P$) track ending is confusable with the mesonic decay of a Λ^0 -hyperfragment. In (6), the ($\Sigma^+ P$) decay may be confused with a Σ^- capture star with two prongs or a hyperfragment non-mesonic decay if the charged decay products are energetic. In (7), the deuteron will have an energy of approximately 8.3 MeV and a range in emulsion of 245μ while the pion will have an energy of about 104.5 MeV. Although this decay mode would be very easy to identify owing to the collinearity of the deuteron and pion tracks, the high energy pion track may be missed in some cases and the event recorded as a Σ^- capture star. The decay-mode (8) is very difficult to miss if it occurs.

In all the three-body decay modes (1), (2), (5) and (6), if one of the charged particles, say the proton, is emitted with an energy less than a certain minimum energy (0.2 MeV for emulsion) the track would not be visible. In such cases (5) and (6) would appear to be normal Σ^+ decays.

$\Sigma^- n$:— The ($\Sigma^- n$) can decay in flight only; on coming to rest it will be captured like a Σ^- hyperon and would be indistinguishable from the latter in its star characteristics.

The decay-mode in flight will be

$$(\Sigma^- n) \rightarrow n + n + \pi^- + 117.6 \text{ MeV} \quad \dots (9)$$

Unless the high energy pion is followed to its end and its energy (and sign of charge) determined, the decay (9) will appear to be an example of Σ^+ or Σ^- hyperon decaying in flight. White *et al* (1958) have followed to rest several lightly ionizing tracks from Σ^\pm hyperon decays in flight. They have found no example of a π -meson of an anomalous range.

An unknown contamination of $(\Sigma^- n)$ fragments in a sample of Σ^\pm hyperons decaying in flight would tend to make the apparent lifetime of these hyperons shorter than the actual value since, for the same measured values of β at the points of emission and of decay, the calculated time of flight would be smaller than the actual time if a smaller value for the mass is used in the calculation. The lifetime of Σ^\pm hyperons decaying in flight has been measured in emulsion by several groups of workers. In each of these measurements, the assumption has been made that the sample of Σ^\pm hyperons consists only of Σ^+ and Σ^- hyperons. The results on lifetime obtained by these different groups do not agree among one another; some groups (Freden *et al*, 1958, Fry, 1957 and Glasser, 1957) report a value for the lifetime of $\sim 0.5 \times 10^{-10}$ second which is shorter than the lifetime of either Σ^+ (0.86×10^{-10} second) or Σ^- (1.83×10^{-10} second) hyperons (Cohen *et al*, 1957) thus indicating the presence of some other effect such as the above-mentioned one; other groups (K^- -stack collaboration, 1957 and Goldhaber 1957) report a value for the lifetime of $0.8-0.9 \times 10^{-10}$ second which, although being higher than the previous result, is much lower than the Σ^- lifetime.

It has been pointed out by Snow (1958) that for a certain binding energy region close to zero the $(\Sigma^- n)$ fragment may be bound, while the $(\Sigma^+ P)$ is unbound due to the extra repulsive force in case of the latter

The considerations made above show that very careful analysis of K^- -stars in emulsion is needed to distinguish the mass-2 hyperfragments from other known particles if such fragments exist and are produced in K^- interactions. The fact that no example of $\Sigma^- n$ fragments and only one example of $(\Lambda^0 P)$ and $(\Sigma^+ P)$ has been reported so far, therefore, does not necessarily mean the non-existence of these fragments.

REFERENCES

- Baldo-Croin, M., Frv, W. F., Greening, W. D. B., Huzita, H. and Limontani, S., 1957, *Nuovo Cim.*, **6**, 144.
 Cohen, E. R., Crowe, K. M., Dumond, J. W. M., 1957, *Fundamental Constants of Physics*, Interscience publishers, Page 91.
 Freden, S. C., Gilbert, F. C. and White, R. S., 1958, *Amer. Phys. Soc. Bull.*, **3**, 25.
 Fry, W. F., Schneps, J., Snow, S. A., Swami, M. S. and Wold, D. C., 1957, *Phys. Rev.*, **107**, 257.
 Glasser, R. G., Seeman, N., and Snow, G. A., 1957, *Phys. Rev.*, **107**, 277.

- George, E. P., Hertz, A. J., Noon, J. H. and Solntseff, N., 1956, *Nuovo Chim.* **2**, 94.
- Goldsack, S. J. and Lock, W. O., 1956, *Nuovo Cim.*, **3**, 600.
- K-stack collaboration, 1957, Padua-Venice Conference Report, Page VIII-10.
- Goldhaber, S., 1957, Padua-Venice, Conference, quoted in 10.
- Pais, A. and Treiman, S. B., 1957, *Phys. Rev.*, **107**, 1396. See also Day, T. B. and Snow, G. A., 1959, *Phys. Rev. Lett.*, **2**, 59.
- Snow, G. A., 1958, *Phys. Rev.*, **110**, 1192.
- Telegdi, V. L., 1957, Rochester Conference Report, Page VIII-6.
- Tripp, R. D., 1958, Geneva Conference Report, Page 184.

A STATISTICAL ANALYSIS TO TEST THE RELIABILITY OF MEASURING ATMOSPHERIC NOISE SUBJECTIVELY BY A SMALL GROUP OF PEOPLE*

B. B. GHOSH

RESEARCH DEPARTMENT, A.I.R., NEW DELHI

(Received, September 30, 1959)

ABSTRACT. A statistical analysis of the results of some preliminary listening tests on the variations of judgement of different groups of listeners for the subjective measurement of atmospheric noise has been described. The possible limits of error committed by a comparatively smaller sample size or group of listeners as compared to that of a large group have been indicated and compared with those obtained from theoretical considerations. On the basis of these findings, a practical procedure to meet the statistical requirement in employing a small group of eight observers for the actual measurement of atmospheric noise by a subjective method like that of Thomas, but suitably modified, for broadcasting services has been discussed.

INTRODUCTION

In any experimental investigation where random events are encountered, a statistical approach has to be adopted for obtaining reliable results. Atmospheric noise, as is well known, constitutes one such random phenomenon and statistical methods have to be employed for its measurements. Usually, two methods of measurements are followed.

The objective method in which noise voltage is observed in a meter or recorded graphically or photographed from oscilloscope and the subjective one in which the minimum signal to over-ride the annoying effect of atmospheric noise is assessed by listening to signals of different strengths mixed with noise. In the first method of measurements, statistical analysis of the observation is required to arrive at the median, higher decile and lower decile values of noise. In the second method also, reliability of assessment by individual listener or a group is required to be known from statistical considerations and any error reduced to a minimum.

In an earlier communication Ghosh and Mitra (1958) have discussed both the methods of measurements and presented the measured data on atmospheric noise at Delhi from 1955 onwards. Thomas method of measuring atmospheric noise has been suitably modified to suit the requirements of broadcasting and a

* Communicated by Prof. S. K. Mitra.

statistical correlation established between the objective noise and subjective assessment of minimum signal required to suppress the noise. Adoption of the Thomas method for subjective evaluation of noise for broadcasting purposes naturally calls for statistical considerations of the range of errors incurred in taking individual or group listening as the correct assessment of minimum satisfactory signal. We have employed 8 people whose collective judgement of this signal has been accepted as accurate enough for all practical purposes. Very elaborate statistical tests were conducted before this minimum number of people, required for the purpose without incurring any significant error, was arrived at. It is the purpose of this paper to determine the range of errors involved in the choice of such a group of persons and to assess the reliability of such measurements. It will be shown that even such a small group is adequate for giving fairly reliable results on subjective assessment within the limits of experimental error.

THEORETICAL CONSIDERATIONS

In the series of tests to determine the size of the group whose collective judgement can be taken as a correct assessment of the minimum satisfactory signal, a number of recorded programmes modulating steady signals which were mixed with atmospheric noise in random proportions, were listened to by a large number

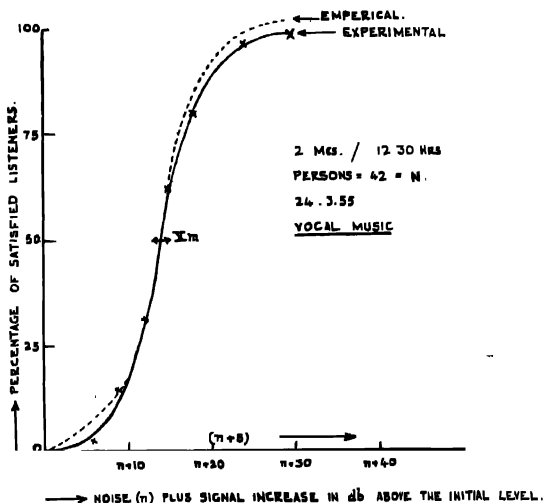


Fig. 1. Shows the variations of the percentage of satisfied listeners, δ , for a group of 42 persons against noise (n) plus signal-increases (S) in db. above the initial level.

of listeners in a group. Each recorded piece contained, therefore, a discrete value of signal to noise ratio and each listener was asked to record his opinion as either

satisfactory or unsatisfactory from the point of view of annoyance caused by the noise.

Here the limited number of listeners in a group represents a sample of the population or universe consisting of all the listeners to broadcast programmes. The characteristic evaluated is the 'estimate' recorded by each individual as either 'satisfactory' or 'unsatisfactory' and is therefore finite and discontinuous. We have sought to determine statistically how, for a given value of S/N ratio, the estimates, random as they are, are distributed. Figure 1 shows the variation of percentage estimate δ with signal increases over a given noise ($n+S$) for a total number of 42 listeners in one group. This is a typical curve for all such distributions where the number of listeners is fairly large and represents a cumulative Gaussian distribution. The curve is of the form represented empirically by

$$\delta = A [1 \pm (1 - e^{-\alpha|x|})] \quad \dots (1)$$

where

δ = % of listener-satisfaction

A, α = constants

x = Deviation in db from 50% satisfaction level

It may be noted that near X_m , the median value of ($n+S$) the curve is very steep indicating that small variation in ($n+S$) produces large changes in δ .

X_m and σ (standard deviation) for a particular universe have fixed values. But if we consider samples within the universe, the values of X_m and σ may vary from sample to sample.

The distribution of X_m for such samples within the population will be normal. We may, therefore, use standard statistical tables for finding out the range of variation of X_m . It can be shown that if the sample consists of N listeners and the tests are repeated, then there is 95% chance that X_m will lie in the range $\pm \frac{1.96\sigma}{\sqrt{N-1}}$ of its correct value. When N is large, (e.g. 42) repeated listening tests will indicate that X_m for such samples will be very near the median value for the entire universe.

We have calculated this range of variations for X_m for different group sizes using the above criterion. The values of σ used for the computation of X_m have been determined by the usual method of finding the mean and squaring the differences from the mean from curves (like figure 1) actually obtained by group listening experiments. The results are described in the next section.

STATISTICAL ANALYSIS

In the first sample considered, total number of listeners was 42 and the variation

of its δ with $(n+S)$ was as shown in figure 1. Its standard deviation σ comes out to be 4.1 and the range of variation of X_m can be found from

$$\overset{\longleftrightarrow}{X_m} = \pm \frac{2\sigma}{\sqrt{N-1}} \quad \dots (2)$$

X_m works out to be ± 1.28 db. If the sample size is increased, $\overset{\longleftrightarrow}{X_m}$ will be further decreased.

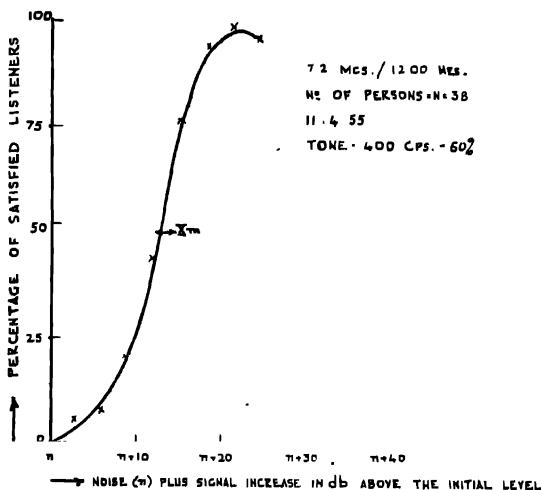


Fig. 2. Shows the variations of δ against $(n+S)$ for a group of 38 persons.

Next we have considered a sample where $N=38$. Its σ comes out from figure 2 to be the same as above and X_m equals ± 1.3 . The experimental results showing the variation of δ are shown in figure 2 for this case and the curve is very similar to figure 1.

Thus, the above two experiments clearly indicate that for large number of listeners of the order of 30 or more, there is not much error involved in the median value of the signal to noise ratio. Our aim, however, is to determine the smallest size of the sample which could be utilised for practical purposes and at the same time the error in estimation by collective listening would not be appreciable. We have, therefore, reduced the size of the sample further and carried out similar analysis.

Figure 3 shows the variation of δ where $N=23$. Its σ is 4.8 and its $\overset{\longleftrightarrow}{X_m}$ is ± 2.0 db. Fig. 4 indicates the situation where $N=18$, its σ is 5.3 and $\overset{\longleftrightarrow}{X_m}$ is ± 2.6 dbs. It would be noted from Fig. 4 that the curve has been steeper and slightly unstable. The border line judgement has become more difficult and

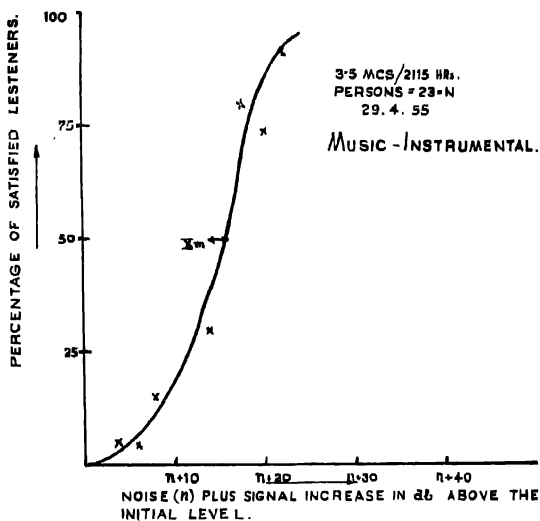


Fig. 3. Shows the variations of δ against $(n+S)$ for a group of 23 persons

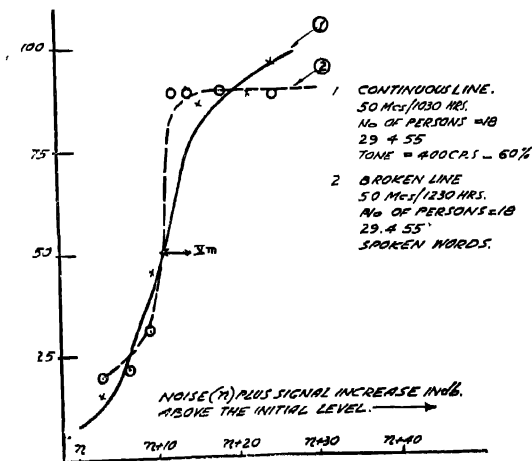


Fig. 4 Shows the variations of δ against $(n+S)$ for a group of 18 persons for two sets of independent group-listening tests.

one or two listeners assessing wrongly have contributed to the change in the shape of the curve at the two ends. This point is illustrated more specifically by the two curves plotted in Fig. 4 corresponding to two independent listening tests. But the significant feature to note is that the median values for both the listening tests (when $N=18$) have remained the same though the shapes of the two curves are slightly different. To conduct each noise measurement subjectively by 18 people at a time is a difficult task specially when one has to carry out these measurements at several hours during the day and each time on several wave frequencies.

Dinger and Paine (1947) from theoretical arguments have arrived at the conclusion that for a random phenomenon like atmospheric noise any method of measurement should be good enough if the results are repeatable within 30%. Thus if we allow 3 to 4 db error in the median values the smallest group size comes out to be about 8, by equation (2), using the above value of $\sigma=5.3$ for $N=18$ for this calculation. Actually this value of σ should be slightly higher for lowering $N=18$ to $N=8$.

Let us now consider the situation when only 8 persons are employed for the listening tests. We have plotted such a curve for 8 from experimental results in figure 5 and the curve is fairly symmetrical about its median and is of the same type as obtained for larger samples.

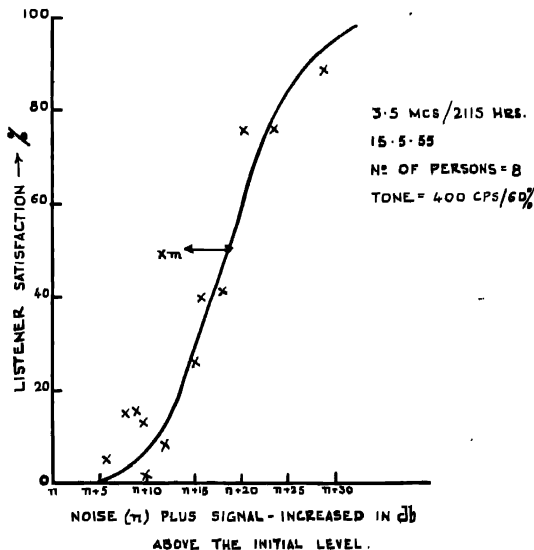


Fig. 5. Shows the variations of δ against $(n+8)$ for a group of 8 persons

σ for this curve is 5.6 about 5% higher than that for $N=18$ and about 35% higher than that for $N=42$ and $\overline{X_m}$ is ± 4.3 db. Thus even from experimental observations, it is proved that when 8 people are employed for such listening tests, it is expected that there is 95% probability that the median of the satisfactory signal as assessed by this group of listeners will lie within a range of ± 4 to 5 db of the correct median value for the universe. In other words, if we can conduct each subjective measurement of atmospheric noise by employing 8 people and take their collective judgement as the measured value of the minimum satisfactory signal, the maximum error we may incur will be about 4 to 5 db.

DISCUSSION

We have shown that for subjective measurements of noise by Thomas method when the annoyance to broadcasting programmes is considered, the collective judgement of 8 people would give a maximum error of the order of 4 to 5 db in the median value of the minimum satisfactory signal as assessed by them. It should be remembered that no such considerations apply to W/T signals where atmospheric noise is assessed from readability of the signals. Personal errors in estimation are thus minimised and may be within 1 or 2 db when experienced persons are employed. But when broadcast programmes consisting of music and talks are used, the assessment of a satisfactory signal in the presence of noise will have a subjective element that may vary from person to person and also on the type of programme used. In fact when 8 people are employed, an incorrect assessment by a single individual will cause a change in the percentage satisfaction by as much as 12.5%. Since these errors in estimation are distributed at random according to a normal law of error, their mean, median or average are the same. Collective judgement of 8 people gives a permissible error in the median (or average) value of the minimum satisfactory signal and therefore, all our subjective measurements have been taken on this basis.

One may ask the question whether an error of 4 to 5 db in the average assessment can be termed negligible. It may be remembered that the main object of the noise measurements, as envisaged by us, is in respect of its utilisation for broadcasting purposes. In planning a broadcasting service, we need to know the signal strength laid down at the target area together with the atmospheric noise existing there. In the calculation of field strengths, an accuracy of 4 to 5 db is indeed difficult to claim. Similarly, if one intends to obtain quantitative estimate of atmospheric noise itself from such subjective assessment, it has already been proved (Ghosh and Mitra—1958) from statistical correlation that a reduction of 40 db will give the noise field. Here again the standard deviation is found to be 6 db. Thus, an accuracy of 4 to 5 db in the assessment of minimum satisfactory signal by a group of 8 persons should be considered adequate for all practical purposes.

We have simplified the problem, without losing further in accuracy in the following way. We know from our experience that at Delhi, noise does not change appreciably from day to day at the same time on the same frequencies, except, of course, during local thunderstorms. As we are interested in monthly and seasonal averages, it would be sufficient to take measurement by a single person and change him from day to day so that when the average figure for the month is considered, we have the assessment of a number of individuals. In our receiving centre at Delhi normally 8 to 10 engineers are in duty taking shift at various times of the day. Their individual assessments, when collectively analysed over a month, represent three to four group listening tests of 8 persons in a group. It is reasonable therefore to consider that the range of error is not likely to exceed 4 to 5 db, on the other hand, may even be less.

The statistical correlation (Ghosh and Mitra 1958) between subjective assessment and objective measurements of noise taken simultaneously is another proof of the reliability of our method of measurement. These two sets of measurements are absolutely independent of each other, even then the figure 40 db ($\sigma=6$ db) has been found to be the most probable value of the protection needed for a satisfactory signal in the presence of atmosphere noise. Had there been greater variability in the assessment by a group of 8 persons, one would not expect a statistically significant protection ratio with a small standard deviation.

ACKNOWLEDGMENT

The present paper forms a part of programme of propagation research of the Research Department of All India Radio, New Delhi. The author is grateful to his colleagues Mr. P. K. Venkatasubramanian and Mr. S. K. Srikanthan for considerable help at the early stages of the investigation.

The paper is published by kind permission of the Chief Engineer, All India Radio.

REFERENCES

- Dinger, H. E. and Pame, H. G., 1947, "Factor affecting the accuracy of radio noise meters" *P.I.R.E.*, **35**, 75.
- Ghosh, B. B. and Mitra, S. N., 1958, "Measurement of Atmospheric Noise", *Jour. I.T.E.*, **5**, 2.

VELOCITY OF SOUND IN WATER AS A FUNCTION OF TEMPERATURE AND PRESSURE

ARVIND MOHAN SRIVASTAVA AND Y. P. VARSHNI

DEPARTMENT OF PHYSICS, ALLAHABAD UNIVERSITY, ALLAHABAD

(Received, July 9, 1959)

ABSTRACT. It is shown that the variation of velocity of sound (u) in water with temperature (t) at different pressures can be represented by $u = a + bt + ct^2$. Using Smith and Lawson's data, maximum velocity temperatures at different pressures have been calculated. The maximum velocity temperatures appear to increase with the increase in pressure but at very high pressures the data is inconclusive.

INTRODUCTION

Water is known to show an abnormal behaviour in many of its physical properties as shown by Partington (1951). And that is also true for the velocity of sound in it. It is known that all pure liquids show a linear variation of sound velocity with temperature and a negative temperature coefficient. Water, on the other hand, displays a maximum velocity (at about 74°C at atmospheric pressure) and the temperature coefficient changes from positive to negative at this temperature (which for the sake of abbreviation we shall call as 'maximum velocity temperature'). Frequently this anomalous behaviour of water is attributed to association, yet methyl alcohol and several other associative compounds do not have a variation similar to that of water.

In recent years considerable attention has been paid to the measurement of sound velocity in water. Willard (1947) has shown that the velocity of sound can be represented as

$$u = 1557 - 0.0245 (74 - t)^2$$

which gives a maximum velocity at 74°C. Greenspan, Tschiegg and Breckenridge (1956) found the maximum velocity temperature to be 73.95°C. On the other hand Salceanu (1957) made measurements of sound velocity at temperatures between 27°C and 81°C at a frequency of 1315 cycles per second and found that the maximum velocity is at about 62°C.

Pancholy (1953) has investigated the velocity of sound in heavy water. Lagemann, Gilley and McLeroy (1953) have determined the velocity of ultrasonics in supercooled water and heavy water. Highly accurate measurements (accuracy one part in 30,000) for the sound velocity in water from 0°C to 100°C have been

recently reported by Greenspan and Tschiegg (1957) who represent their results by a fifth degree polynomial.

Recently determination of sound velocity in water has also been made at high pressures. Holton (1951) has reported measurements on the velocity of sound in water as a function of pressure up to 6000 Kg/cm² at two different temperatures. Smith and Lawson (1954) using an ultrasonic echo technique have carried on similar measurements at hydrostatic pressures varying up to 9600 Kg/cm². Martin (1957) has determined the velocity of high frequency sound waves in distilled water and in standard sea water at 25°C between 0 and 1000 atm. pressures using a pulse technique.

The measurements of Holton and those of Smith and Lawson show an important discrepancy as regards the behaviour of the maximum velocity of sound as a function of temperature as the pressure is increased. Holton concludes from his measurements that this temperature decreases with increasing pressure while Smith and Lawson finds an opposite behaviour. The latter authors have given graphs (their figure 4) showing that the maximum velocity temperature increases gradually with increasing pressure, though no precise analysis of the data is given.

In this paper we have examined Smith and Lawson's data by analytical methods to find the exact behaviour of maximum velocity temperature and maximum velocity with increase in pressure.

It was found that the variation of the velocity of sound (u) with temperature at different pressure can be adequately represented by

$$u = a + bt + ct^2$$

where (t) is the temperature in Centigrade degrees and a, b, c are constants.

Smith and Lawson's values at six different pressures were used to evaluate the constants a, b and c by the method of least squares. The values thus determined are produced in Table I. The calculated and experimentally observed values of u are shown in Tables II to VII. The maximum velocity temperature is given by $-b/2c$. Its calculated values as well as maximum velocities are recorded in Table VIII.

TABLE I

No	Pressures Kg/cm ²	a	b	c
1	1	1407.546	4.24663	-.0295928
2	435	1492.542	3.62012	-.0218743
3	1039	1605.788	3.21895	-.0181010
4	5544	2262.727	1.49529	-.00785982
5	7370	2484.108	0.068427	+ .00144287
6	9410	2617.304	1.32011	-.0073539

TABLE II
For pressure of 1 Kg/cm²

No.	<i>t</i> °C	<i>u</i> , Calculated	m/sec. Observed	Difference <i>u</i> (calc) — <i>u</i> (obs)
1	0	1407.5	1403	+ 4.5
2	22.5	1488.1	1488	+ 0.1
3	24.2	1493.0	1494	— 1.0
4	26.6	1499.6	1504	— 4.4
5	27.0	1500.6	1505	— 4.4
6	27.6	1502.2	1504	— 1.8
7	45.4	1539.3	1539	+ 0.3
8	55.1	1551.7	1547	+ 4.7
9	65.5	1558.7	1555	+ 3.7
10	74.7	1559.6	1557	+ 2.6
11	83.2	1556.0	1557	— 1.0
12	93.8	1545.5	1549	— 3.5

TABLE III
For pressure of 435 Kg/cm²

No.	<i>t</i> °C	<i>u</i> , Calculated	m/sec. Observed	Difference <i>u</i> (calc) — <i>u</i> (obsd)
1	22.5	1562.9	1563	— 0.1
2	57.6	1628.5	1628	+ 0.5
3	66.9	1636.8	1637	— 0.2
4	77.0	1641.6	1642	— 0.4
5	86.7	1642.0	1642	0.0
6	96.5	1638.2	1638	+ 0.2

TABLE IV
For pressure of 1039 Kg/cm²

No.	$t^{\circ}\text{C}$	u , calculated	m/sec. observed	Difference $u(\text{calc}) - u(\text{obsd})$
1	26.5	1678.3	1677	+1.3
2	44.2	1712.5	1714	-1.5
3	55.4	1728.3	1729	-0.7
4	63.4	1736.7	1737	-0.3
5	70.5	1742.3	1742	+0.3
6	75.5	1745.1	1745	+0.1
7	80.4	1747.0	1746	+1.0
8	88.1	1748.2	1748	+0.2
9	96.4	1747.0	1747	0.0
10	104.6	1743.5	1744	-0.5

TABLE V
For pressure of 5544 Kg/cm²

No.	$t^{\circ}\text{C}$	u , calculated	m/sec. observed	Difference $u(\text{calc}) - u(\text{obsd})$
1	0.0	2262.7	2264	-1.3
2	22.6	2292.5	2290	+2.5
3	57.4	2322.7	2324	-1.3
4	66.5	2327.4	2327	+0.4
5	76.3	2331.1	2331	+0.1
6	85.9	2333.2	2335	-1.8
7	96.1	2333.8	2333	+0.8
8	103.3	2333.3	2334	-0.7
9	103.4	2333.3	2332	+1.3

TABLE VI
For pressure of 7370 Kg/cm²

No.	<i>t</i> °C	<i>u</i> , calculated	m/sec. observed	Difference <i>u</i> (calc) - <i>u</i> (obsd)
1	19.1	2485.9	2485	+ 0.9
2	42.8	2489.7	2492	- 2.3
3	51.1	2491.4	2491	+ 0.4
4	63.4	2494.2	2495	- 0.8
5	69.7	2495.9	2495	+ 0.9
6	84.0	2500.0	2497	+ 3.0
7	95.6	2503.8	2506	- 2.2

TABLE VII
For pressure of 9410 Kg/cm²

No.	<i>t</i> °C	<i>u</i> , calculated	m/sec. observed	Difference <i>u</i> (calc) - <i>u</i> (obsd)
1	56.5	2668.4	2671	- 2.6
2	62.4	2671.0	2669	- 2.0
3	70.2	2673.7	2672	+ 1.7
4	82.7	2676.2	2676	+ 0.2
5	97.4	2676.1	2678	- 1.9
6	98.4	2676.0	2676	0.0
7	128.9	2665.3	2664	+ 1.3
8	129.0	2665.2	2666	- 0.8

TABLE VIII

No.	Pressure Kg/cm ²	Maximum Velocity Temperature °C	Maximum Velocity
1	1	71.75	1559.9
2	435	82.75	1642.3
3	1039	88.48	1748.2
4	5544	95.12	2333.8
5	7370	×	×
6	9410	89.76	2676.5

DISCUSSION

Though Smith and Lawson (1954) have not given the uncertainty in their values it appears that the values differ by 2 m/sec from their values given in figure 6. Tables 2-7 show that the average difference in the calculated and observed values of the sound velocity is 1.4 m/sec. This is within the limits of experimental error postulated above

The results for pressure of 7370 Kg/cm² do not show a maxima because it is found that the constant c in this instance is positive whereas for other pressures its values are negative. Also the values of a and b for this pressure do not follow the general trend in their variation with pressures as seen in Table I. It is, therefore, suspected that the experimental values for this pressure are not sufficiently accurate

The constant a represents the velocity of sound at 0°C. Its variation with pressure is seen in Table I and figure 1. Fortunately, Smith and Lawson have

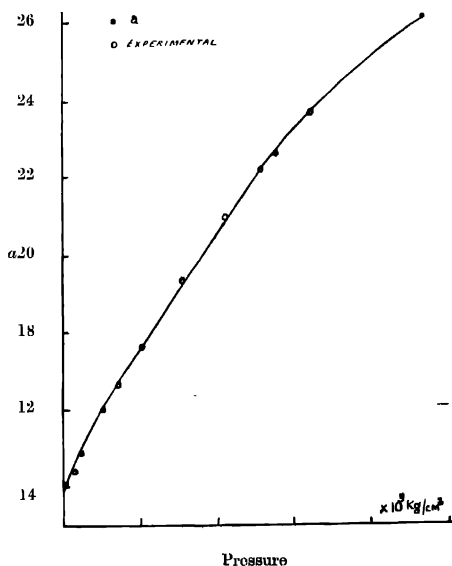


Fig. 1. Shows variation of a with pressure.

experimentally determined the variation of velocity with pressure at 0°C. Some of their experimental points are shown in figure 1 by open circles. As expected

both the above sets of points lie on a smooth curve. Point corresponding to a pressure of 7370 Kg/cm² is not considered.

Behaviour of constants b and c is shown in Figure 2. The values of b and c are observed to decrease smoothly with pressure.

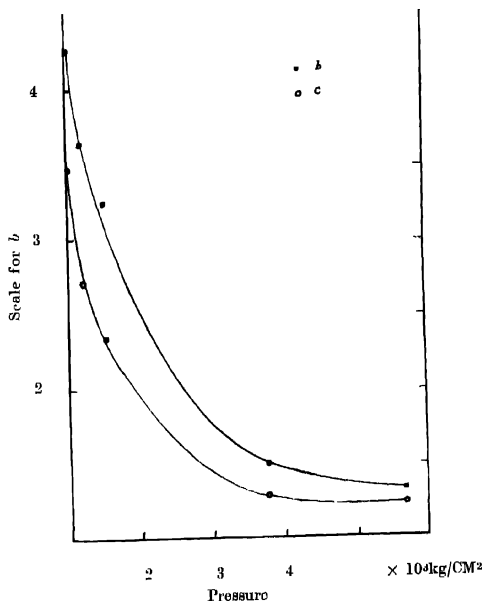


Fig. 2. Shows variation of constants b and c with changes in pressures.

Maximum velocity temperature as determined with the above theoretical expression at a pressure of 1 Kg/cm² is 71.75°C. The value determined by Greenspan *et al* (1956) at atmospheric pressure i.e. 1.03 Kg/cm² is 73.95°C. There is thus a difference of 2.2°C. The discrepancy at other higher pressures is bound to be greater in magnitude. The maximum velocity temperature increases with pressure up to 5544 Kg/cm² but the value at 9410 Kg/cm² is found to be lower than the previous value. It has been pointed out that the value at 7370 Kg/cm² is not sufficiently accurate. The temperature gradient at higher pressures is very small (Table 6, 7) and hence even small error in measurements can seriously vitiate the position of the maxima. The experimental uncertainty of ± 2 m/sec at higher pressures can be responsible for a variation of about 5°C in the value of maximum velocity temperature from the correct value.

The trend of maximum velocity temperature is to increase with pressure, yet we do not consider it safe to draw any precise conclusion from this fact regarding the numerical variation. Perhaps the value at 5544 Kg/cm² is a bit too large and that at 9410 a bit too small.

REFERENCES

- Greenspan, M., Tschegg, C. E. and Breckenridge, F., 1956, *J. Acoust. Soc. Amer.*, **28**, 500.
- Greenspan, M. and Tschegg, C. E., 1957, *J. Res. Nat. Bur. Stand.*, **59**, 249.
- Holton, G., 1951, *J. App. Phys.*, **22**, 1407.
- Lagemann, R. T., Gilley, L. W. and McLeroy, E. G., 1953, *J. Chem. Phys.*, **21**, 819.
- Martin, A. V. J., 1957, *Ann. Geophys.*, **13**, 307.
- Pancholy, M., 1953, *J. Acoust. Soc. Amer.*, **25**, 1003.
- Partington, J. R., 1951, *Advanced Treatise on Physical Chemistry*, vol. II. Properties of Liquids, p. 41.
- Smith, A. H. and Lawson, A. W., 1954, *J. Chem. Phys.*, **22**, 351.
- Suleanu, C., 1957, *C. R. Acad. Sci.*, **245**, 1371.
- Willard, G. W., 1947, *J. Acoust. Soc. Amer.*, **19**, 235.

SOME POSSIBLE ARRANGEMENTS OF PARAMETRIC AMPLIFIERS EMPLOYING LOWER FREQUENCY PUMPING

N. B. CHAKRABARTI† AND K. D. DIKSHIT

J. K. INSTITUTE OF APPLIED PHYSICS, UNIVERSITY OF ALLAHABAD, ALLAHABAD

(Received, August 16, 1959)

ABSTRACT. An analysis of certain parametric amplifiers using lower frequency pumping in lumped constant circuits is presented. Two cases (i) combination of a mixer and an amplifier using one pump and two idlers and (ii) combination of a mixer and an amplifier using two pumps and two idlers, have been treated in detail. The phase and power relations at signal frequency, pump and idling frequencies have been discussed. The expressions for negative resistance, gain, band-width and noise figure for each case have been derived.

Two other possible cases have been mentioned. It is shown that the multi-idler circuits offer no added advantage.

1. INTRODUCTION

In recent years good deal of work has been done on parametric amplifiers which are of great importance in low noise work. In most of the work done. (Bloom and Chang, 1957, Heffner and Wade, 1958) higher frequency pumping requiring pumping power at a frequency higher than that of the signal, has been utilised for signal amplification. The limitation of such amplifiers is that of power at higher frequencies. In the centimetric region, in particular, it would be good to be able to use a lower frequency pumping source. One case of lower frequency pumping has been treated by Chang and Bloom (1958) wherein they have employed two pumps and an idler. They have used reversed-biased junction diodes or nickel-manganese ferrite exhibiting non-linearity of the cubic order as a non-linear coupling reactance.

In this paper some possible arrangements of parametric amplifiers using lower frequency pumping in lumped constant circuit arrangements and employing quadratic non-linearity of the coupling reactance are suggested. Those include (i) combination of a mixer and an amplifier using one pump and two idlers and (ii) combination of a mixer and an amplifier using two pumps and two idlers. The phase and power relations at signal frequency, idler and pump frequencies

* For an excellent bibliography see Bloom and Chang (1957).

† Now at Institute of Radio Physics and Electronics, Calcutta.

have been discussed. Expressions for negative resistance, gain band-width and noise figure have been derived.

II. PARAMETRIC AMPLIFICATION*

It is known that energy can be extracted from a source driving an energy storage element such as an inductor or a capacitor and fed to the fields of a resonant circuit which is suitably coupled to the energy storage element. This fact can be used for amplifying signals. The amplifiers based on this principle are called variable parameter or parametric amplifiers, because here the amplification is achieved by the variation of a parameter of the system.

The principle of a parametric amplifier can be best understood by considering the case of higher frequency pumping. In the system of figure 1, a variable

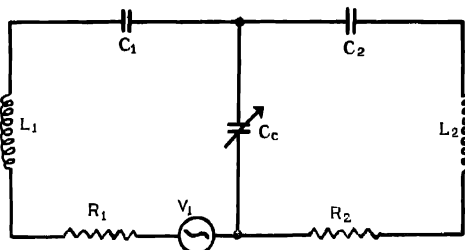


Fig. 1 Schematic representation of a single pump single idler parametric amplifier having a variable non-linear capacitor as the coupling element

non-linear reactance couples two series resonant circuits—one called the signal circuit having its angular resonant frequency ω_1 and other called the idler having its angular resonant frequency $\omega_2 = \omega_1 + \omega_p$, where ω_p is the angular frequency of the pumping source driving the non-linear element. The power at the frequency ω_p mixes with that at ω_1 and causes a current at the idling frequency ω_2 to flow in the coupling reactance. The flow of power at the idling frequency throws a negative resistance to the signal circuit. Amplification of the signal is thus achieved.

The parametric amplifiers using lower frequency pumping, to be treated here, can be considered as a combination of mixers and amplifiers. We shall consider only the following cases :

- (i) combination of a mixer and an amplifier using one pump and two idlers (Hogan *et al*, 1958).
- (ii) combination of a mixer and an amplifier using two pumps and two idlers,
- (iii) combination of two mixers and one amplifier using two pumps and two idlers and

(iv) combination of one mixer and two amplifiers using two pumps and three idlers.

Other arrangements employing more idlers do not offer additional advantages. We shall treat the first two cases in detail and shall briefly discuss the other two cases

III. ANALYSIS OF CASE 1

(1) *Phase Relations*. Let us consider the case of a mixer and an amplifier with frequency relations

$$\omega_1 = \omega_2 + \omega_p \quad (\text{mixer}) \quad \dots (1.a)$$

$$\omega_p = \omega_2 + \omega_3 \quad (\text{amplifier}) \quad \dots (1.b)$$

The subscript 1 denotes signal, subscripts 2, 3 and 4 denote idlers and the subscripts p and q denote the pumps. The coupling reactance taken is a non-linear inductor. The analysis would, however, apply equally well to a system employing a non-linear capacitor as the coupling element.

The idlers ω_2 and ω_3 take power from pumping source ω_p , ω_2 in turn combines with ω_p to supply power at the signal frequency ω_1 .

Consider the resonant circuit shown in figure 2 and suppose that :

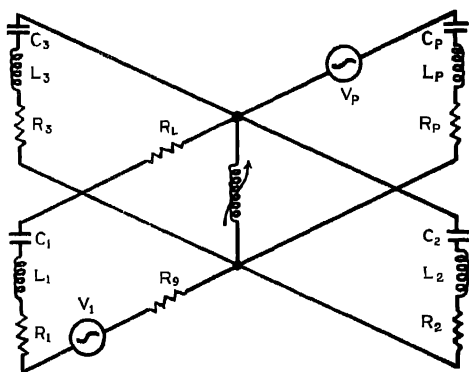


Fig. 2. Schematic representation of a single pump two idler parametric amplifier having a variable non-linear inductor as the coupling element.

L_K = inductance of the k -th circuit,

C_K = capacitance of the k -th circuit,

R_2, R_3, R_p = resistances of the 2nd, 3rd and p -th circuit respectively,

R_1 = coil resistance of the signal circuit,

R_L = load resistance,

R_q = internal resistance of the signal source,

$V_1(e^{j\omega_1 t} + e^{-j\omega_1 t})$ = voltage generated by the signal source.
 and $V_p(p^{j\omega_p t} + e^{-j\omega_p t})$ = voltage generated by the pump source.

The coupling reactor is an inductor with quadratic non-linearity, that is, the flux varies with the instantaneous current $i_{(t)}$ as given by equation (2)

$$\phi = L_0 i_{(t)} - L i_{(t)}^2 \quad \dots (2)$$

where

L = coefficient of non-linearity,

L_0 = linear portion of the inductance,

$i_{(t)}$ = total instantaneous current at time t

$$= \sum_{k=1,2,3,p} (I_k e^{j\omega_k t} + I_k^* e^{-j\omega_k t}),$$

*denotes the conjugate.

The voltage across the reactor at any instant will be given by

$$\begin{aligned} v_{(t)} &= \frac{d\phi}{dt} = L_0 \frac{di_{(t)}}{dt} - 2L i_{(t)} \frac{di_{(t)}}{dt} \\ &= L_0 \sum_{k=1,2,3,p} j\omega_k (I_k e^{j\omega_k t} - I_k^* e^{-j\omega_k t}) \\ &\quad - 2L \sum_{k=1,2,3,p} j\omega_k (I_k e^{j\omega_k t} - I_k^* e^{-j\omega_k t}) \times \sum_{k=1,2,3,p} (I_k e^{j\omega_k t} + I_k^* e^{-j\omega_k t}). \quad \dots (3) \end{aligned}$$

If we designate the voltage at a frequency ω_k as v_k , the various components of the voltages at different frequencies will be

$$v_1 = j\omega_1 L_0 I_1 e^{j\omega_1 t} - j2\omega_1 L I_2 I_p e^{j\omega_1 t} \quad \dots (4.a)$$

$$v_2 = j\omega_2 L_0 I_2 e^{j\omega_2 t} - j2\omega_2 L [I_1 I_p^* - I_p I_3^*] e^{j\omega_2 t} \quad \dots (4.b)$$

$$v_3 = j\omega_3 L_0 I_3 e^{j\omega_3 t} - j2\omega_3 L I_p I_2^* e^{j\omega_3 t} \quad \dots (4.c)$$

$$v_p = j\omega_p L_0 I_p e^{j\omega_p t} - j2\omega_p L [I_1 I_2^* + I_2 I_3] e^{j\omega_p t} \quad \dots (4.d).$$

Supposing the idler circuit (3) to be resonant at ω_3 , we have

$$R_3 I_3 = j2\omega_3 L I_p I_2^* \quad \dots (5)$$

Let us write $I_k = I_k' e^{j\theta_k}$

where

θ_k = the phase difference between the applied voltage and the resulting current.

We now have

$$R_3 I_3' e^{j\theta_3} = j2\omega_3 L I_p' I_2' e^{j(\theta_2 - \theta_3)}$$

Hence the phases will automatically be adjusted such that

$$\theta_3 = \theta_p - \theta_2 + \pi/2 \quad \dots (6)$$

Similarly for the idler circuit (2) resonant at ω_2 ,

$$R_2 I_2' e^{j\theta_2} = j2\omega_2 L I_p' [I_1' e^{j(\theta_1 - \theta_2)} + I_3' e^{j(\theta_3 - \theta_2)}]$$

Using equation. (6)

$$R_2 I_2' e^{j\theta_2} = 2\omega_2 L I_p' [I_1' e^{j(\theta_1 - \theta_2 + \pi/2)} + I_3' e^{j\theta_2}] \quad \dots (7)$$

This requires the phases to be adjusted such that

$$\text{either} \quad \theta_1 - \theta_2 = \theta_2 + \pi/2 \quad \text{and} \quad I_3' > I_1' \quad \text{if} \quad I_2' R_2 < 2\omega_2 L I_p' I_3' \quad \dots (8.a)$$

$$\text{Or} \quad \theta_1 - \theta_2 = \theta_2 - \pi/2 \quad \text{if} \quad I_2' R_2 > 2\omega_2 L I_p' I_3' \quad \dots (8.b)$$

Taking relation (8.a)

$$\begin{aligned} v_1 &= j\omega_1 L_0 I_1' e^{j(\omega_1 t + \theta_1)} - j2\omega_1 L_2' I_p' e^{j(\omega_1 t + \theta_1 - \pi/2)} \\ &= j\omega_1 L_0 I_1' e^{j(\omega_1 t + \theta_1)} - 2\omega_1 L I_2' I_p' e^{j(\omega_1 t + \theta_1)} \end{aligned}$$

The negative sign before the second term in the above equation indicates that the power should be given to the signal circuit. In other words the signal power should be amplified at the cost of the pump power. On the other hand if the phase relations are given as in eqn. (8.b), the power should be extracted from the source and the signal would be attenuated instead of being amplified. Thus the amplification can be achieved only if

$$R_2 I_2' < 2\omega_2 L I_p' I_3' \quad \{\text{vide equation. (8.a)}\}$$

Substituting the value of I_3' , the condition of amplification becomes

$$R_2 < \frac{4\omega_2 \omega_3 L^2 I_p'^2}{R_3} \quad \dots (9)$$

This is verified in section III(3).

(2) *Power Relations* : The last terms on the right hand side of the equations

(4) give the powers at different frequencies entering the coupling reactor. Denoting the power entering the coupling reactor at frequency ω_k as P_k , we find

$$P_1 = 2L\omega_1 |I_1 I_2 I_p| \quad \dots \quad (10.a)$$

$$P_2 = -2L\omega_2 [|I_1 I_2 I_p| + |I_2 I_3 I_p|] \quad \dots \quad (10.b)$$

$$P_3 = -2L\omega_3 |I_2 I_3 I_p| \quad \dots \quad (10.c)$$

$$P_p = -2L\omega_p [|I_1 I_2 I_p| - |I_2 I_3 I_p|] \quad \dots \quad (10.d)$$

From equations (10), we obtain

$$\frac{P_p}{\omega_p} - \frac{P_2}{\omega_2} + \frac{2P_3}{\omega_3} = 0 \quad \dots \quad (11.a)$$

$$\frac{P_1}{\omega_1} + \frac{P_2}{\omega_2} - \frac{P_3}{\omega_3} = 0 \quad \dots \quad (11.b)$$

These are the Mauley-Rowe (1956) relations for this case

(3) *Negative Resistance*. The signal frequency will not always be ω_1 , instead it may be, in general, ω'_1 where $\omega'_1 = \omega_1 + \Delta\omega$. The idling frequencies will then be

$$\omega'_2 = \omega_2 + \Delta\omega \quad \text{and} \quad \omega'_3 = \omega_3 - \Delta\omega$$

Under the assumption that the Q 's of the circuits are quite high and the frequencies are well separated, we can write the general voltage current relations as given below

$$V_1 = Z_1 I_1 - j2\omega_1 L I_2 I_p \quad \dots \quad (12.a)$$

$$0 = Z_2 I_2 - j2\omega_2 L [I_1 I_p^* + I_3^* I_p] \quad \dots \quad (12.b)$$

$$0 = Z_3 I_3 - j2\omega_3 L I_2^* I_p \quad \dots \quad (12.c)$$

$$V_p = Z_p I_p - j2\omega_p L [I_2 I_3 + I_1 I_2^*] \quad \dots \quad (12.d)$$

where

$$\begin{aligned} Z_1 &= R_T + jX_1 = (R_1 + R_L + R_g) + jX_1 \\ &= R_T + j \left[\omega'_1 (L_0 + L_1) - \frac{1}{\omega'_1 C} \right] \\ &= R_T \left[1 + j2Q_1 \frac{\Delta\omega}{\omega_1} \right] \quad \dots \quad (13.a) \end{aligned}$$

$$Z_2 = R_2 \left[1 + j2Q_2 \frac{\Delta\omega}{\omega_2} \right] \quad \dots \quad (13.b)$$

$$Z_3 = R_3 \left[1 - j2Q_3 \frac{\Delta\omega}{\omega_3} \right] \quad \dots \quad (13.c)$$

$$Z_p = R_p \left[1 + j2Q_p \frac{\Delta\omega}{\omega_p} \right] = R_p \quad \dots (13.d)$$

The effective self impedance Z_{11} for the signal circuit can be obtained by eliminating idling currents from equation. (12.a) and will be given by equation (14)

$$Z_{11} = \frac{V_1}{I_1} \\ = Z_1 - \frac{4\omega'_1\omega'_2L^2|I_p|^2}{\frac{4\omega'_2\omega'_3L^2|I_p|^2}{Z_3^*} - Z_2} \quad \dots (14)$$

From this we infer that in order to obtain negative resistance and hence amplification of the signal, it is necessary that

$$Z_2 < \frac{4\omega'_2\omega'_3L^2|I_p|^2}{Z_3^*}$$

and at resonance

$$R_2 < \frac{4\omega_2\omega_3L^2|I_p|^2}{R_3} \quad \dots (15)$$

which is in conformity with the condition {equation. (9)} of amplification obtained from phase consideration in section III(1). Equation. (14) can be written as

$$Z_{11} = (R_T - R) + j(X_1 - X) \quad \dots (16)$$

where the negative resistance R and the reactance X are given by equations, (17)

$$R = \frac{R_T Q_1 Q_2 \beta_{1p} \beta_{2p} (Q_2 Q_3 \beta_{2p} \beta_{3p} - 4Q_3^2 \frac{\Delta\omega^2}{\omega_3^2} - 1)}{\left(Q_2 Q_3 \beta_{2p} \beta_{3p} + 4Q_2 Q_3 \frac{\Delta\omega^2}{\omega_2 \omega_3} - 1 \right)^2 + 4\Delta\omega^2 \left(\frac{Q_2}{\omega_2} + \frac{Q_3}{\omega_3} \right)^2} \quad \dots (17a)$$

$$X = \frac{2\Delta\omega R_T Q_1 Q_2 \beta_{1p} \beta_{2p} \left(\frac{Q_2}{\omega_2} + \frac{Q_2 Q_3 \beta_{2p} \beta_{3p}}{\omega_3} + \frac{4Q_2 Q_3 \Delta\omega^2}{\omega_2 \omega_3^2} \right)}{\left(Q_2 Q_3 \beta_{2p} \beta_{3p} + 4Q_2 Q_3 \frac{\Delta\omega^2}{\omega_2 \omega_3} - 1 \right)^2 + 4\Delta\omega^2 \left(\frac{Q_2}{\omega_2} + \frac{Q_3}{\omega_3} \right)^2} \quad \dots (17.b)$$

where

$$\beta_{kp} = 2 \frac{L|I_p|}{L_k} \cdot \frac{\omega'_k}{\omega_k} \quad \dots (18)$$

At resonance i.e. for $\Delta\omega = 0$, the negative resistance becomes

$$R_{res} = \frac{4\omega_1\omega_2L^2|I_p|^2}{\frac{4\omega_2\omega_3L^2|I_p|^2}{R_3} - R_2} \quad \dots (19.a)$$

$$\text{or} \quad R_{res} = R_T Q_1 Q_2 \beta_{1p} \beta_{2p} / (Q_2 Q_3 \beta_{2p} \beta_{3p} - 1) \quad \dots (19.b)$$

(4) *Gain and Band-width*: The power gain of the amplifier is defined as

$$G = \frac{P_{out}}{P_{in}} = \frac{R_L |I_1|^2}{|V_1|^2 / 4R_g} \quad \dots (20.a)$$

Substituting the value of $|I_1|^2 / |V_1|^2$ from equation. (16)

$$G = \frac{4R_g R_L}{|Z_{11}|^2} = \frac{4R_g R_L}{(R_T - R)^2 + (X_1 - X)^2} \quad \dots (20.b)$$

The gain will be maximum at resonance and will be given by

$$G_{max} = 4R_g R_L / (R_T - R_{res})^2 \quad \dots (21)$$

The normalized gain ($= G/G_{max}$) can be written as

$$\frac{G}{G_{max}} = \left[\frac{R_T - R_{res}}{|Z_{11}|} \right]^2 \quad \dots (22)$$

The band-width of the amplifier will be equal to the difference of the roots of the equation.

$$\frac{G}{G_{max}} = \frac{1}{2} \quad \dots (23)$$

that is

$$\begin{aligned} & 2 \left[1 - \frac{Q_1 Q_2 \beta_{1p} \beta_{2p}}{Q_2 Q_3 \beta_{2p} \beta_{3p} - 1} \right] \\ &= \left[1 - \frac{Q_1 Q_2 \beta_{1p} \beta_{2p} \left(Q_2 Q_3 \beta_{2p} \beta_{3p} - 4Q_3^2 \frac{\Delta \omega^2}{\omega_3^2} - 1 \right)}{\left(Q_2 Q_3 \beta_{2p} \beta_{3p} + 4Q_2 Q_3 \frac{\Delta \omega^2}{\omega_2 \omega_3} - 1 \right)^2 + 4\Delta \omega^2 \left(\frac{Q_2}{\omega_2} + \frac{Q_3}{\omega_3} \right)^2} \right]^2 \\ &+ \left[2\Delta \omega \left\{ \frac{Q}{\omega_1} - \frac{Q_1 Q_2 \beta_{1p} \beta_{2p} \left(\frac{Q_2}{\omega_2} + \frac{Q_2 Q_3^2 \beta_{2p} \beta_{3p}}{\omega_3} + \frac{4Q_2 Q_3^2 \Delta \omega^2}{\omega_2 \omega_3^2} \right)}{\left(Q_2 Q_3 \beta_{2p} \beta_{3p} + 4Q_2 Q_3 \frac{\Delta \omega^2}{\omega_2 \omega_3} - 1 \right)^2 + 4\Delta \omega^2 \left(\frac{Q_2}{\omega_2} + \frac{Q_3}{\omega_3} \right)^2} \right\} \right]^2 \end{aligned} \quad \dots (24)$$

If the value of Q 's and β 's be known, the value of $\frac{1}{|Z_{11}|^2}$ can be plotted against $\Delta \omega$ and the band-width can be determined.

It is obvious that the value of maximum gain and band-width for a particular value of inductance variation is entirely governed by the negative resistance. Larger is the value of R the larger is the gain. From expression (17.b) it is seen that R can be increased by increasing the value of Q_1 and Q_2 and decreasing the value of Q_3 . The increased values of ω_2 and ω_3 will also have similar effect. The value of inductance variation required for annulling the total circuit resistance can be written from equation (19.b) as

$$Q_1 Q_2 \beta_{1p} \beta_{2p} = Q_2 Q_3 \beta_{2p} \beta_{3p} - 1 \quad \dots (25.a)$$

$$\text{or} \quad 2LI_p = \left(\frac{R_1 R_2 R_3}{\omega_2 \omega_3 R_1 - \omega_1 \omega_2 R_3} \right)^{\frac{1}{2}} \quad \dots (25.b)$$

It is therefore seen that for the values of $2LI_p$ given by equationn. (26)

$$\left(\frac{R_2 R_3}{\omega_2 \omega_3} \right)^{\frac{1}{2}} \leq 2LI_p \leq \left(\frac{R_1 R_2 R_3}{\omega_2 \omega_3 R_1 - \omega_1 \omega_2 R_3} \right)^{\frac{1}{2}} \quad \dots (26)$$

the system is unstable and the sustained oscillations will take place. In order to use the combination as an amplifier the adjustment is such that the value of $2LI_p$ approaches

$$\left(\frac{R_1 R_2 R_3}{\omega_2 \omega_3 R_1 - \omega_1 \omega_2 R_3} \right)^{\frac{1}{2}}$$

but still

$$Q_1 Q_2 \beta_{1p} \beta_{2p} < (Q_2 Q_3 \beta_{2p} \beta_{3p} - 1)$$

Such an adjustment will give maximum gain

Usually in practice Q_1 , the loaded Q of the signal circuit, is quite small, that is, $Q_1 Q_2 \beta_{1p} \beta_{2p}$ is a small fraction and hence for large values of gain we can assume

$$(Q_2 Q_3 \beta_{2p} \beta_{3p} - 1) < < 1 \quad \dots (27)$$

With this assumption, the band-width can approximately be written as

$$2\Delta\omega = \frac{Q_2 Q_3 \beta_{2p} \beta_{3p} - 1}{\frac{Q_2}{\omega_2} + \frac{Q_3}{\omega_3}} \quad \dots (28)$$

(5) *Noise Figure* We shall now find out the noise figure of the amplifier under the assumption that the signal to be amplified is precisely at resonant frequency ω_1 of the tank circuit (1). Noise figure is written as

$$\begin{aligned} F &= \frac{S_i/N_i}{S_o/N_o} \\ &= \frac{1}{\text{Power gain}} \times \frac{1}{KT_0 \Delta f} N_o \quad \dots (29) \end{aligned}$$

where

$\frac{S_i}{N_i}$ = available signal to noise ratio at the input

$\frac{S_0}{N_0}$ = available signal to noise ratio at the output

K = Boltzmann's constant

T_0 = Standard noise temperature = $290^\circ K$, and

Δf = the noise band-width of the amplifier.

In order to calculate N_0 , we return to original equations (12) and replace the signal voltages by noise voltages as shown in figure 3.

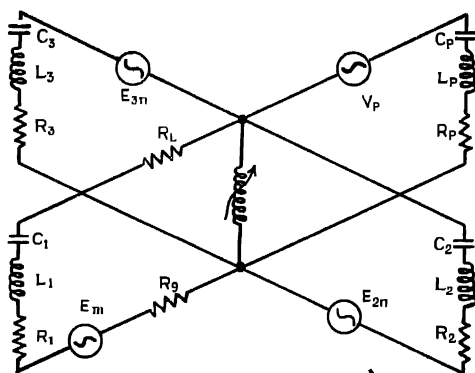


Fig. 3. Figure 2 redrawn to indicate noise sources.

We can find the individual contribution to noise power by any one circuit by putting all the noise voltages except the one under consideration, equal to zero and then eliminating the idling currents. The total* noise current square is

$$[I_1]_n^2 = \sum_{k=1,2,3} [I_1]_{kn}^2$$

$$= \left[\left(\frac{E_{1n}}{|Z_1| - R} \right)^2 + \left(\frac{E_{2n}R}{2\omega_2 L |I_p|} \cdot \frac{1}{|Z_1| - R} \right)^2 + \left(\frac{E_{3n}}{|Z_3|} \cdot \frac{R}{|Z_1| - R} \right)^2 \right] \quad \dots \quad (30)$$

where

$[I_1]_{kn}^2$ = noise current squared in the k -th circuit

$$N_0 = \frac{R_L}{(|Z_1| - R)^2} \left[E_{1n}^2 + \left(\frac{E_{2n}R}{2\omega_2 L |I_p|} \right)^2 + \left(\frac{E_{3n}}{Z_3} \cdot R \right)^2 \right]$$

* It may be noted that we have neglected the noise voltage E_{pn} due to R_p because it is very small as compared to the pump voltage V_p . We have also taken no account of the noise voltage due to the fluctuations of the pump circuit.

As E_{kn} are the thermal noise voltages, we can write

$$E_{1n}^2 = 4K\Delta f(R_g T_0 + R_1 T) \quad \dots (31.a)$$

$$E_{2n}^2 = 4KT\Delta f R_2 \quad \dots (31.b)$$

$$E_{3n}^2 = 4KT\Delta f R_3 \quad \dots (31.c)$$

Substituting these values we get

$$N_0 = \frac{4K\Delta f R}{(|Z_1| - R)^2} \left[(R_g T_0 + R_1 T) + \frac{R_2 T R^2}{4\omega_2^2 L^2 |I_p|^2} + \frac{R_3 T R^2}{|Z_3|^2} \right] \quad \dots (32)$$

$$\text{and} \quad F = \frac{4R_g R_L}{G} \cdot \frac{1}{R_g} \cdot \frac{T}{T_0} \left[R_g \frac{T_0}{T} + R_1 + \frac{R_2 R^2}{4\omega_2^2 L^2 |I_p|^2} + \frac{R_3 R^2}{|Z_3|^2} \right] \quad \dots (33.a)$$

From equation. (20) we have

$$G = \frac{4R_g R_L}{|Z_{11}|^2} = \frac{4R_g R_L}{(|Z_1| - R)^2}$$

Therefore,

$$F = 1 + \frac{T}{T_0} \left[\frac{R_1}{R_g} + \frac{R_2}{R_g} \left(\frac{R}{2\omega_2 L |I_p|} \right)^2 + \frac{R_3}{R_g} \left(\frac{R}{|Z_3|} \right)^2 \right] \quad \dots (33.b)$$

Equation. (33.b) can be rewritten as

$$\left[(F-1) \frac{T_0}{T} - \frac{R_1}{R_g} \right] \frac{R_g R_3}{R_T^2} = \frac{R^2}{R_T^2} \left[\frac{1}{Q_2 Q_3 \left(\frac{\omega_2}{\omega_3} \frac{4L^2}{L_2 L_3} \right) |I_p|^2} + 1 \right] \quad \dots (33.c)$$

Denoting the left hand side of equation. (33.c) by η , we have

$$\eta = \frac{R^2}{R_T^2} \left[\frac{1}{Q_2 Q_3 \left(\frac{\omega_2}{\omega_3} \frac{4L^2}{L_2 L_3} \right) |I_p|^2} + 1 \right] \quad \dots (33.d)$$

The variation of η with pump current I_p is depicted in figure 7.

Before proceeding to analyse the next case, it is worthwhile to note that if we use non-linear capacitance as shown in figure 4, instead of non-linear inductance, the method of analysis will remain unchanged. Thus, if we assume that the voltage across the coupling capacitor is given by

$$V_{(t)} = \int [\mathcal{S}_0^2(t) - \mathcal{S}_1^2(t)] dt \quad \dots (34)$$

where, $S = 1/C$, we can write any one of the above relations simply by replacing $2j\omega L$ by $S/j\omega$ or $1/j\omega C$ in the relations derived for inductance coupling case. For

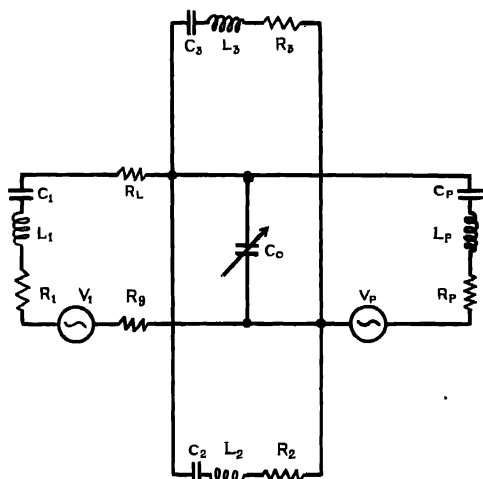


Fig. 4. Schematic representation of a single pump two idler parametric amplifier having a variable non-linear capacitance as the coupling element.

example, the expression for effective self impedance of the signal circuit will be given by

$$Z_{11} = Z_1 + \left[\frac{\frac{S^2 |I_p|^2}{\omega_1 \omega_2}}{Z_2 - \frac{S^2 |I_p|^2}{\omega_2 \omega_3 z_3^*}} \right] \quad \dots (35)$$

III. ANALYSIS OF CASE II

(1) *Phase relations*: Consider the combination of a mixer and an amplifier employing two pumps and two idlers. The frequency relations in this case are

$$\omega_1 = \omega_2 + \omega_p \quad (\text{mixer}) \quad (36.a)$$

$$\omega_q = \omega_2 + \omega_3 \quad (\text{amplifier}) \quad (36.b)$$

The pumping source at frequency ω_q supplies power to ω_2 and ω_3 . The power at ω_2 mixes with that at ω_p to give power at ω_1 . An analysis similar to case I will give following phase relations;

$$\theta_3 = \theta_q - \theta_2 + \pi/2 \quad (37)$$

and

$$\theta_1 - \theta_p = \theta_2 + \pi/2 \quad \text{and} \quad I_q' I_s' > I_1' I_p' \quad \dots (38.a)$$

or

$$\theta_1 - \theta_p = \theta_2 - \pi/2 \quad \dots (38.b)$$

In this case too, although the amplification of the signal will be achieved if the phase relations are those as given by equation (38.a), the possibility of attenuation is not ruled out and the signal will suffer attenuation if equation (38.b) instead of (38.a) holds good.

(2) *Power relations* The power relations are given by equations. (39)

$$P_1 = 2\omega_1 L |I_1 I_2 I_p| \quad \dots (39.a)$$

$$P_2 = -2\omega_2 L [|I_1 I_2 I_p| + |I_2 I_3 I_q|] \quad \dots (39.b)$$

$$P_3 = -2\omega_3 L |I_2 I_3 I_q| \quad \dots (39.c)$$

$$P_p = -2\omega_p L |I_1 I_2 I_p| \quad \dots (39.d)$$

$$P_q = 2\omega_q L |I_2 I_3 I_q| \quad \dots (39.e)$$

(3) *Negative resistance* : Proceeding exactly in the same way as in case I one can write the effective self impedance of the signal circuit as

$$Z_{11} = \frac{V_1}{I_1} = Z_1 - \frac{4\omega_1' \omega_2' L^2 |I_p|^2}{4\omega_2' \omega_3' L^2 |I_q|^2} - Z_2 \quad \dots (40)$$

The negative resistance and reactance, in general, are given by the following equations :

$$R = \frac{R_T Q_1 Q_2 \beta_{1p} \beta_{2p} \left(Q_2 Q_3 \beta_{2q} \beta_{3q} - 4Q_3^2 \frac{\Delta\omega^2}{\omega_3^2} - 1 \right)}{\left(Q_2 Q_3 \beta_{2q} \beta_{3q} + 4Q_2 Q_3 \frac{\Delta\omega^2}{\omega_2 \omega_3} - 1 \right)^2 + 4\Delta\omega^2 \left(\frac{Q_2}{\omega_2} + \frac{Q_3}{\omega_3} \right)^2} \quad \dots (41.a)$$

$$X = 2R_T \Delta\omega \left[\frac{Q_1 Q_2 \beta_{1p} \beta_{2p} \left(\frac{Q_2}{\omega_2} + \frac{Q_2 Q_3^2 \beta_{2q} \beta_{3q}}{\omega_3} + \frac{4Q_2 Q_3^2 \Delta\omega^2}{\omega_2 \omega_3^2} \right)}{\left(Q_2 Q_3 \beta_{2q} \beta_{3q} + 4Q_2 Q_3 \frac{\Delta\omega^2}{\omega_2 \omega_3} - 1 \right)^2 + 4\Delta\omega^2 \left(\frac{Q_2}{\omega_2} + \frac{Q_3}{\omega_3} \right)^2} \right] \quad \dots (41.b)$$

At resonance

$$R_{res} = \frac{R_T Q_1 Q_2 \beta_{1p} \beta_{2p}}{Q_2 Q_3 \beta_{2q} \beta_{3q} - 1} \quad \dots (41.c)$$

where

$$\beta_{kq} = \frac{2L}{L_k} \cdot |I_q| \frac{\omega_k'}{\omega_k} \quad \dots (42)$$

The variation of fractional negative resistance at resonance is depicted in figure 5.

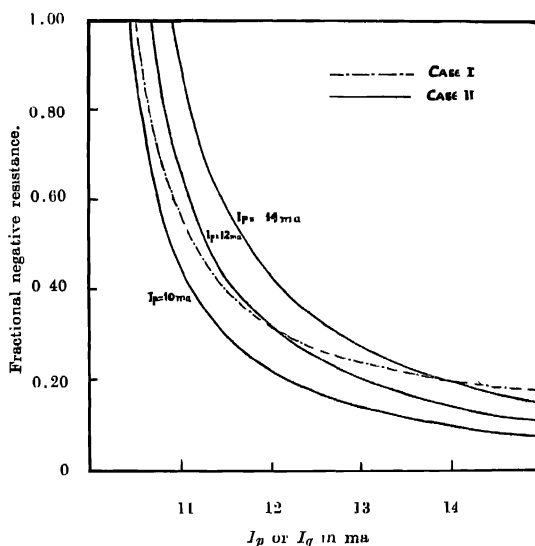


Fig. 5. Plots of variation of fractional negative resistance with pump currents, assuming that,

$$10Q_1 \frac{2L}{L_1} = Q_2 \frac{2L}{L_2} = Q_3 \frac{2L}{L_3} = 100/mA$$

It is clear from the expression of the negative resistance at resonance that the same value of gain or negative resistance can be achieved by a number of combinations of I_p and I_q . Writing

$$\gamma_1 = Q_1 Q_2 \beta_{1p} \beta_{2p} \quad \text{and} \quad \gamma_2 = Q_2 Q_3 \beta_{2q} \beta_{3q}, \quad \text{we have}$$

$$\frac{R_{res}}{R_T} = \alpha = \frac{\gamma_1}{\gamma_2 - 1}$$

Hence

$$\gamma_2 = 1 + \frac{\gamma_1}{\alpha} \quad \text{or} \quad \frac{\gamma_2}{\gamma_1} = \frac{1}{\gamma_1} + \frac{1}{\alpha} \quad \dots (43)$$

This relation is depicted in figure 6. It is easy to see from figure 6 that the large values of negative resistance are obtained by choosing small values of the ratio

$\frac{\gamma_2}{\gamma_1}$. It is also obvious that $\frac{\gamma_2}{\gamma_1}$ (or $\frac{I_g^2}{I_p^2}$) is smaller, the larger is γ_1 (or I_p^2).

Therefore, the condition of large gain demands a small value of the ratio $\frac{I_g^2}{I_p^2}$ and a large value of I_p^2 .

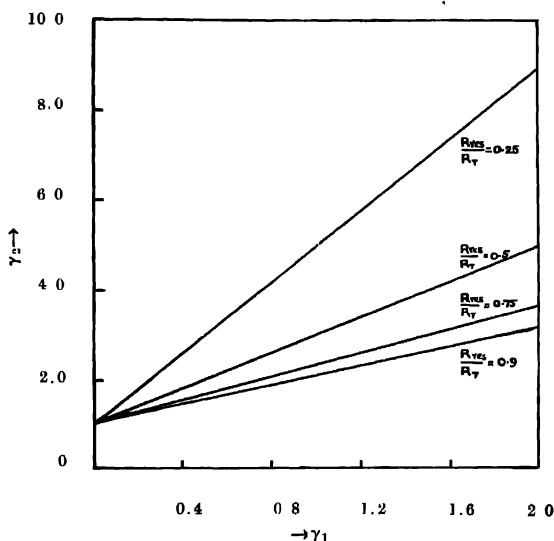


Fig. 6. Plots of variation of γ_2 with γ_1 for different values of fractional negative resistance [see equation (43)].

(4) *Gain and band-width*: The expressions for gain of a parametric amplifier employing a combination of a mixer and an amplifier is not much different from the previous case. We have, in this case

$$G = \frac{4R_g R_L}{(R_T - R)^2 + (X_1 - X)^2} \quad \dots \quad (44)$$

and

$$G_{max} = \frac{(R_T - R_{neg})^2}{(R_T - R)^2 + (X_1 - X)^2} \quad \dots \quad (45)$$

The band-width will be equal to the difference of the roots of the equation.

$$\frac{G}{G_m} = \frac{1}{\alpha} \quad \dots (46.a)$$

that is,

$$2 \left[1 - \frac{Q_1 Q_2 \beta_{1p} \beta_{2p}}{Q_2 Q_3 \beta_{2q} \beta_{3q} - 1} \right]^2 R_T^2 = (R_T - R)^2 + (X_1 - X)^2 \quad \dots (46b)$$

(5) *Noise figure*: The ultimate noise figure is analogous to that of case I, and can be written as

$$F = 1 + \frac{T}{T_0} \left[\frac{R_1}{R_g} + \frac{R_2}{R_g} \left(\frac{R}{2\omega_2 L |I_p|} \right)^2 + \frac{R_3}{R_g} \left(\frac{R}{|Z_3|} \right)^2 \left(\frac{|I_q|}{|I_p|} \right)^2 \right] \quad (47)$$

The equation (47) can be rewritten as

$$\left[(F-1) \frac{T_0}{T} - \frac{R_1}{R_g} \right] \frac{R_g R_3}{R_T^2} = \frac{R^2}{R_T^2} \left[\frac{1}{Q_2 Q_3 \left(\frac{\omega_2}{\omega_3} \cdot \frac{4L^2}{L_2 L_3} \right) |I_p|^2} + \left(\frac{|I_q|}{|I_p|} \right)^2 \right] \dots (48a)$$

or

$$\eta = \frac{R^2}{R_T^2} \left[\frac{1}{Q_2 Q_3 \left(\frac{\omega_2}{\omega_3} \cdot \frac{4L^2}{L_2 L_3} \right) |I_p|^2} + \left(\frac{|I_q|}{|I_p|} \right)^2 \right] \dots (48.b)$$

The variation of η with pump currents is depicted in figure 7.

The expression (48) indicates that the noise figure can be reduced by choosing a small value of the ratio $\frac{\omega_3}{\omega_2}$ and of $\frac{I_q}{I_p}$. It should be noted that the requirements of a small value of I_q/I_p and a large value of I_p demanded by equation (48) for a small noise figure are consistent.

IV. ANALYSIS OF CASES III & IV

(1) *Phase relations*: For the combination of two mixers and an amplifier the frequency relations are

$$\omega_1 = \omega_2 + \omega_p \quad (\text{mixer}) \quad \dots (49.a)$$

$$= \omega_3 + \omega_q \quad (\text{mixer}) \quad \dots (49.b)$$

$$\omega_q = \omega_2 + \omega_3 \quad (\text{amplifier}) \quad \dots (49.c)$$

ω_2 and ω_3 receive powers from the pumping source ω_q and after mixing with ω_1 and ω_q respectively, deliver power at the frequency ω_1 with the result that the signal power is amplified.

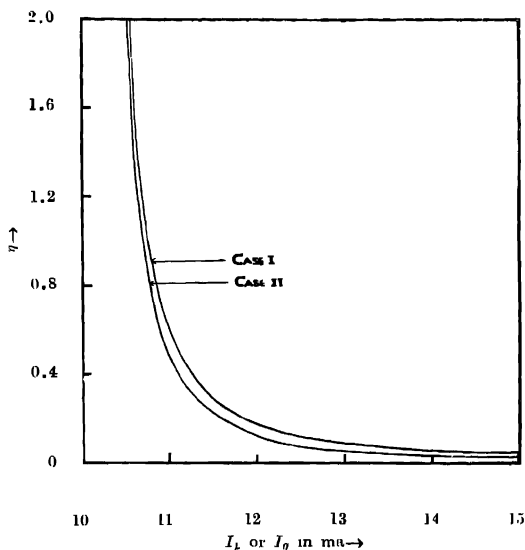


Fig. 7. Plots of $\eta = \left[(F - 1) \frac{T_0}{T} - \frac{R_1}{R_g} \right] \frac{R_g R_s}{R_T^2}$ with pump currents, assuming that,

$$Q_2 Q_3 \left(\frac{\omega_2}{\omega_3} \cdot \frac{4L^2}{L_2 L_3} \right) = 10,000 / (mA)^2$$

In order to achieve amplification of the signal one of the following phase relations should be satisfied.

$$\begin{aligned}
 (\text{a}) \quad & \theta_3 = \theta_1 - \theta_q + \frac{\pi}{2} \\
 & = \theta_q - \theta_2 + \frac{\pi}{2} \\
 & \theta_2 = \theta_1 - \theta_p - \frac{\pi}{2}
 \end{aligned}
 \quad \left. \vphantom{\begin{aligned} \theta_3 = \theta_1 - \theta_q + \frac{\pi}{2} \\ \theta_2 = \theta_1 - \theta_p - \frac{\pi}{2} \end{aligned}} \right\} \dots (50.a)$$

and $I'_2 I'_p > I'_3 I'_q > I'_1 I'_p$

$$\begin{aligned}
 \text{(b)} \quad \theta_3 &= \theta_1 - \theta_q - \frac{\pi}{2} \\
 &= \theta_q - \theta_2 + \frac{\pi}{2}
 \end{aligned} \tag{50.b}$$

$$\begin{aligned}
 \theta_2 &= \theta_1 - \theta_p - \frac{\pi}{2} \\
 \text{and} \quad I_3' I_q' &> I_1' I_p' \quad \text{and} \quad I_2' > I_1'
 \end{aligned}$$

(2) *Power relations*. The power relations are given by the following equations.

$$P_1 = 2L\omega_1[|I_1 I_2 I_p| + |I_1 I_3 I_q|] \quad \dots \tag{51.a}$$

$$P_2 = 2L\omega_2[|I_1 I_2 I_p| + |I_2 I_3 I_q|] \quad \dots \tag{51.b}$$

$$P_3 = 2L\omega_3[|I_1 I_3 I_q| + |I_2 I_3 I_q|] \quad \dots \tag{51.c}$$

$$P_p = -2L\omega_p |I_1 I_2 I_p| \quad \dots \tag{51.d}$$

$$P_q = 2L\omega_q[|I_2 I_3 I_q| - |I_1 I_3 I_q|] \quad \dots \tag{51.e}$$

(3) *Negative resistance* The negative resistance at resonance is given by equation. (52)

$$R_{res} = \frac{4\omega_1\omega_2 L^2 |I_1|^2 R_3 + 4\omega_1\omega_3 L^2 |I_q|^2 R_2 \pm 16\omega_1\omega_2\omega_3 L^3 |I_p| |I_q|^2}{\omega_2\omega_3 L^2 |I_q|^2 - R_2 R_3} \quad \dots \tag{52.a}$$

$$= \frac{R_p [Q_1 Q_2 \beta_{1p} \beta_{2p} + Q_1 Q_3 \beta_{1q} \beta_{3q} \pm 2Q_1 Q_2 Q_3 \beta_{1p} \beta_{2q} \beta_{3q}]}{\dots} \quad \dots \tag{52.b}$$

The negative and the positive signs correspond to phase conditions given by equations. (50.a) and (50.b) respectively. Therefore, the amplification will be greater when the phase conditions are those given by equation. (50.b).

CASE IV.

(1) *Phase relations*: This is a multi-idler case and employs a combination of a mixer and two amplifiers. The frequency relations are as given below:

$$\omega_1 = \omega_2 + \omega_p \quad (\text{mixer}) \quad \dots \tag{53.a}$$

$$\omega_p = \omega_2 + \omega_3 \quad (\text{amplifier}) \quad \dots \tag{53.b}$$

$$\omega_q = \omega_3 + \omega_4 \quad (\text{amplifier}) \quad \dots \tag{53.c}$$

The idlers ω_2 and ω_4 receive powers from pumping sources ω_p and ω_q respectively, while the idler ω_3 receives power from both the pumps. ω_2 mixes

with ω_p to give power at frequency ω_1 and thus the amplification of the signal results.

The phase relations resulting in amplification are given below.

$$\left. \begin{aligned} \theta_4 &= \theta_q - \theta_3 + \frac{\pi}{2} \\ \theta_3 &= \theta_p - \theta_2 + \frac{\pi}{2} \\ \theta_2 &= \theta_1 - \theta_p - \frac{\pi}{2} \\ I_3' &> I_1' \end{aligned} \right\} \quad \dots (54)$$

and

(2) *Power relations* : The powers at various frequencies entering the reactor are given by the following equations.

$$P_1 = 2L\omega_1[|I_1I_2I_p|] \quad \dots (55.a)$$

$$P_2 = -2L\omega_2[|I_1I_2I_p| + |I_2I_3I_p|] \quad \dots (55.b)$$

$$P_3 = -2L\omega_3[|I_2I_3I_p| + |I_3I_4I_q|] \quad \dots (55.c)$$

$$P_4 = -2L\omega_4[|I_3I_4I_q|] \quad \dots (55.d)$$

$$P_p = -2L\omega_p[|I_1I_2I_p| - |I_2I_3I_p|] \quad \dots (55.e)$$

$$P_q = 2L\omega_q[|I_2I_3I_q|] \quad \dots (55.f)$$

(3) *Negative resistance* : The self impedance Z_{11} in this case is given by

$$Z_{11} = Z_1 - \frac{\omega_1' \omega_2' L^2 |I_p|^2}{\omega_2' \omega_3' L^2 |I_q|^2} - Z_2 \quad \dots (56)$$

$$Z_3^* - \frac{\omega_3' \omega_4' L^2 |I_q|^2}{Z_4}$$

At resonance the negative resistance is

$$R_{res} = - \frac{\omega_1 \omega_2 L^2 |I_p|^2}{\omega_2 \omega_3 L^2 |I_q|^2} - R_2 \quad \dots (57.a)$$

$$R_3 - \frac{\omega_3 \omega_4 L^2 |I_q|^2}{R_4}$$

$$= R_T \frac{Q_1 Q_2 \beta_{1p} \beta_{2p}}{Q_2 Q_3 \beta_{2q} \beta_{3q}} - 1 \quad \dots (57.b)$$

$$1 - Q_3 Q_4 \beta_{3q} \beta_{4q}$$

In concluding it would be good to compare the expressions of fractional negative resistance of all the parametric amplifiers so far evolved. The expression of the fractional negative resistance for single pump and single idler as well as two pumps and single idler case (Bloom and Chang, 1958) using third order non-linearity are given below.

$$(i) \quad R_{res} = \frac{\omega_1 \omega_2 L^2 |I_p|^2}{R_s} \quad \dots (58)$$

$$(ii) \quad R = \left[\frac{3}{2} L \left| \frac{V_{p1}}{Z_{p1}} \right| \left| \frac{V_{p2}}{Z_{p2}} \right| \right]^2 \frac{R_d}{R_d^2 + X_d^2} \omega(p_1 + p_2 - \omega) \quad \dots (59.a)$$

Corresponding expressions for different cases considered in this paper are to be found in equations (19.b), (41.c), (52 b) and (57.b).

It will be observed that the negative resistance in case of multi-idler circuit is less than that obtained in other cases and therefore, they offer no added advantage. The third case viz. the lower frequency pumping parametric amplifier considered as a combination of two mixers and one amplifier using two pumps and two idlers, seems to be the best one with regard to gain.

Writing expression (59.a) in terms of equivalent inductance and according to the symbols used in this text we have,

$$R_{res} = \frac{1}{4} \frac{L_p^2 L_q^2 \omega_1 \omega_2}{R_2} \quad \dots (59.b)$$

$$= \frac{1}{4} R_T Q_1 Q_2 \beta_{1p} \beta_{2q} \quad \dots (59.c)$$

Remembering the equation (27) it is easily seen that for the same values of I_p and I_q the negative resistance obtained in our combinations is greater than that obtained in the above one [vide equation (59.c)]. We, therefore, anticipate that the gain will also be larger in the present combinations.

V. AN ALTERNATIVE METHOD OF ANALYSIS

If the coupling reactor is assumed varying at the pump frequency, that is, if the inductance $L_{(t)}$ is given by equation (60), the analysis will remain unaltered except that we have to substitute L_p for $-2LI_p$ and L_q for $-2LI_q$ in each of the equations. The inductance $L_{(t)}$ is given by

$$L_{(t)} = L_p [e^{j(\omega_p t + \theta_p)} + e^{-j(\omega_p t + \theta_p)}] \quad \dots (60.a)$$

for one pump case, and

$$L_{(t)} = L_p[e^{j(\omega_p t + \theta_p)} + e^{-j(\omega_p t + \theta_p)}] \\ + L_q[e^{j(\omega_q t + \theta_q)} + e^{-j(\omega_q t + \theta_q)}] \quad \dots \quad (60.b)$$

for two pump case.

ACKNOWLEDGMENTS

The authors wish to thank Prof. K. Banerjee, Head of the Department of Physics, University of Allahabad and Dr. S. N. Ghosh, Professor, Institute of Applied Physics, University of Allahabad, for their constant encouragement and keen interest. One of the authors (Dikshit) extends thanks to the Government of India for the award of Senior Research Training Scholarship.

REFERENCES

- Bloom, S., and Chang, K. K. N., 1957, *R. C. A. Rev.*, **18**, 578.
 Heffner, H., and Wade, G., 1958, *J. App. Phys.*, **29**, 1321.
 Chang, K. K. N. and Bloom, S., 1958, *Proc. I. R. E.*, **46**, 1383
 Bloom, S. and Chang, K. K. N., 1958, *J. App. Phys.*, **29**, 594.
 Manley, J. M. and Rowe, H. E., 1956, *Proc. I. R. E.*, **44**, 904.
 Hogan, C. L., Jepsen, R. L. and Vartanian, P. H., 1958, *J. App. Phys.*, **29**, 422.

ELECTRON TEMPERATURE IN ELECTRODELESS DISCHARGE SUBJECTED TO A TRANSVERSE MAGNETIC FIELD

S. N. GOSWAMI*

INSTITUTE OF RADIO PHYSICS AND ELECTRONICS, CALCUTTA UNIVERSITY.

(Received, September 18, 1959)

ABSTRACT. Values of electron temperature in molecular gases subjected to electrodeless discharge have been obtained from mobility and its variation with pressure. The apparent discrepancy with the published data is shown in two cases, namely, effect of magnetic field and high value of X/p .

The electron temperature in gaseous discharges has been measured by a number of workers (Seeliger and Hirschert, 1931; Killian, 1930; Sommermeyer, 1934; Druyvesteyn, 1933) with different discharge currents and gas pressures. In view of the fact that almost all the data, available in the literature, refer to the rare gases, and very few to molecular gases, we report here some results of measurement of the electron temperature in molecular gases within a limited range of pressures. The values of the electronic mobility as were reported (Goswami, 1958) in electrodeless discharge subjected to a magnetic field, have been used in evaluating the electron temperature. The values of electron temperature may be determined from mobility and its variation with pressure from a simple relation derived below. Starting with the relation

RESULTS AND DISCUSSION

$$\frac{1}{2} mc^2 = \frac{3}{2} KT_e \quad \dots (1)$$

we can write

$$mu^2 = KT_e \quad \dots (2)$$

where $c^2 = u^2 + v^2 + w^2$, the symbols having their usual significance.

In a gas subjected to an electrical discharge and in thermal equilibrium we can write (Huxley, 1957) for the drift velocity

$$W = \frac{2}{3} \cdot \frac{X \cdot e}{m} \cdot \frac{l}{\bar{c}} = \mu_e X \quad \dots (3)$$

and

$$\bar{u} = \frac{\bar{c}}{1.6} \quad \dots (4)$$

* Now at the Central Calcutta College, Calcutta.

where \bar{v} = mean velocity; l = mean free path; X = electric field and μ_e = electronic mobility.

From (2), (3) and (4) we can write

$$T_e = \frac{l^2}{\mu_e^2} \times 3.35 \times 10^{18} \quad \dots (5)$$

Eqn.(5) can be used to ascertain the variation of T_e with pressure by using the values of electronic mobility determined earlier (Deb and Goswami, 1956; Goswami,

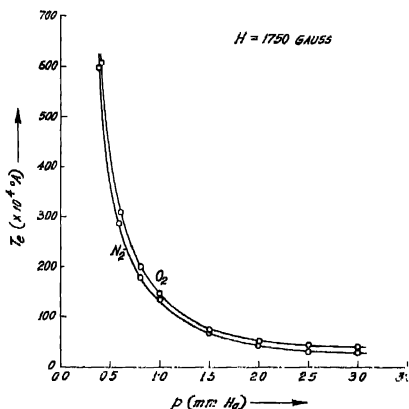


Fig. 1

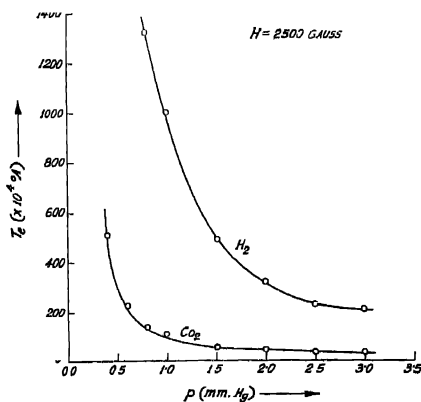


Fig. 2

1958). Standard values of l at 1 mm. Hg for such gases are taken from Loeb (1939) and those corresponding to other pressures are found out from the relation $pl = \text{constant}$. The results are shown graphically in figures 1 and 2. The qualitative variation of T_e with p is as expected and in conformity with the data given in Handbuch der Physik (1953), and Guthrie and Wakerling (1949). Quantitatively, however, it may appear that the results obtained here are one order of magnitude higher. This apparent discrepancy can, however, be traced to two causes. Firstly, T_e depends on H markedly and it increases apparently with increasing magnetic field (Figure 3). T_e as obtained here is thus a bit higher,

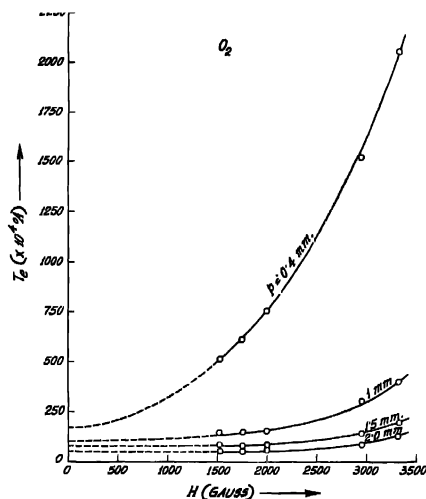


Fig. 3

as measurements are made in the presence of a fairly strong magnetic field. Secondly, in our experimental set-up the value of X/p was high (≈ 1000). In order to illustrate the possible contribution due to these two causes we proceed as follows. Values of T_e for a given gas and discharge tube are plotted against magnetic field with pressure as the parameter and the corrected value is obtained by extrapolation to zero value of H (figure 3). The extrapolated values thus deter-

mined are plotted as a function of X/p (Figure 4). This latter curve shows that T_e increases with X/p . From this trend of variation of T_e as observed in figure

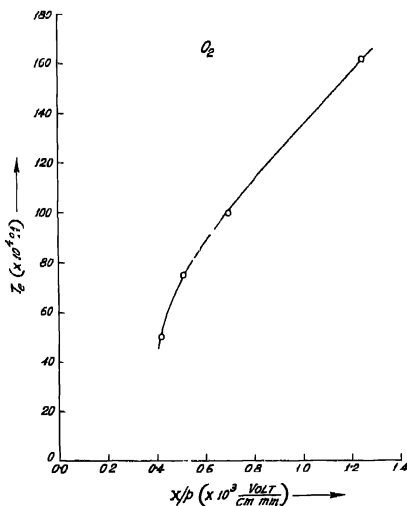


Fig. 4

† it is easily seen that the experimental values may be higher by an order due to the two causes mentioned above, viz., effect of magnetic field and high X/p value.

ACKNOWLEDGMENTS

The work was carried out in the Department of Radio Physics and Electronics. The author is very much indebted to Professor J. N. Bhar for his kind interest and permission to work in the Institute of Radio Physics and Electronics and to Dr. S. Deb for constant guidance.

REFERENCES

- Deb, S. and Goswami, S. N., 1956, *Sci. and Cult.*, **22**, 283.
- Druyvesteyn, M. J., 1933, *Z. Physik*, **81**, 571.
- Goswami, S. N., 1958, *Ind. J. Phys.*, **32**, 241.
- Guthrie, A. and Wakerling, R. K., 1949, *Characteristics of Electrical Discharge in Magnetic Fields*, McGraw-Hill Book Company, Inc., 267.
- Handbuch der Physik, Vol XXII, Gas Discharges II, 1956.
- Huxley, L. G. H., 1957, *Aus. J. Phys.*, **10**, 118.
- Killian, T. J., 1930, *Phys. Rev.*, **35**, 1238.
- Loeb, L. B., 1939, *Fundamental Processes of Electrical Discharge in Gases*, John Wiley & Sons, Inc., 241.
- Seßliger, R. and Hirschert, R., 1931, *Ann. der Phys.*, **11**, 817.
- Sommermeyer, K., 1934, *Z. Physik*, **90**, 232.

Letters to the Editor

The Board of Editors will not hold itself responsible for opinions expressed in the letters published in this section. The notes containing reports of new work communicated for this section should not contain many figures and should not exceed 500 words in length. The contributions must reach the Assistant Editor not later than the 15th of the second month preceding that of the issue in which the paper is to appear. No proof will be sent to the authors.

9

PRELIMINARY REPORT ON THE CRYSTAL STRUCTURE OF ANTHRONE

SURENDRA NATH SRIVASTAVA

DEPARTMENT OF PHYSICS, ALLAHABAD UNIVERSITY, ALLAHABAD. (INDIA)

(Received, September 28, 1959)

The crystal structure of Anthrone is determined by means of two dimensional Fourier Synthesis in the 010 plane. This plane is chosen as the molecule is well resolved in projection on this plane according to the trial structure. The space group of anthrone together with other crystallographic data has already been published by Srivastava (1957). However the axial lengths were again determined with the values of Bragg angles, obtained after correcting them for film shrinkage errors by the author's method (Srivastava, 1959). The revised values thus obtained are

$= 15.80 \text{ \AA}; \quad b = 3.998 \text{ \AA}; \quad c = 7.86 \text{ \AA}.$ The space group being $P2_1/a-C_{2h}^5$.

The values of the atomic coordinates which were obtained after the third refinement of F_0 synthesis are given in the table, taking the X and Z coordinates from the projection, and deriving the y coordinates from the standard inter-atomic distances. The value of the reliability index

$$R = \frac{\sum | |F_0| - |F_c| |}{\sum |F_0|}$$

came out to be 0.267.

(The symbol 0 refers to the Oxygen atom and all other letters refer to carbon atoms.)

TABLE I

Atom	X in AU	Y in AU	Z in AU
A'	2.12	3.65	3.10
B'	0.89	3.08	2.67
C'	0.44	2.56	1.34
E	1.33	2.60	0.46
F	2.65	3.18	0.89
G	3.08	3.70	2.14
D	0.98	2.05	-0.93
O	1.70	2.09	-1.61
A	-2.12	0.35	-3.10
B	-0.89	0.92	-2.67
C	-0.44	1.44	-1.34
E'	-1.33	1.40	-0.46
F'	-2.65	0.82	-0.89
G'	-3.08	0.30	-2.14
D'	-0.98	1.95	0.93

The molecule is assumed to be planar, and the origin is chosen at the centre of symmetry. The atomic scattering factors for carbon atoms were taken as

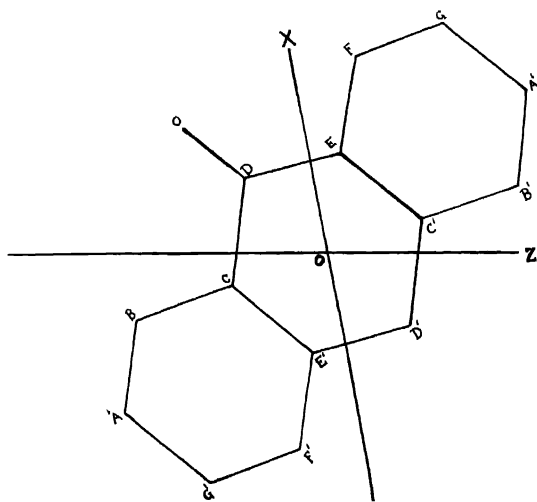


Fig. 1.

those for the general carbon atom for the anthraquinone, and for oxygen atom as that taken in the case of oxygen of anthraquinone by Murty (1957), since the

two structures are strikingly very similar. Refinement of the structure by the Difference Synthesis is in progress.

The author is much indebted to Professor K. Banerjee for his guidance throughout the progress of this work and is thankful to Dr S. C Chakraborty, and Shri S. K Joshi for their help.

REFERENCES

- Murty, B. V. R., 1957, D.Phil. Thesis of Allahabad University.
Srivastava, S. N., 1957, *Indian J. Phys.*, **31**, 644.
Srivastava, S. N., 1959, *Acta Cryst.*, **12**, 412.

10

ON THE CRYSTAL STRUCTURE OF METHANOL AT -180°C

G. S. R. KRISHNA MURTI

OPTICS DEPARTMENT, INDIAN ASSOCIATION FOR THE CULTIVATION OF SCIENCE,
CALCUTTA-32.

(Received, September 30, 1959)

The crystal structure of methanol has been studied by Tauer and Lipscomb (1952) by studying the Weissenberg and precession photographs of the crystal at -110°C and at -160°C . They reported that the crystal has a transition at -115°C the high temperature modification being orthorhombic conforming to the space group D_{2h}^{17} . The Weissenberg photographs taken for the crystal at -160°C show that the low temperature phase consists of small crystallites of low symmetry but not of a single crystal. They observed that the possible unit cell which accounts for all but a few weak reflections is monoclinic with two molecules in the unit cell having dimensions $a = 4.53 \text{ A.U.}$, $b = 4.69 \text{ A.U.}$, $c = 4.91 \text{ A.U.}$ and $\beta = 90^{\circ} \pm 3^{\circ}$. The space group C_{2h}^2 was assigned to the crystal although they suggested the presence of some weak reflections indicating a super lattice. An attempt has been made to find out whether the crystal retains this symmetry at still lower temperatures upto -180°C .

The Debye-Scherrer pattern due to the crystal at -180°C was photographed by the method used earlier (Krishna Murti and Sen, 1956). The spacings calculated from the pattern obtained for the crystal at -180°C are given in Table I. The pattern has been analysed by trial and error method and it has been found that the crystal is monoclinic with the unit cell dimensions as $a = 4.59 \text{ A.U.}$, $b = 4.68 \text{ A.U.}$, $c = 4.92 \text{ A.U.}$ and $\beta = 97^{\circ}30'$. The density of the crystal at -180°C

TABLE I
Spacings of crystals of methanol

at -160°C (Tauer and Lipscomb, 1952)			at -180°C		
Indices	Calculated spacings in A.U.	Observed structure factor (F_o)	Observed spacings in A.U. and Intensities	Calculated	
				spacings in A.U.	Indices
001	4.90	<4	4.86 (m)	4.88	001
100	4.52	9	4.55 (w)	4.55	100
10 $\bar{1}$	3.41	18	3.56 (vw)	3.57	10 $\bar{1}$
011	3.39	18	3.38 (s)	3.38	011
110	3.26	24	3.26 (vs)	3.26	110
101	3.24	18	3.13 (m)	3.13	101
			2.84 (w)	2.84	111
			2.60 (w)	2.60	111
002	2.45	5			
020	2.345	—	2.335 (m)	2.34	020
			2.28 (w)	2.28	201
				2.275	200
200	2.26	5			
021	2.115	<4	2.11 (w)	2.11	021
102	2.11	8		2.05	210
			2.04 (w)	2.04	102
120	2.08	6			
210	2.04	6		1.97	211
201	2.01	9	1.98 (vw)	1.96	201, 121
121	1.93	8			
121	1.90	8	1.87 (w)	1.87	112, 121
			1.82 (w)	1.81	211
022	1.695	4		1.69	022
21 $\bar{2}$	1.64	7	1.68 (w)	1.67	212
003, 220	1.63	4	1.63 (vw)	1.63	12 $\bar{2}$ 220, 003
212	1.53	7		1.52	300
103		6	1.51 (w)		
300	1.51	4		1.51	113, 301
031	1.40	7		1.485	031
130	1.48	7	1.48 (w)	1.43	212, 130
301	1.46	6		1.47	103

is found to be 0.98. The number of molecules in the unit cell is two. The extinction of *oko* for *k* odd places this crystal in the space group C_{2h}^2 or C_2^2 . The agreement between the calculated and observed spacings is shown in Table I.

Thus the space group remains the same at -180°C , but the angle β increases slightly. This increase in the angle β and in the primitive translation along *a*-axis, with lowering of the temperature from -160°C to -180°C , explains the changes in the intensities of reflection observed for certain planes (Table I)

The author is grateful to Professor S. C. Sirkar, D.Sc. F.N.I., for his kind interest and to the National Institute of Sciences of India for the award of a Fellowship.

REFERENCES

- Krishna Murli, G. S. R. and Sen, S. N., 1956, *Ind. J. Phys*, **30**, 242.
Tauer, K. J. and Lipscomb, W. N., 1952, *Acta Cryst*, **5**, 606

ACTION PRINCIPLE AND LAGRANGIAN WITH HIGHER ORDER DERIVATIVES

S. P. MISRA

MATHEMATICS DEPARTMENT, R. COLLEGE, CUTTACK

(Received, July 16, 1959)

ABSTRACT. We have obtained here certain commutation relations of field quantities (field operators and their derivatives) for space-like separation of the points when the Lagrangian density contains derivatives of field operators of order higher than first by using Schwinger's operator principle of Stationary Action. The commutators thus obtained are quite complicated, and the consistency of this procedure can only be discussed in individual cases.

1. INTRODUCTION

In a series of interesting papers, Schwinger has considered quantum field theory in a very general way (Schwinger (1951), (1953) and (1954)). The starting point of this series was a further generalisation of the Action Principle by using the ideas of quantum mechanics. However, all these considerations were confined to the case of a Lagrangian containing only the first order derivative of the field operators. We shall try to generalise this procedure further when the Lagrangian contains derivatives of the field operators of any finite order. We note that this gives rise to a lot of complications even for a single field without spin, and we are able to only write down a number of commutation relations for space-like separation of the field quantities. The consistency of the many such relations that we deduce is not possible to prove; but they are necessary conclusions from the Action Principle and the fundamental ideas of quantum mechanics. We shall have occasion to demonstrate this method in greater detail for the case when the Lagrangian contains only second order derivatives of the field operators and gives rise to a particularly simple type of field equations proposed by Bhabha (1950) and Thirring (1950).

We shall first very briefly outline the Action Principle that we are going to utilise.

Let us consider two space-like surfaces σ_1 and σ_2 on which the dynamical variables are known. On σ_1 and on σ_2 , we construct complete set of commuting observables ξ_1 and ξ_2 respectively which have corresponding eigenvalues ξ_1' and ξ_2' . Thus, we can write the state vectors on the surfaces σ_1 and σ_2 in terms of these eigenvalues as $|\xi_1, \sigma_1\rangle$ and $|\xi_2', \sigma_2\rangle$. The transformation function here is,

$$\langle \xi_1, \sigma_1 | \xi_2, \sigma_2 \rangle$$

A variation of this transformation function is given as

$$\delta \langle \xi'_1, \sigma_1 | \xi_2, \sigma_2 \rangle = i \langle \xi_1, \sigma_1 | \delta W_{12} | \xi_2, \sigma_2 \rangle \quad (1)$$

also

$$\delta W_{13} + \delta W_{32} = \delta W_{12}, \quad \dots \quad (2)$$

$$\delta W_{11} = -\delta W_{31} \quad \dots \quad (3)$$

and

$$\delta W_{12} = \delta W_{12} \quad \dots \quad (4)$$

Since the state vectors on any surface form a complete orthonormal set, when we normalise these state vectors to unity we obtain,

$$\sum_{\xi'} |\xi', \sigma\rangle \langle \xi', \sigma| = 1. \quad \dots \quad (5)$$

Consistent with the properties (2) to (4), we assume that there exists a hermitian function L of the field operators such that

$$W_{12} = \int_{\sigma_1}^{\sigma_2} L(x) dx$$

where

$$\delta W_{12} = \delta(W_{12}).$$

The above L is the Lagrangian density and will give us the complete information about the dynamical system. The operator sets ξ_1 and ξ_2 are similarly constructed from the field variables on the two surfaces σ_1 and σ_2 and in the neighbourhood of these surfaces.

We can get a variation of W_{12} in equation (6) by varying the field operators and their derivatives on the surfaces σ_1 and σ_2 and in the region interior to them, and also by varying the surfaces σ_1 and σ_2 themselves. Now, as a result of such variation, let the new and the old state-vectors be related by the unitary transformation

$$|(\xi + \delta_0 \xi)', \sigma + \delta \sigma\rangle = \bigcup | \xi', \sigma \rangle \quad \dots$$

Writing $\bigcup = \exp(-iF) \simeq 1 - iF$, where $F = F(\xi, \delta_0 \xi; \sigma, \delta \sigma)$ is hermitian and the generator of the infinitesimal transformation on the surface σ due to the above type of variations, we obtain,

$$\delta | \xi', \sigma \rangle = -iF(\xi, \delta_0 \xi; \sigma, \delta \sigma) | \xi', \sigma \rangle$$

which, in conjunction with equation (1) gives us,

$$\delta W_{12} = F(\xi_1, \delta_0 \xi_1; \sigma_1, \delta \sigma_1) - F(\xi_2, \delta_0 \xi_2; \sigma_2, \delta \sigma_2) \quad \dots \quad (7)$$

Now, in postulate (8), we have, (for definiteness, with σ_1 later than σ_2)

$$\begin{aligned}\delta W_{12} &= \delta \int_{\sigma_2}^{\sigma_1} L(x) d^4x \\ &= \int_{\sigma_2}^{\sigma_1} \delta L d^4x + \int_{\sigma_2}^{\sigma_1 + \delta\sigma_1} L d^4x + \int_{\sigma_2 + \delta\sigma_2}^{\sigma_2} L d^4x \\ &= \int_{\sigma_2}^{\sigma_1} \delta L d^4x + \left(\int_{\sigma_1} - \int_{\sigma_2} \right) L \delta x_\mu d\sigma_\mu \quad \dots \quad (8)\end{aligned}$$

where x_μ lying either on σ_1 or σ_2 changes to $x_\mu + \delta x_\mu$ due to the variation of the surfaces, and $d\sigma_\mu = n_\mu d\sigma$ with $d\sigma$ denoting an element of the surface σ and n_μ being the normal to the surface in the time-increasing direction.

2. ACTION PRINCIPLE WHEN THE LAGRANGIAN DERIVATIVES OF ORDER HIGHER THAN THE FIRST

We now proceed to apply the Action Principle to the case when the Lagrangian contains derivatives of the field operators of order higher than the first. We consider for simplicity $L(x)$ to be a function of a single field operator $\phi(x)$ and its derivatives of any finite order. This is not a loss of generality in obtaining the field equations or the commutation rules, as will be clear from what follows. We shall further also restrict our considerations to the case of a scalar or a pseudo-scalar field such that they remain unchanged under rotations, and the complications due to the transformations of field operators with spin are eliminated. Thus we write,

$$L = L(\phi, \partial_\mu \phi, \partial_\mu \partial_\nu \phi, \dots).$$

$$\left(\partial_\mu = \frac{\partial}{\partial x_\mu} \right)$$

Then we obtain δL due to a variation $\delta_0 \phi$ of the field operator ϕ as

$$\delta L = \frac{\partial L}{\partial \phi} \delta_0 \phi + \frac{\partial L}{\partial (\partial_\mu \phi)} \delta_0 (\partial_\mu \phi) + \frac{\partial L}{\partial (\partial_\mu \partial_\nu \phi)} \delta_0 (\partial_\mu \partial_\nu \phi) + \dots \quad \dots \quad (9)$$

We now use the fact that $\delta_0 (\partial_\mu \partial_\nu \dots \phi) = \partial_\mu \partial_\nu \dots (\delta_0 \phi)$ and find, with

$$\partial_\mu \partial_\nu \partial_\lambda \dots (n \text{ times}) = \partial^{(n)}_{\mu\nu\lambda} \dots \quad \dots \quad (10)$$

an n -th order partial differential operator, that, for any function $f_{\mu\nu\lambda} \dots(x)$ symmetric in all its indices,

$$\begin{aligned} f_{\mu\nu\lambda} \dots (x) \partial^{(n)}_{\mu\nu\lambda} \dots (\delta_0 \phi) &= (-1)^n \partial^{(n)}_{\mu\nu\lambda} \dots f_{\mu\nu\lambda} \dots (x) \delta_0 \phi \\ &+ \partial_\mu f_{\mu\nu\lambda} \dots (x) \partial^{(n-1)}_{\nu\lambda} \dots (\delta_0 \phi) \\ &- \partial_\nu f_{\mu\nu\lambda} \dots (x) \partial^{(n-2)}_{\lambda} \dots (\delta_0 \phi) \\ &+ \partial^{(2)}_{\nu\lambda} f_{\mu\nu\lambda} \dots (x) \partial^{(n-3)} \dots (\delta_0 \phi) \\ &- \dots + (-1)^{(n-1)} \partial^{(n-1)}_{\nu\lambda} \dots f_{\mu\nu\lambda} \dots (x) (\delta_0 \phi) \end{aligned} \quad \dots \quad (11)$$

Hence, putting

$$f_{\mu\nu\lambda} \dots (x) \equiv \frac{\partial L}{\partial (\partial_\mu \partial_\nu \partial_\lambda \dots \phi)},$$

we obtain from relations (9) and (11), on rearranging the terms on the right hand side such that the coefficients of $\delta_0 \phi$, $\partial_\mu (\delta_0 \phi)$, ... are conveniently separated in the term with ∂_μ ,

$$\begin{aligned} \delta L &= \left[\frac{\partial L}{\partial \phi} - \partial_\mu \frac{\partial L}{\partial (\partial_\mu \phi)} + \partial_\mu \partial_\nu \frac{\partial L}{\partial (\partial_\mu \partial_\nu \phi)} - \dots \right] \delta_0 \phi \\ &+ \partial_\mu [\pi_\mu (\delta_0 \phi) + \pi_{\mu\nu} \partial_\nu (\delta_0 \phi) + \pi_{\mu\nu\lambda} \partial_\nu \partial_\lambda (\delta_0 \phi) + \dots], \end{aligned} \quad \dots \quad (12)$$

where

$$\begin{aligned} \pi_\mu &= \frac{\partial L}{\partial (\partial_\mu \phi)} - \partial_\nu \frac{\partial L}{\partial (\partial_\mu \partial_\nu \phi)} + \partial_\nu \partial_\lambda \frac{\partial L}{\partial (\partial_\mu \partial_\nu \partial_\lambda \phi)} - \dots, \\ \pi_{\mu\nu} &= \frac{\partial L}{\partial (\partial_\mu \partial_\nu \phi)} - \partial_\lambda \frac{\partial L}{\partial (\partial_\mu \partial_\nu \partial_\lambda \phi)} + \dots \end{aligned} \quad \dots \quad (13)$$

Applying Gauss theorem to the term with ∂_μ in the expression (12), we now obtain from equation (8),

$$\delta W_{12} = \int_{\sigma_1}^{\sigma_2} \left[\frac{\partial L}{\partial \phi} - \partial_\mu \frac{\partial L}{\partial (\partial_\mu \phi)} + \partial_\mu \partial_\nu \frac{\partial L}{\partial (\partial_\mu \partial_\nu \phi)} - \dots \right] (\delta_0 \phi) d^4x + F(\sigma_1) - F(\sigma_2) \quad (14)$$

where

$$F(\sigma) = \int_\sigma [\pi_\mu (\delta_0 \phi) + \pi_{\mu\nu} \partial_\nu (\delta_0 \phi) + \pi_{\mu\nu\lambda} \partial_\nu \partial_\lambda (\delta_0 \phi) + \dots + \delta x_\mu] d\sigma_\mu \quad \dots \quad (15)$$

Comparing expression (14) with (7), the operator* principle of Stationary Action asserts that W_{12} must be stationary for the variation of the field operators in the

interior of the volume bounded by σ_1 and σ_2 . This gives rise to the field equation for the operator ϕ as

$$\frac{\partial L}{\partial \phi} - \partial_\mu \frac{\partial L}{\partial (\partial_\mu \phi)} + \partial_\mu \partial_\nu \frac{\partial L}{\partial (\partial_\mu \partial_\nu \phi)} - \dots = 0 \quad \dots (16)$$

When the field equations are satisfied, we obtain for the variation of W_{12}

$$\delta W_{12} = F(\sigma_1) - F(\sigma_2) \quad \dots (17)$$

with the definition of $F(\sigma)$ given by equation (15). We note that the principle of Stationary Action gives us the same form (7) of δW_{12} as demanded by quantum mechanics

We shall now consider equation (15) in detail, since this is the equation that gives the possible commutation relations and also the energy-momentum tensor. For this purpose we need to write the right hand side integral of equation (15) in terms of the *independent* variations of different quantities on the surface σ . However, we note that once the value of $\delta_0 \phi$ on the surface is determined, the variations $\partial_\mu(\delta_0 \phi)$, $\partial_\mu \partial_\nu(\delta_0 \phi)$, ... are not completely arbitrary, but their variations only in the normal direction are arbitrary. In order to separate the arbitrary increments corresponding to the surface we first define

$$\partial^{(0)} = n_\mu \partial_\mu, \quad \partial_{t\mu} = \partial_\mu + n_\mu \partial^{(0)} \quad \dots (18)$$

such that

$$n_\mu \partial_{t\mu} = \partial^{(0)} + n_\mu n_\mu \partial^{(0)} = 0, \quad (n_\mu n_\mu = -1).$$

We may note that the normal n_μ to a space-like surface is a time-like four-vector, and is exactly defined, with $d^{(0)}x_\mu$ a displacement normal to the surface,

$$n_\mu = \frac{d^{(0)}x_\mu}{\sqrt{(dx_0)^2 - (d\vec{x})^2}}.$$

In equation (18), $\partial_{t\mu}$ indicates the differential operator in the tangential direction at any point of the surface σ , and similarly, $\partial^{(0)}$ indicates the normal (time-increasing) directional derivative at any point. We shall henceforward either take the surfaces σ_1 and σ_2 as plane surfaces, or, as will be sufficient for our purpose, as surfaces such that the tangential derivatives of the normal vanishes upto a sufficiently large but finite order. Let us further introduce the notation for the partial tangential derivative of the k -th order as

$$\partial^{(t,k)}_{\nu\lambda} \dots (k \text{ indices}) \equiv \partial_{t\nu} \partial_{t\lambda} \dots (k \text{ times}) \quad \dots (19)$$

in addition to notation (10). Then, if the Lagrangian density contains upto the N -th order partial derivatives of the field operator, we assume that

$$\partial^{(t,k)}_{\nu\lambda} \dots (n_\mu) = 0 \quad \text{for } 1 \leq k \leq N-1$$

In these notations, of course, the zeroth order partial derivative as usual is the unity operator.

To obtain commutators, we shall also further take that

$$(\partial^{(0)})^k(\delta_0\phi)$$

approaches zero sufficiently rapidly for infinite spatial distances, so that, for any $f_\nu(x)$ on σ ,

$$\int_{\sigma} \partial_{\nu} [f_{\nu}(x)(\partial^{(0)})^k(\delta_0\phi)] d\sigma = 0 \quad \dots (20)$$

whenever

$$k \leq N-1.$$

Now, once we know $(\partial^{(0)})^k(\delta_0\phi)$ on the surface σ , $\partial_{\nu}(\partial^{(0)})^k(\delta_0\phi)$ is determined, and hence only $(\partial^{(0)})^{k+1}(\delta_0\phi)$ is arbitrary. Hence, we shall have to find out the coefficients of $(\partial^{(0)})^k(\delta_0\phi)$. $0 \leq k \leq N-1$, on the right hand side of equation (15), these being independent variations on the surface

Now, with $n \leq N-1$,

$$\begin{aligned} & \int_{\sigma} \pi_{\mu\nu\lambda} \dots (n+1 \text{ indices}) \partial_{\nu\lambda}^{(n)} \dots (\delta_0\phi) d\sigma_{\mu} \\ &= \int_{\sigma} \pi_{\mu\nu\lambda} \overline{(n+1 \text{ indices})} (\partial_{\nu} - n_{\nu} \partial^{(0)}) (\partial_{\lambda} - n_{\lambda} \partial^{(0)}) \dots \text{to } n \text{ factors } (\delta_0\phi) d\sigma_{\mu} \\ &= \int_{\sigma} (-1)^n [\partial^{(t,n)}_{\nu\lambda} \dots \pi_{\mu\nu\lambda} \dots (x)(\delta_0\phi) + \binom{n}{1} n_{\nu} \partial^{(t,n-1)}_{\lambda} \dots \pi_{\mu\nu\lambda} (x)(\partial^{(0)})(\delta_0\phi) + \dots \\ &+ \binom{n}{k} n_{\nu} n_{\lambda} \dots (k \text{ terms}) \partial^{(t,n-k)}_{\alpha} \pi_{\mu\nu\lambda} \dots \alpha \dots (x)(\partial^{(0)})^k(\delta_0\phi) \\ &+ \dots + \binom{n}{n} n_{\nu} n_{\lambda} \dots \pi_{\mu\nu\lambda} \dots (x)(\partial^{(0)})^n (\delta_0\phi)] d\sigma_{\mu} \quad \dots (21) \end{aligned}$$

In deducing equation (21) we have utilised the symmetry of $\pi_{\mu\nu\lambda} \dots$. The consecutive terms from the last backwards of this formula have been obtained by partial integration with the help of equation (20) mentioned earlier.

Thus, in equation (15) we have, collecting coefficients of $(\partial^{(0)})^k(\delta_0\phi)$ separately,

$$F(\sigma)$$

$$\begin{aligned} &= \int_{\sigma} \sum_{n=0}^{N-1} \pi_{\mu\nu\lambda} \dots \overline{(n+1 \text{ indices})} \partial^{(n)}_{\nu\lambda} \dots (\delta_0\phi) d\sigma_{\mu} \\ &= \int_{\sigma} \sum_{n=0}^{N-1} (-1)^n \sum_{k=0}^n \binom{n}{k} n_{\nu} n_{\lambda} \dots (k \text{ terms}) \\ &\quad \times \partial^{(t,n-k)}_{\alpha} \pi_{\mu\nu\lambda} \dots \alpha \dots (x)(\partial^{(0)})^k(\delta_0\phi) d\sigma_{\mu} \end{aligned}$$

$$\begin{aligned}
&= \int_{\sigma} \sum_{k=0}^{N-1} \sum_{n, k}^{N-1} (-1)^{n_{\mu} n_{\lambda}} \dots (k \text{ terms}) \partial_{\alpha}^{(\ell, n-k)} \pi_{\mu \nu \lambda} \dots \alpha \dots (x) (\partial^{(0)} (\delta_0 \phi) d\sigma_{\alpha} \\
&\equiv \int_{\sigma} \sum_{k=0}^{N-1} \pi_{\mu}^{[\sigma, k]}(x) (\partial^{(0)k} (\delta_0 \phi) d\sigma_{\mu} \dots \quad (22)
\end{aligned}$$

where

$$\begin{aligned}
&\pi_{\mu}^{[\sigma, k]} \\
&= \sum_{n=k}^{N-1} (-1)^n \binom{n}{k} n_{\mu} n_{\lambda} \dots (k \text{ times}) \partial_{\alpha}^{(\ell, n-k)} \pi_{\mu \nu \lambda} \dots \alpha \dots (x) \dots \quad (23)
\end{aligned}$$

The $\pi_{\mu}^{[\sigma, k]}$ are the fields conjugate to $(\partial^{(0)})^k \phi$ with $0 \leq k \leq N-1$. When $N=1$ such that we have only $\pi^{[\sigma, 0]}$, there is only one field conjugate to $\phi(x)$.

The fact that $\pi_{\mu}^{[\sigma, k]}(x')$ are conjugate fields can be obtained when we find the commutation relationships of these with the field operators $(\partial^{(0)})^l \phi(x)$ for space-like separation of the points x and x' . To obtain these, we require the variation $\delta_0 \phi(x')$ on the surface and in its immediate neighbourhood (which determines $(\partial^{(0)})^k (\delta_0 \phi) = \delta_0 ((\partial^{(0)})^k \phi)$ on the surface σ as arbitrary variations). Also, we take $\delta x_{\mu} = 0$ so that displacement of the surface is not considered. Now, let any operator G suffer a change $G \rightarrow G + \delta G$ due to this variation. This change in the operator is also associated with the change in the state-vector as we have seen previously. Thus we have,

$$\begin{aligned}
&\delta \langle \zeta', \sigma | G | \zeta'', \sigma \rangle = \langle \zeta', \sigma | \delta G | \zeta'', \sigma \rangle \\
&= (\delta \langle \zeta', \sigma |) G | \zeta'', \sigma \rangle + \langle \zeta', \sigma | G (\delta | \zeta'', \sigma \rangle) \\
&= i \langle \zeta', \sigma | [F(\sigma), G] | \zeta'', \sigma \rangle
\end{aligned}$$

such that

$$[G, F(\sigma)] = i \delta G. \quad \dots (24)$$

Hence, taking $G = (\partial^{(0)})^l \phi(x)$, $0 \leq l \leq N-1$, by equation (24) we get,

$$[(\partial^{(0)})^l \phi(x), F(\sigma)] = i \delta_0 ((\partial^{(0)})^l \phi(x)) \quad \dots (25)$$

where now we have

$$\begin{aligned}
&F(\sigma) \\
&= \int_{\sigma(x)} \sum_{k=0}^{N-1} \pi_{\mu}^{[\sigma, k]}(x') \delta_0 ((\partial^{(0)})^k \phi(x')) d\sigma_{\mu}(x') \quad \dots (26)
\end{aligned}$$

where $\sigma(x)$ is a space-like surface passing through a point x . Equations (25) and (26) are explicitly written as

$$\sum_{k=0}^{N-1} \int_{\sigma(x)} [(\partial^{(0)})^l \phi(x), \pi_{\mu}^{[\sigma, k]}(x') \delta_0 ((\partial^{(0)})^k \phi(x'))] d\sigma_{\mu}(x') = i \delta_0 ((\partial^{(0)})^l \phi(x)). \quad \dots (27)$$

In equation (27), we now take $\delta_0((\partial^{(0)})^l \phi(x))$ on the surface as nonzero only at very small neighbourhood of the point x , and also that $\delta_0((\partial^{(0)})^k \phi(x')) = 0$ for $k \neq l$.

Then we obtain,

$$\begin{aligned} & [(\partial^{(0)})^l \phi(x), \pi_\mu^{[0l]}(x') \delta_0((\partial^{(0)})^k \phi(x'))] \\ & = i \delta_\mu^{(0)}(x-x') \delta_0((\partial^{(0)})^l \phi(x)) \end{aligned} \quad \dots (28)$$

where $\delta_\mu^{(u)}(x-x')$ is the surface δ -function such that for any regular function $f(x')$ defined on the surface,

$$\int_{\sigma(x)} f(x') \delta_\mu^{(u)}(x-x') d\sigma_\mu(x') = f(x) \quad \dots (29)$$

It may be emphasized that this delta function originates since we are at liberty to take arbitrary variations $\delta_0((\partial^{(0)})^l \phi(x'))$ as not equal to zero only at a very small neighbourhood of the point x .

Let us now take $\delta_0((\partial^{(0)})^k \phi(x'))$ as arbitrary where $k \neq l$ and $\delta_0((\partial^{(0)})^l \phi(x')) = 0$. Then we obtain, for $k \neq l$

$$[(\partial^{(0)})^l \phi(x), \pi_\mu^{[0k]}(x') \delta_0((\partial^{(0)})^k \phi(x'))] = 0 \quad \dots (30)$$

Combining equations (28) and (30), we must have, for space-like separation of the points x and x' ,

$$[(\partial^{(0)})^l \phi(x), \pi_\mu^{[0k]}(x') \delta_0((\partial^{(0)})^k \phi(x'))] = i \delta^{kl} \delta_\mu^{(u)}(x-x') \delta_0((\partial^{(0)})^l \phi(x)), \quad \dots (31)$$

where δ^{kl} is the Kronecker delta.

At present we do not have any reason to say that the many commutators in equation (31) are consistent with each other. However, from the Action Principle and basic ideas of quantum mechanics, the above commutators are obtained, and only those fields for which they are self-consistent should be taken.

ACKNOWLEDGMENTS

The author wishes to acknowledge his sincere thanks to Prof. D. Basu, Indian Association for the Cultivation of Science, for suggesting the problem.

REFERENCE

- Schwinger, J., 1951, *Phys. Rev.*, **82**, 914.
Schwinger, J., 1953, *Phys. Rev.*, **91**, 713.

X-RAY SMALL ANGLE MEASUREMENTS ON 1% SOLUTION OF HAEMOGLOBIN CORPUSCULAR PROTEIN

T. RATHO

UTKAL UNIVERSITY, F. M. COLLEGE, BALASORE

(Received, September 14, 1959)

INTRODUCTION

ABSTRACT. The small angle scattering due to 1% solution of haemoglobin in 0.85% solution of NaCl has been investigated. It has been observed that the scattering curve in the region from 600 Å to about 900 Å is fairly horizontal showing the absence of interparticular interference and molecular association

A sample of 1% solution of haemoglobin in 0.85% solution of NaCl from Behring Works, Germany (Handels' product), was investigated with the help of the well-known small angle scattering camera of Prof. Kratky (1958) in order to find out whether any remarkable feature is observable in the innermost portion of the scattering curve. In the case of interparticular interference this part of the curve will slope down, whereas in the case of molecular association the slope will be of the opposite nature.

EXPERIMENT

The experimental arrangement consisted of the well-known small angle scattering camera of Prof. Kratky fitted with a Geiger Muller counter tube together with the beam measuring apparatus of the firm Siemens and Halske. The source of X-radiation was a standard Phillips unit with a tube of copper anticathode. Before proceeding with the measurements on haemoglobin the Siemens apparatus was tested for its stability by taking a standard solution of colloidal gold as the scatterer. The beam-intensity was kept constant by stabilising the primary voltage supplied to the X-ray unit. Keeping the diffracting angle constant the intensity of the scattered ray was measured by using a nickel filter. By registering 6000 impulses each time over consecutive intervals of time it was found that the experimental fluctuation of intensity was in the neighbourhood of the statistical value $100/\sqrt{6000}$ in percentage, thus proving the stability of the apparatus. The natural counts due to cosmic rays were very much reduced by surrounding the counter tube with a very thick cylinder of lead. In order to prove the accuracy of the whole arrangement the full scattering curve of colloidal

gold in mandol oil was obtained by the filter difference method. This curve was compared with the curves, after reduction to proper scale, obtained by anti-coincidence measurements of M. Bishop and by photographic-photometer measurements of Dr. Krutz. The superposition of the later two curves with the one obtained in the present procedure showed very good agreement among them thus providing the accuracy of the adjustment. Measurement of the sample 1% solution of haemoglobin in NaCl was now undertaken. The blind curve with 0.85% solution of NaCl in a mark capillary of 0.75 mm diameter was first obtained by using Co and Ni filters. Then the same capillary was used as the container for 1% solution of haemoglobin in 0.85% solution of NaCl and the curve due to the sample was obtained. The difference-curve gives the scattering due to the pure sample itself. As haemoglobin is very sensitive all arrangements were made to keep the temperature of the sample constant throughout the measurements by using a good refrigerator for cooling the whole chamber. A fresh solution from Behring Works Germany was thus examined.

RESULTS AND DISCUSSION

The blind measurements due to 0.85% solution of NaCl are given in Table I, and the corresponding curve B is shown in figure 1. Table II gives the measurements due to 1% solution of haemoglobin in 0.85% solution of NaCl, the relative curve is marked as P in the above figure. Curve D is the difference curve i.e., the scattering due to the protein molecules themselves. It is evident from figure

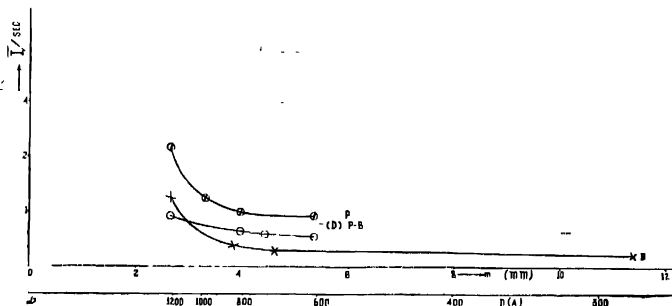


Figure 1.

1 that the difference curve runs horizontal from about 900 Å to 600 Å. The true nature of the scattering curve with low concentration is therefore purely due to particle scattering and is in good agreement with the theory of Debye (1915). Thus there is no interparticular interference nor any molecular association. A very small rise in the scattering curve at about 1200 Å is probably due to small

amounts of association. It is rather very difficult to ascertain the exact nature of the curve in the close vicinity of 1200\AA (Kratky, 1958) as this is the lowest approachable limit of the improved types of cameras. Further measurements are necessary to check up the curve in this region

TABLE I

Blind measurements for 1% haemoglobin in 0.85% solution of NaCl.

Z_H	$m(mm)$	I	t	I/t	Ni-Co	Filter
441	1.16	837	900	0.93	0.33	
371	0.46	927	900	1.03	0.35	
361	0.36	1000	900	1.12	0.46	Ni
352	0.27	2162	900	2.40	1.24	
441	1.16	539	900	0.60		
371	0.46	612	900	0.68		
361	0.36	504	900	0.66		Co
352	0.27	1044	900	1.16		

$S_1 = 5/100$ mm. $S_1' = 10$ mm. $S = 7/100$ mm. $S' = 8$ mm. $Z_{H_0} = 328.5$

TABLE II

Sample, 1% Haemoglobin in 0.85% NaCl

Z_H	$m(mm)$	I	t	I/t	a.R.	Ni-Co	Remark*
352	0.27	2.10^4	5290	3.78		2.21	
358	0.33	2.10^4	8380	2.30		1.18	Ni
365	0.40	1.10^4	4566	2.19		1.01	
361	0.40	1.5×10^4	3966	3.78		...	$S = 16/100$
375	0.54	1.10^4	2793	3.58	2.071	0.97	$F = 0.579$
352	0.27	2.10^4	12732	1.57			Co
358	0.33	2.10^4	16581	1.21			
365	0.40	1.10^4	8475	1.18			
361	0.40	1.5×10^4	8502	1.76	$S = 16/100$
375	0.54	1.10^4	6080	1.64	1.10		$F = 0.6701$

* Filter, Slit width, Reduction factor (F). a.R. = after reduction.

$S_1 = 5/100$ mm. $S_1' = 10$ mm. $S = 7/100$ mm. $S' = 8$ mm. $Z_{H_0} = 328.5$.

$$m = Z_H - Z_{H0} + S/2$$

m is measured in mm. It is the height of the center of the counter window from the center of the direct beam.

$$m = \chi a/D$$

a — distance of the film or the counter tube from the scatterer.

χ = wave length.

D = Bragg's value in Å.

Z_H = Height of the counter tube.

Z_{H0} = Zero position of the counter tube i.e., the center of the primary beam.

S = Width of the slit of the counter window

S' = Length of the slit of the counter window.

S_1 = Width of the entrance slit.

S'_1 = Length of the entrance slit

\tilde{I} = Verschmierte intensity measured in impulses, (Intensity not corrected for collimation error.)

ACKNOWLEDGMENTS

This work was done in the Institute of Physical Chemistry, University of Graz, Austria, under the guidance of Prof Dr. O. Kratky to whom my sincere thanks are due

REFERENCES

- Debye, P., 1915. *Ann. Physik*, **46**, 809.
 Kratky, O. and Scala, Z., 1958, *Z. für Elektrochemie*, **62**, part 1, 73.
 Kratky, O. and Porod, G., 1949. *J. Of colloidal Science*, **4**, 35.
 Kratky, O., 1958, *Z. für Elektrochemie Bd.*, **62**, Heft. 1.
 Porod, G. and coworkers, 1957, *Z. für Elektrochemie, Bd.*, **61**, Heft. 10.
 Ratho, T., 1959 Doctorate Thesis, University of Graz.

SPECTROSCOPIC CONSTANTS OF MOLECULES VII. RELATION BETWEEN FORCE CONSTANT AND EQUILIBRIUM INTERNUCLEAR DISTANCE FOR HYDRIDE DIATOMS

YATENDRA PAL VARSHNI, SHASHANKA SHEKHAR MITRA* AND
RAMESH CHANDRA SHUKLA

DEPARTMENT OF PHYSICS, ALLAHABAD UNIVERSITY, ALLAHABAD

(Received, May 15, 1959)

ABSTRACT For hydride diatoms a relation between the force constant k_r and equilibrium internuclear distance r_e has been suggested: $k_r r_e^3 = C$, where C is a constant depending on the type of the linkage. The validity of the relation for ground and excited states of various hydride diatoms has been examined

INTRODUCTION

It is well known that in a particular molecule the force constant and the internuclear distance vary in an inverse fashion, and numerous relations have been suggested connecting the two. Recently Varshni (1958) has given a brief survey of the different relations (see also Baughan, 1957). In the present paper we will investigate a formula connecting k_r and r_e for all states (ground as well as excited) of the various hydride diatoms.

Hydride diatoms differ somewhat from other diatoms in the fact that they show regular variation in properties, not only in a molecular group, but also in is molecular period (Clark 1936, Clark and Stoves 1936, Berriman and Clark 1938, Clark 1950a,b, Sheline 1950). The same is true for deuterides (Clark 1949,

TABLE I

Nomenclature	Diatoms covered
$s\sigma$	HH, 1a-II, 1b-H
$d\sigma$	CaH, SrH, BaH
$p\sigma$	BeH, MgH, ZnH, CdH, HgH, 3b-H
$p\pi$	4b-H, 5b-H, 6b-H, 7b-H
$7a-H$	MnH, etc.
$8-H$	CoH, NiH, etc.

* Now at Division of Pure Chemistry, National Research Council, Ottawa, Canada,

1950b). Clark (1936) has classified hydride diatoms and diatom ions according to the type of linkage. As we will make use of his classification, we summarize it in Tables I (neutral hydrides) and II (ionized hydrides).

TABLE II

Nomenclature	Diatoms covered
$s\sigma$	BeH ⁺ , MgH ⁺ , ZnH ⁺ , CdH ⁺ , HgH ⁺
$p\sigma$	3b-H ⁺ , 4b-H ⁺
$p\pi$	5b-H ⁺ , 6b-H ⁺ , 7b-H ⁺

Clark's classification of MnH is uncertain, and he has not classified CoH and NiH. We have put the last two together.

The various relations which have been proposed between k_r and r_e have been given by Herzberg (1950) and Varshni (1955, 1958). Here we quote only a few of them, which have been applied on sufficient number of hydrides.

Badger (1934) :

$$k_r(r_e - d_{ij})^3 = \text{const} \quad \dots (1)$$

where d_{ij} is a constant depending on molecular period.

Clark (1935) .

$$\omega_e r_e^3 n^{\frac{1}{2}} = k - k' \quad \dots (2)$$

where n is the group number, equal to the total number of valency electrons of the atoms concerned (e.g. 2 for H_2 , 5 for CH etc.), and $(k - k')$ is a constant.

Allen and Longair (1935) :

$$k_e r_e^6 = \text{const.} \quad \dots (3)$$

where the constant is assumed to be the same for all molecules of a molecular period.

Huggins (1935, 1936) .

$$r_e = r_{12} - (2.303 \log C)/a \quad \dots (4)$$

where

$$C = 5.85 \times 10^{-6} \mu \omega_e^2 / (a^2 - aa')$$

$$a' = (2.0625a^2 + 0.7154 \mu \omega_e x_e)^{\frac{1}{2}} - 1.75a$$

Clark and Stoves (1939) have compared the above four equations. Their calculations of r_e by various formulae on about 50 states of hydride diatoms and diatom ions showed that Clark's formula gives the best results.

NEW FORMULA

Birge (1925) and Mecke (1925) have observed that for the different electronic states of one and the same molecule, the following relation holds :

$$\omega_e r_e^2 = \text{const.} \quad \dots (5)$$

It has been found that a modification of this relation can be successfully used for hydride diatoms and diatom ions for ground as well as excited states.

The modified relation is

$$k_e r_e^4 = C = \text{constant} \quad (6)$$

The constant depends on the type of binding and the molecular period to which that diatom in question belongs

The values of C , for neutral diatoms (when k_e is in 10^5 dynes/cm. and r_e in Angstroms), for different types of binding as classified by Clark (1936), have been given in Table III.

TABLE III

Period	Type of binding					
	$s\sigma$	$p\sigma$	$p\pi$	$d\sigma$	$7\sigma-H$	$8\ H$
HH	2.03					
KH	6.634	7.2	6.8			
LH	9.91	11.4	13.5			
MH	14.56			15.1	11.63	11.035
$\bar{M}H$	9.9	10.4	16.45			
NH	16.16			18.7		
NH	12.1	12.7	20.79			
OH	18.08			20.4		
OH	14.9	13.4	17.1			

Values of the constant C for ionized hydrides have been tabulated in Table IV

TABLE IV

Period	Type of binding		
	$s\sigma$	$p\sigma$	$p\pi$
HH ⁺	1.973		
KH ⁺	7.80	6.75	5.466
LH ⁺	11.95	10.52	10.08
MH ⁺	10.3		
NH ⁺	12.7		
OH ⁺	14.2		

Clark's equation was tested by Clark and Stoves (1939) by using the molecular constants then available. Some of these values have changed, in some

cases appreciably, with improved determinations in recent years. Hence to see the relative merits of our equation and that of Clark, it was necessary to re-determine the constant in Clark's equation. The new values of $(k-k')$ are shown in Tables V and VI.

The constants ' C ' and $(k-k')$ were determined as follows

Equation (6)—In most of the cases, constant C was determined by taking the mean value of $k_e r_e^{-4}$ of the states of a particular type of binding (in some cases the 4th significant figure has been rounded up). But states showing abnormal value of $k_e r_e^{-4}$ were left out, viz., one state in each of LiH, NaH, KH, RbH, CsH, CaH, SrH, and CH⁺.

Clark's equation (2)—The constant $(k-k')$ was also determined by taking the mean of $\omega_e r_e^{-3n^2}$ of the states of a particular type of binding, except the following cases—ground state of H₂, 1 excited state in each of alkali hydrides, CaH and SrH. This point is discussed more fully later on

Numerical results by the two equations have been reported in Tables VII and VIII where only one state was available for determining the constant, 'calculated r_e ' has been omitted. Uncertain values are enclosed in parentheses. Percentage errors in brackets have not been taken into account for calculating average percentage errors.

RESULTS

All data have been taken from Herzberg (1950). Data in square brackets refer to the lowest vibrational level, or the two lowest, or three lowest. Usually we have not considered such states, tabulated by Herzberg, for which the constants appear to be too much uncertain.

TABLE V
Constant $(k-k')$ for neutral hydride diatoms
(ω_e in cm⁻¹ and r_e in Å.)

Period	Type of binding					
	$s\sigma$	$p\sigma$	$p\pi$	$d\sigma$	$7a-H$	$8-H$
HH	3899					
KH	8066	8636	8952			
LH	11139	13756	17005			
MH	15740			17419	21867	19689
MH	8849	11346	21188			
NH	17569			20426		
NH	10460	15683	26957			
OH	19540			22757		
OH	11297	15994	23768			

TABLE VI
Constant ($k-k'$) for hydride diatom ions

Period	Type of binding		
	$s\sigma$	$p\sigma$	$p\pi$
H Γ^+	2736		
KH $^+$	7896	7529	7886
LiH $^+$	11840	11847	15420
MH $^+$	9579		
NH $^+$	11557		
OH $^+$	11377		

TABLE VII
Hydride Diatoms

Period	Diatom and type	State	Eq. (6) This paper						Clark eqn.		
			ω_e	k_e	r_e obs.	r_e calc.	% Error	r_e calc.	% Error		
III	H ₂ <i>sσ</i>	<i>v</i>	(2339)	(1.625)	(1.072)	1.057	-1.41	1.056	-1.49		
		<i>w</i>	2322	1.601	1.057	1.061	+0.38	1.059	+0.19		
		<i>k</i>	2336	1.620	1.067	1.058	-0.84	1.057	-0.94		
		<i>h</i>	2395.2	1.702	1.045	1.045	0	1.048	+0.29		
		<i>d</i>	2371.6	1.669	1.050	1.051	+0.09	1.052	+0.19		
		<i>e</i>	2195.8	1.431	1.107	1.091	-1.44	1.079	-2.53		
		<i>a</i>	2664.8	2.107	0.9887	0.9908	+0.21	1.012	+2.36		
		<i>c</i>	2465.0	1.803	1.038	1.030	-0.77	1.038	0		
		<i>D</i>	2325.1	1.604	1.034	1.060	+2.51	1.059	+2.42		
		<i>J</i>	[2220]	[1.463]	(1.077)	1.085	+0.74	1.075	-0.19		
		<i>I</i>	2265.2	1.523	1.060	1.074	+1.32	1.068	+0.75		
		<i>H</i>	2588.9	1.989	1.012	1.005	-0.69	1.021	+0.89		
		<i>G</i>	2442.7	1.771	1.033	1.035	+0.19	1.041	+0.77		
		<i>B</i>	1356.9	0.5467	1.293	1.388	+7.35	1.267	-2.01		
		<i>A</i>	1395.2	5.735	0.7417	0.7713	+3.99	0.856	(+15.41)		
	KH	LiH <i>sσ</i>	<i>A</i>	* 231.11	0.02851	2.596	3.906	(+50.46)	2.898	(+11.63)	
			<i>X</i>	1405.65	1.025	1.595					
		BeH <i>pσ</i>	<i>B</i>	[2133.1]	[2.430]	[1.321]	1.312	-0.08	1.327	+0.45	
			<i>A</i>	2087.7	2.317	1.333	1.327	-0.45	1.337	+0.30	
		BH <i>pσ</i>	<i>X</i>	2058.6	2.262	1.343	1.336	-0.52	1.343	0	
			<i>B</i>	(2400)	(3.132)	1.215	1.231	+1.32	1.216	+0.08	
		CH <i>pσ</i>	<i>I</i>	(2344)	(2.987)	1.226	1.246	+1.63	1.226	0	
			<i>X</i>	(2366)	(3.045)	1.232	1.240	+0.65	1.222	-0.81	
		CH <i>pπ</i>	<i>C</i>	2824.1	4.366	1.113	1.117	-0.36	1.123	+0.90	
			<i>B</i>	2512.5	3.539	1.186	1.178	-0.67	1.163	-1.94	
			OH	<i>I</i>	2921.0	4.672	1.103	1.098	-0.45	1.124	+1.90
				<i>X</i>	2861.6	4.485	1.120	1.110	-0.80	1.119	-0.09
				<i>C</i>	2612	3.777	[1.125]	1.158	+2.93	1.119	-0.53
<i>pπ</i>	<i>I</i>			(3300)	(6.030)	1.037	1.030	-0.67	1.035	-0.19	
	<i>a</i>			[3186]	[5.619]	[1.044]	1.049	+0.48	1.047	+0.29	
<i>X</i>	<i>A</i>			(3300)	(6.030)	1.038	1.030	-0.77	1.035	-0.29	
	<i>I</i>			3180.6	5.648	1.0121	1.047	+3.46	1.021	+0.88	
<i>pπ</i>	<i>X</i>			3735.2	7.791	0.9706	0.9665	-0.42	0.9676	-0.31	
	<i>X</i>			4138.5	9.654	0.9171	0.9171	-0.11	0.9145	-0.28	
<i>pπ</i>											
3											

TABLE VII (contd.)

Period	Diatom and type	State	ω_e	k_e	r_e obs.	Eq. (6) This paper		Clark eqn.	
						r_e calc.	% Error	r_e calc.	% Error
OH	CsII	A	204.0	0.02451	3.869	5.212	(+34.71)	4.076	(+5.35)
	s σ	X	890.7	0.4673	2.494				
	BaH	C	1323	1.031	2.18	2.109	-3.21	2.149	-1.42
	d σ	K	1231	0.8928	2.198	2.186	-0.55	2.202	+0.18
		B	1088	0.6977	2.271	2.326	+2.42	2.294	+1.01
		X	1172	0.8097	2.232	2.241	+0.40	2.238	-0.27
$\bar{\text{O}}\text{H}$	AuH	A	1669.5	1.646	1.673	1.735	+3.71	1.685	+0.72
	s σ	X	2305.0	3.136	1.524	1.477	-3.08	1.513	-0.72
	Li ₂ H	A	2065.8	2.522	1.586	1.518	-4.29	1.647	+3.85
	p σ	X	1387.09	1.137	1.740	1.853	+6.50	1.881	+8.10
	TiH	C	[1269.5]	[0.9519]	1.944	1.936	-0.41	1.847	-4.99
	p σ	X	1390.7	1.142	1.877	1.851	-1.39	1.792	-4.53
	PbII	X	1564.1	1.444	1.839	1.855	+0.87	1.894	+2.99
	p π								
	BiH	C	[1313.6]	[1.019]	1.96	2.024	+3.06	1.947	-0.66
		B	(1728)	(1.763)	1.780	1.765	-0.84	1.777	-0.17
	p π	A	1739.4	1.786	1.788	1.759	-1.62	1.774	-0.78
		X	1898.9	1.706	1.809	1.779	-1.66	1.788	-1.16
Average							+1.48	1.20	

TABLE VIII
Hydride diatom—ions

Period	Diatom and type	State	ω_e	k_e	r_e obs.	Eq. (6)		Clark eqn.	
						r_e calc.	% Error	r_e calc.	% Error
HH ⁺	HH ⁺	X	2297	1.563	1.060				
	s σ								
KH ⁺	BeH ⁺	A	1476.1	1.163	1.609	1.609	0	1.558	-3.17
	s σ	X	2221.7	2.636	1.312	1.311	-0.08	1.360	+3.66
	BH ⁺	A	(2235)	(2.717)	1.256	1.255	-0.08	1.248	-0.64
	p σ	X	(2435)	(3.226)	1.215	1.203	-0.99	1.213	-0.16
	CH ⁺	A	1850.0	1.875	1.234	1.377	(+11.59)	1.267	+2.67
	p σ	X	[2739.5]	[4.111]	1.131	1.131	0	1.112	-1.68
	OH ⁺	X	[2955]	4.875	1.029				
LiH ⁺	MgH ⁺	A	1132.7	0.731	2.006	2.011	+0.25	1.948	-2.89
	s σ	X	1695.3	1.638	1.649	1.643	-0.36	1.703	+3.27
	AlH ⁺	A	(1753)	(1.758)	1.591	1.564	-1.70	1.574	-1.07
	p σ	X	(1610)	(1.483)	1.602	1.632	+1.87	1.620	+1.12
	CH ⁺	A	1605.8	1.488	1.514	1.613	+6.54	1.537	+1.52
	p π	X	2675.4	4.130	1.315	1.250	-4.94	1.206	-1.44
MH ⁺	ZnH ⁺	A	1365	1.089	1.716	1.754	+2.21	1.706	-0.58
	s σ	X	1916	2.146	1.514	1.480	-2.25	1.523	+0.59
NH ⁺	CdH ⁺	A	1252	0.9223	1.865	1.927	+3.32	1.869	+0.21
	s σ	X	1775	1.855	1.667	1.617	-3.00	1.664	-0.18
$\bar{\text{O}}\text{H}^+$	HgH ⁺	A	1621.0	1.552	1.092	1.739	+2.78	1.706	+0.83
	s σ	X	2033.9	2.442	1.594	1.552	-2.63	1.581	-0.82
Average							+1.94	1.47	

DISCUSSION

Equation 6—When the values are calculated according to equation 6, it will be observed that, except the eight cases where the percentage errors are large ($>10\%$) (errors shown in parentheses), the agreement between the calculated and the observed values is quite satisfactory. The mean percentage error for 80 states of neutral diatoms is 1.48 and that for 17 states of ionized diatoms 1.94.

But when they are calculated according to Clark equation (2) the results are slightly better than our equation. The mean percentage error for 79 states of neutral diatoms is 1.29 and that for 18 states of ionized diatoms 1.47. Errors enclosed in brackets have not been taken into account for calculating the mean percentage errors.

TABLE IX

Formula	No of neutral diatom states	Average % error	No of diatom ion states	Average % error	Total no of states	Average % error
Equation 6 (Present work)	80	1.48	17	1.94	97	1.56
Clark eqn. 2	79	1.29	18	1.47	97	1.33
From Clark and Stoves' paper.						
Allen-Longan	41	4.41	11	6.24	52	4.79
Badger	41	3.37	11	4.53	52	3.61
Huggins	41	2.60	11	2.36	52	2.55
Clark	39	1.17	10	1.48	49	1.23

The percentage errors by the two equations are summarized in Table IX. To give some idea of the results by other equations, average percentage errors for the different equations as calculated from the results given in Clark and Stoves (1939) paper are also given in Table IX. Their results on deuterides and excited states of alkali hydrides were left out. It may be emphasised that these results refer to the molecular constants then available.

Force constants of corresponding states of isotopic molecules are same and the internuclear distances are also almost the same (r_e for hydrides and corresponding deuterides rarely differ by more than 0.001Å). Hence formula (6) will be equally applicable to isotopic molecules like deuterides.

The cases for which large percentage errors have been found are interesting.

Alkali hydrides—For the sake of uniformity the values of constants in both equations were found from the ground state only. The percentage errors for the excited states are shown in Table X.

TABLE X

Diatom	State	% error Eq. (6)	% error Clark eqn.
LiH	A	+50.46	+11.63
NaH	A	+14.22	— 8.42
KH	A	+23.82	— 1.97
RbH	A	+24.89	— 0.14
CsH	A	+34.71	+ 5.35
CaH	D	—19.46	—21.34
SrH	D	—20.42	—23.55

It is known that all the five excited states of alkali hydrides are abnormal in that their $\omega_e x_e$ is negative. The coincidence that equation (6) gives uniformly high positive errors for them is of some significance.

CaH and SrH—Both C and D states of these are known to show strong perturbations. Both the equations give high negative errors for state D (Table X) of each. Corresponding state of BaH has not been observed. It may be that when this state is observed, it may also show perturbations.

One state of CH⁺ gives large error by eq. (6) and so is the case for the ground state of H₂ by Clark equation.

Finally, from these and the previous results it may be concluded that Clark equation still retains its best merit with equation (6) giving a much closer approach to it than others.

ACKNOWLEDGMENTS

One of the authors (Y.P.V.) is thankful to the U.P. Scientific Research Committee for a research grant. Thanks are also due to Mr. S. N. Srivastava for checking some of the results.

REFERENCES

- Allen, H. S. and Longair, A. K., 1935, *Phil. Mag.*, **19**, 1032.
 Badger, R. M., 1934, *J. Chem. Phys.*, **2**, 128.
 Baughan, E. C., 1957, *Trans. Faraday Soc.*, **53**, 1046.
 Borriman, R. W. and Clark, C. H. D., 1938 *Proc. Leeds Phil. Soc.*, **3**, (8), 465.

- Birge, R. T., 1925, *Phys. Rev.*, **25**, 240 (Formula quoted by Morse, P. M., 1929, *Phys. Rev.*, **34**, 57)
- Clark, C. H. D., 1935, *Phil. Mag*, **19**, 476.
- Clark, C. H. D., 1936, *Proc. Leeds Phil. Soc.*, **3**, (4), 218.
- Clark, C. H. D., 1949, *Proc. Leeds Phil. Soc.*, **5**, 244.
- Clark, C. H. D., 1950a, *Nature*, **165**, 1011.
- Clark, C. H. D., 1950b, *Proc. Leeds Phil. Soc.*, **5**, 318.
- Clark, C. H. D. and Stoves, J. L., 1936, *Proc. Leeds Phil. Soc.*, **3**, (4), 221.
- Clark, C. H. D. and Stoves, J. L., 1939, *Phil. Mag.*, **27**, 389.
- Hatzberg, G., 1950, Spectra of Diatomic Molecules (D Van Nostrand Co. Inc., New York).
- Huggins, M. L., 1935, *J. Chem. Phys.*, **3**, 473.
- Huggins, M. L., 1936, *J. Chem. Phys.*, **4**, 308.
- Mecke, R., 1925, *Z. Phys.*, **32**, 823.
- Sheline, R. K., 1950, *J. Chem. Phys.*, **18**, 927.
- Varshni, Y. P., 1955, Thesis, Allahabad University.
- Varshni, Y. P., 1958, *J. Chem. Phys.*, **28**, 1081.

STUDIES ON THE MAGNETIC SUSCEPTIBILITY OF SOME V^{3+} ALUMS AND Ti^{3+} CAESIUM ALUM IN THE RANGE 300°K TO 100°K

S. K. DUTTA-ROY, A. S. CHAKRAVARTY AND A. BOSE

INDIAN ASSOCIATION FOR THE CULTIVATION OF SCIENCE, CALCUTTA-32

(Received, October 31, 1959)

ABSTRACT The paper describes the details of the difficult process of obtaining large single crystals of four alums of V^{3+} and one of Ti^{3+} and the measurements of their magnetic susceptibility in the range 300° to 100°K. All the salts are apparently found to obey Curie law very well. But a theoretical analysis of the data on modern lines shows that in all the salts variations of the effective mean moment square P_f^2 with temperature are to be expected owing to (1) change in the trigonal crystalline splitting with temperature and (2) change in the Boltzmann distribution of the population of the different close lying levels with temperature. Evidently, the variations in the liquid air range are not sufficient to produce a deviation from linearity of $P_f^2 - T$ curves, though deviations in their slopes against T axis as also the intercepts with P_f^2 axis from the theoretical expectations are observed. In Ti^{3+} the change in crystalline field with temperature is considerable at very low temperatures. In V^{3+} alums there is also an appreciable change in crystalline fields from one salt to another.

1. INTRODUCTION

In an earlier paper, one of us (Dutta-Roy, 1956) has discussed the dependence of the crystalline electric fields on the change in structure, in a large number of Cr^{3+} alums. It was found that the mean susceptibility at room temperature changed quite appreciably from one class of alum to another and in a given alum with temperature owing to a phase change of some sort taking place.

The isomorphous V^{3+} and Ti^{3+} alums are expected to behave in a much more complicated way than the Cr^{3+} alums, since in both the former cases triplet orbital states lie lowest in the crystalline Stark pattern as against a singlet for Cr^{3+} . As such, in the former the additional *induced* distortion of the Jahn-Teller cluster arising from distant atoms should be of about the same importance as the primary Jahn-Teller distortion itself, in producing the anisotropy of the cluster (Van Vleck, 1939) whereas, in Cr^{3+} the effect of the distant atoms is practically the only one.

In the present paper we have measured very accurately the mean susceptibilities of four V^{3+} alums containing the alkali cations NH_4^+ , Rb^+ , Tl^+ and Cs^+ and the Cs^+ alum of Ti^{3+} , all with SO_4^{2-} as acid radicals, with the help of the refined techniques of magnetic measurements described in details in an earlier paper

(Dutta-Ray, 1955 ; also Thesis 1958). Only a summary of the main points of note 2st in the experiments are given here and also the details of the rather difficult technique of preparation of the salts.

2. METHOD OF PREPARATION OF THE ALUMS

(a) *V³⁺ alums*. A solution of $V_2(SO_4)_3$ in water when exposed to air is very easily oxidised to vanadyl sulphate, so that the usual method of crystallisation, by evaporation of aqueous solutions of equimolecular proportions of component salts in air, cannot be adopted. Even the product sold in bottles as vanadic sulphate really consists nearly entirely of vanadyl sulphate. Hence, we have adopted the electrolytic method for reducing V^{4+} to V^{3+} in an electrolytic cell modified to suit our requirements. The electrolytic cell consisting of a 250 c.c. pyrex beaker is divided into an inner anode and an outer cathode chamber by a small unglazed porcelain pot passing through a stopper closing the mouth of the beaker. A platinum strip about 6 cm. \times 2 cm. and a closely wound platinum spiral of $\frac{1}{8}$ mm. diam. wire, 1 cm. spiral diameter and 6 cm. length are used as cathode and anode respectively. A continuous stream of CO_2 is circulated in the cathode chamber throughout the entire operations following. The anode chamber contains dilute H_2SO_4 (100 c.c. of water and 25 c.c. of 50% acid) and the cathode chamber contains a nearly saturated solution of equimolecular proportion of vanadyl sulphate and an alkali sulphate (NH_4 , Rb, Tl or Cs as the case may be) very carefully prepared in oxygen free water, filtered and acidulated with about 1 c.c. of dilute H_2SO_4 (same strength as above). The electrolytic cell is kept inside an ice bath and during the whole operation the temperature is never allowed to rise above 5°C. About 0.4 amps. of current taken from a 6 volt storage cell is passed through the cell.

Soon reddish violet crystals of the alum as observed in transmitted light, appear in the cathode chamber, and after about 4 hours of operation sufficient quantity of microcrystals for our purpose is deposited. These are removed from the solution and washed with ice-cold acetone. The crystals are dried and then dissolved in oxygen free cold water at about 10°C, just below saturation. The solution is transferred to two or three small clean crystallizing dishes and allowed to crystallize in a desiccator filled with CO_2 using conc. H_2SO_4 as desiccant, placed in a vibration free ice-box in which the temperature is maintained at about 5°C. After about 24 hours a few large (5 mm across) well developed octahedral single crystals of the alum may be picked up from the solution. The crystals are washed with ice cold acetone and after drying dipped in a dilute solution of collodion for protection. The crystals are tested under polarizing microscope and immediately used for magnetic measurements in the cryostat. It is noted that the NH_4 and Tl alum crystals show a tendency to melt in their water of crystallization near room temperature and also of decomposing comparatively quickly, and hence the collodion coating and quick action in measurements are essential near this

temperature. The Rb and Cs salts are much more stable and can be preserved in CO_2 atmosphere even at room temperatures and without coating for a few months. The crystals can be preserved indefinitely in sealed tubes containing CO_2 in a refrigerator. With due precautions no change in the crystals have been observed in the course of several hours, which are needed to finish a series of magnetic measurements, as shown by the reproducibility of the curves for the data with falling and rising temperatures.

(b) Ti^{3+} alums. We could prepare only one of these, namely, the titanium caesium sulphate alum. For the preparation of this alum, the basic material required is titanous acid hydrate, which is prepared by precipitation from a solution of TiCl_3 in dilute HCl with NH_4OH . The precipitate of $\text{Ti}(\text{OH})_3$ is carefully washed several times with warm water to ensure complete removal of NH_4Cl . The precipitate is then heated to about 80°C and dried in a vacuum desiccator and a weighed quantity of it is dissolved in $(4N)\text{H}_2\text{SO}_4$. The reduction of Ti^{4+} to Ti^{3+} is done in an electrolytic cell as in the case of V^{3+} alums in CO_2 atmosphere, using a current of 0.2 amperes for about 12 hours, keeping the temperature at about 0°C with a low salt content freezing mixture. The complete reduction is marked by the change of the colourless solution to violet and also a rapid fall in the cell current.

The alum is prepared by adding equimolecular proportion of Cs_2SO_4 to the reduced solution. A slow current of CO_2 is passed through the solution to prevent oxidation. The alum is then precipitated from the solution with ice-cold acetone and filtered in a suction filter. The precipitate is next boiled in dilute H_2SO_4 (100 c.c. of water in 25 c.c. of 20% H_2SO_4) in CO_2 atmosphere. The precipitate is thus dissolved and CO_2 bubbled through solution till the solution is clear violet. The solution is then transferred back to the electrolytic cell and a small current is passed for 2 to 3 hours to ensure complete reduction in case some titanous salt had been formed during previous operations. The solution is then transferred to a flat bottom conical flask and CO_2 bubbled through it for a little while. The flask is then put in a CO_2 filled desiccator with conc. H_2SO_4 as desiccant and the whole put away in the ice box for crystallisation. After about 48 hours small shining deep violet crystals of the alum appear at the bottom. The bigger crystals about 3mm. across are picked out, washed with acetone, coated with a thin layer of collodion and are immediately used for magnetic measurements. The time required for a complete low temperature run for magnetic measurements did not decompose the crystals appreciably, as shown by the reversibility and reproducibility of the data curve.

3. A SUMMARY OF THE EXPERIMENTAL TECHNIQUES FOR SUSCEPTIBILITY MEASUREMENT

A modified form of Curie balance, consisting of a light thin horizontal glass tube suspended near the middle with a fine vertical quartz fibre attached at the

upper end to a graduated vernier torsion head (reading to 0.1°), is used to balance the horizontal magnetic translational force on the specimen, attached to one end of the balance arm. The electromagnet is turned on its side so that the pole pieces are horizontal and one above the other. The pole-gap is shaped, following Sucksmith (1939), with about 6° inclination in the central one-third portion of the pole-pieces, while the remaining two-thirds, one portion on either end, are parallel, giving a vertical field in the central region and a horizontal gradient along the length of the pole-pieces. The balance arm with the specimen goes into the central region at right angles to the length of the pole-pieces (Dutta Roy, 1955). An automatic liquid air cryostat developed in this laboratory (Bose, 1947) placed horizontally enclosing the specimen, provides temperatures accurate to more than 0.1°K (measured with a calibrated Cu-constantan thermocouple) for magnetic measurements.

The translational motion of the specimen is optically magnified with the help of a bifilar mirror provided with a suitable oil damping arrangement, attached to the other end of the balance beam, and a telescope and scale arrangement. The force on the specimen is balanced accurately to more than 0.1% by twisting the quartz fibre suspension till the zero position of the image of the scale in the telescope is restored. With the Sucksmith shape of pole-gap the uniformity of the force is within 0.1% over a volume of about 1 c.c. in the central region so that the mounting and positioning of the specimens and standard substance (chromium potassium alum already standardised by earlier experiments; Dutta Roy, 1955) of smaller volumes need not be very critical. The arrangement gives the susceptibility along the field direction, i.e. the vertical. But in the present the alums being of the cubic class the mode of orientation of crystal in the field is immaterial. The balance is enclosed within a suitable draught and moisture proof box, with a side tube to cryostat, a top tube to enclose the fibre suspension and a front glass panel for the observation of the image of the scale from the bifilar mirror. Details of measurement are omitted. Under the conditions of measurement described at room temperature 300°K , we have

$$\chi = \frac{\theta}{\theta_s} \cdot \frac{m}{m_s} \left(\chi_s - \frac{k_a}{\rho_s} \right) + \frac{k_a}{\rho} \quad \dots (1)$$

in which χ 's are the mass susceptibilities of crystal along the field direction, θ 's the angles of twist of torsion fibre to balance the magnetic force on specimen, m 's the masses, ρ 's densities, symbols with and without the subscript 's' referring to the standard and the unknown crystal specimen respectively, and k_a is the volume susceptibility of surrounding air. At any other temperature T (degrees Kelvin),

$$\chi_T = \chi \cdot \frac{\theta_T}{\theta} \left[1 + \frac{k_a}{k} (1 - \gamma \cdot 300) \left(1 - \frac{300}{T} \right) \right] \quad \dots (2)$$

in which k is the volume susceptibility of the crystal at 300°K. and γ is its volume coefficient of expansion. The measurements are taken at 15° or 20°K intervals or even closer in the range 300°K to 100°K. The treatment of the results is as in the earlier papers and the final values for mean susceptibilities are given at 20° intervals, being obtained from the mean curve for the product $\theta_T \times T$ against T . The individual values for three different specimens of each salt do not deviate by more than 0.2% from the mean curve. The gm. molecular susceptibilities χ_M corrected for diamagnetism of the molecule, the squares of

the effective moments in Bohr magneton μ_J^2 the (using $\mu_J^2 = \frac{3k\chi_M T}{N\beta^2} = 7.995.\chi_M T$)* at different temperatures, which are same as the mean ionic values P_J^2 , are given in the Tables I-V.

TABLE I
V.NH₄(SO₄)₂.12H₂O

Temp °K	$\chi_M \times 10^6$	P_J^2 (Obs.)	P_J^2 (Calc.)
300	3025	7.254	7.264
280	3234	7.240	7.243
260	3476	7.226	7.222
240	3759	7.211	7.201
220	4084	7.183	7.180
200	4482	7.167	7.160
180	4967	7.148	7.138
160	5569	7.124	7.117
140	6334	7.089	7.096
120	7364	7.054	7.072
100	8780	7.020	7.040

TABLE II
V.Rb(SO₄)₂.12H₂O

Temp °K	$\chi_M \times 10^6$	P_J^2 (Obs.)	P_J^2 (Calc.)
300	3080	7.387	7.387
280	3293	7.372	7.362
260	3533	7.340	7.335
240	3812	7.313	7.309
220	4140	7.281	7.282
200	4533	7.247	7.257
180	5015	7.216	7.229
160	5627	7.191	7.203
140	6391	7.157	7.176
120	7440	7.139	7.150
100	8912	7.125	7.125

* Using values of the physical constant by Diamond & Cohen, (1948).

TABLE III
V.Tl(SO₄)₂.12H₂O

Temp. °K	$\chi_M \times 10^6$	P_f^2 (Obs.)	P_f^2 (Calc.)
300	3083	7.394	7.394
280	3292	7.370	7.384
260	3542	7.362	7.375
240	3834	7.357	7.365
220	4181	7.353	7.355
200	4596	7.348	7.348
180	5104	7.345	7.339
160	5736	7.336	7.330
140	6545	7.324	7.321
120	7625	7.314	7.311
100	9141	7.308	7.302

TABLE IV
V.Cs(SO₄)₂.12H₂O

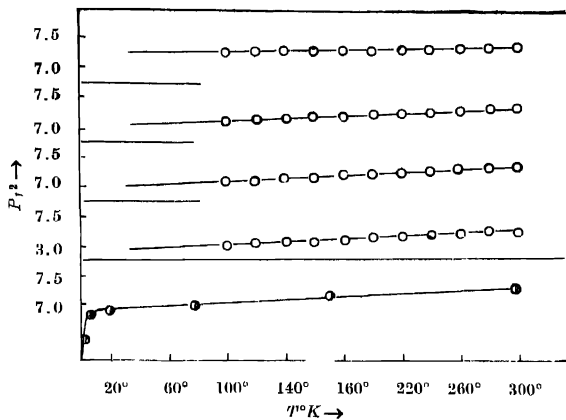
Temp. °K	$\chi_M \times 10^6$	P_f^2 (Obs.)	P_f^2 (Calc.)
300	3078	7.382	7.397
280	3295	7.372	7.372
260	3536	7.350	7.347
240	3281	7.331	7.322
220	4152	7.310	7.296
200	4552	7.278	7.271
180	5034	7.244	7.245
160	5643	7.218	7.219
140	6425	7.191	7.194
120	7471	7.168	7.169
100	8921	7.132	7.143

TABLE V
Cs.Tl(SO₄)₂.12H₂O

Temp. °K	$\chi_M \times 10^6$	P_f^2 (Obs.)	P_f^2 (Calc.)
300	1188	2.848	2.855
280	1270	2.843	2.943
260	1357	2.832	2.829
240	1456	2.819	2.815
220	1581	2.803	2.801
200	1728	2.787	2.787
180	1911	2.775	2.773
160	2142	2.764	2.760
140	2434	2.748	2.745
120	2822	2.731	2.731
100	3369	2.717	2.718

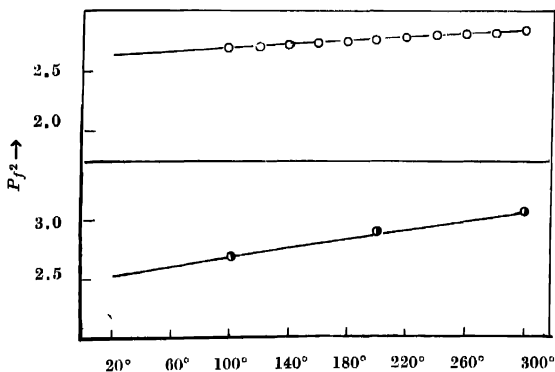
4. DISCUSSION OF THE RESULTS ON V^{3+} ALUMS(a) Variation of P_f^2 from salt to salt and with temperature.

It will be seen on a general survey of the table of values of P_f^2 in V^{3+} alums that the values are about 8 to 12% less than the "spin only" value of 8 squared Bohr magnetons. The values of P_f^2 for Rb, Cs and Tl alums at 300°K are practically the same, whereas, the value for NH_4 alum at 300°K is about 2% less than the previous group. It can be seen from figures 1(a) and (b) that the temperature

Fig. 1a. $P_f^2 - T$ curves for V^{3+} sulphate alums

O present measurements by Dutta Roy

● Leiden measurements.

Fig. 1b: $P_f^2 - T$ curves for Ti^{3+} sulphate alum.

O present measurements by Dutta Roy

● Leiden measurements.

variation curve of P_f^2 for all the alums in our range of temperatures are rectilinear with appreciable slopes against temperature axis, which are very nearly the same for Rb and Cs alums as also for the NH_4 alum though the room temperature value lies lower for the latter. In Tl alum the slope is appreciably smaller than the others though the room temperature value is the same as Rb and Cs alums

P_f^2 values for all the salts in this range appear to obey a Curie Law of the form $P_f^2 = AT+B$ quite well, but with somewhat different A and B values as indicated in the table 6 below. Measurements on V^{3+} ammonium alum by Van den Handel & Siegert (1937) give P_f^2 as 7.290 at 297.4°K, 7.169 at 169.8°K and 7.002 at 77.7°K, and agree well with our values in this range.

TABLE VI
Empirical P_f^2-T parameters for the different alums

	Vanadium alum				Titanium alum
	NH_4	Rb	Cs	Tl	Cs
B	6.949 (6.921)	6.995	7.015	7.136	2.650
$A \times 10^4$	11.4 (13.1)	13.1	12.5	8.2	6.6
g	1.864 (1.860)	1.870	1.872	1.888	1.880

The values in the parentheses are from Van den Handel's data.

The measurements of Van den Handel for the NH_4 salt extend down to 1.465°K and the P_f^2-T curve here is found to deviate from Curie Law slowly at first above 20°K and then more quickly and then very rapidly at 4°K tending towards a very low value near 0°K. This is shown in figure 1(a). The curvature at low temperatures apparently does not seem to have an appreciable effect on the behaviour in the liquid air range. Significance of all these facts is to be fitted into a satisfactory scheme.

(b) *Crystalline field theory of V^{3+} alum.*

In order to explain the experimental results of Van den Handel and Siegert on V^{3+} ammonium alum (1937) mentioned in the previous section, Siegert (1937) postulated a breakdown of the Russel-Saunders coupling between the individual orbital and spin moments of the 3d electrons in the V^{3+} ion (free ion ground state $3d^2\ ^3F$) under the influence of the major cubic component of the crystalline field arising from the trigonally elongated octahedron formed by the six water molecules immediately surrounding the V^{3+} ion (Beevers and Lipson, 1935). Since

the separations of the energy levels under the cubic field are of the order of 10^4 cm^{-1} Siegert considered only the lowest orbital triplet level Γ_4 (figure 2a) and fur-

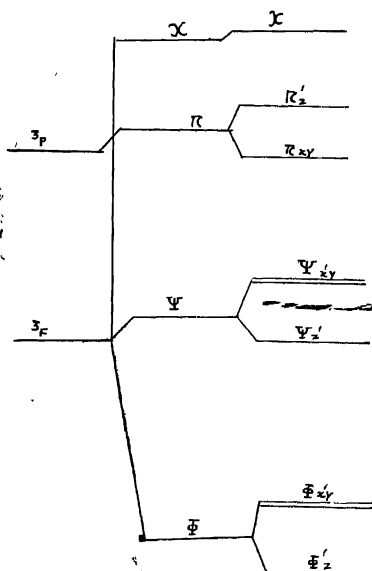


Fig. 2a: Energy level diagram for V^{3+} (not drawn to scale).

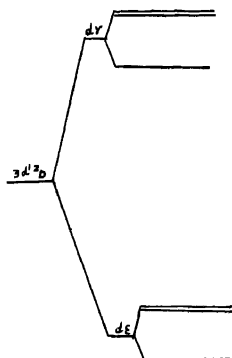


Fig. 2b: Energy level diagram for Ti^{3+} (not drawn to scale).

ther assumed that under the trigonal field and the spin-orbit perturbation this level is split up so as to make a nonmagnetic singlet state lie lowest, with a doublet close above it and other levels at several hundred cm^{-1} above. Thus assuming the trigonal splitting coefficient $\Delta = -700 \text{ cm}^{-1}$, the spin splitting, $D = 4.76 \text{ cm}^{-1}$, but the spin-orbit coupling coefficient $\zeta = +64 \text{ cm}^{-1}$ instead of the free ion value of $+104 \text{ cm}^{-1}$ (Laporte, 1928) he obtained a fairly good fit (a) with the experimental deviation of P_f^2 from the spin only value, (b) with the nearly linear form of the $P_f^2 - T$ curve above 20°K and (c) with the quick drop in this curve near liquid helium temperatures, tending to very low values of P_f^2 . Then, his theoretical high frequency term came out as $3.63 \times 10^{-3}T$ as against the experimental value $1.31 \times 10^{-3}T$ (obtained from the straight portion of the $P_f^2 - T$ curve at high temperatures, see Table VI).

The basic objections to the above theory appear to be the *ad hoc* assumption of the complete breakdown of $R-S$ coupling (Van Vleck, 1939; Owen, 1955) and the neglect of the upper cubic levels and also the components of the 3P multiplet which are sufficiently close to the ground level to affect its contributions to the effective magnetic moment.

In a recent paper one of us (Chakravarty, 1959) has applied the method of Abragam and Pryce (1951) to the problem of V^{3+} alums, without recourse to any special postulate regarding $R-S$ breakdown and, taking into consideration the contributions of all the upper levels, has obtained for the square of the effective moment,

$$P_f^2 = \frac{2A^2 + 16B^2kT/D[\exp(D/kT) - 1]}{2 + \exp(D/kT)} + \frac{3kT}{N\beta^2} K_c$$

$$= \frac{3kT}{N\beta^2} K_c + 2g_{\parallel}^2 + \frac{2D}{3kT} (g^2 - g_{\perp}^2) \quad \dots (3)$$

to a sufficient degree of approximation, in which $A^2 = g_{\parallel}^2$, $B^2 = g_{\perp}^2/4$ and $g = \sqrt{\frac{1}{3}(g_{\parallel}^2 + 2g_{\perp}^2)}$ is the mean spectroscopic splitting factor and K_c is the high frequency susceptibility, D , the spin splitting and other symbols have the usual meanings. The complicated functions of Δ , ζ and α and α' the Lande splitting factors in the crystal (Chakravarty, 1959). Expression (3) gives good fit with the experimental results of Van den Handel *et al* (1937) and Datta-Roy (1958) on NH_4 alum, over the entire range of temperatures (Table VII) taking by trial and error the values of the parameters of $t = 1.820$, $g = 1.870$ as against the experimental leading to $g_{\parallel} = 1.960$, $g_{\perp} = 1.80$ cm^{-1} and $\frac{3k}{N\beta^2} K_c = 1.98 \times 10^{-3}$ as against the mean value $g = 1.864$, $D = 4.80$

TABLE VII
 $V.NH_4(SO_4)_2.12H_2O$.

T°K.	P_f^2 (Theo.)	P_f^2 (Expt.)*
100	7.016	7.040
200	7.002	7.160
300	7.128	7.264

* Fit with Van den Handel's results are not shown because these have been discussed in details by Chakravarty (1959).

experimental value 1.23×10^{-3} (Table VI). It is further found that in the range 300°K to 100°K the contribution of the term of the order $1/T$ (equation (3)) is below the limit of experimental errors of $\pm 0.2\%$. In fact, even at 10°K this contribution amounts to a little over 1% only. The other two terms in equation (3) are of the form $AT + B$, which explains why the empirical curve in the high temperature range is appreciably a straight line. It is to be remarked, however, that

the theoretical slope of the line given by $\frac{3k}{N\beta^2} \cdot K_r$ is somewhat different from

the experimental, even considering the comparatively large error in determining this small term (about $\pm 5\%$). This is probably due to the fact that g and hence Δ the trigonal field splitting coefficient changes a little with temperature which is not sufficient to produce a deviation from linearity but effectively causes an appreciable change in the experimental slope. Thus, evidently the theoretical g value taken to fit the empirical straight line represents really the average value in the given temperature range.

It would be very nice if the actual values of g and D could be determined directly by paramagnetic resonance at each temperature, so that we could account for even the small misfit in K_r value. But, unfortunately, the large spin-splitting $D = 4.8 \text{ cm}^{-1}$ makes it impossible to induce transitions between the lowest levels unless microwaves of 2 mm. or less wavelengths are used, which has not been as yet done.

(c) The crystal field parameters

In the paper mentioned earlier, Chakravarty has shown that the values of parameters $g_{||}$, g_{\perp} , D and K_r , Δ , α , α' and ζ must be chosen so as to be consistent with the cubic field coefficient ($G = 39000 \text{ cm}^{-1}$ and 3P multiplet separation in crystal, $E_p = 9300 \text{ cm}^{-1}$ obtained from optical absorption measurements (Hartmann and Schlafer, 1951) and with a reasonable set of values of the second order and fourth order trigonal field coefficients H and I , namely, 3500 cm^{-1} and 3400 cm^{-1} respectively (Abragam and Pryce 1951). It is worth noticing that

experimental parameters g_{\parallel} and g_{\perp} are uniquely fixed, at least in theory, even from mean susceptibility when D is fixed from the low temperature measurements and g and K_c are found from the intercept and the slope of the high temperature curve where the effect of D may be considered zero, provided the value of ζ has been fixed. In view of what has been said earlier the values of g and K_c have to be slightly adjusted and a number of trials with different ζ values made till the values of Δ , α and α' correspond to reasonable values of H and I . It is found in this way that though there may be other sets of values of ζ , Δ , α and α' which satisfy the experimental parameters g , D and K_c , H and I are rather sensitive to changes in these and become quite unreasonable if these values are changed to any considerable extent, and the best set of values are found as given above. It would have saved much trouble in finding g_{\parallel} , g_{\perp} and D by trial and error if these could have been obtained directly from paramagnetic resonance data. But these are not available for the reasons already mentioned. It is interesting to remark that the 40% reduction in the value of ζ from free ion value, also needed in Siegert's theory, suggests that a fairly large overlap, $f^2 = 0.60$ of the $3d$ wave functions of V^{3+} with both the s - and p -wave functions of attached water-oxygens, exists in these alums (Owen, 1955). On the other hand, the value of Δ found by us is about double than that obtained by Siegert, namely, -700 cm^{-1} .

Now it is very probable that the covalency factor of 0.60 and hence ζ is practically the same in all these alums, since this arises from the semi covalent bond between the 6 water molecules surrounding the V^{3+} ion in everyone of the alums and may not be much influenced by the long range lattice structure; moreover, the values of α and α' representing effect of upper levels, also should not be very different. Then we may make an attempt to estimate the values of Δ , D , g and K_c for the three alums other than NH_4 alum. Of these the Rb and Cs alums appear to behave practically identically and only a little different from NH_4 , whereas the Tl alum is appreciably different. In view of the roughness in the trial and error calculations and the labour involved, it may not be worthwhile to perform these for Rb and Cs salts separately.

We find that for the Tl alum the parameters $\Delta = -1440 \text{ cm}^{-1}$, $\zeta = +64 \text{ cm}^{-1}$, $\alpha = 1.084$, $\alpha' = 1.380$ give $D = 4.812 \text{ cm}^{-1}$, $g_{\parallel} = 1.990$, $g_{\perp} = 1.819$, $g = 1.878$ and $\frac{3k}{N\beta^2} K_c = 1.759 \times 10^{-3}$. The theoretical values of P_f^2 calculated from the above and the experimental values are given for comparison below. The g value gives good fit with experimental value of 1.886 and the contribution of the $1/T$ term is quite negligible as required by the linearity of the P_f^2 - T curve in our range. The large difference with the experimental $\frac{3k}{N\beta^2} \cdot K_c$ term 0.82×10^{-3}

TABLE VIII
V.Tl(SO₄)₂.12H₂O

T°K.	P_f^2 (Theo.)	P_f^2 (Expl.)
300	7.506	7.394
200	7.365	7.348
100	7.230	7.308

indicates the effect of the appreciable variation of g value with temperature. Δ value in Tl alum is appreciably larger than the NH₄ alum and is the main reason for the observed larger g value. It is evident qualitatively that the parameters for the Rb and Cs alums are intermediate between the NH₄ and Tl alums.

5. (a) Variation of P_f^2 for Ti³⁺ alum with temperature

It will appear from the table 5 that P_f^2 for Ti³⁺ alum at 300°K is $\sim 5\%$ less than the spin only value and falls linearly to $\sim 9\%$ less than the spin only value 3, at 100°K, so that the data may be very well represented by the empirical formula

$$P_f^2 = 6.6 \times 10^{-4} \times T + 2.650 \quad \dots (4)$$

It will be seen from our expression (4) above that the A term contributes about 5% of the total P_f^2 at 300°K while B contributes the bulk of $\sim 95\%$. There is no trace of any nonlinear term.

The Leiden measurements on mean susceptibility of this alum by Van den Handel (Thesis 1940) for four different samples in the range 300°K to 1.2°K are so inconsistent amongst one another that it is difficult to put much reliance upon them (see also remarks by Van Vleck, 1940). Even for one of the samples for which the room temperature value is fairly close to ours the entire temperature variation of P_f^2 is of the form $P_f^2 = 14.6 \times 10^{-4}T + 2.784 - 42.3/T \quad \dots (5)$ Apart from the fact that the Leiden high frequency term is too large the $1/T$ term also cannot be fitted with any theory as will be seen later.

(b) Theory for Ti³⁺ ion in crystalline fields of trigonal symmetry

Under a crystalline field of cubic symmetry with a small superposed trigonal component as occurs in the alums the original $3d^1 \ ^2D$ ground state of a free Ti³⁺ ion together with the spin orbit coupling is split as shown in figure 2b. Each orbital level has a twofold Kramers degeneracy which is slightly split to $\sim 0.002 \text{ cm}^{-1}$ only, by the effect of the very small exchange and dipole coupling existing even in these highly magnetically diluted salts, as shown by adiabatic demagnetization experiments (Kurti and Simon, 1935). But we may neglect this for our present purpose. The Kramers doublet can be further split appreciably only by the magnetic field and thus P_f^2 should strictly obey a Curie Law between 1°K to 300°K,

unless the trigonal field separation Δ between the basic orbital singlet and the next higher doublet is comparable to any value of kT in this range

Bleaney *et al* (1955) have found from paramagnetic resonance measurements that $g = 1.25$, $g_{\perp} = 1.14$, so that $g = 1.176$, at helium temperature only, since at higher temperature the spin lattice relaxation time is of the order of 10^{-6} – 10^{-10} sec. making measurements impossible. In order to reconcile this abnormally low value of g and also the departure of Leiden P_f^2 from Curie law shown by eqn (5) these workers assume a high degree of charge overlap, between the d -orbitals of Ti^{3+} and s and p orbitals of the surrounding water-oxygens, represented by a factor $K = 0.7$ and find that $\Delta \approx 30 \text{ cm}^{-1}$. On the other hand, the paramagnetic absorption measurements at 90°K and 2°K give relaxation times $\sim 10^{-9}$ and $\sim 10^{-3}$ sec. respectively (de Haas *et al* 1938; Gorter *et al*, 1938), from which assuming the usual structural model of the alums (Beccers and Lipsou, 1935) Van Vleck (1940) has shown that 'Raman Process' is predominant for relaxation phenomenon in Ti^{3+} alum and Δ is $\sim 1000 \text{ cm}^{-1}$ and $\sim 200 \text{ cm}^{-1}$ at 90°K and 2°K respectively.

TABLE IX
 $Ti.Cr(SO_4)_2.12H_2O$

$T^\circ\text{K.}$	P_f^2 (Theor.)	P_f^2 (Expt.)
300	2.849	2.875
240	2.793	2.807
200	2.763	2.775
140	2.724	2.680
100	2.693	2.625

We have shown in an earlier note (1959) that starting with the molecular orbital theory, as applied by Van Vleck (1935), Stevens (1953) and others (Pryce *et al*, 1958) in many transition group salts, and assuming that the Ti^{3+} and O^{2-} charge overlap is anisotropic in character, Bleaney *et al*'s (1955) abnormal g value at low temperatures and our own P_f^2 value at high temperatures may be fitted into a scheme consistent with the picture given by the paramagnetic absorption as well as optical absorption measurements.

We find that in the liquid air range $g_{\parallel} = 1.919$, $g_{\perp} = 1.775$, $g = 1.823$ as against experimental value 1.880, and $\Delta = 800 \text{ cm}^{-1}$, $k_{\parallel} = 0.800$, $k_{\perp} = 0.580$, (anisotropic overlap factors). $\frac{3k}{N\beta^2} \cdot K_c = 15.3 \times 10^{-4}$ as against experimental value 6.6×10^{-4} ,

give fairly good fit with the experimental P_f^2 values (Table IX), while any value of $\Delta = 200 \text{ cm}^{-1}$ to 30 cm^{-1} may be fitted with the resonance g values, in liquid helium

range, other parameters remaining about the same. The fitting is not improved much by readjusting the parameters within reasonable limits. The whole explanation of the magnetic behaviour thus lies in the fact that Δ decreases rather quickly from below 100°K. owing to decrease in the spin lattice interaction. But the consequent curvature of the P_f^2 curve is to a considerable extent balanced by the variation of the moment caused by thermal depopulation of the upper orbital levels as the temperature falls, so that the P_f^2 curve is apparently straight except perhaps much below liquid air range. These variations, though much smaller in the liquid air range, influence the observed slope of the line as also its intercept

on P_f^2 axis and makes them different from the theoretical values given by $\frac{3k}{N\beta^2} \cdot K$,

and g respectively. These are also the reasons why there is a small persistent deviation of the theoretical and experimental P_f^2 values. Whether this is a purely thermal expansion effect or due to a change in crystal phase cannot be ascertained for the lack of suitable data.

Measurements below liquid air temperatures are in progress in order to verify all the details of the theory which have been communicated in a separate paper.

REFERENCES

- Abragam, A. and Pryce, M. H. L., 1951, *Proc. Roy. Soc. A.*, **205**, 135.
 Beevers, C. A. and Lipson, H., 1935, *Proc. Roy. Soc. A.*, **148**, 604.
 Blewney, B., Bogle, G. S., Cocke, A. H., Duffus, R. J., O'Brien, M. C. M. and Stevens, K. W. H., 1955, *Proc. Phys. Soc. A.*, **78**, 57.
 Bose, A., 1947, *Ind. J. Phys.*, **21**, 275.
 Bose, A., Chakravarty, A. S. and Chatterjee, R., 1959, *Ind. J. Phys.*, **33**, 325.
 Bose, A., Chakravarty, A. S. and Chatterjee, R., 1959, *Proc. Roy. Soc.* (communicated).
 Chakravarty, A. S. 1958, *Ind. J. Phys.*, **32**, 447.
 Chakravarty, A. S., 1959, *Proc. Phys. Soc.*, (in press).
 De Haas, W. J. and Du Pre, F. K. 1938, *Physica*, **5**, 964.
 Dimond, J. W. M. and Cohen, E. R., 1948, *Rev. Mod. Phys.*, **20**, 82.
 Dutta Roy, S. K., 1955, *Ind. J. Phys.*, **29**, 429.
 Dutta Roy, S. K., 1956, *Ind. J. Phys.*, **30**, 169.
 Dutta Roy, S. K., 1958, Thesis, Calcutta University.
 Gorter, C. J., Teunissen, P. and Dijkstra, L. J., 1938, *Physica*, **5**, 1013.
 Handel, J. Van den, 1940, Thesis, Leiden University.
 Handel, J. Van den and Siegert, A., 1937, *Physica*, **4**, 871.
 Kurti, N. and Simon, F., 1935, *Proc. Roy. Soc. A.*, **140**, 152.
 Laporte, O., 1928, *Zets. f. Phys.*, **47**, 761.
 Owen, J., 1955, *Proc. Roy. Soc. A.*, **227**, 183.
 Pryce, M. H. L. and Runoiman, W. A., 1958, Discussions of Farad Soc. No. 20, 34.
 Siegert, A., 1937, *Physica*, **4**, 138.
 Stevens, K. W. H., 1953, *Proc. Roy. Soc. A.*, **219**, 542.
 Sucksmith, W., 1939, *Proc. Roy. Soc. A.*, **17**, 551.
 Van Vleck, J. H., 1935, *J. Chem. Phys.*, **3**, 807.
 Van Vleck, J. H., 1939, *J. Chem. Phys.*, **7**, 61.
 Van Vleck, J. H., 1940, *Phys. Rev.*, **57**, 426.

ON THE ABSORPTION OF 3.18 CM MICROWAVES IN ETHYLENE CHLORHYDRIN AND ITS SOLUTIONS*

T. J. BHATTACHARYYA

OPTICS DEPARTMENT, INDIAN ASSOCIATION FOR THE CULTIVATION OF SCIENCE, CALCUTTA-32

(Received, November 6, 1959)

ABSTRACT. The absorption of microwaves of length 3.18 cm in pure ethylene chlorhydrin and its solutions in carbon tetrachloride and methyl cyclohexane have been studied in the temperature ranges from -70°C to 115°C , from -50°C to 80°C and from -80°C to 85°C respectively. In the case of the pure liquid the absorption starts at -40°C and increases rapidly with rise of temperature without showing any tendency to remain constant. In the case of the solution in CCl_4 absorption has been found throughout the temperature range from -50°C to 80°C with a maximum value at 10°C . In the case of solution in methyl cyclohexane the absorption is much feebler. It starts at -20°C and gradually increases with the rise of temperature but much less rapidly than in the case of the pure substance. The results have been explained on the assumption that the pure liquid consists of dimers formed through two types of intermolecular hydrogen bonds, one through $\text{O-H}\cdots\text{O}$ and the other through $\text{O-H}\cdots\text{Cl}$ linkage.

INTRODUCTION

In a previous investigation on the absorption of microwaves in *o*-chlorophenol (Ghosh, 1955) it was observed that the liquid does not show any absorption in the 3-cm region, from which he concluded that the OH group of the molecule in the liquid state has no freedom of rotation about the C-O bond and this was expected from Pauling's hypothesis that most of the molecules in the liquid exist as dimers (Pauling, 1945). In a later investigation (Bhattacharyya, 1958) it was observed that when the substance is dissolved in CCl_4 the solution absorbs microwaves in the 3-cm region, indicating that the OH group has freedom of rotation about the C-O bond and confirming the results of investigations on the infrared spectra reported by Sirkar *et al* (1958).

The infrared spectra of the solutions of ethylene chlorhydrin and of the pure liquid were studied recently by Mazumder (1959) and it was concluded by him that the pure liquid consists of two types of dimers while solutions in hydrocarbons contain both single molecules and dimers. This conclusion could be tested by studying the absorption of microwaves by the liquid and its solutions and the present investigation was undertaken for that purpose.

EXPERIMENTAL

The experimental arrangements and procedure were similar to those in a previous investigation (Bhattacharyya, 1958).

* Communicated by Prof. S. C. Sirkar.

The pure sample of ethylene chlorhydrin was dehydrated by mixing it with anhydrous Na_2SO_4 powder and then distilling it in a triple-bulb distillation apparatus under reduced pressure. The first portion of the distillate was rejected and the middle portion boiling at 128.8°C at atmospheric pressure was used for the experiment. It was found in the preliminary investigation that the sample absorbed highly 3.18 cm microwaves at the room temperature (30°C) and also at higher temperatures. To be sure that this absorption was not due to presence of water in the sample another sample of the pure substance was taken and mixed with requisite quantity of benzene and the mixture was subjected to fractional distillation. The portion boiling at 128.8°C at normal pressure was taken. It was expected to be pure. The liquid thus obtained was again mixed with anhydrous magnesium sulphate and distilled in a triple bulb under reduced pressure. The purity of the distillate used for the experiment was tested by the boiling point test. The absorption of the microwaves in this sample at temperatures ranging from -70°C to 115°C was then studied.

The temperatures below the room temperature were obtained by putting the water-tight cell containing the samples in a bath of alcohol in which liquid oxygen was added slowly.

The absorption was studied in pure ethylene chlorhydrin, in a 15% solution of the substance in CCl_4 and in a 7.5% solution in methyl cyclohexane. As a maximum was observed only in the case of the solution in CCl_4 the static dielectric constant ϵ_1 , refractive index and η , the viscosity of the solution at room temperature were measured and the values of these constants at 10°C were found out by extrapolation. These values were used for the calculation of the radius of the rotor from Debye's formulac

$$\omega\tau = \frac{\epsilon_0 + 2}{\epsilon_1 + 2} \sqrt{\frac{\epsilon_1}{\epsilon_0}}, \quad a^3 = \frac{kT}{4\pi\eta} \tau$$

where ϵ_0 the dielectric constant at very high frequencies, τ the relaxation time and $\omega/2\pi$ is the frequency of the microwaves.

RESULTS AND DISCUSSION

Figure 1 shows the temperature dependence of $\log_e I_0/I$ observed in the case of the pure substance and also in the solutions. Here I indicates the micro-meter reading due to the microwaves transmitted by the cell filled with the sample and I_0 that due to the microwaves transmitted by the empty cell.

It is seen that the pure liquid begins to show absorption of the microwaves above -30°C and there is very little absorption below -30°C . As the substance melts at -70°C the absorption was studied up to this temperature. No absorption maximum was found in this case in the range from -70°C to 115°C .

In the case of the solution in CCl_4 the absorption starts at -50°C , gradually increases with the increase of temperature and after attaining a maximum value

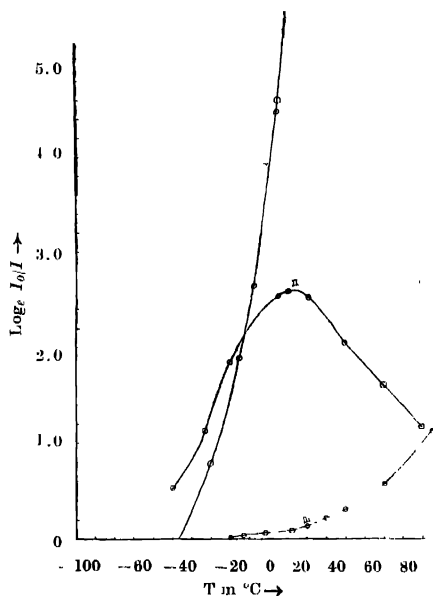


Fig. 1. Curve I shows temperature dependence of $\log_e I_0/I$ for ethylene chlorhydrin.

Curve II shows the same for 15% solution of the liquid in CCl_4

Curve III shows the same for 7.5% solution of the liquid in methyl cyclohexane.

at 10°C it gradually diminishes. The value of $\log_e I_0/I$ at 10°C was as high as 14.00 for the solution. The values of refractive index, dielectric constant and coefficient of viscosity of the solution determined experimentally as well as the value of the radius of the rotor calculated from Debye's formulae are given in Table 1.

TABLE I

Substance	$\omega/2\pi$ Mc/sec	$\sqrt{\epsilon_0}$	ϵ_1	T°K	$\tau \times 10^{11}$ sec.	$100 \times \eta$	$a \times 10^8$ cm
15% solution in CCl_4	9415	1.46	5.01	283°K	4.9	3.4	1.54

This value of a , the radius of the rotor, is identical with that observed in the case of ethylene dichloride by Ghosh (1953). So, the rotor is the C-Cl group in the present case also. Thus the C-Cl group is free in the solution in CCl_4 . This

is indicated also by the results of investigations on the infrared spectra of the solution of ethylene chlorhydrin in CCl_4 (Mazumder, 1959), because if the OH group of the molecule is attached to the Cl atom of the solvent molecule by the formation of $\text{OH}\cdots\text{Cl}$ bond, as postulated by him, the chlorine atoms at the other end of each of the molecules will remain free. This bond is fairly strong, as indicated by the results of investigations on infrared spectra and therefore there is not much increase in absorption with rise of temperature beyond 10°C . This result thus confirms the conclusion drawn by Mazumder.

The fact that there is no absorption in the case of pure ethylene chlorhydrin at very low temperatures indicates that the molecules are in a form in which neither the hydroxyl group nor the C-Cl group is free. This may be due to the formation of either the gauche configuration in all the molecules or associated groups. The existence of such groups of two types in the liquid was postulated by Mazumder (1959). Of these, the groups formed through the weak bond $\text{O}-\text{H}\cdots\text{O}$ is less stable than the group formed through $\text{O}-\text{H}\cdots\text{Cl}$ bond. At temperatures above -40°C the absorption increases rapidly with increase of temperature. This indicates that the associated groups formed through $\text{OH}\cdots\text{O}$ bond break up and the hydroxyl group begins to be free with the rise of temperature. If the molecules were of gauche configuration they would not change into the trans configuration so rapidly to produce the observed rapid increase of absorption with rise of temperature.

Curve III in figure 1 shows the temperature dependence of $\log_e I_0/I$ for the 7.5% solution of ethylene chlorhydrin in methyl cyclohexane. Like the pure substance this solution also does not show any absorption at low temperatures. The absorption starts at -20°C and increases with rise of temperature of the solution, but the rate of increase is much slower than that in the case of pure substance. In this case also the absorption maximum is absent. The investigation was carried out through a range of temperatures from -80°C to 85°C . At 85°C the value of I_0/I is 3.1. Evidently, in the solution of the substance in the hydrocarbon the dimers formed through $\text{OH}\cdots\text{Cl}$ bond do not break up but those formed through $\text{OH}\cdots\text{O}$ bond may break up into single molecules, because the latter bond is weaker. Some of them may reunite through $\text{OH}\cdots\text{Cl}$ bond. This may be the reason for the very small absorption found in the case of the solution of the substance in methyl cyclohexane. Similar results were obtained by Mazumder (1959) in his investigations on the Raman spectra and infrared absorption spectra of pure ethylene chlorhydrin and its solution in heptane. He observed that the nature of the absorption peak due to the solution of ethylene chlorhydrin in heptane is almost the same as that due to the pure liquid, but the magnitude of absorption in the solution is smaller. He assumed the persistence in the solution of the dimers of two types formed in the pure liquid. The

results of the present investigation are thus in good agreement with the conclusions drawn by him.

ACKNOWLEDGMENT

The author is indebted to Professor S. C. Sirkar, D. Sc., F.N.I., for his constant guidance throughout the progress of the work.

REFERENCES

- Bhattacharyya, T., 1958, *Ind. J. Phys.*, **32**, 573.
Ghosh, D. K., 1953, *Ind. J. Phys.*, **27**, 511.
„ „ 1955, *Ind. J. Phys.*, **29**, 450.
Mazumder, M. M., 1959, *Ind. J. Phys.*, **33**, 346.
Pauling, L., 1945, *Nature of Chemical Bond*, p. 324.
Sirkar, S. C., Deb, A. R. and Banerjee, S. B., 1958, *Ind. J. Phys.*, **32**, 345.

Letters to the Editor

The Board of Editors will not hold itself responsible for opinions expressed in the letters published in this section. The notes containing reports of new work communicated for this section should not contain many figures and should not exceed 500 words in length. The contributions must reach the Assistant Editor not later than the 15th of the second month preceding that of the issue in which the paper is to appear. No proof will be sent to the authors.

11

RELATIONSHIP BETWEEN ULTRASONIC VELOCITY AND OTHER PHYSICAL PROPERTIES OF PURE ORGANIC LIQUIDS

SATISH CHANDRA SRIVASTAVA

DEPARTMENT OF PHYSICAL CHEMISTRY, INDIAN ASSOCIATION FOR THE CULTIVATION OF
SCIENCE, CALCUTTA-32

(Received, September 30, 1959)

While investigating the possibility of finding out a relation between ultrasonic velocity (V) and concentration of solutions, specially solutions of electrolytes, the author found a relation between V and the internal pressure P as :

$$V\rho^{\frac{1}{2}} = kR^{\frac{1}{2}}P \quad \dots (1)$$

where ρ is the density of the liquid and R is molar refraction. K is a constant equal to (7 ± 1) . Internal pressure may be related with boiling point of the liquids

$$P = (-1400 + 24.5T)4.5/V_m \quad \dots (2)$$

where V is molar volume and T is the boiling point of the liquid in degrees absolute. The relation has been verified for 75 liquids (from the data of Parthasarthy given by Vigoreaus (1952) and of Natta (1949) and has been found to be true for as many as 60 liquids. In the remaining 15 liquids 8 are alcohols, 2 acetone, and the rest water, etc. for which there is a deviation probably because of high association or polarit

A better relation is observed when data are compared in the similar class of liquids. For a few of them average ratio of $V\rho^{\frac{1}{2}}/R^{\frac{1}{2}}P$ has been shown in Table I which may also be termed as constant of linearity between $V\rho^{\frac{1}{2}}$ and $R^{\frac{1}{2}}P$. The range of variation has also been shown in each case.

Equation (1) may also be kept with the help of equation (2) as

$$V\rho^{\frac{1}{2}} = k_1 R^{\frac{1}{2}} V_m^{-1} (k_2 T - 1)$$

where k_1 and k_2 are constants
and will automatically hold good, if (1) is true.

TABLE I

Class of Liquids H	No. of Liquids	Mean slope (average ratio $V\rho^{\frac{1}{2}}/R^{\frac{1}{2}}P$)	Range of variation of mean slope
Mono Olefins	8	7.52	+ .25, - .29
Paraffins	12	7.53	+ .19, - .09
Alkyl Chlorides	4	7.56	+ .32, - .19
Aliphatic Esters	6	7.85	+ .41, - .30
Alkyl Bromides*	3	7.11	+ .08, - .07

The equation may be helpful in deriving an equation for the velocity of ultrasonic waves in solutions.

The author owes his sincere thanks to Prof. S. R. Palit for his valued suggestions and keen interest in the problem.

REFERENCES

- Vigoreaus, P., 1952, *Ultrasonics*, Chapman and Hall.
Natta, G. and Baccaredda, M., 1949, *Die Makromole Chemie*, **14**, 134.

* Bromoform has abnormally low ratio of $V\rho^{\frac{1}{2}}/R^{\frac{1}{2}}P$ and therefore has not been included.

N.B. Six alcohols were also tested and have the mean ratio $V\rho^{\frac{1}{2}}/R^{\frac{1}{2}}P$ as 6.06 with a wide variation as +1.10, - .70 which is beyond the desired value.

THE EVALUATION OF THE ELECTRONIC TRANSITION MOMENT FOR THE $b^3\Sigma^+ - a^3\pi$ SYSTEM OF CO.

N. R. TAWDE AND B. S. PATIL*

DEPARTMENT OF PHYSICS, KARNATAK UNIVERSITY, DHARWAR

(Received, October 21, 1959)

ABSTRACT. The integrated intensities obtained by Barrow, Gratzner and Malherbe for $\text{CO}(b^3\Sigma^+ - a^3\pi)$ have been used to determine the dependence of electronic transition moment $R_e(r)$ upon the internuclear distance r , with the aid of Frank-Condon factors $q_{v'v''}$ and $r_{0v'v''}$ (r -centroids). For this purpose, the r -centroids have been calculated independently and the relation connecting R_e and \bar{r} evolves in the form $R_e = C(1 - 0.6433\bar{r})$ for this system. The theoretical intensities under the assumptions of R_e as constant are then corrected for variation of R_e with \bar{r} , by the above relation and they have been discussed in the light of the available integrated intensity data. It is noticed that disharmony between theory and experiment is considerably reduced as a result of the introduction of $R_e(r)$ factor.

INTRODUCTION

Barrow, Gratzner and Malherbe have obtained the integrated intensities of the bands belonging to three progressions in the system $b^3\Sigma^+ - a^3\pi$ of carbon monoxide and have indicated therein certain tendencies, which are not quite in harmony with theoretical predictions. He suggested that this disharmony may be a consequence of the variation of electronic transition moment (R_e) with internuclear distance not assumed in the theory. In view of the recent elucidation of some theoretical aspects concerning the electronic transition moment in the treatment of vibrational transition probabilities, it occurred to us to attempt the evaluation of the contribution due to the variation in electronic transition moment in this molecular band system and see how far the disharmony could be removed by using the available measurements of Barrow and others on the integrated intensities.

THEORETICAL

The vibrational transition probability is usefully expressed as

$$P_{v'v''} = |\psi_{v'} R_e \psi_{v''} d\tau|^2 \quad \dots (1)$$

* Formerly Senior Research Assistant of the C.S.I.R. in the Department of Physics and now Head of the Department of Science, Chhatrapati Shivaji College, Satara.

On the r -centroid concept introduced by Fraser (1954), it is possible to rewrite the expression (1) by separating $R_e(r)$ from the bracketted expression so that

$$P_{v'v''} = R_e^2(\bar{r}_{v'v''}) |\psi_{v'}' \psi_{v''}|^2 dr \quad \dots (2)$$

Here, if the electronic transition moment $R_e(\bar{r}_{v'v''})$ is assumed to be constant, we obtain the transition probability $P_{v'v''}$ to be proportional to the Frank-Condon factor $|\psi_{v'}' \psi_{v''}|^2$ which may be expressed in brief as $q_{v'v''}$.

Now, in practice, if experimental results of transition probabilities are compared with theoretical data on the basis of above consideration, we generally obtain some disagreement. In order to trace its source, one must obviously go into the problem of the nature of the variation of the quantity $R_e(\bar{r}_{v'v''})$ with r .

The intensity of a band $v' \rightarrow v''$ in emission is given by

$$I_{v'v''} = KN_{v'} v_{v'v''}^4 P_{v'v''} \quad \dots (3)$$

where the quantities on the right hand side have their usual meaning.

Since $P_{v'v''} = R_e^2(\bar{r}_{v'v''}) q_{v'v''}$ as stated earlier, we get

$$I_{v'v''} = KN_{v'} v_{v'v''}^4 R_e^2(\bar{r}_{v'v''}) q_{v'v''} \quad \dots (4)$$

It is possible to correlate this with intensity $I_{v'n}$ for another vibrational transition $v' \rightarrow n$ and obtain an expression connecting both as follows :

$$\frac{R_e^2(\bar{r}_{v'v''})}{R_e^2(\bar{r}_{v'n})} = \frac{I_{v'v''}}{v_{v'v''}^4 q_{v'v''}} \bigg/ \frac{I_{v'n}}{v_{v'n}^4 q_{v'n}} \quad (5)$$

Here $\bar{r}_{v'v''}$ which is usually defined as r -centroid needs to be evaluated.

(a) Evaluation of r -Centroid

The transition moment $R_e(\bar{r}_{v'v''})$ corresponds to a particular distance $\bar{r}_{v'v''}$. This distance, on considerations of Fraser (1954) and Nicholls and Jarman (1956) is designated as r -centroid. They have evolved it in the form :—

$$\bar{r}_{v'v''} = \int \psi_{v'}' r \psi_{v''} dr / \int \psi_{v'}' \psi_{v''} dr \quad \dots (6)$$

It is defined as the average internuclear separation associated with the transition $v' \rightarrow v''$. Nicholls and Jarman (1956) have indicated several methods of evaluating it and from the results obtained by them, this quantity appears to be an important property in a system, as it is shown to bear a definite relation with $\lambda_{v'v''}$, the wavelength of the band ($v'v''$) in certain band systems studied by them. In evaluating the contribution of the transition moment, we have incidentally verified this relation in the present case too, by deriving the r -centroids for the bands of two v'' -progressions ($v' = 0, 1$) of $b^3\Sigma^+ \rightarrow a^3\Pi$ system of CO by one of the three methods given by them, viz., the graphical method. The values obtained are given in Table I side by side with $\lambda_{v'v''}$.

TABLE I

r -Centroides and wave lengths for CO, $b^3\Sigma^+ \rightarrow a^3\Pi$
 $r'_e = 1.088 \text{ \AA}$; $r''_e = 1.2093 \text{ \AA}$

Transition	Wave length	r -Centroids
$v' v''$	$\lambda_{v'v''} \text{ \AA}$	$\bar{r}_{v'v''} \text{ \AA}$
0, 3	3305.7	1.048
1, 4	3242.1	1.062
0, 2	3134.4	1.081
1, 3	3079.9	1.090
0, 1	2977.4	1.108
1, 2	2930.0	1.118
0, 0	2833.1	1.135
1, 1	2793.1	1.142
1, 0	2665.0	1.156

The variation of $\bar{r}_{v'v''}$ with λ within the present range $1.048 < 1.156$ should follow the general rule established for the two cases, (i) $r'_e > r''_e$ or (ii) $r'_e < r''_e$ by Nicholls and Jarman (1956). For the latter i.e. case (ii) which is applicable here, the $\bar{r}_{v'v''}$ should decrease linearly with λ increasing and this is what has been found here.

Having verified this important property and being in possession of data on r -centroids for the bands of the system, it is possible to use equation (5) above, to obtain the variation of R_e with $\bar{r}_{v'v''}$.

(b) *Determination of electronic transition moment (R_e).*

If the intensities $I_{v'v''}$ and $I_{v'n}$ preferably the integrated intensities are known, the ratio

$$R_e(\bar{r}_{v'v''})/R_e(\bar{r}_{v'n})$$

can be evaluated from equation (5) for any v'' -progression to which the measured bands (v', v'') and (v', n) refer, since the values of λ are known for a given transition. The variation of R_e with $\bar{r}_{v'v''}$ is ultimately obtained from a smooth curve by the least square criterion, as there is generally a scatter of points as a result of (i) experimental error in the intensity measurements and (ii) the nature of precision in the calculation of Frank-Condon factors. For arriving at this variation, the integrated intensities measured by Barrow, Grazer and Malherbe (1956) and Frank-Condon factors calculated by them on the basis of Morse potential

model, have been used. The results have been ultimately obtained in terms of $R_e(\bar{r}_{v'v''})/R_e(\bar{r}_{00})$. These are calculated for $v' = 0, 1$ progression, as well as read from smoothed curve prepared in the manner indicated above. The calculated values could be arrived at in two ways, i.e. either from (a) rescaling procedure or from (b) the ratio $(I/v^4)/(\Sigma I/v^4)$ for bands. Each of these sets are then subjected to graphical plot and a smooth curve determined. In doing so, it was found that the results obtained from rescaling procedure gave a large scatter of points as to make the course of smoothed curve uncertain. But in the case of values resulting from the ratio $(I/v^4)/(\Sigma I/v^4)$, the scatter was within the permissible limits, to make the determination of smoothed curve much more certain. For this reason, we are inclined to place more reliance on these latter results. These are recorded in Table II.

TABLE II

Variation of electronic transition moment in CO ($b^2\Sigma^+ \rightarrow a^2\Pi$) system.

$v' \quad v''$	$R_e(\bar{r}_{v'v''})/R_e(\bar{r}_{00})$	$R_e(\bar{r}_{v'v''})/R_e(\bar{r}_{00})$	$v' \quad v''$
	Calculated	from smoothed curve	
0, 3	1.196	1.207 ₄	1.048
0, 2	1.053	1.028 ₇	1.081
0, 1	1.010	1.064 ₄	1.108
1, 2	1.009	1.040 ₅	1.118
0, 0	1.000	1.000 ₈	1.135
1, 1	0.662	0.983 ₃	1.142
1, 0	1.114	0.949 ₉	1.156

The relation representing the quantities in column 3 and 4 is satisfied by a linear equation of the form

$$R_e = c(1 + \rho \bar{r})$$

Where the ρ value for the system under investigation works out to be -0.6433 within the range of bands examined. This value of ρ seems to be of right order considering similar results on other molecules. Thus, in the present case,

$$R_e = c(1 - 0.6433\bar{r}) \quad \dots (7)$$

RESULTS AND DISCUSSION

With the relation (7) obtained as above and with the values of integrated intensity obtained by Barrow, Gratzner and Malherbe for $v' = 0$ progression, we can now proceed to introduce the correction for R_e in the theoretical derivation of intensity obtained by Barrow. Rewriting equation (4) by taking

$K N_{v'} = K'$, we get

$$I = K' \nu^4 R_e^2 (\bar{F}_{v'v''}) q_{v'v''}$$

i.e.,

$$I \propto R_e^2 (\bar{F}_{v'v''}) q_{v'v''}$$

Now when it is a question of comparing the experimental value of intensity with similar theoretical derivation, it is necessary to multiply transition probability value by ν^4 of the particular band. This procedure was not, however, followed by Barrow and collaborators in studying this experimental intensity in the light of the theory, but they compared directly the experimental intensity values with the transition probability figure, i.e. Frank-Condon factors.

We have, however, obtained our results on considerations given above, viz., by taking account of ν^4 . Table III incorporates the relevant experimental and theoretical data thus derived.

TABLE III

Band $v' v''$	Integrated intensities (Barrow, Gratzor and Malherbe)	$q_{v'v''}$ (Barrow, Gratzor and Malherbe)	Relative theoretical intensities taking R_e as constant $I' = q_{v'v''} \times \nu^4$	Corrected relative theoretical intensities $I = I' \times R_e^2$ $\rho = 0.64$
0, 0	1.00	1.00	1.000	1.000
0, 1	2.00	2.39	1.954	2.216
0, 2	2.42	3.27	2.179	2.773
0, 3	2.67	3.35	1.806	2.632 ₄

In the column 2 above, we have Barrow's experimental data of integrated intensities followed in column, 3, by Frank-Condon factors $q_{v'v''}$ derived by him. These latter are converted to theoretical intensity values in the next column 4. It is to be noted that these values of theoretical intensities emerge on the assumption of the constancy of electronic transition moment. One could see from the trend of experimental values of column 2 that they change more rapidly with v'' in the progression than theoretical values, (column 4). This disharmony between theoretical predictions and experimental results is to be traced to the failure to bring the Frank-Condon factors to the proper scale of intensity data uniform with experimental values. The last column (Table I) gives the theoretical intensity value as corrected for the variation of electronic transition moment in the manner shown above. It would be seen from the corrected results (column 5) that they give, in general, a better approach because of the large disparity being removed particularly in the higher member of the progression, viz, the (0, 3) band. Hence the conclusion is inevitable that the variation of electronic transition moment

with internuclear separation contributes significantly to the vibrational transition probability as suggested by Schuler (1950) and Nicholls (1954).

ACKNOWLEDGMENT

The work was carried out under a research scheme sponsored by the C.S.I.R., New Delhi, and one of us (B.S. Patil) is highly indebted to the organisation for the award of a Senior Research Assistantship. We are also thankful to our colleague, Shri M. I. Savadatti, for checking some of the calculations and for the help rendered in the preparation of the manuscript.

REFERENCES

- Barrow, R. F., Gratzner, W. B. and Malherbe, J. F., 1956, *Proc. Phys. Soc., A*, **69**, 574.
Fraser, P. A., 1954, *Can. Jour. Phys.*, **32**, 515.
Fraser, P. A., 1954, Approximate calculations of electronic transition moment, Scientific Report No. 17, Department of Physics, University of Western Ontario. Contract A.F. 19 (122), 470.
Nicholls, R. W., 1956, *Proc. Phys. Soc., A*, **69**, 741.
Nicholls, R. W. and Jarman, W. R., 1956, *Proc. Phys. Soc., A*, **69**, 253.
Schuler, K. E., 1950, *Jour. Chem. Phys.*, **18**, 1221.
Turner, R. G. and Nicholls, R. W., 1954, *Can. Jour. Phys.*, **32**, 475.

TEMPERATURE VARIATION OF DIELECTRIC RELAXATION IN SIX POLAR LIQUIDS

J. SOBHANADRI

PHYSICS DEPARTMENT, ANDHRA UNIVERSITY, WALTAIR

(Received, October 14, 1959)

ABSTRACT The temperature variation of dielectric relaxation is studied in six polar molecules in dilute solution using *n*-heptane as solvent over the temperature range 0°C to 80°C. The molecules investigated are Chloro benzene, *O*-Chloro toluene, 2,6 Dichloro toluene, Methyl *n*-butyl ketone, Methyl *n*-amyl ketone and Methyl phenyl ketone (Acetophenone). The energy of activation for dipole relaxation for each liquid is compared with the corresponding value for viscous flow. The results are examined in the light of Eyring's theory of absolute reaction rates.

INTRODUCTION

The phenomenon of dielectric relaxation is generally regarded as a rate process involving the rotation of the dipolar molecules about two mean equilibrium positions and separated by a potential energy barrier with a certain probability of jumping from one equilibrium position to another. If $1/\tau$ is the jump rate or the mean number of jumps made by a dipole in unit time and E_τ is the energy of activation, then

$$\begin{aligned} 1/\tau &\propto e^{-E_\tau/kT} \\ \text{or} \quad \tau &= A \cdot e^{E_\tau/kT} \end{aligned} \quad \dots (1)$$

where A is the constant of proportionality.

Eyring (1941) identified the constant A as equal to h/kT , where h is the Planck's constant, and k is the Boltzmann constant, T being the absolute temperature, while according to Frohlich (1949), it is c/ω_a , where c is temperature dependent to some extent and π/ω_a is the average time required by an excited molecule to turn from one equilibrium direction to the other. As experimental investigations seem to indicate that the constant of proportionality is dependent on $1/T$, Saxton (1952) has written equation (1) in the form

$$\tau = A/T \cdot e^{E_\tau/kT} \quad \dots (2)$$

It is evident from this equation that if values for the relaxation time are determined at different temperatures, the energy of activation for dipolar rotation may be obtained. If a graph is drawn between $\log T\tau$ and $1/T$ the slope of the straight line thus obtained gives E_τ/k , from which E_τ , the energy of activation

may be calculated. The value of A may also be determined and compared with that (h/k) derived by Eyring.

Dielectric relaxation and viscosity of liquids are often treated in an analogous manner. The analogy between the molecular motion occurring in dipole orientation and that involved in the process of viscous flow was shown (1946, 1948) by the similarity in appearance of the plots for $\log \eta$ against $1/T'$ to those for $\log \tau$ against $1/T'$. If viscous flow is pictured as the movement of one layer of molecules with respect to another layer (involving translational as well as rotational motion of the molecules) and E_η is the activation energy required to pass over a hindering potential energy barrier, the following relation is obtained.

$$\eta = B.e^{E_\eta/kT} \quad \dots (3)$$

Eyring identified B with the factor hN/V , where h is Planck's constant, N is Avagadro's number and V is the molar volume.

Whiffen and Thompson (1946) investigated the effect of temperature on dielectric relaxation by carrying out measurements of τ in dilute solutions of Chloroform, Camphor, and four other polar substances in heptane. They used the linear relationship between the logarithm of the relaxation time and the reciprocal of absolute temperature for obtaining the energy of activation. They pointed out, however, that a slight curvature to the graph, expected on the basis of Eyring's theory, could not be detected due to insufficient accuracy in their experimental results. Their observations indicated further an approximate equality of E_τ and E_η , with E_η exceeding E_τ by an amount up to a few hundred calories.

Using the arc plot method for obtaining the relaxation times at different temperatures, Smyth and his collaborators (1948) also investigated the absorption of certain organic halides, and obtained values for the energies of activation for dielectric relaxation as well as viscous flow. They further observed that the curve for E_τ plotted against the number of carbon atoms in the molecular chain is rather similar in form but somewhat lower than the corresponding curve for viscous flow. The ratio E_τ/E_η was close to 0.6 over the range of liquids investigated, and this difference (between E_τ and E_η) is attributed to the fact that dielectric relaxation primarily requires molecular rotation, while viscous flow requires translation in addition to rotation. The effect of temperature on the distribution of relaxation times was also considered and it has been observed that the distribution parameter α decreases with increasing temperature.

Saxton (1952) used the linear relationship between $\log T\tau$ and $1/T'$ for estimating the height of the potential barrier in the case of Methyl and Ethyl alcohols and water. Though a linear relationship was observed between $\log T\tau$ and $1/T'$ in the case of Methyl and Ethyl alcohols, a curvature was observed in the case of water. Similar result was observed for water when the $\log \eta$ versus $1/T'$ plot

was studied. However, for all these three liquids, the relationship between $\log T\tau$ and $\log \eta$ was a perfect straight line with slope unity, showing that E_τ and E_η are identical.

Gopalakrishna (1958) carried out experiments in dilute solution on benzo-phenone, Ethyl benzoate, and α -nitro naphthalene in heptane and on ethyl adipate in both heptane and decalin. It was observed that in all the cases, the plot of $\log T\tau$ against $1/T$ was a straight line indicating that E_τ is a constant independent of temperature. He also calculated the value of the factor A at each temperature from equation (2) using the value of E_τ obtained from the slopes of the plots of $\log T\tau$ against $1/T$. It was observed that the values of A are fairly constant for each liquid, and they are of the same order of magnitude but not in agreement with the value predicted by Eyring.

A study of these observations on the effect of temperature on dielectric relaxation indicates that Eyring's theory on dipole rotation is yet open to discussion and a good deal of experimental data are needed before any attempt is made to draw definite conclusions on this subject. It would be of interest to investigate a number of points (1) whether the factor A is a constant and same for all liquids, as suggested by Eyring, being equal to h/k (2) whether the value of A obtained from equation (2) for a particular substance is the same for the pure liquid and in solution (3) whether E_τ and E_η are equal or different (4) whether the same type of relation between E_τ and E_η exist in solution and for the pure liquid as well etc.

A systematic investigation is therefore considered essential to have a better understanding of dielectric relaxation as a rate process. With this purpose the author has undertaken a programme of studying the temperature variation of dielectric relaxation for a number of molecules of different sizes and shapes, both in pure liquid state and in solution over a range of temperature and frequency. It is necessary in such a work to determine τ with as high an accuracy as is possible. Perhaps Cole and Cole's method based on measurements at different frequencies is the most suitable. In the present work, however, as a first step, the method of Whiffen and Thompson is adopted and six molecules are investigated. Values of relaxation time are determined in the temperature range 0°C to 80°C from measurements at a single frequency. E_τ is obtained in each case and compared with the E_η values for viscous flow. The factors A and B are also determined and compared. The molecules investigated are chloro benzene, chloro toluene, dichloro toluene, methyl butyl ketone, methyl amyl ketone and methyl phenyl ketone comprising three aromatic and three aliphatic compounds for which such data have not been recorded previously.

EXPERIMENTAL

All the measurements were made at a wavelength of 1.22 cm using the standing wave method of Roberts and von Hippel (1946). *n*-Heptane was used as the

nonpolar solvent because of its low freezing point and high boiling point. The Debye equation for the complex dielectric constant ϵ^* as a function of frequency for a dilute solution of a polar compound in a non-polar solvent is given as

$$\frac{\epsilon^* - 1}{\epsilon^* + 2} = \frac{\epsilon_\infty - 1}{\epsilon_\infty + 2} + \frac{4\pi n\mu^2}{9kT} \frac{1}{1 + i\omega\tau} \quad \dots (4a)$$

with the usual notation, n being the number of dipole molecules per c.c.

From this equation, by separating the real and imaginary parts, the dielectric constant ϵ' and loss factor ϵ'' of the solution, are given by the relation

$$\frac{3\epsilon''}{(\epsilon' + 2)^2 + \epsilon''^2} = \frac{4\pi n\mu^2}{9kT} \frac{\omega\tau}{1 + \omega^2\tau^2} \quad \dots (4)$$

ϵ''^2 may be neglected in comparison with $(\epsilon' + 2)^2$, so that, by rearranging, equation (4) may be written as

$$\tan \delta = \frac{(\epsilon' + 2)^2}{\epsilon'} \frac{4\pi n\mu^2}{27kT} \frac{\omega\tau}{1 + \omega^2\tau^2} \quad \dots (5)$$

ϵ' only changes from 1.9 to 2.0 so that the factor $\frac{(\epsilon' + 2)^2}{\epsilon'}$ may be taken as independent of temperature, changing only from 8.0 to 8.005 over the range of temperatures investigated. Rewriting this equation

$$\frac{T \tan \delta}{c} = \frac{(\epsilon' + 2)^2}{\epsilon'} \frac{4\pi N\mu^2}{27k} \frac{\omega\tau}{1 + \omega^2\tau^2} \quad \dots (6)$$

$$\frac{T \tan \delta}{c} = X \frac{\omega\tau}{1 + \omega^2\tau^2} \quad \dots (6)$$

where $X = \frac{(\epsilon' + 2)^2}{\epsilon'} \frac{4\pi N\mu^2}{27k}$ is a constant independent of temperature.

The graph of $\frac{T \tan \delta}{c}$ against temperature shows a maximum when $\omega\tau = 1$, so that the value of τ at that particular temperature is 6.5×10^{-12} sec. (at 1.22 cm, $\omega\tau = 1$ when $\tau = 6.5 \times 10^{-12}$ sec.). At any other temperature the ratio of the value of $\frac{T \tan \delta}{c}$ to its maximum value will be $\frac{2\omega\tau}{1 + \omega^2\tau^2}$ in which τ is the relaxation time at that temperature. The values of τ at various temperatures may thus be obtained. The choice between the two possible values of τ for one value of this ratio is determined by examining whether the temperature is above or below that corresponding to the maximum value. This was the method used by Whiffen

and Thompson in their experiments. A similar procedure is adopted in this investigation.

The value of the dipole moment is obtained from the maximum value of $T \tan \delta/c$, since, according to equation (6), it is then equal to $X/2$ from which μ be evaluated

The experimental set-up is that conventionally used consisting of a Raytheon type 2K 33B klystron oscillator with a frequency range 22,000 to 25,000 Mc/s, and is fed by the klystron signal source of the Sperry Gyroscope Company (Model 555). The klystron is followed by a variable attenuator, a matching unit, a standing wave indicator, and a silvered dielectric cell. The cell is mounted vertically to facilitate introduction of the temperature baths without disturbing the main set up. A Dewar flask is used to contain the temperature baths (hot water, ice).

The dielectric cell is designed with two long vertical side tubes for introducing the liquid and is separated from the rest of the set up by means of a mica window. This mica window also minimises the effect of evaporation at higher temperatures. A piece of waveguide connected between the standing wave indicator and the cell reduced to a great extent the transfer of heat to the crystal. In addition, a stream of air was blown continuously at the extension guide to prevent it from getting heated or cooled.

The accuracy of the measurements of $\tan \delta$ is estimated to be within $\pm 3\%$, while the relaxation times are accurate to within $\pm 5\%$.

All the substances were supplied by Light and Co. and were freshly distilled before use.

RESULTS

The experimentally obtained values of $\tan \delta$ at different temperatures together with the values of $T \tan \delta/c$, τ , $\log T\tau$, and $1/T$ obtained on calculation are given in Table I. The weight fraction 'w' of the solute for each liquid is given in brackets. In Table II values of μ and τ obtained from this investigation (at 20°C) are given along with the literature values at the same temperature as far as these are available, for comparison. The results are in good agreement.

Graphs of $\log T\tau$ against $1/T$ for each liquid are drawn and obtained as straight lines, indicating a linear relationship (refer figure 1, for Chlorobenzene; the others are similar and not shown). Both E_τ and A may hence be regarded as constant and independent of temperature their values being obtained from the slope and intercept respectively of the straight line. The individual values of A for each temperature for all the molecules are also calculated and shown in the last column of table I, to illustrate the constancy. The variations in the values are considered to be within experimental error. The mean values of A are shown in table III.

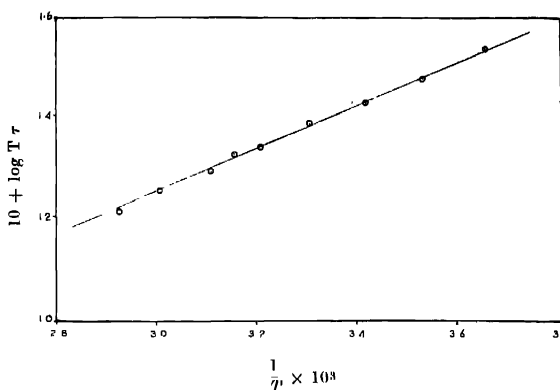


Fig. 1. Plot of $\log T\tau$ vs $\frac{1}{T}$ for chlorobenzene

It is seen that these are widely divergent from the calculated value from Eyring's expression h/k , which comes out to be 4.8×10^{-11} . A similar feature is seen in the case of methyl and ethyl alcohols for which Saxton's experimental results are 41×10^{-11} and 17×10^{-11} . Though these are observed to be fairly constant over the temperature range -10°C to 50°C they are much greater than Eyring's value. In this particular case the large deviation may be the effect of association. Gopalakrishna's experiments also have led to the conclusion that the experimental value of A is larger than h/k . It will be of interest to investigate whether A will be the same or different for the pure liquid and dilute solution. Experiments on these molecules in pure liquid state are in progress.

TABLE I

Temp. $^\circ\text{C}$.	$\tan \delta$	$\frac{T \tan \delta}{c} \times 10^{-3}$	$\tau \times 10^{12}$ sec.	$\log T\tau$ (+10)	$\frac{1}{T} \times 10^3$	A
(1) <i>Chloro benzene</i> ($w = 0.0703$)						
0	0.0264	16.81	12.6	1.539	3.66	10.67
10	0.0272	18.27	10.8	1.486	3.53	10.67
20	0.0277	19.45	9.3	1.435	3.41	10.64
30	0.0275	20.16	8.2	1.396	3.30	10.40
40	0.0269	20.63	7.1	1.348	3.20	10.84
45	0.0263	20.73	6.5	1.335	3.15	10.72
50	0.0257	20.69	6.2	1.304	3.10	10.64
60	0.0244	20.46	5.6	1.261	3.00	10.91
70	0.0227	19.89	4.8	1.219	2.92	10.09
(2) <i>O-Chloro toluene</i> ($w = 0.0865$)						
0	0.0194	10.29	15.9	1.638	3.66	12.75
10	0.0208	11.57	13.4	1.576	3.53	12.50
20	0.0215	12.57	11.6	1.531	3.41	12.65

TABLE I (contd.)

Temp. °C.	$\tan \delta$	$\frac{T' \tan \delta}{c} \times 10^{-4}$	$\tau \times 10^{12}$ sec.	$\log T' \tau$ (+10)	$\frac{1}{T'} \times 10^3$	$A \times 10^{11}$
30	0.0218	13.33	10.2	1.491	3.30	12.88
40	0.0217	13.97	9.0	1.452	3.20	12.97
50	0.0215	14.45	7.9	1.411	3.10	13.03
60	0.0210	14.72	7.0	1.368	3.00	12.91
65	0.0207	14.77	6.5	1.341	2.96	12.68
70	0.0202	14.75	6.2	1.327	2.92	12.70
80	0.0190	14.54	5.4	1.281	2.83	12.47
(3) 2,6 Dichloro toluene ($w = 0.0767$)						
0	0.0102	7.75	12.9	1.549	3.66	9.86
10	0.0107	8.55	10.8	1.486	3.53	9.65
20	0.0108	9.08	9.3	1.437	3.41	9.71
30	0.0107	9.43	8.2	1.397	3.30	9.48
40	0.0104	9.65	7.2	1.352	3.20	8.92
45	0.0102	9.71	6.5	1.331	3.15	9.42
50	0.0099	9.68	6.3	1.309	3.10	9.42
60	0.0094	9.61	5.6	1.269	3.00	9.46
70	0.0088	9.35	4.9	1.226	2.92	9.00
(4) Methyl n-butyl ketone ($w = 0.02952$)						
0	0.0425	53.69	10.1	1.441	3.66	11.14
10	0.0432	57.49	8.2	1.367	3.53	11.06
20	0.0422	58.56	6.9	1.306	3.41	10.82
26	0.0412	59.14	6.5	1.286	3.35	10.54
30	0.0403	59.00	6.0	1.259	3.30	10.73
40	0.0379	58.15	5.4	1.226	3.20	10.82
50	0.0355	56.82	4.9	1.196	3.10	10.84
60	0.0325	54.68	4.3	1.158	3.00	10.73
70	0.0299	52.38	3.9	1.128	2.92	10.87
(5) Methyl n-amyl ketone ($w = 0.03480$)						
0	0.04144	51.34	10.6	1.459	3.66	11.20
10	0.0424	54.89	8.8	1.399	3.53	11.04
20	0.0421	56.97	7.5	1.343	3.41	10.96
30	0.0407	57.62	6.5	1.293	3.30	10.86
40	0.0387	57.37	5.9	1.266	3.20	10.94
50	0.0365	56.33	5.2	1.227	3.10	10.91
60	0.0340	54.66	4.7	1.191	3.00	10.91
70	0.0320	53.09	4.3	1.168	2.92	11.19
(6) Methyl phenyl ketone ($w = 0.0335$)						
0	0.0383	50.71	14.4	1.504	3.66	12.11
10	0.0403	56.18	12.2	1.537	3.53	12.05
20	0.0414	60.50	10.5	1.488	3.41	12.05
30	0.0417	63.93	9.1	1.442	3.30	12.08
40	0.0409	66.12	8.2	1.403	3.20	12.19
50	0.0402	67.47	7.1	1.361	3.10	12.13
55	0.0397	67.78	6.5	1.345	3.05	12.25
60	0.0391	67.74	6.3	1.324	3.00	12.19
70	0.0368	66.95	5.5	1.278	2.92	11.94

TABLE II
Temperature = 20°C

Temperature — 20°C.

Substance	Present investigation		Literature	
	$\tau \times 10^{12}$ sec.	μD	$\tau \times 10^{12}$ sec.	μD
Chloro benzene	9.3	1.58	8.9	1.56
<i>o</i> -Chloro toluene	11.6	1.34	11.1	1.33
2,6 Dichloro toluene	9.3	1.09	.	1.09
Methyl <i>n</i> -butyl ketone	6.9	2.69	.	2.72
Methyl <i>n</i> -amyl ketone	7.5	2.66	.	2.72
Methyl phenyl ketone	10.5	2.85	9.6	2.88

TABLE III

Substance	$E_\tau \times 10^{13}$ ergs	$E_\eta \times 10^{13}$ ergs	$A \times 10^{11}$	$B \times 10^5$
Chloro benzene	1.31	1.36	10.7	14.5
<i>O</i> -Chloro toluene	1.33	1.36	12.9	14.5
2,6 Dichloro toluene	1.35	1.36	9.7	14.5
Methyl <i>n</i> -butyl ketone	1.19	1.36	10.9	14.5
Methyl <i>n</i> -amyl ketone	1.22	1.36	11.0	14.5
Methyl phenyl ketone	1.31	1.36	12.1	14.5

Table III contains also the values of E_τ determined from the slopes of the linear plots for these molecules. Whiffen and Thompson determined E_τ assuming Eyring's expression for A . The author has preferred to adopt the values derived from the graphs. In column (2) and (4), the values of E_η and B are shown. These are derived from the data on the viscosities of heptane at different temperatures (taken from the table of "Physico-Chemical Constants", Timmermans). Though E_η and E_τ are approximately the same, E_τ is lower than E_η particularly in the case of aliphatic molecules. This feature is consistent with the explanation proposed that while viscous flow involves both rotation and translation, dipole orientation involves only rotation. Smyth and others (1948) also made the same observation from their experiments on certain halides.

The value of B is found to be 14.5×10^{-5} which is much greater than hN/V (Eyring's expression) calculated at 20°C, which comes to 2.7×10^{-5} . Saxton's values of B for methyl and ethyl alcohols are 8.7×10^{-5} and 4.5×10^{-5} respectively, compared to the calculated values of 10×10^{-5} and 6.9×10^{-5} .

Further investigations on these and other different molecules in liquid and solution conditions are in progress and will form the subject of subsequent papers.

ACKNOWLEDGMENTS

The author is deeply indebted to Prof. K. R. Rao for his kind and valuable guidance throughout the progress of the work. He is also grateful to the Government of India for the award of a scholarship.

REFERENCES

- Eyring, H., Glasstone, S. and Laidler, K. J., 1941, *The theory of rate process*, New York, McGraw-Hill Co., pp. 548.
- Frohlich, H., 1949, *Theory of Dielectrics*, Clarendon Press, Oxford, pp. 80.
- Gopala Krishna, K. V., 1958, *Ind. J. Phys.*, **32**, 387.
- Roberts and von Hippel, 1946, *J. Appl. Phys.*, **17**, 610.
- Saxton, J. A., 1952, *Proc. Roy. Soc.*, **213A**, 473.
- Smyth, C. P., Hemmelly, E. J. and Heston, W. M., 1948, *J. Amer. Chem. Soc.*, **70**, 4102.
- Wluffen, D. H. and Thompson, H. W., 1946, *Trans. Farad. Soc.*, **42A**, 114.

APPLICATION OF SCHWINGER'S ACTION PRINCIPLE TO QUANTISE A FOURTH ORDER MESON FIELD

S. P. MISRA

MATHEMATICS DEPARTMENT, R. COLLEGE, CUTTACK

(Received, September 22, 1959)

ABSTRACT. We have here applied Schwinger's Action Principle to the case of a fourth order meson equation proposed by Bhabha and Thirring. The result obtained thus is not new, but the method illustrates with the simplest model the difficulties of applying Action Principle when the Lagrangian contains even the second order derivatives of the field operator, and gives a concrete and complete example of the generalisation of the Action Principle when the Lagrangian contains higher order derivatives as given by the author in a recent paper.

INTRODUCTION

The fourth order meson equation proposed by Bhabha (1950) and Thirring (1950) has been considered in some detail, including field quantisation, by Thirring (1950). Here, however, we shall employ the general Action Principle of Schwinger (1951, 1953) in quantising this field, and obtaining a symmetric energy-momentum tensor of the same. The result obtained thus is not new, but the method illustrates with the simplest model the difficulties of applying Action Principle when the Lagrangian contains even the second order derivatives of the field operator, and gives a concrete and complete example of the generalisation of the Action Principle when the Lagrangian contains higher order derivatives as given by the author in a recent paper (Misra, 1959 ; hereafter to be referred as P1).

The above meson equation has been found useful in explaining anomalous magnetic moments of nucleons (Misra and Deo (1956) and is interesting since it gives rise to convergent contributions in many physical processes which involve meson propagator. The fourth order calculations of the matrix elements for the nuclear forces with this fourth order meson equation also gives rise to many conclusions of theoretical interest (Misra ..., to be published).

The free field fourth order meson equation is

$$(\square - \kappa^2)\phi(x) = 0 \quad \dots (1)$$

where

$$\square \equiv (\vec{\nabla}^2 - (\partial_0)^2) \equiv g_{\mu\nu} \partial_\mu \partial_\nu.$$

Equation (1) can be obtained by using the invariant Lagrangian density

$$L(x) = -\frac{1}{2\kappa^2} (\Box \phi)(\Box \phi) - (\partial_\mu \phi)(\partial_\mu \phi) - \frac{k^2}{2} \phi^2 \quad \dots (2)$$

which gives us the Action Integral W_{12} for any two space-like surfaces σ_1 and σ_2 as

$$W_{12} = \int_{\sigma_2}^{\sigma_1} L(x) d^4x.$$

This gives us, when the field equation (1) is satisfied,

$$\delta W_{12} = F(\sigma_1) - F(\sigma_2) \quad \dots (3)$$

where, by equation (15) of PI,

$$F(\sigma) = \int_\sigma [\pi_\mu \delta_\sigma \phi + \pi_{\mu\nu} \partial_\nu (\delta_\sigma \phi) + L \delta x_\mu] d\sigma_\mu. \quad \dots (4)$$

In the above, by equation (13) of PI,

$$\begin{aligned} \pi_\mu &= \frac{\partial L}{\partial(\partial_\mu \phi)} - \partial_\nu \frac{\partial L}{\partial(\partial_\mu \partial_\nu \phi)} \\ &= -2\partial_\mu \phi + \frac{1}{\kappa^2} \partial_\mu \Box \phi \end{aligned} \quad \dots (5)$$

and

$$\begin{aligned} \pi_{\mu\nu} &= \frac{\partial L}{\partial(\partial_\mu \partial_\nu \phi)} \\ &= -\frac{1}{\kappa^2} g_{\mu\nu} \Box \phi \end{aligned} \quad \dots (6)$$

COMMUTATION RELATION

Let us now substitute

$$\pi_{(0)} \equiv n_\mu \pi_\mu = -2\partial^{(0)} \phi + 1/\kappa^2 \partial^{(0)} \Box \phi \quad \dots (7)$$

and

$$\pi_{(00)} \equiv n_\mu n_\nu \pi_{\mu\nu} = 1/\kappa^2 \Box \phi. \quad \dots (7')$$

Then, by equation (23) of PI we obtain,

$$\begin{aligned} n_\mu \pi_\mu^{[\sigma, 0]} &= n_\mu (\pi_\mu - \partial_{t\nu} \pi_{\mu\nu}) \\ &= n_\mu \pi_\mu = \pi_{(0)} \end{aligned} \quad \dots (8)$$

and

$$\begin{aligned} n_\mu \pi_\mu^{[0,1]} &= n_\mu (-n_\nu \pi_{\mu\nu}) \\ &= -\pi_{(00)} \end{aligned} \quad \dots \quad (9)$$

Hence equation (27) of P1 gives us

$$[\phi(x), \int_{\sigma} \{\pi_{(0)}(x') \delta_0 \phi(x') - \pi_{(00)}(x') \delta_0((\partial'^{(0)})\phi(x'))\} d\sigma(x')] = i\delta_0 \phi(x) \quad \dots \quad (10)$$

and

$$[\partial^{(0)}\phi(x), \int_{\sigma} \{\pi_{(0)}(x') \delta_0 \phi(x') - \pi_{(00)}(x') \delta_0((\partial'^{(0)})\phi(x'))\} d\sigma(x')] = i\delta_0(\partial^{(0)}\phi(x)) \quad \dots \quad (11)$$

Hence, using equation (31) of P1, we obtain, with the notation $\delta_\alpha(x-x') = n_\mu \delta_\mu^{(\alpha)}(x-x')$,

$$\begin{aligned} [\phi(x), \pi_{(0)}(x') \delta_0 \phi(x')] &= i\delta_\alpha(x-x') \delta_0 \phi(x), \\ [\phi \partial^{(0)}\phi(x), \pi_{(00)}(x') \delta_0(\partial'^{(0)}\phi(x'))] &= -i\delta_\alpha(x-x') \delta_0(\partial^{(0)}\phi(x)), \end{aligned} \quad \dots \quad (12)$$

and

$$\begin{aligned} &[\phi(x), \pi_{(00)}(x') \delta_0(\partial'^{(0)}\phi(x'))] \\ &= [\partial^{(0)}\phi(x), \pi_{(0)}(x') \delta_0 \phi(x')] = 0. \end{aligned} \quad \dots \quad (12')$$

When we take

$$\begin{aligned} |[\phi(x), \delta_0 \phi(x')]| &= |[\phi(x), \delta_0(\partial'^{(0)}\phi(x'))]| \\ &= |[\partial^{(0)}\phi(x), \delta \phi(x')]| \\ &= |[\partial^{(0)}\phi(x), \delta_0(\partial'^{(0)}\phi(x'))]| = 0, \end{aligned} \quad \dots \quad (13)$$

which have to be satisfied if we assume that the variations of the field operators allowed are such that the commutators or their derivatives do not change, then we obtain the commutation relationships for space-like separation of the points x and x' as

$$[\phi(x), \pi_{(00)}(x')] = [\partial^{(0)}\phi(x), \pi_{(0)}(x')] = 0 \quad \dots \quad (14)$$

and

$$\begin{aligned} |\phi(x), \pi_{(0)}(x')| &= i\delta_\alpha(x-x'), \\ |[\partial^{(0)}\phi(x), \pi_{(00)}(x')]| &= -i\delta_\alpha(x-x'). \end{aligned} \quad \dots \quad (15)$$

Hence making use of equations (7) we obtain the commutation relations for space-like separation of the points

$$[\phi(x), -2\partial'^{(0)}\phi(x') + \frac{1}{\kappa^2} \partial'^{(0)} \square' \phi(x')] = i\delta_\alpha(x-x'),$$

$$[\phi(x), -\square' \phi(x')] = 0,$$

$$[\partial^{(0)}\phi(x), -2\partial'^{(0)}\phi(x') + \frac{1}{\kappa^2} \partial'^{(0)} \square' \phi(x')] = 0$$

and

$$[\partial^{(0)}\phi(x), -\frac{1}{\kappa^2} \square' \phi(x')] = i\delta_n(x-x'). \quad \dots \quad (16)$$

Let us now put, for *any* two space-time points x and y ,

$$[\phi(x), \phi(y)] = C(x-y), \quad \dots \quad (17)$$

where the right hand side is a function of the differences of the coordinates since it has to be invariant under translations. Using this, we obtain that in equations (16), while operating on the commutator $C(x-x')$, $\partial'^{(0)} = -\partial^{(0)}$ and $\square' = \square$. Also, since n_μ is sufficiently stationary at any point of the surface, $\partial'^{(0)}\square' = \square'\partial'^{(0)}$. Hence, by straight-forward simplification, equations (16) with x and x' having space-like separation, reduce to

$$\begin{aligned} \partial^{(0)}\square C(x-x') &= -i\kappa^2\delta_n(x-x'), \\ \partial^{(0)}C(x-x') &= \square C(x-x') = 0. \end{aligned} \quad \dots \quad (18)$$

and

$$2(\partial^{(0)})^2 C(x-x') - \frac{1}{\kappa^2} (\partial^{(0)})^2 \square C(x-x') = 0. \quad \dots \quad (19)$$

Our equations now are sufficiently simple for us to obtain the value of $C(x-y)$ for arbitrary separation of the points x and y , which we had been unable to do in the general case of PI. For this purpose, we shall use the solution of the field operator in terms of the advanced and retarded Green's functions of the field equation (1) (Jauch and Rohrlich (1955)). The equations that these Green's functions satisfy are

$$(\square - k^2)^2 G_{R,A}(x-x') = -\delta_4(x-x'), \quad \dots \quad (20)$$

where

$$G_R(x-x') = 0 \quad \text{when} \quad x'_0 > x_0,$$

and

$$G_A(x-x') = 0 \quad \text{when} \quad x'_0 < x_0. \quad \dots \quad (21)$$

Replacing x by x' in the field equation (1) and using equation (20) we obtain,

$$\begin{aligned} \phi(x) &= \int_{\sigma_2}^{\sigma_1} [G_{R,A}(x-x')(\square' - \kappa^2)^2 \phi(x') - (\square - k^2)^2 G_{R,A}(x-x')\phi(x')] d^4x' \\ &= \int_{\sigma_2}^{\sigma_1} [G_{R,A}(x-x')(\square'^2 - 2\kappa^2\square')\phi(x') - (\square^2 - 2\kappa^2\square)G_{R,A}(x-x')\phi(x')] d^4x' \end{aligned} \quad \dots \quad (22)$$

where σ_1 and σ_2 are two space-like surfaces with σ_1 later than x and σ_2 earlier than x in time, such that the point x lies between them. To simplify the right hand side of equation (22), we first note that

$$\begin{aligned} G_{R,A}(x-x')\square'^2\phi(x') - \square'^2 G_{R,A}(x-x')\phi(x') \\ = \partial'_\mu [G_{R,A}(x-x')\partial'_\mu \square'\phi(x') - \partial'_\mu G_{R,A}(x-x')\square'\phi(x') \\ + \square' G_{R,A}(x-x')\partial'_\mu \phi(x') - \partial'_\mu \square' G_{R,A}(x-x')\phi(x')] \quad \dots \quad (23) \end{aligned}$$

and

$$\begin{aligned} G_{R,A}(x-x')\square'\phi(x') - \square' G_{R,A}(x-x')\phi(x') \\ = \partial'_\mu [G_{R,A}(x-x')\partial'_\mu \phi(x') - \partial'_\mu G_{R,A}(x-x')\phi(x')] \quad \dots \quad (24) \end{aligned}$$

We apply Gauss theorem to the right hand side of equation (22), and use the invariance of Green's functions and the equations (21). These Green's functions vanish for space-like separation of the points x and x' , and thus the integral j over the surface joining σ_1 and σ_2 for infinite space-like separation also vanishes. Hence we get,

$$\begin{aligned} \phi(x) = \int_{\sigma_1} [G_{R,A}(x-x')\partial'_\mu \square'\phi(x') - \partial'_\mu G_{R,A}(x-x')\square'\phi(x') \\ + \square' G_{R,A}(x-x')\partial'_\mu \phi(x') - \partial'_\mu \square' G_{R,A}(x-x')\phi(x') \\ - 2\kappa^2 G_{R,A}(x-x')\partial'_\mu \phi(x') + 2\kappa^2 \partial'_\mu G_{R,A}(x-x')\phi(x')] d\sigma_\mu(x') \\ - \int_{\sigma_2} (\text{the same integrand}) d\sigma_\mu(x'). \quad \dots \quad (25) \end{aligned}$$

In solution (25) of $\phi(x)$ in terms of the surface integrals, on using equation (21) for advanced and retarded Green's functions, we obtain,

$$\begin{aligned} \phi(x) = \int_{\sigma_1} [G_A(x-x')\partial'_\mu \square'\phi(x') - \partial'_\mu G_A(x-x')\square'\phi(x') \\ + \square' G_A(x-x')\partial'_\mu \phi(x') - \partial'_\mu \square' G_A(x-x')\phi(x') \\ - 2\kappa^2 G_A(x-x')\partial'_\mu \phi(x') + 2\kappa^2 \partial'_\mu G_A(x-x')\phi(x')] d\sigma_\mu(x') \quad \dots \quad (26) \end{aligned}$$

$$= - \int_{\sigma_2} (\text{the same integrand with } G_A \text{ replaced by } G_R) d\sigma_\mu(x') \quad \dots \quad (27)$$

We now substitute

$$G(x-x') = G_R(x-x') - G_A(x-x'), \quad \dots \quad (28)$$

such that, on the surface σ_1 , $G = -G_A$ and on the surface σ_2 , $G = G_R$. Hence we obtain for any surface σ which does not contain x

$$\begin{aligned} \phi(x) = - \int_{\sigma} [G(x-x')\partial_{\mu}'[\Box'\phi(x') - \partial_{\mu}'G(x-x')\Box'\phi(x')] \\ + \Box'G(x-x')\partial_{\mu}'\phi(x') - \partial_{\mu}'\Box'G(x-x')\phi(x') \\ - 2\kappa^2 G(x-x')\partial_{\mu}'\phi(x') + 2\kappa^2 \partial_{\mu}'G(x-x')\phi(x')] d\sigma_{\mu}(x') \end{aligned} \quad \dots (29)$$

Let us now assume that the above space-like surface σ contains the point y . Hence we get, by equation (29),

$$\begin{aligned} [\phi(x), \phi(y)] = \int_{\sigma} \{ -G(x-x')\partial_{\mu}'[\Box'\phi(x'), \phi(y)] \\ + \partial_{\mu}'\Box'G(x-x')[\phi(x'), \phi(y)] - \Box'G(x-x')\partial_{\mu}'[\phi(x'), \phi(y)] \\ + \partial_{\mu}'\Box'G(x-x')[\phi(x'), \phi(y)] + 2\kappa^2 G(x-x')\partial_{\mu}'[\phi(x'), \phi(y)] \\ - 2\kappa^2 \partial_{\mu}'G(x-x')[\phi(x'), \phi(y)] \} n_{\mu}(x') d\sigma(x'), \end{aligned}$$

which on rearrangement becomes, by definition (17),

$$\begin{aligned} C(x-y) \\ = \int_{\sigma} \{ G(x-x')(2\kappa^2 \partial'^{(0)} C(x'-y) - \partial'^{(0)} \Box' C(x'-y)) \\ - \partial'^{(0)} G(x-x')(-\Box' C(x'-y) - 2\kappa^2 C(x'-y)) \\ - \Box' G(x-x')\partial'^{(0)} C(x'-y) + \partial'^{(0)} \Box' G(x-x')C(x'-y) \} d\sigma(x'). \end{aligned}$$

Using equations (18), the above relationship reduces to

$$C(x-y) = \int_{\sigma} G(x-x') \{ i\kappa^2 \delta_{\sigma}(x'-y) \} d\sigma(x')$$

such that

$$C(x-y) = i\kappa^2 G(x-y) \quad \dots (30)$$

We shall now write down explicitly the retarded and advanced Green's functions as contour integrals. We have,

$$G_R(x) = \frac{-1}{(2\pi)^4} \int_{\sim} \frac{e^{i(\vec{k} \cdot \vec{x} - k_0 x_0)}}{(k^2 + \kappa^2)^2} d^3k dk_0 \quad \dots (31)$$

where the contour C_R is defined by figure 1a in the complex k_0 plane. This can be easily seen when we notice that

$$\int \frac{e^{-ik_0 x_0}}{(k^2 + \kappa^2)} dk_0$$

over an infinite semi-circle in the upper half plane vanishes when $x_0 < 0$. Hence by Cauchy's theorem the right hand side of equation (31) vanishes when $x_0 < 0$, which corresponds to the first of equations (21). We can write in a similar way, with C'_A defined by figure 1a.

$$G_A(x) = \frac{-1}{(2\pi)^4} \int_{C'_A} \frac{e^{i(k \cdot x - k_0 x_0)}}{(k^2 + \kappa^2)^2} d^3 k dk_0 \quad \dots (32)$$

which can be shown to satisfy equation (21) by considering the vanishing of the above integral over an infinite semi-circle in the lower half complex k_0 plane.

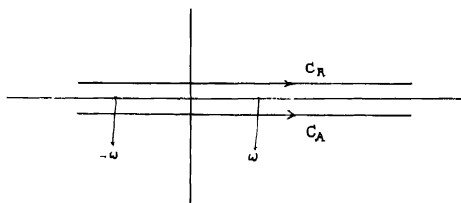


Fig. 1(a)

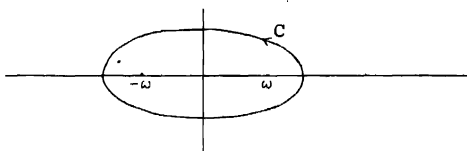


Fig. 1(b)

Thus we have,

$$G(x) = \frac{1}{(2\pi)^4} \int_C \frac{e^{i(k \cdot x - k_0 x_0)}}{(k^2 + \kappa^2)^2} d^3 k dk_0, \quad \dots (33)$$

where C is the contour of figure 1b. Integrating for k_0 this result gives us,

$$G(x) = \frac{1}{2(2\pi)^3} \int \frac{d^3 k}{\omega^3} e^{ik \cdot x} [\omega x_0 \cos(\omega x_0) - \sin(\omega x_0)] \quad \dots (34)$$

with

$$\omega = + \sqrt{k^2 + \kappa^2}$$

We can now verify that $C(x-x') = i\kappa^2 G(x-x')$ satisfies equations (18) and (19) for space-like separation of the points x and x' . This is directly demonstrated when we evaluate the left hand side of the covariant equations (18) and (19), substituting the value of $C(x-x')$ according to equations (30) and (34), and then proving the validity of equations (18) and (19) with the special coordinate system $x_0-x'_0=0$. Equation (19), which was not used to deduce equation (30), may be specially seen to be satisfied

ENERGY-MOMENTUM TENSOR

We can also obtain the energy-momentum tensor for this particular case from the generator $F(\sigma)$ on the surface σ . For this purpose we first recollect the equation

$$F(\sigma) = \int_{\sigma} [\pi_{\mu} \delta_0 \phi + \pi_{\mu\nu} \delta_0 (\partial_{\nu} \phi) + L \delta x_{\mu}] d\sigma_{\mu}$$

Now, let $\delta\phi$ be the total variation of ϕ due to the intrinsic variation $\delta_0\phi$ on the surface σ and also due to a rigid displacement of the surface by δx_{μ} . Then we have,

$$\delta\phi = \delta_0\phi + \phi(x + \delta x) - \phi(x) = \delta_0\phi + (\partial_{\kappa}\phi)\delta x_{\kappa} \quad \dots (35)$$

such that

$$\partial_{\nu}(\delta\phi) = \partial_{\nu}(\delta_0\phi) + (\partial_{\nu}\partial_{\kappa}\phi)\delta x_{\kappa} + (\partial_{\kappa}\phi)(\partial_{\nu}(\delta x_{\kappa})). \quad \dots (36)$$

Hence, using the above two equations we obtain,

$$\begin{aligned} F(\sigma) = \int_{\sigma} [\pi_{\mu} \delta\phi + \pi_{\mu\nu} \partial_{\nu}(\delta\phi) + L \delta x_{\mu} - \pi_{\mu}(\partial_{\nu}\phi)\delta x_{\nu} - \pi_{\mu\nu}(\partial_{\kappa}\phi)\delta x_{\kappa} \\ - \pi_{\mu\nu}(\partial_{\kappa}\phi)\partial_{\nu}(\delta x_{\kappa})] d\sigma_{\mu} \quad \dots (37) \end{aligned}$$

We now note that for a rigid displacement of the surface, since two neighbouring points on the original surface and on the displaced surface will remain at the same distance, we shall have,

$$\partial_{\kappa}(\delta x_{\mu}) + \partial_{\mu}(\delta x_{\kappa}) = 0 \quad \dots (38)$$

But the above is the condition that the transformation $x_{\mu} \rightarrow x'_{\mu} = x_{\mu} + \delta x_{\mu}$ is an infinitesimal Lorentz transformation. This gives us the equivalence of the rigid displacement to a Lorentz transformation.

Let us now consider an infinitesimal Lorentz transformation (or a rigid displacement) $x_{\mu} \rightarrow x_{\mu} + \delta x_{\mu}$, and take the intrinsic variation $\delta_0\phi$ such that the total variations $\delta\phi$ and $\delta(\partial^{(0)}\phi)$ vanish. Then, for such intrinsic variations, the field operators will remain the same on the surfaces σ and $\sigma + \delta\sigma$. The expression for the generator on the surface σ now becomes

$$F_{\delta x}(\sigma) = \int [L \delta x_{\mu} - \pi_{\mu}(\partial_{\nu}\phi)\delta x_{\nu} - \pi_{\mu\kappa}(\partial_{\nu}\partial_{\mu}\phi)\delta x_{\nu} - \pi_{\mu\kappa}(\partial_{\nu}\phi)\partial_{\kappa}(\delta x_{\nu})] d\sigma_{\mu} \quad \dots (39)$$

The above formula does not contain any spin-dependent term since we have taken a scalar field and thus the formula (35) did not involve any expression for the change due to a rotation in the coordinate space that the δx_μ contains.

The expression (39) on the right hand side depends only on the transformation or displacement given by δx_μ . It also involves an integration over σ of functions of field operator. However, since the total variations $\delta\phi$ and $\delta(\partial^{(0)}\phi)$ are zero, these field operators do not change for an infinitesimal displacement of the surface and hence remain the same for a succession of such displacements of the surface. A succession of such displacements is equivalent to a number of infinitesimal Lorentz transformations, under which our theory is invariant. Hence the generator $F(\sigma)$ given by equation (39) is the same for all surfaces, and depends only on δx_μ .

In order to obtain a symmetrical energy-momentum tensor, we need at this stage some further manipulations similar to the treatment of the term due to spin by Schwinger (1951). Equation (38) gives us

$$\pi_{\mu\kappa}(\partial_\nu\phi)\partial_\kappa(\delta x_\nu) = \frac{1}{2}\chi_{\mu\kappa\nu}\partial_\kappa(\delta x_\nu)$$

where

$$\chi_{\mu\kappa\nu} = [\pi_{\mu\kappa}(\partial_\nu\phi) - \pi_{\mu\nu}(\partial_\kappa\phi)] \quad \dots \quad (40)$$

We now define

$$2f_{\mu\kappa\nu} = \chi_{\mu\kappa\nu} - \chi_{\mu\nu\kappa} + \chi_{\nu\mu\kappa} = \chi_{\mu\kappa\nu} + \chi_{\kappa\nu\mu} + \chi_{\nu\mu\kappa} \quad \dots \quad (41)$$

Clearly,

$$f_{\kappa\mu\nu} = -f_{\mu\kappa\nu}, \quad \dots \quad (42)$$

and

$$\frac{1}{2}\chi_{\mu\kappa\nu}\partial_\kappa(\delta x_\nu) = f_{\mu\kappa\nu}\partial_\kappa(\delta x_\nu). \quad \dots \quad (43)$$

Using equations (6) and (7'), we now obtain, by equations (40) and (41) and on simplification,

$$f_{\mu\kappa\nu} = [\pi_{\kappa\nu}(\partial_\mu\phi) - \pi_{\mu\nu}(\partial_\kappa\phi)]. \quad \dots \quad (44)$$

Consistent with earlier notations, let the suffix (0) denote the normal component of any tensor at any point of the surface and the suffix ($t\mu$) denote the tangential component of any tensor at any point of the surface. Then we have,—

$$\begin{aligned} \int_\sigma \partial_\kappa(f_{\mu\kappa\nu}\delta x_\nu)d\sigma_\mu &= \int_\sigma \partial_\kappa(f_{(0)\kappa\nu}\delta x_\nu)d\sigma \\ &= \int \partial_{(t\kappa)}(f_{(0)(t\kappa)\nu}\delta x_\nu)d\sigma + \int \partial_{(0)}(f_{(0)(0)\nu}\delta x_\nu)d\sigma = 0 \end{aligned}$$

provided that $f_{(0)(ik)\nu}\delta x_\nu$ vanishes sufficiently rapidly at the boundary of the surface σ , which we assume to be the case. Hence in equation (39) we obtain,

$$\begin{aligned} \int_{\sigma} \pi_{\mu\lambda}(\partial_\nu\phi)\partial_\lambda(\delta x_\nu)d\sigma_\mu &= \int_{\sigma} f_{\mu\lambda\nu}\partial_\lambda(\delta x_\nu)d\sigma_\mu \\ &= - \int_{\sigma} \partial_\lambda(f_{\mu\lambda\nu})\delta x_\nu d\sigma_\mu = \int_{\sigma} \partial_\lambda(f_{\lambda\mu\nu})\delta x_\nu d\sigma_\mu \end{aligned}$$

and thus we finally get,

$$\begin{aligned} &-F_{\delta x}(\sigma) \\ &= - \int_{\sigma} [g_{\mu\nu}L - \pi_{\mu}(\partial_\nu\phi) - \pi_{\mu\lambda}(\partial_\nu\partial_\lambda\phi) - \partial_\lambda(f_{\lambda\mu\nu})]\delta x_\nu d\sigma_\mu = \int T_{\mu\nu}\delta x_\nu d\sigma_\mu \quad \dots \quad (45) \end{aligned}$$

where

$$\begin{aligned} T_{\mu\nu} \\ = \pi_{\mu}(\partial_\nu\phi) + \pi_{\mu\lambda}(\partial_\nu\partial_\lambda\phi) + \partial_\lambda(f_{\lambda\mu\nu}) - Lg_{\mu\nu}. \end{aligned} \quad \dots \quad (46)$$

This gives us, on substitution of the values in our particular case, by equations (7), (7') and (44),

$$\begin{aligned} T_{\mu\nu} = g_{\mu\nu} \left[-\frac{1}{2\kappa^2} (\Box\phi)(\Box\phi) - \frac{1}{\kappa^2} (\partial_\lambda\Box\phi)(\partial_\lambda\phi) + (\partial_\lambda\phi)(\partial_\lambda\phi) + \frac{\kappa^2}{2} \phi^2 \right] \\ + \frac{1}{\kappa^2} [(\partial_\mu[\Box\phi])(\partial_\nu\phi) + (\partial_\nu[\Box\phi])(\partial_\mu\phi)] - 2(\partial_\mu\phi)(\partial_\nu\phi). \end{aligned} \quad \dots \quad (47)$$

The above $T_{\mu\nu}$ is obviously symmetric in μ and ν , and we shall presently see that it represents the energy-momentum tensor. For this purpose, let

$$\delta x_\mu = \epsilon_\mu + \epsilon_{\mu\nu}x_\nu \quad \dots \quad (48)$$

be the infinitesimal Lorentz transformation associated with the rigid displacement. Then the momentum and angular momentum operators are defined by (Jauch and Rohrlich (1955) p.12)

$$U = 1 + iK = 1 + i(P_\nu\epsilon_\nu + \frac{1}{2}J_{\nu\lambda}\epsilon_{\nu\lambda})$$

where the state-vector transforms by the unitary operator U , and thus we have,

$$K = -F_{\delta x}(\sigma) = P_\nu(\sigma)\epsilon_\nu + \frac{1}{2}J_{\nu\lambda}(\sigma)\epsilon_{\nu\lambda}, \quad \dots \quad (49)$$

where the total energy-momentum four-vector is given as

$$P_\nu(\sigma) = \int_{\sigma} T_{\mu\nu}d\sigma_\mu \quad \dots \quad (50)$$

and the total angular momentum tensor is given as

$$J_{\nu\lambda}(\sigma) = \int_{\sigma} M_{\nu\lambda}d\sigma_\mu \quad \dots \quad (51)$$

with

$$M_{\mu\nu\lambda} = (T_{\mu\nu}x_\lambda - T_{\mu\lambda}x_\nu). \quad (52)$$

The conservation laws follow from the earlier remark that the generator $F_{0x}(\sigma)$ is independent of the surface σ , since a displacement of the surface is equivalent to a Lorentz transformation, and our theory is Lorentz invariant.

Here we may note a difficulty of this theory. The energy density of the field for a flat surface $t = x_0 = \text{const.}$ is given as

$$\begin{aligned} T_{00} &= (\vec{\nabla}\phi)^2 + (\partial_0\phi)^2 + \frac{\kappa^2}{2} \phi^2 \\ &= \frac{1}{2\kappa^2} (\Box\phi)(\Box\phi) - \frac{1}{\kappa^2} (\vec{\nabla}\Box\phi) \cdot (\vec{\nabla}\phi) - \frac{1}{\kappa^2} (\partial_0\Box\phi)(\partial_0\phi). \quad \dots \quad (53) \end{aligned}$$

The above expression is *not* a positive definite function of the field operators. This leads to the suspicion that this theory may lead to inconsistent results associated with "ghost" states. However, such states are known to exist in the exact solutions of the semi-relativistic Lee model (Kallen and Pauli, 1955) and are also suspected to be present even in quantum electrodynamics (Landau, 1955). Since this defect seems to be rather a persistent feature of field theory, we consider it worthwhile to see the effect of this theory on nuclear forces when the mesons occur in the virtual state. This might be interesting since it has been pointed out by Ferreti (1958) that it is possible to eliminate negative energy states for real particles in case of Lee model.

In any case, this is an interesting application of Action Principle to the case when the Lagrangian contains second order derivatives of the field operator

ACKNOWLEDGMENTS

The author wishes to express his sincere thanks to Prof. D. Basu for his guidance and to Dr. B. B. Deo and Dr. T. Pradhan for valuable discussions.

REFERENCES

- Bhabha, H. J., 1950, *Phys. Rev.*, **77**, 665
- Ferreti, B., 1958, *Nouv. Chim.*, **12**, 393
- Jauch, J. M. and Rohrlich, F., 1955, *The theory of Photons and electrons*, Addison-Wesley Publ. Comp.
- Kallen, G. and Pauli, W., 1955, *Dan. Mat. Fys. Medd.*, **30**, no. 7.
- Landau, L. D., 1955, *On the Quantum theory of Fields, Niels Bohr and Development of Physics*, Pergamon Press, London.
- Misra, S. P. and Deo, B. B., 1956, *Ind. J. Phys.*, **30**, 16.
- Misra, S. P., 1959, *Ind. J. Phys.*, **33**, 461
- Schwinger, J., 1951, *Phys. Rev.*, **82**, 914
- Schwinger, J., 1953, *Phys. Rev.*, **91**, 713.
- Thirring, W., 1950, *Phil. Mag.*, **41**, 653.

A SHORT NOTE ON THE CRYSTALLINE ELECTRIC FIELDS IN HYDRATED Co^{2+} SALTS

A. S. CHAKRAVARTY AND R. CHATTERJEE

DEPARTMENT OF MAGNETISM, INDIAN ASSOCIATION FOR THE CULTIVATION OF SCIENCE
CALCUTTA-32

(Received, November 10, 1959)

ABSTRACT The paper gives a preliminary account of the theory of the susceptibility and anisotropy of hydrated Co^{2+} salts using Abragam and Pryce's Hamiltonian. It is seen that the experimental anisotropies and susceptibilities can be well fitted with theory on the assumption that the anisotropic crystalline electric field changes quite appreciably from salt to salt and with temperature.

The magnetic susceptibility of Co^{2+} salts have been investigated by Schlapp and Penney (1932) on the basis of Van Vleck's (1932) theory of crystalline electric fields. This investigation, however, assumes a single Co^{2+} ion in the unit cell of the salts and deals with only two extreme cases of the magnitude of the asymmetric part of the electric field as compared to the spin-orbit coupling. Uryu (1956) has recently attempted to explain the experimental principal susceptibilities of $\text{Co}(\text{NH}_4\text{SO}_4)_2 \cdot 6\text{H}_2\text{O}$ crystal (Jackson 1924, Bose 1948) using the method of Abragam and Pryce (1951). The main drawback of this attempt is that it takes into consideration only the three lowest Kramer's doublets, and contains a serious mistake in the fundamental assumptions regarding the energy levels.

On the basis of the limited X-ray structural data (Hofmann, 1931) and paramagnetic resonance data (Bleaney and Ingram, 1951) on the Co^{2+} Tutton salts, we have assumed an approximate tetragonal symmetry of the $(\text{Co}^{2+}, 6\text{H}_2\text{O})$ octahedron of which there are two ions in the unit cell, with the tetragonal axes inclined at $\sim 34^\circ$ to the χ_1 magnetic axis of the crystal, and following Abragam and Pryce's method have developed a general expression for the susceptibilities of the Co^{2+} ion in the crystals which is a complicated function of Δ , the tetragonal fields splitting parameter, α and α' , the effective Lande splitting factors in the crystals and ζ the spin-orbit coupling coefficient.

We find that in order to fit the experimental principal susceptibilities and anisotropies (Jackson, 1924; Bose, 1948), it is enough to take α , α' to be more or less the same in each of the different salts but Δ is quite different. Moreover, for a given salt Δ is found to vary appreciably with temperature in the entire range studied.

(Table I). Similar variations in Δ have been observed by us in Ti^{3+} caesium alum (Bose *et al.*, 1959) and to a smaller extent in Cu^{2+} (Bose *et al.*, 1957), Ni^{2+} (Bose *et al.*, 1958), Cr^{3+} (Dutta Roy, 1956) and V^{3+} (Dutta Roy *et al.*, 1959) salts and are ascribed to the changes in structure from salt to salt and due to thermal expansion of the lattice. It is interesting to note that ζ is the same for all the salts and has the same value as for the free ion, indicating that the covalent overlap of $3d$ -orbitals of the Co^{2+} ion and the s - and p - orbitals of the surrounding water oxygens is negligible (Owen, 1955). The values of Δ , α , α' are found to be different from those obtained by Abragam and Pryce (1951). Owing to very short relaxation times in the Co^{2+} salts, the paramagnetic resonance values for g_{\parallel} and g_{\perp} could be obtained only at -20°K (Bleaney and Ingram) with which the theoretical values are in reasonable agreement.

We give below (Table I) the parameters for the different salts taken to give the best fits of the theoretical square of the moments P_{\parallel}^2 and P_{\perp}^2 along and perpendicular respectively to the tetragonal axis of the Co^{2+} ion at different temperatures with the experimental values (Table II). In view of fairly large uncertainties in the existing experimental data, it is not very useful to refine the theoretical parameters

The details will be published elsewhere shortly.

ACKNOWLEDGMENT

The authors wish to express their gratefulness to Prof. A. Bose for suggesting the problem and for helpful discussions and suggestions

TABLE I

Salts	α	α'	Temp °K.	Δ cm ⁻¹ at different	g -values at 20°K			
				Tempera- tures	Experimental		Theoretical	
					$g_{ }$	g_{\perp}	$g_{ }$	g_{\perp}
Co(NH ₄ SO ₄) ₂ ·6H ₂ O	1.08	1.53	290	1030	6.45	3.00	6.2	2.9
			77.2	1230			(for Δ = 1250	
			14.5	1265			Cm ⁻¹)	
Co(NH ₄ BeF ₄) ₂ ·6H ₂ O	1.095	1.46	296.7K	864	No resonance value			
			185.8	740				
			86.8	720				
Co(KSO ₄) ₂ ·6H ₂ O	1.245	1.28	300	280	6.56	2.96	6.60	2.71
			200	300			(for Δ = 720	
			100	320			cm ⁻¹)	

(for $\Delta = 1250$
 cm^{-1})

(for $\Delta = 720$
 cm^{-1})

TABLE II

$\text{Co}(\text{NH}_4\text{SO}_4)_2 \cdot 6\text{H}_2\text{O}$			$\text{Co}(\text{NH}_4\text{BeF}_4)_2 \cdot 6\text{H}_2\text{O}$			$\text{Co}(\text{KSO}_4)_2 \cdot 6\text{H}_2\text{O}$		
T°K.	$P_{ }^2$	P_{\perp}^2	T°K.	$P_{ }^2$	P_{\perp}^2	T°K.	$P_{ }^2$	P_{\perp}^2
200	29.22 (29.19)	18.78 (18.75)	296.7	29.40 (29.66)	19.40 (19.59)	300	29.31 (29.49)	21.88 (22.08)
77.2	34.44 (34.33)	11.19 (10.88)	185.8	30.39 (29.58)	18.24 (17.56)	200	30.79 (30.14)	20.11 (19.42)
14.5	30.12 (29.80)	7.05 (6.65)	86.8	28.81 (28.09)	14.32 (13.65)	100	29.31 (29.23)	15.56 (15.19)

The values in the parenthesis indicate the experimental results.

REFERENCES

- Abraham, A. and Pryce, M. H. L., 1951, *Proc. Roy. Soc. A.*, **205**, 135; *Proc. Roy. Soc. A.*, **206**, 173.
 Bose, A., 1948, *Ind. J. Phys.*, **22**, 276.
 Bose, A., Mitra, S. C., and Dutta, Sunil K., 1957, *Proc. Ry. Soc., A*, **239**, 165, 1958, *Proc. Roy. Soc. A.*, **248**, 153.
 Bose, A., Chakravarty, A. S. and Chatterji, R., 1959, *Proc. Roy. Soc.* (communicated).
 Bleaney, B. and Ingram, D. J. E., 1951, *Proc. Roy. Soc. A.*, **208**, 143.
 Dutta Roy, S. K., 1956, *Ind. J. Phys.*, **30**, 169.
 Dutta Roy, S. K., Chakravarty, A. S. and Bose, A., 1959, *Ind. J. Phys.* (in press).
 Hofmann, W., 1931, *Z. Kristallogr.*, **78**, 279.
 Jackson, L. C. 1924, *Trans. Roy. Soc. A.*, **224**, 1.
 Owen, J., 1955, *Proc. Roy. Soc. A.*, **227**, 183.
 Schlapp, R. and Penney, W. G., 1932, *Phys. Rev.*, **42**, 666.
 Uryu, N., 1956, *Jour. Phys. Soc. Japan*, **11**, No. 7, 770.
 Van. Vleck, J. H., 1932, *Phys. Rev.*, **41**, 208.

INFLUENCE OF INTERATOMIC RESONANCE ON THE FREQUENCY OF RE-EMITTED RESONANCE RADIATION*

G. S. KASTHA

OPTICS DEPARTMENT, INDIAN ASSOCIATION FOR THE CULTIVATION OF SCIENCE, CALCUTTA-32

(Received, November 6, 1959)

ABSTRACT. The presence of radiations of changed frequencies, reported earlier, in the spectra of the resonance radiation of sodium and mercury filtered by the vapour of the corresponding element, has been explained on the hypothesis of resonance interactions between two excited atoms of the element. It has been pointed out that, according to this hypothesis, the maximum separation between the components of the transmitted doublet in the case of D_2 line of sodium would be twice that in the case of the D_1 line. This agrees fairly with the relative values of the maximum separation between the components of the doublets in these cases, reported previously.

INTRODUCTION

It was observed by Kastha (1949, 1953), that when almost monochromatic resonance radiation of sodium and mercury are filtered through vapour* of the corresponding elements at different temperatures and pressures, the resonance lines are not fully absorbed by the vapours and the transmitted lines appear as weak doublets. It was also found that the separation between the intensity-maxima in the doublet in each case increases with increase in the pressure of the absorbing vapour and their intensity decreases rapidly with the increase in the separation. It was further observed that the separation between the two components of the doublet observed in the case of D_2 line of sodium was about one and half times that in the case of the D_1 line. It has been concluded, from these results, that fluorescence radiations of changed frequencies, not present in the incident radiations, are created during the process of absorption and re-emission of the absorbed radiations by atoms of the absorbing vapour at suitable pressures. It was pointed out that the change in the frequency observed in these cases are much larger than those due to Doppler effect and Van der Waals forces.

As a qualitative explanation of the change of frequency of the re-emitted resonance line it was suggested that the emission might have taken place at the instant of collision between the excited atom and another neighbouring atom. In the present paper, the problem has been examined from quantum mechanical point of view and attempt has been made to explain the observed change in the frequency of the transmitted lines in the different cases.

*Communicated by Prof. S. C. Sirkar.

INFLUENCE OF RESONANCE BETWEEN TWO NEIGHBOURING EXCITED ATOMS ON THE FREQUENCY OF
EMITTED RADIATION

If a photon of proper frequency is incident on a system consisting of two atoms close to each other, one of the atoms may be excited through absorption of the radiation, but it is difficult to ascertain which of the two atoms is excited. Hence a resonance between the two atoms takes place. As a result, the energy level of the normally excited atom is slightly changed. The magnitude of this perturbation has been worked out by Margenau and Watson (1936). They have also shown that, due to variation in the distance of approach between the two interacting atoms, the perturbed energy states of the system containing the two atoms, instead of being discrete, are broadened symmetrically about its unperturbed position. If now continuous radiation is incident on the system consisting of such a pair of atoms the absorption of radiations by the pair would take place at frequencies slightly different from the frequency corresponding to the normal excited energy level of the atom.

In the present case, however, only the resonance radiation of definite frequency was incident on the atoms of the absorbing vapour, and therefore, any pair of atoms in resonance could not be excited by this radiation. The isolated atoms, however, could absorb the radiation and pass on to the excited state. We can postulate the following process of emission by the excited atoms, in which a change in the wavelength of the emitted radiation can be produced by the influence of the neighbouring atoms on each other.

Let us consider two such atoms 1 and 2, excited by absorption of resonance radiation incident on them while they were sufficiently apart from each other, and also, that at a certain instant before one of the two atoms is about to radiate, they come sufficiently close enough. Such an assumption is justified, as would be evident from the following considerations.

Corresponding to the pressure of the absorbing mercury vapour at 373°K , the number of atoms per c.c. is about 7.10^{15} , and consequently, the average distance between two atoms of mercury is of the order of 500 A.U. Since the average velocity of mercury atom at this temperature is about 3.10^4 cm/sec., the time required for two excited atoms separated by this distance to come close together is about 10^{-10} sec., which is small compared to the life time of 10^{-7} sec. of the excited state of the mercury atom (Garrett, 1932). Similarly, in the case of sodium vapour at about 560°K , the average distance between two neighbouring atoms is about 1000 A.U., and as the average velocity of the sodium atom at this temperature is about 10^6 cm/sec, the time required for two excited atoms of sodium separated originally by this distance to come closer together is about 10^{-10} sec. This is small compared to the life time of the excited state which is about 10^{-8} sec (Minkowski, 1926).

If we consider that the two excited atoms form a system, the system may be described by the composite wavefunction $\psi'(1)\psi'(2)$, where $\psi'(1)$ and $\psi'(2)$ are the excited state wave functions of the isolated excited atoms 1 and 2 respectively. There are two possibilities by which the system can return to the unexcited state. Either, both the atoms may radiate simultaneously or, they can do so one after another. Since the probability of the first process is small, we shall consider the second process only. In this case, an intermediate state of the system may be represented by either of the two following wave functions (Margenau and Watson 1936),

$$\psi' = \frac{1}{\sqrt{2}} [\psi(1)\psi'(2) + \psi'(1)\psi(2)]$$

$$\psi'' = \frac{1}{\sqrt{2}} [\psi(1)\psi'(2) - \psi'(1)\psi(2)]$$

while the final state can be written simply as $\psi(1)\psi(2)$. The linear combination of terms like $\psi(1)\psi'(2)$ takes account of the fact that either of the atoms may finally be in the unexcited state represented by ψ -function without prime. As pointed out by Margenau and Watson (1936), since the radiation from the initial state to the intermediate state and also from this state to the final state takes place through electric dipole radiation, the state given by ψ'' is excluded, for the transition moments due to transition to and from this state vanish. The energy of the initial state of the system, given by $\psi'(1)\psi'(2)$, will be $2E_0$, where E_0 is the energy of the normally excited atom, but the intermediate state will have a perturbation energy besides E_0 . The change in the energy was calculated by Margenau and Watson (1936) and is given by

$$\Delta\epsilon = -\frac{2}{3} \frac{e^2}{R^3} |r_{12}|^2 \quad \text{for } m = 0$$

$$\text{and} \quad \Delta\epsilon = +\frac{1}{3} \frac{e^2}{R^3} |r_{12}|^2 \quad \text{for } m = \pm 1$$

where R is the distance between the two atoms 1 and 2 and the m 's refer to the magnetic quantum number of the excited state, $|r_{12}|^2$ is given by $|r_{12}|^2 =$

$\frac{3\hbar f\lambda}{8\pi^2 c m_e}$, where $|r_{12}|$ denotes the linear transition moment, m_e the electronic mass,

λ the wave length of the resonance radiation, f the oscillator strength connected with this radiation and the other quantities have usual significance.

The energy of the radiated quantum will thus be $2E_0 - (E_0 + \Delta\epsilon) = E_0 - \Delta\epsilon$, where $\Delta\epsilon$ has one of the values indicated above. From this intermediate state the system can return to the ground state with the emission of a further quantum

with an energy of $E_0 + \Delta\epsilon$, slightly different from E_0 , as shown in figure 1. Thus the maximum frequency-shift on either side of the centre of the resonance radiation, would be $\frac{\Delta\epsilon}{hc} = \frac{e^2 f \lambda}{4\pi^2 c^2 R^3 m_0}$ cm⁻¹. Since the value of $\Delta\epsilon$ depends on R , the radiated energies of changed frequencies would not be discrete but would have

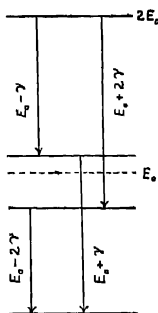


Fig. 1. Schematic energy levels of a pair of atoms in resonance.

a continuous nature, for R may have all possible values. It is also evident that those events, in which R will have a small value, will be rare compared to those in which the value of R is large, and accordingly, the intensity of radiations with relatively large frequency shifts will also be small. Moreover, as the probability of the excited atoms coming closer increases with the increase of temperature and pressure of the absorbing vapour, the extent by which the frequency of the emitted radiation changes also increases. It might, however, be mentioned that the probability of occurrence of the second process would depend on the availability of a large number of excited atoms, and therefore, the following conditions should be fulfilled:

- (1) The f -value, i.e. the oscillator strength of the resonance radiation of the element concerned must be large, and
- (2) the number of atoms per c.c. of the given element at a given temperature should be sufficiently high.

It is seen that $\Delta\epsilon$ varies directly as the value of the oscillator strength and therefore, the value of $\Delta\epsilon$ for D_1 and D_2 lines of sodium should be different. The values of f for D_1 and D_2 lines are 0.333 and 0.667 respectively, and so the value of $\Delta\epsilon$ for D_2 is expected to be double that for D_1 . It is interesting to note, as was previously reported (Kastha, 1953), that actually the separations for D_2 and D_1 are in the ratio 3 : 2. This is in fair agreement with the explanation given above.

All the radiated energies of changed wavelengths would not be transmitted by the vapour of the absorbing element, but a part of it would be absorbed due to resonance broadening of the absorption level of pairs of neighbouring atoms of the element

If we put $\gamma = e^2 h f \lambda / 8 \pi^2 R^3 c m_e$, the energy of the radiation emitted, during transition from the initially excited state to the intermediate state, is either $E_0 + 2\gamma$ or $E_0 - \gamma$, as can be seen from figure 1. Further, transition from this latter state to the unexcited final state creates radiations of energy equal to either $E_0 + \gamma$ or $E_0 - 2\gamma$. Hence, the radiations due to the former transition can not be absorbed by a pair of atoms in resonance and separated by the same distance R as in the case of emission, although there is some probability of absorption of the radiations due to transition from the intermediate state to the ground state. Even in the latter case, some fraction of the total intensity will escape. Hence, the maximum separation between the components of the transmitted radiations is expected to be $4\gamma/hc \text{ cm}^{-1}$. If the observation is made in a particular direction, while the radiation takes place in all directions, the intensity is expected to be small and this may be another reason for the observed weakness of the doublets.

It would be interesting to calculate the distance of closest approach between two atoms of sodium and between two atoms of mercury in the respective vapour from the magnitude of the separations between the components of the transmitted doublets observed in these cases (Kastha, 1949, 1953)

The value of R is calculated with the help of the following two formulae,

$$\Delta\nu(\text{cm}^{-1}) = \frac{2}{3} \frac{e^2}{chR^3} |r_{12}|^2$$

$$\text{and} \quad |r_{12}|^2 = \frac{3hf\lambda}{8\pi^2 cm_e}$$

The values of all the quantities used are in C. G. S. units. The calculated values of R , together with other relevant data, are given in Table I

TABLE I

Element	Wavelength of the Resonance Radiation in A.U.	Oscillator Strength f	$\Delta\nu$ in cm^{-1}	Distance R in A.U.
Na	5895.9(D_1)	1/3	1.125	50
	5889.9(D_2)	2/3	1.575	56
Hg	2536.6	1/35	0.3	8.2

It is seen from the above table that the value of R in the case of mercury is much smaller than that observed with sodium. Though the vapour pressure of mercury (273 mm) at 373°K is much larger than that of sodium at 563°K (9.1×10^{-3} mm), this alone may not be sufficient to explain the small value of R obtained in the former case. However, in the investigation with resonance radiation of mercury, the absorption cell through which the radiation was filtered contained nitrogen at a pressure of about one atmosphere (Kastha, 1949), and the small value of R may be due to local inhomogeneity in the distribution of atoms in the mixture.

ACKNOWLEDGMENT

The author's thanks are due to Prof. S. C. Sirkar, D.Sc., F.N.I., for his kind interest and valuable discussions and also to Prof. D. Basu, Ph.D., for helpful suggestions

REFERENCES

- Garrett, P. H., 1932, *Phys. Rev.*, **40**, 779.
Kastha, G. S., 1949, *Ind. J. Phys.*, **23**, 247.
„ 1953, *Ind. J. Phys.*, **27**, 67.
Margenau, H. and Watson, W. W., 1936, *Rev. Mod. Phys.*, **8**, 22.
Minkowski, R., 1926, *Z. f. Phys.*, **36**, 839.

EFFECT OF ANNULAR SOLAR ECLIPSE OF 19TH APRIL, 1958 (AT SUNRISE) ON THE F_2 LAYER OF THE IONOSPHERE

S. N. MITRA

RESEARCH DEPARTMENT, ALL INDIA RADIO, NEW DELHI

AND

B. C. NARASINGA RAO

SENIOR SCIENTIFIC ASSISTANT, C.S.I.R., ALL INDIA RADIO, TRIVANDRUM

(Received, October 30, 1959)

ABSTRACT. The paper describes the effect of the annual Solar Eclipse of 19th April, 1958 on the ionisation density of the F_2 layer over Trivandrum, Tiruchirapalli and Madras (South India). The eclipse occurred near sunrise at all the three places and its magnitude at maximum phase was 75 to 83%. Analysis of $(foF_2)^2$ values during control period and eclipse day showed a marked decrease in the ionisation density with the progress of the eclipse at all the three places. Theoretical considerations of the effect of an eclipse at sunrise on the ionisation density of the F_2 layer are discussed which have also led to the determination of the value of attachment co-efficient at 350 km. as approximately 10^{-5} sec^{-1} over Trivandrum.

INTRODUCTION

It is well known that an eclipse of the sun produces a decrease in the ionisation density in the E and F_1 layers. But such an effect is not so clearly marked in the F_2 layer, nor it is expected to be so from theoretical considerations. However, when the eclipse occurs around ground sunrise at any particular location, interesting results can be obtained of its optical effect on the F_2 layer. The annular solar eclipse of 19th April, 1958 occurred near sunrise in the south of India and special investigations of the ionosphere were carried out at Trivandrum, Tiruchirapalli and Madras Stations of All India Radio. The present paper deals with these observations. The circumstances of the eclipse are shown in Table I below.

It would be noted from Table I that the eclipse occurred very near to ground sunrise at all the three locations. Ionospheric observations have also shown interesting results

EXPERIMENTAL PROCEDURE

The equipment for ionospheric observations at all the three places are exactly identical. The pulse transmitter is manually operated and is capable of sweeping

through a frequency range of 1.5 to 18 Mc/s. The radiated power is of the order of one kilowatt. The echoes are received in a receiver modified for pulse reception and displayed on a cathode ray oscillograph in the usual way. A height calibrator provides height marks at intervals of 40 or 20 km. A suppressor unit has been provided to suppress the strong ground pulse for facilitating the measurement of E layer characteristics. The transmitting and the receiving acrials are conventional inverted deltas oriented at right angles to each other.

The effect on the F_2 layer of the solar eclipse of 19th April 1958 was investigated in the following way. The control period was taken as 8 days each preceding and following the eclipse day. The half hourly measurements of layer heights and critical frequencies of E and F_2 layers for this period were utilised as control observations. On the eclipse day itself, measurements were taken once every 15 minutes. (The accuracy in height measurements was ± 20 or ± 10 km and critical frequency ± 0.1 Mc/s). Measurements on E layer were vitiated by the appearance of Es and those on the F_2 layer will only be discussed.

TABLE I

Circumstances of the eclipse of 19th April '58.

	Trivandrum	Tiruchirapalli	Madras
	(8°29'N, 76°57'E)	(10°49'N, 78°42'E)	(13°05'N, 80°17'E)
Eclipse begins	0604 IST	0606 IST	0609 IST
Eclipse maximum	0711 ..	0714 ..	0718 ..
Eclipse ends	0829 ..	0834 ..	0838 ..
Ground sunrise	0612 ..	0603 ..	0555 ..
Magnitude	83%	79%	75%

(1ST = GMT + 5½ hours).

RESULTS

The average behaviour of the F_2 layer is determined from the observations during the control days (± 8 days centred on the eclipse day) and compared with those on the eclipse day. The layer heights did not show any significant behaviour and therefore, only $f_o F_2$ values will be considered.

(a) Trivandrum

Figure 1 shows the variation of $(foF_2)^2$ from 0430 to 0930 IST on the control days and on the eclipse day. The eclipse and sunrise timings are indicated in the figure. It would be seen from this figure that there was a steady and rapid increase in ionisation from about 0530 to 0830 IST during the control period. This type of rapid increase in early morning is well known at equatorial latitudes

and is also regularly observed at all the three stations. The day-to-day variation is only in the level of ionisation. On the eclipse day, the initial level of ionisation

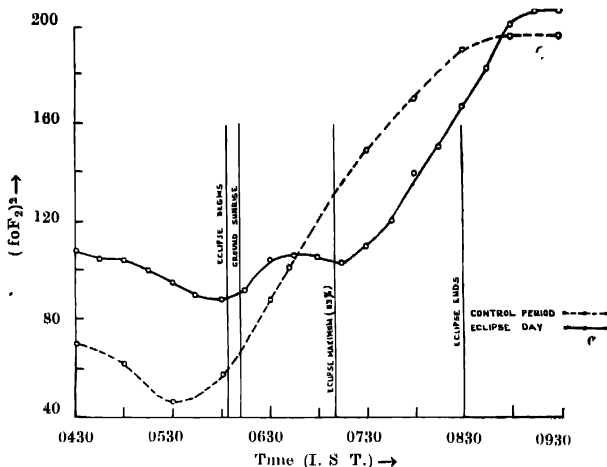


Fig. 1 Variation of ion density, Trivandrum

was itself high as would be seen from figure 1. At about 0600 IST, the ionisation density started increasing and followed its usual trend upto about 0630 IST. Thereafter, it remained more or less stationary as the eclipse progressed. It showed a slight decrease at 0715 IST. Thus, the usually observed rapid rise in the ionisation density was arrested with the obscuration of the solar disc. During the recovery period i.e. after the maximum of the eclipse, there was a rapid increase in ionisation density to reach the normal level by about 0900 IST. It may be noted that the decrease in ionisation density near the maximum of the eclipse, as compared to the level on control days, is quite considerable.

(b) Tiruchirapalli

Figure 2 shows the variation of $(foF_2)^2$ for Tiruchirapalli. The eclipse timings were a few minutes later than those at Trivandrum. The same trend, as observed in the case of Trivandrum, is also apparent here; the initial level of ionisation was high on the eclipse day, it remained practically constant from 0645 to 0745 IST, a small decrease at 0800 IST and thereafter a rapid rise to a constant level at 0845 IST. During the control period, there was a steady but rapid increase in ionisation density from 0600 to 0830 IST which is, however, a regular feature at this station. The minimum in ionisation density occurred about 45 minutes after the eclipse maximum. Here also, the decrease in the ionisation density with the onset and progress of eclipse was quite considerable.

(c) *Madras*

Figure 3 shows the variation of $(foF_2)^2$ for Madras and the same trend in the behaviour of the ionisation density was observed as was in the case of Tiruvandrum and Tiruchirapalli. On the eclipse day, the values of foF_2 at 0430.

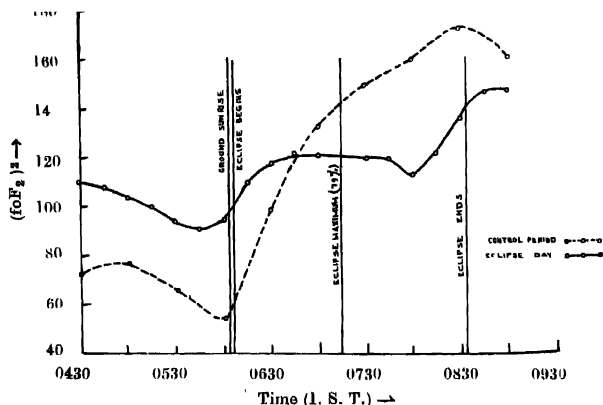


Fig. 2. Variation of ion density, Tiruchirapalli.

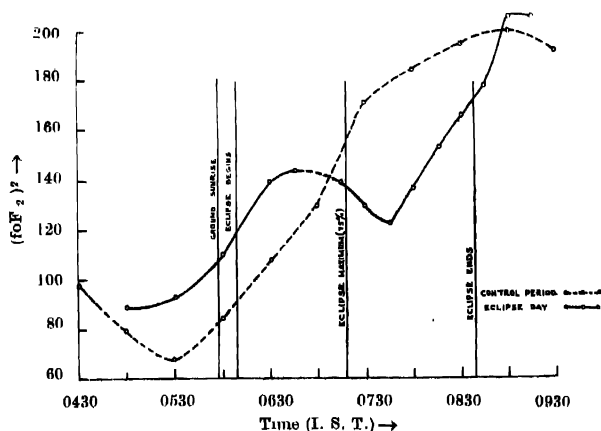


Fig. 2. Variation of ion density, Madras.

0445, 0515, 0545 and 0615 IST were doubtful and have been excluded from the mean curve. During the control period, the ionisation density increased rapidly from 0530 to 0900 IST. On the eclipse day, the increase was maintained till

0645 and then the ionisation decreased gradually to reach a minimum at 0745 IST. Thereafter, the increase was rapid till a constant level was reached at 0900 IST. The minimum in the ionisation density was quite considerable and was displaced from the eclipse maximum by about 27 minutes.

DISCUSSION

It is apparent from the variation of $(foF_2)^2$ as shown in figures 1, 2 and 3 that the eclipse did bring down the ionisation density along with the obscuration of the solar disc. It is also noticed that the ionisation density did not vary very appreciably as the solar disc was gradually covered and its minimum did not coincide with the maximum obscuration. But in all the three cases, the increase in ionisation density had been very rapid soon after the maximum of the eclipse. As the eclipse had occurred shortly after sunrise, the difference in the behaviour of the ionisation before and after the maximum of the eclipse can be explained qualitatively in the following way. During the obscuration of the solar disc, though the intensity of the solar radiation was gradually decreasing $\cos \chi$ (χ = solar zenith angle) was on the increase. These two effects were apparently balancing each other so as to retain the ionisation density at a fairly constant value. On the other hand, after the maximum of the eclipse, both the intensity of radiation as well as $\cos \chi$ were increasing with the result that the ionisation density showed a rapid rise.

We have mentioned earlier that the effect of eclipse in the F_2 layer of the ionosphere has not been so regularly observed as in the case with the E and F_1 layers. But when the eclipse occurs near ground sunrise the situation is different and a clear effect on the F_2 layer should be observable. Wells (1952) has reported well-marked effects of solar eclipse of September 1, 1951 which occurred near sunrise along the coast of United States.

It is interesting to note that the variation in the ionisation density during the progress of the eclipse, as observed by Wells, is very similar to what has been observed by us and described in this paper. Theoretical interpretation of the effect of eclipse near sunrise is discussed below.

The ionisation density of the F_2 layer at times other than sunrise is not wholly determined by χ but is greatly influenced by large scale movements of electrons. Ratcliffe (1956) has shown that if the electrons in the F_2 layer disappear by attachment process, its co-efficient γ varying with height, being given by

$$\gamma(Z) = 10^{-4} \exp \left[\frac{300 - Z(km)}{50} \right] \text{ sec}^{-1} \quad \dots (1)$$

then the time constant of the electrons at different heights would be 3 hours at 300 km, 7.5 hours at 350 km and 20 hours at 400 km. In the present case,

the eclipse lasted for about 2 hours and the layer height was about 350 km. Thus, if the same considerations are to hold good, the effect of the eclipse should be nil.

But the eclipse occurring near sunrise brings about a significant difference. Assuming that the peak electron production rate is at the height (Z_m) of maximum electron density (N_m) as in a Chapman layer, the variation of N_m with time during solar eclipse is governed by :

$$\frac{dN_m(t)}{dt} = A Q_0 \cos \chi - \gamma(Z_m) N_m(t) \quad \dots (2)$$

Where A = fraction of the solar disc exposed,

Q_0 = peak electron production rate when the solar rays are vertical.

The motion of electrons in the F_2 layer represented by a function $M(t)$ gives an additional term $N_m M(t)$ (Ratcliffe, 1956). But near sunrise, $\frac{dN_m(t)}{dt}$ is large and $\gamma(Z_m) N_m(t)$ and $N_m M(t)$ are small, so that N_m is mostly determined by $A Q_0 \cos \chi$. Thus, when an eclipse occurs near sunrise, its effect should manifest itself in a distinct decrease of the ionisation density in synchronism with the obscuration of the solar disc.

It will be noted from figure 1 that $\frac{dN_m}{dt} \approx 0$ from 0630 to 0715 IST.

From equation (2) we get, for this time interval,

$$A Q_0 \cos \chi = \gamma(Z_m) \cdot N_m \quad \dots (3)$$

Assuming probable values of Q_0 , $\gamma(Z_m)$ was found to be of the order of 10^{-5} sec^{-1} when the height of the maximum ionisation density was 350 km. This value of the attachment co-efficient is in good agreement with the same obtained elsewhere.

ACKNOWLEDGMENTS

The work described in this paper forms a part of programme of ionospheric research of Research Department of All India Radio, and also forms a part of the programme of the Indian National Committee for International Geophysical Year. The paper is published by permission of the Chief Engineer, All India Radio.

We are grateful to Mr. P. Ramankutty Nair, Mr. Y.N.G. Rao and Mr. S. S. Kohli, Station Engineers, All India Radio at Trivandrum, Tiruchirapalli and Madras for the supervision and to the CSIR staff at the stations for taking observations. The eclipse parameters have been obtained from the Indian Ephemeris and Nautical Almanac, 1958, published by the Director General of Observatories, New Delhi.

REFERENCES

- Ratcliffe, J. A., 1956, *Solar Eclipses and the Ionosphere*, Pergamon Press, 1.
Wells, H. W., 1952, *J. Geophys. Res.*, 57, 201.

Letters to the Editor

The Board of Editors will not hold itself responsible for opinions expressed in the letters published in this section. The notes containing reports of new work communicated for this section should not contain many figures and should not exceed 500 words in length. The contributions must reach the Assistant Editor not later than the 15th of the second month preceding that of the issue in which the paper is to appear. No proof will be sent to the authors.

12

A NOTE ON THE SPECTRUM OF Br IV

Y. BHUPALA RAO

O. N. G. COMMISSION, DEHRA DUN

(Received, November 21, 1959)

With the help of the extensive data on the spark spectrum of bromine obtained in connection with the analyses of Br II and Br III spectra (Bhupala Rao, 1956 and 1958), an attempt has been made to extend the analysis of the spectrum of trebly ionised bromine, which was worked out only partially by A. S. Rao and S. G. Krishna Murty (1934). A few additional lines have been classified and the scheme of classification suggested previously has been observed to be correct. The newly classified lines are listed below.

TABLE I

Intensity Cond. dis.	λ (air) \AA	ν (vac) cm^{-1}	Classification	
3	3380.56	30473.9	5s $3P^0_3 - 5p$	$3D_2$
7 H	2907.71	34381.3	5s $3P^0_2 - 5p$	$3D_3$
0	2874.57	34777.6	5s $3P^0_1 - 5p$	$3D_1$
6	2842.88	35165.3	5s $3P^0_1 - 5p$	$3D_2$
8 H	2772.62	36056.4	5s $3P^0_0 - 5p$	$3D_1$
7 H	2570.83	38886.3	4d $3P^0_1 - 5p$	$3P_1$
5	2411.64	41452.9	4d $3P^0_1 - 5p$	$3P_2$
7	2257.24	44288.1	4d $3P^0_2 - 5p$	$3D_3$
7	2204.50	45347.6	4d $3P^0_2 - 5p$	$3P_2$

Calculated with respect to the ground level $4p^2\ ^3p_0$ as zero the newly identified levels are

$$\begin{aligned} 5p\ ^3D_1 &= 216674 \\ &\quad 388 \\ ^3D_2 &= 217062 \\ &\quad 3907 \\ ^3D_3 &= 220969 \end{aligned}$$

REFERENCES

- Bhupala Rao, Y., 1956, *Ind. J. Phys.*, **30**, 371.
 Bhupala Rao, Y., 1958, *Ind. J. Phys.*, **32**, 497.
 Rao, A. S. and Krishna Murty, S. G., 1934, *Proc. Phys. Soc.*, **46**, 351.

13

ON THE MAGNETIC PERTURBATION OF AN
ELECTRON BEAM

S. YAMAGUCHI

THE INSTITUTE OF PHYSICAL AND CHEMICAL RESEARCH, 31 KAMIFUJI (HONGO), TOKYO,
JAPAN

(Received, November 12, 1959)

A sharp edge of the usual razor blade of hard steel was employed as a specimen for the experiment. The remanence of this specimen was about 10^4 gaussos. A fine electron beam (diameter of the cross-section being 0.05 mm nearly) grazed the edge of the specimen of the maximum gradient of the magnetic field. An electron diffraction pattern here obtained is shown in figure 1. In this figure we see that the diffraction rings are abnormally perturbed. The central spot found in figure 1 was optically 12 times enlarged in order to investigate the perturbation suffered by the incident beam in passing through the magnetic gradient. This perturbation is recognizable in figure 2. In this figure we see that a unique incident beam is splitted into many a beam. This singular phenomenon should be elucidated in the present study.



Fig. 1. Diffraction pattern obtained from the edge of permanent magnet. The diffraction rings are perturbed. (Wavelength . 0.0328 Å Camera-length : 495 mm. Positive enlarged 2.3 times)

It is known that an electron beam spreads in passing through a magnetic field with gradient. As a matter of fact, all the splitted beams found in figure 2



Fig. 2. The central spot in figure 1 is 12 times enlarged. The incident beam is splitted into many a beam.

show the spreading. From this spreading, ΔZ , we can estimate the magnetic gradient $|\partial H_z / \partial Z|$ existing at the edge of the specimen according to the following equation:

$$\Delta Z = e \left| \frac{\partial H_z}{\partial Z} \right| \cdot \Delta X \cdot \frac{\lambda L}{h} \quad \dots (1),$$

where e is the electron charge (1.6×10^{-20} emu), ΔX is the diameter of the cross-section of the intact incident beam, λ is the wavelength of the electrons (0.0328) Å, L is the magnetic path of the electrons (about one micron), L is the camera length

(495 mμ), and h is the Plank's constant (6.6×10^{-27} erg. sec). In figure 2 we measure $\Delta Z/\Delta X \simeq 3$. Therefore, we obtain $|\partial H_z/\partial Z| \simeq 10^6$ gauss/cm. This magnetic gradient is steep enough to polarize the electrons according to the Stern-Gerlach's process. The separation between the parallel and the antiparallel electron spin, which results from the Stern-Gerlach's process, is given by replacing ΔX by λ in Eqn. (1). Therefore, the force for this separation is weak as compared with that for the spreading caused by the magnetic gradient so that the former is overwhelmed by the latter. This implies that the spin separation can not directly be observed in the present process (1).

Any splitted electron beam observed in figure 2 contains the polarized electrons. As there are many fine zigzag edges in the specimen (figure 3), a re-

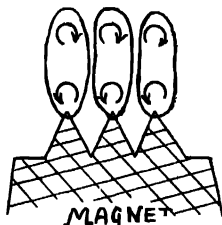


Fig. 3. Any splitted beams in figure 2 contains the polarized electrons. A repulsion occurs between the polarized electrons.

pulsion occurs between the polarized beams, which corresponds to a repulsion between the magnetic moments. In figure 3, the sign of the arrow means the spin directions contained in the polarized beams. In this way the splitting of the electron beams in figure 2 is elucidated as the indirect result of the polarization caused by the behaviour of electron spin.

REFERENCES

- Mott, N. F., 1929, *Proc. Roy. Soc. A.*, **124**, 440.
 Mott, N. F. and Massey, H. S., 1950, "The Theory of Atomic Collisions" II. Ed. (Oxford), pp. 61.
 Van der Spuy, E., 1956, *Nuovo Cimento*, **4**, 1349.